METHODS IN MOLECULAR BIOLOGY™ 312

# Calcium Signaling Protocols

## Second Edition

Edited by

David G. Lambert

HUMANA PRESS

# Calcium Signaling Protocols

# METHODS IN MOLECULAR BIOLOGY™

## *John M. Walker,* SERIES EDITOR

**325. Nuclear Reprogramming:** *Methods and Protocols,* edited by *Steve Pells, 2006*

**324. Hormone Assays in Biological Fluids,** edited by *Michael J. Wheeler and J. S. Morley Hutchinson, 2006*

**323. Arabidopsis Protocols,** *Second Edition,* edited by *Julio Salinas and Jose J. Sanchez-Serrano, 2006*

**322. *Xenopus* Protocols:** *Cell Biology and Signal Transduction,* edited by *X. Johné Liu, 2006*

**321. Microfluidic Techniques:** *Reviews and Protocols,* edited by *Shelley D. Minteer, 2006*

**320. Cytochrome P450 Protocols**, *Second Edition,* edited by *Ian R. Phillips and Elizabeth A. Shephard, 2006*

**319. Cell Imaging Techniques**, *Methods and Protocols,* edited by *Douglas J. Taatjes and Brooke T. Mossman, 2006*

**318. Plant Cell Culture Protocols**, *Second Edition,* edited by *Victor M. Loyola-Vargas and Felipe Vázquez-Flota, 2005*

**317. Differential Display Methods and Protocols**, *Second Edition,* edited by *Peng Liang, Jonathan Meade, and Arthur B. Pardee, 2005*

**316. Bioinformatics and Drug Discovery**, edited by *Richard S. Larson, 2005*

**315. Mast Cells:** *Methods and Protocols,* edited by *Guha Krishnaswamy and David S. Chi, 2005*

**314. DNA Repair Protocols:** *Mammalian Systems, Second Edition,* edited by *Daryl S. Henderson, 2005*

**313. Yeast Protocols:** *Second Edition,* edited by *Wei Xiao, 2005*

**312. Calcium Signaling Protocols:** *Second Edition,* edited by *David G. Lambert, 2005*

**311. Pharmacogenomics:** *Methods and Applications,* edited by *Federico Innocenti, 2005*

**310. Chemical Genomics:** *Reviews and Protocols,* edited by *Edward D. Zanders, 2005*

**309. RNA Silencing:** *Methods and Protocols,* edited by *Gordon Carmichael, 2005*

**308. Therapeutic Proteins:** *Methods and Protocols,* edited by *C. Mark Smales and David C. James, 2005*

**307. Phosphodiesterase Methods and Protocols,** edited by *Claire Lugnier, 2005*

**306. Receptor Binding Techniques:** *Second Edition,* edited by *Anthony P. Davenport, 2005*

**305. Protein–Ligand Interactions:** *Methods and Applications,* edited by *G. Ulrich Nienhaus, 2005*

**304. Human Retrovirus Protocols:** *Virology and Molecular Biology,* edited by *Tuofu Zhu, 2005*

**303. NanoBiotechnology Protocols,** edited by *Sandra J. Rosenthal and David W. Wright, 2005*

**302. Handbook of ELISPOT: Methods and Protocols,** edited by *Alexander E. Kalyuzhny, 2005*

**301. Ubiquitin–Proteasome Protocols,** edited by *Cam Patterson and Douglas M. Cyr, 2005*

**300. Protein Nanotechnology:** *Protocols, Instrumentation, and Applications,* edited by *Tuan Vo-Dinh, 2005*

**299. Amyloid Proteins:** *Methods and Protocols,* edited by *Einar M. Sigurdsson, 2005*

**298. Peptide Synthesis and Application,** edited by *John Howl, 2005*

**297. Forensic DNA Typing Protocols,** edited by *Angel Carracedo, 2005*

**296. Cell Cycle Control:** *Mechanisms and Protocols,* edited by *Tim Humphrey and Gavin Brooks, 2005*

**295. Immunochemical Protocols,** *Third Edition,* edited by *Robert Burns, 2005*

**294. Cell Migration:** *Developmental Methods and Protocols,* edited by *Jun-Lin Guan, 2005*

**293. Laser Capture Microdissection:** *Methods and Protocols,* edited by *Graeme I. Murray and Stephanie Curran, 2005*

**292. DNA Viruses:** *Methods and Protocols,* edited by *Paul M. Lieberman, 2005*

**291. Molecular Toxicology Protocols**, edited by *Phouthone Keohavong and Stephen G. Grant, 2005*

**290. Basic Cell Culture Protocols**, *Third Edition,* edited by *Cheryl D. Helgason and Cindy L. Miller, 2005*

**289. Epidermal Cells**, *Methods and Applications,* edited by *Kursad Turksen, 2005*

**288. Oligonucleotide Synthesis**, *Methods and Applications,* edited by *Piet Herdewijn, 2005*

**287. Epigenetics Protocols**, edited by *Trygve O. Tollefsbol, 2004*

**286. Transgenic Plants:** *Methods and Protocols,* edited by *Leandro Peña, 2005*

**285. Cell Cycle Control and Dysregulation Protocols:** *Cyclins, Cyclin-Dependent Kinases, and Other Factors,* edited by *Antonio Giordano and Gaetano Romano, 2004*

**284. Signal Transduction Protocols,** *Second Edition,* edited by *Robert C. Dickson and Michael D. Mendenhall, 2004*

**283. Bioconjugation Protocols,** edited by *Christof M. Niemeyer, 2004*

**282. Apoptosis Methods and Protocols,** edited by *Hugh J. M. Brady, 2004*

**281. Checkpoint Controls and Cancer, Volume 2:** *Activation and Regulation Protocols,* edited by *Axel H. Schönthal, 2004*

**280. Checkpoint Controls and Cancer, Volume 1:** *Reviews and Model Systems,* edited by *Axel H. Schönthal, 2004*

**279. Nitric Oxide Protocols,** *Second Edition,* edited by *Aviv Hassid, 2004*

METHODS IN MOLECULAR BIOLOGY™

# Calcium Signaling Protocols

*Second Edition*

Edited by

**David G. Lambert**

*Department of Cardiovascular Sciences,*
*Division of Anaesthesia, Critical Care, and Pain Management,*
*Leicester Royal Infirmary, Leicester, UK*

HUMANA PRESS TOTOWA, NEW JERSEY

999 Riverview Drive, Suite 208
Totowa, New Jersey 07512

**www.humanapress.com**



This publication is printed on acid-free paper. ♾
ANSI Z39.48-1984 (American Standards Institute) Permanence of Paper for Prined Library Materials.

Production Editor: Nicole E. Furia

Cover design by Patricia F. Cleary

For additional copies, pricing for bulk purchases, and/or information about other Humana titles, contact Humana at the above address or at any of the following numbers: Tel.: 973-256-1699; Fax: 973-256-8341; E-mail: orders@humanapr.com; or visit our Website: www.humanapress.com



Printed in the United States of America. 10 9 8 7 6 5 4 3 2 1

eISBN 1-59259-949-4

ISSN 1064-3745

Library of Congress Cataloging-in-Publication Data

Calcium signaling protocols / edited by David G. Lambert.-- 2nd ed.
p. ; cm. -- (Methods in molecular biology ; v. 312)
Includes bibliographical references and index.
ISBN 1-58829-442-0 (alk. paper)
1. Calcium--Laboratory manuals. 2. Calcium--Research--Methodology. 3. Calcium channels--Research--Methodology. 4. Cellular signal transduction--Research--Methodology.
[DNLM: 1. Calcium--pharmacokinetics. 2. Calcium Channels--pharmacokinetics. 3. Calcium Signaling--physiology. 4. Signal Transduction. 5. Spectrometry, Fluorescence--methods. QV 276 C14443 2006] I. Lambert, David G. II. Series: Methods in molecular biology (Clifton, N.J.) ; v. 312.
QP535.C2C2665 2006
572'.516--dc22

2005005383

# Preface

In the first edition of *Calcium Signaling Protocols* I began by writing "The regulation of intracellular $Ca^{2+}$ is a common theme presented in many papers over the last 20 or so years and the description of the $Ca^{2+}$-sensitive indicator dye fura-2 in 1985 resulted in a massive increase in these types of studies." This statement is as true in 2005 as it was in 1999, but 20 or so years is now 30 years!

There has been some reorganization of the volume such that there are now 22 chapters including five new ones, all written by experts in their field. These new chapters include use of the FlexStation and electrophysiological measurement of $Ca^{2+}$ channel activity. The book is broken into six parts. Part I is a general coverage of basic theory and the simplest use of fluorescent indicators. Part II covers specialist measurement systems and Part III covers measurement of $Ca^{2+}$ channel activity. Assessment of release of stored $Ca^{2+}$ is covered in some detail in Part IV, with Parts V and VI covering specialist measurement techniques and $Ca^{2+}$-sensitive targets.

Putting a book like this together, even as a second edition, takes time and I am, again, indebted to the individual authors for their help and patience. I am also very grateful to Professor John M. Walker, the series editor, for his continued help and advice over the course of this project.

I would like to end this preface, much as in the final paragraph of the first edition, by sincerely hoping that the specialist will find *Calcium Signaling Protocols: Second Edition* useful and that readers contemplating moving into studies on the regulation of intracellular $Ca^{2+}$ for the first time will find it a source of both theoretical and practical information.

***For Elizabeth***

***David G. Lambert***

# Contents

# Contributors


Izzy Boyfield • *Neurology Centre of Excellence for Drug Discovery, GlaxoSmithKline Pharmaceuticals Ltd, Harlow, Essex, UK*

Paul J. Brighton • *Department of Cell Physiology and Pharmacology, University of Leicester, Leicester, UK*

María F. Cano-Abad • *Departamento de Farmacologia, Facultad de Medicina, Universidad Autonoma de Madrid, Madrid, Spain*

Shamshad Cockcroft • *Department of Physiology, University College London, London, UK*

Ian D. Forsythe • *Department of Cell Physiology and Pharmacology, University of Leicester, Leicester, UK*

Antonio G. García • *Departamento de Farmacologia, Facultad de Medicina, Universidad Autonoma de Madrid, Madrid, Spain*

Robert J. Gillies • *Departments of Physiology and Biochemistry, University of Arizona Health Sciences Center, Tucson, AZ*

Atticus H. Hainsworth • *Pharmacology Research Group, Leicester School of Pharmacy, De Montfort University, Leicester, UK*

Charlotte Harrison • *Division of Anaesthesia, Critical Care, and Pain Management, Leicester Royal Infirmary, University of Leicester, Leicester, UK*

Kazuyoshi Hirota • *Department of Anesthesiology, University of Hirosaki School of Medicine, Hirosaki, Japan*

Robert A. Hirst • *Department of Child Health, Division of Anaesthesia, Critical Care, and Pain Management, Leicester Royal Infirmary, University of Leicester, Leicester, UK*

Aldebaran M. Hofer • *Department of Surgery, Harvard Medical School, Boston, MA*

Hideo Kanaide • *Division of Molecular Cardiology, Research Institute of Angiocardiology, Faculty of Medicine, Kyushu University, Fukuoka, Japan*

Danuta Kosk-Kosicka • *Department of Anesthesiology, Johns Hopkins University School of Medicine, Baltimore, MD*

David G. Lambert • *Department of Cardiovascular Sciences, Division of Anaesthesia, Critical Care, and Pain Management, Leicester Royal Infirmary, University of Leicester, Leicester, UK*

Manuela G. López • *Departamento de Farmacologia, Facultad de Medicina, Universidad Autonoma de Madrid, Madrid, Spain*

Ronald M. Lynch • *Department of Physiology, University of Arizona Health Sciences Center, Tucson, AZ*

Ian C. B. Marshall • *Neurology Centre of Excellence for Drug Discovery, GlaxoSmithKline Pharmaceuticals Ltd., Harlow, Essex, UK*

Raul Martinez-Zaguilan • *Department of Physiology, Texas Tech University Health Sciences Center, Lubbock, TX*

Martin R. McAinsh • *Department of Biological Sciences, Institute of Environmental and Natural Sciences, Lancaster University, Lancaster, UK*
Terence J. McCann • *Department of Orthodontics and Paediatric Dentistry, United Medical and Dental Schools, Guy's Hospital, London, UK*
Shaun McNulty • *Neurology Centre of Excellence for Drug Discovery, GlaxoSmithKline Pharmaceuticals Ltd, Harlow, Essex, UK*
Anthony J. Morgan • *Physiology Group, Vascular Biology Research Centre, Biomedical Sciences Division, King's College London, London, UK*
Adriaan Nelemans • *Department of Molecular Pharmacology, University Centre for Pharmacy, University of Groningen, Groningen, The Netherlands*
Carl K.-Y. Ng • *Department of Botany, University College Dublin, Dublin, Ireland*
Leong L. Ng • *Pharmacology and Therapeutics Group, Department of Cardiovascular Diseases, Leicester Royal Infirmary, University of Leicester, Leicester, UK*
Davina E. Owen • *Neurology Centre of Excellence for Drug Discovery, GlaxoSmithKline Pharmaceuticals Ltd., Harlow, Essex, UK*
Paulene A. Quinn • *Division of Clinical Pharmacology, Department of Medicine and Therapeutics, University of Leicester, Leicester, UK*
Andrew D. Randall • *Neurology Centre of Excellence for Drug Discovery, GlaxoSmithKline Pharmaceuticals Ltd, Harlow, Essex, UK*
Rajendra K. Sharma • *Department of Pathology, Saskatoon Cancer Centre, College of Medicine, University of Saskatchewan, Sakatoon, Saskatchewan, Canada*
Alec W. M. Simpson • *Department of Human Anatomy and Cell Biology, University of Liverpool, Liverpool, UK*
Alison Skippen • *Department of Physiology, University College London, London, UK*
Darren Smart • *Neurology Centre of Excellence for Drug Discovery, GlaxoSmithKline Pharmaceuticals Ltd., Harlow, Essex, UK*
Alessandro Stefani • *IRCCS Fondazione Santa Lucia, Rome, Italy*
Philip Swigart • *Department of Physiology, University College London, London, UK*
Andrew P. Thomas • *Department of Pathology, Cell Biology and Anatomy, Thomas Jefferson University, Philadelphia, PA*
Linda S. Tompkins • *Department of Physiology, University of Arizona Health Sciences Center, Tucson, AZ*
Stephen C. Tovey • *Department of Pharmacology, University of Cambridge, Cambridge, UK*
Mercedes Villarroya • *Departamento de Farmacologia, Facultad de Medicina, Universidad Autonoma de Madrid, Madrid, Spain*
Robert A. Wilcox • *Department of Neurology, Flinders Medical Centre, Bedford Park, Adelaide, Australia*
Gary B. Willars • *Department of Cell Physiology and Pharmacology, University of Leicester, Leicester, UK*

# I

# General

# 1

## Fluorescent Measurement of $[Ca^{2+}]_c$

*Basic Practical Considerations*

**Alec W. M. Simpson**

### 1. Introduction

It is extremely difficult to write a prescriptive account of how to measure cytosolic-free $Ca^{2+}$ ($[Ca^{2+}]_c$) that will suit all potential investigators. The problem arises because of the wide diversity of fluorescent $Ca^{2+}$ indicators that are now available, the variety of cells to be investigated, and the range of detection equipment that can be used. Consequently, this chapter is designed to provide the user with an overview of the technology in order that he or she can move toward developing a protocol that will suit the experimental objectives, the cells, and the equipment available to the investigator.

The main approaches to measuring $[Ca^{2+}]_c$ before the synthesis of fluorescent $Ca^{2+}$ indicators involved using the $Ca^{2+}$-activated photoprotein aequorin, $Ca^{2+}$-selective microelectrodes, or absorbance indicators ***(1)***. The use of aequorin and microelectrodes was generally restricted to large cells (usually from invertebrates) that were easy to handle and manipulate with micropipets. With a few notable exceptions (e.g., injection of hepatocytes and myocytes with aequorin by Cobbold and colleagues ***[2,3]***), these approaches were not applied to the wide diversity of cells present in mammalian tissues. The use of absorbance dyes did not become widespread because they are not very sensitive to the typical $[Ca^{2+}]_c$ found in cells, and did not offer any real potential for investigating $[Ca^{2+}]_c$ in monolayers or single cells.

The synthesis of quin2 by Tsien ***(4,5)*** in the early 1980s heralded a new era in the measurement of $Ca^{2+}$ by making available fluorescent probes that could be readily introduced into living cells. The most commonly used fluorescent $Ca^{2+}$ indicator has been fura-2, which, along with indo-1, formed the first gen-

From: *Methods in Molecular Biology, vol. 312: Calcium Signaling Protocols: Second Edition*
Edited by: D. G. Lambert © Humana Press Inc., Totowa, NJ

eration of ratiometric indicators also designed by Tsien and colleagues ***(6)***. In recent years, the fluo-based indicators have been widely used because of their high fluorescence, favorable $K_d$s, and suitability for 488 laser line excitation.

The $Ca^{2+}$-binding properties of these indicators is formed by the presence of a tetracarboxylic acid core as found in the $Ca^{2+}$-chelator ethylene glycol tetraacetic acid (EGTA). The original $Ca^{2+}$ indicator quin2 and its successors were designed around an EGTA derivative, BAPTA, also synthesized by Tsien ***(7)***. For a compound to act as an intracellular $Ca^{2+}$ indicator, selectivity of the indicator for $Ca^{2+}$ over other physiologically important ions is essential. EGTA already showed a much greater selectivity for $Ca^{2+}$ over $Mg^{2+}$, $Na^+$, and $K^+$, but unfortunately, its $Ca^{2+}$ binding is very pH sensitive. Cells undergo physiological changes in pH ***(8)***, which in the case of an EGTA-like chelator would affect the reported $[Ca^{2+}]_c$. Calibrating a pH-sensitive $Ca^{2+}$ indicator is difficult, because small changes in pH of the calibration solutions affect the measured fluorescence and the $K_d$ for $Ca^{2+}$. The synthesis of BAPTA, a largely pH-insensitive $Ca^{2+}$ chelator, was therefore an important step in the development of fluorescent probes for measuring $[Ca^{2+}]_c$ ***(7)***.

Since the introduction of quin2, fura-2, and indo-1, numerous other fluorescent $Ca^{2+}$ indicators have been synthesized, each with varying fluorescence characteristics and $K_d$s for $Ca^{2+}$ (*see* **ref. *9***; **Tables 1–3**). The fundamental properties of these indicators are similar in that the binding of $Ca^{2+}$ produces a wavelength shift in either the excitation or emission fluorescence spectra ***(6,9)***. When there is little or no shift in the excitation spectra, a $Ca^{2+}$-dependent change in the emission intensity is used to report changes in $Ca^{2+}$ ***(5,9)***. This can arise from $Ca^{2+}$-dependent changes in the intensity of absorbance or quantum efficiency.

In terms of fluorescence properties, the indicators can be divided into two main groups, those that are excited by near ultraviolet (UV) wavelengths 330–380 nm (e.g., quin2, fura-2, indo-1, and their derivatives) and those that are excited with visible light at or above 450 nm (e.g., fluo-indicators, Calcium Green, rhod-2; *see* **refs. *9*** and ***10***). The fluorophores for the visible indicators tend to be fluoroscein and rhodamine derivatives. This is advantageous because a great deal of fluorescence instrumentation has been designed for use with fluoroscein- and rhodamine-based dyes.

## 2. Synthetic $Ca^{2+}$ indicators

### *2.1. Single Excitation Indicators*

The first of this family is quin2 ***(5)***, Tsien's original fluorescent $Ca^{2+}$ indicator. When excited at 340 nm, an increase in emission intensity peaking at 505 nm is observed on binding $Ca^{2+}$. Under physiological conditions quin2 has a $K_d$ of 115 n*M*, making it useful for measuring $[Ca^{2+}]_c$ changes at or close to those

found in unstimulated (resting) cells. However, the dye is of little use in monitoring changes in $[Ca^{2+}]_c$ in excess of 1 μ*M*. Poor quantum efficiency has limited the use of this indicator, especially after the introduction of the more fluorescent ratiometric probes. However, quin2 does have some useful properties; like BAPTA, it is a very good buffer of $[Ca^{2+}]_c$, and its use has allowed $Ca^{2+}$-independent phenomena to be observed ***(11,12)***. Subsequently improved single-excitation indicators have been developed that are more fluorescent and have $K_d$s for $Ca^{2+}$ between approx 200 n*M* and 320 μ*M* ***(9,10,13)*** (*see* **Table 1**). These indicators include the fluo derivatives ***(10)***, and the Calcium Green and Calcium Orange series of indicators. With these indicators there is little or no shift in either the excitation or emission spectra; however, a marked increase in fluorescence intensity can be observed on $Ca^{2+}$ binding. Calcium Green-2 has a $K_d$ of 550 n*M* (*see* **Table 1**) and produces approx 100-fold increase in fluorescence between being $Ca^{2+}$-free and $Ca^{2+}$-saturated. For fluo-3 this increase is reported to be approx 200-fold. It can of course be problematic if the resting $Ca^{2+}$ signal is so low that cells cannot be readily identified or a reliable calibration achieved. Fluo-4 has a similar $K_d$ to fluo-3 but is more fluorescent with 488 nm excitation and appears to load more readily ***(9)***. The fluo and Calcium Green indicators all have peak excitation spectra at or close to 490 nm (*see* **Table 1**), allowing them to be readily used with argon-ion lasers (488 nm excitation). Peak emission lies close to 530 nm. There are $Ca^{2+}$ indicators that can be excited even at longer wavelengths, e.g., rhod derivatives, the Calcium Crimson and Calcium Orange series, and KJM-1 (*see* **Table 1**). Rhod-2 is excited at 520 nm, with a peak emission at 580 nm ***(10)***, and has been used to measure mitochondrial $Ca^{2+}$ rather than $[Ca^{2+}]_c$ ***(9,14)***. Fura-Red (strictly a ratiometric indicator), when excited at wavelengths close to 480 nm, can be used in combination with fluo-3 to obtain a ratio derived from their respective 530- and 650-nm emission signals. Thus, combinations of visible excitation indicators can be used to obtain ratio measures of $[Ca^{2+}]_c$ ***(15,16)***.

### *2.1.1. Visible Excitation Indicators*

Visible wavelength indicators are attractive because they can avoid problems, such as light absorbance by optical elements and cellular autofluorescence. The lower excitation energies of the longer wavelengths also means that photobleaching is reduced. The visibly excited dyes are more suited to the laser-based illumination systems used in confocal microscopy and flow cytometry. The advantage of having a range of indicators that can be excited at different wavelengths is that combinations of ion indicators can be used together. Thus, $Ca^{2+}$ can be monitored simultaneously with other physiologically important ions, such as $Na^+$ or $H^+$ ***(17–19)***. Moreover, $Ca^{2+}$ can be monitored using indicators in separate domains as with simultaneous measurements of intracellular and extracellular $Ca^{2+}$ ***(20)***.

**Table 1**
**Single Excitation Wavelength Indicators**

| Indicator | Source | UV/V | $K_d$ n*M* (or µ*M* where indicated) | AM Loading | Absorbance –$Ca^{2+}$ | Absorbance +$Ca^{2+}$ | Emission –$Ca^{2+}$ | Emission +$Ca^{2+}$ | Comments |
|---|---|---|---|---|---|---|---|---|---|
| quin2 | MP/TL | UV | 60 [a] (115) [b] | ✓ | 352 | 332 | 492 | 498 | High intracellular buffering. |
| methoxyquin2MF | MP | UV | 65 [a] | ✓ | 352 | 332 | 492 | 498 | MethoxyquinMF[19] for NMR. |
| Oregon Green 488 BAPTA-1 | MP | V | 170 [a] | ✓ | 494 | 494 | 523 | 523 | Designed for argon-ion lasers. Dextran conjugate available. |
| Calcium Orange™ | MP | V | 185 [a] (380) [c] | ✓ | 549 | 549 | 575 | 576 | *See* **ref. *13*** |
| Calcium Crimson™ | MP | V | 185 [a] (221) [c] | ✓ | 590 | 589 | 615 | 615 | *See* **ref. *13*** |
| Calcium Green-1 | MP | V | 190 [a] (221) [c] | ✓ | 503 | 506 | 534 | 533 | *See* **ref. *13***, Fluorescence lifetime measurements and multi-photon applications. Brighter than fluo-3. Dextran conjugates available. |
| Calcium Green$C_{18}$ | MP/TL | V | 280 [a] (62) [d] | × | 509 | 509 | 530 | 530 | Near-membrane $Ca^{2+}$ indicator, $K_d$ affected by lipids, *see* **ref. *59*** |
| Fluo-4 | MP | V | 345 [a] | ✓ | 491 | 494 | | 516 | Absorbance peak is close to 488 nm argon-ion laser line. Highly suited to applications using argon-ion lasers. AM ester and $Ca^{2+}$ free forms are only weakly fluorescent. Large increase in fluorescence on $Ca^{2+}$-binding. Dextran conjugates available. |
| Fluo-3 | MP/TL | V | 390 [a] | ✓ | 506 | 506 | 526 | 526 | AM ester and $Ca^{2+}$ free forms are only weakly fluorescent. Large increase in fluorescence on $Ca^{2+}$-binding. |
| FLUO-LOJO™ | TL | V | 440 [e] | ✓ | 491 | 491 | 515 | 515 | Leakage resistant analogue of fluo-4. |
| FLUO-KOJO™ | TL | V | 500 [e] | ✓ | 506 | 506 | 525 | 525 | Leakage resistant analogue of fluo-3. |
| KJM-1 | TL | V | 500 [f] | ✓ | 560 | 560 | Em 640 | | |

| | | | | | | | | | |
|---|---|---|---|---|---|---|---|---|---|
| Calcium Green-2™ | MP | V | 550 [a] | ✓ | 503 | 503 | 536 | 536 | AM ester and $Ca^{2+}$ free forms are only weakly fluorescent. Large increase in fluorescence on $Ca^{2+}$-binding. |
| FluoLR | TL | V | 550 [f] | ✓ | 506 | 506 | 531 | 531 | Leakage resistant indicator. |
| Rhod-2 | MP/TL | V | 570 [a] | ✓ | 549 | 552 | 571 | 571 | Can be loaded as dihydro-derivative. Will locate in mitochondria and peroxisomes. |
| Oregon Green 488 BAPTA-2 | MP | V | 580 [a] | ✓ | 494 | 494 | 523 | 523 | Designed for argon-ion lasers. |
| X-rhod-1 | MP | V | 700 [a] | ✓ | 576 | 580 | | 602 | |
| FLUO-MOMO™ | TL | V | 710 [g] | ✓ | 491 | 491 | 515 | 515 | Lipophilic fluo-4 derivative for measurement of near membrane $Ca^{2+}$ |
| FLUO-NOMO™ | TL | V | 800 [g] | ✓ | 506 | 506 | 525 | 525 | Lipophilic fluo-3 derivative for measurement of near membrane $Ca^{2+}$ |
| FLUO-535 | TL | V | 800 [g] | ✓ | 535 | 535 | 560 | 560 | |
| X-rhod-5F | MP | V | 1.6 µ*M* [a] | ✓ | c576 | c580 | | 602 | |
| Oregon Green 488 BAPTA-6F | MP | V | 3 µ*M* [a] | ✓ | 494 | 494 | 523 | 523 | |
| Fluo-5F | MP | V | 2.3 µ*M* [a] | ✓ | 491 | 494 | 518 | 518 | Weakly fluorescent in $Ca^{2+}$ free. |
| Magnesium Green™ | MP | V | 6 µ*M* [a] | ✓ | 506 | 506 | 531 | 531 | $K_d$ determined in 0-$Mg^{2+}$, indicator will be $Mg^{2+}$-sensitive. |
| Fluo-4FF | MP | V | 9.7 µ*M* [a] | ✓ | 491 | 494 | 516 | 516 | |
| Calcium Green-5N™ | MP | V | 14 µ*M* [a] | ✓ | 506 | 506 | 532 | 532 | |
| X-rhod-FF | MP | V | 17 µ*M* [a] | ✓ | 576 | 578 | | 602 | |
| Rhod-FF | MP | V | 19 µ*M* [a] | ✓ | 548 | 552 | | 577 | Weakly fluorescent in $Ca^{2+}$ free. Designed to locate in mitochondria. |
| Calcium Orange-5N™ | MP | V | 20 µ*M* | ✓ | 549 | 549 | 582 | 582 | Exhibits fast kinetics suitable for millisecond time resolution. *See* **ref. *108***. Product discontinued. |

*Continued on next page*

**Table 1 *(Continued)***
**Single Excitation Wavelength Indicators**

| Indicator | Source | UV/V | $K_d$ n*M* (or µ*M* where indicated) | AM Loading | Absorbance | | Emission | | Comments |
|---|---|---|---|---|---|---|---|---|---|
| | | | | | –$Ca^{2+}$ | +$Ca^{2+}$ | –$Ca^{2+}$ | +$Ca^{2+}$ | |
| Orange Green 488 BAPTA-5N | MP | V | 20 µ*M* [a] | ✓ | 494 | 494 | 521 | 521 | Designed for Argon-ion lasers. |
| Fluo-3FF | TL | V | 41 µ*M* [g] | ✓ | Ex 515 | 526 | 526 | | |
| Fluo-5N | MP | V | 90 µ*M* [a] | ✓ | 491 | 493 | | | |
| Rhod-5N | MP | V | 320 µ*M* [a] | ✓ | 549 | 551 | | 577 | Weakly fluorescent in $Ca^{2+}$ free. |

UV, ultraviolet; V, visible; AM, acetoxymethyl ester; MP, Molecular Probes; TL, Available exclusively through Teflabs; MP/TL, Molecular Probes, Teflabs and other suppliers.

[a] $K_d$ determined in 100 m*M* KCl, pH 7.2 at 22°C.

[b] $K_d$ determined in 100 m*M* KCl, pH 7.05 at 37°C.

[c] Values taken from **ref. *13***.

[d] $K_d$ reported to be 230 n*M* at 0.1 *M* ionic strength, pH 7.2 at 22°C and 62 n*M* in the presence of phospholipid vesicles. *See* **ref. *59***.

[e] $K_d$ is an estimate based on the ratio of the $K_d$s of fura-PE3 and fura-2 being applied to the $K_d$s for fluo-3 and fluo-4. Emission spectra data suggests the $K_d$ may be lower than estimated.

[f] $K_d$ Determined at pH 7.2 and 22°C.

[g] Conditions for $K_d$ determination not defined.

**Table 2**
**Dual Excitation Indicators**

| Indicator | Source | UV/V | $K_d$ n*M* (or µ*M* where indicated) | AM Loading | Absorbance –$Ca^{2+}$ | Absorbance +$Ca^{2+}$ | Emission –$Ca^{2+}$ | Emission +$Ca^{2+}$ | Comments |
|---|---|---|---|---|---|---|---|---|---|
| Fura Red | MP | V | 140 [a] | ✓ | 472 | 436 | 657 | 637 | Low quantum yield. Used in combination with single excitation indicators to obtain ratio values. |
| Fura-2 | MP/TL | UV | 145 [a] (224) [b] | ✓ | 363 | 335 | 512 | 505 | |
| Fura-$C_{18}$ | MP | UV | 150 [a] | × | 365 | 338 | 501 | 494 | Lipophilic near-membrane $Ca^{2+}$ indicator. $K_d$ may be affected by membrane environment. |
| Fura PE3 | TL | UV | 269 [c] | ✓ | 364 | 335 | 502 | 495 | Leakage resistant indicator. |
| Bis-fura | MP | UV | 370 [a] (550 [d]) | ✓ | 364 | 335 | 508 | 500 | Is brighter and has lower affinity than fura-2. Not available as cell permeant ester. |
| FFP18 | TL | UV | 400 [a] | ✓ | 364 | 335 | 502 | 495 | Lipophilic near-membrane $Ca^{2+}$ indicator. $K_d$ affected by membrane environment. |
| Fura-5F | MP | UV | 400 [a] | ✓ | 363 | 336 | 512 | 506 | |
| Fura-4F | MP | UV | 770 [a] | ✓ | 366 | 336 | 511 | 505 | |
| Fura-6F | MP | UV | 5.3 µ*M* [a] | ✓ | 364 | 336 | 512 | 505 | |
| Fura-FF | MP | UV | 5.5 µ*M* [a] | ✓ | 364 | 335 | 510 | 506 | |
| BTC | MP | V | 7 µ*M* [a] | ✓ | 464 | 401 | 533 | 529 | Visible-excitation ratiometric indicator. |
| MagFura-2 (Furaptra) | MP | UV | 25 µ*M* [a] | ✓ | 369 | 329 | 511 | 508 | $K_d$ determined in 0-$Mg^{2+}$, indicator will be $Mg^{2+}$-sensitive. |
| Magfura-5 | MP | UV | 28 µ*M* [a] | ✓ | 369 | 330 | 505 | 500 | $K_d$ determined in 0-$Mg^{2+}$, indicator will be $Mg^{2+}$-sensitive. |
| Fura-2FF | TL | UV | 35 µ*M* [c] | ✓ | 364 | 335 | 512 | 505 | |
| Fura-FF-$C_{18}$ | MP | UV | — | × | 337 | 366 | 504 | 495 | Lipophilic near-membrane $Ca^{2+}$ indicator. $K_d$ affected by membrane environment. $K_d$ not determined. |

UV, ultraviolet; V, visible; AM, acetoxymethyl ester; MP, Molecular Probes; TL, Available exclusively through Teflabs; MP/TL, Molecular Probes, Teflabs and other suppliers.

[a] $K_d$ determined in 100 m*M* KCl, pH 7.2 at 22°C.

[b] $K_d$ determined in 100 m*M* KCl, pH 7.05 at 37°C.

[c] Values taken from **ref. *13***.

[d] Conditions the same as footnote *a* except with 1 m*M* $Mg^{2+}$ present.

**Table 3**
**Dual Emission Ratiometric Indicators**

| Indicator | Source | UV/V | $K_d$ n*M* (or µ*M* where indicated) | AM Loading | Absorbance | | Emission | | Comments |
|---|---|---|---|---|---|---|---|---|---|
| | | | | | $-Ca^{2+}$ | $+Ca^{2+}$ | $-Ca^{2+}$ | $+Ca^{2+}$ | |
| Indo-1 | MP/TL | UV | 230 [a] (250 [b]) | ✓ | 346 | 330 | 475 | 401 | |
| IndoPE3 | TL | UV | 260 [c] | ✓ | 346 | 330 | 475 | 408 | Leakage resistant indicator. |
| FIP18 | TL | UV | 450 [c] | ✓ | 346 | 330 | 475 | 408 | Lipophilic near-membrane $Ca^{2+}$ indicator. $K_d$ affected by membrane environment |
| Indo-5F | MP | UV | 470 [a] | ✓ | 347 | 331 | 475 | 412 | |
| Indo-1FF | TL | UV | 33 µ*M* [c] | ✓ | Ex 348 | 475 | 408 | | |
| MagIndo-1 | MP | UV | 35 µ*M* [d] | ✓ | 349 | 328 | 480 | 390 | $K_d$ determined in 0-$Mg^{2+}$, indicator will be $Mg^{2+}$-sensitive. |

UV, ultraviolet; V, visible; AM, acetoxymethyl ester; MP, Molecular Probes; TL, Available exclusively through Teflabs; MP/TL, Molecular Probes, Teflabs and other suppliers.

[a] $K_d$ determined in 100 m*M* KCl, pH 7.2 at 22°C.

[b] $K_d$ determined in 115 m*M* KCl, 20 m*M* NaCl, 10 mM K-MOPS, pH 7.05, 1 m*M* $Mg^{2+}$ at 22°C.

[c] Conditions for $K_d$ determination not defined.

[d] $K_d$ determined in 100 m*M* KCl, 40 m*M* HEPES, pH 7.0 at 22°C.

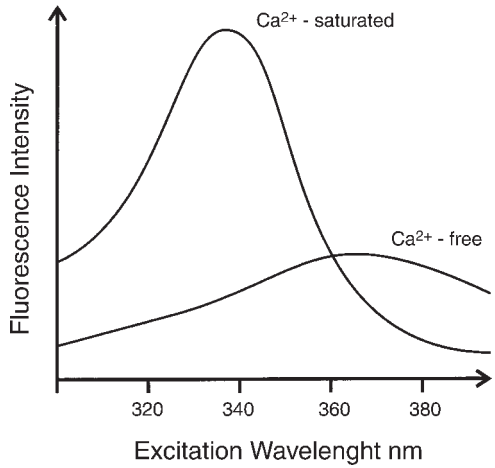


Fig. 1. The $Ca^{2+}$-free and $Ca^{2+}$-saturated spectra of fura-2. The two spectra coincide at 360 nm, the isobestic (or isoemissive) point. It can be seen that when $Ca^{2+}$ binds, the fluorescence signal will increase when the indicator is excited at 340 nm, stay the same when it is excited at 360 nm, and decrease when it is excited at 340 nm.

### *2.1.2. Caged Compounds*

Bioactive molecules can be incorporated into physiologically inert (caged) molecules and subsequently released in a controlled manner by photolysis of the chemical "cage." Introduction of the visible excitation indicators has allowed $[Ca^{2+}]_c$ to be measured during UV-induced flash photolysis of caged compounds, such as caged Ins(1,4,5)$P_3$ and Nitr-5 (caged $Ca^{2+}$) ***(21–23)***. This advance has enabled second messengers to be manipulated in a controlled manner while simultaneously monitoring $[Ca^{2+}]_c$.

## *2.2. Dual Excitation Indicators*

Fura-2 is the archetypal dual excitation $Ca^{2+}$ indicator ***(6)***. In low $Ca^{2+}$, fura-2 shows a broad excitation spectrum between 300 and 400 nm, with a peak at approx 370 nm. On $Ca^{2+}$ binding, the excitation peak increases in intensity and also shifts further into the UV (**Fig. 1**). Consequently, if the dye is excited at 340 nm (emission monitored at 510 nm), $Ca^{2+}$ binding will produce an increase in fluorescence, whereas a decrease in the fluorescent signal is observed when the dye is excited at 380 nm (**Figs. 1** and **2**). When the dye is excited in quick succession at 340 and 380 nm, a ratio of the respective emission signals can be used to monitor $[Ca^{2+}]_c$. Ratiometric measurements have a number of advantages over single wavelength probes. The ratio signal is not dependent on dye concentration, illumination intensity, or optical path length.

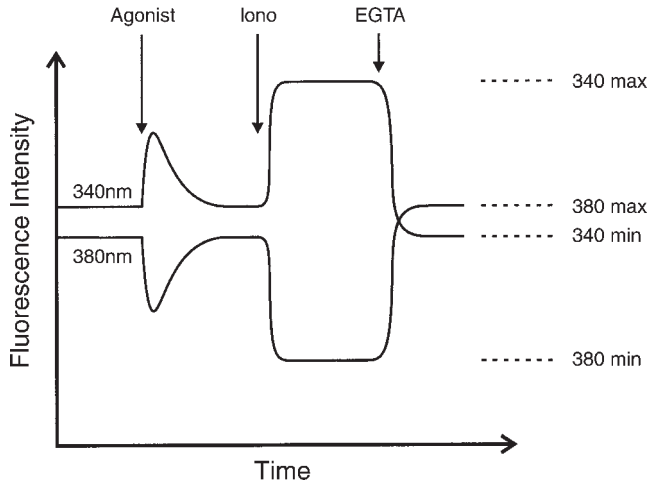


Fig. 2. Typical signals obtained from a fura-2-loaded cell when it is excited at 340 and 380 nm. Agonist stimulation will cause an increase in the 340-nm signal and a decrease in the 380-nm signal. Addition of an ionophore (Iono) in the presence of $Ca^{2+}$ will give $F_{340max}$ and $F_{380min}$, whereas subsequent addition of EGTA will give $F_{340min}$ and $F_{380max}$. The time taken to reach $F_{340min}$ and $F_{380max}$ ($R_{min}$) after the addition of ionophore and EGTA can vary and may be in excess of 30 min. Curve fitting the decay towards $R_{min}$ has been suggested as a strategy to speed up the calibration process ***(36)***. The long time period to required to obtain $R_{min}$ is not ideal for imaging experiments because the dimensions of the cells may change during the calibration.

Therefore, spatial variations in these parameters will not affect the estimations of $[Ca^{2+}]_c$. Such factors are especially important if the dyes are to be used for imaging of $[Ca^{2+}]_c$ where illumination intensity and optical properties vary across the field of view ***(6,24)***. Dye leakage and photobleaching frequently lead to a loss of indicator during an experiment; thus, the active indicator concentration cannot be assumed to be constant ***(25,26)***. Under such conditions, a ratiometric indicator gives a more stable measure of $[Ca^{2+}]_c$ than could be obtained from a single excitation indicator. Ratiometric measurements also produce an additional increase in sensitivity.

A further useful property of ratiometric indicators is the presence of an isobestic or isoemissive point. For example, when fura-2 is excited at 360 nm, no $Ca^{2+}$-dependent change in fluorescence occurs, because at this wavelength, the $Ca^{2+}$-saturated and $Ca^{2+}$-free excitation spectra coincide (*see* **ref. *6***; **Fig. 1**). If $Mn^{2+}$ is used to quench fura-2 fluorescence, excitation at 360 nm can be used to measure its influx (*see* **ref. *27***; **Fig. 3**). Thus, $Mn^{2+}$ can act as a surrogate for

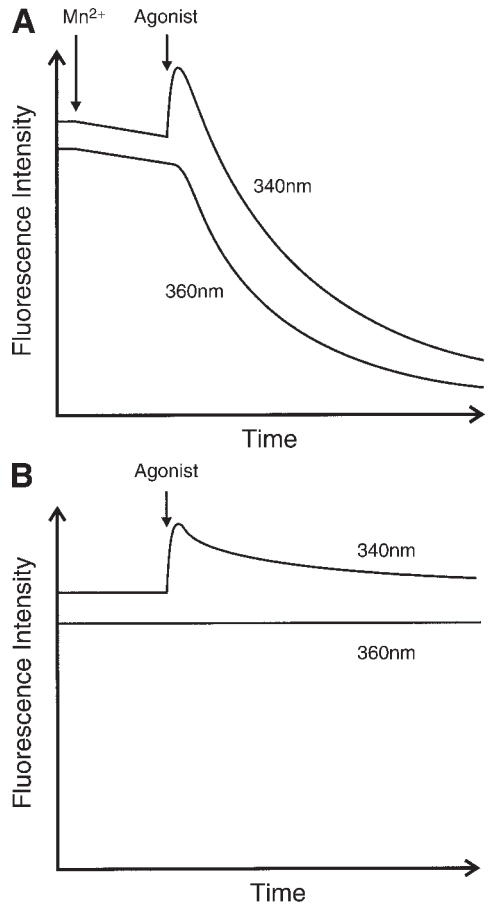


Fig. 3. **(A)** The effect of $Mn^{2+}$ on fura-2 fluorescence when the dye is excited at 340 and 360 nm. Addition of $Mn^{2+}$ will often initiate a slow quench of fura-2 that is markedly enhanced when the cell(s) is/are stimulated with an agonist. The 360-nm signal represents the $Mn^{2+}$ quench, whereas the 340-nm trace is influenced by the increase in $[Ca^{2+}]_c$, as well as by subsequent $Mn^{2+}$ entry. **(B)** The control experiment that should be carried out when using $Mn^{2+}$ quench to follow influx. In the presence of $Ca^{2+}$, although the 340-nm signal will reflect changes in $[Ca^{2+}]_c$, the 360-nm signal should not change when the cells are stimulated with an agonist. The exact isobestic point should be determined for each cell type and each fluorescence system.

$Ca^{2+}$ in influx studies. Excitation at 360 nm will also reveal the intracellular distribution of fura-2 (**ref. *26***; *see* **Subheading 2.5.**). If the cytosolic indicator is lost by permeabilizing the plasma membrane (or quenched using $Mn^{2+}$), the localization of compartmentalized dye will be unveiled ***(25)***.

### 2.3. Dual Emission Indicators

The $Ca^{2+}$ indicator indo-1 shows a shift and an increase in the peak of its emission spectra when $Ca^{2+}$ binds, whereas the excitation spectra remains unaltered ***(6)***. Thus, the dye is excited at a single wavelength between 338 and 350 nm and emission is monitored at 400 and 450 nm, the respective peaks of the $Ca^{2+}$-bound and $Ca^{2+}$-free spectra. Indo-1 has a $K_d$ for $Ca^{2+}$ of 250 n*M* under physiological conditions; indo-5F has a $K_d$ of 470 n*M* (*see* **Table 3**). Another indicator in this class is mag-indo-1. It was originally designed for monitoring $Mg^{2+}$; however, because $Mg^{2+}$ generally changes very little, these indicators have been used as low-affinity $Ca^{2+}$ indicators (*see* **Table 3**). The dual emission indicators are ideal for simple photometric measurements of $Ca^{2+}$ from cells. They need only a monochromatic light source (which could come via an interference filter) and a beam-splitting dichroic mirror on the emission side to separate the emission signals (400 and 450 nm for indo-1). Two photomultiplier tubes (PMTs) running simultaneously can be used to monitor the emission signals. This arrangement gives the apparatus a very rapid time resolution that is limited by the kinetic properties of the indicators. However, these dyes are not ideal for conventional fluorescence imaging experiments, because either two cameras are required or some method of rapidly changing an emission filter is needed. Aligning the image frames is not easy, and introducing additional optical elements on the emission pathway is not desirable because the amount of light per pixel on the camera is much less than that hitting the photocathode of a PMT tube. That said, the current generation of line scanning confocal microscopes equipped with optics for resolving separate and variable emission bands are ideally suited for emission ratioing. In addition, indo-1 is, suited for the expanding technology of two- or multiphoton-photon confocal imaging (*see* **Subheading 2.14.**).

### 2.4. Loading of $Ca^{2+}$ Dyes

#### 2.4.1. Loading Using Acetoxymethyl Esters

The $Ca^{2+}$ indicators, by their very nature, are charged molecules that cannot cross lipid membranes. However, they can be readily introduced into cells by esterifying the carboxylic acid groups, making them lipophilic and therefore membrane-permeant ***(4)***. Fortuitously, cells contain many esterases that remove the ester groups, leaving the charged $Ca^{2+}$ indicator trapped inside. Suppliers of the indicators usually sell them as the acetoxymethyl (AM) esters, as well as in free acid or salt form. Introducing the dyes into cells involves incubating them with 1–10 μ*M* of the esterified indicator with incubation times varying, usually between 15 min and 2 h. Loading is best achieved in a physiological buffer, but it can also be carried out in serum or culture media, although there will be a certain degree of extracellular esterase activity ***(28)***. Some cells may

show poor esterase activity; in others, the esterified indicator accumulates in intracellular compartments, where hydrolysis may be incomplete ***(25,26,28–30)***. As a result, signals from cells may not be entirely derived from the cytoplasm. Recently this "problem" with loading has been used to good effect to actually monitor $Ca^{2+}$ inside organelles ***(15,31)***. The multidrug-resistance transporters (widely expressed in some tumor cells) will remove the esterified indicator directly from the plasma membrane ***(32)*** thereby reducing the loading efficiency. Optimizing the loading protocol is discussed in **Subheading 2.6.**

### *2.4.2. Microinjection and the Patch Pipet*

The introduction of the patch-clamp technique for recording whole-cell and single ion channel currents has provided a great deal of information on the properties of the many selective and nonselective ion channels that are present in the plasma membrane. Some of these channels are $Ca^{2+}$-permeable whereas many others can be regulated by $Ca^{2+}$. Therefore, it was extremely useful to combine $[Ca^{2+}]_c$ measurements with simultaneous recordings of ion channel activity ***(29,33)***. When recordings are made in the whole-cell configuration, the contents of the patch pipet are continuous with the cytoplasm of the cell. This allows the contents of the patch pipet to diffuse out and equilibrate within the cell. Hence, the patch pipet becomes a convenient way of introducing $Ca^{2+}$ indicators and buffers into the cytoplasm of cells, avoiding the hazards of ester loading. Typically, the indicator is introduced at concentrations in excess of 50 μ*M* in the patch pipet. Because the internal volume of the pipet is much larger than that of the cell, the concentration of the dye in the patch pipet will eventually be reflected within the cell.

Microinjection can be used to introduce $Ca^{2+}$ indicators into the cell nucleus, as well as into the cytoplasm. Typically the indicators are introduced at concentrations in the order of 1 m*M* to allow for the small nanoliter volumes that are microinjected. Introduction by patch pipet or microinjection is necessary if either the dextran conjugates of the indicators or other impermeable indicators, such as *bis*-fura-2, are to be used. This fura-2 derivative has a lower affinity for $Ca^{2+}$ (370 n*M*) and is more fluorescent than fura-2, but unfortunately, it is not available as a cell-permeant ester (**Table 2**).

### *2.4.3. Reversible Permeabilization*

There are a number of ways in which the plasma membrane can be made temporarily permeable to $Ca^{2+}$ indicators. Streptolysin O, electroporation, and adenosine triphosphate $(ATP)^{4-}$ have all been used successfully ***(28,34–36)***. The advantage of these techniques is that cytoplasmic loading of poor or impermeant indicators can be carried out on cell populations. However, the amount of loading may be small, and damage to the cells is an inherent risk.

Usually, millimolar concentrations of the acidic indicator are needed, which is expensive and therefore, will tend to limit the loading volume and hence the number of cells that can be loaded in this way.

### 2.5. Subcellular Localization of the $Ca^{2+}$ Indicators

A number of reports have revealed that the synthetic $Ca^{2+}$ indicators can become localized within intracellular compartments ***(25,26,28–31)***. In some cases, these compartments appear to be mitochondria, or even the endoplasmic reticulum (ER). If signals from the cytosolic indicator can be eliminated, then selective monitoring of organelle $Ca^{2+}$ is possible. However, when one wants to measure $[Ca^{2+}]_c$, obtaining $Ca^{2+}$-dependent fluorescence from other compartments is clearly a problem. Incomplete hydrolysis can be an additional complication with compartmentalized indicators ***(25)***, although in many respects, a constant background fluorescence signal is easier to subtract than one that may change with time and $[Ca^{2+}]$. Experimental approaches that can be used to optimize the cytosolic loading of the indicator are discussed in the following **Subheading 2.6.**

### 2.6. Optimization of Loading

There are a number of procedures that can increase the loading of the ester into cells, the likelihood of the dye being cytoplasmic, and, finally, improve the retention of the indicator by the cells. One problem with the esterified indicators is their relatively poor solubility in physiological media. This can be improved by using Pluronic F-127, a nonionic detergent, and by including bovine serum albumin in the loading buffer ***(36)***. Pluronic F-127 (25% w/v in dimethyl sulfoxide) is most effective when it is mixed directly with the indicator before they are added together to the loading buffer. Loading is impaired when the esterified indicator is removed from the plasma membrane by the P-glycoprotein multidrug transporter ***(32)***. If this transporter is saturated with another substrate, such as verapamil (10 μ*M*), then introduction of the ester into cells is enhanced.

Compartmentalization of the indicator within cells can be reduced if the loading temperature is decreased from 37°C to room temperature ***(25,26)***. This is most likely mediated through a reduction in endocytosis, a process that will cause the indicators to accumulate in endosomes and topologically related organelles. When reducing the loading temperature, the loading period usually has to be increased. Thus, a balance of optimal temperature and loading period should be found for each cell type.

Once inside a cell, the hydrolyzed indicator should not escape easily; however, rapid decreases in signal intensities during experiments often occur. The cause can be twofold: photobleaching and transport of the indicators out of the

cell. Retention of the indicators can be enhanced by the presence of anion exchange inhibitors, such as sulphinpyrazone and probenecid ***(37,38)***. These agents should be present during both the loading period with the ester and afterward during the actual experiment. Fura-PE3, indo-PE3, and fluo-LR are derivatives of fura-2, indo-1, and fluo-3 that are resistant to leakage. The PE3 indicators form a zwitterion from a piperazine nitrogen and an adjacent carboxylic acid that apparently enhances their retention ***(39)***. Fortuitously, they too are available as cell-permeant AM esters.

### *2.7. Organelle Targeting*

Although loading procedures may be designed to optimize the presence of the indicators in the cytosol, selective localization of the indicators may provide useful information about $Ca^{2+}$ regulation in specific organelles or cellular domains ***(14,31,40)***. Indo-1 has been used to monitor mitochondrial $[Ca^{2+}]_m$ after the cytosolic dye was quenched using $Mn^{2+}$ ***(40)***. The indicator rhod-2 was found to load preferentially into the mitochondria of some cells ***(14)***. This probably resulted from the fact that it is highly charged and is readily retained by the polarized mitochondria. The dihydro derivative of rhod-2 also locates preferentially into mitochondria and lysosomes because it can be oxidized within these organelles ***(9,10,14)***. Fluo-3 has been reported to coload into the cytosol and mitochondria of endothelial cells such that simultaneous recordings could be made from separate mitochondrial and cytosolic domains identified by confocal microscopy ***(41)***.

Low-affinity $Ca^{2+}$ indicators are needed to measure $Ca^{2+}$ in the ER ($[Ca^{2+}]_{ER}$) because even the most conservative estimates suggest that the concentration is likely to be in excess of 5 μ*M* ***(31,42–44)***. Recent evidence places the $[Ca^{2+}]_{ER}$ around 500 μ*M* ***(45)***. At these concentrations, indo-1 and fura-2 will be saturated with $Ca^{2+}$. Mag-fura-2 (Furaptra) has been used to monitor $[Ca^{2+}]_{ER}$ ***(46)***. Although it was designed as a $Mg^{2+}$ indicator ***(44)***, it is in effect a low-affinity $Ca^{2+}$ indicator ***(47–49)***, given that $Mg^{2+}$ is unlikely to change dramatically. Other low-affinity indicators include fura-2FF, indo-1FF, fluo-3FF ***(31,39)***, and the "5N" indicator derivatives produced by molecular probes (**Tables 1–3**). The problem of loading such indicators selectively into the ER is not easily solved, although "normal" loading with esterified indicator at 36°C is reportedly sufficient to locate fura-2 in the mitochondria ***(41)***, and Furaptra and fura-2FF in the sarco/ER ***(29)***. Screening both cells and loading conditions allowed Hofer and colleagues to find a cell model where $[Ca^{2+}]_{ER}$ to be monitored ***(50)*** by simple loading of the esterified fura-2. Another approach is to load permeabilized cells with indicators, thus allowing the ester greater access to the organelle membranes and the "cytosolic" dye to diffuse out of the cell ***(46)***. Unfortunately, cell permeabilization can dramatically change the ultra-

structure of the ER ***(51)***, which is not at all desirable. Information on $[Ca^{2+}]_{ER}$ has also been obtained by isolating the cell nuclei along with the nuclear envelope that is continuous with the ER. These isolated nuclei are subsequently loaded with esterified indicators ***(52)*** to give measurements of $[Ca^{2+}]$ in the perinuclear ER, whereas incubation of the nuclei with indicator-dextran conjugates allows the $[Ca^{2+}]$ to be monitored in the nucleoplasm.

Injection of dextran-conjugated indicators into the nucleus itself would allow selective measurements of nuclear $[Ca^{2+}]$. This could be combined with another indicator–dextran conjugate that could be injected into the cytoplasm, allowing selective monitoring of $Ca^{2+}$ from the two subcellular regions in an intact cell. For the nucleus and cytoplasm, confocal microscopy offers an alternative approach to monitoring $[Ca^{2+}]$, in that the spatial resolution is such that the cytoplasm and nucleus are separated in single confocal planes. Hence, as long as one can identify the region from which the signal originated, nuclear and cytosolic $Ca^{2+}$ can be monitored by a single, freely diffusable $Ca^{2+}$ indicator ***(53)***.

There is continuing evidence for microdomains of $[Ca^{2+}]_c$ within cells ***(54,57)***. The $Ca^{2+}$ indicators are, by their nature, $Ca^{2+}$ buffers that can diffuse freely within cells. As such, they can act to buffer microdomains, making them harder to resolve. If the $Ca^{2+}$ buffers are made immobile or their diffusion is restricted, more dramatic localized changes in $Ca^{2+}$ should be observed (*see also* **Subheading 2.8.**). One approach along these lines has been to add a lipophilic tail allowing the indicator to be attached to membranes ***(58–60)***. Such indicators include fura $C_{18}$, Calcium Green $C_{18}$ (Molecular Probes), and FFP18, FIP18, and Fluo-FP-18 (Teflabs). When injected into the cell, they locate to the cytoplasmic faces of lipid membranes. Thus, peri-ER and subplasmalemmal $Ca^{2+}$ can be monitored. It has been reported that when added extracellularly, they can be used to monitor $Ca^{2+}$ efflux ***(60)***, although I have found it difficult to obtain sensible data with Calcium Green $C_{18}$. An elegant refinement of this approach has been to conjugate fura-2 with the specific oligopeptides allowing the indicator to be geranyl geranylated ***(61)***. A lipid tail added by prenylation (common to Ras proteins) would allow such indicators to monitor subplasmalemmal $Ca^{2+}$ selectively. Genetically engineered protein indicators for $Ca^{2+}$ allow very selective targeting of $Ca^{2+}$ indicators to cellular organelles. Their potential is discussed in more under **Subheadings 2.12.** and **2.13.**

### *2.8. Indicator Mobility and Buffering of $Ca^{2+}$*

Fura-2 is a relatively high-affinity indicator that will tend to buffer $Ca^{2+}$. As indicated under **Subheading 2.7.**, restricting the mobility of the $Ca^{2+}$ buffer will also restrict the mobility of $Ca^{2+}$ and potentially aid its detection. In intact cells, $Ca^{2+}$ is not believed to diffuse freely owing to the presence of endo-

genous $Ca^{2+}$ buffers and stores capable of rapidly sequestering $Ca^{2+}$ ***(62)***. Thus, freely mobile indicators, such as fura-2, can act to dissipate naturally occurring $Ca^{2+}$ gradients and microdomains of elevated $[Ca^{2+}]_c$. This is, of course, disadvantageous when the aim is to investigate local changes in $[Ca^{2+}]_c$. When fura-2 is introduced at high concentrations so that it is the dominant $Ca^{2+}$ buffer, changes in fluorescence actually report the $Ca^{2+}$ flux. At low concentrations when buffering is minimal, fura-2 will reflect the actual changes in $[Ca^{2+}]_c$ more faithfully ***(63)***. Using a slow buffer, such as EGTA buffer, in combination with a fast $Ca^{2+}$ indicator (fura-2) makes it easier to resolve sites of $Ca^{2+}$ events ***(57)*** because $Ca^{2+}$ released by the indicator is effectively "mopped up" by the slower chelator rather than indicator molecules distant from the source of $Ca^{2+}$.

**Tables 1–3** list some of the common indicators ranked in order of their $K_d$ values. The lower-affinity buffers will of course be better suited to monitoring $[Ca^{2+}]_c$ without increasing intracellular buffering. A potential problem with using immobile indicators is that if they saturate with $Ca^{2+}$ or photobleach, the ability to monitor $[Ca^{2+}]_c$ at a specific location is lost because nonsaturated or unbleached indicator cannot easily replace the impaired dye. As such, this could negate any beneficial effects that localized indicators may confer in the reporting of local changes in $[Ca^{2+}]_c$. Lower-affinity probes may avoid this problem because they would not readily saturate with microdomains of high $[Ca^{2+}]_c$. All said, dramatic images of elementary $Ca^{2+}$ events can be resolved quite adequately with freely mobile buffers ***(54)***.

### *2.9. Calibration*

There are a number of factors that can influence calibration that users of the fluorescent $Ca^{2+}$ indicators need to be aware of. The $K_d$ for $Ca^{2+}$ will vary with temperature, pH, and ionic strength, and for some indicators, the presence of $Mg^{2+}$ will affect the $K_d$ for $Ca^{2+}$ ***(6,7,9,18,19,25,64)***, Viscosity also affects the signals ***(25,65)***. It is therefore advisable to calculate the $K_d$ under conditions that mimic, as far as possible, the expected environment in which the dye is to be used. Not all of the published $K_d$ values will relate to the ionic conditions or temperature that may be chosen for experiments; many values have been determined at 22°C and in the absence of $Mg^{2+}$ (*see* **Tables 1–3**). Apparently, the $K_d$s of the dextran-conjugated indicators vary from batch to batch ***(9)***, so their values would have to be checked. It is, of course, hard to predict precisely what effect the internal cellular environment will have on the $Ca^{2+}$ indicators; however, it is unlikely that the $K_d$ will vary significantly as long as the key parameters outlined here remain constant.

If the $K_d$ is known, all that is required to calibrate a single excitation wavelength indicator is to determine the maximum and minimum fluorescence val-

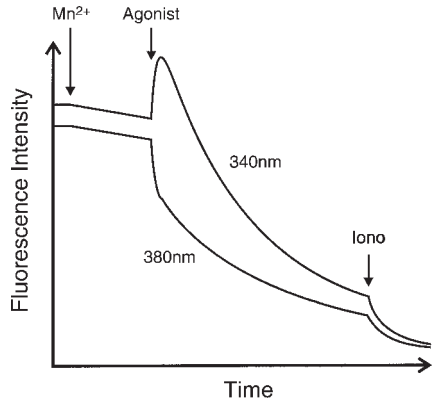


Fig. 4. The effect of adding $Mn^{2+}$ to a cell excited at 340 and 380 nm that is subsequently stimulated by an agonist. The $Mn^{2+}$ quenches both the 340- and 380-nm signals. Usually a steady state is reached when the cytosolic indicator has been quenched. The remaining fluorescence is derived from compartmentilized indicator plus autofluorescence. The intensity values of the 340- and 380-nm signals at this stage represents the background fluorescence. Subsequent addition of an ionophore allows $Mn^{2+}$ to quench the compartmentilized indicator revealing the autofluorescence at 340 and 380 nm.

ues ($F$) of the indicator ($F_{max}$ and $F_{min}$) when it is $Ca^{2+}$-saturated and $Ca^{2+}$-free, along with any background fluorescence ***(5)***. After subtracting the background fluorescence from the signals, $[Ca^{2+}]_c$ can be calculated as follows:

$$[Ca^{2+}]_c = K_d \times (F - F_{min})/(F_{max} - F)$$

When the cells are in suspension, leaked dye will contribute to the background signal particularly if extracellular $Ca^{2+}$ is present, since the extracellular indicator will be saturated with $Ca^{2+}$. The contribution of the extracellular dye to the signal can be determined either by centrifuging the cells and measuring the fluorescence arising from the supernatant or by adding $Mn^{2+}$ and measuring the instantaneous drop in the signal. This latter approach will only work when using those indicators that are quenched by $Mn^{2+}$. When adjusting for extracellular dye in this way, the $Ca^{2+}$-saturated signal from extracellular dye should be subtracted from $F_{max}$ and from the $F$ obtained during the experiment. A $F$ equivalent to that from $Ca^{2+}$-free extracellular dye should be subtracted from $F_{min}$. Usually, this latter component is small and can be ignored unless the indicator gives a relatively large $Ca^{2+}$-free signal. A major source of background signals is cellular autofluorescence, which is more pronounced when the cells are excited in the UV. The signal from unloaded cells can be used to estimate the background fluorescence, as can certain $Mn^{2+}$ quench protocols as indicated in **Fig. 4.**

For single excitation indicators, optical path length and dye concentration are critical and must remain constant. Consequently in cell suspensions, lysing the cells and determining $F_{max}$ and $F_{min}$ works well because the overall dye concentration in the sample chamber does not change, nor does the optical path length. If the measurements are being made on cover slips, then on lysis the dye will diffuse out of the cells and, therefore, out of the focal plane. For such adherent cells, a $Ca^{2+}$ ionophore can be used to estimate $F_{max}$. Obtaining $F_{min}$, however, is more difficult, because even in the presence of extracellular EGTA, sufficient $Ca^{2+}$ may remain within the cell to affect the estimation of $F_{min}$. When calibrating with a suspension, sufficient EGTA must be added to chelate all the 1 m*M* initial $Ca^{2+}$ that is present in many experiments (with adherent cells, the bathing buffer can simply be replaced). This means that there has to be at least a 10-fold excess of EGTA to $Ca^{2+}$ in the cuvet ***(6,65)***. When adding EGTA to $Ca^{2+}$ (or vice versa), it should be remembered that 1 m*M* $Ca^{2+}$ bound to EGTA will liberate 2 m*M* $H^+$. These protons can be removed by adding *tris* base or by adding the EGTA as an alkali solution (pH 8.0–9.0). Fluo-3 can be calibrated using the $Mn^{2+}$-quenched signal to estimate both $F_{min}$ and $F_{max}$ ***(10,66)***. In other instances, it may be simpler to normalize the fluorescence signal to $F_{max}$. For imaging with a single wavelength indicator, the normalization has the added benefit that it can be carried out *in situ* on a pixel-to-pixel basis. During calibration of adherent cells, a potential problem is that increased dye leakage may lead to an underestimate of $F_{max}$ and $F_{min}$ in relation to the $F$ values obtained prior to the calibration. When using a ratiometric indicator, this would not be such a problem because ratio values $(R)_{max}$ and $R_{min}$ are not affected so dramatically by dye leakage.

With the ratiometric dyes, such as fura-2, the calibration is similar to that for the single wavelength indicators ***(6)***. The maximum and minimum $R$s, $R_{max}$ and $R_{min}$, are required instead of $F_{max}$ and $F_{min}$. Because the ratio is not made with reference to the isobestic point (360 nm) but, usually, to the 380-nm signal (to improve the signal-to-noise ratio), a scaling factor, the $F_{380max}/F_{380min}$ ratio is also required. At 360 nm, this factor would be equal to 1. Therefore:

$$[Ca^{2+}]_c = K_d\,[(R - R_{min})/(R_{max} - R)](F_{380max}/F_{380min})$$

where $R = F_{340}/F_{380}$.

With adherent cells, $R_{max}$ and $R_{min}$ are best determined *in situ*. $R_{max}$ is relatively easy to obtain using $Ca^{2+}$ ionophores, such as ionomycin and Br-A23187 (*see* **refs. *36*** and ***64***). The same problems in obtaining a reliable $R_{min}$ apply to the ratiometric probes, as well as to obtaining $F_{min}$ with the single wavelength indicators. Consequently, the calibration protocol is essentially the same as that described for single excitation indicators. With fura-2, the $Ca^{2+}$-saturated signal, determined by addition of ionophore in the presence of 1–10 m*M* extracel-

lular $Ca^{2+}$, will give the $F_{340max}$ and $F_{380min}$ ($R_{max}$). However, problems can arise if the $F_{380min}$ signal is close to autofluorescence, because dividing by zero or small numbers can play havoc with the software and generate very large erroneous $R_{max}$ values. This is a particular problem when using older 8-bit cameras, since auto-fluorescence values are likely to be close to zero. $R_{min}$, which is $F_{340min}/F_{380max}$, is obtained by incubating the cells with ionophore in the presence of relatively large amounts of EGTA as previously outlined for the single excitation indicators. Note, however, that Br-A23187 is reported to be more effective at transporting $Ca^{2+}$ at acid pH values than ionomycin ***(36,64)***.

**Figure 2** is a schematic diagram of the 340- and 380-nm signals of fura-2 during agonist stimulation and calibration.

With fura-2, $Mn^{2+}$ quench of the 340- and 380-nm excitation signals can be used to determine the background fluorescence at each wavelength (*see* **Fig. 4**). Some groups use ionomycin and $Mn^{2+}$ to determine background fluorescence; however, this approach would also quench signals coming from dye trapped inside organelles. To quench the cytosolic signal, it is better to use a maximal concentration of an agonist (or thapsigargin) so that $Mn^{2+}$ rapidly enters the cytosol. Thus, any remaining signal will represent compartmentalized dye and autofluorescence. Ionomycin can be added subsequently to reveal autofluorescence alone, if desired.

When imaging, the calibration should ideally be carried out on a pixel-to-pixel basis (including background subtraction) ***(67,68)***. However, the dimensions of a cell may change between the beginning and the end of an experiment, making perfect calibration virtually impossible. Frequently, the $R_{max}$ and $R_{min}$ values are averages determined for the entire field of view rather than on a pixel-to-pixel basis, although there are analysis packages that allow pixel-to-pixel generation of $R_{max}$ and $R_{min}$ values. I generally use photometric data gained by summing the signal arising from each cell. In this case, it is sufficient to subtract the total background fluorescence originating from each cell.

When calibrating $R_{max}$ and $R_{min}$ on an imaging system, one problem is that 8-bit cameras only just manage to cover the dynamic range of the indicator. Thus, when the gain and black level are optimized, $F_{340min}$ may be on scale, but $F_{340max}$ may saturate the camera and vice versa with the 380-nm signals. It is more than likely that although gain settings may suit some cells in the field of view, for other cells the setting will mean that they are either too bright or too dim. Twelve and 16-bit cameras alleviate this problem. Where possible, cameras should show a linear response to light ***(24,68)***. Confocal microscopes using PMTs should have a very large dynamic range (typically from $10^1$ to $10^6$ counts per second for PMTs), but this will depend on the analog-to-digital converter within the system.

### 2.10. Calcium Flux Measurements

In addition to providing information on $[Ca^{2+}]_c$, the fluorescent indicators can be used to provide data on $Ca^{2+}$ fluxes. Where influx and efflux are abolished (e.g., by $La^{3+}$), or where the cells have been permeabilized, the indicators can give kinetic information on the release of $Ca^{2+}$ from intracellular stores ***(69,70)***. When information is required on $Ca^{2+}$ influx, an easy approach is to use the $Mn^{2+}$ quench of fura-2 signals (**Fig. 3**). If $Mn^{2+}$ is used as a surrogate for extracellular $Ca^{2+}$, its influx into cells can be followed using fura-2 excited at 360 nm ***(27)***. Monochromator-based light sources are best for these experiments because they allow accurate excitation at the isobestic point. If excitation occurs slightly to the right of the isobestic point (i.e., >360 nm), a $Ca^{2+}$-dependent decrease in fluorescence can be confused with $Mn^{2+}$ entry.

The relative permeability of $Ca^{2+}$ influx pathways to $Mn^{2+}$ may be of interest alone ***(71–73)***. This quench technique can be used to investigate the rapid kinetics of cation entry by stopped flow fluorescence ***(73)***. In experiments investigating capacitative or store-operated $Ca^{2+}$ entry, $Ba^{2+}$ and $Sr^{2+}$ have also been used as surrogates for $Ca^{2+}$. These ions actually behave like $Ca^{2+}$ when they bind to fura-2, and do not quench the signal ***(74)***. Barium is also poorly removed from the cell, making it a good indicator of unidirectional fluxes. Interestingly, $Sr^{2+}$ does not appear to enter via store-operated channels but will enter in response to vasopressin, indicating that selective use of permeant cations can be used to distinguish between different influx pathways ***(72)***.

The indicators can be used to monitor $Ca^{2+}$ efflux whether it is a release from vesicles, $Ca^{2+}$ stores in permeabilized cells, or extrusion from an intact cell. Efflux can be measured from individual cells by either restricting the extracellular volume ***(75)*** or using indicator-dextran conjugates to generate a gel around the cells ***(20)***. This restricts the diffusion of $Ca^{2+}$ away, thereby aiding its detection. Alternatively, we have used low concentrations of extracellular fura-2 to monitor $Ca^{2+}$ efflux using cell suspensions ***(76,77)*** where sufficient $Ca^{2+}$ is transported to allow detection by the indicator. With the wide variety of $Ca^{2+}$ indicators now available, it is, of course, possible to combine $Ca^{2+}$ efflux studies using one indicator with measurements of $[Ca^{2+}]_c$ at the same time using another indicator ***(20)***.

### 2.11. Dextran-Conjugated Indicators

Many of the $Ca^{2+}$ indicators are now available as dextran conjugates ***(9)***. They are supplied as 3000, 10,000, and 70,000 molecular weight (MW) dextrans containing poly-(α-D-1,6-glucose) linkages making them resistant to cellular glucosidases. The dextran indicators have a number of useful properties owing to the following:

1. Have a restricted mobility.
2. Are not transported out of cells.

3. Remain cytosolic.
4. Are less likely to bind proteins.
5. Can be linked to peptides to allow specific targeting by peptide signal motifs.

### 2.12. Luminescent Protein Indicators for $Ca^{2+}$

The re-emergence of aequorin as a modern indicator for $Ca^{2+}$ occurred after it was shown that cells could be transfected with aequorin cDNA, allowing specific expression of the photoprotein in intracellular compartments ***(78,79)***. Selective targeting of aequorin to specific organelles or cellular domains, such as the mitochondria ***(78,79)*** nucleus ***(80)***, ER ***(43,45)***, or plasma membrane ***(81)***, meant that intracellular, domain-specific $[Ca^{2+}]$ could be measured. Luminescent probes have a number of advantages including: a large signal-to-noise ratio; avoidance of cell and reagent autofluorescence; and the requirement of simple photomultiplier technology for the detection of signals. In order to use recombinant aequorin, the apoprotein that is expressed in cells has to be reconstituted into functional aequorin by incubation with a prosthetic agent, coelenterazine ***(1,82)***. Aequorin extracted from the jelly fish already contains the prosthetic group. Coelenterazine is triggered to emit light when $Ca^{2+}$ binds to aequorin and during the luminsecent reaction coelenterazine is oxidized to coelenteramide ***(1,82)***. The apoaequorin expressed by cells has only to be incubated with coelenterazine for the functional aequorin to be regenerated. This regeneration requires the presence of molecular oxygen and low $Ca^{2+}$. In the presence of elevated $Ca^{2+}$ the rate of discharge will exceed the rate of regeneration ***(45)***. For wild-type aequorin, regeneration can easily be achieved in the presence of 100 n*M* $[Ca^{2+}]_c$ but regeneration of the luminescent protein in the ER presents a number of difficulties ***(45)***. Wild-type aequorin is effective for measuring $Ca^{2+}$ in the range of 0.2–50 μ*M* ***(1)***. However, when $[Ca^{2+}]_c$ exceeds approx 10 μ*M*, the large consumption of aequorin hampers steady-state measurement of $Ca^{2+}$. Recombinant aequorin was calculated to have an apparent $K_d$ close to that of wild-type aequorin, around 13–16 μ*M* at room temperature ***(83)***. At 37°C the value is around 10 μ*M* ***(1,83)***. In order to measure $Ca^{2+}$ in compartments with a high $Ca^{2+}$ the $K_d$ of the photoprotein for $Ca^{2+}$, was reduced by introducing a point mutation (42). The resulting mutated aequorin has a $K_d$ of around 130 μ*M*. Coelenterazine analogues that undergo a much slower light reaction have been synthesized ***(82)***. When used in combination with the mutated aequorin it is possible to measure steady state $[Ca^{2+}]$ of in the order of 700 μ*M* albeit for a few minutes ***(45)***. Using *n*-coelenterazine and reduced affinity aequorin subplasmalemmal $[Ca^{2+}]$ has been recorded at approx 50 μ*M* ***(81)***, the $[Ca^{2+}]_{ER}$ at 700 μ*M* ***(45)*** and spikes in mitochondrial $[Ca^{2+}]$ at approx 50 μ*M* ***(84)***.

Calibration of aequorin relies on determining the fractional rate of consumption that is proportional to the $[Ca^{2+}]$. This relationship, first reported by Blinks

***(84)***, is widely used to calculate $Ca^{2+}$ signals recorded by aequorin ***(1,45,79)***. In order to monitor $Ca^{2+}$ with any great effect, only a small proportion of the total photoprotein must be consumed at any one moment. Also, during experimentation the total amount of light emitted has to be recorded so that at each time interval the signal as a proportion of the total amount of signal available can be calculated. This means that when using aequorin, the raw count rate as viewed during the experiment is a poor indicator of the actual $[Ca^{2+}]$. A large spike in counts at the beginning of the experiment may actually be smaller in terms of $Ca^{2+}$ that a small spike toward the end of the experiment. At the end of the experiment any remaining aequorin has to be discharged (by cell lysis in the presence of $Ca^{2+}$) to establish the total amount of light emitted. The use of recombinant aequorin is ideally suited to photometry. Although it is possible to image $Ca^{2+}$ using aequorin, it has not been used to any great extent for this purpose. Simply, there is not enough light emitted for imaging because one molecule of aequorin will emit only one photon. That said, targeting of aequorin allows the average $[Ca^{2+}]$ to be recorded from within restricted domains where it would be difficult to obtain good spatial and temporal resolution using fluorescence imaging techniques. For example, aequorin can be used to measure the mean $[Ca^{2+}]$ in a cell population adjacent to adenylyl cyclase ***(85)***.

### *2.13. Fluorescent Protein Indicators for $Ca^{2+}$*

A number of fluorescent protein indicators for $Ca^{2+}$ have now been generated ***(44,86–88)***. These probes have all the targeting advantages associated with using aequorin, but allow visualization of $Ca^{2+}$ and nondestructive approximation of $[Ca^{2+}]$. Initial probes were based on the observation that fluorescence resonance energy transfer (FRET) can take place between the blue- or cyan-emitting mutants of the green fluorescent protein (GFP) and the green- or yellow-emitting GFP mutants ***(44,86–89)***. The cyan fluorescent protein (CFP) and yellow fluorescent protein (YFP) pairing lead to the yellow cameleon (YC) family of probes ***(44)***. The fusion protein consists of two GFP mutants separated by calmodulin (CaM) attached to a CaM-binding peptide. When $Ca^{2+}$ binds to the CaM, the complex binds to the $Ca^{2+}$-CaM-binding peptide, bringing the GFP mutants sufficiently close for FRET to take place. Thus, when the camelion-1 is excited at 380 nm, there is an increase in the 510/445 nm emission ratio on $Ca^{2+}$ binding.

Mutation of the CaM domain allowed the $Ca^{2+}$ sensitivity to be manipulated: YC2 is effective from 0.1 to 10 μ*M* $Ca^{2+}$; YC3, 0.5 to 100 μ*M* $Ca^{2+}$, and YC4, 10 to 1000 μ*M* $Ca^{2+}$ ***(44)***. These probes have been further improved. YC2.1, 3.1, and 4.1 are much less pH sensitive ***(90)***. pH sensitvity has limited the applicability especially for the desired use of measuring $[Ca^{2+}]_{ER}$. Unfortunately, modifying the probes to decrease their pH sensitivity led to slower matu-

ration of the probe, poor folding at 37°C. and a decreased dynamic range for YC4.1 compared with YC4. Using the "citrine" mutation of enhanced yellow fluorescent protein (EYFP), the GFP variants were further improved to possess greater pH tolerance, increased photostability, decreased sensitvity to halides, and improved protein folding ***(91)***. Incorporation of the citrine mutation of YFP into the YC probes generated the citrine cameleon, YC3.3. The Venus cameleon (YC2.12) incorporating the Venus mutant of YFP into YC2.1 rapidly matures within cells and is effective over [$Ca^{2+}$] from 0.1–10 μ*M* ***(92)***. Further cameleons include the CKKp cameleon (YC6.1) and Red Cameleon. The architecture of YC6.1 differs from the other cameleons in that the CaM-binding domain of CaM-dependent kinase has been inserted in the linker region between the N- and C-terminal portions of CaM. This configuration leads to increased FRET ***(93)***.

Other FRET-based $Ca^{2+}$ probes have been developed. Persechini and colleagues ***(94)*** generated the FIP-$CA_n$ series based on blue- and red-shifted GFP (BGFP and RGFP). The donor and acceptor pairing are separated by a $Ca^{2+}$-binding domain from smooth muscle myosin light-chain kinase (FIP-$CB_{SM}$ ) and tethered to variants of N- and C-terminal inverted calmodulin (CaMCN). The resulting probes bind $Ca^{2+}$ with $K_d$ of 100 and 280 n*M* at 37°C and have a monophasic relationship with $Ca^{2+}$. They are excited at 380 nm and emission monitored at 440 and 505 nm. The 440/505 nm ratio changes from approx 1.5 to 2.5 from $Ca^{2+}$-free to $Ca^{2+}$-saturated. An interesting development from the group is a probe ($BSCaM_A$) that measures CaM rather than $Ca^{2+}$ ***(95)***. The design has a CaM-binding domain linking the donor and acceptor GFP variants. In $BSCaM_A$ the calmodulin binding domain derived from neuromodulin binds both apocalmodulin ($Ca^{2+}$-free) and $Ca^{2+}$-CaM allowing the measurement of CaM availability. The probe is excited at 430 nm and emission monitored at 530 and 470 nm to give a ratiometric response. Thus, when $[Ca^{2+}]_c$ increases the available $CaM_A$ decreases because CaM will bind to target effector molecules. Simultanaeous measurement of CaM and $[Ca^{2+}]_c$ (the latter with indo-1) allows the relationship between $Ca^{2+}$-bound and free CaM to be determined.

GFP-based indicators for $Ca^{2+}$ have been developed that do not rely on FRET. These include the Camgaroo, Pericam, and G-CaMP probes ***(96–98)***. Tsien and colleagues ***(96)*** found that interchanging the N and C terminal portions of GFP variants around amino acids in the region between 142 and 229 (circular permutation) could yield a fluorescent protein. Surprisingly, whole protein sequences could be introduced at residue 145 and the resulting chimeric protein was still fluorescent. Camgaroo-1 was constructed by inserting CaM between amino acids 145 and 146 of EYFP ***(96)***. $Ca^{2+}$ binding can lead to a sevenfold increase in fluorescence of the probe. A desire to improve camgaroo-1 led to the genera-

tion of camgaroo-2 containing the Q69M mutation ***(91)***. Insertion of this mutation into EYFP resulted in the YFP variant citrine mentioned previously. Consequently, camgaroo-2 has many of the improved properties associated with citrine and YC3.3.

The Pericams were constructed from circular permutations of YFP around amino acid 145 and the introduction of CaM and M13 domains at that point ***(97)***. Three main probes were generated: Flash Pericam, Ratiometric Pericam, and Inverse Pericam. Pericams give a much larger change in fluorcesence on $Ca^{2+}$ binding compared with the Cameleons. When excited at 490 nm, flash pericam gives a eightfold increase in fluorescence with a $K_d$ for $Ca^{2+}$ of 0.7 $\mu M$. Emission peaks at 514 nm. Ratiometric Pericam needs to be excited around 415–418 nm (405 nm for an Ar-ion laser) and 494 nm with emission being monitored at close to 513 nm. Inverse Pericam should be excited around 490–503 nm and emission monitored at about 514 nm. With Inverse Pericam, fluorescence decreases on $Ca^{2+}$ binding with a $K_d$ of 0.2 $\mu M$. The Pericams have been used with great effect to measure $[Ca^{2+}]_c$ and $[Ca^{2+}]_m$ in cultured myocytes ***(99)***. Although the Cameleon probes have proved difficult to target to some organelles, such as mitochondria, organelle targeting of the Pericam does not appear to be a problem ***(97,99)***. Generally, the Pericams fold better than the early Cameleons; Inverse and Ratiometric Pericam do so independently of temperature, whereas Flash Pericam folds better at 28–30°C. Because the Pericams are based on EYFP (V68L/Q69K) they show a tendency for pH sensitivity that was eliminated from the later Cameleons. Significantly Ratio Pericam gives a tenfold increase in $R_{max}$ to $R_{min}$ compared with under twofold for the Cameleons.

G-CaMP is based on circularly permutated EGFP with M13, circularly permutated EGFP, and CaM arranged in series running from the N to the C terminus of the chimera ***(98)***. The probe is excited around 490 nm with emission peak at about 530 nm. The fluorescence increase on $Ca^{2+}$ binding is monophasic with a $K_d$ of 235 nm. This probe—like many of the recombinant $Ca^{2+}$ probes—is pH sensitive.

The fluorescent protein indicators clearly represent another huge step forward in our ability to monitor intracellular $Ca^{2+}$. They avoid some of the common problems, such as dye leakage, compartmentation, and nonspecific loading associated with the synthetic $Ca^{2+}$ indicators. The targeting advantages of these probes are substantial. They also, by and large, share the same instrumentation for detection as synthetic indicators. The synthetic $Ca^{2+}$ indicators allow $Ca^{2+}$ determinations in most isolated and cultured cells, and can be used to some extent in tissues. The incubation period with synthetic $Ca^{2+}$ indicators is generally tens of minutes to a few hours at the most. Another highly useful feature of some synthetic probes is their ability to bind $Mn^{2+}$, $Ba^{2+}$, and $Sr^{2+}$

allowing the investigation and characterization of $Ca^{2+}$ influx pathways. In comparison, recombinant protein probes require a suitable gene expression system. Plasmid transfection techniques are not readily suited for freshly isolated or quiesencent cells. On the other hand viral vectors offer much wider access of the probes to cells and tissues. The main drawback with recombinant probes is that appropriate molecular biological facilities are required and apart from YC2.1, there is also delay in the order of 24 h between infection and measurement. For freshly isolated cells this delay may be reduced if the probe can be introduced into the tissue sometime before the cells are isolated. As ever, choosing a probe depends on the specific aims and objectives of the experiment. The synthetic probes offer a fast and reliable approach with well-documented limitations. The recombinant probes open new horizons, but also come with their own limitations. There is no reason why synthetic and recombinant protein indicators cannot be used in combination as long as appropriate steps are taken with the instrumentation to avoid signal overlap.

### *2.14. Detection of Fluorescence Signals*

In its simplest form, measurement of $[Ca^{2+}]_c$ using fluorescent indicators requires only an appropriate light source and a PMT detector. A xenon lamp used in combination with interference filters or monochromators can be used to excite the UV and most of the visible indicators. More sophisticated light sources involving beam-splitting optics are needed for dual excitation indicators and multiple excitation of indicators used in combination. Photomultipliers are commonly attached to microscopes for photometric detection of $[Ca^{2+}]_c$ in single cells or from the field of view. Conventional imaging using a low-light intensified charged-coupled device camera attached to the fluorescence microscope is now common. This technique provides very good photometric data from individual cells within the field of view; however, improved spatial resolution of $[Ca^{2+}]_c$ is provided by confocal microscopy.

A major limitation of conventional imaging has been that even the high numerical aperture objectives used to gain sufficient light for detection also collect light from out-of-focus planes. This has a blurring effect on the resulting image. Confocal microscopy avoids this problem by exciting the indicator and collecting the emission via a pinhole or sometimes a narrow slit ***(100)***. The geometry is such that light originating from an out-of-focus plane cannot pass through the pinhole. To construct an image, the "confocal spot" has to be scanned over the object in view. This is achieved by generating a series of line scans over the image.

The use of confocal microscopy (usually confocal laser-scanning microscopy) to view fluorescent $Ca^{2+}$ indicators is now becoming widespread (For a review of confocal microscopy $Ca^{2+}$-imaging and biphotonics *see* **refs.**

***100,101***; *also* Chapter 4). The increased spatial resolution and rapid response time in the line-scan mode has revealed elementary $Ca^{2+}$ release events in excitable and nonexcitable cells ***(15,16,102)***. The increased resolution provided by these microscopes is particularly advantageous when the indicator has been targeted to a particular domain of the cell ***(31,44,58,61)***. In addition to confocal laser-scanning microscopy, there are a number of approaches that can give similar spatial resolution and, in some cases, potentially faster whole-frame data acquisition. Mathematical deconvolution using a series of image planes in the *z*-axis to calculate the blurring effect of the out-of-focus planes is one method ***(103,104)***. Using a calculated point spread function for the objective is another variation on this approach. Other optical methods include the Nipkow disc and a variation described by Wilson ***(105)*** that has a greater light throughput. These systems can give confocal-like images without the need to use lasers. The advantage would be that a monochromator-based excitation source could be used, allowing excitation at any desired wavelength or combination of wavelengths.

Two- and three-photon confocal microscopy can also be applied to fluorescence $Ca^{2+}$ indicators ***(64,69,70,100,106,107)***. Here, the indicator is excited at a longer wavelength and either two or three coincident photons (depending on the dye and excitation wavelength) are able to excite the indicator. Indo-1 is normally excited at approx 350 nm, but can also be excited by light close to 700 nm. The resolution over conventional imaging is enhanced, because statistically the arrival of coincident photons only occurs in a very narrow focal plane. Excitation by longer wavelengths reduces autofluorescence and photobleaching, and therefore, the technique has some advantages over other methods. The longer wavelengths allows deeper penetration of the sample in the *z*-axis owing to reduced scatter and absorbance by the tissue and chromophore. The principal handicap at present is the cost of the infrared (IR) lasers. The current generation of IR femtosecond pulse lasers supplied by Spectra Physics and Coherent can be tuned higher than 700 nm to approx 1000 nm. At the high end of this range, absorption of IR by water is a problem.

## 3. Summary

During the last decade or so, the range of fluorescent indicators for $Ca^{2+}$ has increased dramatically, so that there are now a host of probes available. Each may offer particular advantages depending on the design of the experiment and the fluorometric equipment available. Careful choice of the indicator is therefore central to achieve a successful outcome. The probe that is chosen will of course depend on the aims of the experiment, how the indicator will be introduced into the cell(s), and the excitation source and detection equipment that are available. I hope that this chapter will not only help investigators choose

the most appropriate indicator but, in addition, give an insight into what can be achieved using fluorescent $Ca^{2+}$ indicators.

## Acknowledgments

I would like to express my thanks to Drs John Quayle and Helen Burrell for reading this manuscript.

## References

1. Ashley, C. C. and Campbell, A. K. (eds.) (1979) *Detection and Measurement of Free Calcium in Living Cells*, Elsevier, Amsterdam, The Netherlands.
2. Woods, N. M., Cutherbertson, K. S. R., and Cobbold, P. H. (1986) Repetitive transient rises in cytoplasmic free calcium in hormone-stimulated hepatocytes. *Nature* **319,** 600–602.
3. Cobbold, P. H. and Bourne, P. K. (1984) Aequorin measurements of free calcium in single heart cells. *Nature* **312,** 444–446.
4. Tsien, R. Y. (1981) A non-disruptive technique for loading calcium buffers and indicators into cells. *Nature* **290,** 527–528.
5. Tsien, R. Y., Pozzan, T., and Rink, T. J. (1982) Calcium homeostasis in intact lymphocytes: Cytoplasmic free calcium monitored with a new intracellularly trapped fluorescent indicator. *J. Cell Biol.* **94,** 325–334.
6. Grynkiewicz, G., Poenie, M., and Tsien, R. Y. (1985) A new generation of $Ca^{2+}$ indicators with greatly improved fluorescence properties. *J. Biol. Chem.* **260,** 3440–3450.
7. Tsien, R. Y. (1980) New calcium indicators and buffers with high selectivity against magnesium and protons: Design, synthesis, and properties of prototype structures. *Biochemistry* **19,** 2396–2404.
8. Nuccitelli, R. and Deamer, D. W. (1982) *Intracellular pH: Its Measurement, Regulation and Utilization in Cellular Functions*, Alan R. Liss, New York, NY.
9. Haughland, R. P. (2002) *Handbook of Fluorescent Probes and Research Chemicals*, 7th Ed., Molecular Probes, Eugene, OR.
10. Minta, A., Kao, J. P. Y., and Tsien, R. Y. (1989) Fluorescent indicators for cytosolic calcium based on rhodamine and fluorescein chromophores. *J. Biol. Chem.* **264,** 8171–8178
11. Hallam, T. J., Sanchez, A., and Rink, T. J. (1984) Stimulus-response coupling in human platelets. *Biochem. J.* **218,** 819–827.
12. Simpson, A. W. M., Hallam, T. J., and Rink, T. J. (1986) Low concentrations of the stable prostaglandin endoperoxide U44069 stimulate platelet shape change in quin2-loaded platelets without a measurable increase in $[Ca^{2+}]_i$. *FEBS Lett.* **210,** 301–305.
13. Eberhard, M. and Erne, P. (1991) Calcium binding to fluorescent calcium indicators: calcium green, calcium orange and calcium crimson. *Biochem. Biophys. Res. Commun.* **180,** 209–215.
14. Hajnoczky, G., Robb-Gaspers, L. D., Seitz, M. B., and Thomas, A. P. (1995) Decoding of cytosolic calcium oscillations in the mitochondria. *Cell* **82,** 415–424.

15. Lipp, P. and Niggli, E. (1993) Ratiometric confocal $Ca^{2+}$ measurements with visible wavelength indicators in isolated cardiac myocytes. *Cell Calcium* **14,** 359–372.
16. Lipp, P. and Niggli, E. (1993) Microscopic spiral waves reveal positive feedback in subcellular calcium signalling. *Biophys. J.* **65,** 772–780.
17. Simpson, A. W. M. and Rink, T. J. (1987) Elevation of pHi is not an essential step in calcium mobilisation in fura-2-loaded human platelets. *FEBS Lett.* **222,** 144–148.
18. Morris, S. J., Weigmann, T. B., Welling, L. W., et al. (1994) Rapid simultaneous estimation of intracellular calcium and pH. Methods *Cell Biol.* **40,** 183–220.
19. Martinez-Zaguilan, R., Parnami, G., and Lynch, R. M. (1996) Selection of fluorescent ion indicators for simultaneous measurements of pH and $Ca^{2+}$. *Cell Calcium.* **19,** 337–349.
20. Belan, P. V., Garasimenko, O. V., Berry, D., Saftenku, E., Petersen, O. H., and Tepekin, A. V. (1996) A new technique for assessing the microscopic distribution of cellular calcium exit sites. *Pflugers Arch.* **433,** 200–208.
21. Kao, J. P. Y., Harootunian, A. T., and Tsien, R. Y. (1989) Photochemically generated cytosolic calcium pulses and their detection by Fluo-3. *J. Biol. Chem.* **264,** 8179–8184.
22. Graham, C. and Ellis-Davies, R. (2003) Development and application of caged calcium. *Methods Enzymol* **360,** 226–238.
23. Ashby, M. C., Craske, M., Park, M. K., et al. (2002) Localized $Ca^{2+}$ uncaging reveals polarized distribution of $Ca^{2+}$ -sensitive $Ca^{2+}$ -release sites: mechanism of unidirectional $Ca^{2+}$ waves. *J. Cell Biol.* **158,** 283–292.
24. Ryan, T. A., Milard, P. J., and Webb, W. W. (1990) Imaging $[Ca^{2+}]_i$ dynamics during signal transduction. *Cell Calcium* **11,** 145–155.
25. Roe, M. W., Lemasters, J. J., and Herman, B. (1990) Assessment of fura-2 for measurements of cytosolic free calcium. *Cell Calcium* **11,** 63–73.
26. Malgoroli, A., Milani, D., Meldolesi, J., and Pozzan, T. (1987) Fura-2 measurements of cytosolic free $Ca^{2+}$ in monolayers and suspensions of various types of animal cells. *J. Cell Biol.* **105,** 2719–2727.
27. Merritt, J. E., Jacob, R., and Hallam, T. J. (1988) Use of manganese to discriminate between calcium influx and mobilization from internal stores in stimulated human neutrophils. *J. Biol. Chem.* **264,** 1522–1527.
28. Rink, T. J. and Cobbold, P. H. (1987) Fluorescence and bioluminescence measurement of cytoplasmic free calcium. *Biochem. J.* **248,** 313–328.
29. Almers, W. and Neher, E. (1985) The $Ca^{2+}$ signal from fura-2-loaded mast cells depends strongly upon the method of loading. *FEBS Lett.* **192,** 13–18.
30. Steinberg, S. F., Belizikian, J. P., and Al-Awqati, Q. (1987) Fura-2 fluorescence is localised to mitochondria in endothelial cells. *Am. J. Physiol.* **253,** C744–C754.
31. Golovina, V. A. and Blaustein, M. P. (1997) Spatially and functionally distinct $Ca^{2+}$ stores in sarcoplasmic and endoplasmic reticulum. *Science* **275,** 1643–1648.

32. Homolya, L., Hollo, Z., Germann, U. A., Pastan, I., Gottesmann, M. M., and Sarkadi, B. (1993) Fluorescent cellular indicators are extruded by the multidrug resistance protein. *J. Biol. Chem.* **268,** 21,493–21,496.
33. Neher, E. (1989) Combined fura-2 and patch clamp measurements in rat peritoneal mast cells, in *Neuromuscular Junction* (Sellin, L. C., Libelius, R., and Thesleff, S., eds.), Elsevier, Amsterdam, pp. 65–76.
34. Steinberg, T. H., Newman, A. S., Swanson, J. A., and Silverstein, S. C. (1987) $ATP^{4-}$ permeabilizes the plasma membrane of mouse macrophages to fluorescent dyes. *J. Biol. Chem.* **262,** 8884–8888.
35. Di Virgilio, F., Fasolato, C., and Steinberg, T. H. (1988) Inhibitors of membrane transport system for organic anions block fura-2 excretion from PC12 and N2A cells. *Biochem. J.* **256,** 959–963.
36. Kao, J. P. Y. (1994) Practical aspects of measuring $[Ca^{2+}]$ with fluorescent indicators. *Methods Cell Biol.* **40,** 155–181.
37. Di Virgilio, F., Steinberg T. H., and Silverstein, S. C. (1990) Inhibition of fura-2 sequestration and secretion with organic anion transport blockers. *Cell Calcium* **11,** 57–62.
38. Di Virgilio, F., Steinberg, T. H., Swanson, J. A., and Silverstein, S. C. (1988) Fura-2 secretion and sequestration in macrophages. *J. Immunol.* **140,** 915–920.
39. Teflabs Catalog (2004) Texas Fluorescence Labs Inc., Austin, TX.
40. Miyata, H., Silvermann, H. S., Sollott, S. J., Lakatta, E. G., Stern, M. D., and Hansford, R. G. (1991). Measurement of mitochondrial free $Ca^{2+}$ concentration in living single rat cardiac myocytes. *Am. J. Physiol.* **261,** H1123–H1134.
41. Donnadieu, E. and Bourguinon, L. Y. W. (1996) $Ca^{2+}$ signalling in endothelial cells stimulated by bradykinin: $Ca^{2+}$ measurement in the mitochondria and the cytosol by confocal microscopy. *Cell Calcium* **20,** 53–61.
42. Kendall, J. M., Dormer, R. L., and Campbell, A. K. (1992) Targeting aequorin to the endoplasmic reticulum of living cells. *Biochem. Biophys. Res. Commun.* **189,** 1008–1016.
43. Montero, M., Brini, M., Marsault, R., Alverez, J., Sitia, R., Pozzan, T., and Rizzuto, R. (1995) Monitoring dynamic changes in free $Ca^{2+}$ concentration in the endoplasmic reticulum of intact cells. *EMBO J.* **14,** 5467–5475.
44. Miyawaki, A., Llopis, J., Heim, R., et al. (1997) Fluorescent indicators for $Ca^{2+}$ based on green fluorescent proteins and calmodulin. *Nature* **388,** 882–887.
45. Alverez, J. and Montero, M. (2002) Measuring $[Ca^{2+}]$ in the endoplasmic reticulum with aequorin. *Cell Calcium* **32,** 251–260.
46. Hofer, A. M. and Machen, T. E. (1993) Technique for *in situ* measurement of calcium in intracellular inositol 1,4,5-trisphosphate-sensitive stores using the fluorescent indicator mag-fura-2. *Proc. Natl. Acad. Sci. USA* **90,** 2598–2602.
47. Raju, B., Murphy, E., Levy, L. A., Hall, R. D., and London, R. E. (1989) A fluorescent indicator for measuring cytosolic free magnesium. *Am. J. Physiol.* **256,** C540–C548.

48. Konishi, M., Hollingworth, S., Harkins, A. B., and Baylor, S. M. (1991) Myoplasmic $Ca^{2+}$ transients in intact frog skeletal muscle fibres monitored with the fluorescent indicator furaptra. *J. Gen. Physiol.* **97,** 271–302.
49. Ogden, D., Khodakhah, K., Carter, T., Thomas, M., and Capoid, T. (1995) Analogue computation of transient changes of intracellular free $Ca^{2+}$ concentration with the low affinity $Ca^{2+}$ indicator furaptra during whole-cell patch clamp recording. *Pflugers Arch.* **429,** 587–591.
50. Hofer, A. M., Landolfi, B., Debellis, L., Pozzan, T., and Curci, S. (1998) Free $[Ca^{2+}]$ dynamics measured in agonist-sensitive stores of single living intact cells: a new look at the refilling process *EMBO J.* **17,** 1986–1995
51. van de Put, F. M. M. and Elliott, A. C. (1996) Imaging of intracellular calcium stores in individual permeabilized pancreatic acinar cells. *J. Biol. Chem.* **271,** 4999–5006.
52. Gerasimenko, O. V., Gerasimenko, J. V., Tepekin, A. V., and Petersen, O. H. (1995). ATP-dependent accumulation and inositol trisphosphate- or cyclic ADP-ribose mediated release of $Ca^{2+}$ from the nuclear envelope. *Cell* **80,** 439–444.
53. Minamikawa, T., Takahashi, A., and Fujita, S. (1995) Differences in features of calcium transients between the nucleus and the cytosol in cultured heart muscle cells: Analyzed by confocal microscopy. *Cell Calcium* **17,** 165–176.
54. Cheng, H., Lederer, W. J., and Cannell, M. B. (1993) Calcium sparks, elementary events underlying excitation-contraction coupling in heart muscle. *Science* **262,** 740–744
55. Rizzuto, R., Brini, M., Murgia, M., and Pozzan, T. (1993) Microdomains with high $Ca^{2+}$ close to $IP_3$-sensitive channels that are sensed by neighbouring mitochondria. *Science* **262,** 744–747.
56. Berridge, M. J. (1997) The AM and FM of calcium signalling. *Nature* 386, 759–760.
57. Zenisek, D., Davila, V., Wan, L., and Almers, W. (2003) Imaging calcium entry sites and ribbon structures in two presynaptic cells. *J. Neurosci.* **23,** 2538–2548.
58. Etter, E. F., Kuhn, M. A., and Fay, F. S. (1994) Detection of changes in near-membrane $Ca^{2+}$ concentration using a novel membrane-associated $Ca^{2+}$ indicator. *J. Biol. Chem.* **269,** 10,141–10,149.
59. Etter, E., Minta, A., Poenie, M., and Fay, F. S. (1996) Near membrane $Ca^{2+}$ transients resolved using the $Ca^{2+}$ indicator FFP18. *Proc. Natl. Acad. Sci. USA* **93,** 5368–5373.
60. Lloyd, Q. P., Kuhn, M. A., and Gay, C. V. (1995) Characterization of calcium translocation across the plasma-membrane of primary osteoblasts using a lipophilic calcium-sensitive fluorescent dye, calcium green-C-18. *J. Biol. Chem.* **270,** 22,445–22,451.
61. Horne, J. H. and Meyer, T. (1997) Elementary calcium release units induced by inositol trisphosphate. *Science* **276,** 1690–1692.
62. Clapham, D. E. (1995) Calcium signalling. *Cell* 80, 259–268.
63. Neher, E. and Augustine, G. J. (1992) Calcium gradients and buffers in bovine chromaffin cells. *J. Physiol.* **450,** 273–301.

64. Williams, D. A. and Fay, F. S. (1990) Intracellular calibration of the fluorescent calcium indicator fura-2. *Cell Calcium* **11,** 75–83.
65. Poenie, M. (1990) Alteration of intracellular fura-2 fluorescence by viscosity: a simple correction. *Cell Calcium* **11,** 85–91.
66. Merrit, J. E., McCarthy, S. A., Davies, M. P. A., and Moores, K. E. (1990) Use of fluo-3 to measure $Ca^{2+}$ in platelets and neutrophils. *Biochem. J.* **269,** 513–519.
67. Tsien, R. Y. and Harootunian, A. T. (1990) Practical design criteria for a dynamic ratio imaging system. *Cell Calcium* **11,** 93–109.
68. Moore, E. D. W., Becker, P. L., Fogarty, K. E., Williams, D. A., and Fay, F. S. (1990) $Ca^{2+}$ imaging in single living cells: theoretical and practical issues. *Cell Calcium* **11,** 157–179.
69. Toescu, E. C. and Petersen, O. H. (1994) The thapsigargin-evoked increase in $[Ca^{2+}]_i$ involves an $InsP_3$-dependent $Ca^{2+}$ release process in pancreatic acinar cells. *Pflugers Arch.-Eur. J. Physiol.* **427,** 325–331.
70. Wilcox, R. A., Strupish, J., and Nahorski, S. R. (1995) Measurement of $Ca^{2+}$ fluxes in permeabilised cells using $^{45}Ca^{2+}$ and fluo-3. *Methods Mol. Biol.* **41,** 215–227.
71. Broad, L.M., Cannon, T.R. and Taylor, C.W. (1999) A non-capacitative pathway activated by arachidonic acid is the major $Ca^{2+}$ entry mechanism in A7r5 smooth muscle cells stimulated with low concentrations of vasopressin. *J. Physiol.* **517,** 121–134.
72. Byron, K. L. and Taylor, C. W. (1995) Vasopressin stimulation of $Ca^{2+}$ mobilization, two bivalent cation entry pathways and $Ca^{2+}$ efflux in A7r5 rat smooth muscle cells. *J. Physiol.* **485,** 455–468.
73. Sage, S. O., Reast, R., and Rink, T. J. (1990) ADP evokes biphasic $Ca^{2+}$ influx in fura-2-loaded human platelets. *Biochem. J.* **265,** 675–680.
74. Hatae, J., Fujishiro, N., and Kawata, H. (1996) Spectroscopic properties of fluorescence dye fura-2 with various divalent cations. *Jpn. J. Physiol.* **46,** 423–429.
75. Tepikin, A. V., Voronina, S. G., Gallagher, D. V., and Petersen, O. H. (1992) Acetylcholine-evoked increase in the cytoplasmic $Ca^{2+}$ concentration and $Ca^{2+}$ extrusion measured simultaneously in single mouse pancreatic acinar cells. *J. Biol. Chem.* **267,** 14,073–14,076.
76. Zolle, O. C., Lawrie, A. M., and Simpson, A. W. M. (2000) Activation of the particulate and not the soluble guanylate cyclase leads to inhibition of $Ca^{2+}$ extrusion through localised elevation of cGMP. *J. Biol. Chem.* **275,** 25,892–25,899.
77. Green, A. K., Zolle, O., and Simpson A. W. M. (2002) Atrial natriuretic peptide attenuates $Ca^{2+}$ oscillations in rat hepatocytes by modulating plasma membrane $Ca^{2+}$ fluxes. *Gastroenterol.* **123,** 1291–1203.
78. Rizzuto, R., Simpson, A.W.M. Brini, M., and Pozzan, T. (1992) Rapid changes of mitochondrial $Ca^{2+}$ revealed by specifically targeted recombinant aequorin. *Nature* **358,** 325–327.
79. Robert, V., Pinton, P., Tosello, V., Rizzuto, R., and Pozzan, T. (2000) Recombinant aequorin as a tool for monitoring calcium concentration in subcellular compartments. *Methods Enzymol.* **327,** 440–456.

80. Brini, M., Marsault, R., Bastianutto, C., Pozzan, T., and Rizzuto, R. (1994) Nuclear targeting of aequorin - a new approach for measuring nuclear $Ca^{2+}$ concentration in intact-cells. *Cell Calcium* **16,** 259–268.
81. Marsault, R., Murgia, M., Pozzan, T., and Rizzuto, R. (1997) Domains of high $Ca^{2+}$ beneath the plasma membrane of living A7r5 cells. *EMBO J.* **16,** 1575–1581.
82. Shimomura, O., Musik, B., and Kishi, Y. (1989) Semi-synthetic aequorins with improved sensitivity to $Ca^{2+}$ ions. *Biochem. J.* **261,** 913–920.
83. Brini M., Marsault, R., Bastianutto, C., Alverez, J., Pozzan, T., and Rizzuto, R. (1995) Transfected aequorin in the measurment of cytoscolic $Ca^{2+}$ concentration ($[Ca^{2+}]_c$). *J. Biol. Chem.* **270,** 9896–9903.
84. Marsault, R., Murgia, M., Pozzan, T., Rizzuto, R. (1997) Domains of high $Ca^{2+}$ beneath the plasma membrane of living A7r5 cells *EMBO J.* **16,** 1575–1581.
85. Cooper, D. M. F. (2002) Calcium-sensitive adenylyl cyclase/aequorin chimeras as sensitive probes for discrete modes of elevation of cytosolic calcium. *Methods Enzymol.* **345,** 105–112.
86. Demaurex, N. and Frieden, M. (2001) Measurements of free lumenal ER $Ca^{2+}$ concentration with targeted "cameleon" fluorescent proteins. *Cell Calcium* **34,** 109–119.
87. Miyawaki, A. (2003) Fluorescence imaging of physiological activity in complex systems using GFP-based probes. *Curr. Opin. Neurobiol.* **13,** 591–596.
88. Miyawaki, A. (2003) Visualization of the spatial and temporal dynamics of intracellular signaling. *Developmental Cell* **4,** 295–305.
89. Miyawaki, A. and Tsien , R. Y. (2000) Monotoring protein conformations and interactions by fluorescence resonance energy transfer between mutants of green fluorescent protein. *Methods Enzymol.* **327,** 472–500.
90. Miyawaki, A., Griesbeck, O., Heim, R., and Tsien, R. Y. (1999) Dymanic and quantitative $Ca^{2+}$ measurements using improved cameleons. *Proc. Natl. Acad. Sci. USA* **96,** 2135–2140.
91. Griesbeck, O., Baird, G. S., Campbell, R. E., Zacharias, D. A., and Tsien, R. Y. (2001) Reducing the environmental sensitivity of yellow fluorescent protein. *J. Biol. Chem.* **276,** 29,188–29,194.
92. Nagai, T. Ibata, K., Park, E. S., Kubota, M., Mikoshiba, K., and Miyawaki, A. (2002). A variant of yellow fluorescent protein with fast and efficient maturation for cell-biological applications. *Nat. Biotechnol.* **20,** 87–90.
93. Truong, T., Sawano, A., Mizuno, H., et al. (2001) FRET-based *in vivo* $Ca^{2+}$ imaging by a new calmodulin-GFP fusion molecule. *Nat. Struct. Biol.* **8,** 1069–1073.
94. Persechini, A., Lynch, J. A. and Romoser, V. A. (1997) Novel fluorescent indicator proteins for monitoring free intracellular $Ca^{2+}$. *Cell Calcium* **22,** 209–216.
95. Black, D. J., Tran, Q.-K., and Persechini, A. (2003) Monitoring the total available calmodulin conentration in intact cells over the physiological range in free $Ca^{2+}$. (2004) *Cell Calcium* **35,** 415–425.
96. Baird, G. S., Zacharias, D. A. and Tsien, R. Y. (1999) Circular permutation and receptor insertion within green fluorescent proteins. *Proc. Natl. Acad. Sci. USA* **96,** 11,241–11,246.

97. Nagai, T., Saweno, A., Sun Park, E., and Miyawaki, A. (2001) Circularly permuted green fluorescent proteins engineered to sense $Ca^{2+}$. *Proc. Natl. Acad. Sci. USA* **98,** 3197–3202.
98. Nakai, J., Ohkura, O., and Imoto, K. (2001) A high signal-to-noise $Ca^{2+}$ probe composed of a single green fluorescent protein. *Nat. Biotechnol.* **19,** 137–141.
99. Robert V., Gurlini, P., Tosello, V., et al. (2001) Beat-to-beat oscillations of mitochondrial [$Ca^{2+}$] in cardiac cells *EMBO J.* **20,** 4998–5007.
100. Schild, D. (1996) Laser scanning microscopy and calcium imaging. *Cell Calcium* **19,** 281–296.
101. Parker, I. and Marriott, G. (eds.) (2003) Biophotonics, Part A. in *Methods in Enzymology,* vol. 360, Academic Press, San Diego.
102. Berridge, M. J. (1997) Elementary and global aspects of calcium signalling. *J. Physiol.* **499,** 291–306.
103. Agard, A. D. (1984) Optical sectioning microscopy: cellular architecture in three dimensions. *Annu. Rev. Biophys. Bioeng.* **13,** 191–219.
104. Monck, J. R., Oberhauser, A. F., Keating, T. J., and Fernandez, J. M. (1992) Thin-section ratiometric $Ca^{2+}$ images obtained by optical sectioning of fura-2-loaded mast cells. *J. Cell Biol.* **116,** 745–759.
105. Juskaitis, R., Wilson T., Neil, M. A. A., and Kozubek, M. (1996) Efficient real-time confocal microscopy with white-light sources. *Nature* **383,** 804–806.
106. Zhang, Z. X., Sonek, G. J., Wei, X. B., Berns, M. W., and Tromberg, B. J. (1997) Continuous wave diode laser induced two-photon fluorescence excitation of three calcium indicators. *Jpn. J. Applied Phys.* **36,** L1598-L1600.
107. Konig, K., Simon, U., and Halbhuber, K. J. (1996) 3D resolved two photon fluorescence microscopy of living cells using a modified confocal laser scanning microscope. *Cell. Mol. Biol.* **42,** 1181–1194.
108. Escobar, A. L., Velez, P., Kim, A. M., Cifuentes, F., Fil, M., and Vergara, J. L. (1997) Kinetic properties of DM-nitrophen and calcium indicators: Rapid transient response to flash photolysis. *Pflugers. Arch.-Eur. J. Physiol.* **434,** 615–631.

# 2

# Measurement of $[Ca^{2+}]_i$ in Whole Cell Suspensions Using Fura-2

**Robert A. Hirst, Charlotte Harrison, Kazuyoshi Hirota, and David G. Lambert**

## 1. Introduction

An elevation in intracellular calcium concentration ($[Ca^{2+}]_i$) acts to trigger a range of cellular events including neurotransmitter release, muscle contraction, and oocyte fertilization ***(1,2)***. The pattern of elevation in $[Ca^{2+}]_i$ and response to that elevation is dependent on the agonist and the cell type.

The introduction of the calcium-sensitive dye fura-2 ***(3)*** revolutionized the measurement of $[Ca^{2+}]_i$ in whole cell suspensions, populations of adherent cells, single cells, and in subcellular regions (*see* **ref. *4***). Fura-2 is a ratiometric dye in that when $Ca^{2+}$ binds, the excitation spectrum shifts rightward. In the presence of $Ca^{2+}$, maximum fura-2 fluorescence (at 510 nm emission) is observed at a wavelength of 340 nm and in $Ca^{2+}$-free conditions at 380 nm. Therefore, it follows that the concentration of free intracellular $Ca^{2+}$ is proportional to the ratio of fluorescence at 340/380. The Grynkiewicz equation describes this relationship ***(3)***.

$$[Ca^{2+}]_i \text{ (n}M) = K_d \times [(R - R_{min})/R_{max} - R)] \times \text{Sfb}$$

where $K_d$ (for $Ca^{2+}$ binding to fura-2 at 37°C) = 225 n$M$, $R$ = 340/380 ratio, $R_{max}$ = 340/380 ratio under $Ca^{2+}$-saturating conditions, $R_{min}$ = 340/380 ratio under $Ca^{2+}$-free conditions, and Sfb = ratio of baseline fluorescence (380 nm) under $Ca^{2+}$-free and -bound conditions. The $K_d$ for $Ca^{2+}$ binding to fura-2 decreases with decreasing temperature.

As noted in Chapter 1, fura-2-free acid is $Ca^{2+}$ sensitive but membrane impermeant. To effect cell loading, cells are incubated with fura-2 pentaacetoxymethyl

From: *Methods in Molecular Biology, vol. 312: Calcium Signaling Protocols: Second Edition*
Edited by: D. G. Lambert © Humana Press Inc., Totowa, NJ

(AM) ester; this form of the dye is $Ca^{2+}$ insensitive. Once inside the cell, esterase enzymes sequentially cleave the AM groups to leave fura-2-free acid trapped inside the cell, where it is able to bind $Ca^{2+}$.

In this chapter the authors will describe the use of fura-2 to measure $[Ca^{2+}]_i$ in suspension of several different cell types (*see* **ref. *4***). The technique is quite straightforward and involves incubating cells with fura-2/AM, a postincubation period to allow full de-esterification and extensive washing.

In cell suspensions, an estimate of global changes in $[Ca^{2+}]_i$ can only be made. This is useful in combination with the currently available pharmacological agents to study sources of $Ca^{2+}$ (intracellular vs extracellular) in a given response and to screen for $Ca^{2+}$ mobilizing drugs and receptors. However, detailed information regarding subcellular localization requires more sophisticated measurements using standard subcellular imaging (*see* Chapter 5) or confocal microscopy (*see* Chapter 6).

## 2. Materials

### 2.1. Cell Culture

1. Undifferentiated SH-SY5Y human neuroblastoma cells (gift from Dr. J. L. Beidler, Sloane Kettering Institute, Rye, NJ).
2. Culture medium for SH-SY5Y cells: minimum essential medium supplemented with 10% fetal calf serum (FCS), 2 m*M* glutamine, 100 IU/mL penicillin, 100 IU/mL streptomycin, and 2.5 µg/mL fungizone (*see* **Note 1**).
3. NG108-15 neuroblastoma X glioma hybrid cells (*see* **Note 2**).
4. Culture medium for NG108-15 cells: Dulbecco's minimum essential medium supplemented with 10% FCS, 2 m*M* glutamine, 100 IU/mL penicillin, 100 IU/mL streptomycin, 2.5 µg/mL fungizone, and HAT (hypoxanthine [0.1 m*M*], aminopterin [0.4 µ*M*], thymidine [16 µ*M*]) (*see* **Note 1**).
5. Chinese hamster ovary (CHO) cells expressing the recombinant δ opioid receptor (gift from Dr. L. A. Devi, Department of Pharmacology, New York University, NY).
6. Culture medium for CHO cells: HAMS F12 medium supplemented with 10% FCS, 100 IU/mL penicillin, 100 IU/mL streptomycin, 2.5 µg/mL fungizone, and 100 µg/mL geneticin (*see* **Notes 1** and **3**).

### 2.2. Buffers

1. Krebs HEPES buffer (for loading and washing): 143.3 m*M* $Na^+$, 4.7 m*M* $K^+$, 2.5 m*M* $Ca^{2+}$, 1.3 m*M* $Mg^{2+}$, 125.6 m*M* $Cl^-$, 25 m*M* $HCO_3^-$, 1.2 m*M* $H_2PO_4^-$, 1.2 m*M* $SO_4^{2-}$, 11.7 m*M* glucose, and 10 m*M* HEPES, pH 7.4 titrated with 10*M* NaOH.
2. Nominally $Ca^{2+}$-free Krebs HEPES buffer, pH 7.4, as in **item 1** omitting $Ca^{2+}$ and adding 0.1 m*M* EGTA. This should be made in plastic beakers as glass leaches significant amounts of $Ca^{2+}$.
3. Low $Na^+$ Krebs HEPES buffer, pH 7.4, for depolarization: 43.3 m*M* $Na^+$, 2.5 m*M* $Ca^{2+}$, 1.3 m*M* $Mg^{2+}$, 125.6 m*M* $Cl^-$, 25 m*M* $HCO_3^-$, 1.2 m*M* $H_2PO_4^-$, 1.2 m*M*

$SO_4^{2-}$, 11.7 m*M* glucose, and 10 m*M* HEPES. With this buffer, 100 m*M* $K^+$ is added (*see* **Note 4**).
4. Cell harvest buffer: 10 m*M* HEPES-buffered 0.9% saline plus 0.05% EDTA, pH 7.4 (with 10 *M* NaOH).

### 2.3. General Reagents

1. Fura-2/AM (Sigma, Dorset, UK). Make up as a stock (1 m*M*) solution by dissolving in dimethylsulfoxide and storing aliquots (10 µL) at –20°C until required.
2. Triton X-100 (Sigma). Make a stock (4%) solution in warmed water.
3. EGTA (Sigma). Make a stock (90 m*M*) solution in 1 *M* NaOH.
4. Probenecid (Sigma). Dissolve at 50 mg/mL (175 m*M*) stock in 1 *M* NaOH. Use at 2.5 m*M* in buffer (*see* **Note 5**).

## 3. Methods

### 3.1. Tissue Culture and Monolayer Harvesting

1. Maintain confluent monolayers (75 $cm^2$) of cells in the appropriate media.
2. Split one flask of confluent cells using trypsin (0.5g/L)-EDTA (2g/L, 5 mL) solution as supplied (*see* **Note 1**) into nine other flasks each containing 20 mL of supplemented media. After 2 d of incubation (37°C, 5% $CO_2$ incubator), remove the media and replace with 25 mL of fresh supplemented media.
3. Culture cells (feed 24 h before use with fresh medium) until confluent (use cells up to 3 d post confluency).
4. On the day of the experiment, remove medium and add 5 mL of harvest buffer to cell monolayer.
5. Remove 5 mL of harvest buffer immediately, and add a further 5 mL of fresh harvest buffer and incubate at 37°C for ~5 min.
6. Gently tap the side of the flask to dislodge the adherent cell monolayer.
7. When all the cells are in suspension, transfer it to a centrifuge tube. Rinse the cells out of the flask by adding approx 15 mL of experimental buffer. Transfer this to the centrifuge tube.
8. Sediment at 1000*g* in a low-speed centrifuge for 3 min.
9. Remove supernatant and resuspend the pellet into 30 mL of fresh experimental buffer. Invert the tube three times and resediment at 500*g* for 3 min.
10. Repeat **step 9** once more, and finally resuspend the pellet in 3 mL of experimental buffer.

### 3.2. Fura-2 Loading and Measurement of Intracellular Calcium

Optimal fura-2 loading time and de-esterification time may vary depending on the cell type used, and hence it is recommended that these times should be adjusted accordingly. The protocol used by the authors in a range of cell types is as follows:

1. Incubate cell suspensions with 3 µ*M* of fura-2/AM in 3 mL (10 µL of 1 m*M* fura-2/AM) for 30 min at 37°C in the dark.

2. Sediment the cells (500*g* for 2 min) and resuspend in 30 mL of Krebs/HEPES buffer.
3. Incubate a further 15 min at room temperature in the dark to allow for de-esterification of the fura-2/AM.
4. Sediment the cells (500*g* for 2 min) and resuspend in 30 mL of Krebs/HEPES buffer twice more.
5. Sediment (500*g* for 2 min) and resuspend in buffer allowing 2 mL per determination (*see* **Note 6**).
6. Place cell suspensions (2 mL) in a quartz cuvet containing a magnetic stirrer and place in the cuvet holder, which is maintained at 37°C with a water jacket.
7. Simultaneously monitor and, if possible, display 340 and 380 excitation intensity (at 510 emission). Signal sampling should be set according to the kinetics of the changes in $[Ca^{2+}]_i$; the authors routinely make one ratio measurement per second (*see* **Note 7**).
8. Following establishment of stable 340 and 380 recordings, add compounds to be tested (*see* **Note 8**).
9. Maintain stock of loaded cells on ice (*see* **Note 9**).
10. Calibrate the fluorescence signal as follows (*see* **Note 10**):
    a. Add 0.1% Triton X-100 to the cuvet to produce cell lysis and liberate fura-2 into a $Ca^{2+}$-containing buffer. Under these conditions, fura-2 saturates with $Ca^{2+}$ and maximum fluorescence ratio ($R_{max}$) is determined (*see* **Note 11**).
    b. 4.5 m*M* EGTA, pH >8.0, to chelate $Ca^{2+}$ and determine minimum fluorescence ratio ($R_{min}$) (*see* **Note 12**).
    c. Substitute $R_{max}$, $R_{min}$, and the derived Sfb along with measured *R* values from cell suspensions into the Grynkiewicz equation ***(3)*** and estimate $[Ca^{2+}]_i$. This can be accomplished using a spreadsheet type program, although the authors use FLDM software associated with the fluorimeter (*see* **Note 7**).

## *3.3. Examples of $[Ca^{2+}]_i$ Measurements Made in Cell Suspensions*

### *3.3.1. Carbachol Stimulation in SH-SY5Y Cells*

SH-SY5Y cells express a homogenous population of $M_3$ muscarinic receptors that are coupled to phospholipase C and increased $[Ca^{2+}]_i$. The authors have shown that this $[Ca^{2+}]_i$ is biphasic, with a peak phase mediated by release from intracellular stores and a plateau phase resulting from $Ca^{2+}$ entry across the plasma membrane ***(4,5)***. A typical experiment is described below:

1. Cells are harvested (*see* **Subheading 3.1., steps 4–10**).
2. Suspensions are loaded with fura-2 as described in **Subheading 3.2.**
3. Following de-esterification and washing, cells are placed into a cuvet and 340/380 nm fluorescence monitored.
4. Stocks of loaded cells are kept on ice.
5. As can be seen in **Fig. 1**, the response to 10 μ*M* carbachol was biphasic (**Fig. 1A**). Also shown for comparison is a typical 340/380 nm recording (**Fig. 1B**) and the derived 340/380 ratio (**Fig. 1C**).

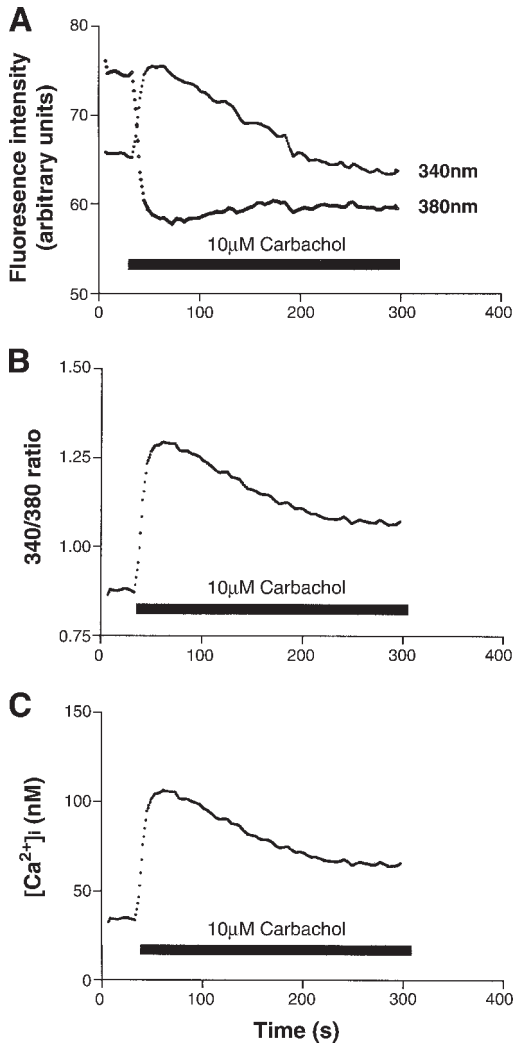


Fig. 1. Carbachol increases $[Ca^{2+}]_i$ in suspensions of SH-SY5Y cells. (**A**) Emission at 340 and 380 nm excitation. Note the antiparallel movement of both traces. (**B**) Derived 340/380 ratio and (**C**) $[Ca^{2+}]_i$ after calibration. In these studies $R_{max}$, $R_{min}$, and Sfb were 4.61, 0.64, and 2.39, respectively. Autofluorescence at 340 and 380 were 1.67 and 3.18 arbitrary units ≲2% of cell signal.

### *3.3.2. $K^+$ Stimulation in NG108-15 Cells*

The authors have previously reported a nifedipine sensitive increase in $[Ca^{2+}]_i$ in NG108-15 cells in response to depolarization with high $K^+$ ***(6)***. A typical experiment is described next:

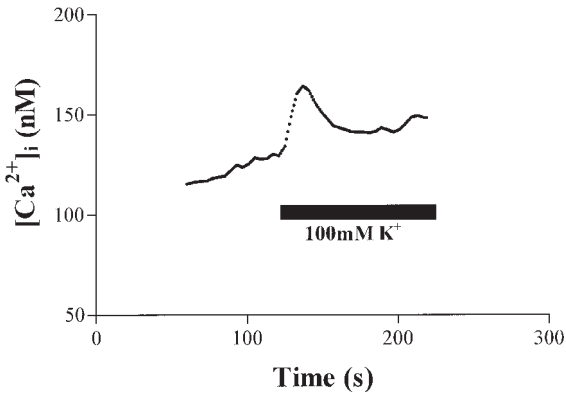


Fig. 2. $K^+$ depolarization (100 m*M*, bar) of NG108-15 cells results in a monophasic increase in $[Ca^{2+}]_i$. Representative trace modified from **ref. *6***.

1. Cells are harvested (*see* **Subheading 3.1., steps 4–10**).
2. Suspensions are loaded with fura-2 as described in **Subheading 3.2.**
3. Following de-esterification and washing in low $Na^+$ buffer (**Subheading 2.2., item 3**), cells are placed into a cuvet and 340/380 nm fluorescence monitored.
4. Cells are challenged with 100 m*M* $K^+$.
5. Stocks of loaded cells are kept on ice
6. As can be seen in **Fig. 2**, depolarization with $K^+$ produces a monophasic increase in $[Ca^{2+}]_i$. This response is mediated by L-type, voltage-sensitive $Ca^{2+}$ channels ***(6)***.

### *3.3.3. D-[Pen$^{2,5}$]enkephalin and Adenosine Triphosphate Stimulation in CHO Cells*

CHO cells have been shown to express low levels of the multidrug-resistance efflux pump, P-glycoprotein ***(7)***. It is possible that this pump is responsible for extrusion of fura-2 from the cell and, hence, increasing baseline measurements. Probenecid is an organic anion transport inhibitor, originally developed to prevent excretion of penicillin from the kidney, that has been shown to block efflux of fura-2 ***(7,8)***. The authors have noted that with the use of CHO cells expressing recombinant opioid receptors (and endogenous purinergic receptors ***[9]***), high rates of fura-2 leakage that can be reduced by inclusion of probenecid (**Fig. 3A**). A typical experiment is described below.

1. Cells are harvested (*see* **Subheading 3.1., steps 4–10**).
2. CHO cell suspensions are loaded, washed, and then de-esterified in the presence of 2.5 m*M* probenecid as noted in **Subheading 3.2.**
3. Cells are challenged with either 1 μ*M* DPDPE or 100 μ*M* adenosine triphosphate (ATP).
4. Between determinations, the stock of loaded cells is kept on ice.

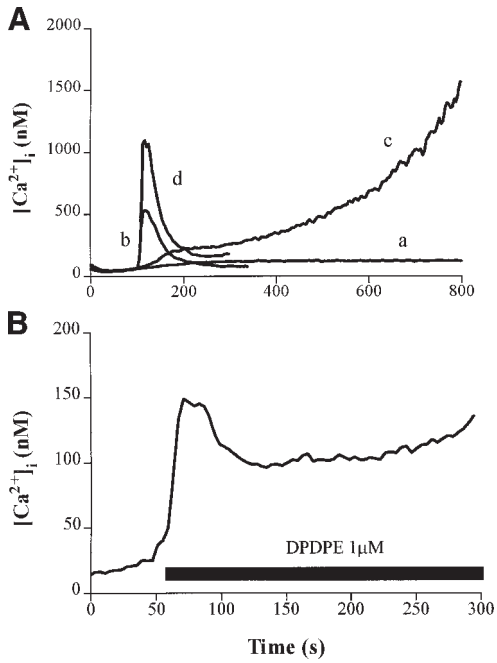


Fig. 3. **(A)** Representative time course showing effects of 2.5 m*M* probenecid in CHO cells expressing the recombinant δ opioid receptor. Probenecid reduced fura-2 leakage in unstimulated cells (A) when compared to unstimulated control (C) and reduced the peak and plateau phases of 100 μ*M* ATP-stimulated (B) when compared to stimulated control (D). **(B)** 1 μ*M* DPDPE increased $[Ca^{2+}]_i$ in CHO cells expressing the recombinant δ opioid receptor. Probenecid was not included in this experiment.

5. As can be clearly seen in **Fig. 3A**, fura-2 leakage was significantly reduced in the presence of probenecid. However, the peak phase response to ATP was also reduced. Careful characterization of the effects of probenecid on the signaling process under study should always be made (*see* **Note 5**).

## 4. Notes

1. All tissue culture media and reagents are supplied by Life Technologies, Paisley, Scotland.
2. From European Collection of Animal Cell Cultures (web site http://www.biotech.ist.unige.it/cldb/cname-dh.html).
3. Where geneticin (G418) or similar is included in cells expressing recombinant receptors and so on as a selection agent, only the stock cultures should be treated. Experimental cultures should be free of selection medium as G418 may inhibit phospholipase C-mediated responses.

4. For varying levels of $K^+$, adjust $Na^+$ accordingly.
5. Probenecid is insoluble at millimolar concentrations in Krebs HEPES buffer. Therefore, a stock solution was made at 50 mg/mL (175 m*M*) in 1 *M* NaOH. This was then diluted in Krebs HEPES buffer prior to addition of $CaCl_2$ (2.5 m*M*). The Krebs HEPES buffer containing probenecid (NaOH) was set at pH 7.4 by the addition of HCl (10 *M*, ~100 µL). Caution should be used when using probenecid to reduce fura-2 leakage as the authors have shown that agonist-induced increases in $[Ca^{2+}]_i$ could be inhibited by this agent (*see* **Fig. 2**).
6. One confluent 75-$cm^2$ flask of SH-SY5Y cells is sufficient to give five determinations (i.e., resuspend in 10 mL of buffer). For larger numbers of determinations, load more flasks. However, remember that as the loaded cells stand they leak fura-2, leading to a time-dependent increase in basal. This can be overcome to some extent by sedimenting and resuspending aliquots of the loaded suspension periodically. Some cells leak fura-2 more than others, notably CHO cells (*see* below).
7. The authors routinely use a Perkin-Elmer LS50B fluorimeter (Beaconsfield, UK) equipped with the software FLDM. Files are saved to disk and 340/380 ratios can be converted to $[Ca^{2+}]_i$ following calibration. It is always advisable to be familiar with the software that controls the configuration and experimental settings of the fluorimeter. Different software packages are available, and for information and troubleshooting the reader is advised to consult the software supplier.
8. For drugs make up 100 times more concentrated so that when 20 µL is added to 2 mL of buffer + cells, the desired concentration is achieved. Additions are made as swiftly as possible to avoid light entering the fluorimeter. All agents used should be tested for fluorescence properties. This can be accomplished by adding to a cuvet containing nominally $Ca^{2+}$-free buffer (containing several micromolar $Ca^{2+}$) and fura-2-free acid (0.5 µ*M*).
9. The authors have noted that de-esterified cells that extrude fura-2 should be maintained on ice between experiments as this reduces the loss of fura-2. In addition, care should be taken to ensure that fura-2-loaded cells are used for experiments immediately after de-esterification.
10. For cells loaded from a single batch of cells, the authors make a single calibration (i.e., they do not calibrate each cuvet of cells), normally the last cuvet used. This needs to be checked for all cell lines and they recommend a comparison of individually calibrated data with all data calibrated from the first and last run of the batch.
11. Addition of Triton X-100 causes complete cell lysis and an increase in 340 and a decrease in 380 nm fluorescence. A globular residue remains in the cuvet, and, therefore, the reusable quartz cuvet should be thoroughly rinsed between experiments using deionized water.
12. Autofluorescence is an important issue for many cell types. This is the fluorescence produced from unloaded cells and can be determined in two ways. First, place an aliquot of unloaded cells into the fluorimeter and measure the fluorescence at 340 and 380 nm (FLDM software has this capability). The main drawback with this method is that the density of unloaded cells should be identical to

the density of cells used for $Ca^{2+}$ measurements. The second method is to add 0.1 m*M* $Mn^{2+}$ to the lysed cell suspension after determination of $R_{min}$. In this protocol, the quenching properties of $Mn^{2+}$ are utilized. In the authors' studies using SH-SY5Y, NG108-15, and CHO cells, they have found the autofluorescence to be negligible when compared to the signal from loaded cells and, therefore, do not routinely subtract autofluorescence (e.g., *see* **Fig. 1**). However, they recommend that whenever using a new cell line, autofluorescence should be assessed.

## References

1. Clapham, D. (1995) Calcium signalling. *Cell* **80,** 259–268.
2. Berridge, M. J. (1993) Inositol trisphosphate and $Ca^{2+}$ signalling. *Nature* **361,** 315–325.
3. Grynkiewicz, G., Poenie, M., and Tsien, R. Y. (1985) A new generation of $Ca^{2+}$ indicators with greatly improved fluorescence properties. *J. Biol. Chem.* **260,** 3440–3449.
4. Lambert, D. G., Wojcikiewicz, R. J. H., Safrany, S. T., Whitham, E. M., and Nahorski, S. R. (1992) Muscarinic receptors, phosphoinositide metabolism and intracellular calcium in neuronal cells. *Prog. Neuro-Psychopharmacol. Biol. Psychiat.* **16,** 253–270.
5. Cobbold, P. H. and Rink, R. J. (1987) Fluorescence and bioluminescence measurement of cytoplasmic free calcium. *Biochem. J.* **248,** 313–328.
6. Hirota, K. and Lambert, D. G. (1997) A comparative study of L-type voltage sensitive $Ca^{2+}$ channels in rat brain regions and cultured neuronal cells. *Neurosci. Lett.* **223,** 169–172.
7. Brezden, C. B., Hedley, D. W., and Rauth, A. M. (1994) Constitutive expression of P-glycoprotein as a determinant of loading with fluorescent calcium probes. *Cytometry* **17,** 343–348.
8. Edelman, J. L., Kajimura, M., Woldemussie, E., and Sachs, G. (1994) Differential effects of carbachol on calcium entry and release in CHO cells expressing the m3 muscarinic receptor. *Cell Calcium* **16,** 181–193.
9. Iredale, P. A. and Hill, S. J. (1993) Increases in intracellular calcium via activation of an endogenous P(2)-purinoceptor in cultured CHO-k1 cells. *Brit. J. Pharmacol.* **110,** 1305–1310.

# 3

# Measurement of $[Ca^{2+}]_i$ in Cell Suspensions Using Indo-1

**Adriaan Nelemans**

## 1. Introduction

Intracellular calcium, in particular the cytosolic free ionized calcium concentration $[Ca^{2+}]_i$, is tightly regulated under physiological conditions. Stimulation of receptors, belonging to almost all the classes so far described, will result in changes in $[Ca^{2+}]_i$. These changes might be directly induced by either $Ca^{2+}$-influx or $Ca^{2+}$-mobilization from intracellular stores, or indirectly by a number of other mechanisms ***(1–4)***. The development of fluorescent indicators of free $[Ca^{2+}]$ that could be loaded into intact cells has contributed enormously to the understanding of cellular $Ca^{2+}$ homeostasis, especially dyes that respond to $Ca^{2+}$ with shifts of excitation or emission spectra ***(5–7)***. By measuring at two selected wavelengths (either dual emission or dual excitation), it is possible to calculate the proportion of dye in the $Ca^{2+}$-bound and $Ca^{2+}$-free forms.

This ion-dependent spectral shift of $Ca^{2+}$ indicators allows them to be used ratiometrically, making $Ca^{2+}$ measurement essentially independent of dye loading, cellular distribution, and photobleaching. Indo-1 shows a shift in its emission maximum on $Ca^{2+}$ binding. It is less suitable for imaging $[Ca^{2+}]_i$ by fluorescence microscopy, and is more often used for single-cell photometer measurements, flow cytometry, and studies in a fluorometer using cells in monolayer or in suspension ***(7,8)***. Further information on the technical and practical aspects of ion measurements using fluorescent indicators can be obtained in Chapter 1 and in **refs. *7–11***.

The method described in this chapter is generally applicable to measurements of intracellular $[Ca^{2+}]$ in cell suspensions, e.g., for a variety of blood cells, but it is based on the author's experience with the smooth muscle cell line $DDT_1$ MF-2. A number of cellular mechanisms have been investigated

From: *Methods in Molecular Biology, vol. 312: Calcium Signaling Protocols: Second Edition*
Edited by: D. G. Lambert © Humana Press Inc., Totowa, NJ

using fluorometric indo-1 detection with this method at various levels in the signal transduction cascade. These include (1) induction of intracellular [$Ca^{2+}$] changes after stimulation of different types of receptors such as α-adrenergic, purinergic, and histaminergic ***(12–15)***; and (2) the effects of arachidonic acid and inhibition of protein kinase C on $Ca^{2+}$ influx ***(16,17)***. The relative contributions of $Ca^{2+}$ influx and $Ca^{2+}$ mobilization to the intracellular changes are determined using $La^{3+}$- or $Ca^{2+}$-free extracellular solution ***(16–19)***. $H_1$ histaminergic and $P_2$ purinergic receptors mobilize $Ca^{2+}$ from separate specific intracellular stores ***(19)*** and use this $Ca^{2+}$ together with inositol tetrakisphosphate to initiate $K^+$ efflux ***(18)***. The alterations in receptor-induced changes in $[Ca^{2+}]_i$ were established on the production of other second messengers ***(14,17,20)***.

## 2. Materials

1. The acetoxymethyl (AM) ester of the fluorescent indicator indo-1 can be obtained from a number of suppliers in varying packaging sizes. In the author's studies on $DDT_1$ MF-2 cells, indo-1/AM from Molecular Probes (Eugene, OR) was used (*see* **Notes 1** and **2**).
2. Cell incubation medium DMEM/FCS: Dulbecco's modified essential medium (DMEM) supplemented with 7 m*M* $NaHCO_3$, 10 m*M* HEPES, pH 7.2, 10% fetal calf serum.
3. Buffered salt solution (BSS): 145 m*M* NaCl, 5 m*M* KCl, 0.5 m*M* $MgSO_4$, 1 m*M* $CaCl_2$, 10 m*M* glucose, 10 m*M* HEPES, pH 7.4.
4. Solutions used for calibration: Triton® X-100 1% aqueous solution (vol/vol); 500 m*M* EGTA, pH 8.0; 1*M* $MnCl_2$.

## 3. Methods

1. Prepare stock solution of 1 m*M* indo-1/AM in dry dimethylsulfoxide (DMSO), mix well to dissolve, distribute into tubes in aliquots sufficient for a single experiment, and freeze at –20°C (*see* **Notes 3–7**).
2. Prepare a stock cell suspension of $2 \times 10^5$ cells/mL in DMEM containing 10% FCS (*see* **Notes 8** and **9**).
3. Prepare fresh indicator solution in DMEM/FCS at a final concentration of 2 μ*M* indo-1/AM just before addition and mix well. Avoid exposure to light as much as possible by wrapping the tube or flask with aluminium foil (*see* **Notes 10** and **11**).
4. Preincubate the cells in DMEM/FCS for 15 min at 37°C (*see* **Note 12**).
5. Take 10 mL of this solution and centrifuge for 5–10 min at 1000*g* (*see* **Note 13**).
6. Resuspend the cell pellet in 2 mL of DMEM/FCS, containing 2 μ*M* indo-1/AM (*see* **Note 14**).
7. Incubate the cells for 45 min at 37°C, preferably in an orbital shaker (100 rpm) (*see* **Notes 15–17**).
8. Wash the cells twice, by centrifugation and resuspension in 2 mL of BSS (*see* **Notes 18–21**).
9. Check for homogeneous cytosolic indo-1 labeling (*see* **Notes 22** and **23**).

10. The cell suspension can now be transferred to a cuvet for fluorometric measurements (*see* **Note 24**).
11. The cell suspension in the cuvet should be continuously stirred, and if applicable the temperature of the solution in the cuvet should be controlled (*see* **Notes 25** and **26**).
12. Most of the commercially available spectrofluorometers have preset parameters for $Ca^{2+}$ measurements with indo-1. However, the following standard settings can be used: excitation wavelength, 325; emission wavelength 1, 405 ($Ca^{2+}$-bound dye); emission wavelength 2, 485 ($Ca^{2+}$-free dye); bandwidth filters 2–10 nm (*see* **Note 27**).
13. The appropriate experiments can now be performed. The fluorescence ratio $R$ = $Ca^{2+}$-bound/$Ca^{2+}$-free should be measured (*see* **Note 28**).
14. Calibrate the fluorescence signal at the end of the experiment as follows. Permeabilize the cells by addition of 30 µL of a 1% Triton X-100 aqueous solution (vol/vol) to cell suspension in the cuvet. Cell lysis may take several minutes. When a stable maximal fluorescence level is obtained, the ratio value under saturating conditions $R_{max}$ is determined. The value under $Ca^{2+}$-free conditions $R_{min}$ is obtained after addition of 200 µL of EGTA solution (500 m*M*, pH 8). After a stable minimal response (within 1 min), background levels are obtained by addition of 30 µL of $MnCl_2$ (1*M*) (*see* **Notes 29–31**).
15. Calculate the intracellular $[Ca^{2+}]$ according to the following equation:

$$[Ca^{2+}] = K_d \times [(R - R_{min})/(R_{max} - R)] \times (S_{f2}/S_{b2})$$

The term $(S_{f2}/S_{b2})$ is the signal ratio of fluorescence measured at emission wavelength 2 in the absence of $Ca^{2+}$ and at $Ca^{2+}$ saturation. The dissociation constant of indo-1 is $K_d$ = 250 n*M* as determined in vitro at 37°C ***(5)*** (*see* **Notes 32** and **33**).

## 4. Notes

1. The use of small pack sizes is recommended to minimize the chance of decomposition.
2. Some companies offer stock solutions of fluorescent dyes in aqueous-free DMSO.
3. AM ester derivatives of $Ca^{2+}$ indicators are not soluble in aqueous solutions.
4. It is advisable to prepare concentrated stock solutions so that minimal amounts of DMSO are present in the loading solution.
5. Stock solutions should be extensively mixed, because remaining undissolved particles will facilitate intracellular compartmentalization of the dye.
6. To avoid indo-1/AM hydrolysis, the stock solution must be kept anhydrous, and aliquots sufficient for a single experiment should be stored desiccated at –20°C.
7. Exposure of indicator containing solutions to light should be avoided.
8. If cells are not grown in suspension, a cell suspension can be obtained by either scraping off the cells from cell monolayers with a rubber policeman (as is the case for $DDT_1$ MF-2 cells), or by detachment from the monolayer using Trypsin/EDTA treatment. Cells growing in monolayer are washed with a $Ca^{2+}$-free physiological salt solution and subsequently treated with a solution of Trypsin 1:250,

0.05% (w/v) and EDTA, 0.02% (w/v) in physiological salt solution. Immediately aspirate this mixture and incubate the cells in monolayer at 37°C for 1–5 min depending on the cell type. Cells are resuspended with at least 5 mL of DMEM containing 10% FCS.

9. The number of cells/mL can vary depending on the type of cells used. For lymphocytes and blood platelets, most often minimal concentrations of $10^7$ cells/mL are used.
10. As an alternative to DMEM/FCS as a loading solution, most other appropriate physiological buffer solutions can be used, although the presence of 2% bovine serum albumin (w/w) is mandatory.
11. For each cell type, optimal parameters should be assessed for $Ca^{2+}$ indicator dye loading, regarding dye concentration, incubation temperature, and time of incubation (*see* **Notes 14–17**).
12. This pre-incubation allows the cells to stabilize and to equilibrate their ion gradients.
13. This is the correct centrifugation procedure for $DDT_1$ MF-2 cells. It can also probably be used for other types of cells. Integrity of the cells should be tested after centrifugation, e.g., by trypan blue dye exclusion assay.
14. Usually loading solutions are used with dye concentrations in the range from 1 to 10 μ*M* indo-1/AM. This concentration should be kept as low as possible to avoid artifacts from overloading, such as incomplete hydrolysis, fluorophore quenching, extreme intracellular $Ca^{2+}$ buffering capacity, or toxicity of formaldehyde produced on AM ester hydrolysis.
15. The time of loading must be kept as short as possible. Optimal incubation time is variable between 15 and 120 min for different cell types and incubation conditions. For experiments with $DDT_1$ MF-2 cells, 45 min is convenient.
16. Accumulation of the dye proceeds rapidly at 37°C, but longer incubation at lower temperature (20–30°C) can reduce redistribution of the dye from the cytosol to various intracellular organelles.
17. Loading is often facilitated by dissolving the AM ester in a solution of the nonionic detergent Pluronic® F-127 in DMSO (20% [w/v]) (*see* **ref. *7***).
18. The procedure to wash away remaining extracellular indo-1/AM after the incubation period will take 20–30 min, which is also necessary to obtain complete hydrolysis of the intracellular esterified dye.
19. Fluorescence spectra before and after esterification are informative not only to follow the process of ester hydrolysis, but also regarding the purity of the dye preparation. The unesterified indo-1/AM has maxima for excitation and emission at 361 and 479 nm, respectively ***(7,8)***.
20. Emission spectra (350–650 nm) can be obtained (at a fixed excitation wavelength, e.g., 325 or 355 nm) with increasing levels of $Ca^{2+}$ or with a saturating concentration of $Ca^{2+}$ obtainable with 1 m*M* excess $CaCl_2$.
21. Assessment of the completeness of AM ester hydrolysis can be achieved by release of indo-1 from the cell by digitonin in $Mn^{2+}$-containing buffer, which will quench almost all the fluorescence of the indicator. Although any BSS can be used, BSS containing 145 m*M* NaCl, 5 m*M* KCl, 0.5 m*M* $MgSO_4$, 1 m*M* $CaCl_2$,

10 m*M* glucose, 10 m*M* HEPES, pH 7.0, is preferred ***(21)***. Autofluorescence is reduced under these conditions in $DDT_1$ MF-2 cells.

22. After establishment of the optimal parameters, a uniformly labeled cytosol should be observed by fluorescence microscopy. Compartmentalization of indo-1 is less likely to occur than for other fluorescent $Ca^{2+}$ indicators ***(8)***.
23. Where compartmentalized dye remains, the experimental data can still be used, by choosing the appropriate calibration procedures. Interaction of digitonin with cholesterol releases only cytosolic $Ca^{2+}$, since most of the cellular cholesterol is present in the plasma membrane (*see* **Note 30**).
24. A cell suspension of 2 mL is sufficient to obtain an undisturbed errorless signal in a standard fluorometric quartz cuvet.
25. Thermostatic control of the cuvet holder enables control of temperatures at which intracellular responses occur. Depending on the study, working at 37°C as the physiological temperature is not always ideal (compared with, e.g., 22°C). Lower temperatures will minimize indo-1 leakage from the cells. With respect to the physiological increases in internal $Ca^{2+}$ concentration induced by receptor stimulation, these develop slower at 22°C in $DDT_1$ MF-2 cells, but responses are of similar magnitude at both temperatures ***(15)***.
26. If despite a uniformly indo-1–labeled cytosol the cells consistently respond to external stimuli with a small increases in internal $Ca^{2+}$ concentration or do not respond at all, it is likely that too much indicator has accumulated in the cell. This will result in a lower signal owing to quenching of the fluorescence signal and/or buffering inappropriate amounts of intracellular $Ca^{2+}$. Re-establish the optimal indo-1/AM loading procedure.
27. Optimal parameters vary slightly between different setups and experimental conditions. Optimal parameters can be obtained from excitation and emission spectra. For measuring intracellular $Ca^{2+}$ changes in $DDT_1$ MF-2 cells with the equipment as described ***(18)***, these parameters were, e.g., 325 nm for excitation and 400 and 480 nm for emission wavelengths, with a bandwidth filter of 10 nm.
28. Many receptor ligands or other drugs have fluorescent properties, and can therefore interfere with fluorimetric measurements. Fluorescence spectra should be determined.
29. A final concentration of 0.015% Triton X-100 is sufficient to lyse $DDT_1$ MF-2 cell suspensions. For other cell types, other optimum concentrations may be necessary. The optimum concentrations should be determined e.g., by Trypan blue exclusion.
30. Alternatively, detergents other than Triton X-100 with minimum light scattering properties can be used. Digitonin (10–100 µg/mL), which primarily affects the plasma membrane, is often used to exclude compartmentalization errors (*see* **Note 23**).
31. $R_{max}$ must be determined when the dye is saturated with calcium ($[Ca^{2+}] > 1$ m*M*). If the experiment is performed in a buffered solution with less $Ca^{2+}$, $CaCl_2$ must be added at this stage.
32. The background or autofluorescence values obtained after addition of $Mn^{2+}$ must be subtracted from the fluorescence intensities before calculation of the ratio.
33. The $K_d$ value at 22°C for indo-1 is 230 n*M* ***(7)***.

## References


1. Himpens, B., Missiaen, L., and Casteels, R. (1995) $Ca^{2+}$ homeostasis in vascular smooth muscle. *J. Vascular Res.* **32,** 207–219.
2. Thomas, A. P., Bird, G. S., Hajnoczky, G., Robb-Gaspers, L. D., and Putney, J. W., Jr. (1996) Spatial and temporal aspects of cellular calcium signalling. *FASEB J.* **10,** 1505–1517.
3. Carl, A., Lee, H. K., and Sanders, K. M. (1996) Regulation of ion channels in smooth muscles by calcium. *Am. J. Physiol.* **271,** C9–34.
4. Cheng, H., Lederer, M. R., Xiao, R. P., Gomez, A. M., Zhou, Y. Y., Ziman, B., Spurgeon, H., Lakatta, E. G., and Lederer, W. J. (1996) Excitation-contraction coupling in heart: New insights from $Ca^{2+}$ sparks. *Cell Calcium* **20,** 129–140.
5. Grynkiewicz, G., Poenie, M., and Tsien R. W. (1985) A new generation of $Ca^{2+}$ indicators with greatly improved fluorescence properties. *J. Biol. Chem.* **260,** 3440–3450.
6. Lipscombe, D., Madison, D. V., Poenie, M., Reuter, H., Tsien, R. W., and Tsien, R. Y. (1988) Imaging of cytosolic $Ca^{2+}$ transients arising from $Ca^{2+}$ stores and $Ca^{2+}$ channels in sympathetic neurons. *Neuron* **1,** 355–365.
7. Haugland, R. P. (2002) *Handbook of Fluorescent Probes and Research Chemicals.* 9th Ed. Molecular Probes Inc., Eugene, OR. Website: www.probes.com
8. Thomas, A. P. and Delaville, F. (1991) The use of fluorescent indicators for measurements of cytosolic-free calcium concentration in cell populations and single cells, in *Cellular Calcium: A Practical Approach* (McCormack, J. G. and Cobbold, P. H., eds.), IRL, Oxford, UK, pp. 1–54.
9. Rawlings, S. R., Theler, J. M., and Schlegel, W. (1994) Monitoring of receptor-mediated changes in intracellular calcium at the cellular and subcellular level by microfluorimetry and imaging, in *Methods in Enzymology*, vol. 238 (Iyengar, R., ed.), Academic, San Diego, pp. 295–308.
10. Demaurex, N., Rawlings, S. R., Krause, K. H., Jaconi, M. E. E., Lew, P. D., and Schlegel, W. (1994) Combination of microfluorimetric monitoring of cytosolic calcium and pH with patch clamp electrophysiological recordings in neutrophil granulocytes, in *Methods in Enzymology*, vol. 238 (Iyengar, R., ed.), Academic, San Diego, pp. 308–320.
11. Silver, R. A., Whitaker, M., and Bolsover, S. R. (1992) Intracellular ion imaging using fluorescent dyes: Artefacts and limits to resolution. *Pflugers Arch. Eur. J. Physiol.* **420,** 595–602.
12. Nelemans, A., Hoiting, B., Molleman, A., Duin, M., and den Hertog, A. (1990) alpha-Adrenoceptor regulation of inositol phosphates, internal calcium and membrane current in $DDT_1$ MF-2 smooth muscle cells. *Eur. J. Pharmacol.* **189,** 41–49.
13. Hoiting, B., Molleman, A., Duin, M., den Hertog, A., and Nelemans, A. (1990) $P_2$ purinoceptor-mediated inositol phosphate formation in relation to cytoplasmic calcium in $DDT_1$ MF-2 smooth muscle cells. *Eur. J. Pharmacol.* **189,** 31–39.
14. Sipma, H., Duin, M., Hoiting, B., den Hertog, A., and Nelemans, A. (1995) Regulation of histamine- and UTP-induced increases in $Ins(1,4,5)P_3$, $Ins(1,3,4,5)P_4$ and $Ca^{2+}$ by cyclic AMP in $DDT_1$ MF-2 cells. *Br. J. Pharmacol.* **114,** 383–390.

15. Sipma, H., Fredholm, B. B., den Hertog, A., and Nelemans, A. (1996) Plasma membrane $Ca^{2+}$ pumping plays a prominent role in adenosine $A_1$ receptor mediated changes in $[Ca^{2+}]_i$ in $DDT_1$ MF-2 cells. *Eur. J. Pharmacol.* **306,** 187–194.
16. van der Zee, L., Nelemans, A., and den Hertog, A. (1995) Arachidonic acid is functioning as second messenger in activating the $Ca^{2+}$ entry process on $H_1$-histaminoceptor stimulation in $DDT_1$ MF-2 cells. *Biochem. J.* **305,** 859–864.
17. Sipma, H., van der Zee, L., van den Akker, J., den Hertog, A., and Nelemans, A. (1996) The PKC inhibitor GF109203X releases $Ca^{2+}$ from internal stores and provokes $Ca^{2+}$ entry in $DDT_1$ MF-2 cells. *Br. J. Pharmacol.* **119,** 730–736.
18. Molleman, A., Hoiting, B., Duin, M., van den Akker, J., Nelemans, A., and den Hertog, A. (1991) Potassium channels regulated by Ins(1,3,4,5)-tetrakisphosphate and internal calcium in $DDT_1$ MF-2 smooth muscle cells. *J. Biol. Chem.* **266,** 5658–5663.
19. den Hertog, A., Hoiting, B., Molleman, A., van den Akker, J., Duin, M., and Nelemans, A. (1992) Calcium release from separate receptor-specific intracellular stores induced by histamine and ATP in a hamster cell line. *J. Physiol. (Lond.)* **454,** 591–607.
20. Sipma, H., den Hertog, A., and Nelemans, A. (1995) $Ca^{2+}$ Dependent and independent mechanisms of cyclic-AMP reduction mediated by bradykinin $B_2$ receptors. *Br. J. Pharmacol.* **115,** 937–944.
21. Hesketh, T. R., Smith, G. A., Moore, J. P., Taylor, M. V., and Metcalfe, J. C. (1983) Free cytoplasmic calcium concentration and mitogenic stimulation of lymphocytes. *J. Biol. Chem.* **258,** 4876–4882.

# II

## Specialist Measurement Systems

# 4

# Confocal Microscopy

*Theory and Applications for Cellular Signaling*

**Stephen C. Tovey, Paul J. Brighton, and Gary B. Willars**

## 1. Introduction

The main aim of this chapter is to introduce some of the basic principles behind the technique of confocal microscopy. Subsequently, we will describe how recent advances in this technology, allied with the continued development of $Ca^{2+}$-sensitive fluorescent probes, have provided us with methodologies for unravelling the complexities of $Ca^{2+}$ signaling at the cellular and subcellular level. Specifically, we will provide a detailed methodology for the study of $Ca^{2+}$ signaling at the single-cell level using a $Ca^{2+}$-sensitive fluorescent indicator in conjunction with confocal microscopy. This chapter also describes a number of confocal-based methodologies that can be used to study other aspects of intracellular signaling, such as immunofluorescent labeling, the use of fluorescently-tagged biosensors for measuring phospholipase C (PLC) activity, and the use of fluorescently-labeled ligands for measuring receptor or ligand internalization. It should be noted that several excellent texts are available that cover the principle and practice of confocal microscopy in relation to biological systems in far greater depth than is possible here ***(1–3)***.

### *1.1. History of Confocal Microscopy*

Marvin Minsky, a postdoctoral fellow at Harvard University, originally developed the concept of the confocal microscope in the early 1950s. In 1957, Minsky filed a patent for his invention. Strangely, it was not until the late 1970s and early 1980s that other scientists took advantage of his invention and developed the first single-beam laser scanning confocal microscope (LSCM) for use in biological research ***(1)***. Over the past decade, the increase in commercially available

From: *Methods in Molecular Biology, vol. 312: Calcium Signaling Protocols: Second Edition*
Edited by: D. G. Lambert © Humana Press Inc., Totowa, NJ

confocal microscopes has led to them becoming commonplace in many life science departments throughout the world. The definition of *confocal imaging* (and hence confocality) is the illumination and detection of a single point within a specimen at a resolution close to the theoretical diffraction-limited maximum ***(1)***. Thus, a confocal microscope allows the nonintrusive optical sectioning of biological specimens in a technique known as "optical slicing." This is achieved by the positioning of two pinholes at appropriate points in the light path. The first is required to produce a sharp intense point of illuminating light (minimizing scatter from excitation light), whereas the second acts to process transmitted light from the specimen. Confocal microscopes are routinely used in the fields of biological research, chemical analysis, and materials testing. In biological research, the confocal microscope has been used extensively to study three dimensional structures in both fixed and live material.

The advent of confocal imaging technology has proven particularly useful in the field of fluorescence, where a wide variety of fluorescent tags and fluorescent indicators are available for the study of biological systems. The main advantage of a confocal microscope over a conventional fluorescence microscope is the ability to visualize a thin optical section within a cell or tissue by virtue of rejecting the out-of-focus light originating from excited fluorophores throughout the rest of the sample. This is obviously of great utility for the study of intracellular $Ca^{2+}$ signals, and the parallel development of both fluorescent $Ca^{2+}$ indicators and confocal techniques has enabled the detection of $Ca^{2+}$ release in defined regions of the cell at spatial and temporal resolutions that were previously unimaginable.

### *1.2. Principles of Confocal Microscopy*

The main benefit of a confocal microscope is the improvement it gives in both horizontal and vertical resolution over conventional fluorescence microscopes. The way in which a confocal microscope achieves this increased resolution (by rejecting out of focus light) inevitably means that a powerful source of illumination is required. Typically, the source of illumination is a continuous-wave gas laser, hence the term LSCM, as lasers represent a bright, stable, and easy-to-focus source of light with minimal divergence. The requirement for a high intensity light source is also one of the main drawbacks of confocal microscopy, as it exacerbates problems such as cytotoxicity of live material and photobleaching of fluorophores. Added to this, conventional lasers (such as Ar, Kr/Ar, or He/Ne) only produce excitation light within a restricted range of the visible spectrum, thereby reducing the fluorescent indicators available for use compared with conventional fluorescence microscopy. However, it should be pointed out that most lasers have more than one excitation line. For example, a Kr/Ar laser can have several lines, including 458, 488, 568, and 647

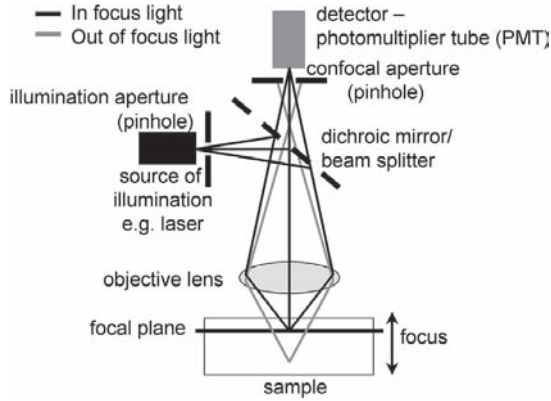


Fig. 1. Simplified light path of a standard laser scanning confocal microscope. Illuminating laser light is reflected onto the objective lens by a dichroic mirror. The objective lens focuses the excitation light onto the sample. In-focus fluorescence that is emitted by the sample passes through the dichroic mirror and is detected by a photomultiplier tube. Out-of-focus fluorescence light is rejected by the confocal aperture. Any illuminating light reflecting back from the sample is reflected away from the detector by the dichroic mirror.

nm. It should also be noted that ultraviolet (UV) lasers are available for confocal microscopes, but they remain expensive and require expensive optics (e.g., UV corrected objectives).

The LSCM works by repeatedly scanning a laser beam across the sample and collecting light emitted from the sample through a pinhole aperture. As described in **Subheading 1.1.**, it is this pinhole aperture that is responsible for giving confocality, in that it is responsible for rejecting the out-of-focus light arising from the rest of the sample (**Fig. 1**). The narrower the pinhole, the thinner the section and the more confocal the image; conversely, if the pinhole is fully open, then confocality is lost. The pinhole also dictates that light can only be collected from a single point within a sample at any given time, so in order to achieve a reconstructed two-dimensional (2D) image of the sample, the laser beam must be scanned across the specimen (so-called "point scanning") with a detector recording the single point outputs as a 2D array. The transmitted light (photons) collected through the pinhole aperture are normally detected by a photomultiplier tube (PMT) and converted into a flow of electrical signals. Images can then be recreated on a computer screen or cathode ray tube and subsequently collated and stored as a digital image or a series of digital images. At present there are three main types of commercially available confocal microscopes that can be categorized by the way in which the excitation light is scanned onto the sample.

### 1.2.1. Standard Scanning

This group of confocal microscopes are the most common and are generally considered to have the best spatial resolution, but they are only capable of relatively modest scan rates (i.e., they have limited temporal resolution). This group includes LSCMs such as the Zeiss LSM 510, Leica TCS, Biorad Radiance 2100, and the Olympus Fluoview FV500. In this case, scanning is usually achieved by the use of two vibrating, mechanically driven mirrors to guide the laser beam across the sample both vertically and horizontally. With these confocal microscopes, the speed of scanning is governed entirely by the mechanical movement of the galvanometric mirrors, leading to a limitation in the time resolution that can be achieved. For most applications this is not a problem, but when studying small but fast subcellular $Ca^{2+}$ release events or even the rapid onset of a whole-cell $Ca^{2+}$ wave, then it is often desirable to achieve a greater temporal resolution. This can be achieved using a line scan, in which a particular region of the sample is repeatedly and rapidly scanned in one dimension (1D) only, meaning the movement of only one mirror is required. Although this method provides high temporal resolution, information may be lost as the image is spatially restricted.

### 1.2.2. Acousto-Optical Deflectors

Increases in temporal resolution can be gained by combining LSCM technology with acousto-optical deflectors (AODs). As described in **Subheading 1.2.1.**, with the standard LSCM, the rate-limiting step is the movement of the galvanometric mirrors. When using confocal microscopes based on AOD technology, such as the Noran *Odyssey* and Noran *Oz*, an AOD device replaces the mirror responsible for horizontal scanning. Thus, the laser beam is rapidly scanned across the sample by nonmechanical deflection through an arrangement of static prisms and AOD devices laid out in 2D. This allows these machines to achieve scanning speeds that approach those achieved with standard video rate fluorescence microscopy. The Noran *Oz* has previously been used to visualize elementary $Ca^{2+}$ release events in a variety of cell types with a temporal resolution of 7.5 Hz (one frame approximately every 133 ms ***[4–6]***), although in 1D line-scanning mode, rates of 60 Hz and greater are theoretically achievable. A disadvantage of this system is that the increase in temporal resolution tends to result in a decrease in the signal-to-noise ratio and consequently a loss of spatial resolution. Although Noran confocal systems are still in use, they are no longer manufactured.

### 1.2.3. Spinning Disk

Confocal microscopes that use multiple pinholes to construct the confocal image (such as the PerkinElmer Ultra*VIEW*) are an alternative to the standard LSCM. In these machines, the light beam is scanned across the specimen using

a rapidly rotating disk containing thousands of pinholes arranged in a spiral pattern (Nipkow disk). In this manner, all parts of the sample are illuminated "quasi-simultaneously" and emitted light returns through the pinholes, thereby rejecting the out-of-focus blur from the rest of the sample. This type of system has the advantage of working with both lasers and other light sources, such as mercury arc lamps, potentially reducing the cost of the light source and removing some of the problems commonly associated with the use of lasers. It also allows the use of real-time color imaging with direct viewing (through an eyepiece, or ocular) as the emitted light does not need to be descanned as with other confocal microscopes. This is because the "quasi-simultaneous" illumination effectively produces a multipoint scanning pattern that allows the image to be formed in real-time and focused onto a charged coupled device (CCD) camera for acquisition.

### 1.3. Applications of Confocal Microscopy With Relation to $Ca^{2+}$ Signaling

The LSCM provides an incredibly powerful and versatile tool for measuring changes in the intracellular $[Ca^{2+}]$ ($[Ca^{2+}]_i$). However, there are many points to consider before using a confocal microscope to monitor changes in $[Ca^{2+}]_i$. One such consideration is whether to use a fluorescent $Ca^{2+}$ dye or a specifically targeted fluorescent protein as the $Ca^{2+}$ sensor; this will, in part, depend on the type of confocal set-up that is available (filters/lasers, etc.). Added to this are the obvious considerations regarding confocal instrumentation and whether spatial or temporal resolution is of paramount importance (or indeed both). It should also be remembered that confocal microscopes are still relatively expensive to purchase, run, and maintain, and so cost may also be a consideration.

#### 1.3.1. Fluorescent $Ca^{2+}$ Indicators

One of the main uses of confocal microscopes has been the study of global and subcellular $Ca^{2+}$ signals using fluorescent indicators sensitive to changes in $[Ca^{2+}]$. Most of these $Ca^{2+}$ indicators are based on the $Ca^{2+}$ chelators, ethylene glycol tetraacetic acid (EGTA) and BAPTA, which have been modified to incorporate fluorescent reporter groups ***(7,8)***. Two main classes of $Ca^{2+}$ indicator have evolved, these being single-wavelength (nonratiometric) and dual-wavelength (ratiometric) indicators. In the former case, increases in $[Ca^{2+}]_i$ are determined by changes in the fluorescence intensity of the indicator (e.g., fluo-3) at a single wavelength, which occurs in the absence of any spectral shift. Generally, there is an increase in fluorescence on binding $Ca^{2+}$, although a decrease is seen with fura red. As an example, the $Ca^{2+}$-bound form of fluo-3 is approx 40 times brighter than the $Ca^{2+}$-free form ***(8)***. The main drawback with single-

wavelength indicators is their reliance on the measurement of fluorescence at a single wavelength as an index of $[Ca^{2+}]$. This means that care must be taken when calculating $[Ca^{2+}]$ from raw fluorescence levels, as this can be influenced by aspects other than changes in $[Ca^{2+}]_i$. This may occur, for example, as a consequence of alterations in cell thickness (e.g., in contractile cells, such as cardiac myocytes), loss of indicator from the cell (owing to leakage or active extrusion), or photobleaching. Photobleaching is the irreversible damage of $Ca^{2+}$-indicator molecules following exposure to the light used for excitation, resulting in a loss of fluorescence related to the duration of exposure to the source of excitation. In the case of dual-wavelength $Ca^{2+}$ indicators, such as fura-2 and indo-1 ***(7)***, changes in $[Ca^{2+}]$ still lead to changes in excitation/emission intensity, but additionally, the $Ca^{2+}$-free and $Ca^{2+}$-bound forms have distinct spectra. With fura-2, $Ca^{2+}$-dependent spectral shifts occur in the excitation spectra, whereas for indo-1, significant shifts are seen in the emission spectra. With dual-wavelength indicators, the $Ca^{2+}$-free and $Ca^{2+}$-bound forms of the indicator have spectral peaks at different wavelengths, and this allows a ratio to be calculated at any given time during an experiment. This ratio is independent of the indicator concentration and, therefore, minimizes some of the artifacts that can arise when using single-wavelength indicators. Despite the obvious advantages of dual-wavelength (ratiometric) indicators, the most popular indicators for confocal $Ca^{2+}$ imaging are undoubtedly single-wavelength indicators, such as fluo-3. In the main, this is because most single-wavelength indicators have excitation maxima in the visible part of the spectrum, making them compatible with the standard laser lines on most confocal microscopes. Conversely, both fura-2 and indo-1 are excited in the UV part of the spectrum, leading to the added expense of a UV laser for excitation and microscope objectives optically corrected for UV light. Indo-1 lends itself more readily for use with confocal microscopes due to the technical difficulties of rapidly switching excitation wavelengths required for the dual excitation of fura-2.

The original single-wavelength $Ca^{2+}$-sensitive indicator was quin-2 ***(9,10)*** but this was superseded by a variety of indicators based on either fluorescein (fluo-3, fluo-4, calcium green) or rhodamine-like chromophores (calcium orange, calcium crimson, rhod-2). The number of single-wavelength indicators seems to increase annually and careful consideration should be given to the choice of indicator for particular experimental purposes. Firstly, the likely amplitude of $Ca^{2+}$ signals should be considered. For example, for low-amplitude $Ca^{2+}$ signals, the affinity of the $Ca^{2+}$ indicator should not be too low, otherwise the signals will be undetectable. Conversely, higher affinity indicators may resolve small signals but saturate with larger signals. The in vitro $K_d$ values of most commercially available $Ca^{2+}$ indicators can be found on the Molecular Probes

website: (http://www.probes.com). One of the main advantages of an indicator, such as fluo-3, is that it has a low level of fluorescence at the resting cytoplasmic [$Ca^{2+}$] and exhibits a large increase in fluorescence on binding $Ca^{2+}$, thus ensuring a large dynamic range for detecting $Ca^{2+}$ signals of varying size ***(11)***. Conversely, indicators such as calcium green and fluo-4 were designed to have a higher level of fluorescence at resting $[Ca^{2+}]_i$, allowing them to be used in cells where subcellular regions need to be identified and clearly defined (e.g., the dendrites and dendritic spines of neurons). The penalty for this increased resting level of fluorescence is a decrease in the dynamic range of the indicator, restricting the amplitude of $Ca^{2+}$ signals that can be visualized. The main difficulties associated with the use of single-wavelength dyes are those of poor indicator loading, dye compartmentalization, dye leakage or extrusion, and, especially in the case of confocal imaging, photobleaching. By definition, having increased confocality means that the signal is being collected from a much smaller volume and, hence, fewer molecules of fluorophore are available for imaging. In addition, a high-intensity light source is required to maintain an adequate signal for detection. Both of these issues dictate that photobleaching can be a major difficulty during confocal imaging of $Ca^{2+}$. To counteract this, dyes including calcium orange and oregon green BAPTA 488 have been developed that are less prone to photobleaching, although many of these have other drawbacks, such as a poor dynamic range ***(11)***.

### *1.3.2. Protein-Based Fluorescent $Ca^{2+}$ Indicators*

As discussed in **Subheading 1.3.1.**, the use of synthetic, small-molecule fluorescent indicators has greatly increased our understanding of $Ca^{2+}$ signals at the single-cell level. However, with the exception of indicators such as rhod-2 that preferentially localizes to the mitochondria, dyes are either difficult to target, or cannot be targeted, to specific intracellular organelles. The $Ca^{2+}$-sensitive chemiluminescent protein aequorin, isolated from the marine jellyfish *Aequoria victoria*, has previously been genetically modified to allow targeting to specific intracellular organelles where it can act as a specific sensor for $Ca^{2+}$ ***(12)***. However, aequorin signals are weak and difficult to measure at the single-cell level ***(13,14)***. This has led to the development of a variety of $Ca^{2+}$ sensors based on another protein isolated from *A. victoria*, namely green fluorescent protein (GFP) and its genetically engineered mutants (e.g., the blue-shifted cyan fluorescent protein (CFP) and the red-shifted yellow fluorescent protein (YFP). GFP has the advantage of having an excitation maxima in the visible spectrum and also of being bright enough to be of use in confocal microscopy. Three main categories of GFP-based $Ca^{2+}$ sensor have been developed and termed "cameleons" ***(15,16)***, "camgaroos" ***(17)***, and "pericams" ***(18)*** (covered in detail in **refs. *13*** and ***14***). All of these sensors are based on the $Ca^{2+}$-binding

properties of the protein calmodulin (CaM), and rely on the fact that when CaM binds $Ca^{2+}$, it undergoes a conformational change. The cameleons are based on a fusion protein of CaM and its target peptide, M13. The fusion protein is tagged at the C-terminus of CaM with CFP and the N-terminus of M13 with YFP ***(15,16)***. On binding $Ca^{2+}$, CaM undergoes a conformational change that brings the two fluorophores closer together allowing fluorescence resonance energy transfer (FRET) to occur (*see* **Note 1**). Hence, an increase in FRET corresponds to an increase in $[Ca^{2+}]_i$ ***(15,16)***. At a similar time to the development of cameleons another sensor, FIP-$CB_{SM}$, based on a similar principle was developed ***(19)***. In this case, the probe is based on the M13 peptide tagged at either end with blue and green varieties of GFP. As $[Ca^{2+}]$ increases, $Ca^{2+}$-bound CaM binds to the M13 peptide leading to a conformational change and a decrease in FRET ***(19)***. Further genetic exploitation of GFP led to the development of the camgaroos and pericams ***(17,18)***. In the case of the camgaroos, the sensor was constructed by inserting the sequence encoding CaM between residues 145 and 146 of YFP. The binding of $Ca^{2+}$ to this sensor leads to a conformational change in the CaM that causes a sevenfold increase in the brightness of YFP ***(17)***. Pericams are the result of further genetic modifications of YFP, in which case a circular variant of YFP was created with the original carboxy and amino terminals fused by a linker peptide. The YFP was then cleaved elsewhere in its sequence, creating new carboxy and amino terminals that were then fused to CaM and the M13 peptide respectively, in effect making a "YFP sandwich" ***(18)***. Subtle mutations in the YFP sequence have led to the generation of several varieties of pericam: the flash pericam that becomes brighter on binding $Ca^{2+}$; the inverse pericam that becomes less bright, and the ratiometric pericam in which there is a spectral shift on binding $Ca^{2+}$ ***(18)***. The cameleons in particular have been successfully targeted to the endoplasmic reticulum ***(15)***, nucleus ***(15)***, mitochondrial-matrix ***(20)***, and the plasma membrane ***(21)***. The advantage of using these sensors to measure $Ca^{2+}$ in specific subcellular compartments is clear, but there are several drawbacks. The signal arising from the cameleons on the binding of $Ca^{2+}$ is relatively small and GFP is also more susceptible to photobleaching than many $Ca^{2+}$-sensitive fluorescent indicators. Probably the biggest concern is that at the relatively high levels of expression required for detection, the CaM part of the probes has the potential to influence $Ca^{2+}$ signaling through buffering or adverse effects on endogenous CaM ***(13,14)***.

### *1.4. Applications of Confocal Microscopy to Other Aspects of Cell Signaling*

#### *1.4.1. Protein-Based Fluorescent Indicators to Measure PLC Activity*

Recently, a number of fluorescently tagged protein biosensors have been developed that allow the real-time imaging of PLC activity ***(22–26)***. Rather

than changes in fluorescence intensity *per se*, the cellular distribution of these biosensors is influenced by the levels of the second messengers, inositol 1,4,5-trisphosphate [Ins(1,4,5)$P_3$] and diacylglycerol (DAG), and alterations in the cellular distribution of the biosensors, therefore, provides an index of PLC activity. Before the advent of these biosensors, studies were restricted to a variety of population-based assays, which, although they provided information about PLC activity, gave no spatial information and only limited temporal resolution. Several biosensors have now been developed, all based on the fusion of a fluorescent reporter molecule (usually fluorescent proteins derived from GFP) with a protein domain that interacts with an intracellular signalling molecule. Thus, the Ins(1,4,5)$P_3$ biosensor is a fusion of the pleckstrin-homology (PH) domain of PLCδ1 with an enhanced form of GFP (eGFP) (eGFP-$PH_{PLC\delta1}$) ***(22,24)***. eGFP is a mutated form of GFP that has an excitation maxima at 488 nm, making it brighter when used with the standard 488 nm laser line available on most confocal microscopes. Under resting conditions, eGFP-$PH_{PLC\delta1}$ is localized to the plasma membrane by the virtue of its high affinity for the membrane lipid phosphatidylinositol 4,5-bisphosphate [PtdIns(4,5)$P_2$]. On activation of PLC, PtdIns(4,5)$P_2$ is hydrolyzed to Ins(1,4,5)$P_3$ and DAG. Ins(1,4,5)$P_3$ competes with PtdIns(4,5)$P_2$ for $PH_{PLC\delta1}$ causing the fusion protein to translocate to the cytosol ***(22,24)***. Thus, an increase in cytosolic fluorescence corresponds to an increase in Ins(1,4,5)$P_3$ production (**Fig. 2A**).

The DAG biosensor is a fusion of the tandem C1 domains ($C1_2$) of protein kinase C (PKC) γwith eGFP (eGFP-PKCγ($C1_2$)) ***(23,26)***. Under resting conditions, eGFP-PKCγ($C1_2$) has a homogeneous distribution across the cell nucleus and cytoplasm, but on activation of PLC and production of DAG it is recruited to the plasma membrane through binding of PKCγ($C1_2$) to DAG. Hence, a decrease in cytosolic fluorescence and an increase in plasma membrane fluorescence is an index of DAG formation and, therefore, PLC activation (**Fig. 2B**). Probes also exist for other parts of the phosphoinositide signalling pathway, for example, PtdIns(3,4,5)$P_3$ ***(27)*** whereas several FRET-based reporters exist for detecting changes in cellular levels of cyclic adenosine monophosphate (cAMP) ***(28,29)*** and cyclic guanosine monophosphate (cGMP) ***(30)***.

### *1.4.2. Determination of G Protein-Coupled Receptor or Ligand Internalization by Confocal Microscopy*

Internalization of plasma membrane G protein-coupled receptors (GPCRs) is a typical response to agonist activation, allowing cells to regulate their sensitivity and responsiveness to subsequent agonist exposures. The current model of GPCR regulation is that following agonist activation, most types of GPCR undergo phosphorylation. Their subsequent internalization is required

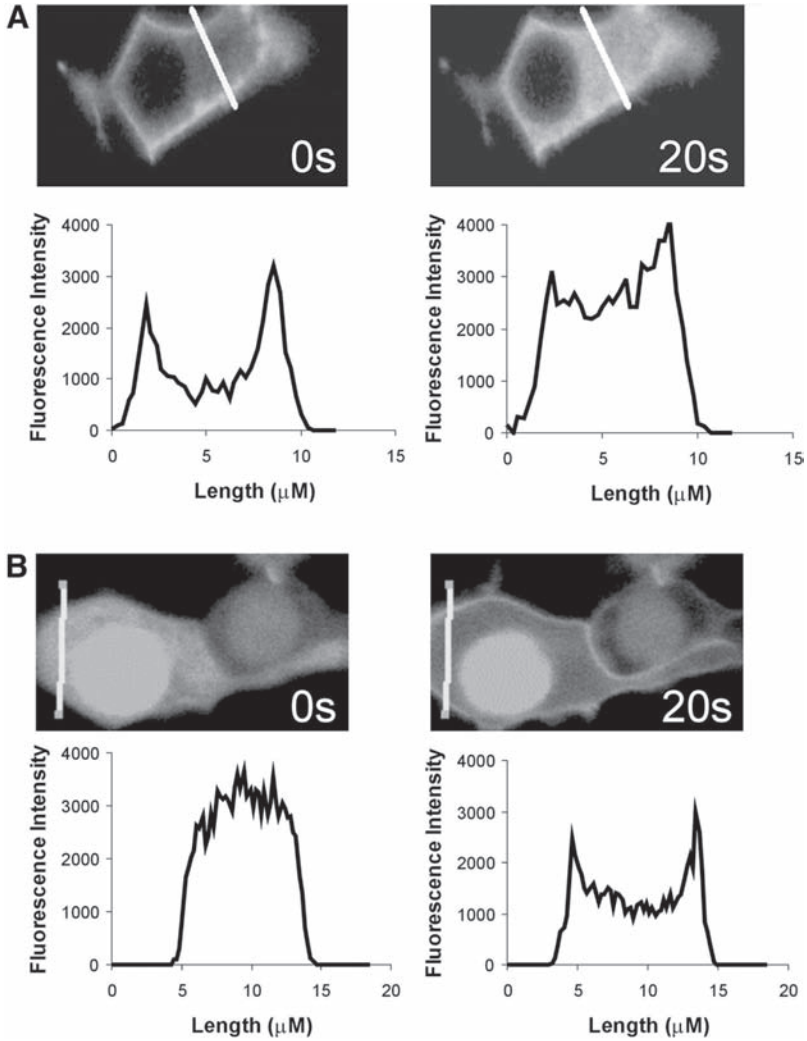


Fig. 2. **(A)** HEK293 cells stably expressing the human muscarinic $M_3$ receptor transfected with eGFP-$PH_{PLC\delta1}$. At rest (0 s), the biosensor is located at the plasma membrane, but after stimulation with 100 μ*M* methacholine (20 s), the biosensor becomes cytoplasmic corresponding to the production of Ins(1,4,5)$P_3$. The change in distribution can be seen clearly in the profiles that represent fluorescence intensity along the lines shown. **(B)** HEK293 cells stably expressing the human muscarinic $M_3$ receptor transfected with eGFP-PKC$\gamma$($C1_2$). At rest (0 s), the biosensor is clearly located homogeneously across the cell but after stimulation with 100 μ*M* methacholine (20 s), the biosensor is recruited to the plasma membrane as diaglycerol is produced. The change in distribution can be seen clearly in the profiles that represent fluorescence intensity along the lines shown.

for dephosphorylation and recycling of resensitized receptors back to the plasma membrane or, alternatively, their proteolytic degradation. Measurements of internalization have been, and continue to be, instrumental in revealing such aspects of receptor regulation. Methods for determining internalization have historically involved the use of radioligands. This has typically involved the measurement of cell surface receptors using a radioligand both before and after a period of agonist exposure to induce internalization. This of course relies on the ability to both remove the agonist that was used to mediate internalization and to measure surface receptors in the absence of further changes caused by processes, such as recycling or further internalization. This can be achieved by, for example, washing to remove the agonist with subsequent binding at a low temperature to block further internalization. For relatively low-affinity agonists, their removal is easily achieved by washing with physiological buffers. However, for high-affinity ligands (e.g., many peptides that have n*M* affinities), removal from the receptor can be more problematic, requiring acidic conditions to cause full dissociation. In contrast to low-affinity ligands, high-affinity ligands often internalize with their receptors and this has also been exploited to measure receptor internalization. Thus, radiolabeled high-affinity agonists can be internalized and following removal of the surface-bound activity, this can be used as a measure of receptor internalization. Despite the relative ease of quantification, these techniques do not allow real-time measurement of receptor internalization, nor do they allow the subcellular localization and trafficking of receptors to be determined. Confocal microscopy offers an alternative means of examining GPCR internalization and, although quantification can be problematic, it provides the prospect of visualizing internalization and other trafficking events at the single-cell level. For example, using dual-label confocal immunocytochemistry, the subcellular localization of receptors can be determined and used to provide information on their trafficking events. As an alternative to visualizing receptors through antibodies and associated fluorophores, the receptors can be tagged directly with fluorophores such as GFP or its variants. Although tagging may itself influence receptor function and trafficking, this approach not only has the potential to allow the subcellular localization of receptors to be determined, it can also allow the real-time visualization of their movement, including internalization. A detailed discussion on the use of GFPs to assess internalization goes beyond the scope of this chapter but has been reviewed elsewhere ***(31)***. In a similar way to which radiolabeled high-affinity agonists can be used to determine receptor internalization, fluorescently labeled agonists and confocal microscopy can also be used. It must be remembered, however, that ligands may dissociate from their receptor as they move into and through the endocytic pathway, and may also recycle and/or degrade independently ***(32)***, providing important con-

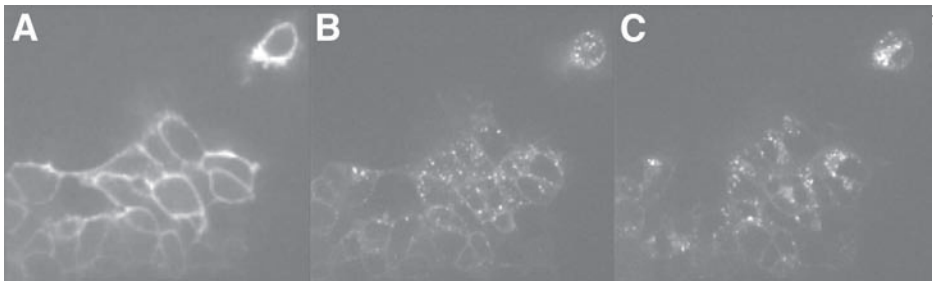


Fig. 3. HEK293 cells stably expressing human neuromedin U (NmU)-receptor-1 were cultured on glass cover slips and mounted onto the stage of an Ultra*VIEW* confocal microscope. The temperature was maintained at 37°C and 10 n*M* Cy3B-pNmU-8 added at 0 s. With excitation at 568 nm, confocal fluorescent images were collected intermittently over a 12-min period. **(A)** Shows membrane localization of fluorescence 180 s following addition of Cy3B-labeled porcine Neuromedin U-8 (Cy3B-pNmU-8). **(B,C)** Images at 300 s and 600 s, respectively, showing internalization in the form of punctate regions of fluorescence.

siderations in the interpretation of data collected using this technique. Although potentially providing real-time visualization of internalization, confocal images are extremely difficult to quantitate and a cautionary approach to interpreting the data is required. Furthermore, photobleaching, quenching, differences in the power of the laser, focal drift, and pixilation of images add to the difficulties of quantification. However, with sensible experimental design and careful analysis, quantification of receptor internalization using confocal microscopy can be achieved. For many, the nature of the investigation means that the images taken of internalization in their own right provide suitable documentation (*see* e.g., **Fig. 3**). Many others have applied different, sometimes complex, methods to quantify internalization of fluorescently-labeled receptor or ligand. A comprehensive discussion of these methods is beyond the remit of this chapter and the reader is referred elsewhere ***(33–36)***. Choosing a fluorophore can be difficult, as there is a wide range that can be conjugated to both non-peptide and peptide ligands. The choice may be limited by the confocal system (e.g., the laser lines and filters available; *see* **Note 2**), the ligand(s) and/or receptor(s) under investigation, and the photobleaching and pH sensitivity of the fluorophore (*see* **Note 3**). It goes beyond the remit of this chapter to discuss the relative merits of all those available. However, Amersham Biosciences (Cardiff, UK; Website: http://www.amershambiosciences.com) supply a range of CyDye, eGFP, and other conjugates, and Molecular Probes (Eugene, OR; Website: http://www.probes.com) supply Alexa Fluor and BODIPY fluorophores and both companies provide further information on their websites. There are also numerous reviews detailing the uses and benefits of different fluorescent labels (e.g., **refs.** ***37*** and ***38***).

## 2. Materials

All chemicals can be obtained from Sigma-Aldrich (Poole, UK) unless otherwise stated, whereas all microscope slides and cover slips are available from VWR International Ltd. (Poole, UK). All cell culture reagents can be obtained from Invitrogen Ltd. (Paisley, UK). All solutions and reagents should be prepared with milli-Q or equivalent grade water ($ddH_20$). When dealing with cells in culture, it is imperative that care should be taken to ensure all reagents are sterile filtered prior to use.

### 2.1. Immunofluorescence

1. Prepare a stock solution of poly-D-lysine hydrobromide at 1 mg/mL (1%) in $ddH_2O$. Store aliquots at –20°C. On the day of use, dilute the stock solution 1:100 in $ddH_2O$ and sterile filter prior to coating cover slips.
2. 10X Phosphate buffered saline (PBS): 101 m*M* $Na_2HPO_4$, 17.6 m*M* $KH_2PO_4$, 26.8 *M* KCl, 1.37 *M* NaCl. To prepare 1 L of 10X PBS, dissolve 14.4 g $Na_2HPO_4$, 2.4 g $KH_2PO_4$, 2 g KCl, and 80 g NaCl in 800 mL of $ddH_2O$ and adjust to pH 7.2. Make up to 1 L with $ddH_2O$ and store at room temperature. Dilute to 1X for use.
3. 4% Paraformaldehyde solution: add 4 g of paraformaldehyde to 100 mL of 1X PBS (*see* **Note 4**).
4. 100% Methanol (cooled to –20°C).
5. Triton X-100: prepare a stock solution of 20% Triton X-100 in 1X PBS. Rotate in a tube overnight at 4°C to dissolve. Dilute the stock solution to 0.2% as required.
6. Blocking buffer: 3% bovine serum albumin (BSA) in 1X PBS (*see* **Note 5**).
7. Antibodies: for general advice on dealing with antibodies *see* **Note 6**.
8. Antibody solutions: antibodies should be used at the concentration recommended by the manufacturer or alternatively at a concentration determined empirically by the user (*see* **Note 6**). Good sources of primary antibodies include Sigma-Aldrich, Santa Cruz Biotechnology Inc. (Santa Cruz, CA), and Abcam (Cambridge, UK). Primary antibodies should be dissolved in an appropriate blocking buffer (*see* **step 6**). To reduce nonspecific labeling, fluorescently labeled secondary antibodies should be prepared in a blocking buffer containing serum from the host animal (e.g., a goat anti-rabbit secondary antibody should be prepared in 1X PBS containing 10% goat serum). Good sources of fluorescently conjugated secondary antibodies include Vector laboratories (Peterborough, UK), Sigma-Aldrich, Abcam, and Jackson ImmunoResearch (West Grove, PA).
9. Commercially available mountants: Vector Shield and Citifluor (Citifluor Ltd., London, UK).

### 2.2. Single-Cell Confocal $Ca^{2+}$ Imaging and the Determination of GPCR or Ligand Internalization by Confocal Microscopy

1. Standard HEK293 growth media: for example, Eagle's minimum essential medium with Glutamax-1 and Earle's salts supplemented with fetal calf serum (10%), non-essential amino acids (1%), 50 U/mL penicillin, and 50 μg/mL streptomy-

cin. Incubate cells in a humidified atmosphere (95% $O_2$, 5% $CO_2$, 37°C) with the culture medium replaced every third day. Passage the cells when they reach approx 80% confluence. Cells transiently or stably expressing receptors or other proteins of interest are generated using standard transfection protocols and, where appropriate, standard selection conditions. Other cell types can of course be used with appropriate culture and transfection conditions.

2. Krebs-HEPES buffer (KHB): 10 m*M* HEPES, 4.2 m*M* $NaHCO_3$, 10 m*M* glucose, 1.18 m*M* $MgSO_4 \cdot 7H_2O$, 1.18 m*M* $KH_2PO_4$, 4.69 m*M* KCl, 118 m*M* NaCl, 1.29 m*M* $CaCl_2$, pH 7.4. To prepare 1 L of KHB, dissolve 2.38 g HEPES, 0.35 g $NaHCO_3$, 2.10 g glucose, 0.29 g $MgSO_4 \cdot 7H_2O$, 0.16 g $KH_2PO_4$, 0.35 g KCl, 6.92 g NaCl, 0.19 g $CaCl_2 \cdot 2H_2O$ in 800 mL $ddH_2O$ and adjust to pH 7.3 with 5 *M* NaOH. Make up to 1 L with $ddH_2O$ and store at 4°C.
3. Stock solutions (1 m*M*) of the acetoxymethyl (AM) ester form of fluorescent $Ca^{2+}$ indicators (e.g., fluo-3) should be prepared in high quality anhydrous dimethylsulphoxide (DMSO) and then dispensed into 20 µL aliquots and stored, well sealed, at –20°C (*see* **Notes 7** and **8**).
4. Cy3B-labeled porcine Neuromedin U-8 (Cy3B-pNmU-8): Cy3B is obtained as the Cy3B-NHS ester (Amersham Biosciences) and attached to the N-terminus of porcine neuromedin U (NmU-8) as per the manufacturer's instructions. Following conjugation the product is purified by high-performance liquid chromatography and tested for biological activity (*see* **Note 9**).

## 3. Methods

### *3.1. Indirect Immunofluorescence Protocol for Adherent Cells*

One technique that is routinely used to examine the subcellular distribution of proteins is indirect immunofluorescence labeling. Adherent cells can be fixed and permeabilized to allow antibodies targeted against specific cellular proteins access to the cell interior. Specific binding of the primary antibody to its target protein can then be detected using a secondary antibody coupled to a fluorophore. Common fluorophores include fluorescein isothiocyanate (FITC), tetramethyl rhodamine isothiocyanate (TRITC) and Texas Red, all of which can be visualized using the standard laser lines on most commercially available confocal microscopes.

#### *3.1.1. Preparation of Cover Slips*

1. Cover slips should be of an appropriate thickness (typically 170 ± 10 µm) for optimal confocal resolution. Cover slips may be stringently cleaned with either acetone or 100% ethanol prior to use and then sterilized by either autoclaving or flaming. Alternatively, for most purposes, cover slips can be sterilized in 70% ethanol and then rinsed in sterile 1X PBS prior to use.
2. To aid cell adhesion, cover slips may be coated with a variety of substances such as fibronectin, gelatin, or poly-D-lysine to provide a substratum for adherence and growth. For example, poly-D-lysine is prepared as a 0.01% solution in sterile

$ddH_2O$ (*see* **Subheading 2.1.**, **step 1**). Depending on size, cover slips can then be coated with between 100 and 500 µL of poly-D-lysine solution. Following 20-min incubation at room temperature, the poly-D-lysine should be removed by suction and the cover slips allowed to air-dry in a tissue culture hood for 20 min prior to the plating of cells. For some cell types, it may also be necessary to wash the cover slips with sterile 1X PBS to remove any excess poly-D-lysine.

### 3.1.2. Immunofluorescence Labeling

1. Cells in the appropriate growth medium should be seeded onto poly-D-lysine coated 22 mm diameter borosilicate glass cover slips contained in 6-well multidishes. Cells should then be returned to the incubator for 24 to 48 h to allow adequate adhesion.
2. Fixation: on the day of experimentation, the growth medium should be removed and the cells washed once with 1X PBS at room temperature. The cells may then be fixed using either 4% paraformaldehyde at room temperature (cross-linking fixation) or 100% methanol cooled to –20°C (protein precipitation fixation) (*see* **Note 5**).
   a. Paraformaldehyde fixation: immerse cover slips in 4% paraformaldehyde at room temperature for 30 min. Wash the cover slips once with 1X PBS. Aspirate the PBS and then permeabilize the cells by addition of 0.2% Triton X-100 in 1X PBS for 5 min at room temperature. Wash the cover slips three times for 5 min each in 1X PBS. Then proceed to the blocking step (**step 3**).
   b. Methanol fixation and permeabilization: immerse cover slips in –20°C methanol for 10 min. Wash the cover slips three times for 5 min each with 1X PBS at room temperature. Then proceed to the blocking step (**step 3**).
3. Blocking: all cover slips should be incubated with blocking buffer (3% BSA in 1X PBS) for 45 to 60 min at room temperature. This step is essential for producing a low level of background staining (*see* **Note 5**). Cover slips should then be washed once in 1X PBS for 5 min.
4. Staining: the primary antibody should be diluted as appropriate in blocking buffer (for example, 3% BSA in 1X PBS). It should be noted that when using a high concentration of antibody it is recommended that the solution is centrifuged for 20 min at ≥12,000*g* at 4°C. This removes aggregated material, thereby reducing nonspecific background staining. The time and temperature for incubation with primary antibody will vary depending on the antibody, but a good starting point is to incubate the cover slips with primary antibody overnight at 4°C with mild agitation (e.g., a rocking platform).
5. Following incubation, aspirate the primary antibody and wash the cover slips three times for 5 min each in 1X PBS at room temperature.
6. Incubate all cover slips with the appropriate concentration of fluorescently labeled secondary antibody in an appropriate blocking buffer (*see* **Subheading 2.1.**, **step 8**) for 45 to 60 min at room temperature in the dark.
7. Aspirate the secondary antibody and wash each cover slip three times for 5 min each with 1X PBS at room temperature in the dark.

8. At this stage the cell nucleus can be counterstained as a cell marker. When using a FITC-conjugated secondary antibody this may be achieved by a 5-min incubation with 2% propidium iodide (PI). It should be noted that PI cannot be used as a counterstain when using either TRITC- or Texas Red-conjugated secondary antibodies, but other counterstains, such as Hoescht or DAPI, may be used if a UV laser is available.
9. Cover slips can then be mounted onto standard microscope slides using a commercially available mountant (*see* **Subheading 2.1., step 9**). Vector Shield (Vector Labs) and Citifluor (Citifluor Ltd.) both contain anti-photobleaching agents that help preserve the lifetime of many common fluorophores. Slides can be stored short-term (several weeks) in the dark at room temperature or alternatively, cover slips can be sealed onto microscope slides using clear nail varnish and stored in the dark at 4°C for several months.
10. Slides are then ready for viewing. For example, the detection of a FITC-conjugated secondary antibody can be achieved by excitation with the 488 nm laser line on most commercially available confocal microscopes. In our case, standard 2D images are taken (512 × 512 pixels) using an Olympus Fluoview or Perkin-Elmer Ultra*VIEW* confocal microscope. Care should be taken when interpreting subcellular staining patterns. For example, it is wise to use a counterstain to mark the position of the cell nucleus and if a protein is thought to be localized to a specific subcellular compartment, then this should be confirmed by co-localization studies with a known marker protein. Adequate controls should also be included, for example, incubation with a blocking peptide to the primary antibody should remove specific staining. A more detailed description of the controls and potential pitfalls surrounding immunofluorescence labeling can be found elsewhere ***(39,40)***.

### *3.2. Dual-Label Immunofluorescence in Adherent Cells*

The dual-labeling immunofluorescence procedure represents an extension of the method discussed in **Subheading 3.1.** In this scenario, the main concern is the selection of both primary and secondary antibodies to allow visualization of two different cellular proteins. It is essential that the primary antibodies have been raised in different species. Most commonly, one antibody is a mouse monoclonal antibody and the other is a polyclonal antibody raised in rabbit. If primary antibodies from the same species were to be used, then the secondary antibodies would bind indiscriminately making an interpretation of the labeling impossible. The main consideration with the secondary antibodies is the choice of fluorophore. It is essential that the fluorophores present on the two different secondary antibodies both excite and emit in different parts of the spectrum in order to reduce bleed-through of light from one channel to the other. The most common combination is probably FITC and Texas Red that absorb maximally at blue and green wavelengths, but emit green and red light, respectively. This combination of fluorophores has previ-

ously been used to show, for example, the subcellular co-localization of type II ryanodine receptors and type II Ins(1,4,5)$P_3$ receptors in atrial myocytes ***(6)***. It should also be noted that care must be taken to select the appropriate laser line for illumination and the correct dichroic mirror and filter sets for detecting emission (*see* **Note 2**).

1. **Steps 1–3** of the single-label immunofluorescence protocol should be followed, i.e., fixation, permeabilization, and blocking.
2. Staining: the primary antibodies should be diluted as appropriate in blocking buffer (for example, 3% BSA in 1X PBS) and added as a mixture to the cover slips of cells. Cover slips should be incubated with the primary antibody solution overnight at 4°C with mild agitation.
3. Following incubation, aspirate the primary antibody solution off and wash the cover slips three times for 5 min each in 1X PBS at room temperature.
4. Incubate all cover slips with an appropriate concentration of the first fluorescently-labeled secondary antibody in an appropriate blocking buffer (*see* **Subheading 2.1., step 8**) for 45 to 60 min at room temperature in the dark.
5. Aspirate the first secondary antibody and wash each cover slip three times for 5 min each with 1X PBS at room temperature in the dark.
6. Incubate all cover slips with an appropriate concentration of the second fluorescently labeled secondary antibody in an appropriate blocking buffer (*see* **Subheading 2.1., step 8**) for 45 to 60 min at room temperature in the dark.
7. Aspirate the second secondary antibody and wash each cover slip three times for 5 min each with 1X PBS at room temperature in the dark.
8. Cover slips can then be mounted onto standard microscope slides using an appropriate anti-photobleaching mountant as described in **Subheading 3.1., step 9**.

### *3.3. Real-Time Confocal Imaging of Intracellular $Ca^{2+}$ Transients in Adherent Cells*

Advances in confocal imaging technology and the concomitant development of fluorescent $Ca^{2+}$ indicators over the past 10 yr or so, have greatly enhanced our understanding of both the spatial and temporal aspects of agonist evoked $Ca^{2+}$ signals at the single-cell level ***(3–5)***. Indeed, there are now a wide variety of fluorescence-based $Ca^{2+}$ indicators available. Several excellent resources exist to aid in the selection of appropriate $Ca^{2+}$ indicators (e.g., Molecular Probes handbook of fluorescent indicators at Website: http://www.probes.com) and there are also several excellent reviews outlining the advantages and disadvantages of many of these indicators ***(11,41)***. The following method is for single-cell $Ca^{2+}$ imaging in HEK293 cells loaded with the AM ester form of fluo-3 (fluo-3 AM) using either an Olympus Fluoview or PerkinElmer Ultra*VIEW* confocal microscope.

1. HEK293 cells in standard growth media should be plated onto 25-mm diameter borosilicate glass cover slips coated with 0.01% poly-D-lysine in 6-well multidishes (2 mL of cells/well). Cells should be seeded at a density that gives approx 80% confluency on the day of experimentation. Cells are then returned to the incubator for between 24 to 48 h to ensure adequate adhesion.
2. On the day of experimentation, aspirate off the growth medium and wash the cells once with KHB at room temperature.
3. Aspirate off the KHB and replace with fresh KHB containing 2 μ*M* fluo-3 AM and 0.02% pluronic F-127. The cells should then be placed in the dark at room temperature for 45 min to allow adequate loading of the $Ca^{2+}$-sensitive indicator (*see* **Notes 7** and **8**).
4. After loading, wash the cells once with KHB. Add 1 mL KHB to each cover slip and incubate in the dark for approx 45 min at room temperature to allow adequate de-esterification of the indicator (*see* **Notes 7** and **8**).
5. Cells on cover slips can then be mounted into a chamber on the stage of an inverted microscope (e.g., Olympus IX50) and maintained at 37°C using a Peltier thermal heating device, and if required, by keeping perfusion buffers in a heated water bath (*see* **Note 10**).
6. Fluo-3 can then be excited using the 488 nm line of an Ar or Kr/Ar laser with emitted fluorescence collected at wavelengths >505 nm.
7. Images (256 × 256 pixels) are typically collected as a time series, with the rate of image capture dependent on the type of experiment and the capabilities of the confocal microscope being used (*see* **Note 11**).
8. On-line image analysis can then be performed using software provided by the confocal microscope manufacturer (e.g., Fluoview software for the Olympus Fluoview and PerkinElmer imaging suite for the Ultra*VIEW*). Alternatively, images can be exported for off-line analysis using other image analysis packages, such as National Institute of Health image (NIH Image/Image J) (*see* Website: http://rsb.info.nih.gov/nih-image/download.html). Raw fluorescence data can be exported to Microsoft Excel and expressed as either the change in fluo-3 fluorescence relative to basal fluo-3 fluorescence ($F/F_o$) or alternatively the raw fluorescence data can be converted into changes in $[Ca^{2+}]$ using the following formula:

$$[Ca^{2+}] = K_d\,[(f - f_{min})/(f_{max} - f)]$$

where $f$ is the fluorescence intensity of fluo-3 at any given time point during the experiment and $f_{min}$ and $f_{max}$ are the minimal and maximal fluorescence intensities of fluo-3, reflecting the calcium-free and the calcium-saturated forms of the indicator. The values of $f_{min}$ and $f_{max}$ are usually determined at the end of each experiment by the addition to the perfusion chamber of a calcium ionophore such as A23187 or ionomycin (≥1 μ*M*) in the presence of either 10 m*M* EGTA or 10 m*M* $CaCl_2$ (for $f_{min}$ and $f_{max}$ respectively). The $K_d$ for fluo-3 as determined in vitro is approx 390 n*M*, although this may differ in a cellular context. For example, the $K_d$ for fluo-3 inside HeLa cells has been determined as approx 810 n*M* ***(11)*** (*see* **Note 12**).

### 3.4. Confocal Imaging of PLC Activity in Adherent Cells Using Protein Biosensors

The methodology described here illustrates the use of two genetically engineered biosensors that can be used to detect the generation of Ins(1,4,5)$P_3$ and DAG, the second messengers produced on activation of PLC. The use of these biosensors has enabled PLC activity to be determined at the single-cell level, both visually and in real-time *(22–26)*. Alternatively, the use of the biosensors in cotransfection experiments has allowed examination of proteins that modulate PLC activity. For example, we have successfully used cotransfection of the biosensors with regulators of G protein signaling (RGS) proteins to determine the impact of RGS proteins on $G\alpha_q$-mediated PLC signalling at the single-cell level. Details of the biosensor constructs can be found in **Note 13**.

1. Plate cells (e.g., HEK293 cells stably expressing the recombinant human muscarinic $M_3$ receptor) in standard growth media into 6-well multidishes containing 25 mm diameter borosilicate glass cover slips coated (where required) with an appropriate substratum (e.g., 0.01% poly-D-lysine as described in **Subheading 3.1.1.**). Ideally, cells should be seeded at a density that gives a confluency of approx 30 to 50% on the day of transfection. Cells should then be returned to the incubator for 24 h to allow adequate cell adhesion.
2. The next day, cells should be transfected with DNA encoding the appropriate biosensor. Cells can be routinely transfected using any one of several commercially available transfection reagents as per the manufacturer's instructions. Suitable transfection reagents include, for example, Fugene 6 (Roche Diagnostics, Lewes, UK), Lipofectamine 2000 (Invitrogen Ltd.) or Genejuice (Calbiochem, Nottingham, UK).
3. Transfection of adherent cells using Fugene 6: add 100 µL of serum-free growth medium to a sterile tube. Add 3 µL of transfection reagent directly into the medium and mix gently. Incubate at room temperature for 5 min.
4. To a fresh sterile tube add 1 µg of the appropriate biosensor DNA (*see* **Note 13**).
5. After the 5 min incubation is complete, add the mixture of medium and transfection reagent drop-wise onto the DNA. Gently mix using a pipet and incubate at room temperature for 15 min.
6. The DNA/Fugene 6 complex should then be added drop-wise to a single well of a 6-well multidish (containing approx 2 mL of fresh media, e.g., change the media on the cells prior to transfection). Cells should then be returned to the incubator for between 24 and 48 h prior to experimentation. For certain cell types it may be necessary to remove the transfection reagent after 8 h to reduce any cytotoxic affects.
7. On the day of experimentation, remove the growth medium and wash the cells once with 2 mL of KHB at room temperature.
8. Cover slips can then be used as the base of a perfusion chamber and mounted on the stage of an inverted microscope. The temperature is maintained by a Peltier

thermal heating device and, if required, by keeping perfusion buffers in a heated water bath.

9. The biosensors can then be visualized by exciting eGFP using the 488-nm line of a standard Ar laser with emitted fluorescence collected at wavelengths greater than 505 nm. Typically, images (256 × 256 pixels) collected every second are sufficient for detecting the movement of the eGFP tagged biosensors.
10. Changes in eGFP fluorescence in response to cellular stimulation can then be expressed as absolute changes in cytosolic eGFP fluorescence or changes in cytosolic fluorescence in relation to the initial basal level of cytoplasmic eGFP fluorescence ($F/F_o$). Changes in the subcellular distribution of eGFP fluorescence can also be determined by measuring pixel intensity across a cell (*see* **Fig. 2**).

### 3.5. Determination of GPCR or Ligand Internalization by Confocal Microscopy

Here we describe a confocal method to monitor the internalization of porcine neuromedin U (pNmU-8), with the fluorophore Cy3B (Amersham Biosciences) conjugated to its N-terminus (Cy3B-pNmU-8). This neuropeptide binds with high affinity to both mammalian forms of its cognate GPCRs (NmU receptor-1 [NmU-R1] and NmU receptor-2 [NmU-R2]) and here we describe a method to use this to visualize internalization of human NmU-R1 expressed as a recombinant protein in HEK293 cells.

1. Receptor-expressing cells (e.g., HEK293 expressing hNmU-R1) should be cultured and plated on poly-D-lysine coated cover slips as described in **Subheading 3.3., Steps 1** and **2**.
2. Cells should then be returned to the incubator for 24 to 48 h to allow adequate cell adhesion. On the day of experimentation, mount a cover slip onto the stage of a PerkinElmer Ultra*VIEW* confocal microscope. Here the cover slip forms the bottom of a chamber to which 250 µL of KHB should be added. Buffer is added at the required temperature, with the temperature maintained using a Peltier heated cover slip holder (*see* **Note 14**).
3. Prior to addition of the fluorescently labeled ligand, obtain a phase image of the cells that can be used subsequently to compare or overlap with the fluorescence image to help with identification of the subcellular localization of the ligand. It is also important to consider the specificity of binding of the fluorescent ligand and any possible contribution of nonspecific binding to cellular fluorescence (*see* **Note 15**).
4. Add directly to the bath 250 µL of KHB containing the fluorescently labeled ligand at twice the required final concentration (20 n*M* Cy3B-pNmU-8) (*see* **Note 16**). The temperature of this addition should be equivalent to the bath temperature. Great care should be taken not to move the chamber or dislodge cells from the cover slip (*see* **Note 17**). As an alternative, ligands can be added through a perfusion system (*see* **Note 18**).
5. Visualization of the fluorescent ligand can be achieved using an appropriate excitation wavelength and suitable filter set (*see* **Note 2**). For example, on a

PerkinElmer Ultra*VIEW* confocal system, Cy3B is excited at 568 nm using a Kr/Ar laser with emitted fluorescence collected with a broad-band RGB emission filter. The intensity of excitation is minimized, using the lowest possible laser setting where images can be seen clearly (*see* **Note 3**).

6. To avoid photobleaching (*see* **Note 3**) of Cy3B, fluorescent images of cells should be collected intermittently (e.g., two to three images every 30 s) during internalization. The time course required will depend on the receptors and the expression system. Alternatively surface-bound fluorescence can be removed by washing following an initial period of internalization (**Note 19**).
7. The images can then be analysed to assess internalization (**Fig. 3**; **Note 20**).

## 4. Notes

1. FRET is a phenomenon characterized by the transfer of energy from one excited fluorophore (the donor, e.g., CFP) to another fluorophore (the acceptor, e.g., YFP). To enable FRET to work the donor fluorophore must have an emission spectrum that overlaps considerably with the excitation spectrum of the acceptor fluorophore. For FRET to occur the donor and acceptor fluorophores must be in close proximity to one another, hence FRET has been used extensively to study protein–protein interactions. A detailed discussion of FRET and its use in biological systems is covered elsewhere ***(42)***.
2. As discussed in **Subheading 1.2.**, confocal microscopes routinely have lasers that produce excitation light in the visible spectrum. Hence, care should be taken when selecting a fluorophore or $Ca^{2+}$-sensitive fluorescent indicator to ensure that it is capable of being used with the instrumentation available. A further consideration is that of dichroic mirrors and emission filters. A wide variety of optical filters and filter blocks are available from companies such as Omega Optical Inc. (Brattleboro, VT; Website: http://www.omegafilters.com) and Chroma Corp. (Rockingham, VT; Website: http://www.chroma.com). These include dual- and triple-coated dichroic mirrors that are suitable for use in dual-labeling experiments.
3. The photobleaching of fluorophores describes the process in which the fluorophore's structure is altered as a result of absorption of excitation light causing it to progressively lose its fluorescence. This problem is often exacerbated with many fluorophores by the need for high excitation light to obtain detectable fluorescence emission. The problem of photobleaching can be minimized by keeping both laser intensity and exposure times to a minimum. Some fluorophores are also extremely sensitive to changes in pH and are more susceptible to photobleaching in a low pH environment. Although this can be exploited experimentally, whereby loss of fluorescence is indicative of receptors/ligands entering the low-pH environment of endosomes and lysosomes, the use of a pH-insensitive fluorescent conjugate (for example, some of the Cy-Dyes [Amersham Biosciences], Alexa Fluor and BODIPY [Molecular Probes]) will limit this problem.
4. Paraformaldehyde should be weighed out in a fume hood while wearing gloves and a protective mask. Paraformaldehyde is insoluble at room temperature and as such the solution should be placed in a shaking water-bath maintained at

60°C until the paraformaldehyde dissolves. The paraformaldehyde solution should then be cooled to room temperature prior to use (this may be achieved rapidly by placing the solution on ice). The paraformaldehyde solution is relatively unstable and should preferably be made fresh on the day of experimentation.

5. Methanol is generally thought to be the quickest and easiest option for fixation, but it is also the most destructive and in general gives poor structural preservation. Methanol solubilizes and precipitates proteins, often leading to the loss of membrane-bound antigens. Methanol treatment also results in the permeabilization of cells, removing the need for a permeabilization step (as is required for paraformaldehyde fixation). Paraformaldehyde works by cross-linking proteins and is generally considered to be the method of choice when the maintenance of cellular structure is of importance (for example, in highly structured cells, such as cardiac myocytes and neurons). After fixation and permeabilization cells should be incubated in an appropriate blocking buffer to reduce background staining. The addition of 0.2% Triton to the blocking buffer may also help to minimize background staining.
6. On receipt of any antibody it is vital to ensure that the data sheet is read thoroughly and that stock antibody solutions are kept at the appropriate temperature (usually either 4°C or –20°C). Preferably, antibodies should be aliquoted into suitable volumes for storage to prevent repetitive freeze/thaw cycles that can lead to loss of antibody function and the formation of inactive antibody aggregates. Secondary antibodies labeled with fluorophores for indirect immunofluorescence studies should be kept in lightproof containers at 4°C unless otherwise stated in the supplier's instructions. The supplier's instructions should be the starting point for determining the appropriate dilution of primary antibody. More detailed discussion on determining the concentration of antibody for use empirically is beyond the scope of this chapter, but several other excellent resources cover this topic ***(39,40)***.
7. Most common fluorescent indicators used for confocal $Ca^{2+}$ imaging are polycarboxylate anions that are lipophilic and hence not cell-permeant. This problem has been overcome by the addition of "protective" AM ester groups to mask the charged carboxyl groups present on the indicator. This makes the AM ester form of, for example, fluo-3, uncharged and consequently cell-permeant. Once inside the cell, endogenous nonspecific esterases cleave off the protecting lipophilic AM ester-groups leaving the original hydrophilic $Ca^{2+}$-sensitive form of fluo-3 trapped inside the cell. It should also be noted that the esterified form of the indicator is also free to cross other cellular membranes, such as those of intracellular organelles like the mitochondria, where esterase activity may result in compartmentalization. The loading of fluo-3 AM into cells is usually aided by the addition of a mild nonionic surfactant, such as pluronic F-127 (0.02%). The pluronic acts as a dispersing agent for the AM esters, aiding their solubility. Pluronic can be added directly to aqueous solutions although it is relatively insoluble and particulate matter should be removed by centrifuga-

tion. Alternatively, make a 20% stock solution of pluronic in DMSO (gentle warming to 40°C may assist with dissolving the detergent) and dilute 1:1000 into aqueous solution. Serum proteins, such as BSA (0.5–1%), can also improve loading efficiency, probably by acting as hydrophobic carriers for the AM esters. It should be noted that as an alternative to AM ester loading, the hydrophilic free acid form of fluo-3 may be introduced into cells by invasive procedures, such as microinjection through a patch pipet ***(41)***.

8. In some instances, there is significant dye loss from cells during and after loading. It is believed that this loss occurs by an extrusion mechanism that expels organic anions and as such can be blocked effectively by inhibitors such as probenecid and sulphinpyrazone ***(43)***. For example, in PC12 cells, sulphinpyrazone has previously been used at a concentration of 100 to 250 μ*M* to aid the loading of fura-2 AM (Dr. Schuichi Koizumi, National Institute of Health Sciences, Tokyo, Japan, personal communication). It should be noted that the loading times mentioned in the methodology (**Subheading 3.3.2.**) are for HEK293 cells and follow basic guidelines issued by the manufacturer (Molecular Probes). Different cell types may require different loading conditions, with possible variables being the concentration of indicator used and the time of loading. Temperature (e.g., 37°C) can also increase the rate of loading, but it can also increase the rate of active extrusion and the degree of compartmentalization. In general, the latter issue of compartmentalization means that indicator loading at 37°C is not recommended.
9. Any potential impact of the fluorescent moiety on ligand binding and/or efficacy should be addressed. Dependent on the nature of the fluorophore, this can be assessed in competition binding and/or functional assays and compared with the properties of the unlabeled ligand. For example, we have demonstrated that the addition of Cy3B to pNmU-8 did not affect potency based on functional assays using recombinantly expressed human NmU-R1 or NmU-R2.
10. The temperature at which $Ca^{2+}$ imaging experiments are performed depends entirely on the user. Carrying out experiments at 37°C is obviously more physiological, but also increases the risk of dye extrusion and compartmentalization. Typically, in our imaging experiments cells are loaded and de-esterified at room temperature, but experiments are performed at 37°C, with the temperature maintained by a Peltier heated cover slip holder. Typically, agonists are added to cells using a pump-driven perfusion system with flow rates of 1 to 5 mL/min. Agonists can then be washed out by perfusion with KHB.
11. Rate of confocal capture: as discussed in the Introduction, the rate of image capture will depend on the confocal microscope. Previously, elementary $Ca^{2+}$ release events ($Ca^{2+}$ puffs) have been visualized using fluo-3 in a variety of cell types with a Noran *Oz* confocal microscope recording a 256 × 256 pixel area at 7.5 Hz (an image every 133 ms) ***(44)***. Using the same system, rapid on-set $Ca^{2+}$ sparks have been visualized in cardiac myocytes recording a 512 × 115 pixel area at 30 Hz ***(6,45)***. Using either an Olympus Fluoview or PerkinElmer Ultra*VIEW* confocal microscope, we more routinely measure whole cell $Ca^{2+}$ transients (256 × 256 pixels) at a frequency of 1 to 2.5 Hz.

12. In vitro $K_d$ values for most fluorescent $Ca^{2+}$ indicators are available from Molecular Probes (http://www.probes.com), as are a variety of in vitro calibration kits that attempt to mimic cellular environments (e.g., high concentrations of KCl). Ideally, the fluorescent indicator chosen should be calibrated in vivo as described elsewhere ***(11)***, and the $f_{min}$ and $f_{max}$ calculated at the end of each experiment. Detailed discussion on the various problems with obtaining in vivo calibrations, not least the difficulty of obtaining accurate values for $f_{min}$ and $f_{max}$, can be found elsewhere ***(11)***.
13. The original eGFP-tagged constructs for detecting Ins(1,4,5)$P_3$ (eGFP-$PH_{PLC\delta1}$) and diacylglycerol (eGFP-PKC$\gamma$($Cl_2$)) production are described by Stauffer et al. ***(22)*** and Oancea et al. ***(23)***, respectively. These constructs were obtained for use from Stefan Nahorski (University of Leicester, UK), but were originally gifts from Tobias Meyer (Duke University Medical Centre, Durham, NC). It should be noted that the success of this technique does appear to be receptor- and cell-dependent. No movement of the eGFP-$PH_{PLC\delta1}$ construct was seen on stimulation of the endogenous muscarinic $M_3$ receptor in wild-type HEK293 cells. This suggests that this technique is a relatively insensitive way of examining cellular signaling compared with the use of $Ca^{2+}$ indicators, where a robust increase in $Ca^{2+}$ can be measured in these cells on muscarinic $M_3$ receptor activation.
14. Ligand-binding and subsequent internalization is, of course, temperature-dependent. Internalization can be substantially reduced by lowering the temperature to less than 16°C. For receptor–ligand combinations where internalization is extremely rapid, making initial visualization of plasma membrane-located fluorescence difficult, the temperature can be kept low (<16°C), using for example a Peltier device, to allow initial image-capture, followed by an increase in temperature during the monitoring of internalization.
15. As with many ligands, the binding of a fluorescently labeled ligand may include a nonspecific component. Indeed many fluorophores are lipophilic and have the possibility of anchoring within the plasma membrane. Such lipophilic properties of the fluorescently labeled ligand and any nonspecific binding can be determined by pre-treating cells with maximal concentrations of other agonists or antagonists for the receptor of interest prior to the addition of the fluorescent ligand. If parental cells are available that do not express the receptor under study, these can also provide excellent controls for nonspecific binding. For example, we have established that parental HEK293 cells that do not express NmU receptors show no detectable fluorescence following the addition of Cy3B-pNmU-8. Furthermore, membrane-associated fluorescence following addition of Cy3B-pNmU-8 is blocked in cells expressing NmU receptors by the pre-addition of a supramaximal concentration (1 $\mu M$) of unlabeled NmU.
16. The concentration of ligand used depends on a number of parameters including: its affinity for the receptor, the level of receptor expression, the fluorescence intensity of the fluorophore, and the sensitivity of the confocal system. For example, we have used a concentration of Cy3B-pNmU-8 (10 n$M$) that will give maximal recep-

tor occupancy. Binding to the cells is easily visible and requires a laser intensity that does not result in rapid and extensive photobleaching (*see* **Note 3**).

17. It is common to lose some cells during washing. The strength at which cells adhere to the cover slip is affected by factors including cell type, the presence of a substratum (e.g., poly-D-lysine), and the amount of time the cells have been left to adhere. Generally, for fluorescence confocal microscopy, cell loss before the experiment has no adverse effect on the experimental outcome because investigations are made at the single-cell level. This can, however, influence the number of cells in the field of view. It is desirable to have a good number of cells (e.g., >5) per field of view. However, cell loss and particularly cell movement can affect later quantification and vigilance throughout an experiment is required.
18. The rate of perfusion required will depend on the bath volume. As an example, we have successfully used a rate of 5 mL/min with a bath volume of approx 0.5 mL and have found this suitable for addition and removal of agonists or test agents in functional studies, such as the measurement of $[Ca^{2+}]_i$. Bath applications are preferred if the ligand is either likely to stick to tubing or is in short supply/expensive. Some peptide ligands can be extremely "sticky" and can adhere to tubes and plastic-ware. This has the potential to affect the final concentration of ligand that reaches the cells. In addition, ligand may leach out of tubing onto cells during subsequent experiments. The inclusion of a carrier protein will help considerably. For NmU, we routinely use 0.01% BSA in the buffer.
19. Following a period of binding and/or internalization it may also be possible to remove a ligand bound to the outer surface of the plasma membrane to allow, for example, easier visualization of subplasmalemmal fluorescence and potential recycling of fluorophore from intracellular sites back to the plasma membrane. High-affinity ligands, such as Cy3B-pNmU-8, require an acid wash to promote dissociation from the receptor. This may be problematic if the acidity changes cellular morphology or influences activity within the endocytic pathway.
20. Direct comparison of images collected immediately after the addition of the fluorescent ligand and following a period to allow internalization will permit a qualitative assessment of internalization (**Fig. 3**). This may be adequate if experimental paradigms are being investigated that may, for example, block internalization. In addition, internalization can be assessed using analysis software. Such software is an integral part of the confocal microscope and permits a variety of on-line and off-line analysis tools that can measure changes in fluorescence. For example, a region of interest within a cell can be selected and changes in fluorescence determined as a function of time. An increase in cytosolic fluorescence will be indicative of ligand internalization. However, internalization most often results in the formation of sparsely distributed punctuate spots and the measurement of increases in cytosolic fluorescence may be a relatively insensitive method for assessing internalization. Alternatively, an area of membrane can be selected as the region of interest and the loss of membrane-associated fluorescence determined as an index of internalization. When measuring such changes, special consideration should be given to the possible contribution of photobleaching to the loss of fluorescence (**Note 3**). The

potential contribution of photobleaching can be assessed by performing the experiment under identical conditions of laser illumination but in which internalization is blocked either chemically or by low temperature. Such experiments can be used to set experimental parameters that minimize photobleaching and can provide data that can be subtracted from experimental data to assess internalization in the absence of an influence of photobleaching. GPCR internalization can be blocked by a variety of methods including hypertonic sucrose, phenylarsine oxide and concanavalin A. Internalization is also essentially blocked at temperatures below 16°C. This can be achieved with a Peltier unit and is a relatively simple method for confocal microscopy. Again, it must be remembered that the technique as described determines the localization of fluorescent ligand. At any one time this may reflect a dynamic equilibrium between extracellular ligand and ligand located within different subcellular compartments. Further, it may not wholly reflect receptor trafficking ***(32)***.

## Acknowledgments

The Wellcome Trust (Grant 061050), Biotechnology and Biological Sciences Research Council; Grants 91/C15897 and 01/A4/C/07909, and GlaxoSmithKline are thanked for financial support.

## References

1. Sheppard, C. J. R. and Shotton, D. M. (1997) *Confocal Laser Scanning Microscopy*. BIOS Scientific Publishers Limited, Oxford, UK.
2. Sheppard, C. J. R. (1999) Confocal Microscopy—principles, practice and options, in *Fluorescent and Luminescent Probes for Biological Activity* (Mason, W. T., ed.), Academic Press, London, UK, pp. 303–309.
3. Lipp, P. and Bootman, M. D. (1999) High resolution confocal imaging of elementary calcium signals in living cells, in *Fluorescent and Luminescent Probes for Biological Activity* (Mason, W. T., ed.), Academic Press, London, UK, pp. 337–343.
4. Berridge, M. J. (1997) Elementary and global aspects of calcium signaling. *J. Physiol.* **499,** 291–306.
5. Bootman, M. D., Berridge, M. J., and Lipp, P. (1997) Cooking with calcium; the recipes for composing global signals from elementary events. *Cell* **91,** 367–373.
6. Lipp, P., Laine, M., Tovey, S. C., et al. (2000) Functional $InsP_3$ receptors that may modulate excitation-contraction coupling in the heart. *Curr. Biol.* **10,** 939–942.
7. Grynkiewicz, G., Poenie, M., and Tsien, R. Y. (1985) A new generation of $Ca^{2+}$ indicators with greatly improved fluorescence properties. *J. Biol. Chem.* **260,** 3440–3450.
8. Minta, A., Kao, J. P., and Tsien, R. Y. (1989) Fluorescent indicators for cytosolic calcium based on rhodamine and fluorescein chromophores. *J. Biol. Chem.* **264,** 8171–8178.

9. Tsien, R. Y. (1980) New calcium indicators and buffers with high selectivity against magnesium and protons: design, synthesis, and properties of prototype structures. *Biochemistry* **19,** 2396–2404.
10. Tsien, R. Y., Pozzan, T., and Rink, T. J. (1982) Calcium homeostasis in intact lymphocytes: cytoplasmic free calcium monitored with a new, intracellularly trapped fluorescent indicator. *J. Cell Biol.* **94,** 325–334.
11. Thomas, D., Tovey, S. C., Collins, T. J., Bootman, M. D., Berridge, M. J., and Lipp, P. (2000) A comparison of fluorescent $Ca^{2+}$ indicator properties and their use in measuring elementary and global $Ca^{2+}$ signals. *Cell Calcium* **28,** 213–223.
12. Rizzuto, R., Pinton, P., Carrington, W., et al. (1998) Close contacts with the endoplasmic reticulum as determinants of mitochondrial $Ca^{2+}$ responses. *Science* **280,** 1763–1766.
13. Rudolf, R., Mongillo, M., Rizzuto, R., and Pozzan, T. (2003) Looking forward to seeing calcium. *Nature Mol. Cell Biol.* **4,** 579–586.
14. Pozzan, T., Mongillo, M., and Rudolf, R. (2003) Investigating signal transduction with genetically encoded fluorescent probes. *Eur. J. Biochem.* **270,** 2343–2352.
15. Miyawaki, A., Llopis, J., Heim, R., et al. (1997) Fluorescent indicators for $Ca^{2+}$ based on green fluorescent proteins and calmodulin. *Nature* **388,** 882–887.
16. Miyawaki, A., Griesbeck, O., Heim, R., and Tsien, R. Y. (1999) Dynamic and quantitative $Ca^{2+}$ measurements using improved cameleons. *Proc. Natl. Acad. Sci. USA* **96,** 2135–2140.
17. Baird, G. S., Zacharias, D. A., and Tsien, R. Y. (1999) Circular permutation and receptor insertion within green fluorescent proteins. *Proc. Natl. Acad. Sci. USA* **96,** 11,241–11,246.
18. Nagai, T., Sawano, A., Park, E. S., and Miyawaki, A. (2001) Circularly permuted green fluorescent proteins engineered to sense $Ca^{2+}$. *Proc. Natl. Acad. Sci. USA* **98,** 3197–3202.
19. Romoser, V. A., Hinkle, P. M., and Persechini, A. (1997) Detection in living cells of $Ca^{2+}$-dependent changes in the fluorescence emission of an indicator composed of two green fluorescent protein variants linked by a calmodulin-binding sequence. A new class of fluorescent indicators. *J. Biol. Chem.* **272,** 13,270–13,274.
20. Arnaudeau, S., Kelley, W. L., Walsh, J. V. Jr, and Demaurex, N. (2001) Mitochondria recycle $Ca^{2+}$ to the endoplasmic reticulum and prevent the depletion of neighbouring endoplasmic reticulum regions. *J.Biol. Chem.* **276,** 29,430–29,439.
21. Emmanouilidou, E., Teschemacher, A. G., Pouli, A. E., Nicholls, L. I., Seward, E. P., and Rutter, G. A. (1999) Imaging $Ca^{2+}$ concentration changes at the secretory vesicle surface with a recombinant targeted cameleon. *Curr. Biol.* **9,** 915–918.
22. Stauffer, T. P., Ahn, S., and Meyer, T. (1998) Receptor induced transient reduction in plasma membrane PtdIns(4,5)$P_2$ concentration monitored in living cells. *Curr. Biol.* **8,** 343–346.
23. Oancea, E., Teruel, M. N., Quest, A. F. G., and Meyer, T. (1998) Green fluorescent protein (GFP)-tagged cysteine-rich domains from protein kinase C as fluorescent indicators for diacylglycerol signalling in living cells. *J. Cell. Biol.* **140,** 485–498.

24. Nash, M. S., Young, K. W., Willars, G. B., Challiss, R. A., and Nahorski, S. R. (2001) Single cell imaging of graded Ins(1,4,5)$P_3$ production following G-protein-coupled-receptor activation. *Biochem. J.* **356,** 137–142.
25. Nahorski, S. R., Young, K. W., Challiss, R. A. J., and Nash, M. S. (2003) Visualizing phosphoinositide signalling in single neurons gets a green light. *Trends Neurosci.* **26,** 444–452.
26. Oancea, E. and Meyer, T. (1998) Protein kinase C as a molecular machine for decoding calcium and diacylglycerol signals. *Cell* **95,** 307–318.
27. Varnai, P., Rother, K. I., and Balla, T. (1999) Phosphatidylinositol 3-kinase-dependent membrane association of the Bruton's tyrosine kinase pleckstrin homology domain visualized in single living cells. *J. Biol. Chem.* **274,** 10,983–10,989.
28. Zaccolo, M., De Giorgi, F., Cho, C. Y., et al. (2000) A genetically encoded, fluorescent indicator for cyclic AMP in living cells. *Nat. Cell Biol.* **2,** 25–29.
29. Zaccolo, M. and Pozzan, T. (2002) Discrete microdomains with high concentration of cAMP in stimulated rat neonatal cardiac myocytes. *Science* **295,** 1711–1715.
30. Honda, A., Adams, S. R., Sawyer, C. L., Lev-Ram, V., Tsien, R. Y., and Dostmann, W. R. (2001) Spatiotemporal dynamics of guanosine 3',5'-cyclic monophosphate revealed by a genetically encoded, fluorescent indicator. *Proc. Natl. Acad. Sci. USA* **98,** 2437–2442.
31. Kallal, L. and Benovic, J. L. (2000) Using green fluorescent proteins to study G-protein-coupled receptor localization and trafficking. *Trends Pharmacol. Sci.* **21,** 175–180.
32. Koenig, J. A., Kaur, R., Dodgeon, L., Edwardson, J. M., and Humphrey, P. P. A. (1998) Fates of endocytosed somatostatin $sst_2$ receptors and associated agonist. *Biochem. J.* **336,** 291–298.
33. Awaji, T., Hirasawa, A., Kataoka, M., et al. (1998) Real-time optical monitoring of ligand-mediated internalization of $\alpha_{1b}$-adrenoceptor with green fluorescent protein. *Mol. Endocrinol.* **12,** 1099–1111.
34. Go, W. Y., Roettger, B. F., Holicky, E. L., Hadac, E. M., and Miller, L. J. (1997) Quantitative dynamic multicompartmental analysis of cholecystokinin receptor movement in a living cell using dual fluorophores and reconstruction of confocal images. *Anal. Biochem.* **247,** 210–215.
35. Maamra, M., Finidori, J., Von Laue, S., et al. (1999) Studies with a growth hormone antagonist and dual-fluorescent confocal microscopy demonstrate that the full-length human growth hormone receptor, but not the truncated isoform, is very rapidly internalized independent of Jak2-Stat5 signaling. *J. Biol. Chem.* **274,** 14,791–14,798.
36. Sneddon, W. B., Syme, C. A., Bisello, A., et al. (2003) Activation-independent parathyroid hormone receptor internalization is regulated by NHERF1 (EBP50). *J. Biol. Chem.* **278,** 43,787–43,796.
37. Daly, C. J. and McGrath, J. C. (2003) Fluorescent ligands, antibodies, and proteins for the study of receptors. *Pharmacol. Therapeut.* **100,** 101–118.

38. Miyawaki, A., Sawano, A., and Kogure, T. (2003) Lighting up cells: labelling proteins with fluorophores. *Nat. Cell Biol.* **Suppl.,** S1–S7.
39. Harlow, E. and Lane, D. (1988) *Antibodies – A Laboratory Manual*. Cold Spring Harbor Laboratory, Cold Spring Harbor, NY.
40. Mongan, L.C., and Grubb, B.D. (2004) Immunocytochemical identification of G-protein-coupled receptor expression and localization, in *Methods in Molecular Biology, vol. 259, Receptor Signal Transduction Protocols*, 2nd Ed. (Willars, G. B. and Challiss, R. A. J. eds.), Humana Press, Totowa, NJ, pp. 67–80.
41. Kao, J. P. Y. (1994) Practical aspects of measuring [$Ca^{2+}$] with fluorescent indicators, in *A Practical Guide to the Study of Calcium in Living Cells* (Nuccitelli, R., ed.), Academic Press, San Diego, CA, pp. 155–180.
42. Bader, J. E. and Beck-Sickinger, A. G. (2004) Fluorescence resonance energy transfer to study receptor dimerization in living cells, in *Methods in Molecular Biology, Vol. 259, Receptor Signal Transduction Protocols*, 2nd Ed. (Willars, G. B. and Challiss, R. A. J., eds.), Humana Press, Totowa, NJ, pp. 335–382.
43. Di Virgilio, F., Steinberg, T. H., and Silverstein, S. C. (1990) Inhibition of Fura-2 sequestration and secretion with organic anion transport blockers. *Cell Calcium* **11,** 57–62.
44. Tovey, S. C., de Smet, P., Lipp, P., et al. (2001) Calcium puffs are generic $InsP_3$-activated elementary calcium signals and are down-regulated by prolonged hormonal stimulation to inhibit cellular calcium responses. *J. Cell. Sci.* **114,** 3979–3989.
45. Mackenzie, L., Bootman, M. D., Laine, M., et al. (2002) The role of inositol 1,4,5-trisphosphate receptors in $Ca^{2+}$ signalling and the generation of arrhythmias in rat atrial myocytes. *J. Physiol. (London)* **541,** 395–409 .

# 5

# Single-Cell and Subcellular Measurement of Intracellular $Ca^{2+}$ Concentration

**Anthony J. Morgan and Andrew P. Thomas**

## 1. Introduction

### *1.1. Why Measure $Ca^{2+}$ at the Single-Cell Level?*

Measurement of the intracellular $Ca^{2+}$ concentration ($[Ca^{2+}]_i$) in populations of cells is an excellent tool to complement population measurements of other cell parameters, but the usefulness of this approach is limited by several problems, not the least of which is temporal averaging. In population studies, agonists often evoke a characteristic peak and plateau type of response irrespective of the stimulus intensity. However, equivalent experiments using single cells can often reveal exceedingly complex patterns, such as oscillations of the cytosolic $Ca^{2+}$ concentration ($[Ca^{2+}]_c$) ***(1)***. By and large these patterns cannot be observed in population studies since cells oscillate out of phase and at different frequencies, resulting in a smooth population average. It is only when cells are electrically well coupled that synchronized, population oscillations can be recorded, but this case is more the exception than the rule.

Temporal averaging will also distort the initial kinetics and peak responses to a given stimulus. In populations, the initial response to submaximal concentrations of agonist is influenced by several factors, such as the latency prior to the initial $[Ca^{2+}]_c$ response (which may vary considerably from cell to cell), the percentage of responding cells and cell to cell differences in sensitivity (which in turn may affect the degree of synchronization and magnitude). Furthermore, with population recording it is difficult to eliminate signals emanating from contaminating cell types or unhealthy cells.

There are also some technical advantages in measuring $Ca^{2+}$ at the single-cell level. For instance, such measurement facilitates microinjection, simulta-

From: *Methods in Molecular Biology, vol. 312: Calcium Signaling Protocols: Second Edition*
Edited by: D. G. Lambert © Humana Press Inc., Totowa, NJ

neous electrophysiological recording, and flash photolysis of caged compounds. Moreover, for those studying $[Ca^{2+}]_c$ in very large cells such as oocytes, single-cell recording has to be the method of choice because of optical limitations imposed by cell thickness.

### 1.2. Why Measure Subcellular $Ca^{2+}$ Responses?

Just as a population $[Ca^{2+}]_c$ recording reflects the average of heterogeneous single-cell responses, so the single-cell response reflects the averaging of heterogeneous subcellular events; it is merely the next level of organization. Such heterogeneity is presumably a consequence of a nonuniform distribution of channel and/or pump activity ***(2,3)*** giving rise to such complex spatial phenomena as the discrete $[Ca^{2+}]_c$ blips and puffs (quarks and sparks) ***(4)***, localized $[Ca^{2+}]_c$ oscillations ***(5)***, right through to full-blown propagating $[Ca^{2+}]_c$ waves (the spatial counterpart of an oscillatory spike) ***(1,4)***. Such rises in heterogeneous $[Ca^{2+}]_c$ have been proposed to afford the cell a means of locally regulating cellular events ranging from polarized fluid secretion, as in pancreatic acini ***(6)***, to the regulation of fertilization in oocytes ***(7)***.

In addition to specialized regions of the cytoplasm forming discrete units, it is now becoming increasingly clear that $Ca^{2+}$ levels fluctuate in a highly controlled manner in subcellular organelles. From the large nucleus ***(8)***, to the smaller mitochondria ***(9,10)*** and secretory vesicles ***(11)***, these membrane-delimited regions of the cell often respond to and in turn influence $[Ca^{2+}]_c$ in a dynamic manner in keeping with their physiological role. It is quite clear then that the $[Ca^{2+}]_i$ response of a cell is far from homogeneous, for which reason one has to examine the subcellular level in order to fully understand $Ca^{2+}$ homeostasis.

### 1.3. $Ca^{2+}$-Sensitive Fluorescence Imaging

The method of choice for monitoring single-cell $[Ca^{2+}]_i$ signals is that using $Ca^{2+}$-sensitive fluorescent probes that have been the subject of previous reviews ***(12,13)***. We shall, nevertheless, briefly discuss their essential features, drawbacks, and practical applications.

Simply stated, this technique relies on the introduction into the cell of a dye whose fluorescent properties change when it binds $Ca^{2+}$. Consequently, by monitoring the emitted light, one thereby monitors the free intracellular $Ca^{2+}$ concentration ($[Ca^{2+}]_i$). The recording of $[Ca^{2+}]_i$ is no different from any other biological assay with a stringent requirement for specificity, sensitivity over an appropriate concentration range (with a near linear output), and, preferably, a large signal-to-noise ratio (SNR). Usually, the modern $Ca^{2+}$-sensitive fluorescent dyes satisfy all of these criteria with the additional advantages of being readily available and easy to use (*see* **Note 1** and **Table 1**).

**Table 1**
**Properties of Commonly Used Low- and High-Affinity $Ca^{2+}$ Indicators**

| | Excitation λ (nm) | Emission λ (nm) | $K_d$ for $Ca^{2+}$ (μM) |
|---|---|---|---|
| Single λ (intensometric) dyes | | | |
| Fluo-3 | 490 | 525 | 0.4 |
| Fluo-3FF | 490 | 525 | 42 |
| Calcium Green-1 | 490 | 525 | 0.19 |
| Calcium Green-2 | 490 | 525 | 0.55 |
| Calcium Green-5N | 490 | 525 | 14 |
| Rhod-2 | 550 | 575 | 0.57–1.0[a] |
| Dual λ (ratiometric) dyes | | | |
| Dual excitation | | | |
| Fura-2 | 340/380 | 510 | 0.22 |
| Fura-2FF | 340/380 | 510 | 35 |
| Mag-fura-2 (furaptra) | 340/380 | 510 | 53 |
| BTC | 480/400 | 540 | 7 |
| Dual emission | | | |
| Indo-1 | 355 | 405/485 | 0.25 |
| Mag-indo-1 | 355 | 405/485 | 35 |

[a] The affinity of rhod-2 for $Ca^{2+}$ is controversial with recent improvements in its purification suggesting a higher affinity than first thought.

## *1.4. Principles of Loading Cells With Fluorescent Dyes*

### *1.4.1. Esterified Dyes*

#### 1.4.1.1. Cytosolic Loading

The most common application of the $Ca^{2+}$-sensitive dyes is to measure $[Ca^{2+}]_c$ in cells loaded with esterified dyes. The whole process of loading the cell cytosol with BAPTA-based dyes is, in principle, extremely simple because of their availability as acetoxymethyl (AM) esters. By masking the four negatively charged carboxyl groups, the ester moieties render the compound cell permeant, and the modified dye readily enters the cell. Once inside, endogenous esterases remove the ester groups, restoring the hydrophilic nature of the dye and thereby trapping the functional dye inside the cell. Consequently, loading is achieved by the simple process of incubating the cells with AM esters for a defined period. This process can concentrate the dye to such an extent that the final intracellular concentration can exceed 100 times the initial extracellular concentration of AM esters. However, bear in mind that deesterification proceeds as a stepwise process and, as such, intermediate, partially hydrolyzed fluorescent species can be generated. Although these species contribute to the fluorescence emission from the cell, they generally do not respond to $Ca^{2+}$, meaning

that they reduce the $Ca^{2+}$-dependent dynamic range and result in errors in the calibration (*see* **Subheading 1.5.**). Sufficient time must, therefore, be set aside after loading to allow for complete deesterification.

In addition, the hydrophobic AM ester tends to form micelles in solution that indiscriminately permeate cellular membranes, and hence pass readily into organelles in which they can be hydrolyzed and report $[Ca^{2+}]$. Thus, the relative activity of the esterases found in cytosolic or other compartments will ultimately determine the distribution of reporting dye. This compartmentalization of dye presents problems when the investigator only wishes to monitor $[Ca^{2+}]_c$ since the signal arises from multiple compartments that may not respond in the same manner.

#### 1.4.1.2. Organellar Loading

Although dye compartmentalization presents a serious problem when monitoring $[Ca^{2+}]_c$ changes, this "drawback" can be turned to advantage since it provides a method of measuring intraorganellar $Ca^{2+}$ changes as long as appropriate conditions and dyes are used. Note, however, that "targeting" the AM ester form of $Ca^{2+}$ indicators to specific intracellular organelles is currently more an art than a science because we do not fully understand why some organelles accumulate more dye than others in a given cell type. Whereas some cellular systems prove to be excellent models for measuring $Ca^{2+}$ concentrations in particular organelles, others display a frustrating resistance to load with dye into the compartment of choice. Consequently, one should always empirically test in which compartment the dye resides. The following merely provides a few basic guidelines.

*1.4.1.2.1. Endoplasmic Reticulum ($Ca^{2+}$ Stores).* Since the free $Ca^{2+}$ concentration of the store lumen ($[Ca^{2+}]_L$) is high (estimates range from 12 μ*M* to several millimolar ***[14]***), the most commonly used high-affinity dyes such as fura-2 ($K_d \approx 0.2$ μ*M*) will be insensitive to lumenal fluctuations. In light of this, many investigators have exploited low-affinity $Ca^{2+}$ dyes such as mag-fura-2, mag-indo-1, and fura-2FF for $[Ca^{2+}]_L$ measurements ($K_d$s range from 35 to 50 μ*M*), with the latter having the added advantage of being more $Ca^{2+}$ selective. High concentrations of indicator AM esters together with loading at 37°C can promote compartmentalization into stores, whether exclusively ***(15)*** or, as is more common, into both stores and cytosol (necessitating elimination of the contaminating cytosolic signal ***[16,17]***).

*1.4.1.2.2. Mitochondria.* In contrast to the ER $Ca^{2+}$ dynamics, changes in the mitochondrial $Ca^{2+}$ concentration ($[Ca^{2+}]_{mito}$) have been estimated to be in the low micromolar range ***(9)***, which means that high-affinity indicators are more suitable. Rhod-2 ($K_d$ 0.5–1 μ*M*), unlike the other fluorescent $Ca^{2+}$ indicators, has a net positive charge in the AM ester form and thereby accumulates

into mitochondria as a function of the mitochondrial membrane potential. With some cell preparations, loading is, fortuitously, exclusively mitochondrial, whereas others give a mixed compartment loading. When the latter occurs, one approach is to allow cytosolic rhod-2 to be actively extruded from the cell after AM ester loading, leaving behind the rhod-2 trapped in the mitochondria ***(10)***. Another approach designed to increase the specificity of mitochondrial targeting is to load cells with the AM ester form of $Ca^{2+}$-insensitive dihydro-rhod-2, the rationale being that its conversion to $Ca^{2+}$-sensitive rhod-2 occurs primarily in the oxidizing environment of the mitochondrion ***(18)***. Rhod-2 is not, however, the only dye to load into mitochondria, as evidenced by $[Ca^{2+}]_{mito}$ recording using fura-2 ***(19)***. Again it depends on the relative ester activities and/or protocols for circumventing cytosolic contamination.

### *1.4.2. Free-Acid Form of Dyes*

There are times when it may be more appropriate to introduce the free-acid form of the dye directly into the cell (using microinjection, via a patch pipet or reversible electroporation). This need may arise either because of problems with compartmentalization or because of the chemical nature of the dye (large mass, or extreme hydrophobicity). Many of the $Ca^{2+}$ indicators are now available conjugated to large inert dextrans (from 5000 to 500,000 $M_r$), which lowers their diffusional mobility and reduces movement between different cellular compartments (e.g., nucleus and cytosol), as well as eliminates loss from the cell over prolonged incubation periods.

In addition to attachment to dextrans, peptide conjugation provides an elegant way of targeting free-acid indicators to specific subcellular locales. Examples of the latter approach are "Nuclear Calcium Green Dextran" targeted to the nucleoplasm by a nuclear localization signal peptide ***(20)*** and "CAAX Green" targeted to internal membranes by virtue of endogenous isoprenylation of a consensus sequence peptide ***(21)***. Another class of so-called near-membrane dyes have been designed that have extended carbon chain tails, anchoring them to lipid bilayers, albeit indiscriminately (e.g., fura-$C_{18}$, Calcium Green-$C_{18}$, FFP-18) ***(22–25)***. Their hydrophobicity is such that they preferentially bind to the extracellular surface rather than permeate the plasma membrane ***(25)***, and therefore their loading into the cell interior has to be effected by a patch pipet.

## *1.5. Calibration of Fluorescence Signals*

Quantitation of fluorescence changes in terms of absolute $[Ca^{2+}]_i$ is both the joy and the burden of $Ca^{2+}$ imaging. In theory it is relatively straightforward to make such a conversion based on a prior knowledge of the dye's characteristics, but therein lies the problem: one has to make the assumption that the prop-

erty of the dye in free solution mirrors that of the dye in the cellular environment, which is not necessarily the case. Nevertheless, careful calibration can provide a reasonable estimate of the $[Ca^{2+}]_i$ changes, even if the absolute values should be treated with some degree of latitude.

### 1.5.1. Principles Underlying Calibration of $[Ca^{2+}]_i$ Signals

Calibration is the process of converting the fluorescence signal into an absolute $[Ca^{2+}]$. Since $Ca^{2+}$ binds to the BAPTA-based indicators with a 1:1 stoichiometry (according to the law of mass action, a normal single-site binding isotherm equation can be used to describe the relationship between free $[Ca^{2+}]$ and the fluorescence signal, be it raw fluorescence intensity for single λ [intensometric] dyes, or ratio for dual λ [ratiometric] dyes). Clearly then, the relationship between $[Ca^{2+}]$ and fluorescence is not linear, which necessitates calibration.

### 1.5.2. Single Wavelength Dyes

$$[Ca^{2+}] = [(F - F_{min})/(F_{max} - F)] \cdot K_d$$

In **Equation 1**, $[Ca^{2+}]$ represents the $Ca^{2+}$ concentration calculated for the fluorescence $F$ at any time; $F_{min}$ and $F_{max}$ are the minimum and maximum fluorescence, respectively; and $K_d$ is the dissociation constant of the indicator.

For a single λ indicator, the simple relationship in **Equation 1** applies. The minimum and maximum fluorescence values represent the limits imposed by the dynamic range of the dye as determined in the absence of $Ca^{2+}$ and in the presence of saturating levels of $Ca^{2+}$, respectively. When calculating $[Ca^{2+}]$, a $K_d$ should be chosen that was determined under the conditions of temperature and ionic composition that most closely mimic the experiment. Calibration simply involves determining these minimum and maximum fluorescence values since the $K_d$ is a known constant.

To calibrate single-cell fluorescence $[Ca^{2+}]_i$ values, an *in situ* calibration has to be effected with the dye trapped inside the cell. (Because fluorescence is also proportional to the dye concentration it is impossible to mimic this in a cell-free system, and the lysis technique is inappropriate since dye will be lost from the recording area.) This is advantageous since it means that the calibration of the dye is carried out in precisely the same environment as in the experimental run. For fluo-3 (with a $K_d$ approx 0.4 μ*M*), the $Ca^{2+}$ ionophore, ionomycin, is usually used to equilibrate extracellular $Ca^{2+}$ concentration across the plasma membrane with the cytosol: for $F_{min}$ this is carried out in the absence of $Ca^{2+}$ and the presence of EGTA, whereas for $F_{max}$ the extracellular medium contains high $Ca^{2+}$ concentration.

This approach works reasonably well with fluo-3 since its $Ca^{2+}$-free fluorescence is very low and its affinity means that it is relatively easy to attain the 5–10 μ*M* $[Ca^{2+}]_i$ needed to saturate the dye. However, for other dyes (especially those with a higher $K_d$), this approach may overestimate the $[Ca^{2+}]_i$ values because there is now good evidence that ionomycin does not efficiently equilibrate $[Ca^{2+}]$ across membranes either *in situ* or in vitro ***(26,27)***, leading to spurious $F_{min}$ and $F_{max}$ values.

### *1.5.3. Dual Wavelength Dyes*

$$[Ca^{2+}] = [(R - R_{min})/(R_{max} - R)] \cdot K_d \cdot (S_{f2}/S_{b2})$$

In **Equation 2**, $R$ represents the ratio of the two wavelengths at any time; $R_{min}$ and $R_{max}$ are the minimum and maximum ratio values, respectively (determined in the absence of $Ca^{2+}$ and in the presence of a saturating concentration of $Ca^{2+}$); and $K_d$ is the dissociation constant of the dye. The expression $s_{f2}/s_{b2}$ (also known as β) refers to the denominator wavelength (i.e., at 380 nm for fura-2 using a 340/380 excitation ratio) as the ratio of the fluorescence in the $Ca^{2+}$-free and $Ca^{2+}$ bound forms. Note that the final units of $[Ca^{2+}]$ will be identical to those used for the $K_d$ since the other two fractions are unitless.

With dual λ indicators, the ratio of two wavelengths is related to $[Ca^{2+}]$ by a similar equation (**Equation 2**) ***(28)***. The great advantage of the ratio technique is that factors such as path length, dye concentration, and instrument sensitivity all cancel out in the final calculation, which makes it possible to avoid tedious *in situ* calibrations. Instead, one calibrates the *hardware* using the free-acid form of the indicator in an in vitro buffer system; similar to **Equation 2**, $R_{min}$ and $R_{max}$ are measured in the absence of $Ca^{2+}$ and in the presence of saturating levels of $Ca^{2+}$. Under these conditions, $s_{f2}$, and $s_{b2}$, respectively, are automatically determined, which makes for a rapid and straightforward process. Normally, this calibration is performed on a day-to-day basis and is particularly crucial when there has been a change in the optical components of the system.

Note, however, that in spite of the fact that the *in vitro* calibration is common practice, it does not take into account subtle effects of the intracellular environment on the dye properties (e.g., viscosity, binding of dye to proteins ***[29]***). To compensate for these effects, in vitro buffers can be modified (e.g., 10% glycerol increases viscosity ***[29]***), or, alternately, $R_{min}$ and $R_{max}$ and β can be determined *in situ* using the ionophore approach described above for single λ dyes.

### *1.5.4. $Ca^{2+}$-Insensitive Fluorescence: Autofluorescence and Compartmentalized Dye*

It should not be assumed that fluorescence emanating from the cell is only derived from a $Ca^{2+}$-sensitive indicator. Owing to the presence of endogenous

molecules that fluoresce, the detected signal will be contaminated to some degree by "autofluorescence" and needs to be accounted for if calibration is to be accurate. How much the autofluorescence contributes to the overall signal depends upon the wavelengths recorded and the cell type. For instance, at the wavelengths commonly used for fura-2 measurements ($\lambda_{ex}$ 340–380 nm; $\lambda_{em}$, 420–600 nm), pyridine nucleotides (NAD(P)H) contaminate fluorescence, whereas flavoproteins are excited at longer wavelengths ($\lambda_{ex}$ 430–500 nm; $\lambda_{em}$, 500–650 nm) and will affect measurements using visible dyes such as fluo-3. Indeed, in hepatocytes, pancreatic β-cells, and adrenal glomerulosa cells, the concentration of these nucleotides is substantial enough to allow the fluctuations in their levels to be fluorescently monitored during $[Ca^{2+}]_i$ spiking ***(10,30)***. However, for most cell types, the weak autofluorescence remains a relatively constant and minor (but significant) percentage of the total signal.

When using in vitro calibration values, the cell-derived autofluorescence is subtracted at the end of the experimental run before converting the ratio to $[Ca^{2+}]_i$. To reveal the autofluorescence value in cells already loaded with a ratiometric indicator, the signal from the dye has to be eliminated; this is most readily achieved by incubating the cells in the presence of $Mn^{2+}$ and ionomycin (to facilitate $Mn^{2+}$ entry). When $Mn^{2+}$ binds to some BAPTA-based dyes (particularly the UV dyes fura-2 and indo-1, but not visible dyes such as fluo-3), it results in a complete quenching (elimination) of the fluorescence at all wavelengths, thereby allowing the residual autofluorescence to be determined.

As stated already, for accurate calibration, one must subtract all $Ca^{2+}$-insensitive fluorescent signals. Therefore, in addition to the autofluorescence, the signal from any $Ca^{2+}$-insensitive dye component should also be subtracted. One such circumstance is when high-affinity $Ca^{2+}$ indicator is compartmentalized into the high-$[Ca^{2+}]$ environment of the $Ca^{2+}$ store in which it will remain saturated and effectively $Ca^{2+}$-insensitive under most physiological conditions. Since ionomycin should allow $Mn^{2+}$ access to dye in all compartments including the stores, it should not be used to determine the $Ca^{2+}$-insensitive fluorescence when there is substantial compartmentalization. Instead, permeabilization of the plasma membrane with digitonin gives a better estimate since it will release cytosolic dye, leaving the mitochondrially derived autofluorescence and compartmentalized dye behind. (It should be ensured that stores be full of $Ca^{2+}$; otherwise this background fluorescence will not be the same as in the intact cell.) However, this is not as gentle as the ionomycin approach and changes in cell shape on permeabilization can lead to problems.

## 2. Materials

1. Fluorescent indicators. These compounds are normally stored desiccated at –20°C for many months. The free-acid forms of the dyes are soluble in water and are

prepared as 1–10 m*M* stocks, whereas the AM esters are normally dissolved in dry dimethysulfoxide (DMSO) at 1 m*M*. Dextran-conjugated dyes are water soluble, but their solubility is inversely proportional to their $M_r$ so it is advisable to follow the manufacturer's guidelines. All stock solutions are stored frozen. To minimise excessive cycles of freeze-thawing, which results in indicator deterioration, stocks should be aliquoted into smaller volumes or purchased in a "special packaging" form in which multiple vials contain small amounts of indicator (e.g., $20 \times 50$ μg). As with the powder form, stocks prepared in hygroscopic DMSO should be desiccated because of their susceptibility to hydrolysis with time. On the day of use, aliquots are thawed and stored on ice and protected from light. DMSO stocks are stable for several weeks with proper storage. (Sources: Molecular Probes, Sigma, Texas Fluorescence Labs (Teflabs) and Calbiochem/Novabiochem.)

2. The nonionic surfactant Pluronic F-127 (free of charge with orders from Molecular Probes) is prepared as a 10% (w/v) solution in DMSO. The solution may be gently warmed to facilitate solubility, and can be stored at room temperature for several weeks.
3. Digitonin is prepared as a 10 mg/mL stock in water. Like Pluronic F-127, the solution should be gently heated to facilitate solubility, and can be stored at room temperature for several weeks.
4. The protease inhibitors leupeptin, antipain, and pepstatin are all prepared as 5 mg/mL stock solutions. Pepstatin is soluble in DMSO whereas the others are prepared in water. These solutions are aliquoted, frozen, and can be stored for a few weeks.
5. MgATP is prepared as a 200 m*M* stock in water and stored frozen for several months. Note that addition to intracellular-like medium (ICM) in this form does not cause pH changes, but stocks should be adjusted to pH 7.2 (with Tris base) when ATP-free acid is favored.
6. Ins(1,4,5)$P_3$ is made as an aqueous solution up to 5 m*M* concentration and aliquots are stored frozen for months at a time.
7. Endothelial balanced salt solution (EBSS): 145 m*M* NaCl, 5 m*M* KCl, 1 m*M* $MgCl_2$, 1 m*M* $CaCl_2$, 10 m*M* HEPES, 10 m*M* glucose, 1% (v/v) bovine serum albumin (BSA), pH 7.4.
8. Hepatocyte balanced salt solution: 121 m*M* NaCl, 4.7 m*M* KCl, 1.2 m*M* $MgSO_4$, 2 m*M* $CaCl_2$, 25 m*M* HEPES, 1.2 m*M* $KH_2PO_4$, 5 m*M* $NaHCO_3$, 10 m*M* glucose, 1–2% (w/v) BSA, pH 7.4.
9. Intracellular medium (ICM): 10 m*M* NaCl, 120 m*M* KCl, 20 m*M* HEPES, 1 m*M* $KH_2PO_4$, pH 7.2 (*see* **Notes 2–4**).
10. Calibration buffer: 10 m*M* NaCl, 120 m*M* KCl, 1 m*M* $MgCl_2$, 20 m*M* HEPES, 200 m*M* EGTA, pH 7.2.

## 3. Methods

### *3.1. Instrumentation*

A single-cell imaging setup can be thought of as an elaborate fluorimeter in which the sample sits on a microscope instead of in a cuvet, but which other-

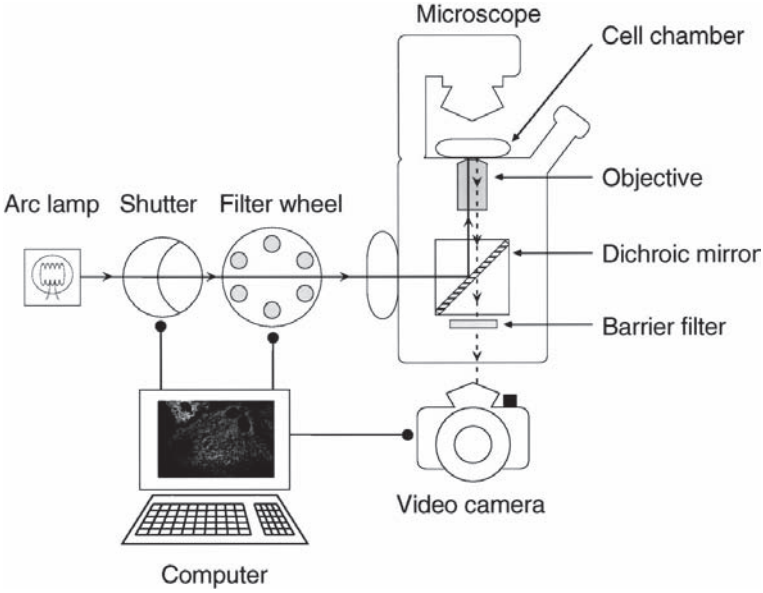


Fig. 1. Schematic representation of a typical $Ca^{2+}$-imaging setup as detailed in **Table 2**.

wise retains the essential components such as excitation light source, wavelength selection devices, and a photosensitive detector for the emitted light. However, the sophistication and cost of a single-cell setup generally exceeds the requirements for crude population measurements, necessitating additional components such as an epifluorescent microscope, dichroic mirrors, and high-sensitivity detectors. A schematic representation of an epifluorescent microfluorimeter is depicted in **Fig. 1**.

### *3.1.1. Microscope*

An epifluorescent microscope differs from other conventional microscopes in several features: an epifluorescent port at the rear that allows introduction of exciting light, and a housing for dichroic mirrors opposite the port and below the objective to reflect light onto the sample. Both upright and inverted microscopes can be used, but in practice the inverted configuration displays many advantages: e.g., cells can be superfused while allowing a short working distance objective to be used, which offers superior optical properties, and the simultaneous use of micropipets is not hindered by the objective, as is the case with the upright microscope. Nevertheless, a long working distance condensor is required to achieve good access to the cells in the inverted microscope configuration.

### *3.1.2. Optics*

The most crucial elements that determine signal quality are the optical properties of the microscope components (especially of the objective) and the nature of the detector. The very fact that many fluorescent indicators are excited in the near UV means that the objective should ideally transmit light down as low as 340–350 nm, e.g., to facilitate ratiometric recording using fura-2. Since quartz objectives are very costly, most workers utilize the less expensive "fluor" nonquartz counterparts, which generally prove more than adequate. Given that the transmitting properties of the objective decreases with the square of the magnification factor, it is advisable to use as low a magnification objective as possible that still gives sufficient resolution. Another important consideration is the numerical aperture (NA) of an objective, which is an index of its light-transmitting properties (the higher the number the more efficient the light transmission). Use of immersion objectives also increases the effective NA, in which an immersion fluid of higher refractive index than air is placed between the objective and the cover slip. Consequently, an objective of high NA will tend to overcome the loss of signal associated with high magnification.

### *3.1.3. Incubation Chamber*

Once cells are loaded with dye, they are mounted in a suitable incubation chamber that sits on the microscope stage. For an inverted configuration, the base of the chamber is usually formed by the glass cover slip itself (no. 1 thickness) to which the cells have previously adhered. Many chamber designs are commercially available, depending on the requirement for access. Open chambers allow microelectrode access and/or manual addition of agents. On the other hand, closed chambers are more conducive to cell superfusion with a laminar flow. Incidentally, superfusion is best effected with a gravity-fed system that circumvents the pulsatile shearing of peristaltic pumps. In addition to housing the cover slip, the chamber serves as the temperature regulator, in which a specialized, regulated heating element in the chamber precisely controls the bath temperature; feedback temperature control is utilized to avoid the undesirable heating and cooling cycles associated with normal thermostats. The temperature of the sample is also affected by the objective itself, which acts as a heat sink. To minimize this problem, the lens can be jacketed with coils of copper or plastic tubing through which water circulates at the specimen temperature.

### *3.1.4. Excitation*

As mentioned above, each fluorescent indicator is excited by and emits light at characteristic wavelengths. The excitation light is provided by a broad spec-

trum source (typically a 75 W xenon lamp) whose output is then narrowed to the wavelengths of choice by one of two methods. One approach is to use a monochromator, which, although costly, is extremely flexible since it can precisely (±1 nm) select any wavelength across the spectrum, using a series of diffraction gratings. Normally this process is relatively slow unless direct motor-driven gratings are used, which allows rapid alternation between wavelengths (within a few milliseconds). Alternatively, a series of appropriate interference filters placed in the light path will serve the same purpose, although without the precision (a bandwidth of ±5 nm is common) or flexibility (each wavelength requires a different filter). However, for most applications the filter system is sufficient and, since it is the more commonly used, will be elaborated on here.

When using intensometric (single λ) dyes (e.g., fluo-3), or dual-emission dyes (e.g., indo-1), a single interference filter placed in the excitation light path makes for the simplest system. However, when dual-excitation dyes (e.g., fura-2) or when simultaneously recording multiple dyes (e.g., fura-2 and rhod-2) are used, one has to alternate rapidly between different excitation wavelengths. To achieve this, a filter wheel system is used with several interchangeable filters that can be rotated to bring the appropriate filter into the light path in a synchronized fashion. In a photomultiplier tube-based system, a rapidly and continuously rotating wheel can allow multiple excitations up to a 50–200 Hz rate. On the other hand, imaging systems utilize a discontinuous rotating wheel system that simply flips between filter positions as required. To prevent burning out filters and/or photobleaching of cells between exposures, a computer-controlled shutter is placed between the filter wheel and the light source. In addition to the interference filter wheel, a second wheel containing a range of neutral density filters can be used to individually regulate the excitation intensity of each wavelength.

As more components are introduced into the system, the potential maximum rate of acquisition will decrease. Therefore, the collection rate for a single-wavelength excitation photometric system will only be limited by the SNR. With indo-1, rates up to 500 Hz are possible since there is no requirement for moving parts to select wavelengths, which otherwise slows down acquisition times. By contrast, a photometric system using a spinning filter wheel has an upper limit of 50–200 Hz governed by the rotation rate of the wheel. On the other hand, imaging-based systems will be slowed down by the movements between filter positions and the additional shutter open/close time. Together with the readout time of the camera, full video rate (25–30 Hz) currently represents the typical maximum rate for single-wavelength recording.

### *3.1.5. Emission*

Having selected the excitation wavelength(s), one has to define the emission wavelength(s). Unlike a simple cuvet, the excitation and emission light paths are partially shared in the inverted epifluorescent microscope; i.e., they both pass through the objective. In essence, the excitation light entering the rear of the microscope via the epifluorescence port is reflected into the objective (and then to the sample) via a dichroic mirror, also known as a dichroic beam splitter. Part of the emitted light (which is given out in all directions) passes back into the objective, through the dichroic mirror and eventually passes into the port housing the detector. Therefore, one crucial component determining the emission wavelength will be the dichroic mirror itself.

In its simplest form, a single dichroic mirror reflects the (excitation) light shorter than a predetermined wavelength, whereas the (emitted) light above this threshold wavelength passes through. This means that the cutoff of the dichroic mirror clearly has to be higher than the excitation wavelengths to prevent exciting light passing directly to and swamping the detector. Although the emission wavelength is primarily dictated by the dichroic mirror cutoff, another filter is often placed below the dichroic mirror to provide a more precise and additional safety margin. This filter may be either a long-pass (LP) filter (allowing all light above a certain wavelength to pass) or a narrow band-pass filter allowing light to pass within a certain range of wavelengths (i.e., it is an LP filter with an upper limit). Clearly, since emitted light is at a premium, it is preferable to collect across as broad a spectrum as possible. Therefore, for imaging with fura-2, one might use 340 and 380 nm excitation filters with a 400-nm dichroic mirror fitted with a 420-LP filter.

To measure multiple dyes whose spectra are sufficiently separated so that there is little cross over, a double dichroic mirror is often required. Unlike simple dichroic mirrors, which have one single threshold above which light is transmitted, double dichroic mirrors allow light to pass within two discrete bands, so there are effectively two thresholds at different parts of the spectrum. The nontransmitting, reflecting bandwidth between these regions permits use of another excitation filter. Again, a band-pass filter is placed after the dichroic mirror for better control, as for single dichroics, although in this instance it would be a double bandpass, defining two spectral regions. For example, for simultaneous fura-2 and rhod-2 measurements; fura-2 is excited at 340/380 nm and emission is measured approx 510 nm, and rhod-2 is excited at 548 nm with emission centered on 590 nm.

For dual-emission dyes such as indo-1, the emission wavelength selection is more complex. Although the geometry of the microscope requires a dichroic mirror irrespective of the dye's characteristics, this time the dichroic mirror is not the main emission wavelength determinant. Rather, the filters placed after

the dichroic mirror are the more important factor. A setup with a beam splitter and two detectors would have separate band-pass filters dedicated to each one (e.g., 405 and 495 nm for indo-1). Given the expense of using two cameras for imaging indo-1, it is more realistic to have one camera with a filter wheel selecting the *emission* filters positioned immediately next to it.

### *3.1.6. Detectors*

The choice of the type of detector for conventional epifluorescence measurements is essentially between photomultiplier tube (PMT) or high-sensitivity camera.

#### 3.1.6.1. Photometric Recording

The advantages of a photometric or PMT-based system are as follows:

1. It is relatively cheap.
2. Its potential for very rapid data acquisition rates.
3. It places little demand on computer memory and data storage.
4. The dynamic range and sensitivity are greater than most camera-based systems.

On the other hand, the primary disadvantages are that only one single cell can be monitored per run and that spatial information is lost in the global cell signal. The geometry of a standard epifluorescent microscope is such that the emitted light from a large fraction of the field of view is sent to the detector port, which means that the signal would be derived from many cells (when using a 20× or 40× objective). To record exclusively from one cell (or even part of a cell), an adjustable aperture or diaphragm is placed immediately before the PMT; thus, with the aid of a side ocular, the investigator can choose to record from a small region of the field of view while the remainder of the field is masked and does not contribute to the fluorescence signal.

#### 3.1.6.2. Imaging

As prices lower and sensitivity increases, epifluorescent camera-based setups are becoming more routinely used for single-cell analysis. The most commonly used camera is a solid-state cooled charge-coupled device (CCD), which provides a reasonable compromise between speed of acquisition and signal sensitivity. At either extreme, "intensifier" cameras are capable of rapid imaging (but with more noisy images), whereas "slow scan" cameras offer superior quality at the expense of speed. Available with microprocessors capable of digitizing images from 8-bit resolution per pixel through to the superior 12-, 14-, or even 16-bit resolution, CCD cameras have been successfully used to monitor subcellular events such as waves, localized oscillations and even more elemental release units.

The pros and cons of using an imaging system are precisely the reverse of those for the photometric system; i.e., its advantages lie in being able to monitor

**Table 2**
**Example of Components Used in a High-Resolution Imaging System That Does Not Employ a Supplementary Frame Grabber**

| Microscope | Nikon diaphot epifluorescent |
|---|---|
| Cell chamber/thermostat | PDMI-2 open perfusion microincubator/TC-202 bipolar temperature controller (Medical Systems, Greenvale NY) |
| Dichroic beam splitter | 400 DM, plus 420 LP filter (Nikon) |
| Camera | Photometrics PXL slow scan cooled CCD, 14 bit (Tucson, AZ) |
| Filter wheel control | Ludl Electronic Products (Hawthorne, NY) |
| Shutter | Uniblitz (Rochester, NY) |
| Computer | Power PC Macintosh (32 MB RAM) |
| Software | Custom written (Paul Anderson, Thomas Jefferson University) |

more than one single cell simultaneously (desirable when there is considerable cell-to-cell heterogeneity) together with little loss of subcellular spatial information when conditions are optimized (*see* **Subheading 3.5.2.**). However, this does require considerable financial outlay, not only for the camera but also for an adequate computer to cope with acquiring and analyzing large imaging files. This accrual of large amounts of data is another practical reason that routine collection rates tend to be slower than the equivalent photometric recordings.

The *spatial* resolution of the CCD camera is directly proportional to the number of pixels per image as defined by the camera's microprocessor. Under conditions in which the signal is weak, and/or spatial resolution is less critical, some cameras offer a "binning"facility, which allows adjacent pixels to be combined into a brighter "super" pixel. This also has the advantage of enhancing the readout time of the chip. The *temporal* resolution of the camera, on the other hand, is primarily determined by the processor readout time and digitization process; i.e., times of 40–2000 ms are typical.

The primary sources of noise for CCD cameras derive from photon-dependent and -independent sources. The former is statistical noise related to the square root of the light intensity, whereas the latter encompasses such phenomena as thermal noise (the dark current) and the readout noise. Since these parameters are light independent, they are relatively constant and will contribute proportionately less to the signal emanating from bright samples; clearly, low-intensity signals will be more heavily contaminated. Lowering the camera temperature reduces the dark current to a very low level and this may be achieved with thermoelectric cooling or even liquid nitrogen.

A typical setup we have in our laboratory to ratiometrically record using fura-2 is illustrated in **Table 2**.

### *3.2. Intracellular Loading of Fluorescent Indicators* (see **Note 5**)

#### *3.2.1. Cytosolic $Ca^{2+}$ ($[Ca^{2+}]_C$) Measurement: Loading Cells With Fura-2/AM*

##### 3.2.1.1. Human Umbilical Vein Endothelial Cells

1. Cell monolayers attached to 24-mm diameter circular no. 1 glass cover slips for 2–5 d are maintained in 30-mm diameter tissue culture grade plastic Petri dishes in 2 mL of culture medium.
2. Loading solution: 80% (v/v) HEPES-buffered Dulbecco's modified Eagle's medium plus 20% (v/v) fetal calf serum containing 1 μ*M* fura-2/AM.
3. Simultaneously load three to five dishes, by removing the culture medium and replacing with 1 mL of loading solution per dish, covering to protect from light and incubating for 30–45 min at room temperature.
4. After the loading period, loading solution is removed and cells are gently washed twice with and then maintained in 2 mL of EBSS at room temperature until use.
5. Cells are left for at least 20 min after loading to facilitate complete deesterification and used within 2 to 3 h after loading.

##### 3.2.1.2. Primary Rat Hepatocytes

1. Cells are seeded overnight onto round polylysine-coated glass cover slips in 2 mL of culture medium.
2. Loading solution: hepatocyte balanced salt solution plus fresh 5 μ*M* fura-2/AM and 0.03% Pluronic F-127.
3. Culture medium is replaced with 2 mL of loading solution, and cells are incubated in a water bath at 37°C for 15–20 min.
4. After loading, cells are washed twice with 1to 2 mL of loading solution *without* dye and detergent and left for 15–20 min to allow deesterification.

### *3.3. Luminal (Stored) $Ca^{2+}$ ($[Ca^{2+}]_L$) Measurement: Loading Cells With Low-Affinity Indicators* (see **Notes 6–9, 14–18**)

#### *3.3.1. Primary Hepatocytes*

1. Hepatocytes are plated overnight onto polylysine-coated glass cover slips in 2 mL of culture medium.
2. Loading solution: hepatocyte balanced salt solution plus fresh 5 μ*M* fura-2FF/AM (or 5 μ*M* mag-fura-2/AM) and 0.03% Pluronic F-127.
3. Culture medium is replaced with 2 mL of loading solution, and cells are incubated in a water bath at 37°C for 60 min.
4. After loading, cells are washed twice with 1 to 2 mL of loading solution *without* dye or Pluronic F-127 and used immediately.

### *3.4. Mitochondrial $Ca^{2+}$ ($[Ca^{2+}]_{mito}$) Measurement: Loading Endothelial Cells With rhod-2/AM* (see **Notes 10–18**)

1. Calf pulmonary artery endothelial cells are seeded onto glass cover slips for ≥2 d prior to use in 30-mm diameter Petri dishes in culture medium.

**Table 3**
**Typical Collection Parameters for Routine $Ca^{2+}$ Imaging on the Setup Used in Table 2**

| | Protocol 1 (ratio) |
|---|---|
| Objective | ×20 |
| Excitation λ | 340/380 |
| Neutral density | 1.6 |
| Image size (pixels) | 128 × 96 |
| Binning | 3 |
| Time of excitation exposure (ms) | 300 |
| Delay between image pairs (ms) | 3000 |

2. Monolayers are loaded with EBSS containing 5 μ*M* rhod-2/AM (plus 0.03% Pluronic F-127) for 10 min at 37°C.
3. After loading, cells are immediately washed gently several times with only EBSS and are ready for use after a 15-min deesterification period.

### *3.5. Experimental Recording* (see **Notes 19–33**)

#### *3.5.1. Single-Cell Recording*

The simplest mode of operation involves recording the *total* fluorescent signal from a single cell without any regard for spatial heterogeneity. With a simple PMT-based photometric system, there is little limitation by acquisition speed, RAM, and data storage as mentioned above, and spinning filter wheel systems mean that multiple wavelengths (at least four) can be simultaneously measured at high temporal resolution (50–200 Hz), depending upon the system configuration. Only one region can be recorded at a time and this can be a cell cluster, single cell, or even part of the cell (depending on the signal strength).

Alternatively, many individual cells can be recorded simultaneously at the expense of temporal resolution by using a video-imaging system. Again, multiple wavelengths can be collected, but in this case there is a restricted amount of data that can be collected. In such cases, acquisition rates of 0.3–1 Hz are typical as given in **Table 3**.

#### *3.5.2. Subcellular Recording*

##### 3.5.2.1. Imaging $[Ca^{2+}]_i$ Waves

The spatial equivalent of a $[Ca^{2+}]_i$ spike is a wave in which $[Ca^{2+}]_i$ rises first in one localized region of the cell and then actively propagates across the rest of the cell, usually (but not always) at a constant velocity at all points

**Table 4**
**Data Acquisition Parameters to Visualize $[Ca^{2+}]_i$ Waves in Primary Cultures of Rat Hepatocytes**

| | Protocol 1 (ratio) | Protocol 2 (single λ) |
|---|---|---|
| Objective | ×20 | ×40 |
| Excitation λ (nm) | 340/380 | 380 |
| Neutral density | 1.6 | 1.0 |
| Image size (pixels) | 128 × 96 | 92 × 72 |
| Binning | 3 | 3 |
| Time of excitation exposure (ms) | 100 | 40 |
| Delay between image sets (ms) | 1000 | 300 |

Cells are loaded with fura-2 according to **Subheading 3.3.** and are mounted in an incubation chamber at 37°C. Repetitive waves can be stimulated with 1–3 μ*M* phenylephrine ***(38)***.

along the wave front. For details of wave types and properties, the reader is referred to several reviews ***(1,4,31,32)***. The speed of the wave is such that rapid data acquisition is required, which often involves making compromises with the data collection parameters (*see* **Notes 19–33**). As an illustration, we have given in **Table 4** the parameters that are suitable for visualizing $[Ca^{2+}]_i$ waves in fura-2–loaded hepatocytes at modest collection rates for ratiometric recording (Protocol 1), and for single λ recording for more rapid measurements (Protocol 2).

#### 3.5.2.2. Measuring Oscillations of $[Ca^{2+}]_L$ in Permeabilized Hepatocytes

A 340/380 ratio pair collected every 2 to 3 s is adequate to resolve spiking. However since the 380-nm changes are small during spiking (~5%, whereas 340 nm is close to the isoemissive λ), these changes will be more readily detected using a PMT or a superior camera-based system (14-bit).

1. Hepatocytes are loaded as above with fura-2FF/AM (**Subheading 3.3.1.**) and used as quickly as possible after loading.
2. On the microscope stage, cells are washed three times with 2 mL of nominally $Ca^{2+}$-free medium containing 100 μ*M* EGTA.
3. Wash cells twice with 2 mL of chelex-treated ICM containing a cocktail of protease inhibitors (1 μg/mL each of leupeptin, pepstatin, and antipain) (*see* **Notes 2–4**).
4. To permeabilize, the above medium is replaced with 3 mL of ICM supplemented with 10 μg/mL of digitonin. Normally, gentle permeabilization is carried out until a new steady-state fluorescence (~30–50% of initial) is attained in the majority of cells (~4 to 5 min). Overpermeabilization results in damage to internal membranes. (Permeabilization is carried out in the absence of ATP since hepatocytes express purinoceptors coupled to phospholipase C.)

5. Digitonin is washed out with two washes of ICM followed by addition of 3 mL of ICM containing 2 m*M* MgATP. Continue incubation for a few minutes to allow complete store refilling.
6. Oscillations can be stimulated by addition of 100–200 n*M* $Ins(1,4,5)P_3$.
7. Total stored $Ca^{2+}$ can be determined with 2 µ*M* ionomycin.

### *3.6. Calibrating $[Ca^{2+}]_c$ Signals*

#### *3.6.1. In Situ Calibration of a Single λ Dye Using Ionophore in Intact Cells*

1. At the end of the run, 5 µ*M* ionomycin is added in nominally $Ca^{2+}$-free EBSS containing 500 µ*M* EGTA; this determines $F_{min}$.
2. In the continued presence of ionomycin, extracellular $Ca^{2+}$ is increased to 10 m*M*. Stable signal gives $F_{max}$.
3. Autofluorescence does not need to be subtracted since it is automatically accounted for in **Equation 1** for single λ dyes when performing an *in situ* calibration.
4. Fluorescence is converted to $[Ca^{2+}]_i$ using **Equation 1** substituting an appropriate $K_d$.

#### *3.6.2. In Vitro Calibration of a Dual λ Dye*

1. Obtain the background fluorescence of the system at both wavelengths using calibration buffer only (**Subheading 2., item 10**). This value should be subtracted from all subsequent measurements.
2. Add 0.5–1 µ*M* free-acid form of the indicator. The ratio will give $R_{min}$, and the fluorescence at the denominator λ is equivalent to $s_{f2}$.
3. Add 1 m*M* $CaCl_2$ to obtain $R_{max}$ and $s_{b2}$ in a similar manner.
4. $[Ca^{2+}]$ is calculated using **Equation 2** substituting the experimentally determined parameters and using the most pertinent $K_d$ value from the literature.

#### *3.6.3. Autofluorescence in Cells With Dye Compartmentalized Into $Ca^{2+}$ Stores*

1. Cells are permeabilized in ICM containing 500 µ*M* EGTA, 250 µ*M* $CaCl_2$, and 5–30 µg/mL of digitonin (free $[Ca^{2+}]$ ~100 n*M*).
2. After permeabilization (~5 min), 2 m*M* MgATP is added for several minutes to refill stores fully.
3. Residual fluorescence is comprised of autofluorescence plus compartmentalized dye.

## 4. Notes

### *4.1. Choosing a Dye*

1. The following represent some of the factors that have to be considered when choosing a $Ca^{2+}$ indicator. As always, there is a compromise between several parameters and the "perfect" dye is not always available.
   a. If possible use a ratiometric rather than an intensometric indicator.
   b. Ensure the $K_d$ is appropriate to the anticipated magnitude of the $[Ca^{2+}]_i$ response in order to prevent dye saturation and to optimize signal changes by working in the most sensitive range of the dye.

c. To avoid excessive buffering by exogenous indicator, use a dye that gives as large a signal change as possible in order to minimize the intracellular concentration of dye.
d. Buffering is less of an issue with lower affinity dyes. In addition, the lower-affinity is usually attributable to a faster dissociation of the $Ca^{2+}$:indicator complex, which means that the rapid kinetics of $Ca^{2+}$ spikes may be less distorted compared to a high-affinity dye.
e. Conjugated dyes with lower mobility reduce artifacts owing to dye diffusion, often crucial for interpreting kinetic and spatial measurements.
f. Visible wavelength dyes circumvent problems associated with poor UV transmission optics and with complicating autofluorescence changes in the UV range and are also used with non-UV confocal scanning microscopes.
g. The AM ester form of the indicator must load predominantly into the compartment of choice; since different dyes do not necessarily distribute between compartments in the same way, the optimal dye and loading conditions are empirically determined on a trial-and-error basis. Alternatively, the free-acid form can be introduced into the cell, although this is technically more demanding.
h. Use a dye that photobleaches (or is extruded from the cell) at an acceptable rate that can only be determined on a trial-and-error basis.
i. Intensometic dyes that are bright at low [$Ca^{2+}$] permit more accurate determination of basal $[Ca^{2+}]_i$ levels and visualization of cells (e.g., Calcium Green-1), whereas dyes that are less bright at low $Ca^{2+}$ levels (e.g., fluo-3) make quantitation more uncertain. However, the fold change in fluorescence on $Ca^{2+}$ binding (and hence the dynamic range) is potentially greater for the latter dye and can provide more "contrasty" images to visualize small, intense events, such as $Ca^{2+}$ sparks and puffs.
j. For multiparameter recording using more than one dye simultaneously, ensure that there is minimal spectral interaction between the indicators.
k. In attempting to overcome the lack of a ratiometric visible dye, cells can be simultaneously loaded with two spectrally distinct probes whose fluorescence is expressed as a ratio: to complement the $Ca^{2+}$ indicator, it is possible to include either a $Ca^{2+}$-insensitive dye, or a $Ca^{2+}$-sensitive one that gives a reciprocal fluorescence change upon $Ca^{2+}$ binding. (It is crucial that the two probes photobleach/leak at a similar rate and reside in the same compartment.) As an example of the former, a mixed dextran conjugated to the indicator Calcium Green-1 and the $Ca^{2+}$-independent Texas Red is available from Molecular Probes. In the second case, coloading cells with the two $Ca^{2+}$ indicators fluo-3 and fura-red gives reciprocal changes reminiscent of fura-2 excited at 340 and 380 nm. However, the latter approach can suffer from problems with cell-to-cell differences in relative AM ester loading and nonlinear behavior of the ratio attributable to the different $K_d$s of the two dyes ***(37)***.

### 4.2. Intracellular Medium

2. A permeabilized cell system is extremely useful since it allows precise control of the composition of the "cytosolic" environment with the additional advantage of facilitating the use of otherwise cell-impermeant agents. For example, investigation of the regulation of the Ins(1,4,5)$P_3$ receptor is ideally suited to this approach (providing permeabilization is carefully carried out ***[34]***) since it allows ready manipulation of both the Ins(1,4,5)$P_3$ and "cytosolic" $Ca^{2+}$ concentration. To mimic the low free $[Ca^{2+}]$ of the cytosol, the ICM is normally supplemented with known quantities of a $Ca^{2+}$ buffer (usually EGTA or BAPTA) and $Ca^{2+}$. The precise concentrations of each needed to yield the required free $[Ca^{2+}]$ can be calculated with software such as Maxchelator (Dr. Chris Patton, Stanford, CA). However, until recently, $Ca^{2+}$ oscillations had never been reported in permeabilized single cells. The breakthrough came when stored $Ca^{2+}$ was measured in an ICM without exogenous $Ca^{2+}$ buffers, which consequently allows the local $Ca^{2+}$ feedback processes at the Ins(1,4,5)$P_3$ receptor to occur unhindered ***(35,36)***. This provides an elegant model system for analyzing $Ca^{2+}$ oscillations but, in the absence of $Ca^{2+}$ buffers, necessitates special preparation of the medium.
3. Since unbuffered nominally $Ca^{2+}$-free ICM is contaminated with at least 5–10 μ*M* $[Ca^{2+}]$, it is necessary to lower this to levels more closely resembling the intracellular concentration. This is achieved by using an exchange resin, Chelex 100 (200–400 mesh, sodium form, Bio-Rad), which can be subsequently separated from the treated medium. Calcium Sponge (Molecular Probes) can also be used, but proves rather expensive for large-scale preparations. The final $[Ca^{2+}]$ can be as low as 50–80 n*M* with careful preparation (as determined fluorimetrically with fura-2 free-acid; *see* **Subheading 1.5.**)
   a. To minimize $Ca^{2+}$ contamination of solutions, all stages are carried out in plasticware and not glassware.
   b. A large (1 L) volume is prepared at a time, for convenience and to reduce the effect of $Ca^{2+}$ contamination at any stage.
   c. The pH of the ICM is adjusted with KOH or Tris base *before* Chelex treatment (note: some batches of Chelex 100 can slightly alter the final pH, which can be accounted for at this stage).
   d. Chelex 100 resin is added directly to the ICM at 50 g/L and the solution is stirred constantly with a magnetic stir bar.
   e. Minimum exchange time is 3 to 4 h at room temperature. Alternatively, overnight at 4°C may be more convenient and seems to be more efficient.
   f. To separate the resin from the ICM, gravity or centrifugal separation is favored over filtration, which can result in $Ca^{2+}$ contamination (but this can be checked for each filtration system).
4. The final free $[Ca^{2+}]$ in the experiment will depend on the extent of $Ca^{2+}$ contamination from the cells and other agents added after treatment (e.g., MgATP, protease inhibitors, Ins(1,4,5)$P_3$). In our hands, a concentration of 200–400 n*M* is typical. Since fura-2 provides significant $Ca^{2+}$ buffering in the absence of any other chelator, this needs to be accounted for in determining the free $[Ca^{2+}]$, by

using low fura-2 concentrations (e.g., 0.1 μ*M*) and/or back-calculation, deriving the amount bound to fura-2.

### 4.3. Cytosolic Dye Loading

5. Minimize AM ester overloading, which results in significant intracellular $Ca^{2+}$ buffering and/or toxicity. Use the lowest intracellular concentration of dye that gives a reliable signal by loading with the lowest possible concentration of AM ester feasible (usually 0.5–10 μ*M* range) for the shortest time (15–60 min is typical). This must be empirically determined for each new cell type tested by comparing the kinetics and magnitude of responses following different loading regimens: buffering manifests itself as more sluggish and/or diminutive responses.
   a. When measuring cytosolic $Ca^{2+}$ responses, dye compartmentalization is best reduced by loading cells at room temperature.
   b. Including a micelle dispersant such as serum (10–20% v/v), BSA (1–2% w/v), or the nonionic surfactant Pluronic F-127 (~0.03% w/v) also can reduce compartmentalization and improve loading.
   c. Serum contains esterases that can hydrolyze the AM ester form of the dye before it enters the cell (especially at 37°C). Since the cell-impermeant free acid is generated, this will reduce the efficiency of loading.
   d. Not all cell types possess efficient intracellular esterase activity, and thus, it may be more practical to load cells at 37°C. But this may in turn give loading problems through active extrusion of the dye from the cell, which occurs more efficiently at higher temperatures (*see* **Subheading 1.5.**). The anion transporters can be inhibited with either 1 m*M* probenicid, 200 μ*M* sulphinpyrazone, or 100 μ*M* bromosulphophthalein, although these are not clean reagents and may have other effects. Another approach is to use fura-PE3 instead of fura-2: this Zwitterionic analogue reportedly leaks from some cells at a slower rate than its congener, since it is less efficiently pumped by the anion transporter ***(23)***.
   e. After incubation in the presence of AM esters, allow sufficient time (≥20 min) for complete deesterification.

### 4.4. Organellar Dye Loading

#### 4.4.1. Store Loading

6. Use high concentrations of indicator (e.g., 3–10 μ*M* AM ester) for longer incubation periods (e.g., 1 h).
7. Loading is best carried out at 37°C. Pluronic F-127 can improve the degree (though probably not the selectivity) of loading.
8. To remove any contaminating cytosolic component, dialyze the cytosol with a patch pipet ***(16)***, and quench cytosolic dye with $Mn^{2+}$ that passively enters the cytosol via plasmalemmal $Ca^{2+}$ channels (e.g., incubate cells in $Ca^{2+}$-free medium containing 100-300 μ*M* $MnCl_2$). Permeabilization of the plasma membrane releases cytosolic dye for $[Ca^{2+}]_L$ measurements ***(15,35,36)***.

9. Dye redistribution between cellular compartments can sometimes occur with time. This may manifest itself as a decrease in the agonist (or Ins[1,4,5]$P_3$)-sensitive component as the reporting dye moves out of the $Ca^{2+}$ store to another apparently nonresponding compartment. Under these circumstances, it is more advisable to load and use cells immediately rather than batch-load many cover slips simultaneously.

### *4.4.2. Mitochondrial Loading*

10. Rhod-2 currently displays the highest selectivity for mitochondria, and short incubation times (≤10 min) with concentrations of AM ester ranging from 2 to 10 μ*M* seem to work well in many cell types. For example, in calf pulmonary artery endothelial cells, >95% of the $Ca^{2+}$ signal is derived from mitochondria.
11. If a significant amount of rhod-2 is cytosolic, it can essentially be eliminated after a short loading protocol by overnight culture of cells in fresh medium without indicator, allowing active extrusion mechanisms to remove cytosolic dye, leaving organellar-trapped dye behind.
12. Dihydro-rhod-2 may load more selectively into mitochondria in some cells (*see* **Subheading 1.4.1.2.**). Dihydro-rhod-2/AM preparation: rhod-2/AM is dissolved as a 1 m*M* stock in DMSO as normal. The smallest amount of $NaBH_4$ solid is added that will make the magenta solution colorless (no more than a few grains). This dihydro-rhod-2/AM solution is always prepared on the day of use since it does not store well.
13. Since mitochondrial conversion is required, loading takes longer with dihydro-rhod-2/AM. For example, hepatocytes are loaded with 1 to 2 μ*M* dihydro-rhod-2/AM for 60 min at 37°C in the presence of 2 m*M* acetoacetate (to shift the mitochondria to a more oxidized redox state via the liver-specific β-hydroxybutyrate dehydrogenase, which favors oxidation of dihydro-rhod-2 ***[10]***). After loading, cells are left for 12–16 h in primary culture to facilitate extrusion of residual cytosolic dye.

## *4.5. How Can Dye Compartmentalization Be Recognized?*

14. Cellular fluorescence is punctate. When a dye is located exclusively in the cytosol, it gives a uniform, diffuse pattern of staining. By contrast, when dye is concentrated in cell organelles, it can appear as punctate, spotty, reticulate, or filamentous fluorescence staining depending on the cell architecture and the organelle in which it is concentrated (e.g., mitochondria, ER). For fura-2, high levels of dye in intracellular stores (in which $Ca^{2+}$ is high) are best viewed at 340 nm, at which fluorescence intensity is proportional to $Ca^{2+}$ concentration. This is always best checked through the microscope binocular since the resolution of many cameras is inferior to the human eye.
15. Low fluorescence of the nuclear matrix*:* In most cells, the nucleus is freely permeable to small molecules such as the $Ca^{2+}$ indicator dyes, thus, as a result, the dye concentration in the nucleus is similar to that in the cytosol (with conventional imaging and no compartmentalization, the nucleus may even appear

*brighter* if it is the thickest part of the cell). By contrast, dye compartmentalized into organelles (e.g., ER, mitochondria) cannot exchange with the nucleus, which consequently appears relatively dim (especially at 340 nm with fura-2).

16. $[Ca^{2+}]_i$ responses are small or apparently negative when cells are stimulated. This occurs when a substantial fraction of dye is contained within the intracellular store itself and reports the fall in the luminal $Ca^{2+}$ levels as the store empties. Clearly this will be less obvious when high-affinity dyes such as fura-2 are used during low-intensity stimulation since they will normally remain saturated in the high $[Ca^{2+}]$ environment of the store lumen (*see* **Subheading 1.4.1.2.1.**). However, more extensive depletion of stores (e.g., with thapsigargin or cyclopiazonic acid, inhibitors of the store $Ca^{2+}$-ATPase) may cause $[Ca^{2+}]_L$ to fall to micromolar or below, which is within the working range for the dye. For low-affinity dyes, the problem is more pronounced because their working range may report $[Ca^{2+}]_L$ changes during physiological stimulation. That aside, caution should always be exercised since even apparently "normal" increases in $[Ca^{2+}]_c$ may be tempered by dye reporting decreases in $[Ca^{2+}]_L$.
17. Empirical determination of compartmentalization: Low concentrations of agents that selectively permeabilize the plasma membrane and release only the cytosolic dye reveal the fraction trapped in intracellular organelles. For example, 5–30 µg/mL of digitonin gently releases cytosolic fluorescence into the medium over 3–5 min. Ideally, this should be monitored at a $Ca^{2+}$-insensitive wavelength (e.g., 360 nm with fura-2); thus the signal is only proportional to dye concentration and not $Ca^{2+}$ concentration. In hepatocytes, up to 50% of ester-loaded dye can be trapped in the ER under appropriate loading conditions.
18. To determine precisely where the dye is located, several structural and functional criteria should be tested. For example, for $[Ca^{2+}]_{mito}$ measurements the pattern of rhod-2 distribution should be compared at as high a resolution as possible with bona fide mitochondrial stains such as JC-1, rhodamine tetramethyl ester, or any of the MitoTracker family (Molecular Probes). Functionally, the resolution afforded by the confocal scanning microscope at high magnification (60×) is able to verify whether $Ca^{2+}$ increases derive solely from a mitochondrial source. In the absence of access to a confocal microscope, a 35-mm single lens reflex camera attached to the appropriate microscope port can offer a finely resolved photographic record. Alternately, $[Ca^{2+}]_{mito}$ changes should be rapidly blocked by mitochondrial inhibitors such as 0.2 µg/mL of antimycin A, 5 µ*M* FCCP/5 µg/ml oligomycin or 1 to 2 µ*M* ruthenium red (which may require microinjection since it does not readily cross the plasma membrane).

## *4.6. Practical Considerations Regarding Experimental Recording*

### *4.6.1. General Considerations* (see also **Table 5**)

19. Single-cell $[Ca^{2+}]_i$ recording can be frustrated by the most fundamental of problems, namely the loss of fluorescent signal and/or cell viability with time. The reduction in the signal strength as a consequence of indicator elimination can be so rapid as to make experimentation impossible, or at least be enough to limit its

**Table 5**
**Troubleshooting Fluorescence Imaging**

| Problem | Notes |
|---|---|
| Calibration | |
| Incomplete dye hydrolysis | Extend postloading incubation period |
| Binding of dye to cell constituents | Perform an *in situ* calibration |
| Dye compartmentalisation | Lower loading temperature; lower loading time; use a dispersant; permeabilization-based calibration |
| Spectral shift *in situ* vs in vitro | Precludes an in vitro calibration, or modify in vitro conditions (e.g., increase viscosity with glycerol) |
| Constant autofluorescence contribution | Determine at end of run by quenching dye with ionomycin plus $Mn^{2+}$ and subtracting residual fluorescence |
| Autofluorescence changes during run | Increase dye loading to swamp endogenous fluorescence (beware of buffering) |
| Saturation of dye when $[Ca^{2+}]_i$ is high | Use a dye of lower affinity |
| Sluggish $[Ca^{2+}]_i$ responses | Reduce dye loading (if buffering); use lower affinity dye; also see compartmentalization |
| Photobleaching | Reduce light exposure (decrease exposure time; increase ND filter); free-radical scavengers such as Trolox; use a different dye |
| Dye leakage | Lower temperature of experimental run; use a less leaky dye; inhibit extrusion pathways |
| Experimental recording | |
| Blooming and streaking of image | Reduce exciting light intensity; adjust camera/filter change synchronization |
| High-frequency extraneous noise at all wavelengths | Change bulb to eliminate lamp flicker |
| Dim image | Increase loading; reduce ND filters; increase exposure time; check lamp alignment |

duration. The first step then is to assess whether photobleaching or leakage (or both) is responsible for the loss of responsive indicator.

20. To resolve this issue, first record the emitted signal for a short time to estimate the rate of change of fluorescence (Intensity 1). The incubation is then continued for a reasonable period (5–10 min) *without* exposing the cells to exciting light.

Subsequently, fluorescence is recorded again, using the same acquisition parameters (Intensity 2). If photobleaching was exclusively responsible for the decline, then intensity 1 = intensity 2. By contrast, if extrusion was exclusively responsible, this would have been unaffected by the light-free period and thus intensity 1 >> intensity 2. Clearly, if both processes contribute to signal loss, some intermediate rate of decline occurs during the light-free period.

21. Irradiation with high-energy light not only degrades the fluorescent indicator but also lowers cell viability and therefore should be reduced to a minimum. As already noted, photobleaching can be reduced to a manageable level in the following ways:
    a. Reduce the intensity and/or duration of the exposure to the exciting light.
    b. Use free-radical scavengers to minimize photodegradation (note, however, the possible biological consequences).
    c. Use a different dye that photobleaches at a slower rate.
22. Leakage, on the other hand, can be countered in different ways:
    a. Inhibit extrusion pathways with agents such as probenicid, sulphinpyrazone and bromosulphophthalein (*see* **Note 5**).
    b. The rate of extrusion is proportional to temperature and is consequently greatest at 37°C. A significant improvement in dye retention can be seen even at 30°C, whereas at room temperature loss of signal can be negligible.
    c. Use a different indicator since they vary in their susceptibility to extrusion (e.g., Calcium Green-1 is less leaky than fluo-3).

### *4.6.2. Nonspatial Recording Mode*

#### 4.6.2.1. Temporal Resolution

23. The highest temporal resolution (up to several hundred hertz acquisition rate) is afforded with a PMT-based system. Camera-based systems run at much slower rates with dual λ indicators (typically 0.3–1 Hz). This means that even nonoptimized recording with the photometric system will offer superior temporal resolution than routine measurement with an imaging system. In this way the rise times of $Ca^{2+}$ spikes measured ratiometrically with fura-2 (of the order of a few seconds or less) can be accurately determined with a PMT-based, but not a camera-based system. (Faster kinetics can be measured with an imaging system if only a single wavelength is recorded, but this compromises the advantages of ratiometric measurements.) However, if initial kinetics are not an issue, the slower collection rate of the imaging system is sufficient.

#### 4.6.2.2. Dynamic Range

24. Again, the detector determines the maximum dynamic range of the system. A PMT has an excellent SNR to allow the resolution of small (~5%) changes in fluorescence intensity. By contrast, 8-bit cameras (especially the intensifier cameras) exhibit an inferior SNR and poor dynamic range (pixel intensity graded from 0 to 255), which makes small changes difficult to detect. However, the

more expensive 14-bit slow-scan cameras, for example, offer excellent image quality, high SNR, and large dynamic range.

#### 4.6.2.3. Heterogeneous Responses

25. When there is considerable cell-to-cell heterogeneity in the response, photometric recording usually proves too time-consuming. This is when imaging comes into its own with the ability to simultaneously record from many tens of cells (depending on magnification and cell diameter).

### *4.6.3. Spatial Recording Mode*

26. There are two complementary approaches to gaining information about how $Ca^{2+}$ is regulated in different subcellular regions: either target the dye to the region of interest and photometrically record the specific signal, or record a homogeneously distributed dye but focus on one cell region (either by optically isolating the region with the masking aperture during recording on a PMT-based system, or by using a camera and performing off-line regional analysis after recording). In other words, *both* systems can provide useful spatial information. These two approaches need not be mutually exclusive.

#### 4.6.3.1. Spatial Resolution Limits

27. The maximal theoretical spatial resolution of light microscopy is governed by **Equation 3**:

$$r = (1.22 \times \lambda_o)/(2 \times \mathrm{NA})$$

In **Equation 3** where ($r$) is the minimum distance by which two points can still be resolved as two points, $\lambda_O$ is the wavelength of light in air, and NA is the numerical aperture of the lens. Therefore, for an objective of NA = 1.4 and light emitted at 510 nm, the maximum resolution will be 0.22 μm (a reasonable rule of thumb is half the wavelength of the emitted light). Although this limit is well below the size of typical somatic cells (10–100 μm), it should still be considered when carrying out high-resolution imaging of small discrete units such as mitochondria or $Ca^{2+}$ elementary release events (blips, spread 1–2 μm) ***(4)***.

#### 4.6.3.2. Optimization of Resolution

28. As detailed in **Subheading 3.**, the maximum resolving power of the imaging system will be determined primarily by the camera (number of pixels per image) and the objective (magnification and NA). Clearly, the highest resolution will be achieved when there is *no* pixel averaging (binning) together with the highest suitable magnification and NA. However, under these conditions the image may be dimmer, which may necessitate increasing the excitation light intensity (by prolonging the exposure time and/or decreasing the number of the neutral density filter), which may cause photodamage or photobleaching.

#### 4.6.3.3. Image Deconvolution

29. Image quality is adversely affected by out-of-focus fluorescence, which reduces contrast and increases the depth of field, resulting in distortion and blurring of the final image. This is particularly problematic as far as cell clusters and intact tissues are concerned. To improve image quality, optical sectioning can be achieved with a confocal microscope which only detects in-focus information. Alternately, application of deblurring algorithms to conventional images can render sectioning mathematically in one of two ways: either a "nearest neighbor" approach ***(33,38)*** or through "no neighbors" processing ***(39)***. The former necessitates multiple image collection at different focal planes to create a 3D stack from which an optical section can be reconstructed. By contrast, the "no neighbors" algorithm mathematically extracts optical sections without the need to acquire multiple sections, which facilitates faster image acquisition since it obviates slow *z* plane stepping.
30. Such "image deconvolution" is advantageous in so far as that ratiometric UV dyes such as fura-2 and indo-1 can be used, otherwise untenable with a single-photon, visible confocal scanning microscope. Even so, there is a downside: with most algorithms discarding a substantial amount of the fluorescent signal, bright specimens and cameras of the highest resolution are a prerequisite. However, this problem has been offset to a degree by the development of a mathematical model that allows restoration of extremely high-quality images with minimal light exposure and sectioning from fewer image planes ***(38)***.

### 4.6.4. Tips on Measuring $Ca^{2+}$ Waves

31. $[Ca^{2+}]_i$ waves generally propagate at a velocity of between 5 and 200 $\mu m \cdot s^{-1}$ ***(1,4,31,32)***. For most somatic cells, this will mean the wave takes ~1–5 s to cross the entire cell. Simply to observe heterogeneous $[Ca^{2+}]_i$ increases and crudely identify wave initiation loci, it is probably sufficient to collect a ratio image every second or so during repetitive waves, such as those in hepatocytes ***(31)***. There is also little need for extremely high-resolution images, so one can increase pixel averaging (binning) and decrease image size to reduce the demand on image storage memory.
32. However, to accurately quantitate the wave velocity, an image will have to be acquired at least every 300 ms, which places demands on the imaging configuration. For rapid visualization of $[Ca^{2+}]_i$ waves (at or approaching video rate, 25–30 Hz), most imaging systems are unable to support ratiometric recording with fura-2, since the time taken to alternate between filter positions introduces a significant delay. For this reason, most rapid analyses of wave fronts are conducted in single $\lambda$ mode to eliminate slow excitation $\lambda$ changes (either at 380 nm with fura-2, which gives a relatively large fluorescence decrease, or with intensometric indicators such as fluo-3 or Calcium Green-1). This method is not ideal and represents yet another example of compromise.
33. Because the time taken to write images to the hard disk of the computer is rate limiting (up to a second depending on the computer and image size), rapid data

collection times can only be achieved when images are stored temporarily in RAM, and written to hard disk after the experimental run has been completed. The only limitation here is that RAM tends to be much smaller than the capacity of the hard disk, so fewer images can be collected. Nonetheless, with computers of 30MB or more of RAM, this imitation should not be too restrictive.

## References


1. Thomas, A. P., St. J. Bird, G., Hajnóczky, G., Robb-Gaspers, L. D., and Putney, J. W. Jr. (1996) Spatial and temporal aspects of cellular calcium signalling. *FASEB. J.* **10,** 1505–1517.
2. Lee, M. G., Xu, X., Zeng, W., Diaz, J., Wojcikiewicz, R. J. H., Kuo, T. H., Wuytack, F., Racymaekers, L., and Muallem, S. (1997) Polarized expression of $Ca^{2+}$ channels in pancreatic and salivary gland cells. *J. Biol. Chem.* **272,** 15,765–15,770.
3. Lee, M. G., Xu, X., Zeng, W., Diaz, J., Kuo, T. H., Wuytack, F., Racymaekers, L., and Muallem, S. (1997) Polarized expression of $Ca^{2+}$ pumps in pancreatic and salivary gland cells. *J. Biol. Chem.* **272,** 15,771–15,776.
4. Berridge, M. B. (1997) Elementary and global aspects of calcium signalling. *J. Physiol.* **499,** 291–306.
5. Thorn, P., Moreton, R., and Berridge, M. B. (1996) Multiple, coordinated $Ca^{2+}$-release events underlie the inositol trisphosphate-induced local $Ca^{2+}$ spikes in mouse pancreatic acinar cells. *EMBO J.* **15,** 999–1003.
6. Ito, K., Miyashita, Y., and Kasai, H. (1997) Micromolar and submicromolar $Ca^{2+}$ spikes regulating distinct cellular functions in pancreatic acinar cells. *EMBO J.* **16,** 242–251.
7. Busa, W. B. and Nuccitelli, R. (1985) An elevated free cytosolic $Ca^{2+}$ wave follows fertilization in eggs of the frog *Xenopus laevis*. *J. Cell. Biol.* **100,** 1325–1329.
8. Gerasimenko, O. V., Gerasimenko, J. V., Tepikin, A. V., and Petersen, O. H. (1996) Calcium transport in the nucleus. *Pflügers Archiv - Eur. J. Physiol.* **432,** 1–6.
9. Rizzuto, R., Brini, M., Murgia, M.. and Pozzan, T. (1993) Microdomains with high $Ca^{2+}$ close to $IP_3$-sensitive channels that are sensed by neighbouring mitochondria. *Science* **262,** 744–747.
10. Hajnóczky, G., Robb-Gaspers, L. D., Seitz, M. B., and Thomas, A. P. (1995) Decoding cytosolic calcium oscillations in the mitochondria. *Cell* **82,** 415–424.
11. Petersen, O. H. (1996) Can $Ca^{2+}$ be released from secretory granules or vesicles? *Trends Neurosci.* **19,** 411–413.
12. Cobbold, P. H. and Rink, T. J. (1988) Fluorescence and bioluminescence measurement of cytoplasmic free calcium. *Biochem. J.* **248,** 313–328.
13. Tsien, R. Y. (1989) Fluorescent probes of cell signalling. *Ann. Rev. Neurosci.* **12,** 227–253.
14. Bygrave, F. L. and Benedetti, A. (1996) What is the concentration of calcium ions in the endoplasmic reticulum? *Cell Calcium* **19,** 547–551.
15. Golovina, V. A. and Blaustein, M. P. (1997) Spatially and functionally distinct $Ca^{2+}$ stores in sarcoplasmic and endoplasmic reticulum. *Science* **275,** 1643–1648.

16. Tse, F. W., Tse, A., and Hille, B. (1994) Cyclic changes in intracellular stores of gonadotropes during gonadotropin-releasing hormone-stimulated $Ca^{2+}$ oscillations. *Proc. Natl. Acad. Sci. USA* **91,** 9750–9754.
17. Hofer, A. M. and Machen, T. E. (1993) Technique for *in situ* measurement of calcium in intracellular inositol 1,4,5-trisphosphate-sensitive stores using the fluorescent indicator mag-fura-2. *Proc. Natl. Acad. Sci. USA* **90,** 2598–2602.
18. Mix, T. C. H., Drummond, R. M., Tuft, R. A., and Fay, F. S. (1994) Mitochondria in smooth muscle sequester $Ca^{2+}$ following stimulation of cell contraction. *Biophys. J.* **66,** A97.
19. Glennon, M. C., Bird, G. S., Takemura, H., Thastrup, O., Leslie, B. A., and Putney, J. W. Jr (1992) In situ imaging of agonist-sensitive calcium pools in AR4-2J pancreatoma cells. Evidence for an agonist- and inositol 1,4,5-trisphosphate-sensitive calcium pool in or closely associated with the nuclear envelope. *J. Biol. Chem.* **267,** 25,568–25,575.
20. Allbritton, N. L., Oancea, E., Kuhn, M. A., and Meyer, T. (1994) Source of nuclear calcium signals. *Proc. Natl. Acad. Sci. USA* **91,** 12,458–12,462.
21. Horne, J. H. and Meyer, T. (1997) Elementary calcium-release units induced by inositol trisphosphate. *Science* **276,** 1690–1693.
22. Etter, E. F., Kuhn, M. A., and Fay, F. S. (1994) Detection of changes in near-membrane $Ca^{2+}$ concentration using a novel membrane-associated $Ca^{2+}$ indicator. *J. Biol. Chem.* **269,** 10,141–10,149.
23. Vorndran, C., Minta, A., and Poenie, M. (1995) New fluorescent calcium indicators designed for cytosolic retention or measuring calcium near membranes. *Biophys. J.* **69,** 2112–2124.
24. Etter, E. F., Minta, A., Poenie, M., and Fay, F. S. (1996) Near membrane $[Ca^{2+}]_i$ transients resolved using the $Ca^{2+}$ indicator FFP-18. *Proc. Natl. Acad. Sci. USA* **93,** 5368–5373.
25. Lloyd, Q. P., Kuhn, M. A,. and Gay, C. V. (1995) Characterisation of calcium translocation across the plasma membrane of primary osteoblasts using a lipophilic calcium-sensitive fluorescent dye, calcium green-$C_{18}$. *J. Biol. Chem.* **270,** 22,445–22,451.
26. Morgan, A. J. and Jacob, R. (1994) Ionomycin enhances $Ca^{2+}$ influx by stimulating store-regulated cation entry and not by a direct action at the plasma membrane. *Biochem. J.* **300,** 665–672.
27. Erdahl, W. L., Chapman, C. J., Taylor, R. W., and Pfeiffer, D. R. (1995) Effects of pH conditions on $Ca^{2+}$ transport catalyzed by ionophores A23187, 4-Br-A23187 and ionomycin suggest problems with common applications of these compounds in biological systems. *Biophys. J.* **69,** 2350–2363.
28. Grynkiewicz, G., Poenie, M., and Tsien, R. Y. (1985) A new generation of $Ca^{2+}$ indicators with greatly improved fluorescence properties. *J. Biol. Chem.* **260,** 3440–3450.
29. Roe, M. W., Lemasters, J. J., and Herman, B. (1990) Assessment of fura-2 for measurements of cytosolic free calcium. *Cell Calcium* **11,** 63–73.
30. Pralong, W. F., Spät, A., and Wollheim, C. B. (1994) Dynamic pacing of cell metabolism by intracellular $Ca^{2+}$ transients. *J. Biol. Chem.* **269,** 27,310–27,314.

31. Thomas, A. P., Renard, D. C., and Rooney, T. A. (1992) Spatial organization of $Ca^{2+}$ signalling and Ins(1,4,5)$P_3$ action. *Adv. Second Messenger Phosphoprotein Res.* **26,** 225–263.
32. Clapham, D. E. and Sneyd, J. (1995) Intracellular $Ca^{2+}$ waves. *Adv. Second Messenger Phosphoprotein Res.* **30,** 1–24.
33. Carrington, W. A., Lynch, R. M., Moore, E. D. W., Isenberg, G., Fogarty, K. E., and Fay, F. S. (1995) Superresolution three-dimensional images of fluorescence in cells with minimal light exposure. *Science* **268,** 1483–1487.
34. Renard-Rooney, D. C., Hajnóczky, G., Seitz, M. B., Schneider, T. G., and Thomas, A. P. (1993) Imaging of inositol 1,4,5-trisphosphate-induced $Ca^{2+}$ fluxes in single permeabilized hepatocytes. *J. Biol. Chem.* **268,** 23,601–23,610.
35. Tanimura, A. and Turner, R. J. (1996) Inositol 1,4,5-trisphosphate-dependent oscillations of luminal $[Ca^{2+}]$ in permeabilized HSY cells. *J. Biol. Chem.* **271,** 30,904–30,908.
36. Hajnóczky, G. and Thomas, A. P. (1997) Minimal requirements for calcium oscillations driven by the $IP_3$ receptor. *EMBO J.* **16,** 3533–3543.
37. Floto, R. A., Mahaut-Smith, M. P., Somasundarum, B., and Allen, J. M. (1995) IgG-induced $Ca^{2+}$ oscillations in differentiated U937 cells: a study using laser scanning confocal microscopy and co-loaded fluo-3 and fura-red fluorescent probes. *Cell Calcium* **18,** 377–389.
38. Agard, D. (1984) Optical sectioning microscopy: cellular architecture in three dimensions. A*nn. Rev. Biophys. Bioeng.* **13,** 191–219.
39. Monck, J. R., Oberhauser, A. F., Keating, T. J., and Fernandez, J. M. (1992) Thin-section ratiometric $Ca^{2+}$ images obtained by optical sectioning of fura-2 loaded mast cells. *J. Cell. Biol.* **116,** 745–759.

# 6

# Ratiometric $Ca^{2+}$ Measurements Using the FlexStation® Scanning Fluorometer

**Ian C. B. Marshall, Izzy Boyfield, and Shaun McNulty**

## 1. Introduction

Many commercial organizations currently use the Fluorometric Imaging Plate Reader (FLIPR®: Molecular Devices, Sunnyvale, CA) to conduct high-throughput measurements of intracellular $Ca^{2+}$ concentration (*see* Chapter 7), taking advantage of its rapid kinetics, reliability, and compatibility for automation. For the majority of industrial applications, the primary limitation of FLIPR (i.e., its requirement for single wavelength fluorescent probes using visible light excitation) is not a significant issue. Indeed, visible light probes offer certain benefits over their ultraviolet (UV)-excited ratiometric counterparts, such as reduced sample autofluorescence and higher absorbance, thereby allowing relatively low concentrations of dye to be used. However, under certain circumstances researchers may prefer to conduct high-throughput experiments with ratiometric dyes, particularly when issues of dye leakage, photobleaching, or signal-to-noise ratio become a concern.

The most commonly used dual-wavelength ratiometric dye for $Ca^{2+}$ measurements is fura-2 ***(1)***. The fluorescence emission from fura-2 (measured at >510 nm) varies with $Ca^{2+}$ concentration depending on the excitation wavelength used. When excited at 340 nm, fura-2 emission rises with increasing $Ca^{2+}$ concentration. However, when excited at 380 nm, fura-2 emission decreases with increasing $Ca^{2+}$ concentration. The ratio of emissions following excitation at 340 and 380 nm is a more reliable indicator of $Ca^{2+}$ concentration than emission from single-wavelength dyes because it is less affected by differences in dye concentration (as may occur during loading), photobleaching, and illumination intensity and offers an improved signal-to-noise ratio. Consequently, fura-2 lends

From: *Methods in Molecular Biology, vol. 312: Calcium Signaling Protocols: Second Edition*
Edited by: D. G. Lambert © Humana Press Inc., Totowa, NJ

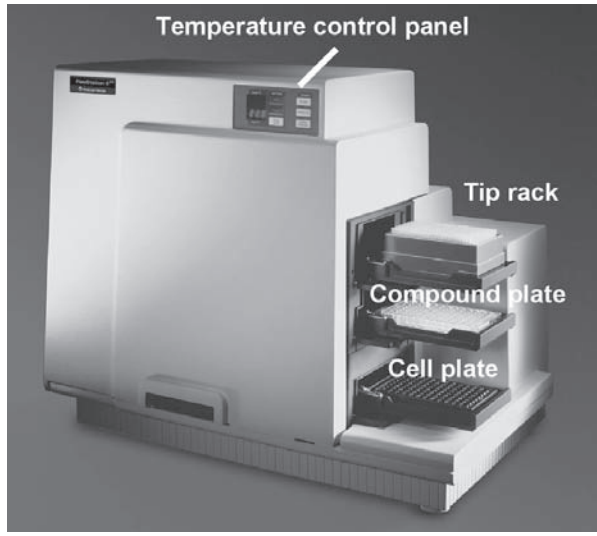


Fig. 1. The FlexStation™ scanning fluorometer (Molecular Devices, Sunnyvale, CA). Critical components of the system are marked.

itself to more accurate calibration of intracellular free $Ca^{2+}$ concentration within cells compared with single-wavelength dyes.

The FlexStation® Scanning Fluorometer (Molecular Devices; **Fig. 1**) is a fluorescence plate reader that can measure intracellular $Ca^{2+}$ concentration using both single- and dual-wavelength fluorescent probes. The FlexStation uses a Xenon flashlamp and monochromators for both excitation and emission light to allow the use of a wide range of fluorescent indicators (excitation range 250–850 nm; emission range 375–850 nm). This flexibility in choosing specific wavelengths also allows the FlexStation to perform excitation and emission scans for characterizing new fluorescent markers. The system incorporates a fluid transfer system for addition of test compounds from a source plate to the cell plate during data acquisition. Both plates are contained within a temperature-controlled unit that can be controlled accurately between room temperature and 45°C. The FlexStation can be configured to read 6-, 12-, 24-, 48-, 96-, and 384-well plates although fluid transfer is currently limited to 96- and 384-well plate format. In contrast to FLIPR, each well is read individually, thereby reducing temporal resolution across the plate. To offset this limitation, compounds are added to the cell plate one column at a time and responses are monitored for the duration of the experiment in each column.

The time interval between successive $Ca^{2+}$ measurements may be a deciding factor in assessing whether the FlexStation is an appropriate tool for ratiometric

$Ca^{2+}$ measurements in a particular study, and it is therefore important for the user to understand fully how the instrument collects ratio pairs during a typical experiment. Once compounds have been added to a single column of the plate, the wells are excited first with 340 nm light and emission is measured down all wells of the column with 0.1-s time resolution between wells. The excitation wavelength is then switched to 380 nm, and emission is measured back up the column, again with a time resolution of 0.1 s. The excitation wavelength is then switched back to 340 nm for the next set of time points until the column has been imaged across the full time course of the experiment. Compounds are then added to the next column of the plate and the cycle is repeated. In practice, this means that the shortest time interval between 340- and 380-nm recordings in a single well varies between 2.2 and 0.75 s depending on whether the well lies at the top or bottom of the column. Also, the shortest time between successive 340-nm recordings within a single well is approx 3 s in a 96-well plate. For very rapid $Ca^{2+}$ transients, this method for collecting 340:380-nm pairs may be unsuitable because peak $Ca^{2+}$ responses are liable to be underestimated. However, slower and more sustained $Ca^{2+}$ transients can be measured without significantly underestimating the peak $Ca^{2+}$ response and with the additional advantages of compensating for uneven dye loading and photobleaching. Here, we describe generic methods for assessing intracellular $Ca^{2+}$ on the FlexStation using ratiometric dyes. These methods are best used as a starting point to which additional modifications relevant to the researchers particular cell system can be made.

## 2. Materials

1. Suitable cell cultures are necessary which may include human embryonic kidney (HEK293) cells and Chinese Hamster Ovary cells.
2. Tyrodes buffer: 145 m*M* NaCl, 2.5 m*M* KCl, 10 m*M* HEPES, 10 m*M* glucose, 1.2 m*M* $MgCl_2$, and 1.5 m*M* $CaCl_2$.
3. Fura-2 acetoxymethyl ester (Molecular Probes, Eugene, OR) dissolved in dimethyl sulfoxide (DMSO) to provide a 2 m*M* stock solution. Aliquots should be stored at –20°C and used once after thawing (*see* **Note 1**).
4. Probenecid (Sigma, Poole, UK) dissolved in 1 *M* of NaOH (5 mL) and diluted 1:1 with Tyrodes buffer to give a 250-m*M* stock (*see* **Note 2**).
5. Pluronic F-127 (Molecular Probes) dissolved in DMSO at 20% (w/v) (*see* **Note 3**).
6. Culture flasks: 75-$cm^2$ (Nunc, Denmark)
7. Cell plates: 96-well, black-walled, clear-base plates with or without poly-D-lysine coating (Corning Inc., High Wycombe, UK).
8. Compound plates: 96-deepwell, clear V-bottom polypropylene plates (Greiner, Stonehouse, UK).
9. Disposable 200 µL non-sterile polypropylene tips (Molecular Devices).
10. Embla plate washer (Molecular Devices).

## 3. Methods

### 3.1. Preparation of Cells for $Ca^{2+}$ Measurements

1. HEK293 cells are typically grown in 75 $cm^2$ flasks in minimum essential medium supplemented with nonessential amino acids, 10% fetal calf serum and 2 m*M* of L-glutamine at 37°C under 5% $CO_2$. Chinese Hamster Ovary cells are grown in Hams-F12 medium supplemented with 10% fetal bovine serum at 37°C under 5% $CO_2$.
2. Cells are typically seeded into black-walled, clear-based, 96-well plates at a density of 25,000 cells per well (minimum volume 100 µL) and cultured overnight (*see* **Note 4**) prior to use.

### 3.2. Preparation of Agonist/Antagonist Plates

1. Prepare agonists and antagonists in clear 96-deepwell plates as follows: make up agonists at 4× and antagonists at 6× their final maximum assay concentrations by dissolving first in appropriate solvent and then diluting in Tyrodes buffer.
2. Apply highest required concentrations of compounds to the end column of plates and perform serial dilutions across the plates as required. Half- or quarter-log dilutions can be performed either manually or using robotics (e.g., Biomek 2000, Beckman Coulter, Fullerton, CA). The final concentrations used are commonly 0.1 n*M*–10 µ*M*. For compounds dissolved in DMSO, the final concentration of DMSO applied to cells should not exceed 1%.

### 3.3. Loading Cells With Fura-2

1. Mix equal volumes of fura-2 stock and pluronic F-127 stock to provide an adequate volume for cell loading.
2. Make up loading medium by adding fura-2–pluronic F-127 mixture to cell culture medium to give a final fura-2 concentration of 2 µ*M*.
3. Remove medium from cell plate and replace with 100 µL loading medium per well. Incubate for between 30 and 120 min at either room temperature or 37°C (*see* **Note 5**). Probenecid (2.5 m*M*) can be included in the loading medium and/or wash medium if required (*see* **Note 2**).
4. Wash cells three times with Tyrodes buffer using an Embla plate washer and leave in 125 µL Tyrodes buffer for antagonist studies or 150 µL for single addition agonist studies as appropriate. Add 25 µL of buffer or antagonist as appropriate from the antagonist plate (this step can be done using a Biomek FX robotic system; Beckman Coulter) and incubate for 30 min to allow antagonists to bind and allow cells to de-esterify intracellular fura-2 acetoxymethyl (AM) dye (*see* **Note 6**).
5. Wash cells three times with Tyrodes buffer using the Embla plate washer and incubate in 150 µL of fresh Tyrode buffer (*see* **Note 7**).
6. Transfer the cell plate, agonist plate, and tip rack to the appropriate drawers in the FlexStation prior to experimentation.

### 3.4. Setting Up the FlexStation for Fura-2 Ratiometric Measurements

1. Open SoftMax Pro® Software and choose the FLEX option under Set-Up.
2. Set the number of wavelengths to two and choose excitation wavelengths of 340 and 380 in LM1 and LM2.

3. For maximum time resolution, set the Readings speed to fast (under Sensitivity) and set Timing Interval to match the minimum interval (3.1 s at highest resolution).
4. Set other parameters as appropriate, including length of experiment, wells to read, compound addition parameters, and assay plate type (*see* **Note 8**).
5. Once parameters have been set, click Read to initiate compound addition and data capture.

### 3.5. Data Analysis

1. Data are automatically stored on disk at the end of the capture. Data may be analyzed using the extensive data calculation and analysis capabilities of SoftMax Pro or off-line by exporting fluorescence values and time points as an ASCII file.
2. Ratio measurements can be converted to intracellular $[Ca^{2+}]$ using the following equation ***(1)***:

$$[Ca^{2+}] = K_d\,[(R - R_{min})/(R_{max} - R)]\;(F_{380max}/F_{380min})$$

where $K_d$ is the dissociation constant of Fura-2, $R_{min}$ and $R_{max}$ are the 340/380 ratios of the $Ca^{2+}$-free and $Ca^{2+}$-bound forms of the dye, respectively, and $F_{380max}$ and $F_{380min}$ are the fluorescence emission intensities of $Ca^{2+}$-free and $Ca^{2+}$-bound dye, respectively, following excitation at 380 nm. $R_{min}$, $R_{max}$, $F_{380max}$, and $F_{380min}$ are determined empirically within the plate by incubating cells either with 10 μM ionomycin (to achieve $R_{max}$ and $F_{380min}$) or with ionomycin and 10 m*M* ethylene glycol tetraacetic acid (EGTA) (to achieve $R_{min}$ and $F_{380max}$).

## 4. Notes

1. Fura-2 acetoxymethyl (AM) is insoluble in aqueous solution. A concentrated stock in DMSO should be divided into small aliquots suitable for individual experiments and stored frozen at –20°C until use. It is essential to mix the DMSO stock well to avoid the formation of particulates that can become compartmentalized during dye loading.
2. Probenecid is an inhibitor of inorganic anion transporters that are able to extrude the hydrolyzed form of fura-2 from the cytosol. It is advisable to compare dye loading in the presence and absence of probenecid to determine whether inorganic anion transporters present a potential problem in the particular cells under investigation.
3. Pluronic F-127 is a non-ionic detergent that is commonly used to improve dispersion of fura-2 AM in aqueous solution. For best results, it should be mixed with fura-2 AM before addition to the aqueous buffer.
4. Weakly adherent cell lines can be used in the FlexStation by using poly-D-lysine coated plates. Suspension cultures can also be used in the FlexStation. However, for these cells it is advisable to centrifuge cells to the bottom of the plate following loading in order to generate a monolayer of cells at the bottom of the well.
5. Optimal dye loading conditions (e.g., concentration of dye, loading time/ temperature, and inclusion of probenecid) should be determined empirically for each cell line.

6. Since the ester and free acid forms of fura-2 have different spectral properties and sensitivities to $Ca^{2+}$, it is important to assist removal of nonhydrolysed ester from the cytosol following loading (i.e., de-esterification). Therefore, a 30-min incubation period is recommended following dye loading to allow both hydrolysis of fura-2 AM or diffusion of fura-2 AM from the cytosol into the wash buffer.
7. The protocol for the Embla plate washer should be optimized for each assay. Adjustments can be made to aspiration and dispensation heights, dispensation speed, the strength of the vacuum and the number of washes per cycle in order to minimize cell disruption. After the final wash step, cells should typically be allowed to recover for an additional 20 min before running on the FlexStation.
8. The parameters for the integrated FlexStation pipetor require optimization for each assay. The dispensation height of the pipetor and the speed of dispensation should be adjusted to ensure optimal delivery of the compounds to the specific plates being used. Optimal delivery should not cause cell disruption but should allow adequate mixing of the compounds in the well. To assist adequate mixing of compounds, the volume of agonist added to the well is typically 25% of the final well volume. The optimal dispenser speed may vary according to how well cells adhere to the bottom of the well. Cells can be checked following dispensation using the plate viewer.

## Reference

1. Grynkiewicz, G., Poenie, M., and Tsien, R. Y. (1985) A new generation of $Ca^{2+}$ indicators with greatly improved fluorescence properties. *J. Biol. Chem.* **260,** 3440–3450.

# 7

# Measuring $Ca^{2+}$ Changes in Multiwell Format Using the Fluorometric Imaging Plate Reader

**Ian C. B. Marshall, Davina E. Owen, and Shaun McNulty**

## 1. Introduction

The Fluorometric Imaging Plate Reader (FLIPR®; Molecular Devices, Sunnyvale, CA; *see* **Fig. 1**) has made a significant contribution to drug discovery programs in the pharmaceutical industry since the first commercial instruments were introduced 9 yr ago ***(1)***. The key advantage of FLIPR over conventional plate readers is its ability to measure fluorescence emission from multiple wells (96- or 384-well) simultaneously and with high temporal resolution. Consequently, FLIPR has been used extensively to record dynamic intracellular processes such as changes in intracellular $Ca^{2+}$ ion concentration, membrane potential, and pH. Since FLIPR is used to measure a functional response in cells, it is rapidly able to distinguish full agonists, partial agonists, and antagonists at a target of interest, making the system a valuable screening tool for interrogation of compound libraries. Typically, FLIPR can be used to screen more than 150 compound plates per day in a high-throughput screening environment equating to more than 50,000 compounds at a single concentration in a 384-well system.

As FLIPR is an excellent tool for monitoring changes in intracellular $Ca^{2+}$ concentration, it is ideally suited to the characterization of ligand-gated ion channels or G protein-coupled receptors (GPCRs) linked to phospholipase C and $Ca^{2+}$ mobilization. However, GPCRs that normally signal through adenylyl cyclase (i.e., receptors coupled to G proteins $G_i$ or $G_s$ which inhibit or activate adenylyl cyclase respectively) can also be studied using FLIPR in recombinant systems through the use of promiscuous "adaptor" ***(2)*** and chimeric G proteins ***(3,4)*** that artificially couple these receptors to the $Ca^{2+}$ release machinery.

From: *Methods in Molecular Biology, vol. 312: Calcium Signaling Protocols: Second Edition*
Edited by: D. G. Lambert © Humana Press Inc., Totowa, NJ

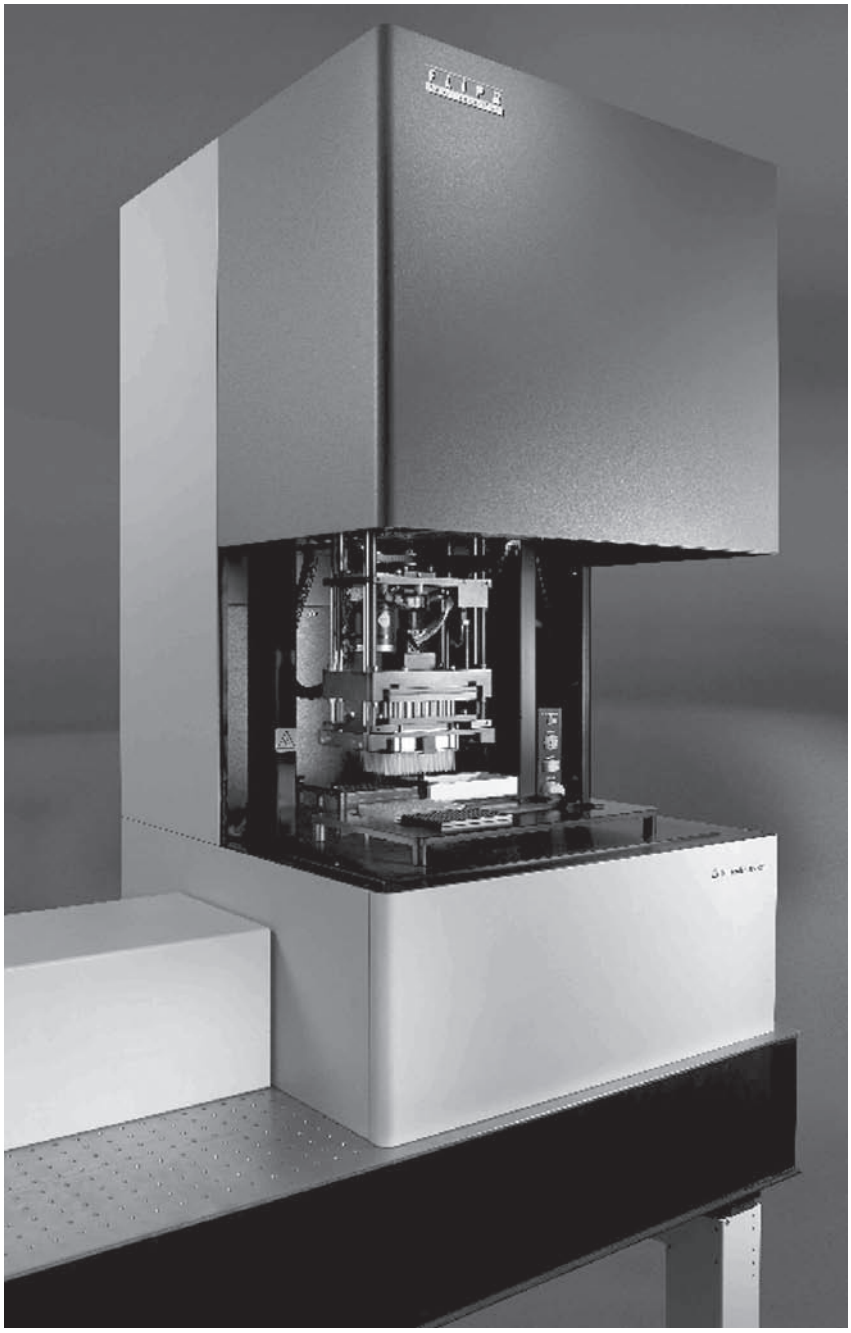

Fig. 1. The Fluorometric Imaging Plate Reader (FLIPR®: Molecular Devices, Sunnyvale, CA.

The FLIPR system uses an argon-ion laser to illuminate each well of a 96- or 384-well plate simultaneously. The laser has two excitation peaks (488 and 510 nm) making the system compatible for a number of nonratiometric $Ca^{2+}$ indicator dyes including fluo-3, fluo-4 and Calcium Green-1. Emitted light from the whole plate is collected through a highly sensitive, cooled charge-coupled device (CCD) camera. Patented excitation optics in conjunction with restricted depth of field of the CCD camera reduce the contribution of background fluorescence owing to extracellular dye. Successive measurements can be taken at 1-s intervals across the whole plate for measurement of transient responses or can be taken over tens of minutes for responses demonstrating longer time courses. During acquisition, a robotic multiwell pipetor adds test compounds to the plate as required, allowing measurements to be taken before and after compound addition. A large number of experimental conditions can be controlled by the user (e.g., laser parameters, camera parameters, time of agonist addition, mixing parameters) to permit optimization of assays for different cells and dye loading protocols. In order to minimize experimental variability caused by inconsistent environmental conditions, the FLIPR system contains a heated stage maintaining the assay and reagent microplates at a constant temperature during experiments.

Recently, the FLIPR$^3$ system has been launched, which offers additional sensitivity and capability to measure luminescence (e.g., some bright luciferase and aequorin). Automated FLIPR systems for ultrahigh-throughput have also become available that employ integrated plate stackers, washers, and specialized stages to allow users to shuttle cell and compound plates from incubators or storage magazines onto the FLIPR system itself.

Here we describe generic methods that can be used to study agonist and antagonist properties of test compounds in recombinant cell systems using standard FLIPR formats. These methods are best used as a starting point to which additional modifications relevant to the researchers particular model system should be made to optimise signal-to-noise ratios.

## 2. Materials

1. Human embryonic kidney (HEK293) cells and Chinese Hamster Ovary (CHO) cells. These are typical cell lines used successfully in FLIPR experiments designed to investigate recombinantly expressed targets (*see* **Note 1**).
2. Tyrodes buffer: 145 m*M* NaCl, 2.5 m*M* KCl, 10 m*M* HEPES, 10 m*M* glucose, 1.2 m*M* $MgCl_2$, and 1.5 m*M* $CaCl_2$.
3. Fluo-3 or fluo-4 acetoxymethyl ester (AM) (Molecular Probes, Eugene, OR) dissolved in dimethyl sulfoxide (DMSO) to give a 2-m*M* stock solution. Aliquots should be stored at –20°C and used once only after thawing (*see* **Note 2**).
4. Probenecid (Sigma, Poole, UK) dissolved in 1 *M* of NaOH (5 mL) and diluted 1:1 with Tyrodes buffer to give a 250-m*M* stock (*see* **Note 3**).

5. Pluronic F-127 (Molecular Probes) dissolved in DMSO at 20% (w/v) (*see* **Note 4**).
6. Culture flasks: 75-cm$^2$ (Nunc, Denmark).
7. Cell plates: 96-well, black-walled, clear-base plates with or without poly-D-lysine or suitable alternative coatings (Corning, High Wycombe, UK).
8. Compound plates: 96-deep-well, clear V-bottom polypropylene plates (Greiner, Stonehouse, UK.).
9. Black, disposable, 200-µL nonsterile polypropylene tips (Molecular Devices Corporation, UK).
10. Embla Plate Washer (Molecular Devices).

## 3. Methods

### 3.1. Preparation of Cells for $Ca^{2+}$ Measurements

1. HEK293 cells are typically grown in 75-cm$^2$ flasks in minimum essential medium supplemented with nonessential amino acids, 10% fetal calf serum, and 2 m*M* of L-glutamine at 37°C under 5% $CO_2$. CHO cells are grown in Hams-F12 medium supplemented with 10% fetal bovine serum at 37°C under 5% $CO_2$.
2. Seed cells into black-walled, clear-based, 96-deep-well plates at a density of 25,000 cells per well (minimum volume 100 µL) and culture overnight prior to experimentation (*see* **Note 1**).

### 3.2. Preparation of Agonist/Antagonist Plates

1. Prepare agonists and antagonists in clear 96-deep-well plates as follows: make up agonists at 4× and antagonists at 6× their final maximum concentrations by dissolving first in appropriate solvent and diluting in Tyrodes buffer.
2. Apply highest required concentrations of compounds to end column of plates and perform serial dilutions across the plates as required. Half- or quarter-log dilutions can be performed either manually or using robotic systems (e.g., Biomek 2000, Beckman Coulter, Fullerton, CA). The final concentration ranges used are commonly between 0.1 and 10 µ*M*. For compounds dissolved in DMSO, the final concentration of DMSO applied to cells should not exceed 1%. Adequate experimental controls must be established to investigate potential solvent effects for each experimental system used.

### 3.3. Loading Cells With Fluorescent Indicator

1. Mix equal volumes of fluorescent indicator (fluo-3/fluo-4) and pluronic F-127 stocks.
2. Prepare loading medium by adding dye–pluronic F-127 mixture to cell culture medium or Tyrodes buffer to obtain a final concentration of 6 µ*M* (fluo-4) or 12 µ*M* (fluo-3).
3. Add 50 µL of loading medium per well. Incubate for 30–120 min at either room temperature or 37°C (*see* **Note 5**). Probenecid (2.5 m*M*) can be included in the loading medium and/or wash medium if required, ensuring adequate dye loading (*see* **Note 3**).

4. Wash the cells four times with 200 µL of Tyrodes buffer using an Embla Plate Washer and leave in 125 µL of Tyrodes buffer (*see* **Note 6**) for antagonist studies or 150 µL for agonist studies requiring a single compound addition.
5. Add 25 µL of buffer or antagonist as appropriate from the antagonist plate (this step can be done using a Biomek FX robotic system; Beckman Coulter) and incubate for 30 min.

### 3.4. Measurement of $Ca^{2+}$ on the FLIPR

1. Transfer the cell plate, agonist plate, and tip rack to the appropriate positions on the FLIPR imaging platform.
2. A signal test should be undertaken to establish effective dye loading and confirm robust cell plating by establishing basal fluorescence prior to experimental initiation. During this process, the CCD camera captures an image of the plate before addition of agonists and the mean fluorescence reading for each well is displayed on the monitor. The signal test allows the user to determine whether cells have loaded with dye uniformly across the plate and also if pre-incubated compounds have elicited any agonist effect on the cells. An optimal signal test should give an average fluorescence intensity value of 8000 to 12,000 fluorescence intensity units (FIU) per well (*see* **Note 7**).
3. If the fluoresence intensity value is too low to obtain a good signal:noise ratio, adjust FIU output if necessary by altering the laser output, the camera aperture or the image exposure length. Typically, the camera aperture is set to F2, the camera exposure to 0.4 s, and the laser output is adjusted between 300 and 800 mW to achieve optimal fluorescence intensity.
4. Adjust FLIPR run protocol as required to control data acquisition parameters and compound additions. During the run, the FLIPR will automatically transfer agonists to the cell plate using an integrated robot and images will be captured before and after the addition of agonist (*see* **Note 8**).
5. Once parameters are set, initiate the experimental run.

### 3.5. Data Analysis

1. Following completion of the FLIPR acquisition, data are automatically stored. For permanent storage of data files, it is recommended that data is transferred via networked connections to a secure server or recordable CD.

1. For each well, fluorescent readings are extracted and tabulated versus time within an ASCII text file. Data can then be exported to a software package for analysis of results and curve fitting. Typically, data are analyzed using an iterative curve-fitting package (e.g., GraphPad Prism) and curves are fitted using a four-parameter logistic equation.
3. Agonist potencies are typically reported as $EC_{50}$ values (concentration yielding half-maximal effect) or $pEC_{50}$ (where $pEC_{50} = -\log [EC_{50}]$) and intrinsic activity (maximal effect as a proportion of the maximal effect of a reference agonist).
4. Antagonist potencies are typically reported as $IC_{50}$ values (molar concentration yielding 50% inhibition of a reference agonist stimulation) or $K_B$ as follows:

$$K_B = IC_{50}/\{1 + [(\text{agonist})/EC_{50}]\}$$

where (agonist) is the molar agonist concentration used and $EC_{50}$ is the molar potency of the agonist.

## 4. Notes

1. Weakly adherent cell lines can be used in the FLIPR by using poly-D-lysine coated plates. Suspension cultures can also be used in FLIPR. However, for these cells it is advisable to centrifuge cells to the bottom of the plate following loading in order to generate a monolayer of cells at the bottom of the well.
2. Fluo-3 acetoxymethyl (AM) and fluo-4 AM are insoluble in aqueous solution. Concentrated stocks in DMSO should be divided into small aliquots suitable for individual experiments and stored frozen at –20°C until use. It is essential to mix the DMSO stock well to avoid the formation of particulates that can become compartmentalized during dye loading.
3. Probenecid is an inhibitor of inorganic anion transporters that are able to extrude the hydrolyzed form of dyes from the cytosol. During assay development, it is advisable to compare dye loading in the presence and absence of probenecid to determine whether inorganic anion transporters are a problem for the particular cells under investigation.
4. Pluronic F-127 is a nonionic detergent that is commonly used to improve dispersion of AM ester forms of fluorescent indicators in aqueous solution. For optimum results, pluronic F-127 should be mixed with dye before addition to the aqueous buffer.
5. Optimal dye loading conditions (e.g., concentration of dye, loading time/temperature, and inclusion of probenecid) should be determined empirically during assay development for each cell line utilized.
6. The protocol for the Embla Plate Washer should be optimized for each assay. Adjustments can be made to aspiration and dispensation heights, dispensation speed, the strength of the vacuum, and the number of washes per cycle in order to minimize cell disruption. After the final wash step, cells should typically be allowed to recover for 20 min before running on the FLIPR.
7. Assays should be optimized to give suitable basal FIU (8000–12,000) and a robust agonist-induced response (typically 8000–25,000 FIU over basal). To achieve this, a number of parameters can be adjusted, including cell density, choice of dye, dye concentration, and loading conditions. Responses should be less than 40,000 FIU to avoid camera saturation (the CCD camera saturates at approx 65,000 FIU).
8. The parameters for the integrated FLIPR pipetor require optimization for each assay. The dispensation height of the pipetor and the speed of dispensation should be adjusted to ensure optimal delivery of the compounds to the specific plates being used. Optimal delivery should cause no cell disruption but should allow adequate mixing of the compounds in the well. To assist adequate mixing of compounds, the volume of agonist added to the well is typically 25% of the final well volume. The optimal dispenser speed may vary according to how well cells

adhere to the bottom of the well. Cells can be checked following dispensation using the plate viewer.

## References

1. Shroeder, K. S. and Neagle, B. D. (1996) FLIPR: A new instrument for accurate, high throughput optical screening. *J. Biomol. Screening* **1**, 75–80.
2. Milligan, G., Marshall, F. and Rees, S. (1996) $G_{16}$ as a universal G protein adapter: implications for agonist screening strategies. *Trends Pharmacol. Sci.* **17**, 235–237.
3. Conklin, B. R., Farfel, Z., Lustig, K. D., Julius, D., and Bourne, H. R., (1993) Substitution of three amino acids switches receptor specificity of $G_q$ to that of $G_{ia}$. *N ature* 363, 274–276.
4. Coward, P., Chan, S. D. H., Wada, H. G., Humphries, G. M., and Conklin, B. R. (1999) Chimeric G-proteins allow a high-throughput signalling assay of $G_i$ coupled receptors. *Anal. Biochem.* **270**, 242–248

# III

# Measurement of $Ca^{2+}$ Channel Activity

# 8

# Measurement of $Ca^{2+}$ Entry Using $^{45}Ca^{2+}$

**Mercedes Villarroya, Manuela G. López, María F. Cano-Abad, and Antonio G. García**

## 1. Introduction

For decades, the measurement of extracellular $Ca^{2+}$ ($^{40}Ca_o^{2+}$) entry into cells, using $^{45}Ca^{2+}$ as carrier, has been a widely used technique. One of the first studies was performed by Hodgkin and Keynes ***(1)*** to measure the rate at which $^{40}Ca^{2+}$ labeled with $^{45}Ca^{2+}$ crosses the surface membrane of resting squid axons, or during nervous activity. In a few large excitable cells, it was also possible to measure $Ca^{2+}$ entry indirectly through the measurement of inward currents through $Ca^{2+}$ channels under voltage-clamp conditions ***(2)***; however, $Ca_o^{2+}$ entry into small excitable cells could only be measured using $^{45}Ca^{2+}$. With the improvement of patch-clamp techniques ***(3)***, $Ca_o^{2+}$ entry was measured via the analysis of single-channel or whole-cell inward currents through $Ca^{2+}$ channels. The first detailed study of $Ca^{2+}$ channel currents in small mammalian excitable cells was performed in 1982 ***(4)*** in bovine adrenal medullary chromaffin cells, in the laboratory of Erwin Neher, where patch-clamp methodologies were developed. As patch-clamp techniques evolved, it seemed that the measurement of $Ca_o^{2+}$ entry using $^{45}Ca^{2+}$ would no longer be useful. Isotopes and scintillation fluids are expensive, administrative controls for good laboratory practices are always increasing, and the manipulation of isotopes becomes a growing nuisance. On the other hand, the time resolution of techniques using $^{45}Ca^{2+}$ entry are in the range of seconds, whereas the patch-clamp measurement of inward $Ca^{2+}$ currents is in the range of milliseconds, three orders of magnitude lower.

Although patch-clamp techniques are available to measure whole-cell currents through $Ca^{2+}$ channels, $^{45}Ca^{2+}$ entry is still used routinely as, on pharmacological grounds, a good correlation between data obtained with the two methodologies has been found. In addition, the use of $^{45}Ca^{2+}$ offers the follow-

From: *Methods in Molecular Biology, vol. 312: Calcium Signaling Protocols: Second Edition*
Edited by: D. G. Lambert © Humana Press Inc., Totowa, NJ

ing advantages: (1) cells can be plated in multiwell plates (12–96 wells) at different densities, so that a screening of the effects of large numbers of drugs and toxins on $^{45}Ca^{2+}$ entry can be systematically performed; (2) direct chemical measurement of the actual $Ca^{2+}$ entering the cells in mol/cell · s can be performed; (3) the time resolution for $Ca^{2+}$ entry can be increased to 1 s; and (4) interference with intracellular $Ca^{2+}$ buffering systems does not occur, since all $^{45}Ca^{2+}$ found in the cells at the end of a given experiment entered such cells from the extracellular space; this contrasts with the measurements of fura-2 $Ca^{2+}$ transients ***(5)*** that do not distinguish between $Ca^{2+}$ entry, intracellular $Ca^{2+}$ sequestration, and/or intracellular $Ca^{2+}$ mobilization.

## 2. Materials

1. Chromaffin cells isolated from the medulla of bovine adrenal glands.
2. $Ca^{2+}$-$Mg^{2+}$-free Locke buffer: 154 m*M* NaCl, 5.6 m*M* KCl, 3.5 m*M* $NaHCO_3$, 11 m*M* glucose, and 10 m*M* HEPES buffer, pH 7.2.
3. Krebs-HEPES solution: 140 m*M* NaCl, 5.9 m*M* KCl, 1.2 m*M* $MgCl_2$, 1 m*M* $CaCl_2$, 11 m*M* glucose, 10 m*M* HEPES, pH 7.2.
4. High $K^+$ solution: Krebs-HEPES containing 70 m*M* KCl with isosmotic reduction of NaCl.
5. DMPP solution: Krebs-HEPES with 100 μ*M* final concentration of the nicotinic receptor agonist dimethylphenylpiperazinium (DMPP).
6. Dulbecco's modified Eagle's medium (DMEM) (Gibco, UK).
7. Collagenase from *Clostridium histolyticum* (Boehringer-Mannheim, Germany).
8. Bovine serum albumin (BSA) fraction V.
9. Soybean trypsin inhibitor.
10. Cytosine arabinoside.
11. Fluorodeoxyuridine.
12. 1,1-dimethyl-4-phenyl-piperazinium (DMPP).
13. EGTA (Sigma, USA).
14. Percoll (Pharmacia, Sweden).
15. Fetal calf serum.
16. Penicillin and streptomycin (Gibco).
17. Scintillation fluid Ready micro (Beckman, USA).
18. $^{45}Ca$ (specific activity 10–40 mCi $mg^{-1}$ calcium, Amersham, UK).
19. All other chemicals are reagent grade.

## 3. Methods

$^{45}Ca^{2+}$ entry has been measured in a large variety of organs, tissues, cells, organelles, and natural or artificial membranes. However, the authors will describe only the model that they most often use—the cultured bovine adrenal medullary chromaffin cell. Many of the issues raised for this model can be extrapolated to other biological models, although the conditions must be defined according to the questions formulated to each system. The authors

use this technique most often to study $Ca^{2+}$ entry through voltage-dependent $Ca^{2+}$ channels in chromaffin cells.

### *3.1. Isolation and Culture of Chromaffin Cells* (see **Note 1**)

The bovine adrenal medullary chromaffin cells are widely used because large quantities of cells can be isolated from a few glands obtained from local abattoirs. In brief, the procedure is as follows (from **ref. *6***, with some modifications):

1. Obtain four adrenal glands from a local slaughtherhouse and bring to the laboratory in ice-cold Locke's buffer. Perform all further steps under sterile conditions.
2. Clean the adrenals of fat and cannulate the adrenal vein. Then, perform several fluid injections.
3. Through the adrenal vein, wash the glands three times with $Ca^{2+}$- and $Mg^{2+}$-free Locke's buffer at room temperature.
4. To carry out medullae digestion, inject, with a syringe, 5 mL of a solution containing 0.25% collagenase, 0.5% BSA fraction V, and 0.01% soybean trypsin inhibitor in $Ca^{2+}$-$Mg^{2+}$-free Locke's buffer, until the glands swell. Then incubate them at 37°C for 15 min; repeat this procedure three times.
5. Wash out the collagenase with a large volume of $Ca^{2+}$-$Mg^{2+}$-free Locke's buffer.
6. Filter the cells first with a 217-µm nylon mesh and thereafter with an 80-µm nylon mesh. Place them on a self-generated Percoll gradient containing 19 mL of Percoll (17.1 mL of Percoll plus 1.9 mL of 10-fold-concentrated $Ca^{2+}$-$Mg^{2+}$-free Locke's buffer at pH 5), plus 21 mL of cell suspension (approx $50–100 \times 10^6$ cells). Final pH of the mixture is 7.2.
7. Centrifuge the mixture at 13,000*g* for 20 min (rotor SS-34, Sorvall centrifuge Model RC-5, Dupont Instruments, USA) at 22°C. Take the lower band of the gradient (enriched in adrenaline-containing cells), wash it once with $Ca^{2+}$-$Mg^{2+}$-free Locke's buffer and a second time with DMEM.
8. Resuspend cells in DMEM supplemented with 10% FCS, 10 µ*M* cytosine arabinoside, 10 µ*M* fluorodeoxyuridine, 50 IU·mL$^{-1}$ penicillin, and 50 µg·mL$^{-1}$ streptomycin.
9. Plate cells on uncoated, 16-mm-diameter plastic culture wells (24 wells/plate), at a density of $5 \times 10^5$ cells/well, or in 5-mm-diameter plastic wells (96 wells/plate), at a density of $2 \times 10^5$ cells/well (in 0.2 mL of DMEM). Maintain cells at 37°C in a humidified incubator under an atmosphere of 95% air and 5% $CO_2$. Change the medium after 24 h, and replace with DMEM without FCS. Subsequently, change the medium every 3 d. Use cells 2–7 d after dissociation.

### *3.2. $^{45}Ca^{2+}$ Entry Studies in Chromaffin Cells Plated in Macrowells*

Most of the studies available on $^{45}Ca^{2+}$ uptake into chromaffin cells have been performed in 24-well plates ***(7–17)***. The procedure comprises the following steps **(Fig. 1)**:

1. Wash the cells (2–7 d in culture) twice with 500 µL of Krebs-HEPES solution, over a 10-min period at 37°C (*see* **Note 2**).

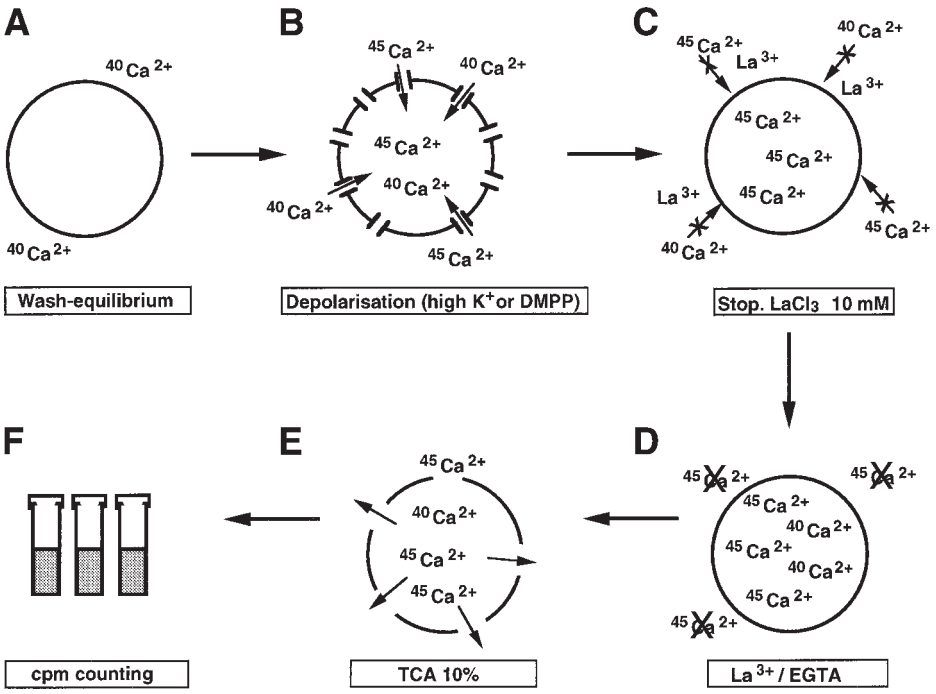


Fig. 1. Steps involved in the procedure used to measure $^{45}Ca^{2+}$ + $^{40}Ca^{2+}$ into chromaffin cells stimulated with high $K^+$ or with the nicotinic receptor agonist DMPP (*see* **Subheading 3.** for details).

2. Incubate the cells at 37°C (*see* **Note 3**) with $^{45}CaCl_2$, at a final concentration of 5 µCi · $mL^{-1}$, with Krebs-HEPES solution (basal uptake), high $K^+$ solution, or DMPP solution (*see* **Note 4**).
3. After a given stimulation time (1–60 s; *see* **Note 5**), rapidly aspirate and stop the reaction by adding 500 µL of cold $Ca^{2+}$-free Krebs-HEPES containing 10 m*M* $LaCl_3$ (*see* **Note 6**).
4. Wash the cells five times more with 500 µL of cold $Ca^{2+}$-free Krebs-HEPES containing 10 m*M* $LaCl_3$ and 2 m*M* EGTA, at 15-s intervals, to remove all extracellular $^{45}Ca^{2+}$ attached to the walls of the well and to the cell surface (*see* **Note 7**).
5. Add 500 µL of 10% trichloroacetic acid and scrape the cells with a plastic pipet tip.
6. Transfer the volume of each well to a polyethylene vial, add 3 mL of scintillation fluid, mix vigorously, and count in a scintillation beta counter (*see* **Note 8**).

### *3.3. $^{45}Ca^{2+}$ Entry Studies in Chromaffin Cells Plated in Microwells*

$^{45}Ca^{2+}$ uptake can also be studied in cells plated in microwells ***(18–21)***. This is especially useful to save cells or when the compounds to be tested are expensive (i.e., ω-conotoxins to block $Ca^{2+}$ channel subtypes, α-conotoxins to block

neuronal nicotinic acetylcholine receptor ion channels). In addition, when large numbers of compounds are to be tested for the blockade or activation of $Ca^{2+}$ channels, or other ionic channels, indirectly responsible for an enhanced $Ca^{2+}$ uptake (i.e., $Na^+$ channels, nicotinic receptor channels, $Ca^{2+}$-activated $K^+$ channels), this method in particular is useful.

**Figure 2** shows the $^{45}Ca^{2+}$ taken up by cells in cpm, when plated at a density of $5 \times 10^4$ cells/well (white columns) or $10^5$ cells/well. Note that doubling the number of cells does not lead to parallel increments of $^{45}Ca^{2+}$ uptake (**Figure 2A**). Hence, basal $^{45}Ca^{2+}$ entry increased by approximately only 20%, whereas doubling of cells enhanced the DMPP response nearly threefold and the $K^+$ response nearly twofold. This indicates that cells cultured at higher densities express more nicotinic receptors and/or voltage-dependent $^{45}Ca^{2+}$ channels.

### *3.4. Calculation of Actual $^{40}Ca^{2+}$ Entry in Weight Units*

$Ca^{2+}$ channel current studies measure charge, and, thus, quantitations cannot be made at lower $[Ca^{2+}]_o$ (i.e., below 1–2 m*M*). On the other hand, fura-2 monitoring of $Ca^{2+}$ entry only measures changes in cytosolic $[Ca^{2+}]$. Thus, the only method that directly determines the amount of $Ca^{2+}$ entering the cell, measured chemically, involves use of $^{45}Ca^{2+}$ as a radiotracer and different concentrations of unlabeled $^{40}Ca^{2+}$ ***(22)***.

**Table 1** summarizes the calculations required to determine various parameters of $Ca^{2+}$ uptake, derived from the uptake (cpm) at the end of an experiment. The data were taken from one experiment similar to that shown in **Fig. 3**, performed in microwells containing $2 \times 10^5$ chromaffin cells. Cells were depolarized for 10 s with a solution containing 100 μ*M* DMPP, 5 $\mu Ci \cdot mL^{-1}$ of $^{45}Ca^{2+}$ as tracer, and 1 m*M* of unlabeled $^{40}Ca^{2+}$. Basal $^{45}Ca^{2+}$ uptake was estimated in parallel wells by incubating the cells in a Krebs-HEPES solution lacking DMPP, and containing similar concentrations of $^{45}Ca^{2+}$ and $^{40}Ca^{2+}$.

Net cpm of $^{45}Ca^{2+}$ taken up by stimulated cells (2310 cpm/$2 \times 10^5$ cells) is obtained by subtracting the cpm in resting cells from the cpm in DMPP-stimulated cells. The specific activity of $^{45}Ca^{2+}$ + $^{40}Ca^{2+}$, estimated by counting an aliquot of 10 μL of Krebs-HEPES medium, is 7805 cpm/nmol. Hence, the 2310 net cpm of $^{45}Ca^{2+}$ found in $2 \times 10^5$ cells is equivalent to 0.296 nmol $^{40}Ca^{2+}$ or 296 pmol/($2 \times 10^5 \cdot$ cells) or 1.48 fmol/cell. Thus, each cell stimulated by DMPP over 10 s took up 1.48 fmol of unlabeled $Ca^{2+}$.

Now the rate of $Ca^{2+}$ entry per unit time can be determined. A 20 μm diameter sphere has 1256 $\mu m^2$ of surface area, or $1.26 \times 10^{-5}$ $cm^2$. Assuming that $^{45}Ca^{2+}$ uptake was linear during the first 10 s of DMPP stimulation, the 1.48 fmol/cell of $Ca^{2+}$ taken up in 10 s becomes 0.15 fmol/(cell · s) or $0.15 \times 10^{-15}$ mol/(cell · s), which, expressed by surface area becomes 11.7 pmol/($cm^2 \cdot$ s).

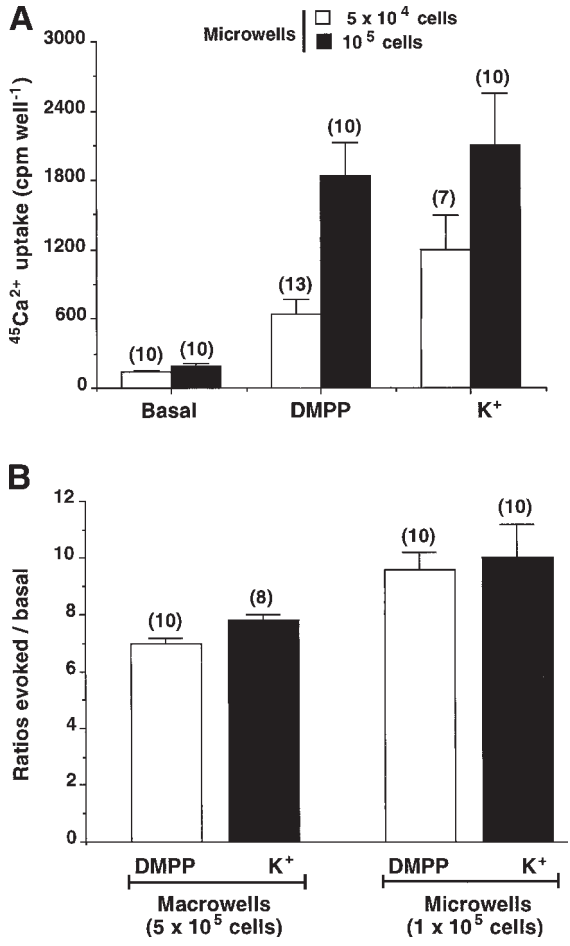


Fig. 2. Comparison of $^{45}Ca^{2+}$ uptake into bovine chromaffin cells cultured in 96-well plates (microwells) or 24-well plates (macrowells). **(A)** cpm of $^{45}Ca^{2+}$ taken up by cells plated in microwells, at a density of $5 \times 10^4$ cells/well (white columns) or at a density of $10^5$ cells/well (black columns). In each case, cells were exposed to the $^{45}Ca^{2+}$ solution (4 μCi · $mL^{-1}$ of $^{45}Ca^{2+}$ in 1 m*M* $^{40}Ca^{2+}$) either in Krebs-HEPES solution (basal), or in Krebs-HEPES containing 100 μ*M* DMPP or high $K^+$ (70 m*M* $K^+$, with isosmotic reduction of $Na^+$). **(B)** The ratios evoked:basal ($^{45}Ca^{2+}$ taken up by cells stimulated with DMPP or $K^+$, vs $^{45}Ca^{2+}$ taken up by resting cells). Data are means ± SEM of the number of wells shown in parentheses, from cells from at least two different cultures.

A third parameter that can be measured is the number of $Ca^{2+}$ ions entering the cell through each individual $Ca^{2+}$ channel in 1 s. Assuming that all $Ca^{2+}$ channels are open during cell depolarization and that the bovine chromaffin

**Table 1**
**Calculation of Rate and Amount of $Ca^{2+}$ Entry Into Single Chromaffin Cells, in Response to a Brief Depolarizing Stimulus (100 μ*M* DMPP for 10 s)** [a]

**Experimental conditions:** microwells (96-well plate) containing $2 \times 10^5$ cells, 3 d in culture. 5 μCi · $mL^{-1}$ of $^{45}Ca^{2+}$ plus 1 m*M* $^{40}Ca^{2+}$ were present in the extracellular solution.

**$^{45}Ca^{2+}$ uptake (in cpm)**

$^{45}Ca^{2+}$ taken up by resting cells: 571 ± 29 cpm $2 \times 10^5$ $cells^{-1}$

$^{45}Ca^{2+}$ taken up by cells stimulated with DMPP (100 μ*M*, 10 s): 2880 ± 225 cpm/$2 \times 10^5$ cells.

Net $^{45}Ca^{2+}$ taken up by DMPP-stimulated cells (evoked/basal/evoked minus basal): 2310 ± 196 cpm/$2 \times 10^5$ $cells^{-1}$

**Conversion of cpm into mass units**

$^{45}Ca^{2+}$ in 10 μL of DMPP-containing Krebs-HEPES (5 μCi · $mL^{-1}$ of $^{45}Ca^{2+}$): 78,047 cpm

$^{40}Ca^{2+}$ present in DMPP-containing Krebs-HEPES medium: 1 m*M*

In 10 μL medium: 10 nmol of $^{40}Ca^{2+}$

In 10 μL of cell extract (cells stimulated with 100 μ*M* DMPP for 10 s): 2310 cpm

$^{40}Ca^{2+}$ in $2 \times 10^5$ cells: 296 pmol or 1.48 fmol of $Ca^{2+}$/cell in 10 s = $1.48 \times 10^{-15}$ mol/cell 10 s

**Rate of $Ca^{2+}$ entry/unit surface area**

Surface area of the cell: 1256 $\mu m^2$ = $1.26 \times 10^{-5}$ $cm^2$

Rate of $Ca^{2+}$ entry = $0.15 \times 10^{-15}$ mol/cell · s/$1.26 \times 10^{-5}$ = $0.117 \times 10^{-10}$ mol/$cm^2$ · s = 11.7 pmol/$cm^2$ · s

**Rate of $Ca^{2+}$entry per single $Ca^{2+}$ channel**

Number of channels in a single chromaffin cell = 10/$\mu m^2$ = 12,560 channels/cell

Rate of $Ca^{2+}$ entry = $0.15 \times 10^{-15}$ mol/cell · s/12,560 channels = $1.19 \times 10^{-20}$ mol/channel · s = 6740 ions/channel · s

**Expected cytosolic $Ca^{2+}$ concentration after 1-s depolarization**

Volume of a single cell: $4 \times 10^{-9}$ mL

$Ca^{2+}$ in 1 mL of cytosol: ($0.15 \times 10^{-15}$ mol/cell · s) × (number of cells in 1 mL) = ($0.15 \times 10^{-15}$) × ($242 \times 10^6$) = $0.036 \times 10^{-6}$ mol/mL = 0.036 mol/L = 36 μ*M*

[a] For these calculations, the chromaffin cell has been considered as a sphere of 20 μm diameter. Data are means ± SEM of nine wells from three different cultures.

cell plasmalemma contains 10 channels/$\mu m^2$ (***4,9,23,24***) 12,560 channels/cell, 6740 ions/(channel · s) enter the cell during DMPP stimulation.

The fourth parameter is the expected cytosolic [$Ca^{2+}$] reached after 1-s depolarization, considering a uniform intracellular distribution without $Ca^{2+}$ buffering. The volume of a cell is $4 \times 10^{-9}$ mL and the $Ca^{2+}$ in 1 mL of cytosol (after 1-s depolarization) will be $0.036 \times 10^{-6}$ mol/mL, which is equivalent to 36 μ*M*. If a cytosolic water space of 50% is considered, this figure is doubled: 72 μ*M*. This calculated [$Ca^{2+}$] is much higher than the few micromolar levels

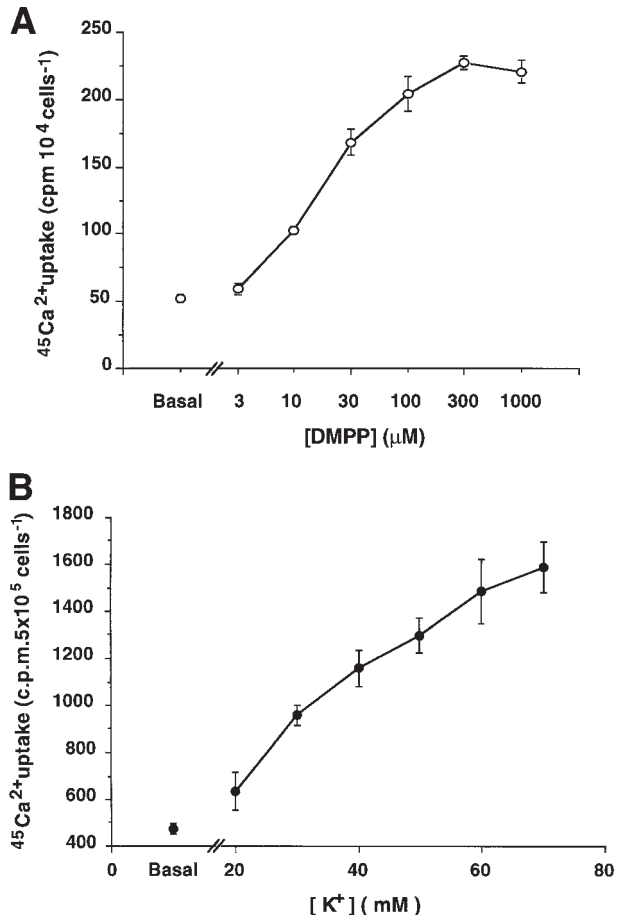


Fig. 3. $^{45}Ca^{2+}$ uptake into bovine chromaffin cells stimulated with increasing concentrations of the agonist for nicotinic acetylcholine receptors, DMPP (**A**) or with $K^+$ (**B**). This experiment was performed following the procedure shown in **Subheading 3.** Cells ($10^5$), plated in microwells (A) were stimulated for 10 s with DMPP; cells ($5 \times 10^5$) plated in macrowells (B) were also stimulated for 60 s with $K^+$. Data are expressed in cpm $^{45}Ca^{2+}$ retained by the cells (ordinate) and are means ± SEM of three to six wells from two different cell cultures.

of $[Ca^{2+}]_i$ increments obtained using $Ca^{2+}$ fluorescent dyes. Of course, it is highly unlikely that this free cytosolic $[Ca^{2+}]_i$ is reached during cell depolarization (except at subplasmalemmal sites near the inner mouth of $Ca^{2+}$ channels); powerful buffers will drastically and quickly reduce the $[Ca^{2+}]_i$. But the calculation using $^{45}Ca^{2+}$ measurements gives a more realistic idea of the huge

amounts of $Ca^{2+}$ that circulate during cell activation; this cannot be estimated from any other technique measuring $Ca^{2+}$ entry.

## 4. Notes

1. Separation and culture of viable adrenaline-containing and noradrenaline-containing cells in large amounts can also be achieved using combined Renografin and Percoll gradients ***(25,26)***. Because these cells have quite different physiological functions, and differ in their relative proportion of $Ca^{2+}$ channel subtypes ***(23)***, this separation can be useful to study $^{45}Ca^{2+}$ uptake in each separate cell population.
2. Cells maintained in the incubator for several days in DMEM solution will need to be equilibrated with the Krebs-HEPES in which the $^{45}Ca^{2+}$ uptake measurement is going to take place. Usually a 10-min period is enough, but this can be extended up to 30 min.
3. Net $^{45}Ca^{2+}$ uptake stimulated by DMPP and $K^+$ is similar in the temperatures range of 24–37°C. However, a physiological temperature is preferable. To keep cells at 37°C the plate is placed on a temperature-controlled water bath, with the bottom submerged in the water 3–5 mm. The solutions to be added are kept at 37°C in assay tubes, also submerged in the water bath.
4. $^{45}Ca^{2+}$ is taken up by cells under resting conditions; thus, in every experiment, control unstimulated cells are always included. Usually, in a single 24-well plate every variable is measured in triplicate; hence eight variables are possible. For instance, if a concentration-response curve with a given toxin that blocks a given $Ca^{2+}$ channel is desired, 3 wells are used to measure basal $^{45}Ca^{2+}$ uptake, another 3 to measure $K^+$-evoked $^{45}Ca^{2+}$ uptake through opened voltage-dependent $Ca^{2+}$ channels, and the remaining 18 wells can be used to measure the effects of up to six concentrations of the toxin on $K^+$-evoked $^{45}Ca^{2+}$ (*see* **ref. *27***).
5. With 1–2-s depolarization times, there is no time to remove the depolarizing solution and replace it with $La^{3+}$ solution. Therefore, it is better to stop the uptake reaction by adding 0.5 mL of a 20 m*M* $LaCl_3$-4 m*M* EGTA solution on top of the depolarizing solution, and then aspirate it slowly. Even in these conditions the process is unreliable at the 1–2-s time range.
6. Rapid aspiration does not mean uncontrolled aspiration of the fluid bathing the cells. If careful aspiration is not performed, cells will detach from the bottom of the well, and unreliable results will be obtained. The authors perform a gentle aspiration using a light vacuum pump connected with a tubing to a glass Pasteur pipet. The tip of the pipet is placed on the wall of the well, without touching the bottom, thus preventing cell aspiration. Triplicates are very important, and if they vary more than 10–20% they should be discarded.
7. More recently the authors have seen that **steps 3** and **4** (**Subheading 3.2.**) of the $^{45}Ca^{2+}$ uptake reaction can be performed as a single step, i.e., adding a washout solution containing 10 m*M* $LaCl_3$ and 2 m*M* EGTA.
8. **Figure 2** shows an example of experiments performed following this protocol. Note that a maximum $^{45}Ca^{2+}$ uptake (expressed as cpm $5 \times 10^{-5}$ $cells^{-1}$ in the ordinates) was reached at DMPP concentrations of 20–50 μ*M*, and at 60–70 m*M* $K^+$.

## References


1. Hodgkin, A. L. and Keynes, R. D. (1957) Movements of labelled calcium in squid giant axons. *J. Physiol.* **138,** 253–281.
2. Hagiwara, S. and Byerly, L. (1983) Calcium channel. *Annu. Rev. Neurosci.* **4,** 69–125.
3. Hamill, O. P., Marty, A., Neher, E., Sakmann, B., and Sigworth, F. J. (1981) Improved patch-clamp techniques for high-resolution current recording from cells and cell-free membranes patches. *Pflügers Arch.* **391,** 85–100.
4. Fenwick, E. M., Marty, A., and Neher, E. (1982) Sodium and calcium channels in bovine chromaffin cells. *J. Physiol.* **331,** 599–635.
5. Grynkiewicz, G. M., Poenie, M., and Tsien, R. Y. (1985) A new generation of $Ca^{2+}$ indicators with greatly improved fluorescence properties. *J. Biol. Chem.* **260,** 3440–3450.
6. Livett, B. G. (1984) Adrenal medullary chromaffin cells in vitro. *Physiol. Rev.* **64,** 1103–1161.
7. Kilpatrick, D. L., Slepetis, R. J., Corcoran, J. J., and Kirshner, N. (1982) Calcium uptake and catecholamine secretion by cultured bovine adrenal medulla cells. *J. Neurochem.* **38,** 427–435.
8. Holz, R. W., Senter, R. A., and Frye, R. A. (1982) Relationship between $Ca^{2+}$ uptake and catecholamine secretion in primary dissociated cultures of adrenal medulla. *J. Neurochem.* **39,** 635–646.
9. Ballesta, J. J., Palmero, M., Hidalgo, M. J., Gutiérrez, L. M., Reig, J. A., Viniegra, S., and García, A. G. (1989) Separate binding and functional sites for ω-conotoxin and nitrendipine suggest two types of calcium channels in bovine chromaffin cells. *J. Neurochem.* **53,** 1050–1056.
10. Gandía, L., Casado, L.-F., López, M. G., and García, A. G. (1991) Separation of two pathways for calcium entry into chromaffin cells. *Br. J. Pharmacol.* **103,** 1073–1078.
11. López, M. G., Fonteríz, R. I., Gandía, L., de la Fuente, M., Villarroya, M., García-Sancho, J., and García, A. G. (1993) The nicotinic acetylcholine receptor of the bovine chromaffin cell, a new target for dihydropyridines. *Eur. J. Pharmacol.* **247,** 199–207.
12. López, M. G., Abad, F., Sancho, C., de Pascual, R., Borges, R., Maroto, R., Dixon, W., and García, A. G. (1991) Membrane-mediated effects of the steroid 17-α-estradiol on adrenal catecholamine release. *J. Pharmacol. Exp. Ther.* **259,** 279–285.
13. Villarroya, M., Gandía, L., Lara, B., Albillos, A., López, M. G., and García, A. G. (1995) Dotarizine versus flunarizine as calcium antagonists in chromaffin cells. *Br. J. Pharmacol.* **114,** 369–376.
14. Gandía, L., Villarroya, M., Sala, F., Reig, J.-A., Viniegra, S., Quintanar, J.-L., García, A. G., and Gutiérrez, L.-M. (1996) Inhibition of nicotinic-receptor mediated responses in bovine chromaffin cells by diltiazem. *Br. J. Pharmacol.* **118,** 1301–1307.

15. Villarroya, M., Gandía, L., López, M. G., García, A. G., Cueto, S., García-Navio, J.-L., and Alvarez-Builla, J. (1996) Synthesis and pharmacology of alkanediguanidium compounds that block the neuronal nicotinic acetylcholine receptor. *Bioorg. Med. Chem.* **4,** 1177–1183.
16. Villarroya, M., de la Fuente, M.-T., López, M. G., Gandía, L., and García. A. G. (1997) Distinct effects of ω-toxins and various groups of $Ca^{2+}$-entry inhibitors on nicotinic acetylcholine receptor and $Ca^{2+}$ channels of chromaffin cells. *Eur. J. Pharmacol.* **320,** 249–257.
17. Michelena, P., de la Fuente, M.-T., Lara, B., López, M. G., Gandía, L., and García, A. G. (1997) Drastic facilitation by α-latrotoxin of chromaffin cell exocytosis without measurable enhancement of $Ca^{2+}$ entry or $[Ca^{2+}]_i$. *J. Physiol.* **502,** 481–496.
18. López, M. G., Montiel, C., Herrero, C. J., et al. (1998) Unmasking the functions of the chromaffin cell $a_7$ nicotinic receptor by using short pulses of acetylcholine and novel selective blockers. *Proc. Nat. Acad. Sci. USA* **95,** 14,184–14,189.
19. Conceiçao, I. M., Lebrun, I., Cano-Abad, M., et al. (1998) Synergism between toxin gamma from the brazilian scorpion Tityus serrulatus and veratridine in chromaffin cells. *Am.J. Physiol.* **274,** C1745–C1754.
20. Villarroya, M., Olivares, R., Ruiz, A., et al. (1999) Voltage inactivation of $Ca^{2+}$entry and secretion associated with N- and P/Q-type but not L-type $Ca^{2+}$ channels of bovine chromaffin cells. *J. Physiol.* **516,** 421–432.
21. de los Ríos, C., Marco, J. L., Carreiras, M. D. C., Chinchón, P. M., García, A. G. and Villarroya, M. (2002) Novel tacrine derivatives that block neuronal calcium channels. *Bioorganic and Medicinal Chemistry* **10,** 2077–2088.
22. Artalejo, C. R., García, A. G., and Aunis, D. (1987) Chromaffin cell calcium channel kinetics measured isotopically through fast calcium, strontium, and barium fluxes. *J. Biol. Chem.* **262,** 915–926.
23. García, A. G., Sala, F., Reig, J. A., Viniegra, S., Frías, J., Fonteríz, R. I., and Gandía, L. (1984) Dihydropyridine Bay K 8644 activates chromaffin cell calcium channels. *Nature* **309,** 69–71.
24. Castillo, C. J. F., Fonteríz, R. I., López, M. G., Rosenheck, K., and García, A. G. (1989) (+)PN200-110 and ouabain binding sites in purified bovine adrenomedullary plasma membranes and chromaffin cells. *J. Neurochem.* **53,** 1442–1449.
25. Moro. M. A., López, M. G., Gandía, L., Michelena, P., and García, A. G. (1990) Separation and culture of living adrenaline- and noradrenaline-containing cells from bovine adrenal medullae. *Analytical Biochem.* **185,** 243–248.
26. Moro, M. A., García, A. G., and Langley, O. K. (1991) Characterization of two chromaffin cell populations isolated from bovine adrenal medulla. *J. Neurochem.* **57,** 363–369.
27. Lomax, R. B., Michelena, P., Núñez, L., García-Sancho, J., García, A. G., and Montiel, C. (1997) Different contributions of L- and Q-type $Ca^{2+}$ channels to $Ca^{2+}$ signals and secretion in chromaffin cell subtypes. *Am. J. Physiol.* **272,(Cell Physiol. 41),** C476–C484.

# 9

# Measurement of [$^3$H]PN200-110 and [$^{125}$I]ω-Conotoxin MVIIA Binding

**Kazuyoshi Hirota and David G. Lambert**

## 1. Introduction

Intracellular $Ca^{2+}$ ($[Ca^{2+}]_i$) can rise primarily via release from intracellular storage sites (e.g., the endoplasmic reticulum) or via entry across the membrane down the steep concentration gradient ***(1–3)***. $Ca^{2+}$ can enter through two main classes of plasma membrane-located $Ca^{2+}$ channels: receptor operated and voltage sensitive ***(4–7)***. Voltage-sensitive $Ca^{2+}$ channels are involved in a wide and diverse array of physiological responses including neurotransmitter release ***(8)***. In addition, many guanine nucleotide protein (G) coupled receptors couple to voltage-sensitive $Ca^{2+}$ channels to reduce $Ca^{2+}$ influx ***(9,10)***.

### *1.1. Voltage-Sensitive $Ca^{2+}$ Channels*

Voltage-sensitive $Ca^{2+}$ channels are classified into low-voltage activated (T-channels) and high-voltage activated (HVA, L-, N-, P/Q-, and R-channels). This further subclassification of LVA channels is based on the interaction of a range of inhibitors and toxins (**Table 1**) ***(4,8,11)***. LVA channels are comprised of four or five distinct subunits ($\alpha_{1/2}\beta\delta\gamma$) arranged in various combinations. The $\alpha_1$-subunit arises from six distinct genes (**Table 1**) and is the pore-forming subunit of the channel. The $\alpha_1$-subunit in the L-channel is also the site to which DHPs bind ***(4)***. In addition, ω-conotoxins bind to the α-subunit(s) ***(12,13)*** of the N-channel.

### *1.2. Radioligand Binding*

Radioligand binding studies enable the properties of drug–receptor interaction to be studied. Two commonly estimated parameters are the total number of receptors/channels expressed in a particular tissue ($B_{max}$) and the affinity

From: *Methods in Molecular Biology, vol. 312: Calcium Signaling Protocols: Second Edition*
Edited by: D. G. Lambert © Humana Press Inc., Totowa, NJ

**Table 1**
**Classification of High-Voltage-Activated $Ca^{2+}$ Channels**

| | L | N | P/Q | R |
|---|---|---|---|---|
| Specific inhibitor | DHPs [a] | ω-CgTx [b] | ω-Aga-IVA[c] | None |
| $\alpha_1$-subunit gene | $\alpha_{1S,1C,1D}$ | $\alpha_{1B}$ | $\alpha_{1A}$ | $\alpha_{1E}$ |

Note: *See also* Chapter 10, p. 162.
[a] DHPs, dihydropyridines.
[b] ω-CgTx, ω-conotoxin GVIA/VIIA.
[c] P-channels blocked by low concentrations and Q-channels blocked by high concentrations.

($K_d$) of a particular drug for a particular receptor/channel. Tissue samples are incubated with various concentrations of radiolabel until binding equilibrium is reached. The tissue and ligand are separated by either filtration or centrifugation and bound ligand is quantified. Receptor/channel binding is determined indirectly as the radiolabel will bind nonspecifically to nonreceptor protein. In practice, nonspecific binding (NSB) is defined by incubating an identical tube in the presence of a high concentration of an unlabeled drug that interacts with the receptor/channel. Specific binding is then the difference between total binding (in the absence of the unlabeled drug) and NSB (in the presence of the unlabeled drug) (**Fig. 1**).

Two types of experiments are commonly used:

1. Saturation in which the concentration of radiolabel increases until specific binding saturates (*see* **Fig. 1**). The saturation curve can be linearized to yield a straight line. $B_{max}$ and $K_d$ can be estimated.
2. Displacement curves enable the affinity of unlabeled drugs to be estimated. A fixed concentration of receptors/channels is labeled with a fixed concentration of label, and increasing concentration of unlabeled drug is added to displace the label (**Fig. 1**). The concentration of unlabeled drug producing 50% displacement is related to its affinity (*see* **Subheading 3.5.**).

In this chapter, the authors will describe a radioligand binding protocol for [$^3$H]PN200-110 binding to L-type channels and [$^{125}$I]ω-conotoxin MVIIA binding to N-channels. This latter toxin is particularly useful because the binding is reversible. Using these protocols, it will be possible to determine channel density and interaction of unlabeled compounds with the radiolabel binding site. Indeed, the authors have recently reported an interaction of a range of iv general and local anaesthetic agents with the [$^3$H]PN200-110 binding site in a variety of tissue preparations ***(14–16)***. For functional studies of $Ca^{2+}$ channel activity *see* Chapter 8.

## 2. Materials

### *2.1. Cell Culture*

1. Undifferentiated SH-SY5Y human neuroblastoma cells (gift from Dr. J. L. Beidler, Sloane Kettering Institute, Rye, NJ).

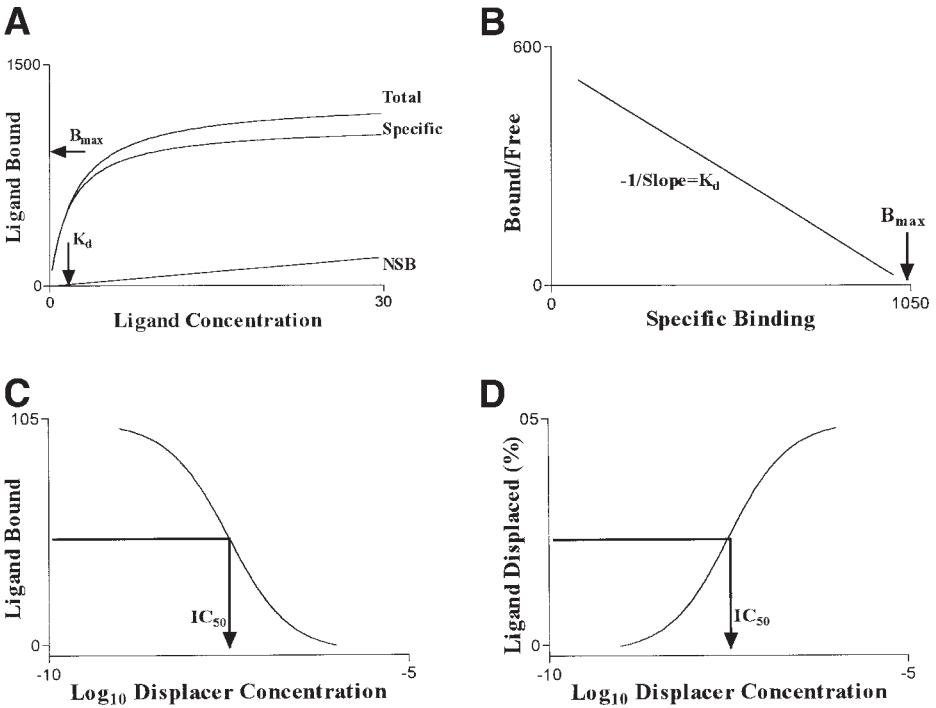


Fig. 1. Stylized saturation type assay used to determine $B_{max}$ and $K_d$ **(A)**. The specific binding curve is shown analyzed according to Scatchard [re] in **(B)**. In **(C)** and **(D)**, a stylized displacement type assay is depicted and used to estimate $IC_{50}$ and calculate $K_{50}$ for an unlabeled drug. Curves **(C)** and **(D)** are mirror images of each other indicating that as the amount bound decreases **(C)** the amount of displacement increases **(D)**.

2. Culture medium for SH-SY5Y cells: minimum essential medium supplemented with 10% fetal calf serum (FCS), 2 m*M* glutamine, 100 IU/mL penicillin, 100 IU/mL streptomycin, and 2.5 µg/mL fungizone (*see* **Note 1**).
3. NG108-15 neuroblastoma X glioma hybrid cells (*see* **Note 2**).
4. Culture medium for NG108-15 cells: Dulbecco's minimum essential medium supplemented with 10% FCS, 2 m*M* glutamine, 100 IU/mL penicillin, 100 IU/mL streptomycin, 2.5 µg/mL fungizone, and HAT (hypoxanthine (0.1 m*M*), aminopterin [0.4 µ*M*], thymidine [16 µ*M*]) (*see* **Note 1**).
5. Cell harvest buffer: 10 m*M* HEPES-buffered 0.9% saline plus 0.05% EDTA, pH 7.4 (with 10 *M* NaOH).

## 2.2. Assay Buffers and Reagents

1. Assay buffer for L-channel binding: 50 m*M* Tris-HCl, pH 7.4.
2. Assay buffer for N-channel binding: 50 m*M* Tris-HCl, pH 7.4, with 0.1% bovine serum albumin (BSA) added.

3. Wash buffer for L- and N-channel binding: 50 m*M* Tris-HCl, pH 7.4.
4. Nifedipine, 50 m*M* stock in dimethyl sulfoxide (DMSO) stored frozen at –20°C in 50-µL aliquots in the dark.
5. [$^3$H]PN200-110 (Amersham International, Bucks, UK).
6. [$^{125}$I]ω-conotoxin MVIIA (NEN Du Pont, Brussels) at a specific activity of 2200 Ci/mmol and reconstituted in distilled water to 50 µCi/mL (*see* **Note 3**).
7. ω-Conotoxin MVIIA, 1-µ*M* stock stored frozen at –20°C in 10-µL aliquots (*see* **Note 4**).
8. Polyethylenimine, 0.1% solution made in distilled water.
9. Cell harvest buffer: 10 m*M* HEPES-buffered 0.9% saline plus 0.05% EDTA, pH 7.4 (with 10 *M* NaOH).

## 3. Methods

### 3.1. Preparation of Rat Brain Membranes

1. Stun and then decapitate female Wistar rats (250–300 g).
2. Rapidly remove the brain, detach the cerebrocortex from its internal structures, and place in 50 m*M* of Tris-HCl, pH 7.4, at 4°C.
3. Homogenize brain tissue using an Ultra Turrax T25 (6 × 5 s bursts on ice).
4. Centrifuge the resulting homogenate at 18,000*g* for 10 min and resuspend the pellet in Tris-HCl buffer.
5. Repeat this procedure three times.
6. Determine membrane protein according to Lowry et al. ***(17)*** and freeze the homogenate in aliquots at –40°C for [$^3$H]PN200-110 binding or use fresh for [$^{125}$I]ω-conotoxin MVIIA binding studies.

### 3.2. Preparation of SH-SY5Y and NG108-15 Cell Membranes

1. Maintain confluent monolayers (75 cm$^2$) of cells in the appropriate media.
2. Split one flask of confluent cells using trypsin (0.5g/L)-EDTA (0.2g/L, 5 mL) solution as supplied (*see* **Note 1**) into nine other flasks each containing 15 mL of supplemented media. After 2 d of incubation (37°C, 5% $CO_2$ incubator), remove the media and replace with 25 mL of fresh supplemented media.
3. Culture cells (feed 24 h before use with fresh medium) until confluent (use cells up to 3 d postconfluency).
4. On the day of the experiment, remove medium and add 5 mL of harvest buffer to the cell monolayer.
5. Remove 5 mL of harvest buffer immediately, and add a further 5 mL of fresh harvest buffer and incubate at room temperature for approx 5 mins.
6. Gently tap the side of the flask to dislodge the adherent cell monolayer.
7. When all the cells are in suspension, transfer to a centrifuge tube. Rinse the cells out of the flask by adding approx 15 mL of harvest buffer. Transfer this to the centrifuge tube.
8. Sediment at 1000*g* in a low-speed centrifuge for 3 min.
9. Resuspend in 50 m*M* Tris-HCl, pH 7.4, at 4°C.

**Table 2**
**[$^3$H]PN200-110 Saturation Binding Assay**
**Addition Table to Determine $K_d$ and $B_{max}$[a]**

| Tube | Buffer | Nifedipine (50 μ*M*) | [$^3$H]PN200-110 (PN1–PN8) | Membranes |
|---|---|---|---|---|
| 1. $Total_{PN1}$ | 700 | — | 200 | 100 |
| 2. $Total_{PN1}$ | 700 | — | 200 | 100 |
| 3. $NSB_{PN1}$ | 500 | 200 | 200 | 100 |
| 4. $Total_{PN2}$ | 700 | — | 200 | 100 |
| 5. $Total_{PN2}$ | 700 | — | 200 | 100 |
| 6. $NSB_{PN2}$ | 500 | 200 | 200 | 100 |

Continue in groups of three to total of 24 tubes using all eight [$^3$H]PN dilutions.

Eight concentrations of [$^3$H]PN200-110 are used with three tubes per concentration set up as duplicate totals and single NSB ($8 \times 3 = 24$ tubes in total)

[a]Assay volume is 1000 μL. 50 μ*M* nifedipine stock is diluted 1:5 when added to the assay to yield a final concentration of 10 μ*M*.

10. Homogenize the suspension using an Ultra Turrax T25 ($6 \times 5$ s bursts on ice).
11. Centrifuge the resulting homogenate at 18,000*g* for 10 min and resuspend the pellet in Tris-HCl buffer.
12. Repeat this procedure three times.
13. Determine the membrane protein according to Lowry et al. ***(17)*** and freeze the homogenate in aliquots at –40°C for [$^3$H]PN200-110 binding or use fresh for [$^{125}$I]ω-conotoxin MVIIA binding studies.

## *3.3. Measurement of [$^3$H]PN200-110 Binding*

### *3.3.1. Saturation Binding Assays to Determine L-Channel Density* (see **Note 5**)

1. Assay volume is 1 mL and one saturation assay uses 24 tubes in total.
2. Dilute nifedipine stock for determination of NSB to give 50 μ*M* in assay buffer (**Subheading 2.2., item 1**). When 200 μL is added to the assay, the final "in the assay" concentration will be 10 μ*M* (200 μL/1000 μL = 1:5 dilution).
3. Make up a working stock of [$^3$H]PN200-110 of approx 2 n*M* in assay buffer (*see* **Note 6**).
4. Make seven serial dilutions of the 2 n*M* [$^3$H]PN200-110 stock by adding equal volumes of assay buffer. This will give eight concentrations as follows: 2, 1, 0.5, 0.25, 0.125, 0.0625, 0.0312, and 0.0156 n*M*.
5. Dilute prepared protein in assay buffer to give approx 200 μg/100 μL of brain membranes (but *see* **ref. *16***), or 800 μg/100 μL for SH-SY5Y and NG108-15 cells.
6. Add reagents to tubes as shown in **Table 2**.
7. Incubate at 20°C in the dark for 90 min.

8. During the incubation, soak Whatman GF/B harvester papers in 0.1% polyethylenimine to reduce NSB.
9. Separate bound and free radioligand by harvesting on a Brandell harvester (*see* **Note 6**).
10. Transfer the filters to scintillation insert vials and add 4.5 mL of scintillant. (The authors use OptiPhase "Safe" [LKB Wallac via Fisons, Loughborough, UK]).
11. Leave the filters for at least 8 h to extract, and then count on a scintillation counter for 3 min per sample.

### *3.3.2. Displacement Binding Assays to Determine Interaction of Unlabeled L-Channel Ligands* (see **Note 8**)

1. Assay volume is 1 mL and uses 24 tubes in total.
2. Dilute nifedipine stock for determination of NSB to give 50 µ*M* in assay buffer (**Subheading 2.2.**, **item 1**). When 200 µL is added to the assay, the final "in the assay" concentration will be 10 µ*M* (200 µL/1000 µL = 1:5 dilution).
3. Make up a working stock of [$^3$H]PN200-110 of approx 0.2 n*M* in assay buffer. Try to keep this consistent between experiments (*see* **Note 6**).
4. Make up dilutions of displacing drugs ensuring that they are five times more concentrated so that when 200 µL is added to 1000 µL a fivefold dilution is made. For a 24-tube assay as shown in **Table 2**, up to 16 displacer concentrations can be included, e.g., in single points, 8 in duplicate, or combinations thereof (*see* **Note 9**).
5. Dilute prepared protein in assay buffer to give approx 200 µg/100 µL of brain membranes (but *see* **ref. *16***), or 800 µg/100 µL for SH-SY5Y and NG108-15 cells.
6. Add reagents to tubes as shown in **Table 3**.
7. Incubate at 20°C in the dark for 90 min.
8. During the incubation, soak Whatman GF/B harvester papers in 0.1% polyethylenimine to reduce NSB.
9. Separate bound and free radioligand by harvesting on a Brandell harvester (*see* **Note 7**).
10. Transfer the filters to scintillation insert vials and add 4.5 mL of scintillant. (The authors use OptiPhase "Safe" [LKB Wallac via Fisons, Loughborough, UK]).
11. Leave the filters for at least 8 h to extract, and then count on a scintillation counter for 3 min per sample.

## ***3.4. Measurement of [$^{125}$I]ω-Conotoxin MVIIA Binding*** (see **Note 10**)

### *3.4.1 Saturation Binding Assays to Determine N-Channel Density*

1. Assay volume is 0.5 mL and uses 24 tubes in total.
2. Dilute ω-conotoxin MVIIA stock for determination of NSB to give 50 n*M* in assay buffer (**Subheading 2.2.**, **item 2**). When 100 µL is added to the assay, the final "in the assay" concentration will be 10 n*M* (100 µL/500 µL = 1:5 dilution). Do not refreeze any unused stock.
3. Defrost [$^{125}$I]ω-conotoxin MVIIA aliquot. Make up a working stock of [$^{125}$I]ω-conotoxin MVIIA of approx 10 p*M* in assay buffer (*see* **Note 11**). Do not refreeze any unused stock.

**Table 3**
**[$^3$H]PN200-110 Displacement Binding Assay Addition Table to Determine Binding Properties of Unlabeled Drugs**

| Tube | Buffer | Nifedipine (50 μ*M*) | Displacer (various) | [$^3$H]PN200-110 (0.2 n*M*) | Membranes |
|---|---|---|---|---|---|
| 1. Total | 700 | — | — | 200 | 100 |
| 2. Total | 700 | — | — | 200 | 100 |
| 3. NSB | 500 | 200 | — | 200 | 100 |
| 4. NSB | 500 | 200 | — | 200 | 100 |
| 5. Displacer 1 | 500 | — | 200 | 200 | 100 |
| 6. Displacer 2 | 500 | — | 200 | 200 | 100 |
| 7. Displacer 3 | 500 | — | 200 | 200 | 100 |
| ↓ | | | | | |
| 20. Displacer 16 | 500 | — | 200 | 200 | 100 |
| 21. Total | 700 | — | — | 200 | 100 |
| 22. Total | 700 | — | — | 200 | 100 |
| 23. NSB | 500 | 200 | — | 200 | 100 |
| 24. NSB | 500 | 200 | — | 200 | 100 |

[a]Assay volume is 1000 μL. 50 μ*M* nifedipine stock and displacer dilutions are diluted 1:5 when added to the assay.

4. Make seven serial dilutions of the 10 n*M* [$^{125}$I]ω-conotoxin MVIIA stock by adding equal volumes of assay buffer. This will give eight concentrations as follows: 5, 2.5, 1.25, 0.625, 0.312, 0.156, 0.078, and 0.039 p*M*.
5. Dilute prepared protein in assay buffer to give approx 5 μg/100 μL of brain membranes, or 100 μg/100 μL for SH-SY5Y and NG108-15 cells.
6. Add reagents to tubes as shown in **Table 4**.
7. Incubate at 20°C in the dark for 30 min.
8. During the incubation, soak Whatman GF/B harvester papers in 0.1% polyethylenimine to reduce NSB.
9. Separate bound and free radioligand by harvesting on a Brandell harvester (*see* **Note 7**).
10. Transfer the dry filters directly to counting tubes suitable for one's γ-counter and count for 1 min/sample.

### *3.4.2. Displacement Binding Assays to Determine Interaction of Unlabeled N-Channel Ligands* (see **Note 8**)

1. Assay volume is 0.5 mL and uses 24 tubes in total.
2. Dilute ω-conotoxin MVIIA stock for determination of NSB to give 50 n*M* in assay buffer (**Subheading 2.2.**, **item 2**). When 100 μL is added to the assay, the final "in the assay" concentration will be 10 n*M* (100 μL/500 μL = 1:5 dilution). Do not refreeze any unused stock.

**Table 4**
**[$^{125}$I]ω-Conotoxin MVIIA Saturation Binding Assay Addition Table to Determine $K_d$ and $B_{max}$[a]**

| Tube | Buffer | ω-conotoxin (10 n*M*) | [$^{125}$I]ω-conotoxin (C1–C8) | Membranes |
|---|---|---|---|---|
| 1. $Total_{C1}$ | 300 | — | 100 | 100 |
| 2. $Total_{C1}$ | 300 | — | 100 | 100 |
| 3. $NSB_{C1}$ | 200 | 100 | 100 | 100 |
| 4. $Total_{C2}$ | 300 | — | 100 | 100 |
| 5. $Total_{C2}$ | 300 | — | 100 | 100 |
| 6. $NSB_{C2}$ | 200 | 100 | 100 | 100 |

Continue in groups of three to total of 24 tubes using all eight [$^{125}$I]ω-conotoxin dilutions.

Eight concentrations of [$^{125}$I]ω-conotoxin MVIIA are used with three tubes per concentration set up as duplicate totals and single NSB ($8 \times 3 = 24$ tubes in total).

[a]Assay volume is 500 µL. 50 n*M* ω-conotoxin MVIIA stock is diluted 1:5 when added to the assay to yield a final concentration of 10 n*M*.

3. Defrost [$^{125}$I]ω-conotoxin MVIIA aliquot. Make up a working stock of [$^{125}$I]ω-conotoxin MVIIA of approx 1 p*M* in assay buffer (*see* **Note 11**). Do not refreeze any unused stock, and try to keep the concentration consistent between experiments.
4. Make up dilutions of displacing drugs ensuring that they are five times more concentrated so that when 100 µL is added to 500 µL a fivefold dilution is made. For a 24-tube assay as shown in **Table 4**, up to 16 displacer concentrations can be included, e.g., in single points, 8 in duplicate, or combinations thereof (*see* **Note 9**).
5. Dilute prepared protein in assay buffer to give approx 5 µg/100 µL of brain membranes, or 100 µg/100 µL for SH-SY5Y and NG108-15 cells.
6. Add reagents to tubes as shown in **Table 5**.
7. Incubate at 20°C in the dark for 30 min.
8. During the incubation, soak Whatman GF/B harvester papers in 0.1% polyethylenimine to reduce NSB.
9. Separate bound and free radioligand by harvesting on a Brandell harvester (*see* **Note 7**).
10. Transfer the dry filters directly to counting tubes suitable for one's γ-counter and count for 1 min per sample.

### *3.5. Data Analysis*

Specific binding is calculated as the difference between total and NSB. $B_{max}$ and $K_d$ are obtained from Scatchard plots ***(18)***. In displacement studies (*see* **Note 12**), the concentrations of displacer producing 50% displacement of specific binding ($IC_{50}$) is obtained by computer-assisted curve fitting (GRAPHPAD-PRISM, *see* **Note 13**) and corrected for the competing mass of radioligand

**Table 5**
**[$^{125}$I]ω-Conotoxin MVIIA Displacement Binding Assay Addition Table to Determine Binding Properties of Unlabeled Drugs**[a]

| Tube | Buffer | ω-conotoxin (50 p*M*) | Displacer (various) | [$^{125}$I]ω-conotoxin (1 p*M*) | Membranes |
|---|---|---|---|---|---|
| 1. Total | 300 | — | — | 100 | 100 |
| 2. Total | 300 | — | — | 100 | 100 |
| 3. NSB | 200 | 100 | — | 100 | 100 |
| 4. NSB | 200 | 100 | — | 100 | 100 |
| 5. Displacer 1 | 200 | — | 100 | 100 | 100 |
| 6. Displacer 2 | 200 | — | 100 | 100 | 100 |
| 7. Displacer 3 | 200 | — | 100 | 100 | 100 |
| ↓ | | | | | |
| 20. Displacer 16 | 200 | — | 100 | 100 | 100 |
| 21. Total | 300 | — | — | 100 | 100 |
| 22. Total | 300 | — | — | 100 | 100 |
| 23. NSB | 200 | 100 | — | 100 | 100 |
| 24. NSB | 200 | 100 | — | 100 | 100 |

[a]Assay volume is 500 µL. 50 n*M* ω-conotoxin MVIIA stock and displacer dilutions are diluted 1:5 when added to the assay.

according to Cheng and Prusoff ***(19)*** to yield the affinity constant ($K_{50}$) (*see* **Note 14**).

## 4. Notes

1. All tissue culture media and reagents are supplied by Life Technologies.
2. From European Collection of Animal Cell Cultures (web site http://www.biotech.ist.unige.it/cldb/cname-dh.html).
3. Pack sizes of 10 and 50 µCi are available. These sizes refer to the stated activity reference date (normally one month after manufacture), which usually means that more is actually supplied if purchased close to the manufacture date. One should check this when ordering. The specific activity does not change because on decay [$^{125}$I]ω-conotoxin MVIIA undergoes decay catastrophe. The reconstituted stock should be frozen at –20°C in small aliquots in a dark lead-lined box. Typically the authors purchase 10 µCi close to the date of manufacture (~16 µCi), reconstitute in 320 µL, and store as 20 µL aliquots (1 µCi/aliquot = $2.22 \times 10^6$ cpm/aliquot).
4. This should be bought in the smallest pack size from Sigma (cat no. C1182) and made up fresh every 4 wk. Take care in preparation as the peptide content varies. Allow product as supplied to warm to room temperature before opening the pack. Avoid storage in a frost-free freezer to minimize freeze-thaw cycles.
5. A typical experiment using this protocol is shown in **Fig. 2** and should be examined in conjunction with **Subheading 3.5.**

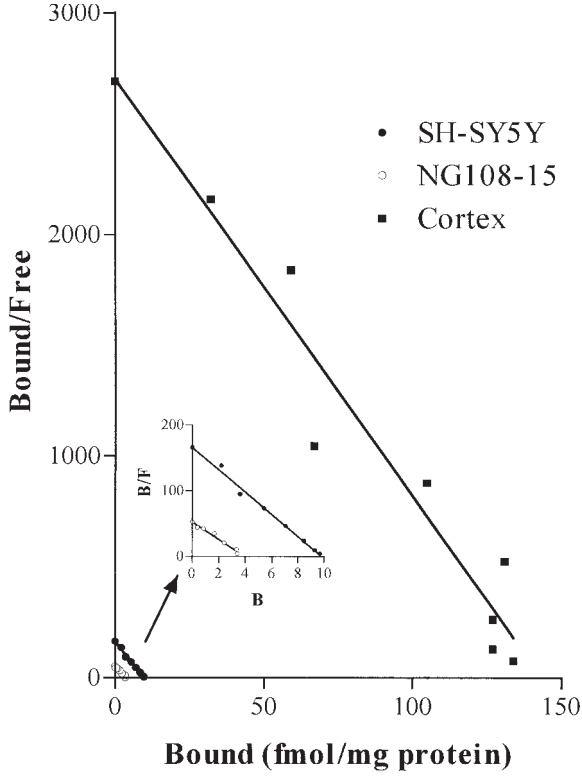


Fig. 2. Typical Scatchard analysis of [$^3$H]PN200-110 binding to rat cerebrocortical, SH-SY5Y, and NG 108-15 membranes. $B_{max}$ and $K_d$ values in each tissue were 143.5 fmol/mg protein and 53 p*M*, 9.9 fmol/mg protein and 60 p*M*, 4.0 fmol/mg protein and 75 p*M*.

6. To do this calculate from the specific activity the number of [$^3$H] DPM that would yield a 1-n*M* solution in an assay volume of 1 mL. This figure will vary for differing specific activities. The authors are currently using a batch that has a specific activity of 81 Ci/mmol. This is equivalent to 1/81 mmol/Ci or 0.01235 mmol/Ci. It is also equal to 0.01235 mmol $\times$ $10^{-6}$ mmol/μCi or 12.35 pmol/μCi. 12.35 pmol in a 1-mL assay is a 12.35-n*M* solution and 1 μCi = $2.22 \times 10^6$ dpm; therefore, a 1-n*M* solution is $2.22 \times 10^6/12.35$ or 179,757 dpm. Then add from [$^3$H]PN200-110 as sold sufficient to give approx 270,000 dpm (or 2 n*M*). The authors add approx 1 μL/mL to begin with and then count 200 μL to determine activity. Depending on the value obtained, either more [$^3$H] or buffer is added so that 200 μL will contain the desired 270,000 dpm. It is important to spend some time getting this right. Remember to make sufficient for the number of tubes set up in the assay and to make serial dilutions.

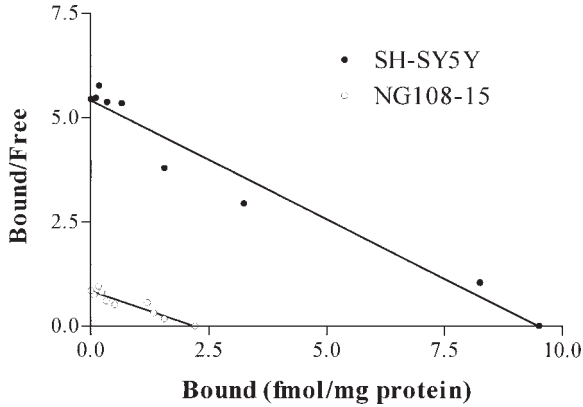


Fig. 3. Typical Scatchard analysis of [$^{125}$I]ω-conotoxin MVIIA binding to SH-SY5Y and NG108-15 membranes. $B_{max}$ and $K_d$ values in each tissue were 9.5 fmol/mg protein and 1.8 p*M*, and 2.2 fmol/mg protein and 2.6 p*M*.

7. All harvesting should be performed with cold (4°C) wash buffer. Initially dispense 4 mL of buffer and deposit the mixture onto the filter papers using the harvester according to the manufacturer's instructions. Wash the filters twice using the harvester. Harvest buffers do not contain BSA because this foams in the harvester waste trap.
8. A typical experiment using this protocol is shown in **Fig. 3** and should be examined in conjunction with **Subheading 3.5.**
9. When making up serial dilutions of displacing drugs, the authors make 10- and 3-fold dilutions. The choice of which concentration range to use depends on the displacer and its expected $IC_{50}$. When plotted on a log scale, this gives an even spread of data points ($\log_{10}$ 3 ~0.5). In addition, the solvent used to make up the displacer should be included to control for a solvent effect. The authors recommend that if a single solvent is used routinely, then a full displacement curve should be constructed. They have performed such an experiment with DMSO and have found that concentrations as high as 1% produce only 3% displacement of [$^3$H]PN200-110.
10. A typical experiment using this protocol is shown in **Fig. 4** and should be examined in conjunction with **Subheading 3.5.**
11. To do this calculate from the specific activity the number of [$^{125}$I] cpm that would yield a 1-p*M* solution in an assay volume of 0.5 mL. This figure will vary for differing specific activities. The batch that the authors are currently using has a specific activity of 2200 Ci/mmol. The calculations are as described in **Note 6**. When 1 p*M* [$^{125}$I]ω-conotoxin MVIIA in a 0.5-mL assay will give 2442 cpm, a 10-p*M* solution should contain 24,420 cpm. Then add from [$^{125}$I]ω-conotoxin MVIIA (as made in **Subheading 2.2.**, **item 6**) sufficient to give approx 24,420 cpm (or 10 p*M*). Count 100 µL to determine activity. Depending on the value obtained, either

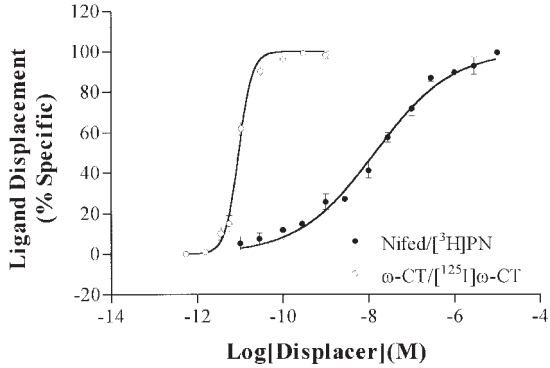


Fig. 4. Displacement of [$^3$H]PN200-110 by nifedipine and [$^{125}$I]ω-conotoxin MVIIA by unlabeled ω-conotoxin MVIIA in rat cerebrocortical membranes. $K_{50}$ values were 3.2 n*M* and 9.2 p*M*. Data are mean ± SEM ($n$ = 5-6). In [$^{125}$I]ω-conotoxin MVIIA binding study, the $IC_{50} = K_{50}$ (*see* **Note 11**) as the radiolabel and the displacer are the same drug (these "isotope dilution" data can also be used to calculate $B_{max}$). Note the steep nature of the ω-conotoxin MVIIA curve; this is consistent with **ref. *20***.

more [$^{125}$I] or buffer is added so that 100 µL will contain the desired 24,420 dpm. It is important to spend some time getting this right. Remember to make sufficient for the number of tubes set up in the assay and to make serial dilutions. Also, as the batch ages while the specific activity remains constant, the absolute activity declines; hence, more stock volume will be required to obtain a 10-p*M* solution.

12. Calculate specific binding by subtracting the average NSB (duplicates at the start and end of the assay). Displacement (%) is calculated as follows:

$$\text{Total}_{(\text{specific counts})} - \text{Displacer}_{(\text{specific counts})}/\text{Total}_{(\text{specific counts})} \times 100$$

Lowest concentration of displacer should give lowest percent displacement (highest counts) and approach total tubes. Highest concentration of displacer should give highest percent displacement (lowest counts).

13. The authors strongly recommend that the instructions manual and help menu are consulted in conjunction with a standard pharmacology text when interpreting data.
14. As the concentration of radiolabel increases, the amount of displacer required to produce 50% displacement increases (hence competitive binding assay). The Cheng and Prusoff ***(19)*** equation [$K_{50} = IC_{50}/(1 + (L/K_d)$] (where $IC_{50}$ is the concentration of displacer producing 50% displacement, $L$ is the concentration of radiolabel, and $K_d$ refers to the radiolabel) corrects the displacement curve to the position it would theoretically occupy in the absence of radiolabel.

## References

1. Tsien, R. W. and Tsien, R. Y. (1990) Calcium channels, stores and oscillations. *Annu. Rev. Cell Biol.* **6,** 715–760.

2. Berridge, M. J. (1993) Inositol trisphosphate and $Ca^{2+}$ signalling. *Nature* **361,** 315–325.
3. Clapham, D. (1995) Calcium signalling. *Cell* **80,** 259–268.
4. Spedding, M. and Paoletti, R. (1992) Classification of calcium channels and the sites of action of drugs modifying channel function. *Pharmacological Rev.* **44,** 363–376.
5. Miller, R. J. (1992) Voltage sensitive $Ca^{2+}$ channels. *J. Biol. Chem.* **267,** 1403–1406.
6. Fasolato, C., Innocenti, B., and Pozzan, T. (1994) Receptor activated $Ca^{2+}$ influx: how many mechanisms for how many channels. *Trends Pharmacol. Sci.* **15,** 77–83.
7. Berridge, M. J. (1995) Capacitative calcium entry. *Biochem. J.* **312,** 1–11.
8. Wu, L.-G. and Saggau, P. (1997) Presynaptic inhibition of elicited neurotransmitter release. *Trends Neurosci.* **20,** 204–212.
9. Miller R. J. (1990) Receptor mediated regulation of calcium channels and neurotransmitter release. *FASEB J.* **4,** 3291–3299.
10. Hille, B. (1994) Modulation of ion-channel function by G-protein coupled receptors. *Trends Neurosci.* **17,** 531–536.
11. Miller, R. J. (1997) Calcium channels prove to be a real headache. *Trends Neurosci.* **20,** 189–192.
12. Ellinor, P. T., Zhang, J.-F., Horne, W. A., and Tsien, R. Y. (1994) Structural determinants of the blockade of N-type calcium channels by a peptide neurotoxin. *Nature* **372,** 272–275.
13. Ichida, S., Wada, T., Akimoto, T., Kasamatsu, Y., Tahara, M., and Hasimoto, K. (1995) Characteristics of specific $^{125}$I-ω-conotoxin GVIA binding and $^{125}$I-ω-conotoxin GVIA labeling using bifunctional crosslinkers in crude membranes from chick whole brain. *Biochem. Biophys. Acta.* **1233,** 57–67.
14. Hirota, K. and Lambert, D. G. (1996) I.v. anaesthetic agents inhibit dihydropyridine binding to L-type voltage-sensitive $Ca^{2+}$ channels in rat cerebrocortical membranes. *Br. J. Anaesth.* **77,** 248–253.
15. Hirota, K. and Lambert, D. G. (1997) Do local anaesthetics interact with dihydropyridine binding sites on neuronal L-type $Ca^{2+}$ channels? *Br. J. Anaesth.* **78,** 185–188.
16. Hirota, K. and Lambert, D. G. (1997) A comparative study of L-type voltage sensitive $Ca^{2+}$ channels in rat brain regions and cultured neuronal cells. *Neurosci. Lett.* **223,** 169–172.
17. Lowry, O. H., Rosebrough, N. J., Farr, A. C., and Randall, R. J. (1951) Protein measurement with Folin phenol reagent. *J. Biol. Chem.* **193,** 265–275.
18. Scatchard, G. (1949) The attraction of proteins for small molecules and ions. *Ann. NY Acad. Sci. USA* **52,** 660–672.
19. Cheng, Y. C. and Prusoff, W. M. (1973) Relationship between the inhibition constant ($K_i$) and the concentration of inhibitor which causes 50% inhibition ($IC_{50}$) of an enzymic reaction. *Biochem. Pharmacol.* **22,** 3099–3108.
20. Stoehr, S. J. and Dooley, D. J. (1993) Characteristics of $^{125}$I-ω-conotoxin GVIIA binding to rat neocortical membranes. *Neurosci. Lett.* **161,** 113–116.

# 10

# Whole-Cell Patch Clamp Recording of Voltage-Sensitive $Ca^{2+}$ Channel Currents

*Heterologous Expression Systems and Dissociated Brain Neurons*

**Atticus H. Hainsworth, Andrew D. Randall, and Alessandro Stefani**

## 1. Introduction

Voltage-sensitive $Ca^{2+}$ channels (VSCC) play a central role in an extensive array of physiological processes. Their importance in cellular function arises from their ability both to sense membrane voltage and to conduct $Ca^{2+}$ ions, two facets that couple membrane excitability to a key intracellular second messenger. Through this relationship, activation of VSCCs is tightly coupled to the gamut of cellular functions dependent on intracellular $Ca^{2+}$, including muscle contraction, energy metabolism, gene expression, and exocytotic/endocytotic cycling.

VSCCs are formed from a core $\alpha 1$ subunit that comprises the $Ca^{2+}$ selective pore, the voltage sensor, and most drug binding sites. Accessory subunits $\alpha 2\delta$, $\beta$, and $\gamma$ modulate channel function by altering biophysical properties and cell surface expression. The primary level of VSCC diversity results from the differing functional and pharmacological properties of $\alpha 1$ subunits (**Table 1**). For VSCC classification, *see* **ref. *1***.

Whole-cell (tight-seal) recording is a form of patch clamp technique, utilizing a glass microlectrode ("pipet") connected to a sensitive amplifier that can record picoamp currents (pA, $10^{-12}$ A). The pipet, filled with the desired intracellular solution, is gently pressed against the surface of a single cell under micromanipulator control. With gentle suction, a tight seal forms between glass and plasma membrane, giving electrical resistance in excess of 1 G$\Omega$ (a "gigaseal"). From this cell-attached mode, stronger suction ruptures the patch of cell membrane

From: *Methods in Molecular Biology, vol. 312: Calcium Signaling Protocols: Second Edition*
Edited by: D. G. Lambert © Humana Press Inc., Totowa, NJ

**Table 1**
**Classification of VSCC α1 CaV Subunits** [a]

| Group | Other group names | α Subunit | Previous nomenclature | Cellular counterpart |
|---|---|---|---|---|
| CaV1 | L-type $Ca^{2+}$ channels, dihydropyridine receptors | CaV1.1 | α1S | L-type |
| | | CaV1.2 | α1C | L-type |
| | | CaV1.3 | α1D | L-type |
| | | CaV1.4 | α1F | L-type |
| CaV2 | Presynaptic $Ca^{2+}$ channels | CaV2.1 | α1A | P/Q-type |
| | | CaV2.2 | α1B | N-type |
| | | CaV2.3 | α1E | R-type |
| CaV3 | Low-voltage activated, low-threshold $Ca^{2+}$ channels | CaV3.1 | α1G | T-type |
| | | CaV3.2 | α1H | T-type |
| | | CaV3.3 | α1I | T-type |

[a] *See* **ref. *1***.

delimited by the pipet mouth and gives access to the cytoplasm. In this whole-cell mode, the transmembrane voltage can be controlled ("clamped") and the net current flow across the cell membrane measured with well-defined external and internal solutions. This level of control over membrane transport parameters at the single-cell level has earned whole-cell recording its deserved popularity as a reporter of ion channel function. Changes in current produced by voltage pulses, varying ion concentrations, or drug application can then be monitored. For further details of patch clamp methods, *see* **refs. *2–6***.

### *1.1. Whole-Cell Recordings of Calcium Currents: The Foundations*

Whole-cell recordings of calcium channel currents were first performed in cultured bovine adrenal chromaffin cells ***(7)*** and snail neurons ***(8)***. Similar techniques were later validated in acutely isolated neurons from adult animals (e.g., rat sympathetic ganglia, **ref. *9***). Recording conditions were refined and channel blockade by divalent ions (e.g., cadmium, cobalt, and nickel) became routine. In addition, several groups began dissecting the biophysical properties of VSCCs, in terms of activation, deactivation, and inactivation ***(10,11)*** and the first studies of pharmacological modulation of whole-cell calcium currents appeared ***(12,13)***. On the basis of gating kinetics, VSCC types were classified as transient (T), sustained or long (S, L) or N (neither T nor L/S) ***(14–16)***. Other types are toxin-resistant (R) or found in Purkinje cells (P/Q), *see* **ref. *13***.

Here we summarize the whole-cell recording methods generally used to characterize macroscopic currents mediated by VSCCs. We describe approaches used to study recombinant VSCCs expressed in cell lines and also native VSCCs in brain neurons isolated by enzymatic treatment.

## 2. Materials

### 2.1. Recording Recombinant VSCC Currents in Cell Lines

1. Maintain in cell-culture a suitable cell line expressing the desired recombinant VSCC subunits (*see* **Note 1**). The cells should be grown on glass cover slips (*see* **Note 2**) for transfer to the recording chamber.
2. HEPES-buffered saline (HBS) is composed of 130 m*M* NaCl, 5 m*M* KCl, 2 m*M* $CaCl_2$, 1 m*M* $MgCl_2$, 30 m*M* glucose, 10 or 20 m*M* HEPES acid pH 7.3 with NaOH, and 310–315 mOsm/L.
3. Extracellular solution for VSCC recordings: 140 m*M* tetraethyl ammonium (TEA) chloride, 10 m*M* HEPES acid, 2.5 (range 2–5) m*M* $CaCl_2$ or $BaCl_2$ (occasionally $SrCl_2$), 5 m*M* CsCl, 10 m*M* glucose, and 1 m*M* $MgCl_2$, pH 7.3 with TEA-OH, osmolarity 310– 315 mOsm/L. Make 200–500 mL; this can be used for a few days if kept in the fridge (*see* **Notes 3–6**).
4. Internal solution: 108 m*M* Cs Me-sulphonate, 24 m*M* HEPES acid, 10 m*M* ethylene glycol tetraacetic acid (EGTA), 4.5 m*M* $MgCl_2$, 0.1 m*M* $CaCl_2$, 4 m*M* Na-adenosine triphosphate (ATP), 0.3 m*M* Na-guanosine triphosphate (GTP), 5 m*M* creatine, 5 m*M* Na-phosphocreatine, 5 m*M* pyruvate, 5 m*M* oxolo-acetate, and 5 μg/mL calpain inhibitor peptide. Make up aliquots of 2–5 mL and freeze them (*see* **Notes 7** and **8**).

### 2.2. Recording Whole-Cell VSCC Currents in Acutely Isolated Neurons

1. The process of dissociating neurons from adult brain is given in **Note 9**. We have studied neurons from diverse brain areas (striatum, sensorimotor cortex, globus pallidus) using the basic protocol given here ***(17–19)***. Points to note in regard to this preparation are given in **Notes 10–12**.
2. HEPES-buffered Hank's balanced salt solution (HBSS): 10 m*M* HEPES acid, 138 m*M* NaCl, 3 m*M* KCl, 1 m*M* $MgCl_2$, and 2 m*M* $CaCl_2$, pH 7.3 adjusted with NaOH, 300 mOsm/L.
3. Na isethionate solution: 140 m*M* Na isethionate, 2 m*M* of KCl, 1 m*M* $MgCl_2$, 23 m*M* glucose, 15 m*M* HEPES acid, 1 m*M* kynurenic acid, 1 m*M* pyruvic acid, 0.1 m*M* nitro-arginine, and 0.05 m*M* glutathione (pH 7.3; 310 mOsm/L).
4. The pipet solution: 185 m*M* *N*-methyl-D-glucamine (NMG), 40 m*M* HEPES acid, 11 m*M* EGTA (or BAPTA), 4 m*M* $MgCl_2$, adjusted to pH 7.2–7.3 with analytical regent-grade phosphoric or sulphuric acid. Aliquots of this solution can be stored in the freezer. On the day of use add: 20 m*M* phosphocreatine, 2–3 m*M* sodium ATP, 0.2 m*M* GTP, and 0.1–0.2 m*M* leupeptin with a final osmolarity 270–280 mOsm/L. Solutions containing BAPTA should be protected from light (*see* **Notes 12** and **13**).
5. The external recording solution: 165 m*M* TEA-Cl, 5 m*M* $CsCl_2$, 10 m*M* HEPES acid, 10 m*M* glucose, and 2.5 or 5 m*M* $BaCl_2$ (as the charge carrier); pH adjusted to 7.35 with CsOH or TEA-OH. If necessary, sucrose is added to bring the osmolality to 305 mOsm/L (*see* **Notes 3, 5–8**).

6. If desired, NaCl can be substituted for TEA as the major cation in external recording solution: 125 m*M* NaCl, 20 m*M* CsCl, 1 m*M* $MgCl_2$, 10 m*M* HEPES acid, 5 m*M* $BaCl_2$, 0.001 m*M* tetradotoxin (TTX), and 10 m*M* glucose (pH 7.3 with TEA-OH; 300–305 mOsm/L).

### 2.3. The Recording Set-Up

Assemble a standard patch clamp apparatus, for both cell lines and dissociated neurons. The core components are as follows:

1. Microscope (inverted style is usual) equipped with simple fluorescence optics if required (i.e., for visualizing fluorescent protein-expressing cells).
2. Antivibration table, though this is not always essential for whole-cell recordings.
3. Some form of recording chamber mounted on the microscope stage (e.g., commercially available Warner chambers).
4. A suitable low-drift micromanipulator (Burleigh, Narishige).
5. A patch clamp amplifier (e.g., Axon Instruments, HEKA-List, Warner, Biologic, Cairn Research).
6. Some form of analog–digital interface (e.g., 1401 black box, CED; Digidata, Axon Instruments).
7. A personal computer with software to acquire data and control experiments (e.g., pClamp, Axon Instruments; Pulse, Strathclyde freeware, Dr J. Dempster; **ref. *20***).

In addition to **items 1–7**, the following should be considered: a Faraday cage surrounding the microscope (these are commonly used but may not be absolutely required for most whole-cell studies), an oscilloscope, some form of temperature controller (if experiments are to be performed away from ambient temperature; *see* **Note 14**), and finally, equipment to perfuse the recording chamber and perform solution exchanges (*see* **Note 15**). For external solution exchange, we favor a local change in extracellular perfusion. To achieve this we use a gravity-fed multibarrel "liquid filament" approach, whereby parallel streams of solutions are translated across the recorded cell in order to produce rapid solution changes (time to completion 30–100 ms). A number of such systems are available commercially (e.g., the relatively inexpensive system sold by Warner Instruments).

## 3. Methods

### 3.1. General Points

Starting VSCC current recording is like planning a mountain climbing trip. Before you can start recording, you have several weeks of preparation ahead. This may feel frustrating but always keep your mind on the goals: beautiful, clean currents, the clear test of your hypothesis and the paper in *Nature Medicine*.

1. Assemble your set-up, such that patch clamp amplifier talks to the recording system, that the computer runs the software smoothly, and that you can play back

recorded currents. Check this by filling a pipet and recording the current response to a 5-mV step voltage first in air, then in bath solution.

2. Plan your extracellular and internal solutions (*see* **Notes 3–8, 12** and **13**). A major concern for VSCC recording is "run-down" of the current with time (*see* **Note 16**). You may need to modify your internal solution in the light of preliminary experiments or even consider perforated patch recording (*see* **Note 17**).
3. Plan the voltage protocols that you will use to answer your question (*see* **Note 18**). You will likely need more than one protocol in any given recording.
4. Learn as much as possible about your cell type and its complement of calcium channels before you begin. Do a literature search, talk to the people who gave you the cells, ask your biochemist friend. For example, does expression begin only at 2 d after plating out? What bath solution is best for gigaseal formation? Are the cells densely packed with Ca-activated anion or K channels?

### 3.2. The Basic Process of Recording Whole-Cell VSCC Currents

1. Choose a suitable smooth, healthy-looking, debris-free cell before you fill the pipet.
2. Pull a pipet and fill with filtered internal solution.
3. Patch clamp amplifier should be in voltage clamp mode, whole-cell capacity compensation, and series resistance compensation turned off, seal test on (small voltage steps, approx 5 mV, to test pipet resistance).
4. Mount filled patch pipet on electrode holder (which is in turn attached to headstage which is attached to micromanipulator (*see* **Note 19**).
5. Apply positive pressure to pipet lumen (*see* **Note 20**).
6. Lower pipet into bath solution, partially remove current offsets using the pipet offset control, check pipet resistance and, if suitable, position pipet tip close to your chosen cell. If necessary re-zero current using pipet offset control.
7. Gently touch cell surface and apply gentle suction. Monitor gigaseal formation by observing current response to small voltage step command, e.g., 5 mV (*see* **Notes 21–22**).
8. If a gigaseal is formed, i.e., >IGΩ resistance, neutralize fast capacitance transients with appropriate controls, then enter whole-cell configuration by brief application of further suction and/or high voltage "zaps" (*see* **Note 23**).
9. If the whole-cell configuration is successfully achieved (this will be apparent by the large whole-cell capacitance transients that appear), then neutralize capacitance transients. Thereby, establish the series resistance value (*see* **Note 24**).
10. If series resistance is sufficiently low for experimental purposes, apply series resistance compensation (typically 70–90%; *see* **Note 25**).
11. After obtaining whole-cell access, the cell is bathed in appropriate external solution for VSCC current recording, using multibarrel, fast, extracellular perfusion (*see* **Note 15**). Recordings typically last for 5-10 min, but can last much longer than this.
12. Start data acquisition. Initially apply a simple square test-pulse to see how much VSCC current is present (**Fig. 1**).

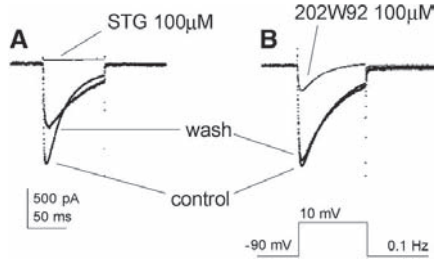


Fig. 1. R-type voltage-sensitive calcium channel currents mediated by human α1E + β3 subunits expressed in human embryonic kidney 293 cells. The currents are induced by 100 mV square pulses of 100-ms duration, applied every 10 s, with 2.5 m*M* of $Ba^{2+}$ as the charge carrier, inward currents plotted downward, by convention. The control currents exhibit clear voltage-dependent inactivation. Application of the lamotrigine analogs sipatrigine (STG) or 202W92 (each at 100 μ*M*) inhibits the voltage-sensitive calcium channel-mediated currents. The peak current amplitude is inhibited >95% by STG and approx 70% by 202W92. After washing out STG, the current recovers partially, but the recording shows signs of poor voltage control, possible owing to declining gigaseal resistance. In the example shown for 202W92, the recording shows almost complete recovery following removal of the drug. (A. H. Hainsworth, unpublished data.)

13. You may then apply your chosen voltage protocol (*see* **Note 18**) and/or expose the cell to the drugs of interest. It is usual to record a few (3–6) currents pre-drug, then exchange the external solution to apply the drug (*see* **Note 15**) and again record a few traces, ideally until a steady-state response is seen. Then wash off the drug and record current responses, ideally showing a near-complete recovery to predrug levels.

## 4. Notes

### *4.1. Recombinant VSCCs in Host Cell Lines and Other Heterologous Expression Systems*

1. Cell types typically chosen for VSCC expression are those lacking endogenous $Ca^{2+}$ currents and regarded as "good" transfection hosts. Most commonly used are epithelial cells such as human embryonic kidney (HEK)-293, Chinese hamster ovary, and COS-7 monkey kidney cells, all of which express very low levels of voltage-gated channels. It must be noted, however, that cell lines from the same original source (i.e., with the same name) can vary considerably in their membrane properties and channel complement. For example there are reports of HEK-293 cells that express, albeit quite small, endogenous VSCC ***(21,22)***, although we have never observed them. An alternative, widely used host for VSCC expression is the Xenopus oocyte, which can be injected with either cDNA or mRNA for VSCC subunits. These are too large for whole-cell methods and require two electrode voltage clamp or the cut-open oocyte technique.

Recombinant VSCCs subunit combinations can be either transiently or stably expressed in host cell lines. With the exception of the CaV3 family, where expression of an α1 subunit alone produces robust VSCC-mediated currents, it is usually necessary to co-express at least a β subunit—and often a β and α2δ—along with an α1 subunit to generate suitable currents. This requirement to express two or three different subunits has made the generation of stable cell lines for CaV1 and CaV2 family channels a substantial although not insurmountable, challenge (examples are reported in **refs. *23*** [α1B], ***24*** [α1A], and ***25*** [α1E]. The inclusion of a visible marker (e.g., green fluorescent protein) to identify transfected cells in studies using transient gene expression permits a much greater number of successful recordings to be made per working day.

2. Other considerations with respect to host cells involve the level of VSCC expression and the cell culture substrate used when plating cells out. The major reason for controlling expression level is to set the size of the VSCC-mediated currents to a level that is suitable for whole-cell recording. An ideal range to aim for would be a current, at the peak of the I–V relationship, of 300–1500 pA in 2 m*M* of $Ca^{2+}$, when stepping from a hyperpolarized holding potential (e.g., –100 mV). Current amplitudes can be manipulated in additional ways, including varying nature or concentration of the permeating divalent ion species (*see* **Note 4**) and altering the test and/or holding potentials employed. Regarding plating of cells, we typically use glass cover slips coated with poly-D-lysine and maintained within standard 35-mm plastic Petri dishes. A range of other substrates, including direct plating onto tissue culture plastic, are also suitable. One advantage of using glass cover slips is they can be readily broken into numerous shards. These can then individually be transferred to the recording chamber, giving numerous individual preparations from a single 35-mm Petri dish.

   With stable VSCC cell lines, expression levels can change with passage number and it is prudent to monitor this and work with passage numbers within a defined window. In addition we have found that expression levels change with time after the final plating. Even with cells that generally have a high level of VSCC expression, we found a proportion with no $Ca^{2+}$ current at all; this may reflect a stage in the cell cycle. Expression levels in both transient and stable expression systems can be further altered by changing culture conditions. For example, the addition of butyrate to culture media increases expression of some cell surface proteins. Changes in culture temperature can also be utilized to promote functional expression of certain VSCCs ***(24)***.

## *4.2. Recording Solutions*

3. There is considerable diversity in the solutions used for whole-cell studies of VSCC function. Usually, the primary goal driving decisions on solution composition reflects the need to eliminate current flow through other ion channels while sparing (or augmenting) current flow through VSCCs. Consequently, these decisions will reflect the ion channel complement of the cell used as an expression host and the level of VSCC expression achieved. Secondary considerations may

reflect specific experimental demands, such as a desire to be as close to the physiological condition as possible or a desire to limit intracellular processes triggered by $Ca^{2+}$ entry; for example, $Ca^{2+}$-dependent VSCC inactivation or $Ca^{2+}$-dependent channel activation.

4. For recombinant VSCCs we have used a very simple extracellular solution based on 140 m*M* TEA chloride and 10 m*M* of HEPES buffer ***(26,27)***. In some studies this is only supplemented with the chloride salt of the permeating divalent species, usually $CaCl_2$ or $BaCl_2$ (occasionally $SrCl_2$). To generate currents of a suitable amplitude for study, the concentration of the permeating divalent ion is set between 1 and 20 m*M* (most usually 2 or 5 m*M*). For CaV1 and CaV2 families $Ba^{2+}$ and $Sr^{2+}$ give currents two to three times larger than equimolar $Ca^{2+}$, whereas for CaV3 channels, currents are of a broadly similar amplitude in all three ions. Over and above the three solution components described here we have, at various times, added CsCl (5 m*M*), glucose (10 m*M*) and $MgCl_2$ (1 m*M*) to the bathing solution. Whatever the precise composition of the extracellular solution we adjust the pH to 7.3 with TEA-OH and aim for a final extracellular osmolarity of 310–315 mOsm. To achieve this latter target make-up, we adjust the TEA-Cl concentration as required by the particular solution composition. Other large cations can be used in place of TEA as the majority extracelluar ion, for example NMDG and choline, indeed, in many systems the more physiological $Na^+$ ion would also be acceptable. Our standard recording method (described in **Note 15**) involves gigaseal formation to be carried out in a simple pseudo-physiological HBS, which is also used to perfuse the recording chamber. This solution is also used to maintain cells after they have been removed from the cell culture incubator.
5. At very low concentrations of divalent cations, VSCCs effectively conduct monovalent ions such as $K^+$, $Na^+$, $Li^+$, and protons ***(28)***. Workers wishing to study such currents should ensure that the extracelluar $Ca^{2+}$ concentration is sufficiently low by using a $Ca^{2+}$ chelator such as EGTA or BAPTA. This is because divalent ion contamination is significant in both double distilled water and commercial NaCl and LiCl (for example, 140 m*M* NaCl made with standard lab chemical and completely divalent-free water would be expected to contain approx 3 μ*M* of $Ca^{2+}$ and 1.5 μ*M* of $Ba^{2+}$).
6. Junction potentials. The combination of bath and electrode solutions used in many VSCC experiments produce significant liquid junction potentials (for example, 14 mV between a Cs Me–sulphonate-based electrode solution and a TEA-Cl-based bath solution). If uncorrected, these potentials can produce significant voltage errors. The magnitude of the liquid junction potential can be measured directly by immersing an open pipet tip in pipet solution, then exchanging this for normal bath solution (HBS) and noting the change in voltage offset.
7. Pipet (internal) solutions should be filtered (0.2 μ*M*) to removed debris. In whole-cell experiments, pipet solution rapidly replaces the intracellular ionic milieu. Pipette solutions for recording VSCCs typically contain $Cs^+$ as their predominant cation, as this eliminates most current through potassium channels. As for the

major anion, a number of species have been adopted. These include $Cl^-$, methanesulphonate, gluconate, aspartate, and glutamate. A significant advantage of the use of chloride is that it results in small junction potentials when used with the common bath solutions. The other main features of pipet solutions are the provision of suitably buffered levels of $Ca^{2+}$ and pH along with some additional provisions to sustain intracellular signalling and limit $Ca^{2+}$ current rundown. $Ca^{2+}$ is usually buffered with either EGTA or BAPTA. If a defined intracellular $Ca^{2+}$ concentration is required, a known amount of $Ca^{2+}$ is included along with the chelators and the actual concentration calculated with appropriate software.

8. Osmolarity. For cell lines, we aim for pipet solutions with a value of 295–300 mOsm for use with bath solutions of 310–315 mOsm. For dissociated neurons, we strongly suggest a greater difference in osmolarity, with external solution around a "physiological" 305 mOsm and the internal solution 270–275 m*M* (including the addition of all final constituents—leupeptin, GTP, ATP, phosphocreatine, etc).

### 4.3. Dissociation of Central Neurons

9. Brain slices are cut on a Vibrotome (300–400 μ*M* thick) and maintained in Krebs at room temperature for up to 6 h. Dissect out the desired brain area under stereomicroscope using a scalpel, to give a microslice. Usually, only one microslice is then incubated in HBSS at 35°C, bubbled with 100% $O_2$. In order to minimize hypoxic damage, the incubation and dissociation media can be supplemented with kynurenic acid (1 m*M*), pyruvic acid (1 m*M*), nitro-arginine (0.1 m*M*), and glutathione (0.05 m*M*; *see* **Subheading 2.**, and **ref. *29***). From 30 to 60 min later, 1 microslice is incubated in HBSS containing 0.5 mg/mL protease pronase E (Sigma protease type XIV, St. Louis, MO; 1 mg/mL at 32-35°C; *see* **Note 11**). The tissue is washed three times with HBSS, then mechanically triturated using three glass Pasteur pipets, flame-polished to successively narrower tip diameter. Alternatively, the tissue may be rinsed in an antioxidizing Na isethionate solution. The cell suspension supernatant is then placed in a Petri dish mounted on the stage of an inverted microscope. Cells are allowed to settle for about 10 min, following which a background flow of HBSS is initiated through the bath (approx 1 mL/min).
10. General notes on dissociation of central neurons. Acute preparations of isolated cells are somewhat variable. Some degree of hypoxia is unavoidable. We have studied the survival of dissociated pallidal neurons and found a dramatic loss of viable cells in aged rats (>2 mo). We routinely use animals younger than 7–8 wk of age, ideally in the 20–35 d postnatal range (assuming they represent fully developed neurons).
11. We have found the nonspecific protease type XIV (pronase E, Sigma) to be most effective (instead of trypsin or papain). This usually gives acutely isolated somata with "enzymatically chopped" long dendrites. The ability to isolate neurons without extensive arborizations is important for adequate voltage clamp control of the whole cell surface ("space-clamp"), at least for quite slow, sustained conductances, such as VSCC. We have used pronase E in the concentration range 0.5–1

mg/mL at 32–35°C, for incubation time between 25 and 40 min. Mody and coauthors were probably the first to suggest pronase E for central neurons ***(30)***, although the enzyme had a previous long history for different preparations (e.g., retina). It should be noted that effects of pronase E on ion channels have been reported, including loss of sodium channel inactivation, reduction of low-threshold calcium current and shifts of voltage-dependence. Some scientists have tried to minimise the effects of proteolysis by means of a "mixed" or purely mechanical mode of dissociation ***(31)***.

12. General rules for whole cell recordings of VSCCs in isolated central neurons. Whole-cell recordings are performed utilizing pipets (glass capillaries from WPI, PG52165-4) pulled on a Flaming-Brown puller and fire-polished just prior to use. Pipet resistance is 3–8 MΩ when filled with internal solution. Aim to limit possible Ca-dependent inactivation, thus entirely replace all external calcium with barium, but maintain some free intracellular calcium (<20–50 n*M*) using EGTA or BAPTA (unless the assessment of calcium-dependent calcium release is a priority). Minimize VSCC current run-down ***(32)***. As a rule, internal 3 m*M* ATP significantly prolongs VSCC survival ***( 33)***. Consider the possible permeability of calcium channel by monovalent cations (e.g., potassium or protons ***[28]***).
13. In dissociated neurons we favor the impermeant cation NMG as the main internal cation in order to impede outward currents. On the other hand, whole-cell recordings from neurons in "intact tissue," such as intraslice patch recording, usually utilize potassium salts, such as sulfonates. Powers and Binder ***(34)***, studying spinal motorneurons in 300 µm slices, are a typical example. To study the full ensemble of physiological currents, they used a pipet solution containing: 146 m*M* $KCH_3SO_4$, 5 m*M* KCl, 2 m*M* $MgCl_2$, 2 m*M* EGTA, 10 m*M* MOPS, 2 m*M* $Na_2ATP$, and 0.2 m*M* $Na_3GTP$, pH 7.3. For recording inward currents in isolation, the pipet solution was: 100 m*M* of CsCl, 20 m*M* of TEA-Cl, 5 m*M* $MgCl_2$, 2 m*M* BAPTA, 10 m*M* HEPES, 5 m*M* $Na_2ATP$, 0.5 m*M* $Na_3GTP$, pH 7.3.

### 4.4. General Whole-Cell Recording Methods

14. Temperature. The majority of patch clamp studies are still performed at room ("ambient") temperature for experimental simplicity. Anyone wanting to draw parallels between the physiological condition and a recombinant preparation, however, may be advised to consider a series of recordings at physiological temperature. Those taking this route should check the pH of all solutions at experimental temperature and correct for altered junction potentials (for example, a combination of intracellular 140 m*M* CsMeSO4, 10 m*M* TEA-Cl, and extracellular 140 m*M* TEA-Cl, and 10 m*M* CsMeSO4, will change junction potential by approx 6 mV between 20 and 37°C). In addition, at higher temperature currents will exhibit faster kinetics and may well be larger. This can affect voltage-clamp fidelity and series resistance.
15. External solution exchange. Some VSCC experiments can be performed in static bath preparations; however, any manipulation that requires changing solutions or

adding drugs will require some form of bath perfusion or cell perifusion device. Although a fairly straightforward approach, completely exchanging the bath solution carries certain disadvantages. First, with bath perfusion it can take some time to effect the desired solution exchange, particularly if there is significant dead space in the perfusion system. This can be minimized by using small volume chambers (or laminar flow chambers) and placing a solution manifold as close as possible to the perfusion entry to the bath. A second disadvantage is that bath exchange can use significant solution volumes, which, although generally not a problem for simple salt solutions, can have cost implications when expensive drugs or toxins are applied. Our favored approach is to use a fast perfusion device (*see* **Subheading 2.3.**) to effect local cell perifusion. Here the cell is locally perifused from 200 to 500 µm glass barrels at flow rates of about 100–200 µL/min$^{-1}$. In addition, the bath is perfused with a single solution at 1–2 mL/min. In many of our experiments the bath perfusate is a simple HBS consisting mainly of NaCl supplemented with glucose and chloride salts of $Ca^{2+}$ and $Mg^{2+}$. We typically form our gigaseals in this NaCl-based solution before turning on the local perifusion (which applies the TEA-based VSCC bath solution described above) and entering the whole-cell configuration.

16. Run-down of VSCC currents. Time-dependent run-down of VSCC-mediated currents is a common problem in whole-cell experiments. One way to reduce this is to use perforated patch methods (*see* **Note 17**). Alternatively, pipet solutions can be supplemented with biochemical reagents proposed to prolong recording lifetime. Most commonly included are ATP and GTP (which also require inclusion of $Mg^{2+}$ to produce any benefit). Some workers include phosphocreatine (and sometimes creatine phosphokinase). Other additions include calpain inhibitor peptide, cyclic adenosine monophosphate, pyruvate and oxaloacetate, and the peptidase inhibitor, leupeptin. To limit current run down in recordings of recombinant human CaV2.3, we have used the pipet solution listed under **Subheading 2.**

    For dissociated neurons, with 0.1 m*M* of EGTA in the pipet, the addition of 3 m*M* of ATP significantly prolongs calcium current ($I_{Ca}$) survival, whereas no further improvement obtained by increasing the ATP to 10 m*M* or replacing ATP with creatine phosphate ***(33)***.
17. Perforated patch recording (e.g., Nystatin, *see* **ref. *35***). Starting from the cell-attached configuration, this method of recording uses antibiotic/antifugal agents (e.g., nystatin and amphotericin) to "perforate" the cell membrane beneath the tip of the patch electrode. This process generates electrical continuity between the pipet and the cytoplasm, thus allowing the macroscopic currents of the entire cell membrane to be recorded. The degree and rate at which the pipet contents exchange with the cell's interior during perforated patch recordings depend on the perforating agent used and how extensively the membrane is perforated. Furthermore, certain perforating agents exhibit selectivity in their ionic permeabilities and, consequently, can be used to preserve the physiological concentrations of certain ions (e.g., gramicidin which is used to preserve physiological Cl-gradients, *see* **ref. *36***). The key feature of perforated patch recording is that is pre-

serves the intracellular biochemistry of the cell. This can prove valuable in reducing the rundown of VSCCs and studying regulation of VSCC function by intracellular signalling cascades. Because $Ca^{2+}$ chelators, such as EGTA and BAPTA, do not pass through most perforating ionophores, perforated patch recording does not allow the investigator to control the level of intracellular $Ca^{2+}$ buffering. Thus, VSCC activation can produce very large internal $Ca^{2+}$ rises that may be poorly controlled—particularly in the epithelial cells typically used as expression hosts which are not "designed" to cope with such $Ca^{2+}$ loads, having no voltage-gated channels of their own.

To an aliquot of standard electrode solution, the perforating agent is added at a suitable concentration (usually from a stock solution in DMSO). Many workers report that the perforating efficacy of agents, such as nystatin, declines with time in solution. Consequently, a new aliquot of electrode solution containing the perforating agent should be prepared every 2 h.

Having prepared solutions, the very tip of the recording pipet is filled with internal solution devoid of perforating agent. It is important not to fill too much of the tip in this way. To achieve this, we fabricate our pipets from microfilament-containing glass (e.g., Clark Electromedical GC120F10). We then immerse the back (i.e., untapped) end of the pipet in electrode solution (this fills the tip by capillary action) for about 5 s, before removing and rapidly blotting the immersed end dry on filter paper. Using a 1-mL syringe and flexible microfilament (WPI microfil), the rest of the pipet is then filled to about half full with pipet solution containing perforating agent. After this the cell-attached configuration is entered in the standard way and fast capacitance neutralization performed. The process of perforation is then monitored by observing the appearance of whole-cell capacitance transients. These will grow in amplitude and narrow in width as the access resistance decreases. When these changes to the capacity transient have stabilized, and if the series resistance has reached a sufficiently low value, recording of whole-cell responses can be initiated.

18. Voltage protocols. The components of a VSCC response to a square voltage command of 100 mV from a holding potential of –90 mV is shown in **Fig. 1**. The response rapidly rises to a peak through a process of time-dependent activation. While the command potential is maintained, a decline from the initial peak is observed for most, if not all, VSCCs. This is a consequence of the process of inactivation (which can be either voltage- or $Ca^{2+}$-dependent).

    The multiple phases of the $Ca^{2+}$ current response to a simple voltage step allows one to measure a range of parameters. The most commonly made measurement is the peak current amplitude during the command pulse; in addition, the amplitude of the tail current can be characterized. The kinetics of activation, inactivation, and deactivation can also be quantified, as can recovery from inactivation. Furthermore, all of these parameters are voltage-dependent and can also exhibit dependencies on each other.

    For a simple first pharmacological experiment with any compound many workers will simply track the time course of the peak $Ca^{2+}$ channel current amplitude

measured at a single test potential applied from a fixed holding potential. The test potential used will often be close to that which produces maximum current amplitude, typically around 0 mV for a high-voltage-activated (HVA) channel and –15 mV for an low-voltage-activated (LVA) channel. The holding potential would usually be set at a level which elicits little steady-state inactivation. (To know where the test and holding potentials lie on the activation and inactivation curves an initial series of I-V relationships and steady-state inactivation curves can be gathered; for protocols *see* below). When using such a protocol we would utilize a P-over-4 leak subtraction method and would store both leak-subtracted and raw data to the computer. It can also be useful to include a "passive" voltage step (e.g., –80 to –90 or –70 mV) in the acquired data trace. The purpose of this is to allow both an assessment of the effectiveness of the P-over-4 leak subtraction and to provide a means to calculate and subtract leak from the raw data if there are concerns about the outcome of the chosen P-over-4 paradigm.

Although many workers use such a protocol simply to measure peak current amplitude versus time, the current trace will also provide information on activation rate, tail current amplitude and deactivation rate. Furthermore, if the test pulse is long enough, the rate of macroscopic inactivation can be estimated. Given that compounds can alter all of these parameters it is suggested that they are at least "eye-balled" for change during an experiment and better still analyzed quantitatively. It is also worth noting that changes in these parameters with time, particularly deactivation kinetics, can be good indicators of changes in the fidelity of the voltage clamp and consequently of recording quality.

For many VSCCs expressed in common host cells (e.g., HEK293, CHO, COS) it is likely that all, or nearly all, the VSCCs will be inactivated in the culture dish prior to obtaining whole-cell access. This is because the resting membrane potential of such host cells is typically very depolarized (e.g., –35 to –5 mV). Consequently, when recordings are started with standard protocols, the current will often run up for a short time as the entire channel population slowly shifts to a new equilibrium in which most channels are in non-inactivated closed states at rest. After this initial period of run-up the current amplitude may, for a while, become steady with respect to time. In most recording scenarios the current will begin to run down at some finite rate, although under the right conditions this run down can be very slow (*see* **Note 16**).

The next most common protocol to be used for VSCC analysis is the current–voltage relationship. In its most common form, this consists of a series of depolarizing steps of incrementally increasing amplitude applied from a negative holding potential. For example, 10 mV test potential increments from –80 mV to +60 mV, all applied from a holding potential of –80 mV. The standard readout is a plot of peak current amplitude vs test potential. With the right protocol the voltage-dependence of activation and inactivation rates and conductance voltage plots can also be obtained.

First, it is well worth including a zero amplitude step as the first pulse (e.g., –80 to –80 mV). The main reason for this is that in subsequent analysis where the

measured "peak" during such a zero amplitude test pulse can be subtracted from all subsequent peaks as a means to remove the effect of background current noise on measured peak current. Indeed it may also be worth including a single hyperpolarizing step at the start or the end of the data set, this can be used to judge the effectiveness of leak subtraction, or as a basis for an ohmic leak subtraction method.

Second, to define the shape of the voltage-dependence of activation, which realistically only spans about 30 mV for most VSCCs, we often include smaller increments in test potential (5 mV or even 3 mV) in the area of the rising phase of the I-V (the downstroke of the U-shape of a typical I-V). For example, for a HVA current, we may include additional test pulses to –35, –25, –15, and –5 mV. In order to keep protocols short we may then leave out test pulses to, –70, –50, +20, and +40 mV, where there is either no channel activation or current amplitude is only a consequence of electrochemical driving force.

Third, some consideration must be given to the length of the test pulses employed. For small depolarizations, channel opening may be very slow, so to obtain a good estimate of the peak current a long pulse will be required. Conversely, for strong depolarizations, peak current will be reached in a few milliseconds and longer pulses will produce some degree of channel inactivation. If one is only interested in studying current activation, the length of the test pulse can be set so that it is just longer than the time required to reach peak macroscopic current. Indeed, this is the best method to use if one it trying to determine peak conductance–voltage relationships from tail current measurements. If one wishes to assess the kinetics of macroscopic inactivation at various test potentials, pulses long enough to induce a reasonable degree of inactivation will be required. As for activation studies these test pulses may need to be of different durations for different test potentials because the rate of inactivation is voltage-dependent. Furthermore, when eliciting significant inactivation during test pulses, sufficient time must be left between test pulses to allow recovery from inactivation to occur (this can be estimated using a standard recovery from inactivation protocol).

Inactivation of VSCCs is another important parameter and one that is often relevant to pharmacology, as many compounds preferentially bind to inactivated states. As mentioned earlier, macroscopic inactivation kinetics can be measured during voltage pulses used to characterize channel activation. However, inactivation (albeit much slower) also occurs at potentials that fail to activate VSCCs significantly. This is easily demonstrated in experiments that characterize steady-state inactivation relationships. Put simply, to gather such data one varies the holding potential employed before applying a brief test pulse to activate the VSCCs. This test pulse is of invariant amplitude, typically to the peak of the I-V relationship, and is usually brief (just long enough to produce peak current). Commonly steady-state inactivation protocols use a conditioning pre-pulse of incremental amplitude applied for a few seconds before the test pulse. Alternatively, after the test pulse the cell is repolarized to the next required holding potential,

which is then maintained until the next test pulse applied. Notably, as the rate of inactivation is faster at more depolarized levels there is a tendency with such methods, to fail to reach a steady-state level of inactivation at the more hyperpolarized holding potentials; however, this rarely has a highly significant effect on the final curve if sufficient points around the mid-point of inactivation are gathered. The output of such experiments is plotted as peak current response in the test pulse vs pre-test pulse-holding potential. The data are typically normalized to current amplitude produced during the maximally effective test pulse. We would recommend that leak subtraction sweeps are gathered after the test pulse, rather than before.

$Ca^{2+}$-dependent inactivation (i.e., channel inactivation caused by cytoplasmic $Ca^{2+}$) is often studied with paired test-pulse protocols. Here, the first test pulse amplitude is varied, such that the level of $Ca^{2+}$ entry changes, and the degree of inactivation thus produced is studied by applying an invariant second test pulse. Having said this, using such protocols it is very difficult to entirely separate $Ca^{2+}$-dependent inactivation from voltage-dependent inactivation, whereas the reverse separation can be achieved by studying the flux of monovalent cations in the absence of $Ca^{2+}$. At extreme depolarizations relatively little $Ca^{2+}$-dependent inactivation is produced (because little $Ca^{2+}$ enters the cell because of driving force considerations) but voltage-dependent inactivation is maximal owing to the strong depolarization.

Inactivated VSCCs recover from voltage-dependent inactivation with a rate that depends on the membrane potential. To characterize recovery from inactivation a paired pulse protocol is typically used. Here a series of paired pulses are applied in which a first test pulse that substantially inactivates the VSCC population is followed, at a varied latency, by a brief, second test pulse. The response to the second pulse is used to monitor what proportion of the channels have recovered from the inactivation produced in the first pulse to a state that allows them to be reactivated. It is good practice to leave sufficient time between individual paired pulse stimuli to allow near complete recovery from inactivation. Furthermore, we recommend that the change in interpulse interval is made in a logarithmic fashion rather than a linear one as the process of recovery from inactivation typically follows an exponential (or often multi-exponential) time course. The voltage dependence of the rate of recovery from inactivation can be determined by performing a series of such experiments in which the holding potential employed between the paired pulses is systematically varied.

The last major biophysical hallmark we shall consider is deactivation, the process through which VSCCs close on membrane repolarization. Like activation and inactivation deactivation is a voltage-dependent process which is speeded at more hyperpolarized potentials. To characterise this voltage-dependence a protocol in which a fixed amplitude test pulse is followed by repolarization to a range of different potentials is employed. Repolarization to potentials at which VSCCs exhibit no measurable opening in activation protocols will produce a large inward tail current that will decline rapidly to the zero current level.

The decline in this current represents the process of deactivation and can be fit with exponential functions, the time constant of which will depend on voltage. The key factor to note is that deactivation is very fast. At room temperature, CaV3 family channels (i.e., LVA T-type channels) deactivate with time constants of the order of 1 ms at –80 mV. HVA channels (CaV1 and CaV2) deactivate perhaps 10 times faster. Indeed, to characterize the rapid deactivation of these channels faithfully, the very best patch clamp practice must be employed to elicit a suitably fast voltage clamp (e.g., large electrodes, very low series resistance, and accurate capacitance compensation). For example in the past we have measured CaV2.2 channel deactivation time constants of around 60 μs, using 0.6 MΩ electrodes and approx 1 MΩ series resistances compensated by approx 90%). Because of the speed and voltage dependence of deactivation, the best tip for tail current measurements—for example, to create conductance–voltage curves—is to use the most depolarized repolarization potential possible (e.g., approx –50 or –60 mV).

We have summarized a range of standard voltage-step protocols for making simple biophysical measurements. Review of the literature will uncover a range of other voltage step protocols including, for example, triple pulse measurements favored by some laboratories for inactivation studies. Of course in the physiological situation VSCC opening and closing is not triggered by square-wave voltage changes, but instead by physiological membrane potential changes. These will include, depending on the VSCC type, action potentials, synaptic potentials, and pacemaker currents. Analysis of how VSCCs are activated by such voltage changes can be revealing when considering how biophysical parameters relate to physiological role. To achieve this goal, recorded real or digitally synthesized physiological voltage transients can be used as voltage commands. Alternatively models of channel gating can be used to simulate the physiological behaviour of VSCCs under various conditions. It is often advisable to complement studies of recombinant channels with analysis of native VSCCs which of course may exhibit somewhat different behaviors owing to their environment or posttranslational modifications.

### *4.5. The Basic Process of Recording Whole-Cell VSCC Currents*

19. The operator should hold an earthed (grounded) lead when touching the headstage. The sensitive amplifier in the headstage input can be damaged by static electricity.
20. Pressure and suction can be applied using a syringe (e.g., 10 mL) or by mouth (through the body of a 1-mL syringe). Pressure line is connected to suction port of the electrode holder via a three-way stopcock and suitable tubing. This allows applied pressure (or suction) to be locked in. We prefer to leave positive pressure on the pipet lumen until we touch the surface of the cell.
21. We visually observe the occurrence of contact between the pipet and the cell surface. You can also detect this by watching the current response of the electrode.

22. In cells that form gigaseals slowly (or with difficulty), we find that seals of 50–500 MΩ can be encouraged to convert to gigaseals by placing the pipet potential at a negative value, e.g., –70 mV and by applying the VSCC bath solution.
23. Certain amplifiers provide a "zap" button that delivers a short-duration, high-amplitude electrical pulse which dielectrically perturbs the membrane with the intent of breaking through to the whole cell configuration. We have used this, although rarely. We find it is most effective when combined with suction rather than used alone.
24. Prior to neutralizing capacity transients and compensating for series resistance it can be useful to check whether the current under study is present in the cell (e.g., by using a single voltage step to a potential where a good-sized current would be expected or, if appropriate, by applying a brief agonist application). There is little point in optimizing recording parameters if there is no current to record. This is particularly applicable when working with transiently transfected cells.
25. Series resistance. In terms of the fidelity of the voltage clamp and lack of voltage errors the best recordings are made with the lowest access resistances. Thus, if there is no reason to work with higher series resistance levels (for example to reduce run down) aim low. The best way to achieve this is to use as low a resistance electrode as is commensurate with getting a decent number of gigaseals and whole cell recordings. For the common host cell lines, such as HEK293s and CHOs, we would generally have series resistance values in the range of 2–5 MΩ and have worked at <1 MΩ. Generally, in such systems we would not work with recordings with an access resistance >10 MΩ and certainly never more than 20 MΩ. Having said this, the most important factor is to marry the level of uncompensated series resistance with the amplitude of the current under study; for example, for a slowly activating current of 100-pA amplitude, an uncompensated series resistance of 15 MΩ may not cause any significant errors for most experiments, whereas a 5-MΩ series resistance and a fast-gating 15-nA current could combine to produce substantial recording errors.

## References

1. Ertel, E. A., Campbell, K. P., Harpold, M. M., et al. (2000) Nomenclature of voltage-gated calcium channels. *Neuron* **25,** 533–535.
2. Sakmann, B. and Neher, E. (1983) *Single-Channel Recording*. Plenum Press, New York, NY.
3. Hamill, O. P., Marty, A., Neher, E., Sakmann, B., and Sigworth, F. J. (1981) Improved patch-clamp techniques for high-resolution current recording from cells and cell-free membrane patches. *Pflugers Arch.* **391,** 85–100.
4. Levis, R. A. and Rae, J. L. (1992) Constructing a patch clamp setup. *Methods Enzymol*. **207,** 14–66.
5. Levis, R. A. and Rae, J. L. (1998) Low-noise patch-clamp techniques. *Methods Enzymol*. **293,** 218–266.
6. The Axon Guide. (Website: http://www.axon.com/MR_Axon_Guide.html). Accessed on April 6, 2005.

7. Fenwick, E. M., Marty, A., and Neher, E. (1982) Sodium and calcium channels in bovine chromaffin cells. *J. Physiol.* **331,** 599–635.
8. Lux, H. D. and Brown, A. M. (1984) Patch and whole cell calcium currents recorded simultaneously in snail neurons. *J. Gen. Physiol.*, **83,** 727–750.
9. Ikeda, S. R., Schofield, G. G., and Weight, F. F. (1986) $Na^+$ and $Ca^{2+}$ currents of acutely isolated adult rat nodose ganglion cells. *J. Neurophysiol.* **55,** 527–539.
10. Matteson, D. R. and Armstrong, C. M. (1984) Na and Ca channels in a transformed line of anterior pituitary cells. *J. Gen. Physiol.* **83,** 371–394.
11. Carbone, E. and Lux, H.D. (1987) Kinetics and selectivity of a low-voltage-activated calcium current in chick and rat sensory neurones. *J. Physiol.* **396,** 547–570.
12. Tsien, R. W., Bean, B. P., Hess, P., Lansman, J. B., Nilius, B., and Nowycky, M. C. (1986) Mechanisms of calcium channel modulation by beta-adrenergic calcium agonists. *J. Mol. Cell Cardiol.* **18,** 691–710.
13. Hille, B. (2001) *Ion Channels of Excitable Membranes*. Sinauer, Sunderland, MA.
14. Hess, P., Lansman, J. B., and Tsien, R. W. (1984) Different modes of Ca channel gating behaviour favoured by dihydropyridine Ca agonists and antagonists. *Nature* **311,** 538–544.
15. Bossu, J. L., Feltz, A., and Thomann, J. M. (1985) Depolarization elicits two distinct calcium currents in vertebrate sensory neurones. *Pflugers Arch.* **403,** 360–368.
16. Dupont, J. L., Bossu, J. L., and Feltz, A. (1986) Effect of internal calcium concentration on calcium currents in rat sensory neurones. *Pflugers Arch.* **406,** 433–435.
17. Stefani, A., Pisani, A., Mercuri, N. B., Bernardi, G., and Calabresi, P. (1994) Activation of metabotropic glutamate receptors inhibits calcium currents and GABA-mediated synaptic potentials in striatal neurons. *J. Neurosci.* **14,** 6734–6743.
18. Stefani, A., Spadoni, F., and Bernardi, G. (1997) Differential inhibition by riluzole, lamotrigine, and phenytoin of sodium and calcium currents in cortical neurons: implications for neuroprotective strategies. *Exp. Neurol.* **147,** 115–22.
19. Hainsworth, A. H., Spadoni, F., Lavaroni, F., Bernardi, G., and Stefani, A. (2001) Effects of extracellular pH on the interaction of sipatrigine and lamotrigine with high-voltage-activated (HVA) calcium channels in dissociated neurones of rat cortex. *Neuropharmacol.* **40,** 784–791.
20. J. Dempster, Strathclyde Electrophysiology software. (Website: http://spider.science.strath.ac.uk/PhyPharm/). Accessed on April 6, 2005.
21. Vasquez, C., Navarro-Polanco, R. A., Huerta, M., et al. (2003) Effects of cannabinoids on endogenous K+ and $Ca^{2+}$ currents in HEK293 cells. *Can. J. Physiol. Pharmacol.* **81,** 436–442.
22. Berjukow, S., Doring, F., Froschmayr, M., Grabner, M., Glossmann, H., and Hering, S. (1996) Endogenous calcium channels in human embryonic kidney (HEK293) cells. *Br. J. Pharmacol.* **118,** 748–754.
23. Bleakman, D., Bowman, D., Bath, C. P., et al. (1995) Characteristics of a human N-type calcium channel expressed in HEK293 cells. *Neuropharmacology* **34,** 753–765.

24. McCool, B. A., Pin, J. P., Harpold, M. M., Brust, P. F., Stauderman, K. A., and Lovinger, D. M. (1998) Rat group I metabotropic glutamate receptors inhibit neuronal $Ca^{2+}$ channels via multiple signal transduction pathways in HEK 293 cells. *J. Neurophysiol.* **79**, 379–391.
25. Pereverzev, A., Klockner, U., Henry, M., et al. (1998) Structural diversity of the voltage-dependent $Ca^{2+}$ channel alpha1E-subunit. *Eur. J. Neurosci.* **10,** 916–925.
26. McNaughton, N. C., Hainsworth, A. H., Green, P. J., and Randall A. D. (2000) Inhibition of recombinant low-voltage-activated $Ca(^{2+})$ channels by the neuroprotective agent BW619C89 (Sipatrigine). *Neuropharmacology* **39,** 1247–1253.
27. Hainsworth, A. H., McNaughton, N. C., Pereverzev, A., Schneider, T., and Randall, A. D. (2003) Actions of sipatrigine, 202W92 and lamotrigine on R-type and T-type $Ca^{2+}$ channel currents. *Eur. J. Pharmacol.* **467,** 77–80.
28. Zeilhofer, H. U., Swandulla, D., Reeh, P. W., and Kress, M. (1996) $Ca^{2+}$ permeability of the sustained proton-induced cation current in adult rat dorsal root ganglion neurons. *J. Neurophysiol.* **76,** 2834–2840.
29. Song, W. J. and Surmeier, D. J. (1996) Voltage-dependent facilitation of calcium channels in rat neostriatal neurons. *J. Neurophysiol.* **76,** 2290–2306.
30. Mody, I., Salter, M. W., and MacDonald, J. F. (1989) Whole-cell voltage-clamp recordings in granule cells acutely isolated from hippocampal slices of adult or aged rats. *Neurosci. Lett.* **96,** 70–75.
31. Matsuo, S., Jang, I. S., Nabekura, J., and Akaike, N. (2003) Alpha 2-Adrenoceptor-mediated presynaptic modulation of GABAergic transmission in mechanically dissociated rat ventrolateral preoptic neurons. *J. Neurophysiol.* **89,** 1640–1648.
32. Kameyama, A., Yazawa, K., Kaibara, M., Ozono, K., and Kameyama, M. (1997) Run-down of the cardiac $Ca^{2+}$ channel: characterization and restoration of channel activity by cytoplasmic factors. *J. Neurophysiol.* **433,** 547–556.
33. Belles, B., Malecot, C. O., Hescheler, J., and Trautwein, W. (1988) "Run-down" of the Ca current during long whole-cell recordings in guinea pig heart cells: role of phosphorylation and intracellular calcium. *Pflugers Arch.* **411,** 353–360.
34. Powers, R. K. and Binder, M. D. (2003) Persistent sodium and calcium currents in rat hypoglossal motoneurons. *J. Neurophysiol.* **89,** 615–624.
35. Horn, R. and Marty, A. (1988) Muscarinic activation of ionic currents measured by a new whole-cell recording method. *J. Gen. Physiol.* **92,** 145–159.
36. Akaike, N. (1994) Glycine responses in rat CNS neurons studied with gramicidin perforated patch recording. *Jpn. J. Physiol.* **44,** S113—S118.

# IV

## Measurement of Ins(1,4,5,)$P_3$ and $Ca^{2+}$ Release From Intracellular Stores

# 11

# Measurement of Phospholipase C by Monitoring Inositol Phosphates Using [$^3$H]Inositol-Labeling Protocols in Permeabilized Cells

**Alison Skippen, Philip Swigart, and Shamshad Cockcroft**

## 1. Introduction

Hormones, neurotransmitters, chemoattractants, and growth factors all elicit intracellular responses on binding to cell surface receptors by activating inositol phospholipid-specific phospholipase C (PLC). Activated PLC catalyzes the hydrolysis of phosphatidylinositol bisphosphate ($PIP_2$), a minor membrane phospholipid, to form two second messengers, diacylglycerol (DAG) and inositol (1,4,5)trisphosphate [Ins(1,4,5,)$P_3$]. DAG is a direct activator of protein kinase C isozymes, and Ins(1,4,5)$P_3$ mobilizes intracellular $Ca^{2+}$. G protein-coupled receptors couple to the PLC-β family via G proteins, and tyrosine kinase receptors activate PLC-γ isozymes ***(1,2)***. Regardless of the PLC isozyme activated, the product is invariantly Ins(1,4,5)$P_3$.

To monitor the activation of PLC enzymes, the authors have established in their laboratory, methods of using permeabilized cells. Permeabilized cells are useful for examining the regulatory components that are essential for Ins(1,4,5,)$P_3$ production. Calcium levels can be rigorously controlled, as well as appropriate regulatory proteins, such as phosphatidylinositol transfer protein (PITP) ***(3–5)***. Permeabilized cells can be used under conditions in which the cytosolic proteins are still present ("acutely permeabilized") and in which the cytosolic proteins have been allowed to leak out of cells. The loss of cytosolic proteins leads to the phenomenon of "run down" in which the ability of guanosine 5-[γ-thio]triphosphate (GTPγS) or a receptor agonist to stimulate PLC is diminished. The response can be "reconstituted" by addition of exogenously added cytosolic proteins ***(3)***. A major reconstituting factor in the cytosol is PITP ***(3–6)***.

From: *Methods in Molecular Biology, vol. 312: Calcium Signaling Protocols: Second Edition*
Edited by: D. G. Lambert © Humana Press Inc., Totowa, NJ

Ins(1,4,5)$P_3$ is rapidly metabolized by phosphatases, and therefore, the authors assay for the production of inositol (poly)phosphates. The stimulus for PLC activation can be a direct activator of G proteins, e.g., GTPγS or an agonist that interacts with an appropriate cell-surface receptor ***(3–6)***. The protocols can be applied to most cell lines. Commonly used cell lines in the authors' laboratory are HL60 cells (both undifferentiated and differentiated) and RBL-2H3, but other cell lines have also been used ***(3–6)***.

The basic principle is the labeling of the inositol lipids by growing the appropriate cell line in culture in the presence of [$^3$H]inositol for 2–3 d. This ensures that the inositol-containing lipids are prelabeled to near equilibrium prior to the experiment. Lithium at 10 m*M* inhibits the degradation of inositol phosphates to free inositol and is used to trap the inositol in the inositol polyphosphate forms. Inositol phosphates can be separated with ease from free inositol by using anion exchange chromatography. Approximately 40–60 samples can be easily processed in a single day.

## 2. Materials

1. Mammalian cells: HL60 available from American Type Culture Collection, Rockville, MD.
2. [$^3$H]inositol is the *myo*-[2-$^3$H]inositol and is obtained from Amersham BioSciences (Buckinghamshire, UK) (cat. no. TRK317).
3. Growth medium: RPMI-1640 available from Sigma-Aldrich as 1X (cat. no. R-0883) or 10X (cat. no. R-1145) solution.
   a. The growth medium at 1X can be stored at 4°C and supplemented with 12.5% heat-inactivated fetal calf serum (FCS) (*see* **Note 1**).
   b. 12 mL of penicillin/streptomycin (P-0906, Sigma) and 25 mL of glutamine solution (G-7513, Sigma)/L when the medium is to be used (*see* **Note 2**).
   c. The supplemented medium can be stored at 4°C for 1–2 wk.
4. Labeling medium: Medium 199 (M199) available as a 10X solution from Sigma-Aldrich (cat. no. M-0650) (*see* **Notes 3** and **4**).
   a. The 1X M199 is supplemented with 12 mL of penicillin/streptomycin and 25 mL of glutamine/L.
   b. Because FCS is excluded, the labeling medium is supplemented with either;
      i. Insulin (I-5500, Sigma) (5 µg/mL final) and transferrin (T-2252, Sigma) (5 µg/mL final) as growth factors at the time of labeling, or
      ii. 12.5% heat-inactivated dialyzed FCS (26400-036, Invitrogen).
5. PIPES buffer: 20 m*M* PIPES, 137 m*M* NaCl, and 3 m*M* KCl, pH 6.8.
   a. Made from stock solutions, 1 *M* PIPES:
      i. Dissolve 302.4 g of PIPES (P6757, Sigma) in 600 mL of $H_2O$ and adjust the pH to approx 6.0 with concentrated NaOH (*see* **Note 5**).
      ii. When the PIPES is fully dissolved, adjust to pH 6.8 and make up the volume to 1 L. The PIPES can be aliquoted and stored at –20°C for several months.

**Table 1**
**Preparation of $Ca^{2+}$ Buffer Stock Solution**

| | Vol (mL) | |
|---|---|---|
| pCa | $Ca^{2+}$ · EGTA | EGTA |
| 7 (100 n*M*) | 0.996 | 7.004 |
| 6 (1 μ*M*) | 4.698 | 3.302 |

6. 20X of NaCl/KCl solution: dissolve 159 g of NaCl and 4 g of KCl in 1 L of $H_2O$ and store at 4°C; stable for months.
   a. For 100 mL of PIPES buffer, take 5 mL of 20X NaCl/KCl stock plus 2 mL of 1 *M* PIPES stock to 100 mL with $H_2O$ checking that the pH is still 6.8.
7. Permeabilization buffer: PIPES buffer supplemented with 1 mg/mL glucose and 1 mg/mL bovine serum albumin (BSA).
8. Streptolysin O (SLO) is obtained from Sigma (cat. no. S-140).
   a. Each bottle contains 40 IU equivalents and is dissolved in 2 mL of $H_2O$ to make a stock solution of 20 IU/mL.
   b. The stock solution is stored at 4°C for 1–2 wk and is used at 0.4–0.6 IU/mL in experiments (*see* **Note 6**).
9. 0.1 *M* MgATP stock solution: dissolve 605 mg of disodium trihydrate adenosine triphosphate (ATP) (Roche, Lewes, East Sussex, UK; cat. no. 127531) in a 10-mL solution containing 2 mL of 1 *M* Tris-HCl and 1 mL of 1-*M* $MgCl_2$ (*see* **Note 7**). The solution is stable at –20°C for 1–2 yr at neutral pH.
10. Calcium buffers: required stock solutions are as follows:
    a. 100 m*M* of ethylene glycol tetraacetic acid (EGTA) prepared in 20 m*M* of PIPES, 137 m*M* of NaCl, 3 m*M* of KCl, pH 6.8.
    b. 100 m*M* $Ca^{2+}$ · EGTA (100 m*M* EGTA, 100 m*M* $CaCl_2$ [*see* **Note 8**]) prepared in 20 m*M* PIPES, 137 m*M* NaCl, 3 m*M* KCl, pH 6.8. These stocks can be stored at –20°C for several months.
    c. To prepare $Ca^{2+}$ buffer (pCa 7 and pCa 6) stock solutions, combine stock solutions of 100 m*M* $Ca^{2+}$ · EGTA and 100 m*M* EGTA to achieve the desired free $Ca^{2+}$ (*see* **Table 1** and **Note 9**).

       These quantities are calculated for a final $[EGTA]_{total}$ = 3 m*M*, $[MgCl_2]$ = 2 m*M* and pH 6.8. Eight milliliters of each buffer stock solution are prepared by mixing the $Ca^{2+}$ · EGTA and EGTA solutions (100 m*M*) in the proportions indicated in **Table 1**. For use the buffer stocks (100 m*M*), which do not contain Mg, are diluted to 3 m*M* $[EGTA]_{total}$.
11. Dimethyl sulfoxide (DMSO) from Sigma (D-5879).
12. 60 mM Dibutyryl cyclic adenosine monophosphate (DbcAMP) (D-0627, Sigma).
    a. Dissolve 100 mg of the powder in 3.08 mL of DMSO.
    b. The DbcAMP is used at a final concentration of 300 μ*M* (1 mL stock to 200 mL cells) to differentiate HL60 cells.

13. 1 *M* LiCl stored at –20°C for several months.
14. Preparation of Dowex 1-X8 anion exchange resin (*see* **Note 10**):
    a. Place 100 g of Dowex resin in a beaker.
    b. Add 400 mL of 1 *M* NaOH and stir with a glass rod.
    c. Allow the resin to settle (1–2 h).
    d. Carefully decant the NaOH solution, add 400 mL of 1 *M* formic acid, and stir with a glass rod.
    e. Allow the resin to settle and decant the formic acid.
    f. Wash the resin five times with 400 mL of $H_2O$. The resin can be left as a 50% slurry in $H_2O$ at 4°C. One milliliter of the slurry is used per column and either Pasteur pipets or purchased columns (Poly-Prep columns, cat. no. 731-1550; Bio-Rad, Hercules, CA) can be used (*see* **Note 11**).

## 3. Methods

### 3.1. Maintenance of HL60 Cell Cultures

1. Dilute HL60 cells to between 0.3 and $0.5 \times 10^6$ cells/mL. Generally, use 50 mL in 75-$cm^2$ tissue culture flasks with a 5% $CO_2$ atmosphere.
2. Grow the cells to confluence (usually takes 2 to 3 d) and dilute to between 0.3 and $0.5 \times 10^6$ cells again (*see* **Note 12**).
3. Use one flask to label, keeping one flask as a seed culture.

### 3.2. Differentiation of HL60 Cells (see **Note 13**)

1. Differentiate a confluent flask of cells in the presence of 300 µ*M* DbcAMP; the cells will be differentiated by 36–40 h.
2. Cells can be prelabeled with [$^3$H]inositol by transferring them to M199 and labeling as described in **Subheading 3.3.** with the addition of the DbcAMP (1 mL of stock DbcAMP to 200 mL of cells).

### 3.3. Preparation of [$^3$H]Inositol-Labeled HL60 Cells (see **Note 14**)

1. HL60 cells can be labeled with [$^3$H]inositol with one of two methods
    a. Procedure 1:
        i. Pellet 50 mL of confluent ($2 \times 10^6$ cells/mL) cells by centrifugation at 1000*g* for 5 min at room temperature (Heraeus Megafuge 1.0; Brentwood, Essex, UK).
        ii. Resuspend the cells in 10 mL of M199 without FCS but with glutamine and penicillin/streptomycin.
        iii. Add the 10 mL of cells to 40 mL of M199 without FCS containing glutamine and penicillin/streptomycin, to which 0.25 mL of a 1 mg/mL sterile solution of insulin and 0.25 mL of a 1 mg/mL sterile solution of transferrin (final concentrations of 5 µg/mL each) have been added.
        iv. Add 50 µCi (1 µCi/mL final) [$^3$H]inositol.
        v. Grow cells for 48 h.
        vi. 50-mL cells are sufficient for 50 incubations.

b. Procedure 2:
   i. Pellet 20 mL of confluent ($2 \times 10^6$ cells/mL) cells by centrifugation at 1000*g* for 5 min at room temperature (Heraeus Megafuge 1.0; Brentwood) (*see* **Note 15**).
   ii. Resuspend the cells in 10 mL of M199 containing glutamine and penicillin/streptomycin with 12.5% heat-inactivated dialyzed FCS.
   iii. Add the 10 mL of cells to 40 mL of M199 with 12.5% dialyzed FCS containing glutamine and penicillin/streptomycin.
   iv. Add 50 µCi (1 µCi/mL final) [$^3$H]inositol.
   v. Grow cells for 48 h.
   vi. 50-mL cells are sufficient for 50 incubations.

### 3.4. PLC Activity in "Acutely Permeabilized" HL60 Cells

1. Centrifuge 50 mL of [$^3$H]inositol-labeled cells at 1000*g* for 5 min at room temperature.
2. Discard the supernatant, which contains most of the radioactivity, and gently resuspend the cells in 40 mL of permeabilization buffer (PIPES buffer plus 1 mg/mL of glucose and 1 mg/mL of BSA).
3. Pellet the cells and wash once more with the permeabilization buffer.
4. After the final centrifugation, resuspend the cells in 2–3 mL of the permeabilization buffer.
5. Equilibrate the washed radiolabeled cells at 37°C for 10–25 min.
6. In a 1.5-mL Eppendorf tube (*see* **Note 16**), and 50 µL of labeled cells to the equivalent volume of permeabilization buffer supplemented with the following:
   a. SLO (0.4 IU/mL final).
   b. MgATP (1 m*M* final).
   c. $MgCl_2$ (2 m*M* final).
   d. $Ca^{2+}$ buffered with 3 m*M* EGTA (pCa6).
   e. LiCl (10 m*M* final) (*see* **Note 17**).
   f. GTPγS (10 µ*M* final).
7. Incubate the mixture at 37°C for 20 min.
8. Place the reactions in an ice bath and terminate the reactions with one of two methods.
   a. Procedure 1:
      i. Quench the assay with 500 µL of (chloroform:methanol [1:1 by v/v]) and vortexing.
      ii. Add 250 µL of $H_2O$ and vortex.
      iii. Centrifuge the samples for 5 min at 1000*g* at 4°C (*see* **Note 18**).
      iv. Use 400 µL of the aqueous phase for inositol phosphate analysis.
   b. Alternative procedure:
      i. Quench the assay with 500 µL of ice-cold saline (0.9% NaCl).
      ii. Centrifuge at 2000*g* to sediment the permeabilized cells.
      iii. Use 400 µL of the supernatant for inositol phosphate analysis.

### 3.5. Separation of Inositol Phosphates by Dowex (see **Note 19**)

1. Load the 400-µL sample containing the radiolabeled inositol phosphates onto the prepared Dowex columns.
2. Allow the sample to gravity flow through the column.
3. Wash the columns with 6 mL of $H_2O$ (*see* **Note 20**).
4. Wash the columns with 6 mL of 5 m*M* sodium tetraborate/60 m*M* sodium formate (*see* **Note 21**).
5. Elute total inositol phosphate with 3 mL of 1-*M* ammonium formate/0.1 *M* of formic acid directly into scintillation vials.
6. Alternatively, if inositol monophosphate (IP1), inositol bisphosphate (IP2), and inositol trisphosphate (IP3) are to be separated, elute step-wise into scintillation vials:
   a. 3 mL of 0.2 *M* ammonium formate/0.1 *M* formic acid (IP1).
   b. 3 mL of 0.4 *M* ammonium formate/0.1 *M* of formic acid (IP2).
   c. 3 mL of 1 *M* ammonium formate/0.1 *M* of formic acid (IP3 and inositol tetrakisphosphate [IP4] if present in the sample) (*see* **Fig. 1A**; *see* **Note 22**).
7. Add scintillant and measure radioactivity (*see* **Note 23**).
8. Regenerate the columns by washing with 6 mL of 2 *M* ammonium formate/0.1 *M* of formic acid followed by extensive washing with $H_2O$ (10–15 mL) (*see* **Note 24**).

### 3.6. Data Handling (see **Note 25**)

The dpm in inositol phosphates provides the level of PLC activity in individual experiments. The amount of dpm found in inositol phosphates is ultimately dependent on the amount of label incorporated by the cells, which can vary from experiment to experiment. The increase in inositol phosphates can also be expressed as a function of the total radioactivity (disintegration/min [dpm]) incorporated into the inositol lipids. This allows results to be calculated as a percentage of the total lipids.

### 3.7. Determination of Radioactivity Incorporated Into the Inositol Lipids

1. Carefully remove the total lipid chloroform extract obtained from the first procedure and transfer it to a clean scintillation vial.
2. Allow the chloroform to evaporate by leaving the vials open in a fume hood overnight.
3. Add 500 µL of methanol to the dried lipids followed by 2 mL of scintillation cocktail and measure dpm.

### 3.8. Establishing Conditions for Rundown of PLC Activity

1. Use 4.5 mL of washed [$^3$H]inositol labeled cells in the permeabilization buffer.
2. Add cocktail (0.5 mL) of SLO (0.4 IU/mL final), MgATP (1 m*M* final), and $Ca^{2+}$, pCa 7 (100 n*M* buffered with 100 m*M* EGTA final) to the cells.
3. At timed intervals, remove 4 × 50 µL-aliquots of cells and transfer to duplicate assay tubes containing 50 µL of a cocktail containing $Ca^{2+}$, pCa 6 (1 µ*M* buffered

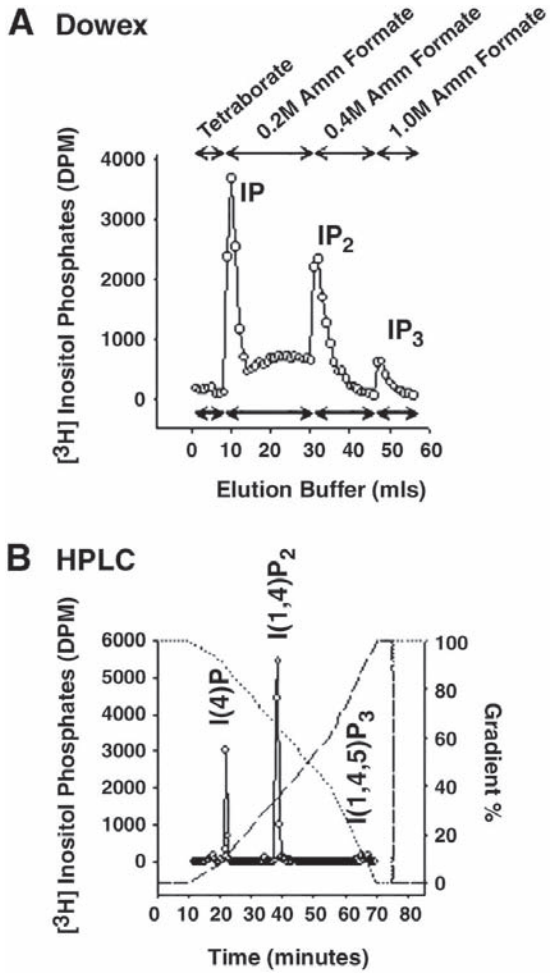


Fig. 1. Comparison of two identical samples analyzed on **(A)** Dowex anion exchange resin and **(B)** anion exchange high-performance liquid chromatography. HL60 cells were radiolabeled for 48 h with [$^3$H]inositol and were permeabilized for 10 min with SLO as described in **Subheading 3.9.** Cells were washed and incubated at 37°C with PITPα (5 m*M*) and GTPγS (10 m*M*). After 20 min, the samples were quenched and the aqueous phase containing the inositol phosphates was analyzed by **(A)** Dowex or **(B)** high-performance liquid chromatography (HPLC.) In **(A)** the sample was loaded onto the Dowex anion exchange resin and the inositol phosphates were eluted in 1-mL fractions using the solutions indicated. In **(B)** the inositol phosphates were analyzed on a Partisil 10 SAX column using a gradient of 1.4 *M* monobasic ammonium phosphate buffer adjusted to pH 3.7 with orthophosphoric acid, and fractions were collected every 0.5 min (*see* **Note 26**).

with 3 m*M* EGTA final), LiCl (10 m*M* final), $MgCl_2$ (2 m*M* final) ± GTPγS (10 μ*M* final).
4. Incubate the samples at 37°C for 20 min.
5. Quench the reaction using one of the two methods described in **Subheading 3.4.** and analyze [$^3$H]inositol phosphates as described in **Subheading 3.5.** (*see* **Note 27**).

### 3.9. Reconstitution of G Protein Stimulated PLC by Cytosolic Factors in Rundown Cells

1. Incubate 4.5 mL of washed [$^3$H]inositol-labeled HL60 cells in permeabilization buffer with 0.5 mL of cocktail containing SLO (0.4 IU/mL final), MgATP (1 m*M* final), and $Ca^{2+}$, pCa 7 (100 n*M* buffered with 3 m*M* of EGTA final) for 10 min (*see* **Notes 28** and **29**).
2. After permeabilization, dilute the cells to 35 mL with ice-cold permeabilization buffer.
3. Centrifuge the cells at 2000*g* for 5 min to pellet the cells (*see* **Note 30**).
4. Resuspend the cell pellet in 2X assay buffer (permeabilization buffer supplemented with $Ca^{2+}$, pCa 6 with 6 m*M* of EGTA final), LiCl (20 m*M* final), MgATP (4 m*M* final), and $MgCl_2$ (4 m*M* final) (*see* **Note 31**).
5. Prepare tubes in advance that contain 25 μL of cytosol, or other reconstituting factors (e.g., PITP) ± GTPγS at 20 μ*M*.
6. Transfer 25 μL of permeabilized cells to assay tubes on ice (*see* **Note 32**).
7. Transfer the assay tubes to a 37°C water bath and incubate the samples for 20 min.
8. Quench the assay as described in **Subheadings 3.4.8.** and **3.5.** and assay for inositol phosphates.

### 3.10. Assaying for PLC Activity Using a Receptor-Directed Agonist in Differentiated HL60 Cells That Express the FMetLeuPhe Receptor

1. Incubate 4 mL of washed differentiated [$^3$H]inositol-labeled HL60 cells in permeabilization buffer with 1 mL of cocktail containing SLO (0.4 IU/mL final), MgATP (1 m*M* final), and $Ca^{2+}$, pCa 7 (100 n*M* buffered with 3 m*M* of EGTA final) for 10 min.
2. After permeabilization, dilute the cells to 35 mL with ice-cold permeabilization buffer.
3. Centrifuge the cells at 2000*g* for 5 min to pellet the cells.
4. Resuspend the cell pellet in 2X assay buffer (permeabilization buffer supplemented with pCa 6 [6 m*M* of EGTA], LiCl [20 m*M*], MgATP [4 m*M*], and $MgCl_2$ [4 m*M*]).
5. Prepare tubes in advance that contain 25 μL of cytosol, or other reconstituting factors ± FMetLeuPhe at 1 μ*M* final and guanosine triphosphate (GTP) at 100 μ*M* final.
6. Transfer 25 μL of permeabilized cells per assay tube on ice.
7. Transfer the assay tubes to a 37°C water bath and incubate the samples for 20 min.
8. Quench the assay as described in **Subheadings 3.4.8.** and **3.5.** and assay for inositol phosphates (*see* **Note 33**).

## 4. Notes

1. FCS from Sera Laboratories International Ltd (EU-000-F): heat inactivate before use by immersing a thawed bottle in a 56°C bath for 1 h.
2. Batches of RPMI-1640 can be stored with FCS added; however, the glutamine and penicillin/streptomycin must be added only as each bottle is needed.
3. Because RPMI-1640 medium contains relatively high levels of inositol, cells are labeled in M199. Concentration of inositol in different media are as follows: 0.05 mg/mL of M199, 35 mg/mL of RPMI-1640, and 7.2 mg/mL of Dulbecco's modified Eagle's medium.
4. FCS is also excluded owing to high levels of inositol.
5. The solution will start out at approx pH 2.5–3.0 and will fluctuate as NaOH is added and the PIPES dissolves. Generally, the PIPES is fully dissolved by pH 6.0–6.2.
6. The solution will become cloudy after a couple of days, but this will not affect permeabilization and can be partially cleared by warming to 37°C before use. Alternatively, the SLO can be aliquoted and stored at –20°C for several months.
7. The use of 200 m*M* Tris-HCl (final) effectively gives a neutral final solution (pH 7.0). This should be checked and adjusted accordingly.
8. High quality EGTA is required from Fluka Chemie AG, Gillingham, Dorset, UK (cat. no. 03779). $CaCl_2$ is analytical-grade from BDH Industries.
9. Values have been obtained using the program "Chelate" for a pH of 6.8 ***(8)***.
10. The Dowex resin (1X8 and mesh size 100–200) is purchased from Sigma-Aldrich in the chloride form and must be converted to the formate form.
11. The Dowex is transferred to Pasteur pipets (0.5 mL bed volume) equipped with a glass wool plug (gloves should be worn when making the glass wool plugs).
12. HL60 cells are generally passed for 50–60 passages, and then fresh cells are thawed from liquid nitrogen. Always make sure that you have stocks from early passages saved for future use.
13. HL60 cells can be differentiated toward neutrophils by the addition of DbcAMP or DMSO. DMSO is flammable and must be kept from open flames.
14. Other cell lines can be used. The authors have successfully labeled and reconstituted RBL-2H3 cells. Cells are labeled with 1 μCi of [$^3$H]inositol/mL being added directly to the medium (Dulbecco's modified Eagle's medium + 5% FCS), and the cells are grown for 48 h. It is preferable to add the label when the cells have just been split.
15. If HL60 cells are to be differentiated with DbcAMP at the same time as labeling with [$^3$H]inositol using Procedure 2, then 30 mL of confluent ($2 \times 10^6$ cells/mL) cells should be pelleted by centrifugation at 1000*g* for 5 min at room temperature.
16. Prepare the Eppendorf tubes with the appropriate reagents in an ice bath and transfer to a 37°C-water bath 5 min prior to the addition of 50 μL cells.
17. LiCl inhibits the conversion of inositol phosphates back to free inositol. It can be kept as a 1-*M* stock at –20°C.
18. The lipids are present in the lower chloroform phase, and the upper aqueous phase contains the water-soluble components including the inositol phosphates.

19. Inositol phosphates can also be analyzed on HPLC. This technique is able to identify the individual inositol phosphate isomers (**Fig. 1B**).
20 This step washes out the [$^3$H]inositol.
21. This step elutes glycerophosphoinositol.
22 Two identical samples were analyzed on Dowex and HPLC for comparison in **Fig. 1**.
23. The scintillation cocktail should be able to accommodate 1 M salt. (Use Ultima-Flo from Packard Bioscience, Pangbourne, Berkshire, UK).
24. The Dowex columns can be used and reused indefinitely if they are regenerated with 2 *M* of ammonium formate/0.1 *M* of formic acid after each use.
25. The increase in inositol phosphate can be expressed as a function of the total radioactivity (dpm) incorporated into the inositol lipids. This allows results to be calculated as a percentage of the total lipids.
26. The sample (**Fig. 1B**) was analysed by anion exchange, HPLC on a Partisil 10 SAX column (250 × 4.6 mm; Hichrom, Reading, UK) with a Partisil 10 SAX guard cartridge (Hichrom). The method used was taken from **ref. *9***. Briefly, the gradient program was set up using a flow rate of 1.25 mL/min and the fraction collector was set up to collect fractions at 0.5 min intervals (750 µL per fraction). The gradient was as follows:

0–1.4 *M* ammonium phosphate/orthophosphoric acid, pH 3.7

| Time (min) | 0 | 10 | 55 | 70 | 75 | 75.5 | 85 |
|---|---|---|---|---|---|---|---|
| % buffer | 0 | 0 | 35 | 100 | 100 | 0 | 0 |

27. Data can be plotted as the extent of GTPγS-stimulated PLC activity and a function of the permeabilization interval. Total run down is typically 80 to 90% for GTPγS-stimulated PLC activity.
28. The permeabilization cocktail can be made up from stocks as follows: 150 µL of pCa7, 150 µL of SLO solution, 50 µL of MgATP, and 150 µL of permeabilization buffer (PIPES + glucose and BSA).
29. Longer permeabilization times (i.e., 40 min) allow many more cytosolic factors to leak out.
30. Care should be taken because the permeabilized cell pellet is quite loose and some cells may be lost when decanting the buffer.
31. 2X Assay buffer can be made up as follows: 62.5 µL of pCa 6, 40 µL of MgATP (0.1 *M*), 10 µL of $MgCl_2$ (0.4 *M*), 20 µL of LiCl (1 *M*), 865 µL permeabilization buffer.
32. The final concentrations during the incubation will be as follows: $Ca^{2+}$, pCa 6 (1 µ*M* final buffered with 3 m*M* EGTA final), LiCl (10 m*M* final), MgATP (2 m*M* final), $MgCl_2$ (2 m*M* final), and GTPγS (10 µ*M* final).
33. The FMLP receptor-driven response can be much weaker than the GTPγS response.

## References

1. Rhee, S. G. (2001) Regulation of phosphoinositide-specific phospholipase C. *Annu. Rev. Biochem.* **70,** 281–312.

2. Rebecchi, M. J. and Pentyala, S. N., (2000) Structure, function, and control of phosphoinositide-specific phospholipase C. *Physiological Revs*. **80,** 1291–1335.
3. Thomas, G. M. H., Cunningham, E., Fensome, A., et al. (1993) An essential role for phosphatidylinositol transfer protein in phospholipase C-mediated inositol lipid signalling. *Cell* **74,** 919–928.
4. Kauffmann-Zeh, A., Thomas, G. M. H., Ball, A., et al. (1995) Requirement for phosphatidylinositol transfer protein in epidermal growth factor signalling. *Science* **268,** 1188–1190.
5. Allen, V., Swigart, P., Cheung, R., Cockcroft, S., and Katan, M. (1997) Regulation of inositol lipid-specific phospholipase Cδ by changes in $Ca^{2+}$ ion concentrations. *Biochem. J.* **327,** 545–552.
6. Cunningham, E., Tan, S. W., Swigart, P., Hsuan, J., Bankaitis, V., and Cockcroft, S. (1996) The yeast and mammalian isoforms of phosphatidylinositol transfer protein can all restore phospholipase C-mediated inositol lipid signalling in cytosol-depleted RBL-2H3 and HL60 cells. *Proc. Natl. Acad. Sci. USA* **93,** 6589–6593.
7. Skippen. A., Jones. D. H., Morgan, C. P., Li, M., and Cockcroft, S. Mechanism of ADP Ribosylation-Factor-stimulated phosphatidylinositol 4,5-bisphosphate synthesis in HL60 cells. *J. Biol. Chem.* **277,** 5823–5831.
8. Tatham, P. E. R. and Gomperts, B. D. (1990) Cell permeabilisation, in *Peptide Hormones—A Practical Approach* (Siddle, K. and Hutton, J. C., eds.), IRL, Oxford, England, pp. 257–269.
9 Bird, I. M. (1998) Phosphoinositidase C activation assay III, in *Methods in Molecular Biology, vol. 105: Phospholipid Signaling Protocols*, (Bird, I. M., ed.) Humana Press, Totowa, NJ, pp. 25–45.

# 12

# Measurement of Inositol(1,4,5)Trisphosphate Using a Stereospecific Radioreceptor Mass Assay

**Darren Smart**

## 1. Introduction

Inositol(1,4,5)trisphosphate [Ins(1,4,5)$P_3$] is an intracellular second messenger that plays an important role in calcium homeostasis and, thus, many diverse cellular processes including neuronal signaling, smooth muscle contraction, fertilization, and sensory perception ***(1)***. Ins(1,4,5)$P_3$ formation is triggered by the activation of a wide variety of seven-transmembrane, G protein-linked receptors, e.g., muscarinic, glutamate, dopamine, and opioid receptors ***(1–3)***, as well as by the activation of the tyrosine kinase-linked growth factor receptors ***(1)***. Ins(1,4,5)$P_3$ is produced by the phospholipase C (PLC)-mediated hydrolysis of phosphatidylinositol 4,5-bisphosphate ***(1,4)***, and is metabolized by 3-kinase and 5-phosphatase ***(5)***, with the actual intracellular concentration of Ins(1,4,5)$P_3$ being dependent on the balance between formation and metabolism. Ins(1,4,5)$P_3$ in turn binds to the Ins(1,4,5)$P_3$ receptor on the smooth endoplasmic reticulum, causing a conformational change that opens the intrinsic calcium channel in the receptor, thus allowing the efflux of calcium ions from the intracellular stores ***(4)***. For further details, see the reviews by Berridge ***(1)*** and Furuichi and Mikoshiba ***(4)***.

Historically, Ins(1,4,5,)$P_3$ was measured in terms of total inositol polyphosphate turnover in the presence of lithium in cells that had been "loaded" with [$^3$H]inositol ***(6,7)***. This technique was subsequently refined by using separation columns or high-pressure liquid chromatography to separate the various inositol polyphosphates and, even to some degree, their isomers ***(7–9)***. However, there are several significant disadvantages associated with these [$^3$H]inositol loading techniques. First, the main assumption of these techniques

From: *Methods in Molecular Biology, vol. 312: Calcium Signaling Protocols: Second Edition*
Edited by: D. G. Lambert © Humana Press Inc., Totowa, NJ

is that all pools of phosphoinositides are labeled to equilibrium under the assay conditions, yet there is very little experimental evidence for this ***(9)***. Second, it is almost inevitable that in [$^3$H]inositol-loaded cells, there would be some degree of agonist-induced changes in the specific radioactivity of the inositol trisphosphates ***(9)***. Third, these [$^3$H]inositol loading techniques do not take into account changes in the metabolism of Ins(1,4,5)$P_3$. For example, in rat acinar cells depolarization with $K^+$ stimulates polyphosphoinositide hydrolysis without affecting Ins(1,4,5)$P_3$ levels, because of a simultaneous enhancement of 3-kinase-mediated Ins(1,4,5)$P_3$ metabolism ***(10,11)***. Finally, the [$^3$H]inositol-loading techniques are less likely to detect small, transient changes in Ins(1,4,5)$P_3$ formation because they make only a minute contribution to total polyphosphate turnover, and this is masked by basal accumulation in the presence of lithium ***(2,3,11)***.

In 1988 a groundbreaking paper by Challiss et al. ***(9)*** was published that described a stereospecific radioreceptor assay for Ins(1,4,5)$P_3$ mass. This assay was superior to the [$^3$H]inositol-loading protocols because it made no assumptions about the establishment of equilibrium of label in various pools of polyphosphoinositides, nor was it susceptible to agonist-induced changes in specific radioactivity ***(9)***. Furthermore, subsequent studies have shown that the radioreceptor assay also takes into account changes in Ins(1,4,5)$P_3$ metabolism ***(10,11)***, and is able to detect small, transient changes in Ins(1,4,5)$P_3$ levels ***(2,3,11)***. This radioreceptor assay is based on the same simple principles as any other radioreceptor assay. The unlabeled Ins(1,4,5)$P_3$ in the sample competes with a fixed amount of [$^3$H]-labeled Ins(1,4,5)$P_3$ for a limited amount of a specific binding protein. The bound and free Ins(1,4,5)$P_3$ are separated by rapid vacuum filtration, and subsequent measurement of the radioactivity in the assay tube enables the amount of unlabeled Ins(1,4,5)$P_3$ in the sample to be determined by interpolation from a standard curve. The fundamental step in developing such an assay is the identification and purification of a suitable binding protein. Challiss et al. ***(9)*** used a relatively crude extract of the Ins(1,4,5)$P_3$ receptor prepared from bovine adrenal cortex. This was a suitable binding protein because the Ins(1,4,5)$P_3$ receptor displays the necessary high affinity and stereoselectivity for Ins(1,4,5)$P_3$, especially compared to Ins(1,3,4)$P_3$ ***(4,9)***, and it is both abundant in and easily extracted from bovine adrenal cortex ***(9)***. Rat cerebellum was also tested as a potential source of the binding protein, but was found to give smaller yields with lower affinity ***(9)***.

In the remainder of this chapter the author will describe how the binding protein is prepared, how the Ins(1,4,5)$P_3$ is extracted from the samples, how the radioreceptor assay is performed, and how the data are processed. Furthermore, the common pitfalls and how to avoid or deal with them will be described.

## 2. Materials

1. Ins(1,4,5)$P_3$ binding protein buffer (BP buffer): 20 m*M* $NaHCO_3$ and 1 m*M* dithiothreitol (DTT; *see* **Note 1**) in distilled water, pH 8.0 (*see* **Note 2**). Store at 4°C (*see* **Note 3**). Two L of this buffer is sufficient to prepare approx 100 mL of binding protein from 10 to 12 adrenal glands.
2. Ten to twelve fresh bovine adrenal glands (*see* **Note 4**).
3. 1 *M* trichloroacetic acid (TCA). This should be stored in a glass-stoppered bottle at 4°C for no longer than 3 mo.
4. 10 m*M* EDTA in distilled water, pH 7.4. This should be stored at 4°C for no longer than 3 mo.
5. Freon/Octylamine (F/O): 1:1 (v/v) mixture of 1,1,2-trichlorofluroethane (Freon) and tri-*n*-octylamine, both of which are available from Aldrich, Poole, UK (*see* **Note 5**).
6. 25 m*M* sodium bicarbonate ($NaHCO_3$) in distilled water. This should be stored at 4°C for no longer than 3 mo.
7. Stock Ins(1,4,5)$P_3$ standard: 1 m*M* D-*myo*-inositol-1,4,5-triphosphate hexasodium monohydrate (Research Biochemicals International, MA) in distilled water. Store in 20-µL aliquots at –20°C (*see* **Note 6**).
8. Stock [$^3$H]Ins(1,4,5)$P_3$: This is obtained from Amersham (Braunschweig, Germany) at 10 µCi/mL. Store at –20°C for no longer than 4 wk past the activity date.
9. Tris-EDTA (TE) buffer: 100 m*M* Tris-HCl and 4 m*M* EDTA in distilled water at pH 8.0. Store at 4°C; keeps virtually indefinitely.
10. Diluent: Mix 3 mL of Krebs/HEPES buffer (*see* **Note 7**), 3 mL of TCA, 1.25 mL of EDTA, and 3 mL of F/O. Vortex well and then centrifuge at 500*g* for 2 min at 4°C. This mixture will now have separated into two distinct phases (layers). Take 5 mL of the upper phase and neutralize with 2.5 mL of $NaHCO_3$. The remainder of the upper phase as well as the lower phase should be discarded. The diluent should be made fresh on the day of use and then kept at 4°C.
11. Wash buffer: 25 m*M* Tris-HCl, 1 m*M* EDTA, 5 m*M* $NaHCO_3$ in distilled water, pH 7.8. This *must* be made fresh on the day of use and kept at 4°C. Two L is sufficient for a 72-tube assay.
12. A Brandell cell harvester and Whatman GF/B filters (Fisons, Loughborough, UK).

## 3. Methods

### 3.1. Preparation of the Ins(1,4,5)$P_3$ Binding Protein

1. Take the adrenal glands, halve longitudinally, remove the medulla (*see* **Note 8**), and then scrape the cortex from the capsule (*see* **Note 9**).
2. Pool the cortex tissue in a 500-mL glass beaker, dilute 1 in 6 with ice-cold BP buffer, and homogenize thoroughly, taking care that there are no lumps of cortex left intact.
3. Centrifuge the homogenate at 2000*g* for 10 min at 4°C (*see* **Note 10**).
4. Carefully decant (*see* **Note 11**) and keep the supernatant. Store the supernatant at 4°C.

5. Rehomogenize the pellet in a minimum volume of BP buffer (*see* **Note 12**) and then centrifuge at 2000*g* for 10 min at 4°C. Decant (*see* **Note 11**) the supernatant and pool it with the supernatant from **step 4**. Discard the pellet.
6. Centrifuge the pooled supernatant at 20,000*g* for 30 min at 4°C (*see* **Note 13**). A soft pellet will form at the bottom of the tube.
7. Carefully decant (*see* **Note 11**) the supernatant into fresh centrifugation tubes and store the pellet at 4°C. Recentrifuge the supernatant at 20,000*g* for 30 min at 4°C (*see* **Note 13**). A smaller soft pellet will form at the bottom of the tube.
8. Repeat **step 7**.
9. Pool all the pellets and resuspend in BP buffer at ~30 mg/mL (*see* **Note 14**).
10. Then dispense the binding protein into 1-mL aliquots and store at –20°C until needed (*see* **Note 15**).

### 3.2. Sample Preparation

1. Incubate the relevant cells with the appropriate agonist for the required time (e.g., *see* **ref. *3***), in a final volume of 0.3 mL in polypropylene tubes (12 × 75 mm; Sarstedt, UK). Terminate reactions by the addition of an equal volume (0.3 mL) of ice-cold 1 *M* TCA (*see* **Note 16**).
2. Next vortex the samples and centrifuge at 500*g* for 10 min at 4°C.
3. Carefully decant the uppermost 500 µL of the supernatant (*see* **Note 17**) into fresh polypropylene tubes. Discard the remaining supernatant and "pellet."
4. Add 125 µL of EDTA and 500 µL of F/O to the supernatant, cap the tubes, vortex, and then centrifuge at 500*g* for 2 min at 4°C. At the end of this process, the samples will have separated into two clearly delineated phases (layers).
5. Take 200 µL of the upper phase, which contains the Ins(1,4,5)$P_3$, and place into fresh tubes. Neutralize this with 100 µL of 25 m*M* $NaHCO_3$, cap, and vortex the tubes. Discard the remaining upper, as well as the lower, phase. The samples should be stored at 4°C for no longer than 1 wk, and must not be frozen.

### 3.3. Radioreceptor Ins(1,4,5)$P_3$ Mass Assay

1. It is essential that the entire assay is carried out on ice. At the start of the assay, make up fresh wash buffer (*see* **Subheading 2.**, **item 11**) and place in a refrigerator to cool.
2. Label the appropriate number of polypropylene tubes (12 × 75 mm; Sarstedt), i.e., the relevant number of samples (single or in duplicate) and the standard curve, consisting of total counts (TOT), nonspecific binding (NSB), and six standards (std. 0.036, 0.12, 0.36, 1.2, 3.6, and 12 pmol tube) in duplicate. These labeled tubes should be placed in a Brandell harvester rack on ice at the start of the assay.
3. Thaw out the correct amount (1 mL/30 tubes) of binding protein (*see* **Note 18**).
4. Make up fresh diluent (*see* **Subheading 2.**, **item 10**) and store on ice.
5. Dilute the stock Ins(1,4,5)$P_3$ standard with diluent in the following manner (*see* **Note 19**):
   a. NSB: 20 µL of stock + 480 µL of diluent.
   b. 12 pmol std: 10 µL of NSB + 990 µL of diluent.

c. 3.6 pmol std: 100 µL of 12 pmol std. + 200 µL of diluent.
d. 1.2 pmol std: 20 µL of 12 pmol std. + 180 µL of diluent.
e. 0.36 pmol std: 20 µL of 3.6 pmol std. + 180 µL of diluent.
f. 0.12 pmol std: 20 µL of 1.2 pmol std. + 180 µL of diluent.
g. 0.036 pmol std: 20 µL of 0.36 pmol std. + 180 µL of diluent.
These standards should be stored on ice until pipetted into the relevant tubes, as described in **step 9**.

6. Prepare the working concentration of the tracer {[$^3$H]Ins(1,4,5)$P_3$} by adding stock [$^3$H]Ins(1,4,5)$P_3$ to TE buffer at 15 µL/mL (*see* **Note 20**). Allow 1 mL of tracer/30 tubes. Store on ice until used.
7. Pipet 30 µL of TE buffer into each of the labeled tubes in the Brandell harvester rack (*see* **Note 21**).
8. Pipet 30 µL of diluent into the two TOT tubes (*see* **Note 21**).
9. Pipet 30 µL of standard/sample into the appropriate tubes (*see* **Notes 21** and **22**).
10. Pipet 30 µL of the working concentration of [$^3$H]Ins(1,4,5)$P_3$ into each tube (*see* **Notes 21** and **23**).
11. Gently vortex all the tubes for a few seconds (*see* **Note 24**).
12. Pipet 30 µL of the binding protein into each tube (*see* **Note 25**).
13. Gently vortex all the tubes for a few seconds, and allow to incubate on ice for 40 min (*see* **Note 26**). At this point the total assay volume is 120 µL.
14. Filter on a Brandell cell harvester (Whatman GF/B filters) with the ice-cold wash buffer (*see* **Note 27**), to separate the bound and free [$^3$H]Ins(1,4,5)$P_3$. Each tube should receive two washes of approx 3 mL, each in quick succession (*see* **Note 28**). The bound material will be clearly visible as a brown deposit on the filter (*see* **Note 29**).
15. The filters should be extracted overnight in a suitable scintillant, e.g., Optiphase Safe (Wallac, UK), and then counted in a β-counter for 3 min per tube.

### *3.4. Data Processing* (see **Note 30**)

1. Calculate the average cpm for each standard, and sample if assayed in duplicate (*see* **Note 31**).
2. Calculate the percent bound for each standard and sample as follows:

$$\% \text{ Bound} = \frac{(\text{Standard/sample dpm} - \text{NSB dpm}) \times 100}{\text{TOT dpm} - \text{NSB dpm}}$$

3. The percent bound for the standards can then be plotted [against the relevant concentration of Ins(1,4,5)$P_3$] to generate a standard curve, using a suitable curve-fitting program (i.e., GraphPad Prism, CA) or by hand on semi-log graph paper. Then, using the relevant percent bound values, the concentrations of Ins(1,4,5)$P_3$ in the samples can be "read off" this curve.

## 4. Notes

1. DTT is harmful and should therefore be handled with all due care. However, its inclusion is essential or the binding protein will rapidly become degraded.
2. Although ideally this buffer should be at pH 8.0, any pH in the range 7.9–8.1 is acceptable.

3. This buffer should be prepared on the day of use, but can be used on the following day if stored at 4°C. Do not store for longer than 24 h prior to use.
4. These are obtained from an abattoir and can come from cattle of any age or either sex. Most abattoirs will allow direct dissection of the adrenal gland, and many will cut out the glands for a small fee. However, it should be borne in mind that the vast majority of abattoir workers do not know what the adrenal gland looks like or where it is located and, therefore, are likely to provide the wrong material. It is preferable to collect intact glands, but "bits" of gland, when the gland has been damaged during the butchery of the cattle, can still be used. The glands must be "fresh," i.e., collected as soon as possible after the cattle have been slaughtered, and must not be frozen. It is best to minimize the delay between the removal of the glands and the preparation of the binding protein, but if this delay is likely to exceed 2 h, the glands (wrapped in a plastic bag) need to be transported on ice.
5. Care should be taken when handling these chemicals and their mixture, as they are potent irritants. The F/O mixture should be made up just prior to use and, being somewhat unstable, cannot be stored for more than a couple of hours. Furthermore, exposure to the F/O mixture does cause some plastics to become extremely brittle, hence the reason that sample preparation and the assay are conducted in polypropylene tubes.
6. The stock Ins(1,4,5)$P_3$ standard must not be thawed and then refrozen, as this causes significant breakdown of the standard, leading to high NSB values and a poor quality standard curve. The stock standard still degenerates slowly even when frozen and thus should be discarded after 2 mo.
7. Or, whatever physiological buffer the cell incubations were performed in can be used.
8. The medulla is the "off white" material in the center of the adrenal gland, and is best removed by pulling it gently upward with a pair of forceps while cutting it away from the underlying cortex using a pair of fine-dissecting scissors. It is essential to remove as much of the medulla as possible, to minimize NSB.
9. The cortex is the reddish-brown material that surrounds the medulla, and is easily scrapped from the semitransparent, tough outer membrane or capsule, using a small metal spatula.
10. It is essential from this moment on that the crude binding protein is kept at 4°C. If all the material in a given step cannot be handled at once, then store any excess on ice or in the refrigerator, until the material can be dealt with.
11. This is best done using a long, fine-pointed, disposable glass pipet, and care must be taken not to suck up any of the pellet. If any of the pellet is decanted, then the pipet and its contents should be discarded, rather than risk contaminating the rest of the supernatant.
12. If there is still material from **step 2** waiting to be rehomogenized, then use this, rather than the BP buffer, to resuspend the pellet. However, note that if this is done then the subsequent pellet will still need to undergo **step 5**, as part of this pellet has not been washed twice.
13. Alternatively, centrifuge at 40,000*g* for 20 min at 4°C.

14. The protein content of the combined pellets resuspended in a minimum volume of BP buffer should be measured using a suitable assay (e.g., Follins-Lowry) prior to the full resuspension. In general, 10–12 adrenal glands should yield ~80 mL of binding protein.
15. The binding protein can be thawed and refrozen once, but repeated freeze/thaw cycles should be avoided. The binding protein will keep for approx 6 mo at –20°C, although it should be noted that the binding protein will gradually degrade over this period, causing the total binding to fall and the NSB values to rise.
16. Once the TCA has been added, the sample can be stored at 4°C for up to 1 h prior to undergoing the rest of the extraction procedure. This allows "batching" of the samples and thus more effective time management.
17. If using a Gilson pipet to decant the supernatant, it is advisable to first remove the waste tip dispeller.
18. Allow the binding protein to thaw slowly. Do not heat the frozen binding protein in a water bath or by other means, as this causes considerable degradation of the binding protein, leading to high NSB values.
19. The standards and NSB are made at these concentrations to obtain the correct final concentrations in the assay, in which there is a 1 in 4 dilution factor.
20. The appropriate procedures for handling radioactivity should be used at all times. The dilution of 15 µL of stock/mL of TE buffer is based on the assumption that the specific activity of the stock [$^3$H]Ins(1,4,5)$P_3$ is approx 40 Ci/mmol. If the specific activity is significantly higher, add proportionally less stock/mL; if the specific activity is significantly lower, then add proportionally more stock/mL.
21. Remember to do all pipetting into the tubes while the tubes are still on ice. Furthermore, care must be taken when pipetting as the volumes involved are very small. The most common problem is drops of the assay components sticking to the sides of the tube. These can be brought down by gently tapping the base of the tube, or by using a fine disposable pipet to blow the drops down.
22. NSB tubes receive 30 µL of the NSB "standard" made in **step 5** of **Subheading 3.3.**
23. All due care should be maintained when pipetting radioactive material.
24. This step is essential for obtaining a smooth standard curve (*see* **Note 31**). If there are any drops on the sides of the tubes, then these must be brought down prior to vortexing (*see* **Note 21**).
25. Particular care must be taken when pipetting out the binding protein. The aliquot of binding protein being used must be vortexed frequently (approximately every minute), to keep the binding protein uniform. Furthermore, as the binding protein is very viscose, it is particularly prone to sticking to the sides of the assay tubes (*see* **Note 21**).
26. Timing of this step is crucial. If the incubation is too short, equilibrium will not have been achieved and there will be a far greater degree of intra-assay variability. On the other hand, if the incubation is too long, there is a tendency toward increased NSB values. Forty minutes is optimal, but anywhere between 38 and 50 min is acceptable.

**Table 1**
**Common Assay Problems and Their Causes**

| Problem | Possible cause |
|---|---|
| High NSB (>10%) | • The stock [$^3$H]Ins(1,4,5)$P_3$ may have degraded. This is usually associated with a low TOT cpm.<br>• The stock standard may have degraded. This is usually associated with a distorted standard curve.<br>• Binding protein may have degraded. This is usually associated with all tubes having low cpm. |
| All tubes have low cpm | • The binding protein has degraded (associated with high NSB) or is too dilute (*see* **Note 29**).<br>• The tracer is too dilute (*see* **Note 20**) or has degraded (usually associated with high NSB) |
| Standard curve is distorted | • Stock standard has degraded (associated with high NSB) or has been diluted incorrectly.<br>• **Step 11** of **Subheading 3.3.** has not been performed. |
| Standards have low cpm, but samples are normal | • Standards were incorrectly diluted, or have degraded (associated with high NSB). |
| TOT > 2500 dpm | • This is often associated with a shallow standard curve.<br>• Tracer has been incorrectly diluted (*see* **Note 20**). |

27. It is advisable to wash the first filter with the wash buffer prior to harvesting the samples. Care must be taken to ensure that the filters are fitted properly to avoid leaking.
28. Do not overfill (more than 3/4) the tubes, or there will be a risk of overflow and the associated loss of material. Be aware that not all tubes will fill at the same rate.
29. If the deposit is somewhat "faded" (i.e., sandy rather than brown) in color, this indicates that the binding protein is not concentrated enough. This is inevitably associated with low total counts (*see* **Note 31**). If this occurs, concentrate the remaining binding protein prior to its use by centrifuging the thawed binding protein at 5000*g* for 15 min at 4°C and then pipetting off 250 µL of the "clear" supernatant. Vortex vigorously to resuspend the binding protein.
30. Most modern counters have packages on them that will automatically plot the standard curve and calculate the sample values.
31. Ideally TOT should lie in the range of 1000–2500 dpm and the NSB should be 5–10%. This is the stage at which most assay problems will become apparent. **Table 1** describes the most common problems and their usual causes. However, it should be borne in mind that other factors will also affect assay performance, most notably temperature and pH. Therefore, at all times it is essential to ensure that the assay is performed on ice, that dilutions are made correctly, and that all the buffers are at the optimal pH.

## References


1. Berridge, M. J. (1993) Inositol trisphosphate and calcium signalling. *Nature* **361,** 315–325.
2. Smart, D., Smith, G., and Lambert, D. G. (1994) Halothane and isoflurane enhance basal and carbachol-stimulated inositol(1,4,5)triphosphate formation in SH-SY5Y human neuroblastoma cells. *Biochem. Pharmacol.* **47,** 939–945.
3. Smart, D., Smith, G., and Lambert, D. G. (1994) μ-Opioid receptor stimulation of inositol(1,4,5)trisphosphate formation via a pertussis toxin-sensitive G protein. *J. Neurochem.* **62,** 1009–1014.
4. Furuichi, T. and Mikoshiba, K. (1995) Inositol 1,4,5-trisphosphate receptor-mediated $Ca^{2+}$ signaling in the brain. *J. Neurochem.* **64,** 953–960.
5. Shears, S. B. (1989) Metabolism of the inositol phosphates upon receptor activation. *Biochem. J.* **260,** 313–324.
6. Kendall, D. A. and Nahorski, S. R. (1984) Inositol phospholipid hydrolysis in rat cerebral cortical slices: II. Calcium requirement. *J. Neurochem.* **42,** 1388–1394.
7. Wojcikiewicz, R. J. H., Lambert, D. G., and Nahorski, S. R. (1990) Regulation of muscarinic agonist-induced activation of phosphoinositidase C in electrically permeabilized SH-SY5Y human neuroblastoma cells by guanine nucleotides. *J. Neurochem.* **54,** 676–685.
8. Yu, V. C. and Sadee, W. (1986) Phosphatidylinositol turnover in neuroblastoma cells: Regulation by bradykinin, acetylcholine, but not μ and δ opioid receptors. *Neurosci. Lett.* **71,** 219–223.
9. Challiss, R. A. J., Batty, I. H., and Nahorski, S. R. (1988) Mass measurements of inositol(1,4,5)trisphosphate in rat cerebral cortex slices using a radioreceptor assay: Effects of neurotransmitters and depolarization. *Biochem. Biophys. Res. Commun.* **157,** 684–691.
10. Zhang, G. H. and Melvin, J. E. (1993) Membrane potential regulates $Ca^{2+}$ uptake and inositol phosphate generation in rat sublingual mucous acini. *Cell Calcium* **14,** 551–562.
11. Smart, D., Wandless, A., and Lambert, D. G. (1995) Activation of phospholipase C in SH-SY5Y neuroblastoma cells by potassium-induced calcium entry. *Br. J. Pharmacol.* **116,** 1797–1800.

# 13

## Measurement of Calcium Fluxes in Permeabilized Cells Using a $^{45}Ca^{2+}$ Uptake and Release Assay

**Robert A. Wilcox**

### 1. Introduction

Many cell surface receptors activate phosphoinositidase(s) C, via G proteins that catalyze the hydrolysis of phosphatidylinositol 4,5-biphosphate to produce the second messengers, inositol(1,4,5)trisphosphate [Ins(1,4,5)$P_3$] and diacylglycerol ***(1)***. Ins(1,4,5)$P_3$ interacts with specific receptor populations of ligand-gated channels to mobilize nonmitochondrial intracellular calcium ($Ca^{2+}$) stores ***(1)***. Because Ins(1,4,5)$P_3$ is very hydrophilic, it cannot readily cross the intact plasma membrane. Consequently, Ins(1,4,5)$P_3$-induced $Ca^{2+}$ release was initially demonstrated in permeabilized pancreatic acinar cells ***(2)***, and all subsequent studies in cells have involved the introduction of Ins(1,4,5)$P_3$ by rendering a cell population permeable ***(3)***, using microinjection techniques ***(4)*** or by the presentation of chemically modified membrane-permeable Ins(1,4,5)$P_3$ analogs, such as photolabile "caged Ins(1,4,5)$P_3$" ***(5)***. An alternative approach involves disruption of the plasma membrane and preparation of microsomes from the intracellular vesicular $Ca^{2+}$ stores ***(6,7)***, however, these preparations exhibit a loss of Ins(1,4,5)$P_3$ responsiveness compared to cells. The author will describe a $^{45}Ca^{2+}$-release assay used to monitor Ins(1,4,5)$P_3$-induced $Ca^{2+}$ mobilization from nonmitochondrial intracellular $Ca^{2+}$ stores using "cytosol-like" buffer (CLB) and permeabilized SH-SY5Y neuroblastoma cell populations.

The $^{45}Ca^{2+}$-release assay is similar to those previously described ***(3,8)*** and involves preloading $^{45}Ca^{2+}$ into the intracellular $Ca^{2+}$ stores of permeabilized cells and then monitoring the resultant release of $^{45}Ca^{2+}$ induced by concentrations of Ins(1,4,5)$P_3$ and other agonists. The author has utilized this assay to assess

From: *Methods in Molecular Biology, vol. 312: Calcium Signaling Protocols: Second Edition*
Edited by: D. G. Lambert © Humana Press Inc., Totowa, NJ

the intrinsic activity of Ins(1,4,5)$P_3$, a wide range of Ins(1,4,5)$P_3$ analogs, and other $Ca^{2+}$-mobilizing agents. The assay can be undertaken at a low cell density to minimize cellular metabolism of the Ins(1,4,5)$P_3$ and other $Ca^{2+}$-mobilizing inositol polyphosphates (CM-IPs), or at high cell density to allow the metabolic sensitivity of the CM-IP to be estimated.

The method described here for monitoring $Ca^{2+}$ fluxes induced by CM-IPs in permeabilized SH-SY5Y cells can be readily modified for other cell types and for testing a wide range of different $Ca^{2+}$-mobilizing agents.

## 2. Materials

1. Ultrapure $H_2O$ derived from a specialist unit (Elgastat, High Wycomb, Bucks, UK, or Millipore, Watford, Herts, UK) (*see* **Note 1**).
2. Fura-2-free acid (Calbiochem-Novabiochem, Nottingham, Notts, UK; Molecular Probes, Eugene, OR) was prepared as a 1-m*M* stock solution.
3. $^{45}CaCl_2$ solution, 77 mBq/mL (CES3, Amersham, Amersham, Bucks, UK).
4. 200 m*M* $CaCl_2$.
5. 200 m*M* EGTA/400 m*M* KOH solution (*see* **Note 2**).
6. HEPES-buffered saline (HBS)/EDTA solution: 0.02% (w/v) $Na_2EDTA$, 0.9% (w/v) NaCl, and 20 m*M* HEPES-free acid, corrected to pH 7.2–7.4 using 20% (w/v) NaOH.
7. Adenosine 5'-triphosphate disodium salt ($Na_2 \cdot ATP$; grade 1, Sigma A-2383, Poole, Dorset, UK).
8. CLB stock should be prepared as a fivefold stock solution in ultrapure $H_2O$, to yield final concentrations of 120 m*M* KCl, 2 m*M* $KH_2PO_4$, 5 m*M* $(CH_2COONa)_2 \cdot 6H_2O$, 2 m*M* $MgCl_2 \cdot 6H_2O$, and 20 m*M* HEPES-free acid. Since the ATP required is relatively unstable in alkaline solutions, the working CLB solution should be prepared just prior to use.
9. EGTA (10 m*M*/20 m*M* KOH).
10. Saponin or β-escin (Sigma) 1 mg/mL solution prepared fresh in working stock CLB.
11. Ionomycin from *Streptomyces conglobatus*; calcium salt (Sigma I-0634, formula wt 747.1) or free acid (Calbiochem-Novabiochem) and antibiotic A23187 (Calbiochem-Novabiochem) are prepared as 2 m*M* (*see* **Note 3**).
12. Silicon oil mixture for separation of the aqueous phase and cell pellet: Dow Corning (British Drug House [BDH], Toronto, Ontario, Canada) silicone fluids 556 (0.98 g/mL; 60%) and 550 (1.07 g/mL; 40%) shaken thoroughly (*see* **Note 4**).
13. 0.4% Azur A (Fluka, Buchs, Switzerland) stock in ATP-free CLB, pH 7.2.
14. Oligomycin (Sigma) 5 mg/mL solution made up in EtOH (*see* **Note 5**).
15. Ins(1,4,5)$P_3$ (CellSignals, Lexington, Semat Technical St. Albans, Herts, UK [UK agents for Research Biochemicals]) 1–2 m*M* 20-µL stock solution (*see* **Note 6**).
16. Lumasolve (Lumac, Landgraaf, The Netherlands) and Emulsifier-safe scintillation cocktail (Packard, Meriden, CT).

17. Fluorescence spectrophotometer (fluorimeter) with variable excitation and emission optics, ideally with a chart recorder or computer interface for fura-2 experiments (*see* **Note 7**).
18. Benchtop microcentrifuge, with a capacity for 24 standard 1.5-mL microcentrifuge tubes (Heraeus, Dusseldorf, Germany, and Desaga, Sarstedt-Gruppe, Wiesloch, Germany).
19. Electroporator (Gene-Pulser, Bio-Rad, Hemel Hampstead, Herts, UK).
20. IBM Pentium PC or compatible with Prism version 2.01 (Graph-Pad Software, San Diego, CA) for computer-assisted curve-fitting calculations (*see* **Note 8**).

## 3. Methods

### 3.1. Preparation of CLB Working Solution and Buffering of $Ca^{2+}$

1. Add the fivefold CLB stock (1 vol) to a container with preweighed $Na_2 \cdot ATP$ (2 m*M* final) and dilute this to 5 vol with $H_2O$ and the correct pH (~5.3) 7.2 using 20% (w/v) KOH and 1 m*M* of HCl.
2. Buffer the contaminating-free $Ca^{2+}$ ($[Ca^{2+}]_{free}$) to a final concentration of between 60 and 120 n*M*, by addition of an appropriate aliquot of EGTA (10 m*M*/20 m*M* KOH) (*see* **Note 9**).
3. Confirm the $[Ca^{2+}]_{free}$ of the CLB using a tracer concentration of fura-2 (100 n*M*). Briefly place a sample of EGTA-buffered CLB (2 mL) in a fluorimeter cuvet with 4 µL of 50 µ*M* fura-2. Determine the fluorescent intensity ($F_{CLB}$) of the buffer at excitation and emission wavelengths of 340 and 510 nm, respectively. Recording the resultant *F* values, add 2 µL of the 200 m*M* $CaCl_2$ solution (200 µ*M* final; $F_{max}$ value), followed by 40 µL of 200 m*M* EGTA (2 m*M* final; $F_{min}$ value), and then calculate $[Ca^{2+}]$ from the Grynkiewicz equation ***(9)*** in which the $K_d$ for fura-2 is approx 139 n*M* at 25°C and 224 n*M* at 37°C (*see* **Note 10**):

$$[Ca^{2+}]_{free}\ (nM) = (F_{CLB} - F_{min}/F_{max} - F_{CLB}) \times K_d$$

### 3.2. Permeabilization of Cells

1. Electropermeabilization ***(10)*** or the cholesterol-specific detergents saponin ***(3)*** and β-escin ***(11)*** are routinely utilized to produce $Ins(1,4,5)P_3$-responsive permeabilized cells. Both of these methods require empirical determination of optimal conditions for each cell type used. The DNA dye Azur A (0.025% [w/v] CLB) can be used to quantify permeabilization, since it is excluded from intact cells but specifically stains the nucleus of permeabilized cells blue. When permeabilized with 20–100 µg/mL of saponin or β-escin or via optimized electropermeabilization, >99% Azur A-stained SH-SY5Y neuroblastoma cells are obtained.
2. Electropermeabilization is rapid and efficiently generates plasma membrane pores, which allow free passage of inositol polyphosphates. Electropermeabilization of SH-SY5Y cells in 0.8 mL volume is accomplished in a Gene-Pulser using 3–12 discharges of a 3-µF capacitor with a field strength of 1.5 kV/cm and a time constant of 0.1 ms (*see* **Note 11**).

### 3.3. $^{45}Ca^{2+}$-Release Assay

1. Produce an inositol polyphosphate dilution series in CLB that is twofold the final required concentration (*see* **Note 12**).
2. Use ionomycin (10 µ*M* final, free acid or calcium salt) and Ins(1,4,5)$P_3$ (20–30 µ*M*) prepared as twofold stocks in CLB as internal controls to define, respectively, the total mobilizable and Ins (1,4,5)$P_3$-sensitive cellular $Ca^{2+}$ pools in permeabilized SH-SY5Y cells.
3. All agents were added as duplicate 50 µL-aliquots to decapped 1.5-mL microcentrifuge tubes, and two duplicate blanks (CLB alone) defined the baseline calcium release (*see* **Note 13**).
4. Wash a postconfluent SH-SY5Y monolayer (175-$cm^2$ flask) once and then harvest using the HBS/EDTA solution (*see* **Note 14**).
5. Resuspend and centrifuge to wash the cell suspension twice in 5 mL of CLB (500*g*, 1 min).
6. Discard the supernatant and add 1.8 mL of CLB to resuspend the cells. Add 200 µL of saponin stock solution (1 mg/mL, ~100 µg/mL final) to the cells, mix gently and leave for 40–60 s, and then centrifuge (500*g*, 2 min).
7. Resuspend the pellet in approx 5 to 6 mL of CLB; for SH-SY5Y cells, this corresponds to a cell density of approx 2–4 × $10^6$ cells/mL, 0.5–0.8 mg/mL protein ***(12)***, or a cellular DNA content of 100–200 µg/mL ***(18)***.
8. Add 1 µL of oligomycin and 1 µL of $^{45}Ca^{2+}$ per 2 mL of permeabilized cells.
9. Quickly and gently vortex the cells and $^{45}Ca^{2+}$ and leave for 15–20 min at 18–20°C, with periodic vortexing (*see* **Note 15**).
10. Using a repeating pipet (Eppendorf-Netleter-Hinz GmbH, Hamburg, Germany), titurate the cell suspension, and then add 50 µL of the cell suspension to 50 µL of the agonist in the decapped 1.5-mL microcentrifuge tubes.
11. Immediately add 300–400 µL of silicon oil mixture, and after 30–90 s, load the tubes into a microcentrifuge and centrifuge the cells through the oil (16,000*g*, 3 min) (*see* **Note 16**).
12. Remove the aqueous phase and most of the silicon oil, but avoid disturbing the cell pellet or "smear" on the opposite side of the tube.
13. Invert the tubes on paper underlayered with foil for 30 min to remove the oil.
14. Add 1 mL of scintillant, and when the pellets are solubilized, vortex the tube and count the retained $^{45}Ca^{2+}$ (*see* **Note 17**).
15. Calculate the percentage release of $^{45}Ca^{2+}$ using the average value of the four CLB blanks, these define the zero $^{45}Ca^{2+}$ release value (or 100% loaded $^{45}Ca^{2+}$ retained in the pellet) (*see* **Note 18**).

### 3.4. Optimizing the $^{45}Ca^{2+}$-Release Assay for Different Cell Lines

$^{45}Ca^{2+}$ assays have been successfully performed using many adherent and nonadherent cell lines, such as L15, L vec, Rat-1, Swiss 3T3 and NIH-3T3 mouse fibroblasts, J774.2 mouse macrophages cell, SaOS-2 human osteoblasts, Yac-1 mouse cells, 1321N1 human astrocytomas, and also primary cultured

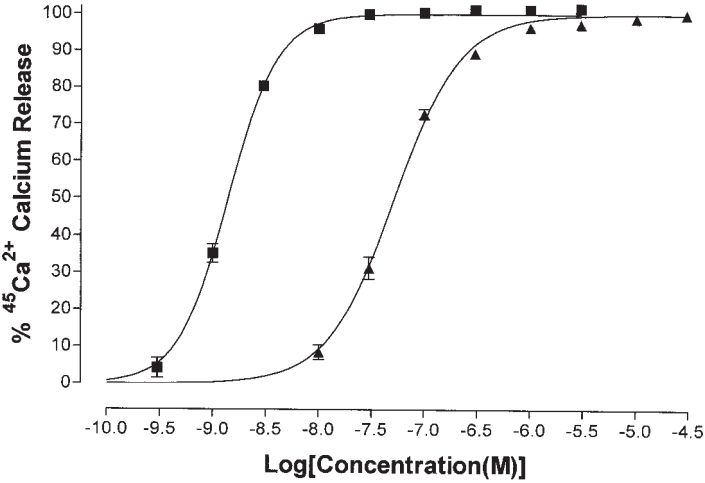


Fig. 1. The percentage $^{45}Ca^{2+}$ released at 20–22°C from the Ins(1,4,5)$P_3$-sensitive intracellular stores of saponin-permeabilized SH-SY5Y cells ($n \geq 4$) by $IP_3$ (▲), and adenophostin A (Ada) (■). AdA is a highly potent metabolically resistant Ins(1,4,5)$P_3$ receptor agonist ***(19)***. It released $^{45}Ca^{2+}$ from SH-SY5Y cells with a $\log_{10}[EC_{50}\ (M)]$ of $-8.857 \pm 0.021$ ($EC_{50} = 1.4$ n*M*) and thus was ~40-fold more potent than Ins(1,4,5)$P_3$ {$\log_{10}[EC_{50}\ (M)] = -7.288 \pm 0.019$ ($EC_{50} = 52.1$ n*M*)}. (Ada was a gift from Prof. Van Boom's laboratory, Leiden, The Netherlands.)

bovine adrenal chromaffin cells. However, it is crucial that the conditions used for each cell type be optimized empirically:

1. Use Azur A staining; confirm that >95% of cells are effectively permeabilized and choose the minimal insult to the cells that effectively produces permeabilization.
2. Select an appropriate cell density, in which $^{45}Ca^{2+}$ release is readily detected, but in which cellular metabolism of inositol polyphosphate is minimal over 2 to 3 min (*see* **Note 19**).
3. Produce a time course for $^{45}Ca^{2+}$ loading and identify the plateau at which an equilibrium loading state is obtained and maintained; for most cells this occurs between 10 and 40 min.

## 4. Notes

1. The most critical consideration is the reduction of $Ca^{2+}$ contamination during the preparation of all solutions, especially CLB. Reagents used must be the highest purity available, especially divalent metal salts such as $MgCl_2 \cdot 6H_2O$. Ultrapure water is essential and all solutions must be prepared and stored in plastic containers—never glass, which leaches significant quantities of metal cations.
2. The solution may require sonication for solubilization.

3. Store as 10-μL stock aliquots in ethanol or dry dimethyl sulfoxide.
4. The efficiency of the silicon oil mix is batch dependent and must be empirically tested as alternative mixing ratios can be more effective. Alternatively, if the cells are pelleted first, then a 1/1 (v/v) mixture will effectively separate the pellet and aqueous phase during the second spin.
5. This acts to exclude $Ca^{2+}$ uptake into the mitochondrial pool. However, the addition of oligomycin is not critical since at $[Ca^{2+}] < 1$ μ*M*, mitochondrial $Ca^{2+}$ uptake (Km ~10 μ*M*) is minimal ***(14)***.
6. Stock solutions of stimulating agonists such as inositol polyphosphates must be checked for calcium contamination, since $Ca^{2+}$ levels exceeding 200–400 n*M* can inhibit $IP_3$-induced $Ca^{2+}$ release ***(15–17)***. Stock solutions can be readily pretreated to remove $Ca^{2+}$ contamination with solid phase $Ca^{2+}$ chelating agents such as chelex-100 (Bio-Rad) or immobilized-BAPTA–based "$Ca^{2+}$-sponges" (Molecular Probes). The author has treated a wide range of inositol polyphosphates with these chelators and have detected no loss owing to adsorption.
7. The author utilizes the model LS5β and LS50β fluorimeters (Perkin Elmer, UK).
8. Prism is an excellent and easy to use program, but many similar curve-fitting programs are also available.
9. Usually 10–20 μL/100 mL of CLB (1 to 2 μ*M* EGTA final) is sufficient.
10. Ideally the $[Ca^{2+}]_{free}$ should be 60–120 n*M*, certainly <200 n*M*, to avoid significant mitochondrial uptake ***(14)*** and $Ca^{2+}$ inhibition of $Ins(1,4,5)P_3$ receptor responses ***(15–17)***. If it exceeds this, then add more 10-m*M* EGTA stock to the CLB, mix well, take a fresh 2-mL sample, and repeat the procedure. Once determined, the $[Ca^{2+}]_{free}$ value should remain relatively stable for a given batch of fivefold CLB stock, and a stable supply of high-purity water.
11. However, under some conditions the process can generate significant concentrations of aluminium ions ($Al^{3+}$) from the disposable cuvets used, and this may affect cellular metabolism of inositol polyphosphates ***(18)***. Consequently, the author has favored saponin and β-escin permeabilization, which generate large plasma membrane pores and offer the flexibility of initiating an experiment with the permeabilization event.
12. For example, $Ins(1,4,5)P_3$ concentrations of 30, 10, 3, 1, 0.3, 0.1, 0.03, and 0.01 μ*M* fully cover the $Ca^{2+}$-release dose response range in most cell types the author has tested.
13. Thus, a typical experiment consisted of 22 to 24 tubes; these were stored on ice and then allowed to come to room temperature for 15 min prior to addition of the permeabilized cells.
14. Cell clumping occurs particularly with fibroblasts and can cause reduced precision; gently titurating the cells two to three times through a 19 G needle generally produces a single cell suspension. Alternatively, trypsinized cells can be used in the assay following deactivation of the trypsin via centrifugation through underlayered fetal calf serum.
15. In SH-SY5Y cells, $^{45}Ca^{2+}$ loading into intracellular $Ca^{2+}$ stores proceeds rapidly and reached equilibrium within 10 min.

16. Alternatively the cells can be pelleted after 1–15 s (16,000*g*, 2 min). The silicon oil is then added and a second centrifugation performed (16,000*g*, 1 min). This procedure was not ideal for time course studies; however, once optimal stimulation times are determined, this procedure yields identical data and the solid and reproducible pellets produce more consistent data values.
17. Large cell pellets may require solubilization in 100 µL of Lumasolve, prior to the addition of scintillation cocktail.
18. Typically in most cells ionomycin (10 µ*M*) mobilizes 90% of the total loaded $^{45}Ca^{2+}$, whereas in SH-SY5Y cells a maximal dose of Ins(1,4,5)$P_3$ mobilizes 70% of the total loaded $^{45}Ca^{2+}$.
19. For SH-SY5Y cells, the author selected a cell density in which 30–50% of the $^{45}Ca^{2+}$ spike (~2 to 3 µ*M*) is incorporated into the intracellular stores. Utilizing fura-2, it was confirmed that the ~2.4 µ*M* of $^{45}Ca^{2+}$ added to CLB supplemented with 2 µ*M* EGTA produces an initial increase in total $[Ca^{2+}]_{free}$ from approx 60–350 n*M*.

## References


1. Berridge, M. J. (1993) Inositol trisphosphate and calcium signalling. *Nature* **361,** 315–325.
2. Streb, H., Irvine, R. F., Berridge, M. J., and Schulz, I. (1983) Release of Ca2+ from a nonmitochondrial intracellular store in pancreatic acinar cells by inositol-1,4,5-triphosphate. *Nature* **306,** 67–69.
3. Strupish, J., Cooke, A. M., Potter, B. V. L., Gigg, R., and Nahorski, S. R. (1988) Stereospecific mobilization of intracellular $Ca^{2+}$ by inositol 1,4,5-triphosphate. *Biochem. J.* **253,** 901–905.
4. Berridge, M. J., and Taylor, C. W. (1988) Inositol triphosphate and calcium signalling, in *Cold Spring Harbor Symposia on Quantitative Biology*. **53**, pp. 927–933.
5. Walker, J. W., Somlyo, A. V., Goldman, Y. E., Somlyo, A. V., and Trentham, D. R. (1987) Kinetics of smooth and skeletal muscle activation by laser pulse photolysis of caged inositol 1,4,5-triphosphate. *Nature* **327,** 249–252.
6. Ely, J. A., Hunyady, L., Baukal, A. J., and Catt, K. J. (1990) Inositol 1,3,4,5-tetrakisphosphate stimulates $Ca^{2+}$ release from bovine adrenal microsomes by a mechanism independent of the inositol 1,4,5-trisphosphate receptor. *Biochem. J.* **268,** 333–338.
7. Joseph, S. K., Hansen, C. A., and Williamson, J. R. (1989) Inositol tetrakisphosphate mobilizes calcium from cerebellum microsomes. *Mol. Pharmacol.* **36,** 391–397.
8. Gershengorn, M. C., Geras, E., Purrello, V. S., and Rebeccchi, M. J. (1984) Inositol trisphosphate mediates thyrotrophin-releasing hormone mobilization of nonmitochondrial calcium in rat mammotrophic pituitary cells. *J. Biol. Chem.* **259,** 10,675–10,681.
9. Grynkiewicz, G., Poenie, M., and Tsien, R. Y. (1985) A new generation of $Ca^{2+}$ indicators with greatly improved fluorescent properties. *J. Biol. Chem.* **260,** 3440–3449.

10. Knight, D. E. and Scrutton, M. C. (1986) Gaining access to the cytosol: the technique and some applications of electropermeabilization. *Biochem. J.* **234,** 497–506.
11. Kobayashi, S., Kitazawa, T., Somlyo, A. V., and Somlyo, A. P. (1989) Cytosolic heparin inhibits muscarinic and α-adrenergic $Ca^{2+}$ release in smooth muscle: Physiological role of inositol 1,4,5-trisphosphate in pharmacomechanical coupling. *J. Biol. Chem.* **264,** 17,997–18,004.
12. Bradford, M. M. (1976) A rapid and sensitive method for the quantitation of microgram quantities of protein utilising the principle of protein-dye binding. *Anal. Biochem.* **72,** 248–254.
13. Labarca, C. and Paigen, K. (1980) A simple, rapid and sensitive DNA assay procedure. *Anal. Biochem.* **102,** 344–352.
14. Carafoli, E. (1987) Intracellular calcium homeostasis. *Annu. Rev. Biochem.* **56,** 395–433.
15. Bezprozvanny, I., Watras, J., and Ehrlich, B. E. (1991) Bell-shaped calcium-response curves of Ins(1,4,5)$P_3$- and calcium-gated channels from endoplasmic reticulum of cerebellum. *Nature* **351,** 751–754.
16. Danoff, S. K., Suppattapone, S., and Snyder, S. H. (1988) Characterization of a membrane protein from brain mediating the inhibition of inositol 1,4,5-trisphosphate receptor binding by calcium. *Biochem. J.* **254,** 701–705.
17. Finch, E. A., Turner, T. J., and Goldin, S. M. (1991) Calcium as a coagonist of inositol 1,4,5-trisphosphate-induced calcium release. *Science* **252,** 443–446.
18. Loomis-Husselbee, J. W., Cullen, P. J., Irvine, R. F., and Dawson, A. P. (1991) Electroporation can cause artifacts due to solubilization of cations from electrode plates. Aluminium ions enhance conversion of inositol 1,3,4,5-tetrakisphosphate into inositol 1,4,5-trisphosphate in electroporated L1210 cells. *Biochem. J.* **277,** 883–885.
19. Takahashi, M., Tanzawa, K., and Takahashi, S. (1994) Adenophostins, newly discovered metabolites of Penicillium brevicompactum, act as potent agonists of the inositol 1,4,5-trisphosphate receptor. *J. Biol. Chem.* **269,** 369–372.

# 14

# Microinjection of *myo*-Inositol(1,4,5)Trisphosphate and Other Calcium-Mobilizing Agents Into Intact Adherent Cells

**Robert A. Wilcox, Ian D. Forsythe, and Terence J. McCann**

## 1. Introduction

Many receptor tyrosine kinases and seven-transmembrane receptors are directly coupled or coupled via G proteins, respectively, to the activation of phosphoinositidase Cs ***(1)***. These enzymes catalyze the hydrolysis of phosphatidylinositol 4,5-bisphosphate to produce the second messengers, *myo*-inositol(1,4,5)trisphosphate [Ins(1,4,5)$P_3$] and diacylglycerol ***(1)***. Ins(1,4,5)$P_3$ interacts with a specific receptor that is a ligand-gated channel that allows mobilization of non-mitochondrial intracellular calcium ($Ca^{2+}$) stores ***(1)***. Because Ins(1,4,5)$P_3$ is plasma membrane impermeant, this phenomenon was first demonstrated in permeabilized pancreatic acinar cells ***(2)***, and all subsequent studies in cells have involved introduction of Ins(1,4,5)$P_3$ by rendering a cell population permeable ***(3)***, using microinjection techniques ***(4)***, or by the presentation of chemically modified membrane-permeable Ins(1,4,5)$P_3$ analogs, such as photolabile "caged Ins(1,4,5)$P_3$" ***(5)***. An alternative approach involves disruption of the plasma membrane and preparation of microsomes from the intracellular vesicular $Ca^{2+}$ stores ***(6,7)***; however, microsomal preparations exhibit a loss of Ins(1,4,5)$P_3$ responsiveness compared to permeabilized and intact cells.

This chapter will outline a semiautomated method for the microinjection of Ins(1,4,5)$P_3$ and other hydrophilic $Ca^{2+}$ mobilizing inositol polyphosphates (CM-IPs) and pharmacological agents. Dynamic $Ca^{2+}$ imaging using fura-2-loaded cells was used to measure $Ca^{2+}$ fluxes at the single cell level. Because microinjected Ins(1,4,5)$P_3$ and CM-Ins(1,4,5)$P_3$ rapidly mobilize intracellular $Ca^{2+}$ stores, the use of fully automated, multiple microinjection was considered

From: *Methods in Molecular Biology, vol. 312: Calcium Signaling Protocols: Second Edition*
Edited by: D. G. Lambert © Humana Press Inc., Totowa, NJ

redundant. However, this is a powerful technique for the injection of more latent agents such as DNA, peptides, and antibodies and has been extensively described elsewhere ***(8–11)***. $Ca^{2+}$ fluxes are acutely examined just prior to the moment of microinjection to obtain a baseline, then followed for several minutes after the microinjection. The authors have utilized a number of different cell types, but have conducted the majority of their experiments with mouse L-fibroblasts overexpressing the type I Ins(1,4,5)$P_3$ receptor (L15 cells) ***(12,13)*** and SaOS-2 human osteoblasts ***(14)***.

## 2. Materials

### 2.1. Reagents and Buffers

1. Ultrapure $H_2O$ derived from a specialist unit (e.g., Elgastat, Elga, High Wycomb, Bucks, UK, or Millipore, Watford, Herts, UK). All solutions are prepared in plasticware and using ultrapure water unless otherwise stated. Glass leaches significant concentrations of ions, including $Ca^{2+}$, into aqueous solutions. Consequently, glassware should be avoided when making nominally $Ca^{2+}$-free buffers, especially for storage of solutions.
2. The fluorescent calcium chelating dye fura-2–free acid (Calbiochem-Novabiochem, Nottingham, Notts, UK, and Molecular Probes, Eugene, OR) is prepared as 0.5 or 1 m*M* stock solutions in $H_2O$, distributed into 10-, 20-, and 50-µL aliquots, and stored at ≤–20°C protected from light in an aluminum foil–covered container. Fura-2/AM, the cell-permeant derivative of fura-2 (Calbiochem and Molecular Probes), is relatively insoluble in $H_2O$ and, thus, should be prepared in dry dimethyl sulfoxide (DMSO) as a 1 to 2 m*M* stock solution and stored at ≤–70°C protected from light. The use of dry DMSO solution is crucial; thus, DMSO (Sigma, Poole, Dorset, UK) should be purchased in small sealed ampules and opened just prior to solubilization of the fura-2/AM.
3. $Ca^{2+}$ calibration top stocks are used for the determination of the $F_{max}$ (fluorescence at saturating [$Ca^{2+}$]) and $F_{min}$ (fluorescence at zero [$Ca^{2+}$]) values of fura-2 and fluo-3, in solution. For $F_{max}$ a 1/400 dilution of 200 m*M* $CaCl_2$ (0.5 m*M* final) fully $Ca^{2+}$ saturates both fluorescent dyes. For $F_{min}$ a 1/100 dilution of 400 m*M* EGTA/400 m*M* KOH, pH 7.2 (4 m*M* final) essentially chelates all available $Ca^{2+}$. The 400 m*M* EGTA/400 m*M* KOH, pH 7.2, solution will require sonication for solubilization of the EGTA. Alternatively a 1/50 dilution of 400 m*M* BAPTA (Molecular Probes and Calbiochem), pH 7.2, will more efficiently and rapidly chelate $Ca^{2+}$. BAPTA readily solubilizes in $H_2O$, but fresh stock must be made every 7 d. All solutions are stored at 4°C between use.
4. $Ca^{2+}$-buffering stocks: EGTA (10 m*M*/20 m*M* KOH, pH 7.2) or BAPTA (10 m*M* aqueous solution, pH 7.2) prepared via aqueous dilution from the $Ca^{2+}$ calibration top stocks.
5. HEPES-buffered saline (HBS)-EDTA solution for removal of adherent cells: 0.02% (w/v) $Na_2EDTA$, 0.9% (w/v) NaCl, and 20 m*M* HEPES-free acid, corrected to pH 7.2–7.4 using 20% (w/v) NaOH.

6. Ins(1,4,5)$P_3$ (CellSignals, Lexington, KY, Semat Technical [UK agent for Research Biochemicals], St. Albans, Herts, UK), L-*myo*-inositol(1,4,5)trisphosphate [L-Ins(1,4,5)$P_3$] (Sigma), and adenophostin A (AdA) (a kind gift from Sankyo, Tokyo, Japan) are prepared as 1–5 m*M*, 20-µL aqueous stock solutions. Aqueous stocks of all CM-IPs are pretreated with Chelex-100 (Bio-Rad, Hemel Hampstead, Herts, UK) to chelate divalent cations and then with BAPTA-based polystyrene-immobilized "$Ca^{2+}$-sponge" (Molecular Probes) to specifically remove contaminating $Ca^{2+}$ (*see* **Note 1**).
7. Glass cover slips (no. 1. thickness, Chance-Propper, Smethwick, Warley, UK) are used. Tissue culture grade plastic slides cannot be used because they exhibit autofluorescence and thus interfere with fura-2 measurements.
8. HEPES-buffered Krebs-Henseleit (K/H buffer): 118 m*M* NaCl, 4.64 m*M* KCl, 1.18 m*M* $KH_2PO_4$, 1.18 m*M* $MgSO_4$, 11.7 m*M* glucose, 4.2 m*M* $NaHCO_3$, 10 m*M* HEPES-free acid, and 1–1.3 m*M* $CaCl_2$ (pH 7.4). Use of HEPES-buffered solutions is crucial in order to ensure that the pH remains stable during the microinjection procedure; bicarbonate-buffered solutions are not used since when open to the air, they rapidly develop a basic pH. $CaCl_2$ is omitted from nominally calcium-free HEPES-buffered Krebs-Henseleit ($Ca^{2+}$-free K/H buffer). The $Ca^{2+}$ contamination present in nominally $Ca^{2+}$-free K/H buffer generally 1–3 µ*M* as assessed using 50 n*M* fluo-3 (*see* **Note 2**).
9. Cells are grown in a variety of growth media, supplemented with 10% fetal calf serum (FCS) and 100 IU/mL penicillin, 100 µg/mL streptomycin, and 2.5 µg/mL fungizone (Gibco, Paisley, Renfrewshire, UK). Mouse L-fibroblasts and transfects overexpressing the type 1 Ins(1,4,5)$P_3$ receptor derived from L-fibroblasts are initially a kind gift from Prof. Mikoshiba (Tokyo, Japan). These are subcultured 1/10–1/20 weekly and grown in HEPES-buffered Dulbecco's modified Eagle's medium (DMEM). SaOS-2 cells from American Type Culture Collection, Rockville, MD (ATCC) are subcultured 1/10 weekly and maintained in a DMEM/Nutrient Mix F12 (1:1)–based growth medium ***(14)***.
10. Confluent adherent cell monolayers (25-$cm^2$ flask) are washed once, then harvested using the HBS/EDTA solution. The cells are washed twice in tissue culture media (5 mL), and sometimes the cells are centrifuged through a layer of 0.5 mL of FCS to remove cell debris.
11. Before cells are plated, the glass cover slips are treated in two steps to clean and then sterilize the surface. All procedures are carried out under sterile conditions in a cell culture class II flow cabinet. First, using fine tip forceps, 22-mm-diameter glass cover slips are dip washed in analytical grade ethanol or methanol to clean the cover slip surface. This removes most of the dust and any organic material (*see* **Note 3**). Second, the cover slips are dipped twice in a 70% ethanol (or methanol)/30% $H_2O$ solution, blotted onto a sterile tissue, flamed briefly using a Bunsen burner, gently air cooled, and then placed into 35-mm-diameter plastic culture dishes (Nunc, Roskilde, Denmark). The prepared cells are diluted and plated in 2 mL volumes, onto the glass cover slips in the culture dishes. Cells are plated to give approx 5% confluence on the glass cover slip and used for microinjection when they have reached 10–15% confluence; usually this takes 1–3 d in culture.

### 2.2. Equipment

1. The most important piece of equipment for successful microinjection is a good quality microscope with some kind of contrast enhancement optics (phase or differential interference). The better the image obtained, the easier it will be to inject the target cells. For adherent cells flattened onto a glass cover slip, a good optical image is especially important. The authors use a Nikon Diaphot (Nikon, Kingston Upon Thames, UK) with phase contrast optics, including a high numerical aperture quartz objective for compatibility with the ultraviolet (UV) wavelengths used to excite the fluorescent dyes. An inverted microscope is essential for injecting adherent cells grown on glass cover slips.
2. Fluorescence spectrophotometer (fluorimeter) with variable excitation and emission optics ideally with a chart recorder or computer interface is used to determine the free $Ca^{2+}$ concentration of solutions including the K/H buffer. The authors utilize the model LS50β fluorimeter (Perkin-Elmer, Beaconsfield, Bucks, UK), which allows large variations in the selection of wavelengths and excitation and emission slit widths, thus permitting fluorescent measurements to be made over a large dynamic range.
3. IBM 486/586 PC or compatible computer. The Perkin-Elmer fluorescence data manager (FLDM) software is used to run the fluorimeter.
4. For single cell fluorimetric analysis of $Ca^{2+}$ fluxes, the authors utilized a Nikon Diaphot 200 fluorescent microscope (Nikon) coupled to a $Ca^{2+}$-imaging system. For the data collection, they used the MiraCal PRO (Life Science Resources, Cambridge, UK), which included an 8-bit digital, cooled charge-coupled device camera, filter wheel and Windows95™-based image acquisition and analysis software. A myriad of other inverted fluorescent microscope and imaging systems are available, but the MiraCal PRO system is flexible and easy to use. New $Ca^{2+}$-imaging systems are continuously being introduced, offering better technological features and generally at decreasing prices. When purchasing a $Ca^{2+}$ imaging system, the authors recommend an extensive and current assessment of several systems, to determine one's personal requirements.
5. Benchtop microcentrifuge, with a capacity for 24 standard 1.5-mL microcentrifuge tubes (Heraeus, Dusseldorf, Germany and Desaga, Sarstedt-Gruppe, Wiesloch, Germany). Prior to loading into the microinjection needles, all stimulants are centrifuged at top speed for 5 min, at 4°C, to pellet any microparticles in the solution. This is a crucial step as microparticles derived from the solution or the air can readily block the narrow tip of the microinjection needle and prevent successful microinjection. The solution should be recentrifuged after the tube has been opened to the atmosphere.
6. Microinjections are accomplished using an integrated system consisting of Eppendorf Micromanipulator 5170 and Microinjector 5242 (Eppendorf-Netheler-Hinz GmbH, Hamburg, Germany), but several other popular microinjection systems are available, e.g., the Picospritzer II (General Valve, East Hanover, NJ). Generally prepulled "femtotip" micropipets with internal filaments and a 0.3–1-μm tip opening diameter are utilized (Eppendorf-Netheler-Hinz, cat. no. 5242-

956.008). Femtotips are favored since they are individually sealed free of microparticles and are sterile, have a standardized length, and can be directly screwed onto the injector capillary holder. Alternatively, it is possible to prepare one's own micropipets, if one has access to a suitable microelectrode puller (e.g., Sutter Instrument, San Rafael, CA; model P-87). Pulling microinjection pipets is an art form in itself ***(15)***, and entire books have been written about this subject ***(16)***. The author's have successfully used thin-walled borosilicate glass capillaries, with an internal filament to aid filling (GC120TF-10, Clark Electromedical Instruments, Reading, Berkshire, UK), to inject cultured mammalian cells. The advantages of making one's own micropipets are primarily cost and flexibility. The cost per micropipet is significantly lower than for femtotips, although the initial investment in a puller is high. In addition, it is possible to prepare micropipets for a variety of applications (e.g., injection, impalement, patch-clamp) from one machine.

7. The micropipets are backloaded with Eppendorf microloader pipet tips (Eppendorf-Netheler-Hinz, cat. no. 5242-956.003). A yellow tip (Anachem, Luton, Beds, UK) is used as a guide to assist threading the thin microloader tip into the rear of the femtotip. Generally, approx 0.5–3 µL of stimulant is loaded. The internal filament in the micropipet increases the capillary flow of the solution, and hence the tip fills easily; gentle tapping or shaking can be used to encourage the solution to flow directly into the tip or to remove bubbles if necessary. Care should be taken to reduce exposure of the microloader to air particles; between loading they are stored in their sealed box in an airtight plastic container (*see* **Note 4**).
8. Magnetic stirrer and control unit for cuvets (Rank Brothers, Bottisham, Cambridge, UK), magnetic stirrer bars for cuvets (Perkin-Elmer), and disposable fluorimetry cuvets (Sarstedt, Leicester, Leicestershire, UK).
9. A temperature-controlled cell perfusion chamber incorporating a cell cover slip holder is constructed in-house (*see* **Fig. 1**). Although normal body temperature is from 36 to 37°C, most imaging and electrophysiological experiments are conducted at room temperature (20–25°C). Even though this has the advantage of slowing rapidly occurring events and increasing temporal resolution, many cellular processes have differing temperature dependence (Q10). In addition, many laboratories have temperatures that vary over the time course of hours and are subject to seasonal fluctuations. When collating results over a period of time, such fluctuations will add further variance to the data. To avoid this source of error, in the authors' experiments, the experimental temperature is precisely controlled by bipolar feedback through Peltier devices. These solid-state heat pumps induce a temperature difference between their two surfaces that is proportional to the magnitude of the electrical current flow through the device. By reversing the current flow, one can change from heating to cooling. By assembling such devices into the stage of the experimental microscope and incorporating some feedback control, one can precisely control the experimental temperature over a range of approx 0°C–50°C. Hence, experiments are performed at any set temperature, independent of the ambient temperature, and including physiologically relevant

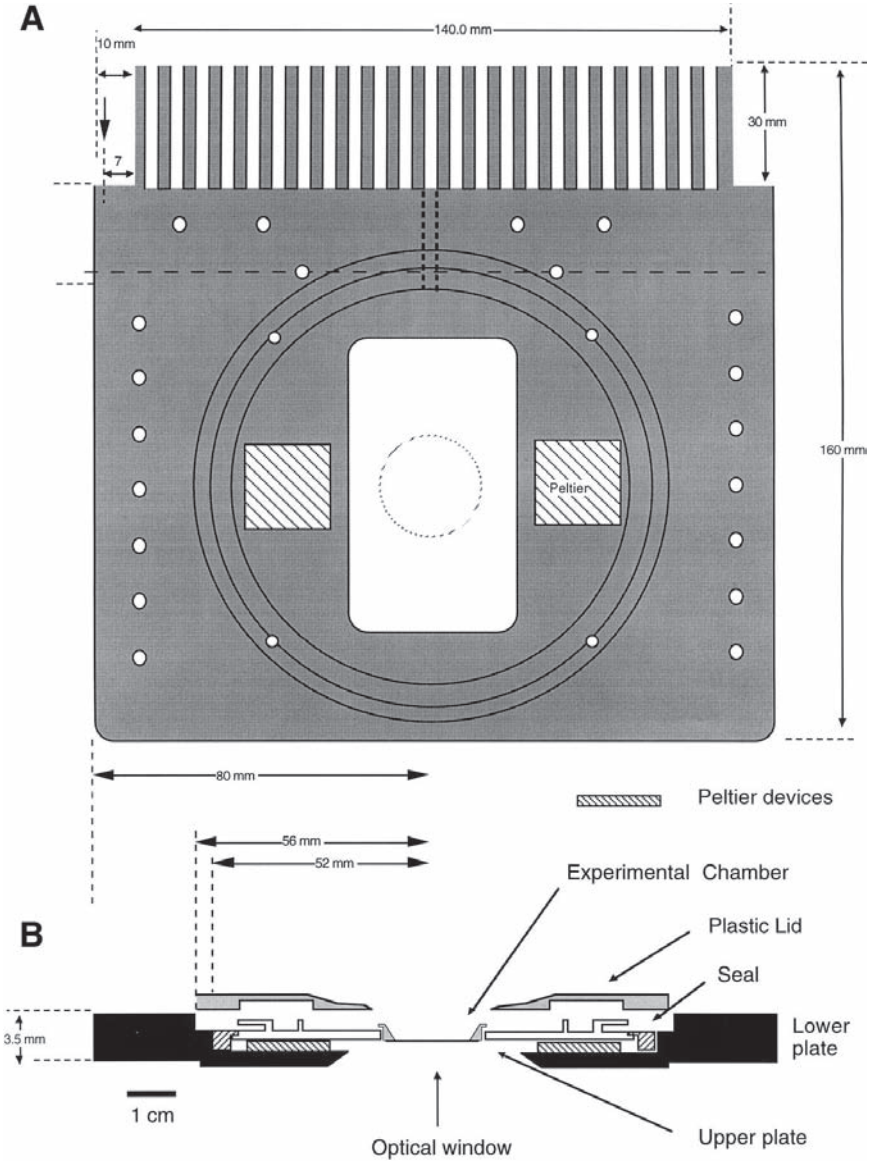


Fig. 1. *(continued on opposite page)* Construction and design plan of the heated perfusion chamber **(A)** Lower plate (material: anodized aluminum). This plate forms the base and is fixed to the microscope stage. It also acts as a heat source or sink for the Peltier devices. **(B)** An exploded side view is shown with all the components in their relative positions. The Peltier devices are effectively sandwiched between the upper and lower plate, with a heat-sink compound used to improve thermal conductivity. An aluminum ring drops into the central hole to form the experimental chamber. **(C)** Upper plate (mate-

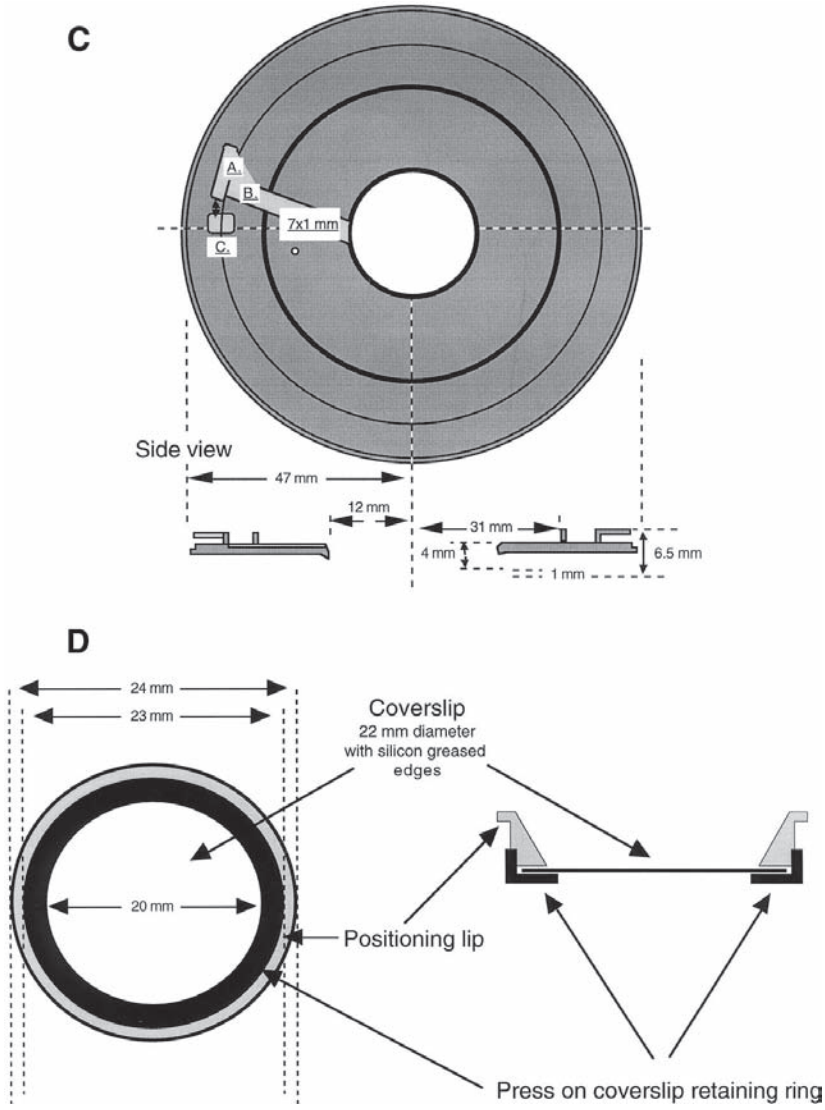


rial: anodized aluminum). The outer lip forms a slot through which plastic tubes carrying saline are coiled forming a heat exchange. The tubes enter at the slot marked "x," pass around 350°, and then pass along a shallow groove (indicated by the gray area) to reach the central hole in the middle of the plate (which receives the experimental chamber; *see* **[B]**). Gas mixture can also be passed over this heat exchange. The top plate is covered by a plastic lid (not shown). The solution delivery tubes can be readily connected to a peristaltic pump, and with the addition of a waste suction tube placed at the opposite side of the bath, a continuous flow of warm fresh solution at variable rates is possible. **(D)** Experimental chamber and cover slip holder (material: aluminum or polypropylene).

temperatures. The design used is based on a previous version ***(17)*** that has been modified for use on either inverted or conventional microscopes. It is suitable for both tissue culture and brain-slice preparations ***(18,19)***. The experimental chamber is formed by an aluminum ring with a glass cover slip forming the optical window. This chamber is secured into an aluminum plate, which forms the heat exchange surface (controlled by the Peltier device). The stage incorporates three elements of temperature control: (1) the experimental chamber is in thermal contact with the heat exchange; (2) the saline passes across the same heat exchange surface; and (3) an air or gas mixture can also be passed over the heat exchange (**Fig. 1**). This latter element is useful for reducing the thermal losses from the saline to the atmosphere because the experimental chamber is open on the upper surface to permit access. Similar temperature-controlled cell perfusion chambers are commercially available (IntraCel, Royston, Herts, UK; Applied Imaging, Sunderland, Tyne and Wear, UK; Medical Systems, NY).

9. The microscope and integrated micromanipulator and microinjection system are mounted on a large antivibration table ("Micro-g" series, Technical Manufacturing, Peabody, MA).

## 3. Methods

### 3.1. Preparation of Cells for Injection

1. Cells are plated at low density onto 22-mm-diameter cover slips in 2 mL of tissue culture medium in 40-mm-diameter tissue culture Petri dishes and grown for 1–3 d prior to loading with fura-2/AM and microinjection (*see* **Subheading 2.1.**, **item 11**). Fura-2/AM loading is conducted within the culture dishes, and the cover slips are washed twice with 2 mL of K/H buffer (pH 7.4) to remove debris and all traces of serum and culture medium. The cover slip cells are then loaded with fura-2/AM (3.3 μ*M*) for 20–40 min at room temperature in 2 mL of K/H buffer. A small magnetic flea is placed in the Petri dish adjacent to the cover slip, and this is used to mix gently the fura-2/AM during the loading (*see* **Subheading 2.2.**, **item 8**).
2. The cover slip is then washed twice with 2 mL of K/H buffer and left for >15 min, to allow for de-esterification of the dye. The cover slip is removed from the culture dish and quickly mounted into the coverslip holder, which was sealed with silicone grease (silicone compound MS4, Dow Corning GmbH, Munich, Germany) to prevent leaks. K/H buffer (37°C, 0.5 mL) is placed in the small chamber to cover the cells, and then the whole chamber is mounted into the heated cell perfusion chamber (37°C). Just prior to setting up the microinjection, the cell chamber should be washed twice with 0.5 mL of 37°C $Ca^{2+}$-free K/H buffer (pH 7.4).

### 3.2. Setting Microinjection Needle Pressures

#### 3.2.1. Compensation Pressure (Pc)

The microinjection needle is subject to capillary suction forces as soon as it is submerged into the buffer bathing the cells. Thus a Pc is applied that pre-

vents that particular buffer from flowing into the needle and diluting the injection solution. Practically a Pc value is set empirically that ensures a permanent slight discharge from the femtotip when in $Ca^{2+}$-free K/H buffer. Eppendorf suggests a Pc range of 30–100 hPa for femtotips depending on the surface tension and viscosity of both the injection and buffer solution. The authors determine their working Pc value by loading 0.5–1 m*M* fura-2-free acid into a femtotip; the femtotip is then immersed in $Ca^{2+}$-free K/H buffer supplemented with 1.3 m*M* $CaCl_2 \cdot 6H_2O$. Using the appropriate oscillating light source and fluorescent microscope system to visualize the tip opening of the femtotip, the Pc value is gradually increased from 30 hPa until fura-2 can be directly observed very slowly discharging into the buffer. In the authors' buffer, a Pc value of 30–40 hPa is appropriate.

#### *3.2.2. Injection Pressure (Pi)*

Pi is generally significantly higher than Pc (but *see* **Note 5**). Eppendorf suggests a Pi of 50–500 hPa for femtotips; however, for small mammalian cells the lower end of this range is more appropriate. Obviously Pi must be higher than the internal pressure of the microinjected cell, but extensive inflation of the cell or nucleus indicates that the set Pi needs to be reduced. The injection time *($t_i$)* defines the period for which Pi will be maintained inside the cell; it is generally set empirically between 0.4 and 1.5 s. For an injection time of 0.5 s, the authors use Pi values between 70 and 160 hPa, at which a barely noticeable cellular inflation accompanies the injections and cellular integrity is maintained.

#### *3.2.3. The Cleaning or Rinsing Pressure (Pr)*

Should the pipet become blocked by solution particles or the tip occluded with cellular debris, a rinsing pressure (Pr ~3000 hPa) can be applied in an attempt to blow the contamination away. Never use the Pr close to a cell monolayer as the high pressure will invariably damage or wash cells away. If several applications of Pr fail to dislodge cell debris, replace the femtotip as subsequent microinjections are usually compromised.

### *3.3. Estimating Microinjection Volume*

Typically microinjected volumes range from 0.01 to 0.05 pL for nuclear injections and 0.1–0.5 pL for cytoplasmic injections into mammalian cells ***(11,20)***. Several methods have been used to quite accurately measure the microinjection volume using fluorescence ***(21)*** or radioactivity ***(22)***. The authors have used a relatively crude method to estimate injected volume because most of their experiments involved a single microinjection of a stimulant at supramaximally effective concentrations. An estimate of the cell volume is made by calculating the volume of freshly harvested "rounded up" cells. A

microscope micrometer is used to measure the average diameter of 100 cells, the average radii *(R)* determined, and the spherical volume *(V)* estimated, using $V = 4\pi R^3/3$. The estimated injection volume is calculated by delivering tens of injections of fura-2 into a cuvet containing 2 mL of K/H buffer. Since the fura-2 added will be completely saturated by the 1.3 m*M* in the K/H buffer, the resulting fluorescence can be directly calibrated against known volumes of fura-2 (10 n*M*) added to K/H buffer. This is a relatively inaccurate calculation owing to population variance in the size of the microinjected adherent cells, but corresponds well with the estimated microinjection volume of 5–10% of cell volume suggested by others ***(11,20)***. Thus microinjected stimulants are loaded into the microinjection needles at 10 to 20-fold the desired final concentration.

### *3.4. Finding the Cell and Aligning Cells for Microinjection*

1. For the initial microinjection, locate a single cell or small group of cells for microinjection, using contrast enhancement optics, and then tilt back the microscope condenser head.
2. Load the micropipet, mount it onto the injection apparatus, and, using the micromanipulator on the high-speed mode, roughly center the tip over the objective and carefully lower it below the buffer surface. Watch out for a meniscus forming around the tip of the micropipet; this indicates that it has entered the solution (shining a beam from a penlight on the solution will make it easier to see the meniscus).
3. As soon as the micropipet tip has been submerged, switch the manipulator to the slow-speed mode and check the centering of the tip over the objective. If possible, carefully tilt the condenser head back to its normal position without hitting the micropipet; again, a penlight will help one to see what is happening (but *see* **Note 6**).
4. Finding the micropipet tip and aligning it above the cells can be frustratingly difficult, but switching to bright field illumination (rather than contrast enhancement) greatly increases the depth of field, making it much easier to locate the micropipet. To do this on a Diaphot with phase contrast optics, rotate the condenser phase annular ring out of the light path and replace it with the aperture diaphragm; one should still see an image of the cells (albeit with little contrast). Reducing the aperture size will further increase the depth of field. Focus initially on the cells and then raise the focal plane a "large" distance above the cells (i.e., focus "up").
5. Now it is necessary to locate the "shadow" of the out-of-focus micropipet. It is easier to detect a moving shadow than a stationary one, so begin by moving the micropipet gently backward and forward in the Y-plane only. When the shaft of the micropipet has been located, move it in the X-plane, in the direction that will bring the tip into the field of view (i.e., "backward"). The shadow of the end of the micropipet should now be visible through the microscope. Initially lower the tip slowly until the focus improves significantly as it enters the focal plane (*see* **Note 6**).

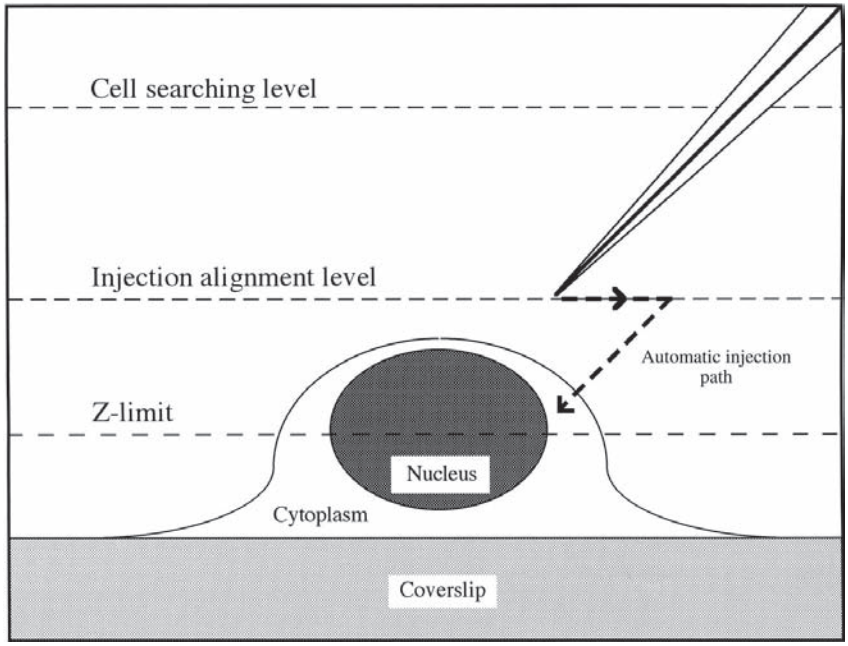


Fig. 2. Microinjection of adherent cells. Note microinjections are preferentially delivered into the thick cytoplasm of the perinuclear region.

6. Switch back to contrast enhancement microscopy and focus "down" toward the cells. Then bring the micropipet slowly down until it comes into focus again. This process is repeated several times until the tip of the micropipet lies above the cell monolayer a distance of about two to three times the maximum cell height of the monolayer. This cell searching level (**Fig. 2**) allows alignment of the tip above cells without the danger of stripping off the cell monolayer (*see* **Note 7**).

### *3.5. Microinjection*

1. Adherent cells usually resemble a fried egg, with the perinuclear region raised above rest of the cell (**Fig. 2**); aim to inject just outside the nucleus where the cell is thickest. The Eppendorf microinjection system permits an axial 45° angle automatic injection process. The tip of the micropipet is aligned immediately above the desired injection point, and when the injection is activated the tip is driven first backward and then axially downward at 45° to the preset "Z-limit," impaling the cell and delivering a microinjection for time $(t_i)$.
2. The micropipet is then axially withdrawn and retraces its path to return to the starting position (*see* **Fig. 2**). Consequently, before a microinjection is possible, a Z-limit (which restricts the downward movement of the tip) must be preset. For

this a cell is sacrificed by lowering the tip of the micropipet into the target cell, or by gently "stroking" the plasma membrane of the cell near the nucleus. The Z-limit function is then activated, and the micropipet is returned to the cell-searching level (*see* **Note 8**).

3. Cells chosen for injection can then be aligned and automatically microinjected as described above (*see* **Subheading 3.5., item 1** and **Note 9**). When imaging $Ca^{2+}$ levels in conjunction with microinjection, work quickly to start recording the experiment, taking care not to disturb the microscope as the light output to the camera port is redirected.

### 3.6. Did the Microinjection Kill the Cell?

Following microinjection damage, a dead cell will appear refractory under phase contrast. Additionally fura-2 will leak out of the cell cytoplasm. But injection of high concentrations of $Ca^{2+}$-releasing agents is often cytotoxic. Consequently, one often takes advantage of the fact that Ins(1,4,5)$P_3$ and many Ins(1,4,5)$P_3$ analogs will pass through gap junctions into adjacent cells. Therefore, $Ca^{2+}$ mobilization in several adjacent cells can be followed, even when the viability of the initially microinjected cell is compromised.

## 4. Notes

1. To effectively measure cellular $Ca^{2+}$ release induced by microinjection, it is crucial that the introduced stimulant is free of contaminating $Ca^{2+}$, which would cause artifacts. Aqueous stocks of all stimulating inositol polyphosphates and AdA are pretreated with Chelex-100 (Bio-Rad) to chelate divalent cations and then with BAPTA-based polystyrene-immobilized "$Ca^{2+}$-sponge" to specifically remove contaminating $Ca^{2+}$. Treatment is repeated until final concentration of contaminated [$Ca^{2+}$] is <10 n*M* at the highest final inositol polyphosphate concentration (10 μ*M*) solubilized in control cytosol-like buffer (CLB). Small columns containing 10–20 mg of Chelex-100 or BAPTA "sponge" are utilized to remove divalent cation contamination. These are made from disposable 250-μL yellow tips or 1000-μL blue tips (Anachem, Luton, Bedfordshire, UK) with a retaining filter in their base made from 40-μm nylon mesh (Plastok Associates, Birkenhead, Merseyside, UK). Alternatively, small volumes of known aqueous stock concentrations of inositol polyphosphates (<40 μL) can be "cleaned" by treatment with 5–10 mg of Chelex-100 or BAPTA "sponge" in microcentrifuge tubes. The tubes are then vortexed for 60 s, centrifuged (13,000*g*, 1 min at 4°C), and the supernatant is harvested and transferred to a fresh tube. Centrifugation of the harvested supernatant is repeated until no chelating beads pellet. Although 5–10% of the volume of the aqueous stock solution is lost using this treatment, the authors have treated a wide range of inositol polyphosphates with these chelators and have detected no loss of compound owing to adsorption.
2. The concentration of contaminating-free $Ca^{2+}$ ($[Ca^{2+}]_{free}$) in the nominally $Ca^{2+}$-free K/H buffer is determined using a tracer concentration of fluo-3 (100 n*M*). Briefly a sample of $Ca^{2+}$-free K/H buffer (2 mL) is placed in a fluorimeter cuvet

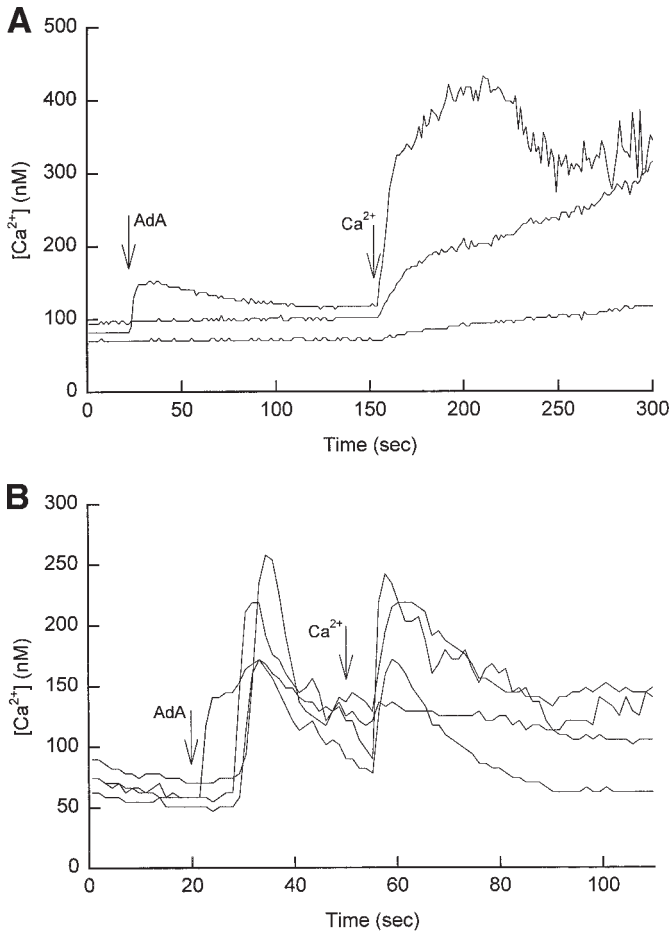


Fig. 3. The effect of microinjecting SaOS-2 cells **(A)** and m3-L15.20 cells **(B)** with a maximally effective concentration of the metabolically resistant Ins(1,4,5)$P_3$ analog, AdA. Cells are initially microinjected with AdA (~2 μ*M*) in $Ca^{2+}$-free KHB and $Ca^{2+}$ is then added to a final concentration of 1 m*M*, where indicated. In SaOS-2 cells, AdA only produced detectable mobilization of intracellular $Ca^{2+}$ stores in 1/3 cells, but some degree of capacitative $Ca^{2+}$ entry was observed on $Ca^{2+}$ add back in all three injected cells. By contrast, L15.20 cells exhibited both $Ca^{2+}$ release from internal stores and significant capacitative $Ca^{2+}$ entry on $Ca^{2+}$ add back in 4/4 injected cells. Significantly, L15.20 cells are derived from L15 cells that were transfected with and stably overexpress the type 1 Ins(1,4,5)$P_3$ receptor ***(12,13)***.

with 4 μL of 50 μ*M* fluo-3. The fluorescent intensity ($F_{CLB}$) of the buffer is determined at excitation and emission wavelengths of 505 and 530 nm, respectively. After recording the resultant *F* values, 5 μL of the 200 m*M* $CaCl_2$ solution ($F_{max}$),

is added followed by 25 µL of 200 m*M* EGTA ($F_{min}$). $[Ca^{2+}]$ is then calculated from the equation of Grynkiewicz ***(23)*** in which the $K_d$ for fluo-3 is approx 400 n*M* at 25°C and 864 n*M* at 37°C ***(24)***:

$$[Ca^{2+}]_{free}\ (nM) = (F_{CLB} - F_{min}/F_{max} - F_{CLB}) \times K_d$$

Ideally the $[Ca^{2+}]_{free}$ at 37°C should be 1–3 µ*M*—certainly <5 µ*M*, to avoid significant $Ca^{2+}$ inflow following microinjection and subsequent $Ca^{2+}$ inhibition of $Ins(1,4,5)P_3$ receptor responses ***(25)***. $[Ca^{2+}]_{free}$ can be reduced by adding an appropriate aliquot of EGTA (10 m*M*/20 m*M* KOH) or BAPTA (10 m*M*); usually 2–10 µL/100 mL of CLB (0.2–1 µ*M* EGTA final) will effectively reduce the $[Ca^{2+}]_{free}$ to below 3 µ*M*.

High concentrations of EGTA and BAPTA are not used to completely chelate $[Ca^{2+}]_{free}$ from the nominally $Ca^{2+}$-free K/H buffer for several reasons. High concentrations of EGTA and BAPTA cause adherent cells to round up and detach from the cover slip, and they also tend to significantly deplete the intracellular $Ca^{2+}$ stores. Additionally, recent evidence suggests that cell membrane resealing following microinjection requires the presence of some extracellular $Ca^{2+}$ ***(26)***.

3. Never touch the surface of a cover slip with ungloved fingers; fingerprints leave smudges that both discourage cell attachment and also absorb light significantly in the UV wavelengths, the wavelength range used to stimulate fura-2.
4. The micropipets are filled just prior to use, rapidly screw mounted on the microinjector head, and the femtotip is quickly lowered into the buffer above the cells. Speed is critical here because exposure to air can rapidly dry out the sample in the end of the femtotip, causing clogging.
5. Pc can be set slightly higher and then utilized for relatively gentle manual microinjection. Essentially the cell can be manually impaled and the injection solution allowed to discharge slowly inside the cell.
6. The focus on the femtotip will never be perfect because it is oriented at 45° to the cell monolayer. Consequently, aim to get a reasonable focus on the very end of the femtotip. Remember it should not be in exactly the same plane of focus prior to injection, or it would be in contact with the cells or cover slip.
7. The cover slip surface is not completely even. Consequently when searching for cells to inject utilizing relatively long X-Y movements, use the slow speed to avoid breaking the tip or stripping off the cell monolayer.
8. Appropriate setting of the Z-limit is crucial: if it is set too high, the cell will not be effectively microinjected; if set too low, the tip can be broken on the cover slip or the injection can be delivered underneath the cell monolayer.
9. The whole microinjection procedure requires practice; while learning expect to break a lot of tips. These tips are quite expensive, so even after breaking a tip it is best to continue practicing with the broken tip until the procedure is mastered.

## Acknowledgments

The authors are most grateful for the expert technical assistance provided by David Jones in the Biological Sciences workshop at the University of Leicester, especially for the construction of the heated perfusion chamber.

## References


1. Berridge, M. J. (1993) Inositol trisphosphate and calcium signalling. *Nature* **361,** 315–325.
2. Streb, H., Irvine, R. F., Berridge, M. J., and Schulz, I. (1983) Release of $Ca^{2+}$ from a nonmitochondrial intracellular store in pancreatic acinar cells by inositol-1,4,5-triphosphate. *Nature* **306,** 67–69.
3. Strupish, J., Cooke, A. M., Potter, B. V. L., Gigg, R., and Nahorski, S. R. (1988) Stereospecific mobilization of intracellular $Ca^{2+}$ by inositol 1,4,5-triphosphate. *Biochem. J.* **253,** 901–905.
4. Berridge, M. J. and Taylor, C. W. (1988) Inositol triphosphate and calcium signalling, in *Cold Spring Harbor Symposia on Quantitative Biology*. **53**, pp. 927–933.
5. Walker, J. W., Somlyo, A. V., Goldman, Y. E., Somlyo, A. V., and Trentham, D. R. (1987) Kinetics of smooth and skeletal muscle activation by laser pulse photolysis of caged inositol 1,4,5-triphosphate. *Nature* **327,** 249–252.
6. Ely, J. A., Hunyady, L., Baukal, A. J., and Catt, K. J. (1990) Inositol 1,3,4,5-tetrakisphosphate stimulates $Ca^{2+}$ release from bovine adrenal microsomes by a mechanism independent of the inositol 1,4,5-trisphosphate receptor. *Biochem. J.* **268,** 333–338.
7. Joseph, S. K., Hansen, C. A., and Williamson, J. R. (1989) Inositol tetrakisphosphate mobilizes calcium from cerebellum microsomes. *Mol. Pharmacol.* **36,** 391–397.
8. Proctor, G. N. (1992) Microinjection of DNA into mammalian cells in culture: theory and practise. *Meth. Mol. Cell. Biol.* **3,** 209–213.
9. Pepperkok, R., Scheel, J., Horstman, H., Hauri, H. P., Griffiths, G., and Kreis, T. E. (1993) β-COP is essential for biosynthetic membrane transport from the endoplasmic reticulum to the Golgi complex in vivo. *Cell.* **74,** 71–82.
10. Pepperkok, R., Herr, S., Lorenz, P., Pyerin, W., and Ansorge, W. (1993) System for quantitation of gene expression in single cells by computerized micro-imaging application to c-fos expression after microinjection of anti-casein kinase II (CKII) antibody. *Exp. Cell. Res.* **204,** 278–285.
11. Pepperkok, R. (1995) Microinjection and electroporation of macromolecules into live cells, in *Cell Cycle—Materials and Methods* (Pagano, M., eds.), Springer, London, pp. 75–86.
12. Miyawaki, A., Furuichi, T., Maeda, N., and Mikoshiba, K. (1990) Expressed cerebellar-type inositol 1,4,5-trisphosphate receptor ($P_{400}$) has calcium release activity in a fibroblast L cell line. *Neuron.* **5,** 11–18.
13. Mackrill, J. J., Wilcox, R. A., Miyawaki, A., Mikoshoba, K., and Nahorski, S. R. (1996) Stable overexpression of the type-1 inositol 1,4,5-trisphosphate receptor in L fibroblasts: Subcellular distribution and functional consequences. *Biochem. J.* **318,** 871–878.
14. Rifas, L., Fausto, A., Scott, M. J., Avioli, L. V., and Welgus, H. G. (1994) Expression of metalloproteinases and tissue inhibitors of metalloproteinases in human osteoblast-like cells—differentiation is associated with repression of metalloproteinase biosynthesis. *Endocrinology.* **134,** 213–221.
15. Ogden, D. (1994) *Microelectrode Techniques: The Plymouth Workshop Handbook*. Company of Biologists, Cambridge, England.

16. Brown, K. T. and Flaming, D. G. (1986) Advanced micropipette techniques for cell physiology. *Methods in the Neurosciences Vol. 9,* John Wiley & Sons, Chichester, UK.
17. Forsythe, I. D. (1991) Microincubator for regulating temperature and superfusion of tissue-cultured neurons during electrophysiological or optical studies, in *Methods in Neurosciences, Vol. 4, Ion Channels and Electrophysiology* (Conn, P. M., eds.), Academic Press, London, UK, pp. 301–320.
18. Forsythe, I. D. (1994) Direct patch recording from identified presynaptic terminals medicating glutamatergic EPSCs in the rat CNS, in vitro. *J. Physiol.* **479,** 381–387.
19. Barnes-Davies, M. and Forsythe, I. D. (1995) Pre- and post-synaptic glutamate receptors at a giant excitatory synapse in rat auditory brain stem slices. *J. Physiol.* **488,** 387–406.
20. Pepperkok, R., Zanetti, M., King, R., Delia, D., Ansorge, W., Philipson, L., and Schneider, C. (1988) Automatic microinjection system facilitates detection of growth inhibitory mRNA. *Proc. Natl. Acad. Sci. USA* **85,** 6748–6752.
21. Lee, G. M. (1989) Measurement of volume injected into individual cells by quantitative fluorescence microscopy. *J. Cell. Sci.* **94,** 443–447.
22. Zavortink, et al. (1983) The distribution of calmodulin in living mitotic cells. *Exp. Cell. Res.* **149,** 367–385.
23. Grynkiewicz, G., Poenie, M., and Tsien, R. Y. (1985) A new generation of $Ca^{2+}$ indicators with greatly improved fluorescent properties. *J. Biol. Chem.* **260,** 3440–3449.
24. Merritt, J. E., McCarthy, S. A., Davies, M. P. A., and Moores, K. E. (1990) Use of fluo-3 to measure cytosolic $Ca^{2+}$ in platelets and neutrophils. *Biochem. J.* **269,** 513–519.
25. Danoff, S. K., Suppattapone, S., and Snyder, S. H. (1988) Characterization of a membrane protein from brain mediating the inhibition of inositol 1,4,5-trisphosphate receptor binding by calcium. *Biochem. J.* **254,** 701–705.
26. Steinhart, R. A., Bi, G., and Alderton, J. M. (1994) Cell membrane resealing by a vesicular mechanism similar to neurotransmitter release. *Science* **263,** 390–393.

# 15

# Measurement of Free [$Ca^{2+}$] Changes in Agonist-Sensitive Internal Stores Using Compartmentalized Fluorescent Indicators

**Aldebaran M. Hofer**

## 1. Introduction

The fact that acetoxymethyl (AM)-ester derivatives of fluorescent $Ca^{2+}$ indicators accumulate not only in the cytoplasm but also in organelles was recognized long ago as a potential source of artifacts during measurements of cytoplasmic [$Ca^{2+}$] ***(1,2)***. Later, it was observed that high-affinity dyes, such as fluo-3 and fura-2, normally saturated in the high-[$Ca^{2+}$] environment of the agonist-sensitive $Ca^{2+}$ store, could register [$Ca^{2+}$] changes in this compartment under special conditions (e.g., when pools were already partially empty) ***(3–6)***. The propensity of indicators to become compartmentalized was fully exploited, however, when investigators began to use lower affinity probes such as mag-fura-2 ***(7)***, to monitor [$Ca^{2+}$] changes in the inositol(1,4,5)trisphosphate [Ins(1,4,5)$P_3$]-sensitive store (a compartment largely accepted to be the endoplasmic reticulum [ER]). Thus, the release and reloading of this organelle with $Ca^{2+}$, as reported by ER-trapped dye, could be directly visualized in single permeabilized cells with high spatiotemporal resolution ***(8,9)***. This basic approach has been adopted by a number of laboratories to investigate phenomena ranging from $Ca^{2+}$ oscillations ***(10–12)*** to quantal release ***(13–15)***, and the subcellular localization of $Ca^{2+}$ storage sites ***(16–19)***.

This chapter provides a guide for the use of compartmentalized fluorescent dyes to measure free [$Ca^{2+}$] in the agonist-sensitive internal store of single cells. The basic steps involve incubating cells with the AM-ester derivative of the appropriate dye (resulting in partitioning of the probe in both the cytoplasm

From: *Methods in Molecular Biology, vol. 312: Calcium Signaling Protocols: Second Edition*
Edited by: D. G. Lambert © Humana Press Inc., Totowa, NJ

and organelles), and then permeabilizing the plasma membrane selectively to release the fluorophore from the cytoplasm. Fluorescence of organelle-trapped indicator is then monitored as with the cytoplasm (*see* **Chapters 2–4**). On completion of the experiment, a calibration can be performed to convert fluorescence into approximate values of intraluminal [$Ca^{2+}$]. Other methods for eliminating cytosolic indicator (such as dialysis via a patch pipet) will also be described. In addition, in some cell types it is possible to apply this approach for the measurement of intrastore [$Ca^{2+}$] in intact cells, based on the preferential retention of indicator in organelles during prolonged loading.

As is the case with the measurement of cytoplasmic [$Ca^{2+}$] using fluorescent indicators, the procedures involved are relatively straightforward. However, the interpretation of data can be confounded by many factors. Therefore, emphasis will be on the problems specific to this method that a beginner may encounter, and how to diagnose and circumvent artifacts.

## 2. Materials

1. Cells: a wide variety of mammalian cell types have been used previously, including hepatocytes, gonadotropes, smooth muscle cells, pancreatic acinar cells, gastric epithelial cells, RBL-1 cells, and BHK-21 fibroblasts (*see* **Note 1**).
2. Selection of dye: spectral compatibility with the equipment is generally the main consideration when choosing a fluorescent indicator. **Table 1** lists dyes that have been used successfully to monitor [$Ca^{2+}$] changes in Ins(1,4,5)$P_3$-sensitive stores and their spectral characteristics (*see* **Note 2**).
3. AM-esters of the chosen indicators (available from Molecular Probes, Eugene, OR, or Teflabs, Austin, TX; *see* **Note 3**) are prepared as 10-m*M* stock solutions in anhydrous dimethyl sulfoxide (DMSO). It is advisable to make 10-µL aliquots of the dye and store in the freezer until use, as repeated freezing and thawing causes degradation of the probe.
4. *N*,*N*,*N*′,*N*′-tetrakis (2-pyridylmethyl)ethylene diamine (TPEN): 10 m*M* in 100% ethanol (Molecular Probes).
5. Ionomycin (Calbiochem, La Jolla, CA): 10 m*M* in DMSO; store in freezer.
6. 4Br-A23187 (Molecular Probes): 10 m*M* in DMSO; store in freezer.
7. Nitrilotriacetic acid (NTA): 1 *M* in $H_2O$ (Sigma).
8. Digitonin: 5 mg/mL in water (Sigma).
9. Ethylene glycol tetraacetic acid (EGTA): 0.5 *M* dissolved in KOH, pH 7.2 (Sigma).
10. 1 *M* $CaCl_2$ (Sigma).
11. Standard Ringer's solution: use a composition appropriate for each cell type. For example: 145 m*M* NaCl, 2.5 m*M* $K_2HPO_4$, 1 m*M* $MgSO_4$, 10 m*M* HEPES, 10 m*M* glucose, 1.8 m*M* $CaCl_2$, pH 7.4.
12. KCl rinse solution: 125 m*M* KCl, 25 m*M* NaCl, 10 m*M* HEPES, 0.2 m*M* $MgCl_2$, pH 7.25.
13. Intracellular buffer: 125 m*M* KCl, 25 m*M* NaCl, 10 m*M* HEPES, 0.5 m*M* $Na_2ATP$, 0.2 m*M* $MgCl_2$, 200 µ*M* $CaCl_2$, 500 µ*M* EGTA to give a final free [$Ca^{2+}$] of

**Table 1**
**Indicators That Have Been Used to Measure [$Ca^{2+}$] in Agonist-Sensitive Internal Stores** [a]

| Indicator | $K_d$ for $Ca^{2+}$ (μ*M*) | Excitation (nm), emission (nm) | Comments |
|---|---|---|---|
| Mag-fura-2 ("furaptra") | 53 | 345/375 ex., 510 em. | Ratiometric |
| Mag-fura-5 | 28 | 340/380 ex., 510 em. | Ratiometric |
| Fura-2-ff | 35 | 340/380 ex., 510 em | Ratiometric; available from Teflabs |
| Mag-indo-1 | 32 | 351 ex., 405/485 em. | Ratiometric (emission) |
| Mag-fura-red | 17 | 488 ex., 630 em. | Fluorescence decreases on $Ca^{2+}$ binding |
| Fluo-3-ff | 41 | 515 ex., 530 em. | Available from Teflabs; fluorescence increases on $Ca^{2+}$ binding |
| Oregon Green BAPTA-5N | 20 | 492 ex., 521 em. | Excited efficiently by 488-nm laser line; fluorescence increases on $Ca^{2+}$ binding |

[a] Dyes are available from Molecular Probes unless otherwise noted.

**Table 2**
**Free [$Ca^{2+}$] of NTA Buffers for *In Situ* Calibration as Calculated by the Computer Program** [a]

| Free [$Ca^{2+}$] (μ*M*) | NTA (m*M*) | [$CaCl_2$] |
|---|---|---|
| 100 | 1 | 489 μ*M* |
| 200 | 1 | 760 μ*M* |
| 300 | 1 | 956 μ*M* |
| 400 | 1 | 1.12 m*M* |
| 600 | 1 | 1.39 m*M* |

[a] Described in **ref. *19***

approx 100 n*M*. Pay careful attention to the pH of this solution (pH 7.25; *see* **Note 4**).

14. Permeabilization solution: Same as the intracellular buffer + 1 μL/mL of digitonin stock solution (final digitonin concentration 5 μg/mL).
15. Calibration solution: for KCl rinse solution add 10 μ*M* ionomycin or 4Br-A23187. For $Ca^{2+}$-free solution, supplement with 1 m*M* EGTA; for high-$Ca^{2+}$ solution, add 10 m*M* $CaCl_2$ (*see* **Note 5**). Intermediate $Ca^{2+}$ concentrations (100, 200, 300 μ*M*, etc.) can be prepared approximately (*see* **Note 6**) by simply adding $CaCl_2$, or if more accuracy is desired, NTA buffers can be used (*see* **Note 7**). Some sample compositions of NTA buffers (calculated from the excellent computer program described in **ref. *20***) are shown in **Table 2**.

## 3. Methods

### 3.1. Loading Cells With Indicators

Add dye directly to cells (in suspension or grown on cover slips) at a final concentration of 2–5 μ*M*, and mix gently. Cultured cells can be put back in the tissue culture incubator. The optimal loading time varies with cell type, but a good starting point is 30 min at 37°C (*see* **Note 8**).

### 3.2. Permeabilizing the Plasma Membrane With Digitonin

A variety of plasma membrane permeabilization techniques have been used previously with good results, e.g., using Streptolysin O (SLO) ***(21)*** or α-toxin ***(15)***. Here, the use of digitonin is described for this purpose:

1. After loading with dye, rinse cells briefly with KCl rinse solution.
2. It is helpful to mount cells into the experimental chamber and follow the permeabilization process on the microscope stage during initial experiments in order to establish optimal permeabilization conditions. Exchange KCl rinse solution with the permeabilization solution containing digitonin. After several minutes cells begin to lose the fluorophore from the cytoplasm resulting in a 60 to 90% drop in fluorescence intensity at 345 nm. When using mag-fura-2 for these measurements, it is usually easier to identify permeabilized cells using the 345-nm excitation, because there will be more contrast between regions of low $Ca^{2+}$ (which yield low fluorescence) and compartments containing high $Ca^{2+}$ (such as the ER). The nucleus, which is devoid of organelles, will be readily apparent as a nonfluorescent central region whereas dye remaining in the periphery should have a reticular distribution (**Fig. 1**).
3. Switch to intracellular buffer without digitonin as soon as the majority of cells have become permeabilized (usually <5 min; *see* **Note 9**).

### 3.3. Measurement of Internal Store [$Ca^{2+}$]

Cells that have been properly permeabilized should have relatively high resting [$Ca^{2+}$] as reported by the fluorophore. Protocols for the measurement of intracellular fluorescence from individual cells (setting of appropriate wavelengths, capture speed, gain, background, and so on) are described in **Chapters 2–4**. Continuous superfusion with intracellular buffer during the experiment is useful to wash away dye that may have leaked from the cells (*see* **Note 10**).

### 3.4. Assessing the Presence of Multiple $Ca^{2+}$ Stores

The AM-ester loading of dyes results in indiscriminate accumulation of indicator into a variety of organelles. When looking at a new cell type for the first time, it is helpful to determine in which functional compartments the dye reports [$Ca^{2+}$] changes. A typical measurement from a mag-fura-2-loaded, digitonin-permeabilized RBL-1 cell is shown in **Fig. 2**.

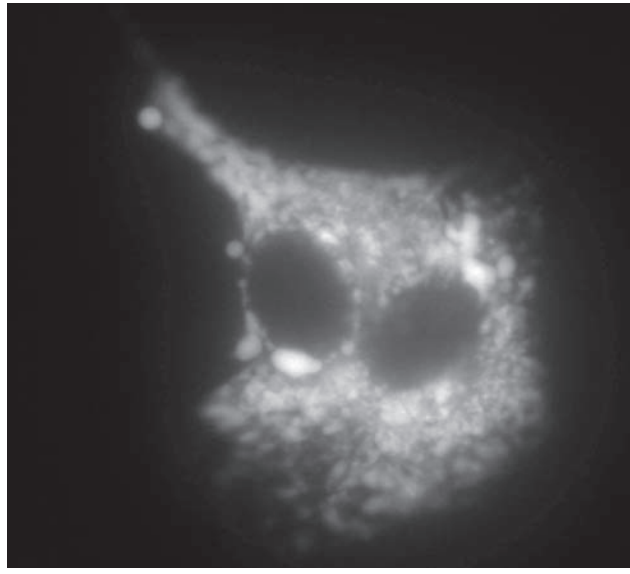

Fig. 1. Fluorescence image of digitonin-permeabilized mag-fura-2-loaded BHK-21 cell. Excitation 345 nm, emission 510 nm.

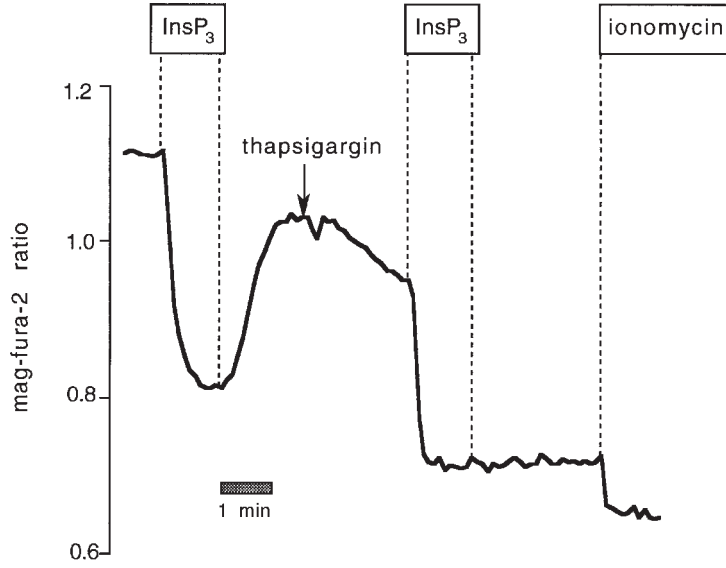


Fig. 2. Typical experimental protocol applied to mag-fura-2/AM-loaded RBL-1 cells to characterize intracellular $Ca^{2+}$ pools (*see* text for details).

1. The cell was superfused continuously with intracellular buffer.
2. Addition of 10 μ*M* $Ins(1,4,5)P_3$ (a supramaximal dose) resulted in a large drop in the ratio owing to the release of $Ca^{2+}$ from internal stores. The ratio recovered when $Ins(1,4,5)P_3$ was removed and the stores were refilled.
3. The cell was next treated with an inhibitor of the internal store $Ca^{2+}$-adenosine triphosphatase, thapsigargin (100 nm). In the absence of active uptake of the cation, a passive outward leak of $Ca^{2+}$ was unmasked. A second stimulation with $Ins(1,4,5)P_3$ released additional $Ca^{2+}$ from the store, but there was no further decrease in the ratio for many minutes, indicating that the $Ins(1,4,5)P_3$ and thapsigargin-sensitive $Ca^{2+}$ pool(s) were empty. At this time, ionomycin was given to release residual $Ca^{2+}$.
4. For this particular cell type, one can conclude that $[Ca^{2+}]$ changes are measured mainly in an $Ins(1,4,5)P_3$- and thapsigargin-sensitive pool, but that a smaller store released only by ionophore is also present (*see* **Note 11**).
5. The contribution of mitochondria (*see* **Note 12**) and acidic $Ca^{2+}$ compartments not accessible to ionomycin (*see* **Note 13**) can be assessed by treating with the appropriate agents. The presence of multiple compartments introduces a particular nonlinearity in the measurement, and complicates the calibration of luminal $[Ca^{2+}]$ ***(9)***.

### *3.5. Calibration*

The most controversial aspect of the technique concerns the quantification of $Ca^{2+}$ in internal stores ***(22)***. Many of the factors affecting the calibration are problems shared by all fluorescent $Ca^{2+}$ indicators (*see* **Chapters 2–4**), e.g., vulnerability of dyes to pH, viscosity, ionic strength, bleaching, dye concentration, and so on. In addition, however, there are some special considerations for calibrating dyes in internal stores. Although the compartmentalized dye approach is an excellent way to monitor dynamic changes in $Ca^{2+}$ stores [such as $Ins(1,4,5)P_3$-induced release], the many problems inherent in the calibration make it unfeasible to make precise quantitative comparisons, particularly among different cell preparations. When only qualitative information is desired, it is often sufficient to express $[Ca^{2+}]$ changes simply as the ratio (or fluorescence intensity changes for single wavelength indicators), keeping in mind that the ratio is not necessarily a linear measure of $[Ca^{2+}]$ (the distortions being more significant at higher $[Ca^{2+}]$ in the case of internal store measurements). Here two basic calibration procedures are described for ratiometric indicators, such as mag-fura-2.

#### *3.5.1. Procedure 1*

This method relies on the relationship originally described by Tsien and collaborators ***(23)*** for calibrating ratiometric probes such as fura-2:

$$[Ca^{2+}] = K_d \cdot (S_{f2}/S_{b2}) \cdot (R - R_{min})/(R_{max} - R)$$

in which the $K_d$ equals the dissociation constant of the probe, $S_{f2}$ is the maximum fluorescence at 375 nm (in zero $Ca^{2+}$), $S_{b2}$ is the minimum fluorescence at 375 nm (in saturating $Ca^{2+}$), R is the measured ratio, and $R_{min}$ and $R_{max}$ are the minimum and maximum ratio in zero and saturating $Ca^{2+}$, respectively.

**Figure 3A** illustrates a typical calibration trace using mag-fura-2-loaded BHK-21 fibroblasts.

1. As in **Fig. 2**, the cells were initially bathed in intracellular buffer, and the Ins(1,4,5)$P_3$-stimulated release was monitored.
2. The minimum ratio ($R_{min}$) was next obtained by treating cells in $Ca^{2+}$-free calibration buffer with 10 μ*M* of ionomycin.
3. $Ca^{2+}$-containing calibration buffer (10 m*M*) was then applied to estimate $R_{max}$.
4. From the raw fluorescence, $S_{b2}$ and $S_{f2}$ are collected.
5. These values are entered into the preceding equation (using a $K_d$ of 53 μ*M*; *see* **Note 14**), to convert ratio data into free [$Ca^{2+}$] (**Fig. 3B**).
6. The apparent resting free [$Ca^{2+}$] of this cell using the standard calibration approach was 490 μ*M*; [$Ca^{2+}$] dropped to 60 μ*M* following Ins(1,4,5)$P_3$ stimulation.
7. A major problem with the preceding approach as applied to compartmentalized low-affinity dyes is that it is frequently quite difficult to obtain a reliable value for $R_{max}$. Ionophores have a limited capacity to equilibrate internal and external [$Ca^{2+}$] (the estimated $K_d$ of ionomycin for $Ca^{2+}$, e.g., is approx 100 μ*M*), and large [$Ca^{2+}$] is required to truly saturate the indicator (10–20 m*M*).
8. An alternative for determination of $R_{max}$ takes advantage of the fact that $Mn^{2+}$ ions (also carried by ionophores) bind the dye with high affinity, and can be used as a surrogate for $Ca^{2+}$ ions. $Mn^{2+}$ quenches fluorescence at both wavelengths, but for mag-fura-2, $Mn^{2+}$ and a saturating [$Ca^{2+}$] cause the same degree of quenching at the $Ca^{2+}$-sensitive wavelength of 375 nm (*see* **Note 15**). $R_{max}$ can be approximated by taking the value of the fluorescence intensity at 345 nm immediately prior to $Mn^{2+}$ addition ($F_{345nm}$), and dividing this by the $Mn^{2+}$-quenched intensity at 375 nm ($F_{375nm}$). It is assumed that the 345-nm intensity will not have changed dramatically over this time. Correspondingly, a more accurate value for $S_{b2}$ (which is the same as $F_{375nm}$) can also be obtained. Using these new values for $R_{max}$ and $S_{b2}$, a second calibrated trace is determined and is shown in **Fig. 3B**. Here the resting [$Ca^{2+}$] was 273 μ*M*, falling to 49 μ*M* after Ins(1,4,5)$P_3$ treatment.

### *3.5.2. Procedure 2*

The second basic calibration approach is the more laborious *in situ* determination, which, in principle, should give more accurate results because the ratio changes are independent of the many factors that can influence the $K_d$ of the dye (viscosity, ionic strength, and so on). One difficulty that remains is the equilibration of internal and external [$Ca^{2+}$], particularly at higher [$Ca^{2+}$] concentrations.

1. Cells were exposed to calibration buffer and ionomycin containing varying free [$Ca^{2+}$]. **Figure 4** shows a typical experiment.

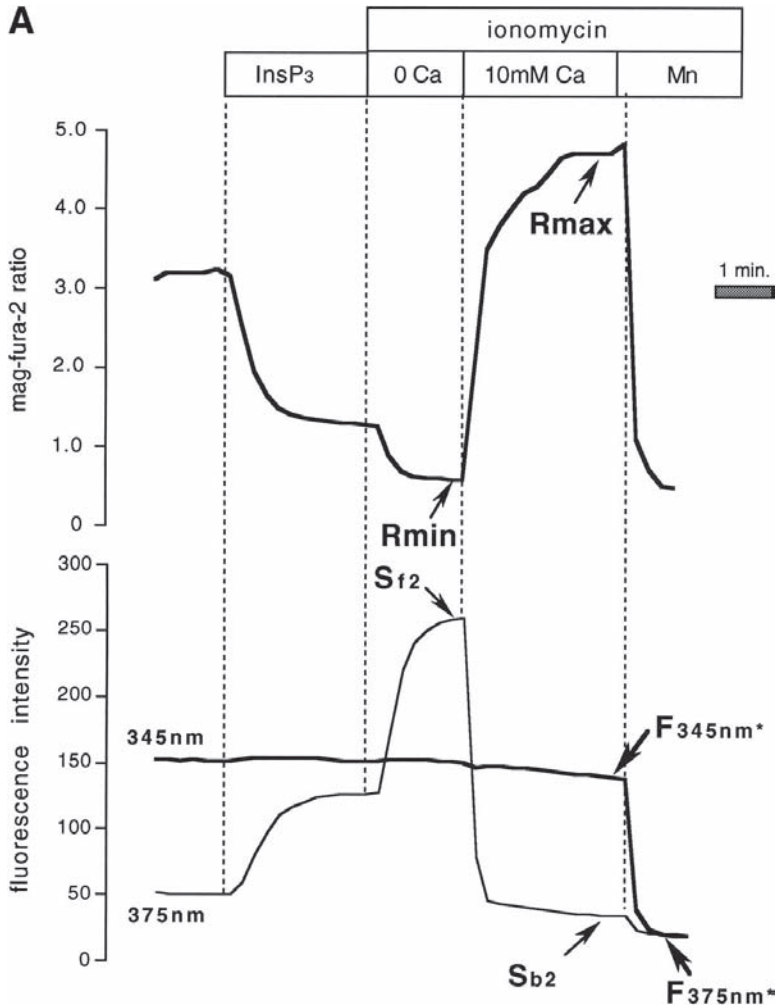


Fig. 3. **(A)** Calibration procedure for mag-fura-2-loaded BHK-21 cells permeabilized with SLO. Determination of $R_{min}$, $R_{max}$, $S_{f2}$, and $S_{b2}$, as well as an estimated $R_{max}$ and $S_{b2}$ based on Mn quenching at 375 nm. The 345-nm wavelength is insensitive to changes in $[Ca^{2+}]$, whereas the 375-nm excitation wavelength is inversely related to $[Ca^{2+}]$. Both wavelengths are quenched by Mn. An alternative way to estimate $R_{max}$ using $F_{345\ nm}/F_{375\ nm}$ may circumvent difficulties in obtaining a true $R_{max}$ with saturating $[Ca^{2+}]$. Note that $F_{375\ nm}$ replaces $S_{b2}$ with this approach. **(B)** *(top, opposite page)* Comparison between calibrated Ins(1,4,5)$P_3$ response using $R_{max}$ and $S_{b2}$ obtained in saturating $[Ca^{2+}]$ ("standard technique;" dotted line) and $R_{max}$ and $S_{b2}$ (the same as $F_{375\ nm}$) obtained with $Mn^{2+}$ ("$Mn^{2+}$ quench technique;" solid trace). Values for $S_{b2}$, $S_{f2}$, and $F_{375\ nm}$ were corrected for bleaching using the 345-nm wavelength prior to calculation of apparent $[Ca^{2+}]$ (*see* **Note 14**).

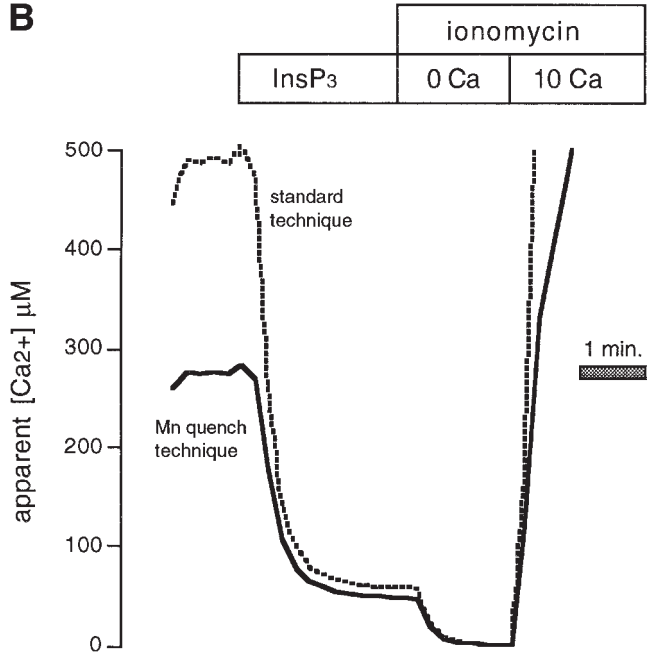


Fig. 3. (**B**)

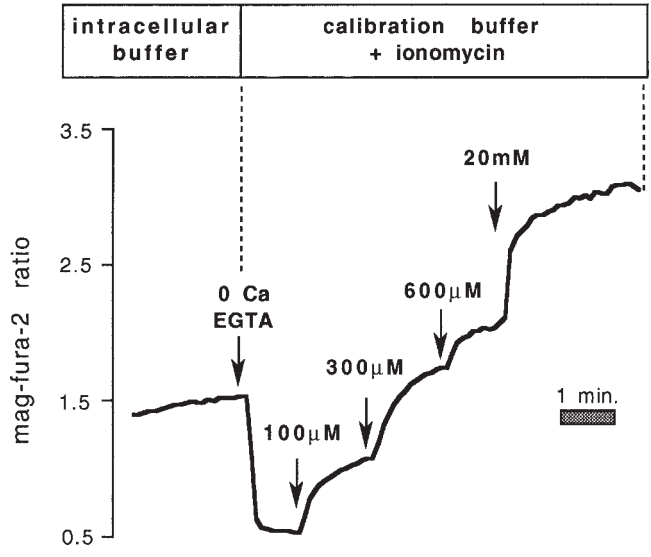


Fig. 4. *In situ* calibration using NTA buffers containing 100, 300, and 600 µ*M* free $Ca^{2+}$. Data from mag-fura-2/AM-loaded BHK-21 fibroblasts permeabilized with SLO (*see* text for details).

2. In this case, there was modest agreement between the $R_{min}/R_{max}$ approach and the values interpolated from the *in situ* data (223 μ*M* starting $[Ca^{2+}]$ vs 147 μ*M*, respectively).

Both calibration procedures are subject to a serious problem: dye may also be present in compartments such as mitochondria in which $[Ca^{2+}]$ is low ("silent compartments"). Therefore, it is not possible to detect $Ca^{2+}$ changes in these organelles (and thereby assess whether they contain dye or not), yet this indicator nevertheless contributes to overall signal, potentially causing underestimation of ER $[Ca^{2+}]$ (*see* **Note 16** and **ref. *22***).

### 3.6. Interference by $Mg^{2+}$ and Heavy Metals

1. Many of the popular indicators used for measuring $[Ca^{2+}]$ in internal stores, such as mag-fura-2, mag-fura-5, mag-indo-1, and mag-fura-red, were, as the names would suggest, originally intended as $Mg^{2+}$ indicators. Several studies have concluded that $[Mg^{2+}]$ changes do not interfere significantly with the measurement of $[Ca^{2+}]$ in Ins(1,4,5)$P_3$-sensitive internal stores ***(9,16,22,24)***, likely because the affinity of these probes for $Ca^{2+}$ is so much higher than for $Mg^{2+}$ (e.g., the $K_d$ of mag-fura-2 for $Mg^{2+}$ in vitro is 1.5 m*M*; *see* **refs. *7*** and ***25***). Nevertheless, it should not be taken for granted that $[Mg^{2+}]$ changes will not be reported by the dye under some conditions. The recent introduction of probes ***(26)*** with reduced sensitivity to $Mg^{2+}$ (e.g., fura-2-ff, fluo-3-ff), provide the possibility to control for such potential artifacts.
2. Another concern is that of heavy metal contamination ***(27,28)***. As is the case with all fluorescent $Ca^{2+}$ dyes, many heavy metals bind the dye molecule with far greater affinity than $Ca^{2+}$ itself (*see* **Note 17**). In the author's experience, the extent to which heavy metals perturb the measurement depends a great deal on the cell type (*see* **Note 18**). Sometimes the spectral effect of these contaminating ions is to mimic $Ca^{2+}$ ions, thus giving a false, high $[Ca^{2+}]$ measurement. Alternatively, many heavy metals quench the fluorescence of indicators, causing a reduction in sensitivity toward $Ca^{2+}$.
3. To diagnose whether these ions are interfering with the measurement of internal store $Ca^{2+}$, supplement the intracellular buffer with a low dose (10 μ*M*) of the membrane-permeant heavy-metal chelator TPEN. In the case of mag-fura-2, the ratio may or may not drop, whereas the individual fluorescence intensities will increase at both wavelengths as the TPEN competes for heavy metals bound to the dye. It may be necessary to perform control experiments in the presence of TPEN to test whether the biological phenomenon under study is influenced by contaminating ions.

It is noteworthy that TPEN also binds $Ca^{2+}$ with relatively low affinity ($K_d$ for $Ca^{2+}$ approx 100–200 μ*M*). High concentrations of TPEN (200–1000 μ*M*) have been used to rapidly and reversibly clamp levels of free $[Ca^{2+}]$ in the internal store without affecting total store $Ca^{2+}$ or causing $Ca^{2+}$ changes in the cytoplasm ***(29–31)***.

### *3.7. Troubleshooting*

Beginners to this technique may experience one or more of the following problems during the course of their experiments:

1. Cells and organelles appear not to load with dye. Check whether the nonpermeabilized cells also have a low fluorescence, which, assuming that the microscope optics and equipment are in proper order, may be improved by increasing dye concentration, changing loading times, changing temperature, or trying a different indicator, if possible.
2. Cells are unresponsive to Ins(1,4,5)$P_3$. Are the cells really permeabilized or might they be overpermeabilized? Excessive loading can also yield poor results because of buffering of [$Ca^{2+}$] changes by the indicator (*see also* **Subheading 3.6.2.**). In the case of cultured cells, it is sometimes necessary simply to use a newer passage of cells, as some cell types seem to lose responsiveness to Ins(1,4,5)$P_3$ and agonists following many generations.
3. The resting $Ca^{2+}$ concentrations in the ER are very low. Check that the background of the measuring system is set appropriately. Also be aware that some lipophilic $Ca^{2+}$-releasing agents, such as thapsigargin and ionomycin, can be extremely pernicious in sticking to plastic elements of the superfusion system (*see* **Note 19**); hence, stored $Ca^{2+}$ may have been inadvertently released before the measurement even started.

### *3.8. Combined Patch-Clamp and Internal Store $Ca^{2+}$ Measurements*

In a whole-cell patch-clamp configuration, it is possible to dialyze the cytoplasmic indicator via the patch pipet, leaving behind organelle-trapped dye and an intact, functional plasma membrane. The combination of these techniques affords a number of exciting experimental possibilities. Tse et al. ***(10)*** used this approach to monitor hormone-induced $Ca^{2+}$ oscillations in internal stores simultaneously with measurements of cytoplasmic $Ca^{2+}$ (assessed indirectly as the activity of a $Ca^{2+}$-activated $K^+$ current). Alternatively, fluorescent indicators with compatible spectral properties can be loaded into the cytoplasm via the patch pipet, permitting simultaneous measurements of [$Ca^{2+}$] in both compartments ***(11,32)***. An example of another type of problem addressed by this approach is shown in **Fig. 5**.

1. A whole-cell current recording of $I_{CRAC}$ (a $Ca^{2+}$ current activated by depletion of internal stores) was monitored concurrently with internal store [$Ca^{2+}$] as measured by compartmentalized fura-2-ff ***(29)***. The time course for the dilution of the probe into the patch pipet is shown in **Fig. 5** (upper records).
2. Treatment with ionomycin resulted in a drop in the fura-2-ff ratio **Fig. 5** (middle record), and the activation of a $Ca^{2+}$ current (bottom record).

### *3.9. Measurements in Intact Cells*

Although agonist-evoked changes of internal store [$Ca^{2+}$] were readily detectable in intact cells in the original mag-fura-2 measurements on gastric epithe-

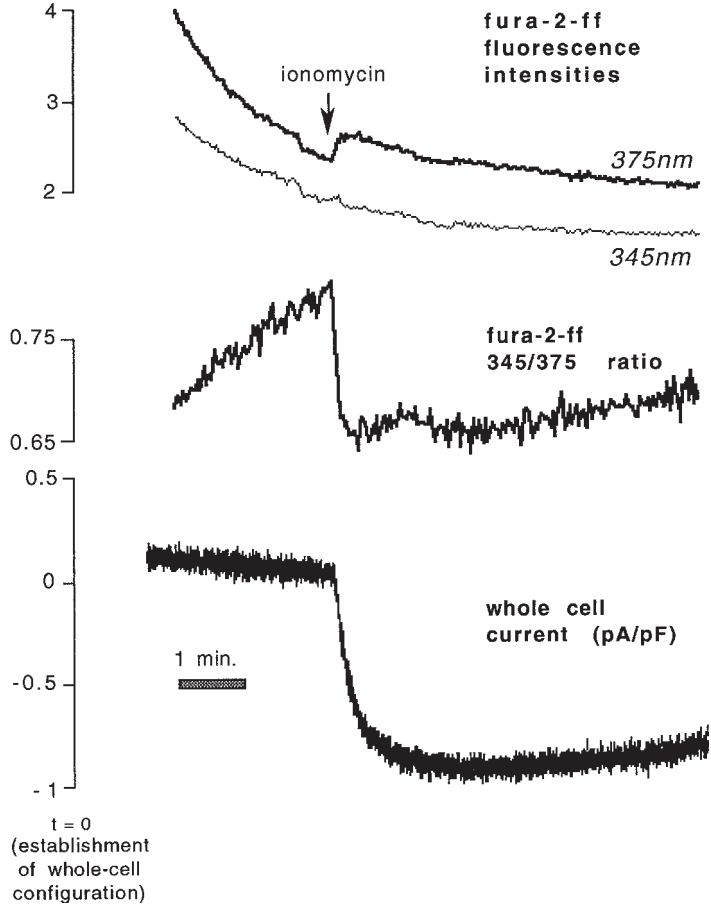


Fig. 5. Simultaneous whole-cell current measurement of $I_{CRAC}$ and 345 nm/375 nm fluorescence ratio from compartmentalized fura-2-ff in RBL-1 cell. Top record shows individual fluorescence intensities, which declined as cytosolic dye was dialyzed into the patch pipet. Ionomycin caused a rapid drop in the ratio (middle record) and activated an inward current (bottom record).

lial cells ***(8)***, releasing cytoplasmic indicator eliminated the large background fluorescence from this dye, and improved the resolution of the measurement enormously. Recently, however, the author and others have observed that in the absence of any special treatment, certain cell types seem to export cytoplasmic dye, resulting in preferential accumulation of mag-fura-2 and other AM-ester indicator derivatives in organelles ***(17,30,33,34)***. For example, in the majority of BHK-21 fibroblasts loaded with 2μ*M* of mag-fura-2 for 45 min to 1 h at 37°C, >85% (and often 100%) of the dye was localized in organelles

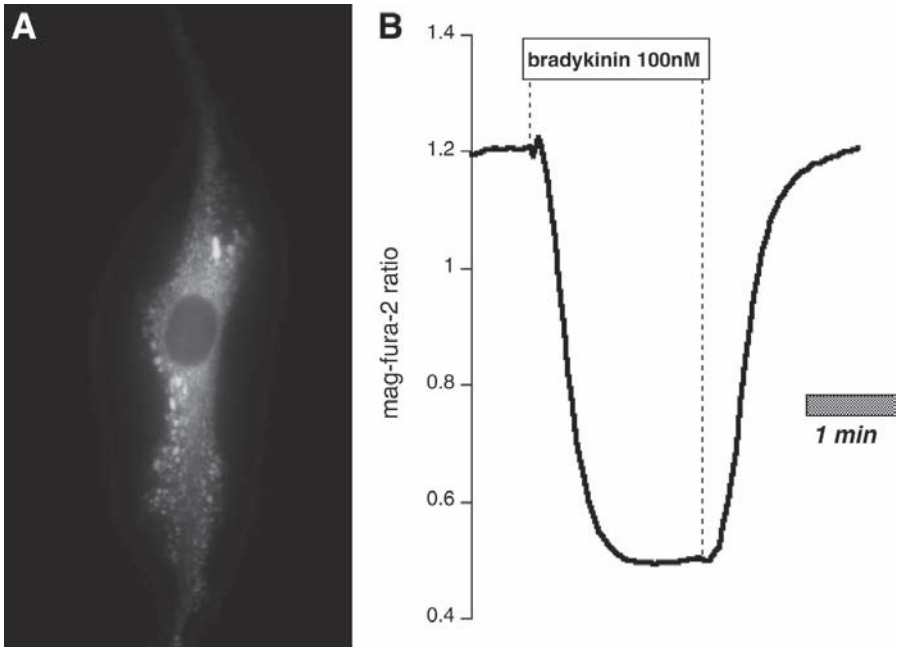


Fig. 6. Intact BHK-21 fibroblast loaded for 45 min at 37°C with 2 μ*M* mag-fura-2 (excitation 345 nm, emission, 510 nm). The mag-fura-2 ratio decreases during treatment with the $Ca^{2+}$-mobilizing hormone bradykinin (100 n*M*).

(*see* **Note 20**). This has allowed high-resolution measurements of free [$Ca^{2+}$] changes in internal stores in response to native $Ca^{2+}$-mobilizing agonists in intact cells ***(30,33,34)***. The typical appearance of an intact mag-fura-2-loaded fibroblast and its response to the $Ca^{2+}$-mobilizing hormone bradykinin is shown in **Fig. 6**.

### *3.10. Conclusions and Future Directions*

Because many laboratories are already equipped for making cytoplasmic [$Ca^{2+}$] measurements with fluorescent probes, such as indo-1 and fura-2, it is straightforward to combine existing equipment with the methodology described in this chapter toward the measurement of [$Ca^{2+}$] in agonist-sensitive $Ca^{2+}$ stores. A major disadvantage of this approach is the nonspecific intracellular localization of dye. Complementary approaches employing ER-targeted probes, such as those based on the $Ca^{2+}$-sensitive photoprotein aequorin ***(35–37)*** have resolved some of these issues, although it is in practice quite challenging to image $Ca^{2+}$ in single cells using this luminescent reporter. In addition, aequorin relies on the incorporation of a cofactor, coelenterazine,

which becomes consumed during the course of the measurement, and restricts the length of experiments.

Recently there has been exciting progress in the development of genetically encoded green fluorescent protein (GFP)-based $Ca^{2+}$ sensors ***(38,39,40)***. Like aequorin, these probes are amenable to targeting to specific subcellular compartments, with the added advantage of a relatively bright fluorescence signal that like mag-fura-2, permits imaging at the single cell level. Currently, Miyawaki, Tsien, and others have produced several generations of targeted GFP-based probes. Among the most promising of these are the "pericam" class of indicator ***(39)***. All three approaches (compartmentalized dye, ER-targeted luminescent, and GFP-based indicators) have thus far yielded excellent qualitative agreement, and reasonably good quantitative concurrence in living cells. Compartmentalized dyes still hold an advantage over these newer probes in at least one regard, because this approach can be applied to primary cells and tissues resistant to DNA transfection. In the future we can hope for improved indicators that combine all of the desirable features of compartmentalized dyes and genetically encoded indicators to permit versatile measurements of ER $Ca^{2+}$ dynamics in any cell type ***(40)***.

## 4. Notes

1. The success of the measurement relies to some extent on cell type, as cells differ greatly with respect to their cytological composition and their handling of dye (*see* **Subheading 3.4.**). For example, much better results have been obtained in our hands with baby hamster kidney (BHK-21) fibroblasts than pancreatic acinar cells or rat basophilic leukemia (RBL) cells. RBL cells appear to have an ER that occupies a very small part of the cell volume, resulting in a poor signal-to-noise ratio.
2. Mag-fura-2 (also called "furaptra"), has been by far the most popular indicator for this purpose to date. This probe is similar to fura-2 in its spectral properties: the 345:375 nm excitation ratio (peak emission at 510 nm) is proportional to free $[Ca^{2+}]$. Mag-fura-2 is extremely bright and loads quite well into cells, generally giving very high levels of intracellular fluorescence.
3. New dyes suitable for this purpose continue to be developed. A good resource for information on new low-affinity $Ca^{2+}$ indicators is the web site provided by Molecular Probes (www.probes.com), which sells most of the fluorescent dyes. Teflabs is also a good source of indicators, including some "unique" products available only through them.
4. One may have to experiment with different intracellular buffer compositions to find the recipe that works best for a given cell type. For example, [ATP] can be varied, or BAPTA may be used as the $Ca^{2+}$ buffer instead of EGTA, the $Ca^{2+}$-buffering properties of which are highly sensitive to pH. The author also observed that organelle morphology is better preserved when a portion of the $Cl^-$ in the intracellular buffer is substituted with an impermeant anion, such as gluconate (added, e.g., as K gluconate, leaving 25 m*M* of NaCl in the solution).

5. Be aware that when EGTA is added to a $Ca^{2+}$-containing solution (and vice versa), many protons are liberated in the process, resulting in dramatic acidification of the medium. Therefore, when making $Ca^{2+}$-free solutions it is best to add EGTA to a nominally $Ca^{2+}$-free buffer (otherwise, be sure to check the pH).
6. Remember that the activity coefficient for $CaCl_2$ in a typical Ringer's solution is considerably less than 1, meaning that, strictly, speaking, the actual free [$Ca^{2+}$] (which is what is seen by the dye) is approx 50 to 80% of the total added $Ca^{2+}$.
7. A good computer program that can calculate free [$Ca^{2+}$] of multiple buffer systems, such as the MaxChelator program ***(20)*** by Chris Patton and colleagues, is indispensable. This superb program is available for free on the website: http://www.stanford.edu/~cpatton/maxc.html. By experimenting with these programs, one often learns many surprising things about the effects of pH, ionic strength, and interactions with other buffer constituents, such as ATP, on the free [$Ca^{2+}$] in solution.
8. There is a lot of variability among the various cell types with respect to optimal loading times. For example, in the case of BHK-21 fibroblasts, loading for extended periods of time or with higher probe concentration does not necessarily yield better results (but *see* **Subheading 3.9.**). In some cells it appears that the probe is degraded or transported to other organelles (perhaps lysosomes), where it remains as a $Ca^{2+}$-insensitive form.
9. To maintain organelle integrity, incubate as briefly as possible with the minimum digitonin concentration. The permeabilization process is accelerated at 37°C. Digitonin appears to lose its membrane permeabilizing properties with excessive agitation.
10. Leaked dye can cause a suppression of mag-fura-2 ratio changes because this probe is bright in its $Ca^{2+}$-unbound form. This means that extravesicular dye will contribute disproportionately to the background (*see* **ref.** ***22*** for details). Measurements in cuvets (in which released dye remains in the medium) may therefore be impractical with probes that share this spectral property.
11. Cell types vary greatly with respect to their organellar constitution and their handling of dye. In contrast to RBL-1 cells, BHK-21 fibroblasts appear to measure [$Ca^{2+}$] changes only in a thapsigargin- and Ins(1,4,5)$P_3$-releasable pool, which greatly simplifies data analysis.
12. Mitochondrial inhibitors such as FCCP plus oligomycin block $Ca^{2+}$ uptake by collapsing the electrochemical gradient across the inner mitochondrial membrane ***(41)***. Ruthenium red blocks the mitochondrial $Ca^{2+}$ uniporter, the principal pathway for $Ca^{2+}$ uptake. Although this organelle is notorious for compartmentalizing AM-esters, the high $K_d$ of indicators, such as mag-fura-2, effectively filters out detection of [$Ca^{2+}$] changes in this space because the resting [$Ca^{2+}$] is generally quite low (however, *see* **ref.** ***9***, and note that mag-fura-2 has been used in many preparations, such as skeletal muscle, to measure very robust cytoplasmic $Ca^{2+}$ transients).
13. Because ionomycin functions as an electroneutral $Ca^{2+}/H^+$ exchanger, it is inefficient at releasing $Ca^{2+}$ from compartments with low pH, such as secretory granules. The combination of monensin (an $Na^+/H^+$ exchanging ionophore) plus

ionomycin is more effective, and may reveal the presence of additional compartments ***(42)***.

14. As is the case with cytosolic indicators, the $K_d$ *in situ* can vary considerably with respect to values determined in vitro ***(24)***. The ability to monitor the $Ca^{2+}$-insensitive wavelength is advantageous because corrections for the decline in intensity at both wavelengths over time (owing to bleaching and dye leakage) can be applied to values obtained for $S_{b2}$ and $S_{f2}$.
15. This assumption should be checked when using indicators other than mag-fura-2.
16. The author has observed that the starting mag-fura-2 ratio values can be quite variable from cell to cell, but that these differences are reduced somewhat when the indicator is calibrated. This variation may be, in part, the result of a form of dye trapped in compartments that is insensitive to $Ca^{2+}$, causing a large background that suppresses the ratio. Although it is quite possible that the actual free luminal [$Ca^{2+}$] may differ from cell to cell, the contribution of silent compartments may also vary, causing an apparent heterogeneity.
17. Mag-fura-2, for example, is exquisitely sensitive to zinc ions ($K_d$ = 20 n*M*; **ref. *43***), and in fact can be used as an indicator for this cation, which is rather abundant in many cell types.
18. RBL-1 cells, for example, have a considerable pool of heavy metals, whereas BHK-21 cells appear to have none as assessed by this technique.
19. Often the offending contaminants will not perturb measurements in intact cells (leading one to believe that their particular regimen of cleaning is adequate), but can pose problems in permeabilized cells, which tend to be much more sensitive to minute traces of these agents. Rinsing thoroughly with the appropriate solvent (e.g., ethanol) is advisable between experiments.
20. Although prolonged dye incubation is key to success with intact cell measurements, overloading of cells does not usually produce desirable results, because indicators appear to be lost from the ER or redistribute to other compartments with time. It is therefore important to determine the time window that optimizes cytosolic exclusion and internal store retention of dye for each cell type. Some cell types (e.g., HEK-293 cells) have not been amenable to this approach whatsoever in our hands.

## Acknowledgments

The author would like to thank the many colleagues who have given help and support over the years, including Drs. Paul Negulescu, Terry Machen, Irene Schulz, Silvana Curci, and Tullio Pozzan.

## References

1. Williams, D. A., Fogarty, K. E., Tsien, R. Y., and Fay, F. S. (1985) Calcium gradients in single smooth muscle cells revealed by the digital imaging microscope using Fura-2. *Nature* **318,** 558–561.
2. Roe, M. W., Lemasters, J. J., and Herman, B. (1990) Assessment of fura-2 for measurements of free cytosolic calcium. *Cell Calcium* **11,** 63–73.

3. Terasaki, M. and Sardet, C. (1991) Demonstration of calcium uptake and release by sea urchin cortical endoplasmic reticulum. *J. Cell Biol.* **115,** 1031–1037.
4. Connor, J. A. (1993) Intracellular calcium mobilization by inositol 1,4,5-trisphosphate: intracellular movements and compartmentalization. *Cell Calcium* **14,** 185–200.
5. Glennon, M. C., Bird, G. St. J., Takemura, H., Thastrup, O., Leslie, B. A., and Putney, J. W., Jr. (1992) In situ imaging of agonist-sensitive calcium pools in Ar4-2J pancreatoma cells. *J. Biol. Chem.* **267,** 25,568–25,575.
6. Short, A. D., Klein, M. G., Schneider, M. F., and Gill, D. L. (1993) Inositol 1,4,5-trisphosphate-mediated quantal $Ca^{2+}$ release measured by high resolution imaging of $Ca^{2+}$ within organelles. *J. Biol. Chem.* **268,** 25,887–25,893.
7. Raju, B., Murphy E., Levy, L. A., Hall, R. D., and London, R. E. (1989) A fluorescent indicator for measuring cytosolic free magnesium. *Am. J. Physiol.* **256,** C540–C548.
8. Hofer, A. M. and Machen, T. E. (1993) Technique for in situ measurement of calcium in intracellular $InsP_3$-sensitive stores using the fluorescent indicator mag-fura-2. *Proc. Natl. Acad. Sci. USA* **90,** 2598–2602.
9. Hofer A. M. and Machen, T. E. (1994) Direct measurement of free $Ca^{2+}$ in organelles of gastric epithelial cells. *Am. J. Physiol.* **267,** G442–G451.
10. Tse, F. W., Tse, A., and Hille, B. (1994) Cyclic $Ca^{2+}$ changes in intracellular stores of gonadotropes during gonadotropin-releasing hormone-stimulated $Ca^{2+}$ oscillations. *Proc. Natl. Acad. Sci. USA* **91,** 9750–9754.
11. Chatton, J.-Y., Liu, H., and Stucki, J. W. (1995) Simultaneous measurement of $Ca^{2+}$ in the intracellular stores and cytosol of hepatocytes during hormone-induced $Ca^{2+}$ oscillations. *FEBS Lett.* **368,** 165–168.
12. Hajnóczky, G. and Thomas, A. P. (1997) Minimal requirements for calcium oscillations driven by the IP3 receptor. *EMBO J.* **16,** 3533–3543.
13. Hirose, K. and Iino, M. (1994) Heterogeneity of channel density in inositol-1,4,5-trisphosphate-sensitive $Ca^{2+}$ stores. *Nature* **372,** 791–794.
14. Sugiyama, T. and Goldman, W. F. (1995) Conversion between permeability states of IP3 receptors in cultured smooth muscle cells. *Am. J. Physiol.* **269,** C813–C818.
15. Steenberger, J. M. and Fay, F. S. (1996) The quantal nature of calcium release to caffeine in single smooth muscle cells results from activation of the sarcoplasmic reticulum $Ca^{2+}$-ATPase. *J. Biol. Chem.* **271,** 1821–1824.
16. Hofer, A. M., Schlue, W. R., Curci, S., and Machen, T. E. (1995) Spatial distribution and quantitation of free luminal [$Ca^{2+}$] within the $InsP_3$-sensitive internal store of individual BHK-21 cells: Ion dependence of $InsP_3$-induced $Ca^{2+}$ release and reloading. *FASEB J.* **9,** 788–798.
17. Golovina, V. A. and Blaustein, M. P. (1997) Spatially and functionally distinct $Ca^{2+}$ stores in sarcoplasmic and endoplasmic reticulum. *Science* **275,** 1643–1648.
18. van de Put, F. H. and Elliott, A. C. (1996) Imaging of intracellular calcium stores in individual permeabilized pancreatic acinar cells: Apparent homogeneous cellular distribution of inositol 1,4,5-trisphosphate-sensitive stores in permeabilized pancreatic acinar cells. *J. Biol. Chem.* **271,** 4999–5006.

19. Park, M. K., Petersen, O. H., and Tepikin, A. V. (2000) The endoplasmic reticulum as one continuous Ca2+ pool: visualization of rapid Ca2+ movements and equilibration. *EMBO J*. **19,** 5729–5739.
20. Bers, D. M., Patton, C. W., and Nuccitelli, R. (1994) A practical guide to the study of calcium in living cells, in *Methods in Cell Biology*, vol. 40 (Nuccitelli, R., ed.) . Academic, San Diego, CA, pp. 3–29.
21. Hofer, A. M., Curci S., Machen T. E., and Schulz I. (1996) ATP regulates the passive leak from agonist-sensitive internal calcium stores. *FASEB J*. **10,** 302–303.
22. Hofer, A. M. and Schulz, I. (1996) Quantification of intraluminal free [$Ca^{2+}$] in the agonist-sensitive internal calcium store using compartmentalized fluorescent indicators: Some considerations. *Cell Calcium* **20,** 235–242.
23. Grynkiewicz, G., Poenie, M., and Tsien, R. Y. (1985) A new generation of $Ca^{2+}$ indicators with greatly improved fluorescence properties. *J. Biol. Chem.* **260,** 3440–3450.
24. Sugiyama, T. and Goldman, W. F. (1995) Measurement of SR free $Ca^{2+}$ and Mg in permeabilized smooth muscle cells with use of furaptra. *Am. J. Physiol*. **269,** C698–C705.
25. London, R. E. (1991) Methods for measurement of intracellular magnesium: NMR and fluorescence. *Annu. Rev. Physiol*. **53,** 241–258.
26. London, R. E., Rhee, C. K., Murphy, E., Gabel, S., and Levy, L. A. (1994) NMR-sensitive fluorinated and fluorescent intracellular calcium ion indicators with high dissociation constants. *Am. J. Physiol*. **266,** C1313–C1322.
27. Arslan, P., Di Virgilio, F., Betrame, M., Tsien, R. Y., and Pozzan, T. (1985) Cytosolic $Ca^{2+}$ homeostasis in Ehrlich and Yoshida carcinomas: a new membrane-permeant chelator of heavy metals reveals that these ascites tumor cell lines have normal cytosolic free $Ca^{2+}$. *J. Biol. Chem.* **260,** 2719–2727.
28. Snitsarev, V. A., McNulty, T. J., and Taylor, C. W. (1996) Endogenous heavy metal ions perturb fura-2 measurements of basal and hormone-evoked $Ca^{2+}$ signals. *Biophys. J*. **71,** 1048–1056.
29. Hofer, A. M., Fasolato, C., and Pozzan, T. (1998) Capacitative $Ca^{2+}$ entry is closely linked to the filling state of internal $Ca^{2+}$ stores: a study using simultaneous measurements of $I_{CRAC}$ and intraluminal [$Ca^{2+}$]. *J. Cell Biol*. **140,** 325–334.
30. Caroppo, R., Colella, M., Colasuonno, A., et al. (2003) A reassessment of the effects of luminal [$Ca^{2+}$] on inositol 1,4,5-trisphosphate-induced $Ca^{2+}$ release from internal stores. *J. Biol. Chem.* **278,** 39,503–39,508.
31. Hofer, A. M. (2001) Using low-affinity fluorescent calcium indicators and chelators for monitoring and manipulating free [$Ca^{2+}$] in the endoplasmic reticulum, in *Calcium Signaling. A Practical Approach* (Tepikin, A., ed.) Oxford University Press, Oxford, UK, pp. 111–124.
32. Mogami, H., Tepikin, A. V., and Petersen, O. H. (1998) Termination of cytosolic $Ca^{2+}$ signals: $Ca^{2+}$ reuptake into intracellular stores is regulated by the free $Ca^{2+}$ concentration in the store lumen. *EMBO J*. **17,** 435–442.

33. Hofer, A. M., Landolfi, B., Debellis, L., Pozzan, T., and Curci, S. (1998) Free [$Ca^{2+}$] dynamics measured in agonist-sensitive stores of single living intact cells: a new look at the refilling process. *EMBO J*. **17,** 1986–1995
34. Landolfi, B., Curci, S., Debellis, L. A., Pozzan, T., and Hofer, A.M. (1998). $Ca^{2+}$ homesostasis in the agonist-sensitive internal store: functional interactions between mitochondria and the ER measured *in situ* in intact cells. *J. Cell Biol*. **142,** 1235–1243.
35. Montero, M., Brini, M., Marsault, R., Alvarez, J., Sitia, R., Pozzan, T., and Rizzuto, R. (1995) Monitoring dynamic changes in free $Ca^{2+}$ concentration in the endoplasmic reticulum of intact cells. *EMBO J*. **14,** 5467–5475.
36. Kendall, J. M., Dormer, R. L., and Campbell, A. K. (1994) Changes in free calcium in the endoplasmic reticulum of living cells detected using targeted aequorin. *Anal. Chem*. **221,** 173–181.
37. Hofer, A. M. and Pozzan, T. (1999*)* Use of compartmentalized calcium indicators and recombinant aequorins in calcium signaling research, in *Methods in Signal Transduction Research* (J.W. Putney, Jr., ed.) CRC Press, Boca Raton, FL, pp. 47–69.
38. Yu, R. and Hinkle, P. M. (2000) Rapid turnover of calcium in the endoplasmic reticulum during signaling–studies with cameleon calcium indicators *J. Biol. Chem*. **275,** 23,648–23,653
39. Miyawaki, A., Mizuno, H., Nagai, T., and Sawano, A. (2003) Development of genetically encoded fluorescent indicators for calcium. *Methods Enzymol*. **360,** 202–225.
40. Tsien, R. Y. (2003) Imagining imaging's future: review. *Nat. Rev. Mol. Cell Biol*. (Suppl), SS16–SS21.
41. Gunter, T. E. and Pfeiffer, D. R. (1990) Mechanisms by which mitochondria transport calcium. *Am. J. Physiol*. **258,** C755–C786.
42. Fasolato, C., Zottini, M., Clementi, E., Zacchetti, D., Meldolesi, J., and Pozzan, T. (1991) Intracellular $Ca^{2+}$ pools in PC-12 cells: three intracellular pools are distinguished by their turnover and mechanisms of $Ca^{2+}$ accumulation, storage, and release. *J. Biol. Chem*. **266,** 20,159–20,167.
43. Simons, T. J. B. (1993) Measurement of free $Zn^{2+}$ ion concentration with the fluorescent probe mag-fura-2 (furaptra). *J. Biochem. Biophys. Methods* **27,** 25–37.

# V

# Specialist Measurement Techniques

# 16

# Measurement of $[Ca^{2+}]_i$ in Smooth Muscle Strips Using Front-Surface Fluorimetry

**Hideo Kanaide**

## 1. Introduction

In regulating the contraction of smooth muscle cells, changes in the cytosolic concentrations of $Ca^{2+}$ ($[Ca^{2+}]_i$) play a primary role as the initiation of contraction is associated with $Ca^{2+}$ binding to calmodulin with the subsequent activation of myosin light chain kinase. During the contraction induced by receptor-mediated stimulation, however, there are temporal changes in the relationship between $[Ca^{2+}]_i$ and the developed tension. Furthermore, the receptor-mediated stimulation also produces a proportionately greater tension for a given change in $[Ca^{2+}]_i$ than does $K^+$ depolarization. Therefore, it is important to measure $[Ca^{2+}]_i$ and tension simultaneously in order to determine the molecular and cellular mechanisms in both the regulation of contraction and relaxation of smooth muscle. For this purpose, front-surface fluorimetry of fura-2, a $[Ca^{2+}]_i$ indicator dye ***(1)***, has been performed on small smooth muscle strips ***(2,3)***.

The technique of front-surface fluorimetry is commonly used for measuring tissue fluorescence. The first and, so far, the only successful technique known to monitor the naturally occurring fluorescence of intact tissue in surface fluorimetry was developed by Chance et al. ***(4)***. Using surface fluorimetry and a perfused rat heart, they reported the depth of penetration of excitation light (366 nm), and hence the detection of fluorescence (460 nm), to be 0.4 mm, and studied the kinetics of mitochondrial flavoprotein and the reduced form of pyridine nucleotide in the myocardium. They also developed a front-surface fluorometer utilizing a bifurcated fiber-optic light source to perform surface fluorimetry of the kidney ***(5)***. The underlying principle of front-surface fluorimetry is simple: the closer the distance between the excitation light source

From: *Methods in Molecular Biology, vol. 312: Calcium Signaling Protocols: Second Edition*
Edited by: D. G. Lambert © Humana Press Inc., Totowa, NJ

(and also the detector) and the object, the easier and more accurate the detection of the emission light becomes.

In the author's front-surface fluorometer, concentric optic fibers are used: the excitation light is guided through quartz optic fibers arranged in an inner circle, and emission light is collected by glass optic fibers arranged in an outer circle. By preparing small-sized specimens of smooth muscle strips, the entire front surface of the sample can be illuminated, and almost the whole fluorescence signal from the front-surface can be detected by the use of concentric optic fibers placed close to the sample.

One of the advantages of using a fura-2 signal is the ratiometric measurement of two excitation wavelengths, which cancels the parallel changes in the intensities of the two emitted light signals induced by the moving artifact produced by the contraction, shortening, or torsion of the sample, and changing or bubbling of the solutions. In addition, since the emitted light from the entire front surface of the sample strip is detected by these confronted optical fibers, the amount of the observed fura-2 dye is thus kept constant, while any possible artifact owing to the movement or changing shape of the strips during contraction is eliminated as far as possible. Therefore, the signals obtained of front-surface fura-2 fluorescence simply indicate the changes in $[Ca^{2+}]_i$ of the smooth muscle cells and not the artifacts owing to either the contraction or movement of the smooth muscle strips.

## 2. Materials

1. $[Ca^{2+}]_i$ indicator dyes: These dyes are all directly purchased in special packaging from the manufacturers. Fura-2/AM (mol wt = 1002; an acetoxymethyl [AM] form of fura-2) is from Molecular Probes (Eugene, OR) and Dojindo Laboratory (Kumamoto, Japan), and fura-PE3/AM (mol wt = 1258) is from TEFLABS (Austin, TX). Small plastic tubes in special packaging contain either fura-2/AM or fura-PE3/AM dry powder, 50 μg each, and are stored at –20°C.
2. Fura-2 loading buffer: Oxygenated (bubbling with a mixture of 95% $O_2$ and 5% $CO_2$), Dulbecco's modified Eagle's medium (Gibco, Grand Island, NY) containing fura-2/AM (or fura-PE3/AM), 5% inactivated fetal bovine serum (FBS) (Gibco), and whenever necessary, pluronic F127 (TEFLABS), cremophor EL (Sigma, St. Louis, MO), and/or probenecid (Sigma), as shown in **Table 1**.
3. Normal physiological salt solution (PSS): 123 m*M* NaCl, 4.7 m*M* KCl, 15.5 m*M* $NaHCO_3$, 1.2 m*M* $KH_2PO_4$, 1.2 m*M* $MgCl_2$, 1.25 m*M* $CaCl_2$, and 11.5 m*M* D-glucose. $Ca^{2+}$-free PSS contains 2 m*M* EGTA instead of $CaC1_2$. High-$K^+$ PSS is of the same composition as normal PSS, except for the equimolar substitution of KCl for NaCl.
4. Quartz organ bath: A quartz cuvet (5 mL; $1 \times 1 \times 5$ cm) is used. Three faces of the cuvet are covered with a quartz water jacket to maintain the experimental temperature, whereas one free face of the cuvet is used for surface fluorimetry.

**Table 1**
**Conditions for Fura-2 Loading on Smooth Muscle Cells** [a]

| Species | Smooth muscle | Concentrations of fura-2/AM (μ*M*) | Incubation time (h) | Other additions |
|---|---|---|---|---|
| Human | Umbilical artery | 50 | 4 | — |
| | Urinary bladder | 25 | 6 | — |
| Bovine | Mid-cerebral artery | 50 | 4 | — |
| | Ophthalmic artery | 50 | 4 | — |
| | Coronary artery | 50 | 4 | — |
| | Pedal artery | 50 | 4 | — |
| Pig | Coronary artery | 25 | 4 | — |
| | Pulmonary artery | 25 | 4 | — |
| | Pulmonary vein | 25 | 4 | — |
| | Renal artery | 50 | 4 | — |
| | Trachea | 50 | 4 | — |
| | Urinary bladder | 40 [b] | 6 | 0.1% Pluronic F127 |
| Rabbit | Basilar artery | 10 | 3 | — |
| | Ear artery | 40 [b] | 4 | — |
| | Femoral artery | 50 | 4 | — |
| | Saphenous vein | 40 [b] | 6 | 0.1% Pluronic F127 |
| | Vein graft | 40 [b] | 6 | 0.1% Pluronic F127 |
| | Corpus cavernosum | 50 [b] | 7 | — |
| Rat | Basilar artery | 25 | 3 | — |
| | Aorta | 25 | 3 | 0.08% Cremophor EL, 1 m*M* probenecid |
| | Myometrium | 40 [b] | 6 | 0.1% Pluronic F127 |
| | Cultured aortic cells | 10 | 1 | — |
| Guinea pig | Taenia coli | 50 [b] | 8 | 0.02% Pluronic F127 |

[a] FBS (5%) is added to all loading solutions and temperature is 37°C.
[b] Instead of fura-2/AM, fura-PE3 is utilized.

5. Force transducer: TB-612T (Nihon Koden, Japan).
6. Front-surface fluorometer (CAM-OF-3) ***(2,3,6)***:
   a. Fluorometer: In collaboration with the Japan Spectroscopic Co. (JASCO, Tokyo, Japan) dual wavelength excitation microscopic fluorometer on the market, a CAM-230 2-λ Microscopic Fluorometer (JASCO), is remodeled into the front-surface fluorometer, CAM-OF-3. The remodeling involves the conversion of the connection of dual wavelength excitation fluorometer to a fluorescence microscope to a configuration with a fiber-optic light guide.

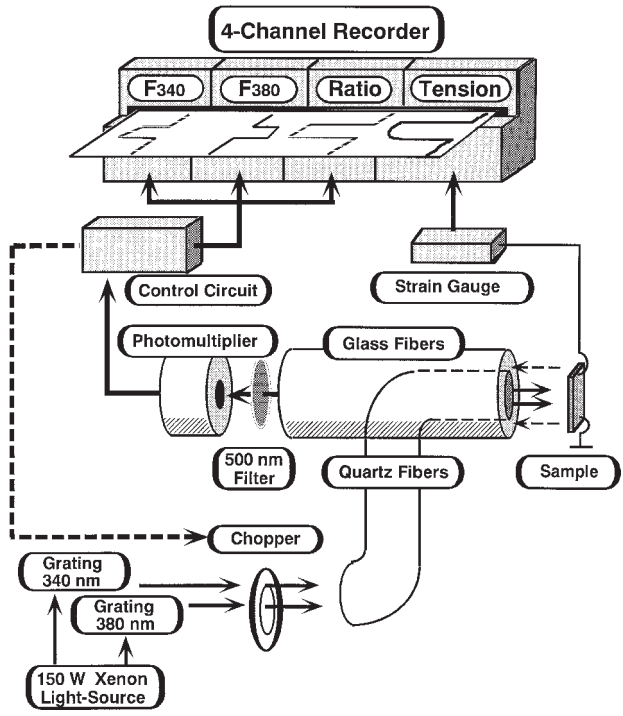


Fig. 1. A block diagram of the front-surface fluorimetry for fura-2 using CAM-OF-3.

b. Optic fibers: In collaboration with FUJITOK Co. (Tokyo, Japan), the fiber-optic light guide Optical Assy 800 (FUJITOK) is specifically designed and made for front-surface fluorimetry. The light guide utilizes a bifurcated fiber-optic light source with quartz fibers (95 fibers [330–340-μm diameter × 500-mm length, ST200D-S]) in one branch and glass fibers (250 fibers [300–310-μm diameter × 800-mm length, S0-230/250-50FE]) in the other branch. Fibers are concentrically arranged at the common end, which faces the samples. The quartz fibers are arranged in an inner circle (3 mm diameter) whereas the glass fibers are arranged in an outer circle (7 mm diameter) at the common end.
c. Photomultiplier, R-268 (Hamamatsu Photonics, Shizuoka, Japan) is utilized.
d. A block diagram of front-surface fluorimetry using CAM-OF 3 is shown in **Fig. 1**. Dual excitation light (340 nm, 380 nm) is obtained using two spectroscopes from a 150-W Xenon light source. Using a chopper wheel, the excitation light is then alternately (400 Hz) guided through quartz optic fibers and directly illuminates the sample strip (5-mm length × 1-mm width × 0.1-mm thickness). The fluorescence of the entire front surface is collected by glass fibers and introduced through a 500-nm band-pass filter into a photomulti-

plier. The ratio of the fluorescence intensities at 340 nm (F340) and 380 nm (F380) excitation, F340/F380, is monitored.

7. Recordings: All data (F340, F380, F340/F380, and tension) are recorded using a computerized data acquisition system (MacLab, Analog Digital Instruments, Castle Hill, Australia; Macintosh, Apple computer, Cupertino, CA), which enables the $[Ca^{2+}]_i$-tension relationship of smooth muscle contraction and relaxation to be studied.
8. To take fluorescent microphotographs of the smooth muscle strips stained with fura-2, a fluorescence microscope (Axioskop, Zeiss, Germany), equipped with a water-immersion objective system (Plan-Neofluor 40, Zeiss) and appropriate combinations of filters (BP 340 for excitation light and BP 500-530 for fluorescence) is utilized.

## 3. Methods

### 3.1. Fura-2 Loading

1. Prior to each measurement, dissolve either 50 µg of fura-2/AM or fura-PE3/AM powder in 50 µL of dimethyl sulfoxide (DMSO), and then dilute with fura-2 loading solution (with the final concentration of DMSO ranging from 1 to 5%) and utilize only once.
2. Incubate smooth muscle strips in oxygenated fura-2 loading buffer using the conditions shown in **Table 1**. Fura-2 (or fura-PE3) loading for smooth muscle cells varies depending on the species and organ.
3. After loading with fura-2, incubate the smooth muscle strips in normal PSS for at least 1 h before starting the measurements, in order to remove the dye in the extracellular space and for the purpose of equilibration (*see* **Notes 1** and **2**).

### 3.2. Measurement of Isometric Tension Development

1. Perform the simultaneous determination of the tension and $[Ca^{2+}]_i$ of the smooth muscle strips at 37°C.
2. At the beginning of the fura-2 equilibration period, mount the strip vertically and connect to a force transducer in a quartz organ bath.
3. During this period, stimulate the strip with 118 m*M* $K^+$ PSS every 15 min and increase the resting tension in a stepwise manner until levels that will induce the maximal tension development are reached (*see* **Note 3**).
4. Record the responsiveness to 118 m*M* $K^+$ PSS before the start of each experimental protocol. The developed tension is expressed in percentages, assuming the values in normal PSS (5.9 m*M* $K^+$) to be 0%, and in 118 m*M* $K^+$ PSS to be 100%.

### 3.3. Front-Surface Fluorimetry

1. To minimize background fluorescence owing to any possible extraneous signals, fluorimetry must be performed in a darkroom (*see* **Notes 4** and **5**).
2. Using front-surface fluorimetry, simultaneously monitor changes in the fluorescence emission (F340, F380, and their ratio, F340/F380) from the entire front

surface and tension development of fura-2-loaded smooth muscle strips (*see* **Note 6**).

3. The fluorescence ratio (F340/F380) is utilized as an index of $[Ca^{2+}]_i$, and is expressed as a percentage, assuming the values in normal (5.9 m*M* $K^+$) and 118 m*M* $K^+$ PSS to be 0% and 100%, respectively. The determination of the 100% levels of tension and fluorescence ratios are performed at the same time just prior to the start of the experimental protocol (*see* **Note 7**).
4. Estimate the absolute values of $[Ca^{2+}]_i$ for the 0% (5.9 m*M* $K^+$) and 100% levels (at the steady state of the contraction induced by 118 m*M* $K^+$-depolarization) of the fluorescence ratio (F340/F380) using separate measurements as follows: After recording the 100% levels of F340/F380 induced by the depolarization with 118 m*M* $K^+$ PSS, apply ionomycin (final concentration: 5 μ*M* for rat aorta, and 25 μ*M* for the porcine coronary artery). Thereafter, F340 further increases until reaching plateau levels ($F340_{max}$). The solution is then changed to $Ca^{2+}$-free PSS, and F340 gradually decreases until reaching a steady state ($F340_{min}$). $[Ca^{2+}]_i$ is calculated according to the following equation, which is the calibration equation for fura-2 using intensity values (F340) at only one wavelength:

$$[Ca^{2+}]_i = K_d\,(F - F_{\,min})/(F_{\,max} - F) \qquad (1)$$

in which Kd is the apparent dissociation constant for $Ca^{2+}$ at 37°C and is assumed to be 224 n*M* ***(1)***, F is the fluorescence signal of F340 expressed in percent, and $F_{\,min}$ and $F_{\,max}$ are $F340_{min}$ and $F340_{max}$, respectively. *F* at 5.9 m*M* $K^+$ and at 118 m*M* $K^+$ depolarization are assigned to be 0 and 100%, respectively. Thus, the $[Ca^{2+}]_i$ levels at *F* = 0% and F = 100% are assigned to be those at the fluorescence ratios (R; F340/F380) of 0 and 100%, respectively (*see* **Note 8**).

## 4. Notes

1. To show evidence that fura-2 is almost exclusively and homogeneously loaded in smooth muscle cells, it is recommended that fluorescence photomicrographs be taken of the sample using a fluorescence microscope (Axioskop).
2. The incubation time and the concentration of fura-2/AM for fura-2 loading appear to be long and excessive in comparison to those reported by other workers (**Table 1**). However, these are the most appropriate conditions to obtain reliable recordings. Under these conditions, the intracellular fura-2 concentration is expected to be approx 13 μ*M*, and the inhibition of tension development owing to $Ca^{2+}$-buffering action of fura-2 is not recognized ***(6)***. The exclusive and homogeneous staining of smooth muscle cells with fura-2 can be confirmed by taking fluorescence photomicrographs. The insufficient loading of smooth muscles with fura-2/AM at its lower concentration or shorter incubation time frequently induces a smaller fluorescence signal with greater optical artifacts during measurements. For easier and homogeneous loading of fura-2, FBS, pluronic F127, cremophor EL, or probenecid ***(7)*** are used either alone, or in various combinations ***(8)*** (**Table 1**).
3. In proximal coronary arterial strips (5 × 1 × 0.1 mm) of the pig, an appropriate resting tension is approx 250 mg.

4. Background fluorescence: To avoid possible extraneous contamination of the signal the strip is suspended in a quartz organ bath and the measurements are performed in a darkroom. In addition, ratiometry continuously negates parallel changes in intensities of F340 and F380. Background fluorescence, if any, is always subtracted.
5. The nature of the autofluorescence of the tissue is pyridine nucleotide (reduced form), flavoproteins, or cytochromes, and is essentially related to energy metabolism. The population of mitochondria is so small that the absorbance of excitation light or the fluorescence by these naturally occurring pigments is negligible in smooth muscle cells. In addition, the extinction coefficient and fluorescence quantum yield of fura-2 is so high that autofluorescence of the tissue is easily overcome.
6. With concentric optic fibers, which have a 3-mm quartz inner circle and a 7-mm glass outer circle at the common end, the most suitable distance between the optical fibers and the strip is approx 8 mm. The shorter the distance, the greater the excitation light and, hence, the emission signal. However, it must be noted that a greater intensity of excitation (ultraviolet) light may also cause a greater degree of tissue injury and photobleaching of the fluorescence dye, which will disturb the experiments over a long time course. Furthermore, if the distance is too close and the common end comes into contact with the strip, the emission from the area of the strip overridden by the inner circle cannot be detected by the outer circle. Thus, the distance and the angle between the common end of the optical fibers and the strip are adjusted to the most appropriate for each measurement. This is one of the most important principles regarding front-surface fluorimetry.
7. The absolute values of the fluorescence ratio, F340/F380, for the fura-2–$Ca^{2+}$-complex can not be obtained when CAM 230 is utilized, because this fluorometer is essentially designed for use in microscopic fluorimetry. The fluorescence intensities are not normalized by the intensity of the excitation light, which directly correlate with the intensities of the 340 or 380 nm signal of the xenon light source. The spectrum of the xenon light source indicates that the intensity of excitation light at 380 nm is much greater (approximately three times) than that at 340 nm. To perform ratiometry with a good balance of excitation between 340 and 380 nm, i.e., to make the F340/F380 reach approx 1 at rest (0%), a combination of appropriately sized metal-optical slits placed in both excitation light paths, in front of and after the grating spectroscopes are used. To estimate the changes in $[Ca^{2+}]_i$ in the experimental protocols, it is not essential to obtain the absolute values of F340/F380.
8. Estimation of the absolute values of $[Ca^{2+}]_i$:
   a. The absolute values of $[Ca^{2+}]_i$ are estimated in separate measurements: In prolonged experimental protocols, although the changes in fluorescence ratio to certain stimulations (such as to high $K^+$ depolarization) are well maintained, the responsiveness of the strips to ionomycin varies depending on the time course of the experimental protocols, and, thus, great variations in the calculated absolute values of $[Ca^{2+}]_i$ are observed. Therefore, it is not recommended

to express the $[Ca^{2+}]_i$ levels with absolute $[Ca^{2+}]_i$ values calculated at the end of each experiment. Only for approximation purposes are the absolute values of $[Ca^{2+}]_i$ at the 0 and at 100% levels of the fluorescence ratio determined in separate measurements. In porcine coronary arterial smooth muscle cells, $[Ca^{2+}]_i$ at the 0 and 100% levels correspond to approx 100 and 900 n*M*, respectively.

b. Ionomycin induces an increase in the fluorescence signal in a concentration-dependent manner. The maximum response is obtained with 5 and 25 μ*M* ionomycin in rat aorta ***(9)*** and porcine coronary artery, respectively.

c. Grynkiewicz et al. ***(1)*** described the following equation to determine the absolute values of $[Ca^{2+}]_i$ in ratiometry:

$$[Ca^{2+}]_i = K_d\,(R - R_{min})/(R_{max} - R)(S_{f2}/S_{b2}) \quad (2)$$

where $K_d$ is a dissociation constant and $R$ is the fluorescence ratio (F340/F380). $R_{max}$ is obtained by the addition of ionomycin in normal PSS (saturating $Ca^{2+}$), and $R_{min}$ is obtained in $Ca^{2+}$-free PSS (zero $Ca^{2+}$). $S_{f2}/S_{b2}$ is the ratio of proportionality coefficients of free fura-2 and $Ca^{2+}$-bound fura-2 at 380 nm, which is influenced by various optical factors, including excitation intensity, path length, and the instrumental efficiency. Therefore, in front-surface fluorimetry using optic fibers, the $S_{f2}/S_{b2}$ values vary depending on the relation between the optic fibers and strips, even though they can be kept constant for each measurement. Since F380 is not stable at the time when F340 reaches $F340_{max}$ and $F340_{min}$, the recordings of $R_{max}$ and/or $R_{min}$ often appear to be difficult, and hence $[Ca^{2+}]_i$ cannot be determined. **Equation 1**, is thus considered to be the most appropriate for determining the absolute values of $[Ca^{2+}]_i$.

d. **Equation 2** is closely analogous to **Eq. 1**. From these two equations, the following form is obtained:

$$(F - F_{min})/(F_{max} - F) = (R - R_{min})/(R_{max} - R)(S_{f2}/S_{b2})$$

The $S_{f2}/S_{b2}$ value can be adjusted to 1 by changing the optical slits in the light paths and/or by changing the relative positioning between the common end of the optic fibers and the strip. Empirically, in the range between $F$ = 0% ($R$ = 0%) and $F$ = 100% ($R$ = 100%), the following equation is obtained:

$$(F - F_{min})/(F_{max} - F) \approx (R - R_{min})/(R_{max} - R)$$

Thus, in the physiological range of changes in $[Ca^{2+}]_i$, one can employ the following equation to calculate the absolute values of $[Ca^{2+}]_i$:

$$[Ca^{2+}]_i \approx K_d\,(R - R_{min})/(R_{max} - R) \quad (3)$$

It has been noted, however, that the $[Ca^{2+}]_i$ values obtained are only an approximation of true $[Ca^{2+}]_i$ values.

## References

1. Grynkiewicz, G., Poenie, M., and Tsien, R. Y. (1985) A new generation of $Ca^{2+}$ indicators with greatly improved fluorescence properties. *J. Biol. Chem.* **269,** 3440–3450.

2. Hirano, K., Kanaide, H., Abe, S., and Nakamura, M. (1990) Effects of diltiazem on calcium concentrations in the cytosol and on force of contractions in porcine coronary arterial strips. *Br. J. Pharmacol.* **101,** 273–280.
3. Abe, S., Kanaide, H., and Nakamura, M. (1990) Front-surface fluorometry with fura-2 and effects of nitroglycerin on cytosolic calcium concentration and on tension in the coronary artery of the pig. *Br. J. Pharmacol.* **101,** 545–552.
4. Chance, B., Salkovitz, I. A., and Kovach, A. G. B. (1972) Kinetics of mitochondrial flavoprotein and pyridine nucleotide in perfused heart. *Am. J. Physiol.* **223,** 207–218.
5. Frank, H., Barlow, C. H., and Chance, B. (1976) Oxygen delivery in perfused rat kidney: NADH fluorescence and renal function state. *Am. J. Physiol.* **231,** 1082–1089.
6. Miyagi, Y., Kobayashi, S., Nishimura, J., Fukui, M., and Kanaide, H. (1995) Resting load regulates vascular sensitivity by a cytosolic $Ca^{2+}$-insensitive mechanism. *Am. J. Physiol.* **268,** C1332–C1341.
7. Di Virgilio, F., Steinberg, T. H., Swanson, J. A., and Silverstein, S. C. (1988) Fura-2 secretion and sequestration in macrophages: A blocker of organic anion transport reveals that these processes occur via a membrane transport system for organic anions. *J. Immunol.* **140,** 915–920.
8. Watanabe, C., Yamamoto, H., Hirano, K., Kobayashi, S., and Kanaide, H. (1992) Mechanisms of caffeine-induced contraction and relaxation of rat aortic smooth muscle. *J. Physiol.* **456,** 193–213.
9. Watanabe, C., Yamamoto, H., Kobayashi, S., and Kanaide, H. (1993) Extracellular $Ca^{2+}$-dependent potentiation by cocaine of serotonin- and norepinephrine-induced contractions in rat vascular smooth muscle. *Circ. Res.* **72,** 1191–1201.

# 17

# Measurement of Calcium and Movement in Heart Cells

**Leong L. Ng and Paulene A. Quinn**

## 1. Introduction

Preparations of calcium-tolerant cardiac myocytes for studies on intracellular calcium ($[Ca^{2+}]_i$) signaling and contraction have been difficult owing to the susceptibility of these cells to the enzymatic digestion process. This often leads to the cells acquiring a bricklike contracted shape with a granular cytoplasm and membrane blebbing. A successful preparation results in single myocytes that do not show spontaneous contractions and that remain relaxed in $Ca^{2+}$-containing buffers, indicating that the sarcolemmal membrane was not damaged during enzymatic digestion and led to membrane depolarization.

A modification of the method of Eckel et al. ***(1)*** was used for isolation of cardiac myocytes ***(2)***. The perfusion with a low-$Na^+$ buffer reduces the influx of $Na^+$ during the digestion process, so that the operation of the cardiac $Na^+$-$Ca^{2+}$ exchanger does not lead to $[Ca^{2+}]_i$ overload and death of the cardiac myocytes ***(3)***. Furthermore, the use of sucrose has a protective effect against the subsequent reintroduction of $Ca^{2+}$ following the $Ca^{2+}$-free perfusion period that precedes introduction of the enzyme solution ***(1)***. This technique can be optimized to improve the yield of cells substantially, and following loading with the $Ca^{2+}$ fluorophore fura-2 ***(4)***, it is possible to monitor changes in $[Ca^{2+}]_i$ and cell contractility using an epifluorescence microscope fitted with an edge detection device to measure movement ***(5)***.

## 2. Materials

1. Type V collagenase (EC 3.4.24.3, from *Clostridium histolyticum*, specific activity 435 U/mg) (*see* **Note 1**).
2. Hyaluronidase Type 1-S (EC 3.2.1.35, from bovine testes, specific activity 340 U/mg).
3. Fatty acid-free bovine serum albumin (BSA).

From: *Methods in Molecular Biology, vol. 312: Calcium Signaling Protocols: Second Edition*
Edited by: D. G. Lambert © Humana Press Inc., Totowa, NJ

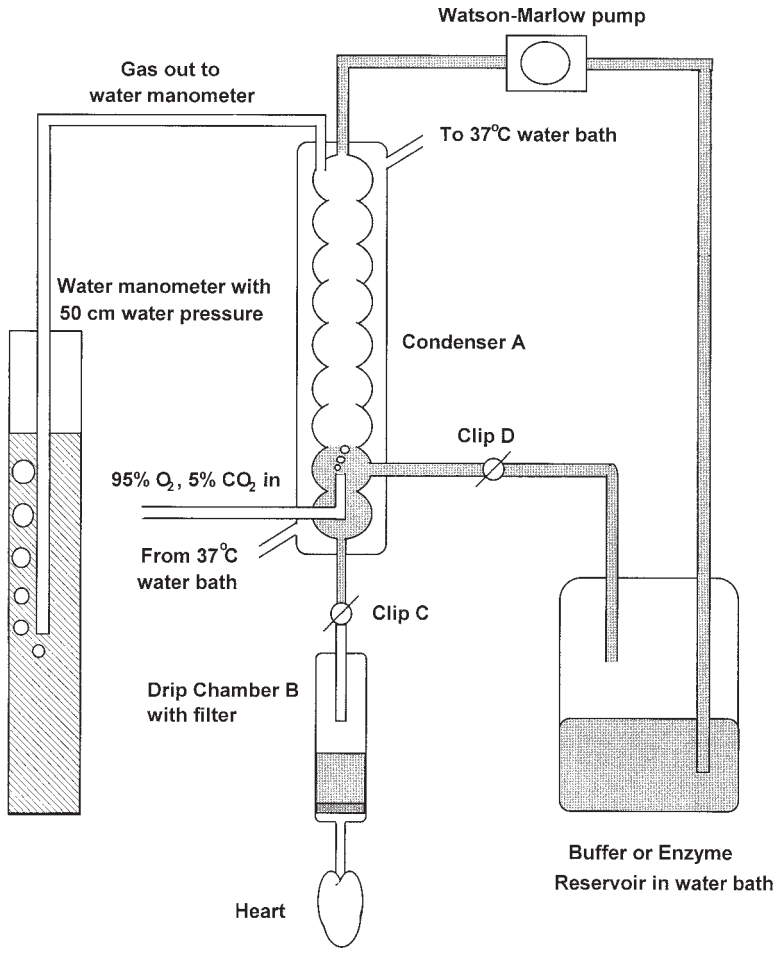


Fig. 1. Schematic representation of the "in-house" Langendorff apparatus.

4. Joklik's Minimal Essential Medium (MEM) were from Sigma, Poole, Dorset, UK.
5. Fura-2 acetoxyl methyl (AM) ester (fura-2/AM) is from Calbiochem, Nottingham, UK.
6. Ionomycin is from Calbiochem.
7. Cell-Tak is from Collaborative Research, Bedford, MA.
8. All other chemicals were of Analar grade and were from BDH, Poole, Dorset, UK.
9. The dual excitation Deltascan single-photon counting fluorometer is from Photon Technology International (PTI), South Brunswick, NJ.
10. The Video Edge Detection Device *(5)* is purchased from Crescent Electronics, Sandy, UT.
11. The Langendorff apparatus (**Fig. 1**) is made locally and consists of a glass condenser (A) for warming and oxygenating the buffer, which was pumped in by a

Watson-Marlow pump. The effluent from A can be recirculated to the buffer reservoir in a 37°C water bath or diverted into the drip chamber (B) cut from an intravenous set (Baxter Healthcare, Thetford, Norfolk, UK) (*see* **Note 2**).

a. 95% $O_2$, 5% $CO_2$ gas mixture is fed into the glass condenser at the bottom inlet and escapes via the top outlet into a manometer filled with water so that a pressure of approx 50 cm of water is maintained in the condenser and the drip chamber in order to perfuse the heart adequately.
b. Flow rate is regulated by a clip (C) just above the heart. Since the rate at which buffer is pumped in at the top of the condenser A will exceed the flow to the heart, any excess buffer that accumulates in the condenser has to be periodically released back into the buffer reservoir in the water bath through clip D.
c. Make a mark near the bottom on the side of the condenser A and the drip chamber B and measure the volume of fluid that is contained within the tubing, the condenser A, and the drip chamber B. This dead space will initially contain buffer A during the $Ca^{2+}$-free perfusion period and must be taken into account when the double-strength enzyme solution is introduced, so that the final enzyme solution that is recirculated during the digestion process becomes single strength enzyme buffer.

12. Buffer A is low-$Na^+$ buffer used for the enzymatic digestion of cardiac myocytes and is composed of 35 m*M*/L NaCl, 4.75 m*M*/L KCl, 1.19 m*M*/L $KH_2PO_4$, 16 m*M*/L $Na_2HPO_4$, 25 m*M*/L $NaHCO_3$, 134 m*M*/L sucrose, 1.2 m*M*/L $MgSO_4$, 10 m*M*/L HEPES, 10 m*M*/L glucose, 5 m*M*/L pyruvate, 20 m*M*/L creatine, 2 mg/mL BSA (pH 7.4 when equilibrated with 95% $O_2$, 5% $CO_2$) (*see* **Note 3**).
13. Double-strength enzyme solution: buffer A with 1 mg/mL Type V collagenase, 2.5 mg/mL hyaluronidase Type 1-S and 100 µ*M*/L $CaCl_2$. A volume equal to the dead space of the Langendorff apparatus is measured into a reservoir and kept gassed and warmed at 37°C.
14. Buffer B is used for studying the $[Ca^{2+}]_i$ transients and consists of 134 m*M*/L NaCl, 4 m*M*/L KCl, 1.2 m*M*/L $MgSO_4$, 10 m*M*/L HEPES, 1.2 m*M*/L $NaH_2PO_4$, 1.8 m*M*/L $CaCl_2$, 11.1 m*M*/L glucose, 2 mg/mL BSA 2 (pH 7.4 when bubbled with 100% $O_2$).

## 3. Methods

### *3.1. Cardiac Myocyte Isolation*

1. Use Wistar rats weighing 250–300 g for isolation of $Ca^{2+}$-tolerant single ventricular myocytes.
2. Kill the animal with an ip injection of pentobarbital.
3. Open the chest and remove the heart quickly, ensuring that there is enough aortic stump to tie the heart onto the Langendorf apparatus without nipping the coronary arteries. Drop the heart immediately into ice-cold preoxygenated buffer A; it should stop beating after a few seconds.
4. Weigh the heart in this cold buffer A (*see* **Note 4**).

5. Start the Watson-Marlow pump running to fill the condenser A (**Fig. 1**) with the $Ca^{2+}$-free buffer A, and adjust the drip rate to approx 3 drops/s (1 mL = 20 drops). Return any buffer that builds up in the condenser to the buffer reservoir in the water bath by opening clip D.
6. Tie a cotton ligature loosely around the cannula and pick up the heart by the aortic stump and quickly tie onto the cannula, ensuring that the origins of the coronary arteries are not nipped in the process.
7. The retrograde perfusion of the heart with warm buffer A will lead to a few contractions that will empty blood from the ventricles, but these contractions rapidly stop owing to the lack of $Ca^{2+}$ (*see* **Note 5**).
8. Adjust the rate of flow through the heart with clip C, so that the rate is maintained at 3 drops/s.
9. As the end of the $Ca^{2+}$-free period approaches, empty the level of the solutions down to the predetermined marks on the side of condenser A and drip chamber B by opening clip D (**Fig. 1**).
10. At 1 min, transfer the tubing from the buffer A reservoir in the water bath to the reservoir containing the premeasured volume of double-strength enzyme solution (the volume being equal to the dead space of the apparatus and the tubing, determined as detailed above).
11. Increase the pump rate to mix the dead space fluid with the double-strength enzyme solution rapidly, returning any excess accumulating in the condenser A to the reservoir by opening clip D (*see* **Note 6**).
12. Maintain the flow rate at 3 drops/min for a period of time (in minutes) equal to approx 1.5 multiplied by the weight of the heart (in grams) (*see* **Note 7**).
13. At the end of this time, the heart should feel soft and can be cut down from the cannula. Then coarsely cut it up on a McIlwain Tissue chopper (approx 1-mm cuts in two dimensions) and transfer the pieces into a plastic tube.
14. To achieve disaggregation, gently pipet (triturate) the pieces up and down in buffer A with a plastic Pasteur pipet with the tip cut off (without any added $Ca^{2+}$, other than the remains of the enzyme solution within the heart).
15. After allowing the large pieces of cardiac muscle to settle by gravity for 30 s, periodically inspect the turbid supernatant under the microscope; it initially contains many rounded granular dead cells or actively contracting rod-shaped cells, which are damaged cardiac myocytes. Following approx 5–10 min of periodic trituration, some rod-shaped cells that are not actively contracting will be released and these supernatants should be saved.
16. Carefully layer the supernatants containing quiescent rod-shaped cells onto buffer A containing 6 g/100 mL of BSA. Allow the cells to settle by gravity for 5 min, and remove the pellet at the bottom of the tube that contains the quiescent rod-shaped cells.
17. This can be performed two to three times to obtain a pellet consisting mostly of live undamaged cardiac myocytes.
18. Combine the pellets into Joklik's MEM (that does not contain $Ca^{2+}$) and recover the cells by centrifugation at 160*g* for 3 min on a benchtop centrifuge.
19. Resuspend the cells in Joklik's MEM at room temperature, add $CaCl_2$ to a final concentration of 0.25 m*M*/L and allow the cardiac myocytes to adjust to this for

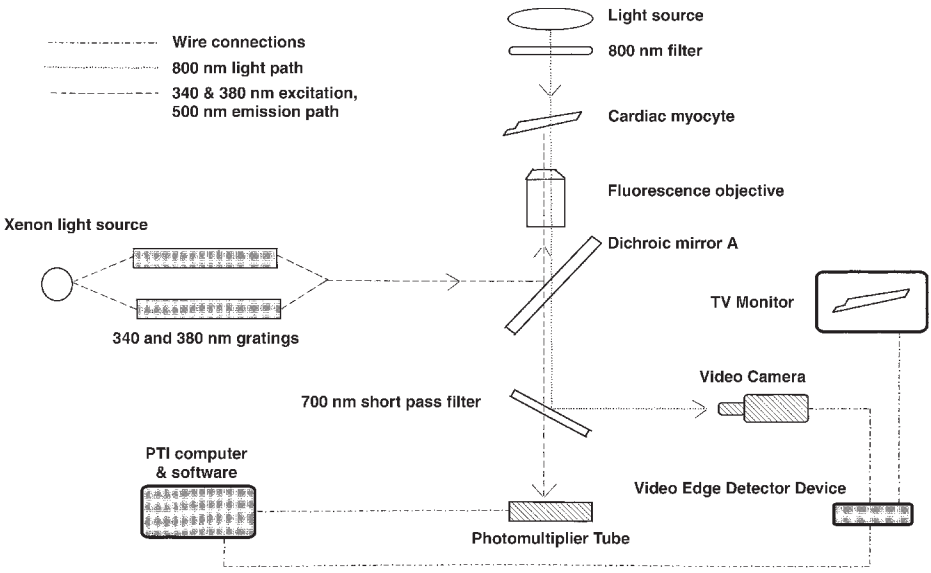


Fig. 2. System alignment for simultaneous measurements of $Ca^{2+}$ and movement in isolated myocytes.

30 min before increasing the $Ca^{2+}$ concentration to 1.8 m*M*/L. The cells should be viable and $Ca^{2+}$ tolerant for approx 24 h.

### 3.2. Measurement of $[Ca^{2+}]_i$ and Movement

1. The cardiac myocytes can then be loaded with fura-2/AM (5 µ*M*/L final concentration, premixed with Pluronic F127 100–200 mg/L before adding the Joklik's MEM containing 1.8 m*M*/L of $CaCl_2$) for 30 min at 37°C.
2. Wash the cells twice to remove fluorophore, and they are left to de-esterify the fura-2/AM for 15–30 min at room temperature.
3. Then layer the cells onto quartz cover slips (Carl Zeiss, Welwyn, UK) that have been coated with Cell-Tak, a tissue adhesive approx 3.5 µg/$cm^2$, and leave to attach for 30 min (*see* **Note 8**).
4. Once cells are attached with the Cell-Tak, it is possible to change the solutions in the incubation chamber without washing off the cells. Buffer B can be used in most applications.
5. Cover slips with the attached cells are then inserted into a specially constructed cover slip holder that is held within a Peltier incubation platform, which maintains the cells at 37°C (*see* **Note 9**).
6. The instrumentation for measurement of epifluorescence emission and movement is detailed in **Fig. 2**.

7. Set dual excitation wavelengths at 340 and 380 nm with a data acquisition time of 50–100 ms (*see* **Note 10**).
8. To simultaneously measure movement, insert a near infrared filter (800 nm) beneath the microscope lamp (**Fig. 2**) so that long-wavelength light can be used to measure the movement of cells without interfering with the fluorescence measurements (*see* **Note 11**).
9. The PTI software allows both the 340/380 fluorescence ratios and the Reference Cell Quantum Counter (RCQC) outputs to be simultaneously displayed, and in this instance, the RCQC output represents myocyte length.
10. Recording of $[Ca^{2+}]_i$ and movement are made simultaneously, using platinum or silver wire electrodes to stimulate the cardiac myocytes to contract.

### 3.3. Calibration of Fura-2 Ratios and Video Edge Detector Outputs

1. Cells are superfused with glucose- and BSA-free buffer B, with the metabolic poisons carbonyl cyanide *m*-chlorophenylhydrazone (an inhibitor of oxidative phosphorylation) 5 μ*M*/L, amytal (an inhibitor of NADH dehydrogenase) 3.3 m*M*/L ***(6)***. After 20 min, the intracellular ATP stores are sufficiently depleted so that manipulation of intracellular calcium does not cause contracture.
2. $R_{max}$ for the fura-2 is determined by addition of the nonfluorescent ionophore ionomycin (10 μ*M*/L) in buffer B (which contains 1.8 m*M*/L of $Ca^{2+}$).
3. $R_{min}$ is obtained by addition of EGTA 10 m*M*/L to chelate the $Ca^{2+}$. Intracellular free $[Ca^{2+}]_i$ can thus be calculated using the equation $[Ca^{2+}]_i = K_d \times (R - R_{min})/(R_{max} - R) \times S_f/S_b$, in which $K_d$ is 225 n*M*/L at 37°C, and $S_f/S_b$ is the ratio of cellular fluorescence emission with excitation at 380 nm for $Ca^{2+}$-free and $Ca^{2+}$-saturated buffers ***(4)***.
4. To calibrate the output from the Video Edge Detector Device, a piece of glass capillary of known outer diameter is visualized at the same magnification as used for the cell measurements, and detection of the edges by changing the thresholds on the edge device would enable an output to the RCQC sockets of the PTI fluorometer to be measured and expressed as an absolute length measurement.

## 4. Notes

1. An alternative crude collagenase is the preparation from Boehringer Mannheim, Mannheim, Germany (collagenase A, cat. no. 103586). Each batch of these enzymes has to be tested for their activity on the preparation of cardiac myocytes and the time of digestion and concentration of the enzyme standardized. Some methods recommend protease (pronase E), which considerably speeds up the digestion, but it is difficult to control and kills the myocytes.
2. The drip chamber enables the flow rate to the heart to be controlled more accurately and also prevents air and particle embolization into the heart, resulting in infarction.
3. The free $Ca^{2+}$ of this buffer is approx 1 μ*M*/L when Milli-Q water is used to make up the buffer. Ensure that the buffer A is fully oxygenated with 95% $O_2$, 5% $CO_2$ at 37°C for 15 min before the rat is killed.

4. The heart weight determines the duration of enzymatic digestion.
5. This $Ca^{2+}$-free perfusion period should be limited to 1 min to disrupt intercalated discs, but must not be continued for much longer since the heart could undergo a $Ca^{2+}$ paradox when the enzyme solution with $Ca^{2+}$ is subsequently introduced, leading to contracture and death of the cells.
6. The enzyme should start perfusing the heart, and it may commence beating for a few minutes.
7. This factor of 1.5 may need to be changed with different batches of collagenase, but is a good starting guide to the length of digestion.
8. The quartz cover slips are necessary since the excitation wavelengths for fura-2 are 340 and 380 nm, and ordinary glass would attenuate the 340-nm illumination.
9. It is also possible to gas the surface of the incubation buffers with air containing 5% $CO_2$ if bicarbonate buffers are used.
10. Dichroic mirror A (Fig. 2) had a half-pass wavelength of 400 nm and reflected the excitation light through the ×20 Nikon fluorescence objective lens onto the cardiac myocyte. The longer wavelength emitted by fura-2 was transmitted by dichroic mirror A. This light was transmitted through a short-pass filter B (half-pass wavelength of 700 nm) mounted at 45° in the side arm of the PTI fluorometer and impinged on the single-photon counting photomultiplier tube. Signals from this tube were collected by the computer, and the PTI software enabled the on-line computation of 340/380 fluorescence ratios. An estimate of the $[Ca^{2+}]_i$ could be read on-line if constants for the equation $[Ca^{2+}] = K_d \times (R - R_{min})/(R_{max} - R) \times S_f/S_b$ ***(4)*** are predetermined as detailed in **Subheading 3.3.** and fed into the software.
11. This long wavelength light was transmitted by dichroic mirror A and was reflected by the short-pass (700 nm) filter B into a video camera. The output from this camera is fed into the Video Edge Detection Device ***(5)***, and the video output from this is then connected to a TV monitor to visualize the cardiac myocyte (the original video input signal) together with the detection windows with the edge points marked. It may be necessary to change the thresholds of the device so that the contrast between the edge of the myocyte and the background can be successfully detected. The output from the Video Edge Detection Device can be fed into the PTI connector box, in the RCQC sockets.

## References

1 Eckel, J., Pandalis, G., and Reinauer, H. (1983) Insulin action on the glucose transport system in isolated cardiocytes from adult rat. *Biochem. J.* **212,** 385–392.
2. Ng, L. L., Davies, J. E., and Quinn, P. (1993) Intracellular pH regulation in isolated myocytes from adult rat heart in $HCO_3^-$containing and $HCO_3^-$-free media. *Clin. Sci.* **84,** 133–139.
3. Tani, M. and Neely, J. R. (1989) Role of intracellular $Na^+$ in $Ca^{2+}$ overload and depressed recovery of ventricular function of reperfused ischemic rat hearts: Possible involvement of $Na^+$-$H^+$ and $Na^+$-$Ca^{2+}$ exchange. *Circ. Res.* **65,** 1045–1056.

4. Grynkiewicz, G., Poenie, M., and Tsien, R. Y. (1985) A new generation of calcium indicators with greatly improved fluorescence properties. *J. Biol. Chem.* **260,** 3440–3450.
5. Steadman, B. W., Moore, K. B., Spitzer, K. W., and Bridge, J. H. (1988) A video system for measuring motion in contracting heart cells. *IEEE Trans. Biomed. Eng.* **35,** 264–272.
6. Li, Q., Altshuld, R. A., and Stokes, B. T. (1987) Quantitation of intracellular free calcium in single adult cardiomyocytes by fura-2 fluorescence microscopy: Calibration of fura-2 ratios. *Biochem. Biophys. Res. Commun.* **147,** 120–126.

# 18

# Simultaneous Analysis of Intracellular pH and $Ca^{2+}$ From Cell Populations

**Raul Martinez-Zaguilan, Linda S. Tompkins, Robert J. Gillies, and Ronald M. Lynch**

## 1. Introduction

Manipulation of cell function through stable transfection of agonist-specific receptors, components of second messenger cascades, or proteins with specific functional activities (enzymes, transporters, channels) has provided the tools to study intra- and intercellular signaling phenomena at a molecular level ***(1–3)***. In addition, cotransfection of cells with sequences coding for fluorescent markers such as green fluorescent protein has facilitated the selection and analysis of transfected cells ***(4,5)***. Techniques are also required to screen for and to monitor the functional changes associated with the genetic manipulation in order to investigate the physiological role of a component within a complex system such as a cell. Hormones and other agonists often elicit changes in intracellular pH ($pH_{in}$) ***(6,7)*** and/or calcium ($[Ca^{2+}]_i$) ***(8,9)*** that modulate cell responses. Thus, methods for comparing steady-state ion concentrations and the regulation of these ions between cell populations in which signaling pathways have been modified can provide an approach to screen for functional changes in signal transduction for selective agonists.

There are several fluorescent indicators for measuring pH and $Ca^{2+}$ ***(10,11)***. These probes are commercially available in acetoxymethyl (AM) ester forms, which allow passive loading of cells with minimal effect on cell physiology ***(10,11)***. Optimally, these probes should be specific for the ion of interest and have a high quantum efficiency, and the affinity of the probe ($K_d$) for the ion of interest should be within the physiological range. To simultaneously monitor $pH_{in}$ and $[Ca^{2+}]_i$, the probes need to have distinct excitation or emission char-

From: *Methods in Molecular Biology, vol. 312: Calcium Signaling Protocols: Second Edition*
Edited by: D. G. Lambert © Humana Press Inc., Totowa, NJ

acteristics. An additional feature required for accurate analyses is that each probe exhibit at least two excitation or emission wavelengths reciprocally sensitive to the ion of interest. The ratio of ion-sensitive wavelengths provides a precise measure of ion levels that is relatively independent of dye concentration. An excitation or emission wavelength that is ion insensitive is also desirable, since analysis of signal intensity at this wavelength allows for simultaneous determination of the efficiency of dye loading, dye leakage from cells, as well as possible interactions between probes including quenching ***(12,13)***.

Two probes that meet the described criteria for simultaneous pH/$Ca^{2+}$ measurements are snarf-1 and fura-2 ***(12,13)***. The ratio of fluorescence emission intensities at 644/584 nm for snarf-1, and the ratio of fura-2 fluorescence excited alternately at 340/380 nm can be used to generate calibration curves for pH and $Ca^{2+}$, respectively. The isoexcitation wavelength (ion insensitive) for fura-2 at 360 nm and the isoemission wavelength of snarf-1 at 600 nm are monitored to determine the stability of dye loading and to alert one to other potential artifacts.

Although changes in both $pH_{in}$ and $[Ca^{2+}]_i$ have been observed in response to a variety of agonists, it is not clear whether these ionic events work independently or are coordinated to lead to a specific physiological response. One of the fundamental problems in studying these ionic events is that changes in $pH_{in}$ modify $Ca^{2+}$ regulatory mechanisms (e.g., $Ca^{2+}$-binding proteins, $Ca^{2+}$ ATPase ***[14]*** $Ca^{2+}$ channels ***[15]***) and changes in $Ca^{2+}$ may modify pH regulation (e.g., $Na^+/H^+$ exchanger ***[16]***, $H^+$-ATPase ***[17]***). Therefore, it is desirable to use a technique that allows concomitant monitoring of these two ions in cell populations with high time resolution. Furthermore, like many $Ca^{2+}$ binding proteins, all $Ca^{2+}$-sensitive fluoroprobes are inherently sensitive to pH owing to competition of $H^+$ for the $Ca^{2+}$-binding sites ***(12,18)***. Thus, changes in pH induced by an agonist can complicate analysis of the activated $Ca^{2+}$ response when using $Ca^{2+}$ fluoroprobes. Similarly, analysis of differences in steady-state $Ca^{2+}$ between unique cell populations can be influenced by differences in resting cell pH. For example, resting pH in neoplastic cells is generally higher compared to normal controls ***(19)***. For most $Ca^{2+}$ fluoroprobes, the sensitivity to $H^+$ is most prevalent at relatively acidic pH values ***(12,18)***. However, many cell lines do exhibit resting pH lower than 7.0, and some perturbations can lower pH into the sensitive range. Fortunately, the effect of pH on the $Ca^{2+}$-binding parameters can be predicted and used to correct the $Ca^{2+}$ signal ***(12,18)***.

This chapter describes experimental paradigms that provide optimum conditions for simultaneous measurement of pH from the fluorescence emission of snarf-1, and $Ca^{2+}$ using fura-2. The fluorescence spectra of these compounds are sufficiently different to allow simultaneous measurement of pH and $Ca^{2+}$ both in vitro and in vivo. Moreover, the ratio of the $H^+$-sensitive wavelengths of

snarf-1 is unaffected by $Ca^{2+}$, or the concomitant presence of fura-2 in cells ***(18)***. Although the fluorescence ratio of fura-2 is insensitive to the presence of snarf-1, it is affected by pH, as indicated above. Therefore, the authors will describe procedures to correct for this effect and to obtain the calibration parameters ($K_d$ or $pK_a$, $R_{min}$ and $R_{max}$) for fura-2 and snarf-1 required to facilitate analysis of pH and $Ca^{2+}$ concentrations within cell populations.

## 2. Materials

1. Three cell lines are used in the studies described:
   a. RIN-38 are an insulin-secreting transformed β cell line ***(20)***.
   b. Endothelial cells were isolated from human umbilical vein endothelium (HUVE) ***(21)***.
   c. HSF cells are fibroblasts isolated from human skin.
2. Cell culture media is Dulbecco's modified Eagle's medium supplemented with 5.6 m*M* glucose, 10% fetal bovine serum (FBS), 1U penicillin/mL, and 0.1 mg/mL streptomycin sulfate.
3. Cells are cultured for experiments on glass coverslips (9 × 22 mm) contained in 10-cm dishes at initial plating densities of approx $5 \times 10^4$ cells/dish. Cells are grown to near confluency for fluorescence experiments.
4. 0 $Ca^{2+}$ buffer (KEGTA): 110 m*M* KCl, 20 m*M* MOPS, 20 m*M* NaCl, and 10 m*M* $K_2H_2EGTA$. The $K_2H_2EGTA$ is obtained by mixing equimolar concentrations of EGTA and $K_2CO_3$. pH is adjusted using KOH.
5. Calcium-saturated buffer (CaEGTA): 110 m*M* KCl, 20 m*M* MOPS, 20 m*M* NaCl, and 10 m*M* $K_2CaEGTA$ obtained by mixing equimolar concentrations of EGTA and $CaCO_3$. The most critical requirement for this buffer is to contain equimolar concentrations of calcium and EGTA in order to achieve a stoichiometric balance. Because EGTA is rarely 100% pure, these buffers normally contain a 5% excess of EGTA by weight (*see* **Note 1**). This excess EGTA in $K_2EGTA$ buffer is not likely to cause problems because the performance of calcium buffers is not very sensitive to total calcium concentration.
6. Standard experimental buffer (EB): 1.3 m*M* $CaCl_2$, 1 m*M* $MgSO_4$, 5.4 m*M* KCl, 0.44 m*M* $KH_2PO_4$, 110 m*M* NaCl, 0.35 m*M* $NaH_2PO_4$, 1 m*M* $NaHCO_3$ , 5 m*M* glucose, 2 m*M* glutamine, and 25 m*M* HEPES, pH 7.15, at 37°C. Experiments can be performed under 5% $CO_2$/95% air if the EB contains $HCO_3^-$ at a concentration set by its equilibrium with $CO_2$ at the desired pH value using **Eq. 1**

$$[HCO_3^-] = pK_a\ (1.52\ mM) \times 10\ (pH - 6.24) \quad (1)$$

   in which 1.52 m*M* is the concentration of $CO_2$ in Hank's balanced salt solution at 37°C, and 5% ambient $CO_2$ (e.g., $pCO_2$ = 38 mmHg); and 6.24 is the pK for the process of $CO_2$ hydration ***(22)***.
7. In vitro pH values used for calibration are obtained with a Beckman (Fullerton, CA) model 71 pH meter, using a Beckman gel-filled combination electrode. The electrode is calibrated at two known pH values using commercially prepared standards from VWR Scientific (San Francisco, CA).

8. Fluorescence measurements are performed in a temperature-controlled cuvet housed in an SLM 8000C fluorometer (SLM, Urbana, IL) using 4-nm band-pass slits and an external rhodamine standard as a reference. Sample temperature is maintained at 37°C by keeping both the water jacket and the buffer at 37°C using a circulating water bath. Spectral data for fura-2 are acquired by scanning the excitation monochrometer between 300 and 500 nm with the emission monochrometer set at 510 nm. Spectra from snarf-1 are acquired by setting the excitation monochrometer at 534 nm and scanning the emission monochrometer between 540 and 700 nm.
9. Cell holder for fluorometric measurements: Two cover slips containing cells are placed back to back (cells on the outside surface), and transferred to the quartz fluorometer cuvet using a holder/perfusion device as described previously ***(23)***. The holder maintains the cover slips upright in the fluorescence light path at an angle of 30° allowing for illumination of a spot at the same position on both cover slips. The use of quartz cuvets is essential when monitoring fluorescence in the ultraviolet region, as with fura-2. Tubing from a dual line peristaltic pump is used to introduce fresh media into the bottom of the chamber while removing an equal volume from the chamber top. Small bore tubing (Masterflex no. 13, Fluid Metering Inc., Syosset, NY) is used as the inlet and larger bore tubing (no. 14) for the outlet line. The cells are continuously perfused at a rate of 3.0 mL/min (*see* **Note 2**). Prototypes of this device with modifications have been published elsewhere ***(23,24)***. A commercially available cover slip holder for fluorescence measurements is also available (Spectronics Instruments, Rochester, NY).
10. Fluorometric data collection for simultaneous pH and $Ca^{2+}$ measurements: Continuous data collection occurs while the emission and excitation modes are alternated as follows. Emission at 510 nm with sequential scanning to excitation wavelengths of 340, 360, and 380 nm (fura-2 conditions), followed by excitation at 534 nm with the emission monochrometer sequentially scanned to 584, 600, and 644 nm (snarf-1 conditions). An individual cycle requires 15 s. Temporal resolution is limited primarily by the slew rate of the monochrometer, and not integration time of the phototube. Data are translated to ASCII format for manipulation and analysis ***(18)***.
11. Data analysis: Conversions of ratio values to both $pH_{in}$ and $Ca^{2+}$ are performed using **Eqs. 2**, **3**, and **6** (**Subheading 3.1.**), and plotted using a commercial software (*see* **Note 3**; Sigmaplot, Statistical Product and Service Solutions, Chicago, IL). Analysis of both in vitro and *in situ* calibration curves, as well as estimation of the $pK_a$s, $R_{max}$, and $R_{min}$ values for snarf-1 and fura-2 are obtained from **Eqs. 1–5** using a simplex method and by least-squares regression analysis (MINSQ, MicroMath Scientific Software, Salt Lake UT, or Sigmaplot).
12. Fluoroprobes are obtained from Molecular Probes (Eugene, OR). For each day of experiments, a fresh batch of dye is used. AM dyes are prepared using anhydrous methylsulfoxide (MSO) as a solubilizing agent. The fluorescent probes can be obtained in 50-µg or 1-mg portions. MSO is removed from its container using a syringe equipped with an appropriate gauge needle, or, for the small volumes required for the 50-µg containers, a Hamilton syringe can be used. If 1-mg quan-

tities are prepared, the stock solution should be aliquoted into smaller portions (10 µL) and stored at –80°C until use. Freeze thawing of probes should be avoided. An alternate source for fluorescent ion indicators is Teflabs (Austin, TX).

13. Unless otherwise stated, all other chemicals were obtained from Sigma.

## 3. Methods

### *3.1. Calculation of pH and $Ca^{2+}$ From the Ratio of Ion-Sensitive Wavelengths*

Excitation or emission wavelengths that increase or decrease on cation binding are monitored. The ratio of fluorescence at the ion-sensitive wavelengths is used to determine the extent of ion-bound dye, and hence the free ion concentration by the following equations:

$$\mathrm{pH} = \mathrm{pK}_a + \log(S_{f2}/S_{b2}) + \log[(R - R_{min})/(R_{max} - R)] \quad (2)$$

$$[Ca^{2+}] = K_d(S_{f2}/S_{b2})[(R - R_{min})/(R_{max} - R)] \quad (3)$$

in which $R$, $R_{min}$, and $R_{max}$ are the measured, minimum, and maximum ratios, respectively. For snarf-1, $R$ increases with pH; hence $R_{max}$ represents the ratio of fluorescence intensity of ion-sensitive wavelengths under fully deprotonated conditions, whereas $R_{min}$ is the ratio for the dye when it is fully protonated. In the case of fura-2, $R$ increases with increasing $Ca^{2+}$; hence $R_{min}$ represents fura-2 in the absence of $Ca^{2+}$ ($Ca^{2+}$ <1 n*M*) whereas $R_{max}$ represents the $Ca^{2+}$-fura-2 chelate. $S_{f2}$ and $S_{b2}$ are the fluorescence values at the denominator wavelengths for the free and bound forms of the dye, respectively. These values are used to correct the titration curve for the fact that denominator and numerator wavelengths are independently sensitive to ion binding. If an ion-insensitive wavelength is used as the denominator, $S_{f2}/S_{b2}$ becomes 1 and the term is eliminated.

Since the ratio of fluorescence at the ion-sensitive wavelengths for fura-2 is affected by pH, corrections for changes in pH during an experiment, or when comparing steady-state values between populations is often warranted. The pH sensitivity of fura-2 can be described by the following equations which rely on data acquired from the calibrations described in **Subheading 3.2.** The effect of pH on the $K_d$ is described by # (pH corrected):

$$K_d\# = (K_{d\,max} + \log10(\mathrm{pH}_{in} - \mathrm{pK}_a) \times K_{d\,min})/\log10(\mathrm{pH}_{in} - \mathrm{pK}_a) + 1 \quad (4)$$

whereas the effect of pH on the $R_{min}$ and $R_{max}$ of fura-2 is determined by

$$R^{\#} = k1 \times (\mathrm{pH})^3 + k2 \times (\mathrm{pH})^2 + k3 \times (\mathrm{pH}) + k4 \quad (5)$$

**Eq. 5** is empirically derived by fitting data acquired from the in vitro calibration curves generated for fura-2 as pH is varied. Thus, pH-corrected $[Ca^{2+}]$ ($[Ca^{2+}]^{\#}$) can be estimated by using the following equation and fitting these parameters into the equation:

$$[Ca^{2+}]^{\#} = K_d\# \times (R - R_{min}{}^{\#})/R_{max}{}^{\#} - R) \quad (6)$$

The accuracy of the [$Ca^{2+}$] estimate relies on the accuracy of *in situ* and in vitro titrations ***(18)***. It also relies heavily on appropriate estimations of pH. In many cases, the $K_d$ of fura-2 for $Ca^{2+}$ in vitro is similar to that measured *in situ*, so this parameter may not be cell-type dependent ***(12,18)***. However, other investigators have reported differences between the in vitro and *in situ* estimated $K_d$ values ***(25,26)***. Moreover, the $R_{max}$ and $R_{min}$ values are likely to be cell-type dependent because the dynamic range of the dyes is determined by viscosity and interactions of dye with intracellular proteins. Thus, the authors emphasize the need for determining the calibration parameters in individual cell types if accurate quantification of [$Ca^{2+}$] is required.

### 3.2. In Vitro Calibration of Snarf-1 and Fura-2

In vitro calibration of dyes allows estimation of pH and $Ca^{2+}$ concentrations from the measured ratio values (**Fig. 1**). However, this calibration is also important to determine the dynamic range of the equipment and which $R_{min}$ and $R_{max}$ ratio values are reasonable. To calibrate the probes, $Ca^{2+}$ concentration is varied at a set pH by combining fixed amounts of KEGTA and CaEGTA buffers that are held at constant and equal pH by strong buffers that do not bind $Ca^{2+}$, such as MOPS. A set of EGTA buffers are prepared between pH 5.5 and 8.0. Equal amounts of fura-2 and snarf-1 are added to each of the initial stock solutions. By serially diluting the KEGTA solution with CaEGTA at a given pH, calibration solutions are prepared with good precision. The magnitude of the increment in $Ca^{2+}$ is determined by the effect of pH on the $K_d$ EGTA; specifically, smaller (tenths of nanomolar increments) are obtained at alkaline pH, whereas larger increments (i.e., hundredths of nanomolar to micromolar) are obtained at acidic pH ***(27)*** (*see* **Note 4**).

1. Fura-2 and snarf-1 in their free acid forms are dissolved to final concentrations of 2 μ*M* and 1 μ*M*, respectively, into 30 mL of the KEGTA buffer held at 37°C and a specific pH between 5.5 and 8.0. pH is titrated using KOH.
2. A 3-mL aliquot is placed into a quartz cuvet, and the initial fura-2 excitation and snarf-1 emission data are acquired (zero $Ca^{2+}$).
3. Three mL of CaEGTA (at the same pH) containing 2 μ*M* fura-2– and 1 μ*M* snarf-1–free acids is added to the remaining 27 mL with stirring; e.g., 9 mmol KEGTA added to 1 mmol CaEGTA. Again, a 3-mL aliquot is taken to acquire fura-2 excitation and snarf-1 emission data.
4. Each 3-mL aliquot removed for fluorescence analysis is replaced with an equal volume of the CaEGTA to provide a continuous variation in $Ca^{2+}$. This procedure provides incremental changes in "cell" $Ca^{2+}$, as described previously ***(12,18)***. The estimated $Ca^{2+}$ concentrations for each of 11 iterations at three distinct pH settings are provided in **Table 1** as an example.
5. Another set of 30-mL starting solutions of KEGTA and CaEGTA are titrated to a unique pH, and the procedure is repeated. Increments of 0.25 pH units are rea-

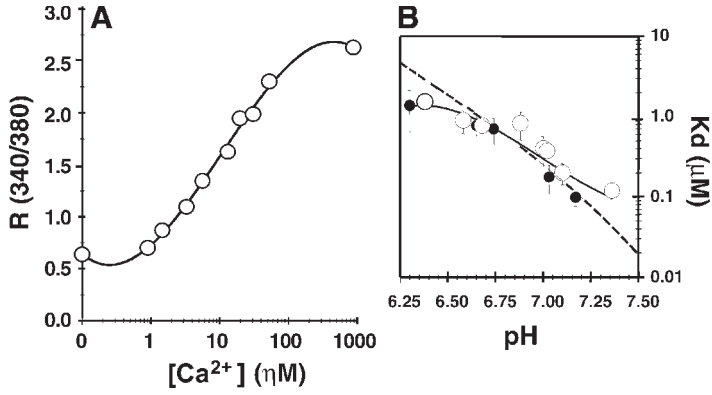


Fig. 1. *In situ* calibration of fura-2 in 3T3 Cells. The 340/380 ratio for fura-2 increases as $Ca^{2+}$ is increased at fixed pH. Similar calibrations were repeated over a range of pH values indicated in the insert. The inset **(B)** shows the effect of pH on the apparent affinity of fura-2 for $Ca^{2+}$ estimated in vitro (i.e., dyes in solution; open circles) and in 3T3 cells (closed circles). Each point represents the mean ± SD of 9–11 different $Ca^{2+}$ concentrations per pH value. $H^+$ and $Ca^{2+}$ dissociation constants were calculated as described earlier. The dashed line indicates the effect of pH on the $K_d$ of EGTA ***(19)***.

sonable for the initial titration. However, subsequent calibrations can be performed using 0.5 pH unit increments.

### *3.3. Loading of Ion-Sensitive Indicators Into Cells*

The ion-sensitive probes in their AM forms are lipophilic and cell permeant. Cellular esterases cleave the ester groups to yield free acids that are relatively impermeant and, therefore, "trapped" within cells ***(10)***. *See* **Note 5** regarding sequestration of probes into subcellular compartments, and **Note 6** regarding cell viability issues.

1. Two cover slips containing confluent or near confluent cell cultures are incubated for 30 min at 37°C in 3 mL of EB containing 7 μ*M* snarf-1/AM and 2 μ*M* fura-2/AM. This can be performed in a single well of a six-well cell culture dish, and all wash solutions can occupy other wells (*see* **Note 7**).
2. After the 30-min loading period, the cells are washed three times with EB containing 0.2% (v/v) FBS, followed by a second incubation in FBS containing EB for 30 min, to allow for the complete hydrolysis of the esters, and leakage of uncleaved dyes from the cells.
3. The two cover slips are placed back to back into the holder/perfusion device, which is subsequently inserted into the fluorometer cuvet for pH/$Ca^{2+}$ measurements.

**Table 1**
**Estimated Concentration of $Ca^{2+}$ at 37°C for Three Sequential Dilutions as Described in Subheading 3.2.**

| Dilution | 1 | 2 | 3 | 4 | 5 | 6 | 7 | 8 | 9 | 10 | 11 |
|---|---|---|---|---|---|---|---|---|---|---|---|
| pH 7.2 | 0 | $1.0e^{-8}$ | $2.11e^{-8}$ | $3.35e^{-8}$ | $4.73e^{-8}$ | $6.25e^{-8}$ | $7.94e^{-8}$ | $9.83e^{-8}$ | $1.19e^{-7}$ | $1.42e^{-7}$ | $1.68e^{-7}$ |
| pH 7.0 | 0 | $3.73e^{-8}$ | $7.88e^{-8}$ | $1.25e^{-7}$ | $1.76e^{-7}$ | $2.33e^{-7}$ | $2.96e^{-7}$ | $3.66e^{-7}$ | $4.45e^{-7}$ | $5.31e^{-7}$ | $6.28e^{-7}$ |
| pH 6.3 | 0 | $4.69e^{-7}$ | $9.9e^{-7}$ | $1.57e^{-6}$ | $2.22e^{-6}$ | $2.93e^{-6}$ | $3.72e^{-6}$ | $4.6e^{-6}$ | $5.58e^{-6}$ | $6.67e^{-6}$ | $7.88e^{-6}$ |

### *3.4.* In Situ *Calibration of Snarf-1 and Fura-2*

*In situ* calibrations are important to compare absolute steady-state concentrations of the ions in different cell populations. This is particularly important when cells are transfected with vectors that influence growth rate, which often is associated with changes in steady-state pH ***(3,28)***. In addition, biological variability between cells must be recognized. By incubating cells in an "intracellular" buffer in the presence of selective ionophores for $H^+$, $K^+$, and $Ca^{2+}$, intracellular ion concentration can be manipulated by changing media concentrations, and therefore, the probes trapped within the cytosolic compartment can be adequately calibrated. 4Br-A23187, a nonfluorescent $Ca^{2+}$ ionophore is used in combination with nigericin/valinomycin in high $K^+$/EGTA buffers to generate physiologically relevant calibration curves for intracellularly trapped fura-2 and snarf-1 (*see* **Note 8**). By varying $pH_{ex}$ between pH 6.0 and 8.0 at 0.25 unit increments, one can obtain the $pK_a$ of snarf-1 from the *in situ* calibration curves. Sequential incubation with media containing incrementally increasing $Ca^{2+}$ concentration ranging from 0 to submicromolar or low micromolar to 250 μ*M* provides a full analysis of $K_d$, $R_{min}$, and $R_{max}$ for fura-2 at each pH.

1. 300 mL of KEGTA containing 2 μ*M* 4Br-A23187, 2 μ*M* valinomycin, and 5 μ*M* nigericin is prepared.
2. Dye-loaded cells on cover slips are transferred to the fluorometer cuvet and perfused in KEGTA buffer at selected pH values. Fluorescence is then continuously recorded until equilibration of extracellular ions with the intracellular space is reached—typically 3–5 min.
3. Fura-2 excitation and snarf-1 emission spectra are acquired (*see* **Note 9**).
4. Sequential dilutions: **Steps 3–5** are identical to those carried out for in vitro calibrations (**Subheading 3.2.**). However, a minimum of 3 min is required for equilibration of ions between media and intracellular space at the new $Ca^{2+}$/pH setting (*see* **Note 10**).

### *3.5. Comparison of Steady-State Ion Concentrations Between Unique Cell Populations*

To evaluate the validity of using *in situ* calibration parameters for estimating pH and $Ca^{2+}$ in each specific experiment, the *in situ* $R_{min}$ and $R_{max}$ for both probes needs to be assessed. For simplicity and reliability, cells are perfused with KEGTA and CaEGTA buffers (containing ionophores) at three distinct pH values (i.e., 6.0, 7.0, and 7.5) to obtain the corresponding *R* values, thereby allowing comparison of the *in situ* titration parameters from a discrete number of points vs those generated from a complete *in situ* titration (*see* **Note 10**).

1. Dye-loaded cells on cover slips are transferred to the fluorometer cuvet and perfused in EB for 2 to 3 min prior to data acquisition. Full emission and excitation spectra are acquired to evaluate the quality of the spectra (*see* **Note 11**).

2. Fluorescence data at ion-sensitive wavelengths are then acquired, and ion-insensitive wavelengths are followed to determine if dye loading is stable or if dye is quenched (*see* **Notes 12** and **13**).
3. The resting ion concentrations are evaluated after a stable signal is obtained (*see* **Note 14**).
4. Full emission and excitation spectra of snarf-1 and fura-2 are acquired to confirm that the spectral characteristics are comparable to the calibration spectra.
5. The perfusion media are changed to KEGTA buffer containing ionophores at a selected pH value (e.g., 6.3; **Table 1**, *see* **Note 9**), and fluorescence is continuously recorded until equilibration of extracellular ions with the intracellular space is achieved—typically 3–5 min.
6. The perfusion media are changed to KEGTA diluted with CaEGTA held at equal pH to obtain a midrange $Ca^{2+}$ concentration (e.g., approx 3 μ*M*, dilution 5; *see* **Note 9**, **Table 1**).
7. The perfusion media are changed to KEGTA diluted with CaEGTA held at equal pH to obtain the maximal $Ca^{2+}$ concentration (dilution 11; *see* **Note 9**, **Table 1**).
8. Sequences 5–7 are repeated at two additional pH values (e.g., *see* **Note 4**).
9. Spectra obtained at each pH/$Ca^{2+}$ value are compared to those obtained during the *in situ* calibrations at the same pH/$Ca^{2+}$ values, to determine the validity of the limited calibration.

### 3.6. Experimental Protocols for Analyzing Ion Homeostasis

Alterations in expression of many specific proteins are translated into differences in cell function. Specific experimental protocols can be designed to test directly for the associated changes in handling of $H^+$ and $Ca^{2+}$. Analyses of these effects are simplified if each cell is used as its own control. However, as we will demonstrate, accurate *in situ* calibration can be crucial for determining the accuracy of a response under specific conditions. Provided in this section are examples that describe methods for testing some specific pathways important for ion homeostasis. In addition, methods for standardizing responses between experiments are described.

#### 3.6.1. $Na^+/Ca^{2+}$ Exchanger

The effect of $Na^+$ removal on $[Ca^{2+}]_i$ can be used to evaluate the activity of the $Na^+/Ca^{2+}$ exchanger ***(21,29,30)***. If the $Na^+/Ca^{2+}$ exchanger is present, $Na^+$ removal results in a rapid increase in $[Ca^{2+}]_i$ owing to reversal of the exchanger. $Na^+$ removal can also result in a decrease in pH owing to inactivation of the $Na^+/H^+$ exchanger, although other pH regulatory mechanisms can compensate to maintain pH constant (i.e., activation of $HCO_3^-$ transport or $H^+$-ATPases).

1. Dye-loaded cells are incubated in EB, and the ion-sensitive ratio for both probes is monitored to determine when a stabile signal is attained.
2. Perfusion media are changed to media in which NaCl has been replaced with 140 m*M* of *N*-methylglucamine-Cl, and the ion-sensitive ratios are monitored continuously.

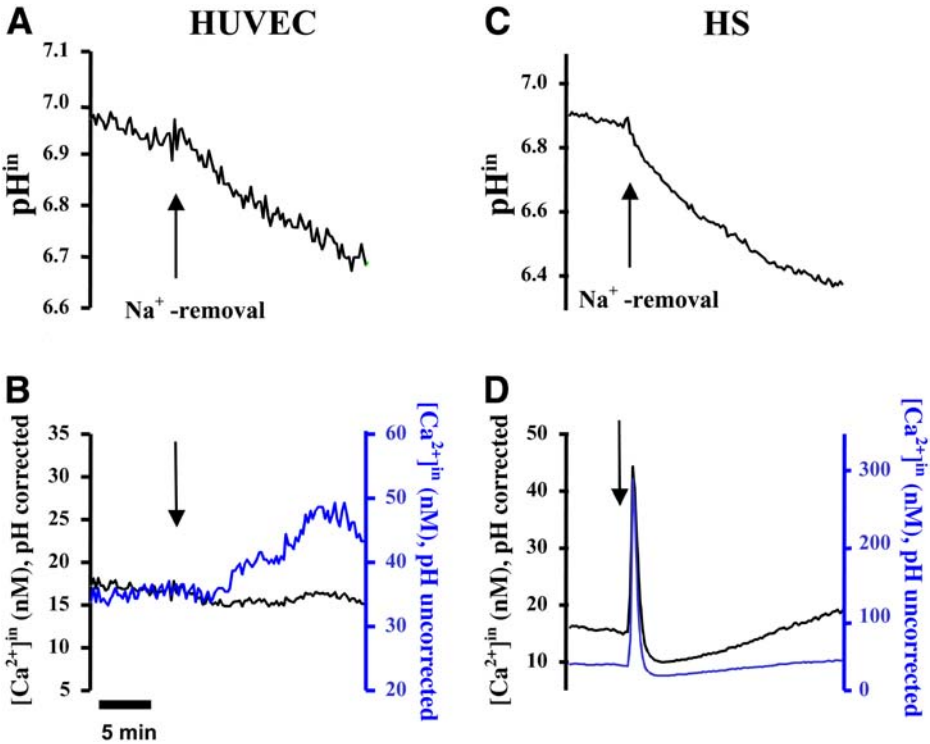


Fig. 2. Effect of $Na^+$ removal on pH and $Ca^{2+}$. Cells were perfused at a rate of 3 mL/min with HBSS, pHex 7.15 at 37°C. At the time indicated (arrow), the $Na^+$ in the media was exchanged for *N*-methyl glucamine; isosmotically substituted. The bottom panels show the $Ca^{2+}$ concentration calculated from a standard calibration curve without correction for the observed changes in pH (light gray lines), and with correction (black lines), as described in **Eq. 6**.

3. At the end of the experiment, 25 m*M* $NH_4Cl$ is added to the perfusion media to elicit a rapid alkalinization.
4. The perfusion media is replaced with $NH_4Cl$-free EB to allow recovery of pH (*see* **Note 15**).

As shown in **Fig. 2**, removal of $Na^+$ resulted in a decrease in pH owing to inhibition of the $Na^+/H^+$ exchanger in both human umbilical vein endothelial cells (HUVEC) and in human skin fibroblasts (HSF). Removal of $Na^+$ also resulted in an increase in the Fura-2 ratio and thereby in apparent changes in $Ca^{2+}$. However, correction for the fura-2 signal response for the change in pH induced by $Na^+$ removal indicates that the increase in $Ca^{2+}$ in HUVEC, which could be interpreted as increase in $Na^+/Ca^{2+}$ exchanger activity, is actually an artifact; i.e., correction of the Fura-2 signal response for changes in pH indicates that there are no significant changes in $Ca^{2+}$ following $Na^+$ removal in HUVEC.

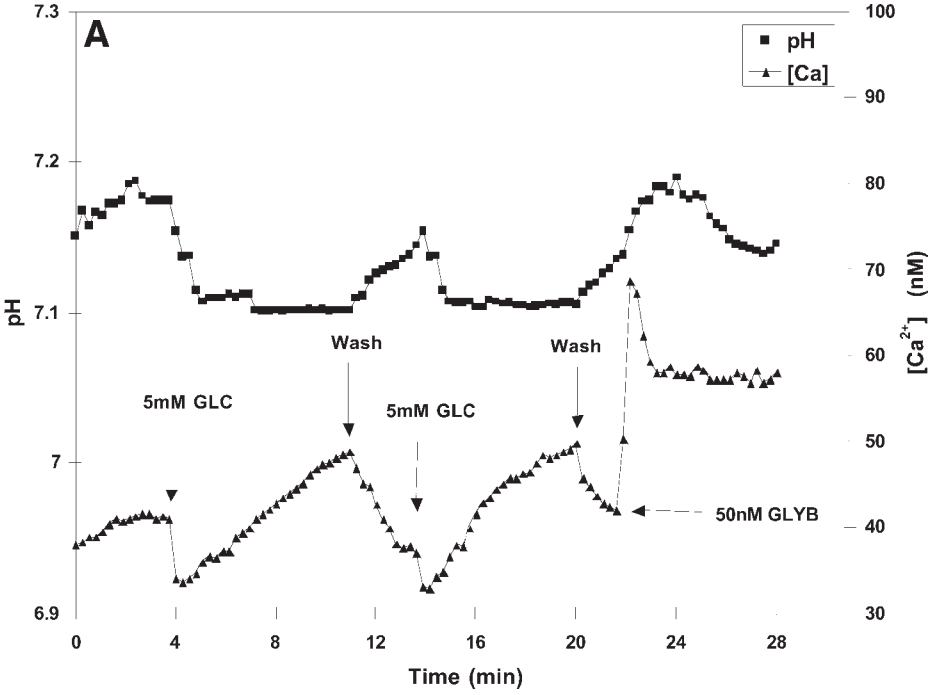
A
pH
[Ca]
5mM GLC
Wash
5mM GLC
Wash
50nM GLYB
pH
[Ca2+] (nM)
Time (min)

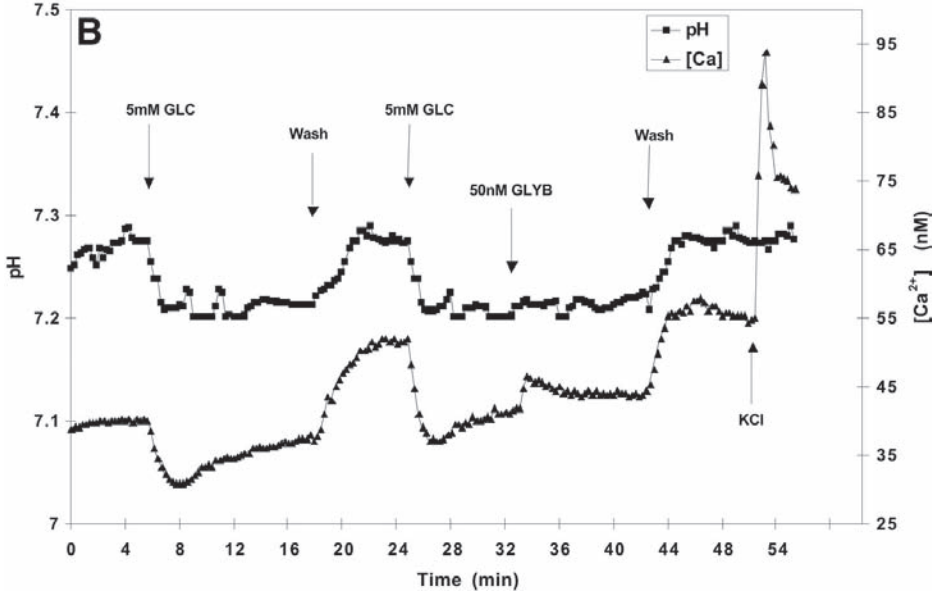
B
pH
[Ca]
5mM GLC
Wash
5mM GLC
50nM GLYB
Wash
KCl
pH
[Ca2+] (nM)
Time (min)

Similar artifactual increases in the fura-2 ratio owing to decreasing pH following $Na^+$ replacement have been observed in ovarian luteal cells ***(30)***. Importantly, $Na^+$ removal in HSF results in apparent increase in $Ca^{2+}$ that is persistent, even after correction for pH effects on Fura-2, indicating that HSF exhibit significant $Na^+/Ca^{2+}$ exchanger activity. The relevance of pH corrections on fura-2 data is difficult to evaluate *a priori*. However, the magnitude of these corrections is clearly larger for acidic than for alkaline pH excursions ***(12,18)***.

### *3.6.2. Normalization of Agonist-Stimulated Responses*

Insulin secretion from pancreatic β-cells is primarily activated by increased metabolism of nutrients and, in particular, glucose with a $K_m$ of approx 15 m*M*. $Ca^{2+}$ is the second messenger that couples secretion to cell activation. Unlike normal β-cells, the RIN-38 cells are excited maximally at 1–5 m*M* glucose. Described is a protocol used to evaluate the effects of modulators of secretion on the glucose-activated response.

1. Dye-loaded cells are incubated in EB containing 0.1 m*M* glucose, and the ion-sensitive ratio for both probes is monitored to determine when a stabile signal is attained.
2. The perfusion media is changed to media containing 5 m*M* glucose, and the ion-sensitive ratios are monitored continuously (**Fig. 3**).
3. After the cell response has peaked, the cells are perfused with low-glucose media to wash out the response.

---

Fig. 3. *(Opposite page)* Glucose induced changes in $Ca^{2+}$ and pH in the insulin secreting β cell line RIN-38 **(A)** Responses of wild-type RIN-38 cells to repetitive challenges with glucose. Cells were incubated in media containing 0.1 m*M* glucose under resting conditions, and were returned to this media to "wash out" the response. After $Ca^{2+}$ returned to baseline, a second response was elicited. The magnitude and rate of response and recovery between the two responses are compared to determine the variability between repetitive activation by the agonist. The effect of a modulator on the agonist-initiated response can be precisely determined by comparing its effect on signaling with that observed in the initial modulator-free response. Also shown is the effect of Glyburide ($10^{-7}$ *M*) on cell $Ca^{2+}$. Glyburide closes nucleotide-sensitive $K^+$ channels ($K_{ATP}$), leading to cell depolarization and enhanced $Ca^{2+}$ influx via voltage dependent channels. **(B)** Effect of knockdown of the sulfonylurea receptor SUR1 in RIN-38 cell signaling. The ability of glucose to elicit an increase in $Ca^{2+}$ is lost in RIN-38 which express limited SUR1, although the initial decrease in cell $Ca^{2+}$ and pH remain indicating that these effects are independent of KATP channel activity. The response to glyburide also is greatly attenuated as expected. The absence of an elevation in $Ca^{2+}$ could be due to loss of dye sensitivity or saturation, which can easily be tested by subsequent addition of KCl; i.e., KCl can be added at the end of an experiment to fully depolarize the membrane in order to estimate the maximal (peak) signal response (*see* **Note 16**).

4. After ion concentrations return to baseline, either a second response is initiated (control), or a modulator is added.
5. In the case for testing the effect of a modulator on a subsequent response, the second agonist (glucose) response is initiated by changing the perfusion media to one containing both glucose and the modulator.
6. At the termination of the experiment, 40–60 m*M* KCl is added to the perfusion media to elicit a maximal signal response.

The second response to elevated glucose is compared to the initial response (% initial) to analyze the effect of modulator. This approach normalizes the effect of a modulator among different experiments independent for differences in absolute signal responses. Comparison among repetitive glucose responses without modulator evaluates the variability of the control response. The KCl pulse provides a measure of the maximal signal response for a given experiment; however, use of this maximal response to normalize between experiments may not be optimal since the sensitivity of the $Ca^{2+}$ dye is sigmoidal.

### *3.6.3. Knockout of the Sulfonylurea Receptor (Isoform 1 [SUR1]) in RIN-38 Cells*

In response to increasing glucose from 0.05 to 5 m*M*, the initial decrease in $Ca^{2+}$ observed in the parental line is maintained, but the secondary elevation in $Ca^{2+}$ that activates the secretory response is absent. Addition of KCl demonstrates that the dynamic range of fura-2 is not limiting the observation of the secondary rise in $Ca^{2+}$ following glucose stimulation. Absence of a response to KCl would be indicative of a problem with dye loading or responsiveness, explaining a similar absence of response to the test agonist. Furthermore, the response after KCl may be used to normalize the original agonist response; i.e., data are analyzed as a percentage of the maximal (KCl) response. However, there are some specific caveats using this approach (*see* **Note 16**).

## 4. Notes

1. Methods to assess the extent of EGTA impurity have been published ***(31)***. The impact of this lack of purity in estimating [$Ca^{2+}$] is larger at high buffer ratios. A simple empirical method for preparing solutions with stoichiometric balance is to assume that EGTA is approx 5% impure. Thus, a 5% excess EGTA is added to the buffer to compensate for the lack of purity ***(31)***.
2. All cells within the population will leak dye into the cuvet medium over time. Therefore, perfusion of the chamber to remove leaked dye is absolutely essential. Buildup of active probe in the medium will obviously lead to spurious results owing to profound differences in extracellular and intracellular ion levels and volumes.
3. Data obtained from simultaneous measurements are further analyzed using SigmaPlot. An advantage of using this system is that data obtained (from either SLM or PTI instruments) can be imported into the SigmaPlot spreadsheet. The

equations needed to estimate pH and $Ca^{2+}$ (i.e., **Eqs. 1–6**) can be written into this format and iteratively solved using built-in algorithms. Then, graph templates can be extracted and used to instantly plot the data. Thus, a plot can be generated in <1 min provided that there are only minor changes in the legends of the figure.

4. Because pH affects the $K_d$ of EGTA for $Ca^{2+}$, i.e., $K_d$ is larger at acidic than alkaline pH (*see* **Fig. 1**), it follows that the magnitude of the $Ca^{2+}$ change for a given titration step is larger at acidic than at alkaline pH. The expected $Ca^{2+}$ concentrations at three distinct pH values (using temperature- and pH-corrected $K_d$ values for $Ca^{2+}$ binding on EGTA) for typical calibration curves outlined in **Subheading 3.2.** (**steps 2** and **3**) are indicated in **Table 1**. The EGTA $K_d$ values used for estimating free $Ca^{2+}$ are 4.22 μ*M*, 336 n*M*, and 90 n*M* for pH values of 6.3, 7.0, and 7.2, respectively.
5. A general assumption related to dye loading is that the probes become localized within the compartment of interest, which, in this case, is the cell cytosol. Access to a fluorescence microscope facilitates the analysis of probe distribution. Unfortunately, depending on exact loading conditions, the ion-sensitive probes can become sequestrated into subcellular compartments. One relatively quick approach is to permeabilize the cell membrane with a detergent (saponin, 0.1%; 1 min), and to measure the level of fluorescence that remains in the cells. Normally >80% of the signal should be lost with this maneuver unless significant compartmentation or autofluorescence is present. Factors that can influence compartmentation of dye are concentration of AM dye in the loading media, the time of loading, and temperature at which loading is carried out. Approaches to specifically load probes into the cytosol have been described in detail ***(32)***, and should be consulted if unwanted compartmentalization of the probes occurs.
6. Dye toxicity: The effect of AM dyes on cell viability and proliferation should be evaluated. In the author's experience, when snarf-1 and fura-2/AM are used at concentrations of <15 μ*M*, there are only minimal effects on cell viability in the more than 40 different cell types they have used. Cell viability can easily be evaluated by trypan blue exclusion. If loss of viability occurs, the time required for cell loading, the temperature at which loading is carried out, or the dye concentration in the loading media can be decreased. On the other hand, even at concentrations as low as 1 μ*M* with incubation times of 5–10 min, followed by washout of the dye, cell proliferation is decreased without any apparent cytotoxic effect ***(18)***. The mechanisms underlying the inhibition in cell division are not apparent but may be related to ATP depletion or to aldehyde formation on cleavage of the AM form of these dyes ***(33)***.
7. To ensure homogeneous loading, the authors recommend the use of a rocker platform (Bellco, Vineland, NJ) or a belly dancer (Sorvall, Greenville, NC), which can be placed in the 5% $CO_2$ incubator, at 37°C. In addition, pluronic acid can be used to assist in dye loading, if problems with limited dye loading occur. Addition of 1 μL of a 20% stock solution of pluronic acid to 1 mL of loading media often facilitates enhanced levels and more uniform loading of AM dyes.

8. Use of nigericin plus valinomycin is essential to fully collapse the pH gradient and, therefore, to adequately calibrate fura-2 *in situ* because in many cells, varying $Ca^{2+}$ levels can affect pH, which, in turn, affects fura-2 fluorescence ***(18)***.
9. If both signals are similar to those observed from in vitro experiments in terms of spectral shape, proceed with the experiment. If anomalous spectra are obtained, investigate whether the aberrant profiles are due to inherent properties of the cell (i.e., autofluorescence). This can be overcome by ensuring proper loading of the cells. Thus, load another set using higher fura-2 or snarf-1 concentrations. In addition, it is critical that the relative fluorescence intensities of fura-2 and snarf-1 are equivalent (<50% difference in either dye is acceptable). Failure to ensure equivalent loading results in the intensity of one dye overwhelming the other due to inevitable spectral overlap, which will preclude correct measurement of both ions. Equal loading can be achieved by increasing/decreasing the concentration of the AM conjugates in the loading.
10. To obtain reliable *in situ* calibration parameters (i.e., $K_d$/pK, $R_{max}$, $R_{min}$) for estimating pH or $Ca^{2+}$, the authors recommend analyses from at least six different pH and $Ca^{2+}$ concentrations (each in triplicate). For $Ca^{2+}$, titrations should be performed at a minimum of five different pH values because the goodness of the fit with **Eqs. 1–6** using nonlinear minimization routines is determined by the number of observations. In some cell types, it is problematic to perform complete *in situ* titrations for $Ca^{2+}$, because high $Ca^{2+}$ levels can induce contractility and/or cell detachment. Similarly, it is often difficult to perform complete titrations at high pH, because most cells do not tolerate prolonged alkaline pH. Thus, it is difficult to obtain reliable ratio values at alkaline pH or high $Ca^{2+}$. Consequently, there is much error in estimates of *in situ* $R_{max}$ values for both $Ca^{2+}$ and pH indicators. One common solution to this problem is the use of the in vitro $R_{max}$, which can be generated to a high degree of accuracy. This phenomenon does not have a significant effect on characterizing the effect of pH on the $K_d$ of $Ca^{2+}$ indicators, because the pK of this effect is quite low, and thus the $K_d$ is relatively insensitive at alkaline pH values. Although it is theoretically possible to partially overcome this problem by linearizing the data (requiring fewer points at high $Ca^{2+}$ or high pH), in the authors' experience, both linear and nonlinear methods provide similar $K_d$/pK and $R_{min}$ values, and more reproducible in situ $R_{max}$ values are obtained from nonlinear methods.
11. If the calculated $R_{min}$ or $R_{max}$ values are distinct (>10%) from those obtained from the complete calibrations, it may indicate that the intracellular environment of the cell population has changed, and therefore new titrations are required. In the authors' experience with 3T3 cells, thawing of new cell cultures and complete *in situ* titrations are generally required every 12 passages. However, this must be tested for every batch and for each individual cell type.
12. On-line analyses of all useful wavelengths is important for correct interpretation of data. The behavior of these wavelengths, and not only ratios, should be continuously monitored during an experiment. Specifically, treatments that elicit increases in pH should elicit distinct increases and decreases in the signal at 644

and 584 without changes in the isoemissive wavelength. Similarly, increases in $Ca^{2+}$ should be associated with increases and decreases in the fluorescence signals at 340 and 380 nm, respectively. This is particularly important when analyzing $R_{min}$ and $R_{max}$ for assessment of absolute ion concentrations.

13. Dye behavior at isoemissive/isoexcitation wavelengths should be assessed throughout an experiment. A drastic drift in the fluorescence signal may indicate that cells are detaching or exhibiting changes in cell volume. The ratio method partially corrects for this; however, if the changes are not symmetric, then the ratio values also are modified. The signals at the isoexcitation and isoemissive point of fura-2 and snarf-1, respectively, are particularly useful for monitoring dye leakage. It is normal to observe a decrease in signal owing to dye leakage/extrusion or photobleaching of the probe. In the ratio mode, this will typically be corrected, and the resulting ratio should be stable.
14. Individual cells within a population of cultured cells can have very heterogeneous resting ion levels, which may be due to many factors, including their state of differentiation. A consideration when attempting to analyze "normal resting" levels is developing an approach to bring all cells to a similar level of activation. For example, RIN-38 cells are mildly activated by amino acids and other nutrient factors. The authors have found that treating these cells with alanine during the AM wash period stabilizes the subsequent responses of cells within the population to glucose, which results in a significant decrease in the variability of response to many agonists, and normalizes resting levels.
15. Addition of activators such as KCl or $NH_4Cl$ at the end of an experiment provides general information regarding dye responsiveness. However, the signal response of the dye exhibits a nonlinear response at high ion concentrations, making such a maneuver difficult to interpret with respect to absolute ion concentration.
16. In cells that express voltage-activated $Ca^{2+}$ channels, KCl can be used to elicit membrane depolarization at the end of an experiment to evaluate absolute maximal $Ca^{2+}$ signal responses for an individual experiment. In the absence of voltage-activated $Ca^{2+}$-dependent channels, or lack of a response to KCl treatment, ionomycin or A23187 can be used to determine the maximal signal response.

## References

1. Becker, T. C., Noel, R. J., Lynch, R. M., Johnson, J. H., Takeda, J., Bell, G. I, et al. (1996) Adenovirus mediated overexpression of glucokinase isoforms in islets: Minimal secretory and metabolic effects relative to hexokinase overexpression. *J. Biol. Chem.* **271,** 390–394.
2. Gillies, R. J., Martinez-Zaquilan, R., Martinez, G. M., Serano, R., and Perona, R. (1990) Tumorigenic 3T3 Cells maintain an alkaline intracellular pH under physiological conditions. *Proc. Natl. Acad. Sci. USA* **87,** 7414–7418.
3. Tompkins, L. S., Murphy, S. M., Nullmeyer, K. D., Weber, C., and Lynch, R. M. (2002) Regulation of secretory granule pH in insulin secreting cell lines. *Am. J. Physiol. Cell Physiol.* **283,** C429–C437.

4. Patterson, G. H., Knobel, S. M., Sharif, W. D., Kain, S. R., and Piston, D. W. (1997) Use of green fluorescent protein and its mutants in quantitative fluorescence microscopy. *Biophys. J.* **73,** 2782–2790.
5. Hanson, G. T., McAnaney, T. B., Park, E. S., Rendell, M..E., Yarbrough, D. K., Chu, S., et al. (2002) Green fluorescent protein variants as ratiometric dual emission pH sensors. 1. Structural characterization and preliminary application. *Biochem.* **41,** 15,477–15,488.
6. Putney, L. K., Denker, S. P., and Barber, D. L. (2002) The changing face of the $Na^+/H^+$ exchanger, NHE1: structure, regulation, and cellular actions. *Annu. Rev. Pharmacol. Toxicol.* **42,** 527–552.
7. Putnam, R. W. (2001) Intracellular pH regulation, in: *Cell Physiology Source Book*, 3rd Ed. (Speralakis, N., ed.) Academic Press, New York, NY, pp. 357–376.
8. Clapham, D. E. (1995) Calcium signaling. *Cell* **80,** 259–268.
9. Berridge, M. J., Bootman, M. D., and Roderick, H. L. (2003) Calcium signaling: dynamics, homeostasis and remodelling. [Review]. *Nat. Rev. Mol. Cell. Biol.* **4,** 517–529.
10. Opas, M. (1997) Measurement of intracellular pH and pCa with a confocal microscope. *Trends Cell Biol.* **7,** 75–80.
11. Tsien, R. Y. (1989) Fluorescent indicators of ion concentration. *Methods Cell Biol.* **30,** 127–156.
12. Martinez-Zaguilan, R., Parnami, G., and Lynch, R. M. (1996) Selection of ion indicators for simultaneous measurement of pH and $Ca^{2+}$. *Cell Calcium* **19,** 337–349.
13. Martinez-Zaguilan, R., Gurule, M., and Lynch, R. M. (1996) Simultaneous measurement of pH and $Ca^{2+}$ in single insulin secreting cells by microscopic spectral imaging. *Am. J. Physiol.* **270,** C1438–1446.
14. Dixon, D. A. and Haynes, D. H. (1990) The pH dependence of the cardiac sarcolemmal $Ca^{2+}$-transporting ATPase: Evidence that the $Ca^{2+}$ translocator bears a doubly negative charge. *Biochem. Biophys. Acta* **1029,** 274–284.
15. Orchard, C. H. and Kentish J. C. (1990) Effects of changes of pH on the contractile function of cardiac muscle. *Am. J. Physiol.* **258,** C967–C981.
16. Sanchez-Armass, S., Martinez-Zaguilan, R., Martinez, G., and Gillies, R. J. (1994) Regulation of pH in rat synaptosomes. I. Role of sodium, bicarbonate, and potassium. *J. Neurophysiol.* **71,** 2236–2248.
17. Van Adelsberg, J. and Al-Awqati, Q. (1986) Regulation of cell pH by $Ca^{2+}$-mediated exocytotic insertion of $H^+$-ATPases. *J. Cell Biol.* **102,** 1638–1645.
18. Martinez-Zaguilan, R., Martinez, G. M., Lattanzio, F., and Gillies, R. J. (1991) Simultaneous measurements of intracellular pH and $Ca^{2+}$ using the fluorescence of snarf-1 and fura-2. *Am. J. Physiol.* **260,** C297–C307.
19. Perona, R. and Serrano, R. (1988) Increased pH and tumorigenicity of fibroblasts expressing a yeast $H^+$ pump. *Nature* **334,** 438–440.
20. Clark, S. A., Burnham, B. L., and Chick, W. L. (1990) Modulation of glucose-induced insulin secretion from a rat clonal B-cell line. *Endocrinology* **127,** 2779–2788.

21. Martinez-Zaguilan, R., Chinnock, B. F., Wald-Hopkins S., Bernas M., Way, D., Weinand, M., et al. (1996). $[Ca^{2+}]_i$ and pH in homeostasis in Kaposi sarcoma cells. *Cell. Physiol. Biochem.* **6,** 169–184.
22. Gillies, R. J. and Martinez-Zaguilan, R. (1991) Regulation of intracellular pH in BALB/c-3T3 cells: Bicarbonate raises pH via $NaHCO_3$/HCl exchange and attenuates the activation of $Na^+/H^+$ exchange by serum. *J. Biol. Chem.* **266,** 1551.
23. Ohkuma, S. and Poole, B. (1978) Fluorescence probe measurement of the intralysosomal pH in living cells and the perturbation of pH by various agents. *Proc. Natl. Acad. Sci. USA* **75,** 3327–3331.
24. Iredale, P. A. and Dickenson, J. M. (1995) Measurement of intracellular free calcium ion concentration in cell populations using Fura-2. *Meth. Mol. Biol.* **41,** 203–213.
25. Konishi, M., Olson, A., Hollingworth, S., and Baylor, S. M. (1988) Myoplasmic binding of fura-2 investigated by steady-state fluorescence and absorbance measurements. *Biophys. J.* **54,** 1089–1104.
26. Bassani, J. W. M., Bassani, R. A., and Bers, D. M. (1995) Calibration on indo-1 and resting intracellular $[Ca^{2+}]_i$ in intact rabbit cardiac myocytes. *Biophys. J.* **68,** 1453–1460.
27. Harrison, S. M. and Bers, D. M. (1989) Correction of proton and $Ca^{2+}$ association constants of EGTA for temperature and ionic strength. *Am. J. Physiol.* **256,** C1250–C1256.
28. Martinez, G. M., Martinez-Zaguilan, R., and Gillies, R. J. (1994) Effect of glucose on pH and $Ca^{2+}$ in NIH-3T3 cells transfected with the yeast p-type $H^+$-ATPase. *J. Cell. Physiol.* **161,** 129–141.
29. Lax, D., Martinez-Zaguilan, R., and Gillies, R. J. (1994) Furazolidone increases thapsigargin-sensitive $Ca^{2+}$-ATPase in chick cardiac myocytes. *Am. J. Physiol.* **36,** H734–H741.
30. Martinez-Zaguilan, R., Wegner, J. A., Gillies, R. J., and Hoyer, P. B. (1994) Differential regulation of $Ca^{2+}$ homeostasis in ovine large and small luteal cells. *Endocrinology* **135,** 2099–2108.
31. Klabusay M. and Blinks, J. R. (1996) Some commonly overlooked properties of calcium buffer systems: A simple method for detecting and correcting stoichiometric imbalance in $Ca^{2+}$ EGTA solutions. *Cell Calcium* **20,** 227–234.
32. Roe, M. W., Lemasters, M. M., and Herman, B. (1990) Assessment of Fura-2 for measurements of cystolic free calcium. *Cell Calcium* **11,** 63–74.
33. Tiffert, T., Garcia-Sancho, J., and Lew, V. (1984) ATP depletion caused by low concentrations of formaldehyde and/or $Ca^{2+}$-chelator esters in human red cells. *Biochim. Biophys. Acta* **773,** 143–156.

# 19

# Measurement of Cytosolic-Free $Ca^{2+}$ in Plant Tissue

**Martin R. McAinsh and Carl K.-Y. Ng**

## 1. Introduction

Several techniques have been used to measure the concentration of cytosolic-free $Ca^{2+}$ ($[Ca^{2+}]_{cyt}$) in plants ***(1,2)***. These include $Ca^{2+}$-sensitive microelectrodes, luminescent photoproteins, cameleons, and fluorescent $Ca^{2+}$ indicators. $Ca^{2+}$-sensitive microelectrodes ***(3)*** can be used only in cells that are able to withstand impalement with two electrodes or a double-barrelled electrode. In addition, microelectrodes suffer from slow response times and difficulties with calibration. These problems are particularly acute in plant cells in which the high turgor often results in partial displacement of the sensor, and the subsequent loss of sensitivity, following impalement. Consequently, the use of $Ca^{2+}$-sensitive electrodes has been limited to only a few studies in plants and algae ***(4,5)***.

Luminescent photoproteins, such as aequorin ***(6)***, emit light on binding $Ca^{2+}$. The luminescence is directly proportional to $[Ca^{2+}]_{cyt}$ and can be measured by either luminometry or imaging techniques. Initially, measurement of plant $[Ca^{2+}]_{cyt}$ using aequorin was restricted to a limited number of cell types owing to the need to microinject this high-molecular-weight protein into cells using pressure ***(7,8)***. More recently, aequorin has been introduced into plants by stable transformation techniques ***(9)*** allowing the protein to be targeted specifically to the cytosol ***(9,10)*** or to organelles ***(10,11)***. This provides a noninvasive method for monitoring whole-plant $[Ca^{2+}]_{cyt}$ and organellar-free $Ca^{2+}$. However, potential limitations with this technique include differences in the stability, distribution, or localization of aequorin in cells, and differences in the permeability of cells to the luminophore coelentrazine. In addition, at present this technique is limited to plant species, such as tobacco and *Arabidopsis*.

From: *Methods in Molecular Biology, vol. 312: Calcium Signaling Protocols: Second Edition*
Edited by: D. G. Lambert © Humana Press Inc., Totowa, NJ

Cameleons are a new green fluorescent protein (GFP)-based $Ca^{2+}$ sensor ***(12,13)*** consisting of a fusion protein comprising a cyan-emitting version of GFP linked to calmodulin and a calmodulin-binding peptide (M13) and an enhanced yellow-emitting GFP. Binding of $Ca^{2+}$ to the calmodulin domain induces a conformational change that can be detected by fluorescence resonance energy transfer (FRET) between the component cyan and yellow fluorescent protein domains. $[Ca^{2+}]_{cyt}$ can therefore be measured by determining the efficiency of FRET. Like aequorin, cameleons can be introduced into plants by stable transformation techniques and have the potential to be targeted to specific cell types or organelles ***(12,14)***. However, to date, as with aequorin, their use has been restricted to species such as *Arabdiopsis* ***(15,16)***.

Fluorescent $Ca^{2+}$-sensitive indicators have been used extensively to measure plant $[Ca^{2+}]_{cyt}$ ***(1,2)***. These fall into two main categories: nonratiometric indicators, which exhibit an increase in fluorescence across the whole of the emission spectra on binding $Ca^{2+}$ (e.g., calcium green); and ratiometric indicators, which exhibit a shift in either their excitation or emission spectra when they bind $Ca^{2+}$. For example, fura-2 exhibits a shift in its excitation maximum (510-nm emission) on binding $Ca^{2+}$, so that the fluorescence at 340 nm increases and the fluorescence at 380 nm decreases with increasing $[Ca^{2+}]_{cyt}$; the 340/380 nm fluorescence ratio is proportional to $[Ca^{2+}]_{cyt}$ ***(17)***. Quantification of $[Ca^{2+}]_{cyt}$ using nonratiometric indicators is complicated by cell-to-cell variation in the concentration and distribution of indicators within cells together with indicator loss during experiments ***(17)***. Therefore, ratiometric measurements of $[Ca^{2+}]_{cyt}$ obtained using either a ratiometric $Ca^{2+}$-sensitive indicator or a combination of nonratiometric $Ca^{2+}$-sensitive indicator co-loaded into cells with a $Ca^{2+}$-insensitive dye, such as Texas Red, are preferred.

A number of techniques are available for loading fluorescent $Ca^{2+}$-sensitive indicators into plant cells, including low-pH loading, ester loading, electroporation, digitonin permeabilization, and microinjection ***(1)***. These have all met with varying degrees of success. Microinjection allows a wide range of compounds to be introduced directly into the cytosol of a cell and has been the most successful method in plants. There are two main techniques for microinjections: iontophoretic injection and pressure injection ***(18)***. Iontophoretic microinjection uses electrical current to carry charged molecules, such as the free acid forms of the $Ca^{2+}$-sensitive indicators, into cells ***(18)***. By contrast, pressure microinjection uses applied pressure to move solutions into a cell. Iontophoretic and pressure microinjection have both been used to load $Ca^{2+}$-sensitive indicators into plant cells ***(1,19–21)***. In addition, patch-clamp techniques have also been used to introduce compounds into plant cell protoplasts in the whole-cell configuration ***(16,23)***.

The $Ca^{2+}$-dependent fluorescence signal of cells loaded with $Ca^{2+}$-sensitive indicators can be quantified using either photometric or imaging techniques.

The equipment required for each of these techniques differs markedly; however, there are four common components. These are:

1. An excitation light source that allows the selection of excitation wavelengths.
2. A specimen holder for the isolation and perfusion of cells.
3. A detector that enables the emission wavelengths to be specified.
4. Signal processing for amplification, recording, and analysis of data ***(1,2,18,24)***.

Ratio photometry detects total fluorescence emissions. This provides quantitative and temporal information about changes in whole-cell $[Ca^{2+}]_{cyt}$. Ratio imaging, employing conventional imaging techniques, uses a video camera to detect the fluorescence emissions, providing additional information about the spatial distribution of $[Ca^{2+}]_{cyt}$. Furthermore, three-dimensional spatial resolution can be achieved using confocal scanning laser microscopy (CSLM) ***(24)*** and/or two-photon laser microscopy ***(25)***.

There are two important factors that must be taken into account when using fluorescent $Ca^{2+}$ indicators to measure $[Ca^{2+}]_{cyt}$ in plants: cell autofluorescence, and the signal-to-noise ratio (SNR). Plant cells are highly autofluorescent at the excitation wavelengths of many of the $Ca^{2+}$-sensitive indicators. Therefore, it is essential to correct for the contribution this makes to the total fluorescence signal at excitation or emission wavelengths. Following autofluorescence correction, the signal from cells loaded with $Ca^{2+}$-sensitive indicators is often low, making measurements extremely noisy. The noise can be reduced by integrating successive fluorescence measurements, increasing the SNR.

Many of the techniques required for the measurement of $[Ca^{2+}]_{cyt}$ in plant tissue—including specimen preparation, microinjection of fluorescent $Ca^{2+}$-sensitive indicators, quantification of the $Ca^{2+}$-dependent fluorescence, and calibration of the fluorescence signal—are illustrated clearly in studies of $[Ca^{2+}]_{cyt}$ in stomatal guard cells ***(19–23,26–38)***. These studies also highlight many of the problems, and their solutions, which are encountered during measurements of plant $[Ca^{2+}]_{cyt}$. This chapter describes a method for measuring $[Ca^{2+}]_{cyt}$ in guard cells of the model species *Commelina communis* using the ratiometric fluorescent $Ca^{2+}$-sensitive indicator fura-2.

## 2. Materials

1. Plant material: *C. communis* L. is grown from seed in Levington M3 potting compost in a temperature-controlled growth room (day/night temperature of 24/19 ± 1°C, 16-h per day, photon flux density of 150 µmol/$m^{-2}$·$s^{-1}$). Maintain the plant free from $H_2O$ stress at all stages of development ***(39)*** (*see* **Note 1**).
2. Isolation buffer: 10 m*M* of 2-(*N*-morpholino)ethanesulfonic acid (MES) in distilled $H_2O$. Adjust to pH 6.2 with KOH. Store at 4°C (*see* **Notes 2** and **3**).
3. Perfusion buffer: 10 m*M* of MES and 10 m*M* of KCl in distilled $H_2O$. Adjust pH 6.2 with KOH. Store at 4°C (*see* **Notes 2** and **3**).
4. Opening buffer: 10 m*M* of MES and 50 m*M* of KCl in distilled $H_2O$. Adjust pH 6.2 with KOH. Store at 4°C (*see* **Notes 2** and **3**).

5. Fura-2: prepare a 10-m*M* stock solution of fura-2 pentapotassium salt (Molecular Probes, Eugene, OR [*see* **Notes 4** and **5**]) in double-distilled $H_2O$. The stock solution of fura-2 should be made up in a 0.5-mL microfuge tube. Check that the pH is approx 7.0 by spotting a small aliquot of the solution onto pH paper. Adjust the pH using very small volumes of pH reagents (*see* **Note 6**). Store at –20°C. Prepare a fresh injection solution of 0.5 m*M* fura-2 daily by diluting the stock solution with 50 m*M* KCl made up in double-distilled $H_2O$ (*see* **Note 7**). Immediately prior to use, centrifuge the fura-2 stock solution at 13,000*g* for 10 min in a microfuge.
6. Cover slips: 18 × 18 and 22 × 64 mm (Chance Propper, Warley, UK).
7. Low-melting point wax can be purchased from Agar Scientific, Essex, UK.
8. Petroleum jelly can be purchased from Chesbrough-Ponds, London, UK.
9. Low-power soldering iron can be purchased from RS Components, Northants, UK.
10. Perfusion system: perfusion is provided under gravity from a temperature-controlled reservoir mounted approx 50 cm above the specimen (*see* **Note 8**). The reservoir consists of a 6-L heated water bath (Grant, Cambridge, UK) and a purpose-built cooling coil. Perfusion media are delivered to the specimen along an insulated pipe. Excess media are removed from the specimen under vacuum ***(29)***. A schematic representation of the perfusion system used during measurements of guard cell $[Ca^{2+}]_{cyt}$ is shown in **Fig. 1** (*see* **Note 9**).
11. Microinjection of fura-2: micropipets are fabricated from quartz glass capillaries (1-mm outside diameter, Sutter Instruments, Novato, CA) using a laser-based microelectrode puller (Sutter Instruments, Novato, CA; Model P-2000 Micropipet Puller) (*see* **Note 10**). Micropipets are positioned using a precision micromanipulator (Leitz-Leica, Milton Keynes, UK). Fura-2 is microinjected by pressure using a modified pressure probe ***(40)*** and using an average pressure of 1.2 MPa. A schematic representation of the system used to microinject guard cells is shown in **Fig. 1** (*see* **Note 11**).
12. Fluorescence microscopy: specimens are viewed using an inverted epifluorescence microscope with ultraviolet (UV) optics (*see* **Note 12**). Additional stage illumination is from a halogen cold-light source (Schott, Cologne, Germany). Fluorescence excitation is from a xenon light source and is transmitted to the microscope via a liquid light guide (e.g., Cairn Research, Kent, UK). Excitation wavelengths (340 and 380 nm, 10-nm bandwidth) are selected using a monochromator or interference filters and a spinning filter changer (e.g., Cairn Research). Emission (510 nm, 20-nm bandwidth) wavelengths are specified using together with a 400-nm dichroic mirror (Nikon) (*see* **Note 13**). A ×40 oil immersion lens (1.30 numerical aperture) (e.g., a Nikon CF Fluor DL ×40, oil immersion lens) and nonfluorescent immersion oil are used for all measurements. A schematic representation of the epifluorescence microscope used in the measurement of guard cell $[Ca^{2+}]_{cyt}$ is shown in **Fig. 1**.
13. Measurement of $[Ca^{2+}]_{cyt}$: fluorescence emissions (510 nm) are quantified using either ratio photometry or ratio imaging techniques. Photometric studies are performed using a Cairn Research spectrophotometer system ***(19–21,29–31,34–37)***.

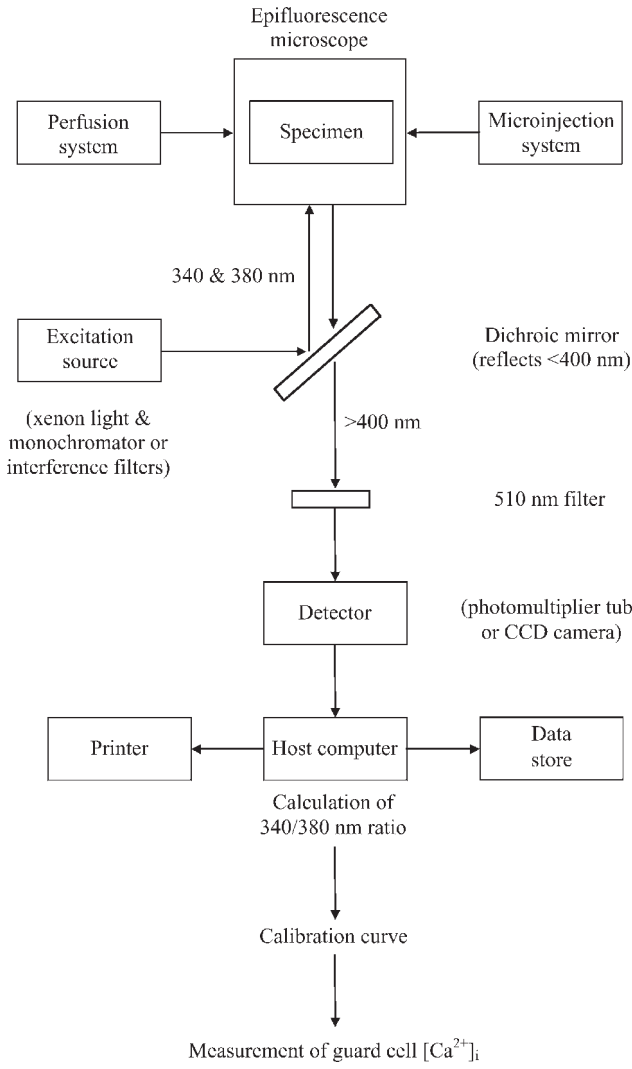


Fig. 1. A schematic representation of the photometric and/or conventional imaging equipment required for measurements of $[Ca^{2+}]_{cyt}$ in stomatal guard cells using fura-2. CCD, charge-coupled device.

Imaging studies are performed using Axon Imaging Workbench ***(37)***. Fluorescence images are recorded using a cooled Extended ISIS-M intensified charge-coupled device camera (Photonic Science, Sussex, UK) ***(29,30,37)***. A schematic representation of the photometric and imaging systems used to quantify the $Ca^{2+}$-dependent fluorescence of fura-2 in guard cells is shown in **Fig. 1** (*see* **Note 14**).

## 3. Methods

### 3.1. Preparation of Leaf Epidermis

1. Detach the leaf to be peeled immediately prior to each experiment *(29)*.
2. Place the leaf on a glass plate and cut it into lamina strips of manageable widths (5-8 mm) with a razor blade or scalpel (*see* **Notes 15–18**).
3. Cut through the upper epidermis near one end, without damaging the lower epidermis, to form a tab in the lamina strip to obtain the abaxial epidermis (*see* **Notes 19** and **20**).
4. Turn the lamina strip over and pull the tab formed in **step 3** gently back with forceps for a few millimeters to separate the tissues.
5. Peel the remaining epidermis off by pulling the tab vertically away from the rest of the lamina, holding the latter in position with a mounted needle (*see* **Notes 21–23**).
6. Float the detached epidermis (cuticle up) on $CO_2$-free isolation buffer at 25°C. Remove the remaining leaf tissue from both ends of the epidermal strip using sharp scissors.

### 3.2. Perfusion System

1. Cut the freshly prepared epidermis in pieces 2 cm in length *(29)* (*see* **Notes 24** and **25**).
2. Mount the epidermal strip cuticle side down in the middle of a long no. 1.5 cover slip (*see* **Notes 26** and **27**).
3. Pipe a ring of petroleum jelly around the epidermal strip using a 1-mL syringe.
4. Secure the epidermal strip around the edge with four smaller cover slips. Press these down firmly on the petroleum jelly (*see* **Note 28**).
5. Attach the securing cover slips to the bottom cover slip using low-melting point wax (*see* **Note 29**) creating a small open perfusion chamber, approx $0.5 \times 1$ cm and the one cover slip-deep, over the center of the strip (*see* **Note 30**).
6. Place a drop of $CO_2$-free perfusion buffer at 25°C in the perfusion chamber to prevent the epidermis from drying out.
7. Mount the perfusion system on the microscope stage, with the exposed epidermis upward, as if it were a standard microscope slide.
8. Place the inlet and outlet of the perfusion system at the front and rear of the perfusion chamber, respectively.
9. Perfuse the specimen continuously (6 mL/min$^{-1}$) with $CO_2$-free perfusion buffer at 25°C in the dark (*see* **Note 31**).

### 3.3. Microinjection of Fura-2

1. Pull injection micropipet (*see* **Notes 10, 32,** and **33**).
2. Fill the tip of the micropipet with fura-2 using a MicroFil nonmetallic syringe needle (World Precision Instruments, Hertfordshire, UK) (*see* **Notes 34**).
3. Back fill the micropipet with hydraulic fluid used in the pressure injection system and insert the microelectrode into the pipet holder (*see* **Note 35**).
4. Position the micropipet in the perfusion chamber close to the guard cell to be microinjected (*see* **Note 36**).

5. Determine the autofluorescence of each guard cell at 340 and 380 nm prior to microinjection as described in **Subheadings 3.4.** and **3.5.**
6. Impale the guard cell with the injection micropipet (*see* **Note 37**).
7. Load the fura-2 in the tip of the injection micropipet into the cytosol of the guard cell using 1.2 MPa for up to 1 min ***(19)***. Monitor the progress of injection at either 340 or 380 nm excitation (*see* **Notes 38** and **39**).
8. Remove the injection micropipet from the cell following microinjection (*see* **Note 40**).
9. Perfuse the fura-2-loaded guard cells in opening buffer at 25°C under conditions of continuous illumination (photon flux density of 1000 μmol/$m^{-2}$·$s^{-1}$) from a halogen cold light source for 1 h to promote stomatal opening (*see* **Note 41**).
10. Select stomata that open to the same aperture as those on the rest of the epidermal strip (6–10 μm) and in which both the injected and noninjected cells of a single stoma exhibit the same increase in turgor for measurements of $[Ca^{2+}]_{cyt}$ (*see* **Notes 25, 40, 42,** and **43**).

### 3.4. Ratio Photometry

1. Use ratio photometry to monitor whole-cell $[Ca^{2+}]_{cyt}$ from a single guard cell (*see* **Note 44**).
2. Sample both the 340- and 380-nm $Ca^{2+}$-dependent fura-2 fluorescence (510-nm emission) at 64 Hz.
3. Average the signal over 1 s following autofluorescence subtraction on-line (**Subheading 3.3., step 5**) (*see* **Note 45**).
4. Calculate the 340/380-nm ratio every second online ***(19–21,28–30,34,35,37)***.

### 3.5. Ratio Imaging

1. Use ratio imaging to monitor spatially localized changes in $[Ca^{2+}]_{cyt}$ (*see* **Note 44**).
2. Measure the camera dark signal prior to each experiment. Subtract this from images online.
3. Record alternate 340- and 380-nm excitation (510-nm emission) images at a minimum resolution of 512 × 512 pixels and digitized to 256 gray levels.
4. Average both signals over individual frames, e.g., eight frames (*see* **Note 45**).
5. Calculate the mean autofluorescence from the cytoplasmic region of an unloaded guard cell at both excitation wavelengths (*see* **Note 46**).
6. Subtract the mean autofluorescence values from each pair of averaged 340- and 380-nm images, pixel by pixel, at the end of the experiment.
7. Divide the autofluorescence-subtracted 340-nm image by the corresponding autofluorescence-subtracted 380-nm image, on a pixel-by-pixel basis, to produce a series of 340/380-nm ratio images.

### 3.6. Calibration

1. Perform an in vitro (external) calibration of the 340/380-nm fluorescence ratio vs $[Ca^{2+}]_{cyt}$ using $Ca^{2+}$ calibration buffers (World Precision Instruments, Hertfordshire, UK) (10, 100, and 1000 n*M* of free $Ca^{2+}$) containing 0.5 μ*M* fura-2 (*see* **Notes 47** and **48**).

2. Determine the autofluorescence of a 20-µL drop of distilled $H_2O$ on a glass cover slip (**Subheadings 3.4.** and **3.5.**).
3. Pipet 20-µL aliquots of each of the calibration buffers onto a glass cover slip.
4. Calculate the 340/380-nm fluorescence ratio for each of the calibration buffers using either ratio photometry (**Subheading 3.4.**) or ratio imaging (**Subheading 3.5.**).
5. Construct a standard curve of the 340/380-nm fluorescence ratio against the concentration of free $Ca^{2+}$ ***(27,29,30,37)***.

## 4. Notes

1. Measurements of $[Ca^{2+}]_{cyt}$ using fluorescent $Ca^{2+}$-sensitive indicators have only been performed on stomatal guard cells of *C. communis* ***(19–21,26–31,34,35,37)***, *Vicia faba* ***(22,23,35,36,38)***, *Arabidopsis thaliana* ***(37)***, and the orchid *Paphiopedilum tonsum* ***(32)***. Growth conditions vary depending on the plant species.
2. Always use tissue culture-grade MES. MES buffers should be aerated with $CO_2$-free air for 1 h before use and during experiments. $CO_2$-free air can be obtained by pumping air through a 15-cm column of soda lime (Sigma, Dorset, UK) ***(28)***.
3. MES buffers tend to become contaminated even when stored at 4°C. This can cause problems with perfusion systems and the microinjection of cells. Therefore, unused buffers should be discarded regularly.
4. The Molecular Probes Handbook of Fluorescent Probes and Research Chemicals ***(41)*** is an invaluable source of reference for researchers. The Molecular Probes website provides up to date information on all Molecular Probes products (http://www.probes.com).
5. This is the maximum concentration to which fura-2 will dissolve in aqueous solution.
6. The pH of the stock solution seldom requires adjustment. If the pH differs markedly from pH 7.0, it should be adjusted using very small volumes of either 5 *M* of KOH or HCl.
7. Refreeze the fura-2 stock solution after use. Fura-2 solutions can be subjected to repeated freeze-thaw cycles without any detrimental effects. However, the fura-2 stock solution should be aliquoted into smaller volumes to minimize the number of times it is thawed and refrozen.
8. The perfusion rate can be adjusted by altering the height of the reservoir and/or the diameter of the perfusion tubing. Typically, a perfusion rate of 6 mL/$min^{-1}$ is used ***(28–31,34)***. However, flow rates of up to 10 mL/$min^{-1}$ have been used in studies of guard cell $[Ca^{2+}]_{cyt}$ ***(35)***. Alterations in the rate of delivery of plant hormones, such as abscisic acid, have been shown to affect stomatal responses ***(42)***.
9. Alternative perfusion systems used in studies of guard cell $[Ca^{2+}]_{cyt}$ include perfusion of guard cell protoplasts in the cell-attached configuration ***(22,23)*** and the exchange of perfusion media using low-noise peristaltic pumps ***(26,27)***.
10. Rigid, extremely sharp micropipets with a small tip diameter are required for the microinjection of plant cells. Micropipets with these characteristics are most

frequently obtained from quartz glass capillaries, although borosilicate and aluminosilicate glass capillaries with a larger outside diameter and thicker walls (i.e., smaller inside diameter) can also be used. The harder quartz glass capillaries require a specialized laser-based micropipet puller (Sutter Instruments, Novato, CA; Model P-2000 Micropipette Puller), whereas aluminosilicate or borosilicate capillaries can be used with conventional vertical and horizontal micropipet pullers. Glass capillaries can be obtained with an outside diameter of 1, 1.2, or 1.5 mm, although larger sizes are available, and with a range of inside diameters. The use of filamented glass capillaries can help with the filling of micropipets.

11. Fura-2 has also been iontophoretically microinjected into guard cells ***(19,20, 26–37)***.
12. The Nikon (Melville, NY) inverted epifluorescence microscopes are often used in $Ca^{2+}$ measuring systems ***(19–21,26–31,33,34,37)***. However, Olympus ***(32)*** and Zeiss ***(22)*** microscopes have both been used to measure guard cell $[Ca^{2+}]_{cyt}$.
13. Fura-2 suffers from photobleaching during prolonged exposure to high-intensity 340- and 380-nm light. This can be reduced by the inclusion of either metal gauze neutral density filters (Cairn Research, Oberkochen, Germany) or quartz neutral density filters (Ealing Electro-Optics, Watford, UK) in the light path. In addition, liquid light guides, such as that supplied by Cairn Research, attenuate the excitation light by up to 40%. Reducing the intensity of excitation to approx 3% of the original value allows extended measurements of guard cell $[Ca^{2+}]_{cyt}$ ***(19–21,29–31,34,37)***.
14. Guard cell $[Ca^{2+}]_{cyt}$ has been measured using commercial and purpose-built photometric ***(19–22,26–31,33–36)*** and imaging, both conventional ***(27,29,30,36–38)*** and CSLM ***(23,32)***, techniques.
15. In the case of *C. communis*, the epidermis is typically peeled from the youngest fully expanded leaf of 4-wk-old plants, although this may vary among species ***(19–23,26–32,34–38)***.
16. Lamina strips are normally used immediately. If not, they are floated on $CO_2$-free isolation buffer at 25°C to avoid desiccation.
17. Turgid leaves are easier to peel than flaccid ones.
18. All experiments are conducted during the middle of the photoperiod, between 10 AM and 6 PM, to minimize the effects of diurnal changes in stomatal responses.
19. Great care should be taken to cut through the leaf only as far as the lower epidermis. This requires practice.
20. Adaxial epidermis can be obtained by cutting through the lower epidermis.
21. Leaving the final few millimeters of leaf tissue attached to the epidermis aids handling.
22. Maximum viability is achieved if the epidermis is peeled from the lamina strip at an even, slow speed, taking care to be consistent in the angle of peeling.
23. Peeling is best performed in a pool of $CO_2$-free isolation buffer at 25°C on a glass plate.
24. Guard cells with a low turgor are more easily microinjected than those with a high turgor. Therefore, it is important to use only epidermal strips in which sto-

mata are open to <1 μm. This can be achieved by maintaining plants in the dark for 1 h before use. Stomatal apertures can be determined by mounting a small piece of epidermis from the epidermal strip in a drop of $CO_2$-free isolation buffer at 25°C on a glass slide. Cover the epidermis with a glass cover slip. Press the cover slip down gently with a mounted needle to expel all the air. The epidermis can then be viewed under the microscope and the stomatal apertures measured using an eyepiece graticule ***(39)***.

25. The use of epidermis in which stomata are open to <1 μm allows the stomata to be opened in $CO_2$-free opening buffer at 25°C following microinjection of fura-2. This provides an indicator of guard cell viability ***(29)***.
26. Transfer the epidermis to a long cover slip by holding one end with a pair of forceps while supporting the other with a mounted needle. If the strip rolls up, it is relatively simple to unroll it on the cover slip.
27. It is essential that the epidermal strip is completely flat on the cover slip. This can be achieved by carefully smoothing the strip with a mounted needle and then blotting it gently with a small piece of tissue.
28. The securing cover slips are fabricated from 18 × 18 mm cover slips. Cut into convenient sizes using a diamond-tipped knife (RS Components). Typically, whole cover slips are used to secure the ends of the strip while the sides are secured with half cover slips.
29. The perfusion chamber is fabricated by using 2-mm strips of low-melting point wax and a low-power soldering iron to solder the cover slips together.
30. Large-volume perfusion chambers introduce a lag period in the changeover of perfusion media during which mixing occurs. This can affect the kinetics of stimulus-induced changes in $[Ca^{2+}]_{cyt}$. The small volume of the perfusion chamber allows rapid, almost instantaneous changeover of the perfusion media.
31. Specimens should be perfused with $CO_2$-free perfusion buffer at 25°C in the dark for at least 10 min before use to determine whether they will retain focus.
32. Micropipets with tip diameters ranging from 0.1 to 1 μm have been used to microinject plant cells ***(1)***. Typically, microelectrodes with a tip diameter of <0.25 μm fabricated from either filamented borosilicate (1.2-mm outside diameter, 0.68-mm inside diameter) ***(28–31,34)*** or 1-mm quartz outside diameter ***(19–21,37)*** glass capillaries are used for the microinjection of guard cells. The tip diameter of a representative sample of microelectrodes is measured by scanning electron microscopy ***(43)***.
33. Glass micropipets tend to go blunt overnight. Therefore, fresh micropipets should be pulled at the start of each experiment.
34. Concentrations of $Ca^{2+}$ indicators that have been used to fill microelectrodes range from 50 μ*M* to 10 m*M* ***(1)***. Increasing the concentration of fura-2 reduces volume required for injection to achieve a given cytosolic concentration of fura-2. In turn, this reduces the potential damage caused by injection.
35. Take care to exclude air bubbles by tapping the micropipet with the tip pointed downward before inserting it into the pipet holder.
36. Positioning the micropipet in the perfusion chamber is a highly exacting task and requires practice. It is often impractical to locate the micropipet down the micro-

scope using low magnifications because of the presence of immersion oil on the cover slip. However, by reducing the level of bright-field illumination using the field diaphragm, the micropipet can normally be located by its shadow at high magnification.

37. Gentle tapping of the injection micromanipulator is often required to achieve penetration of guard cells.
38. Fura-2 loaded into the cytosol of guard cells gives a discrete pattern of fluorescence around the edge of cells and in the region of the nucleus ***(27,28)***. However, $Ca^{2+}$ indicators loaded into the guard cell vacuole give a uniform fluorescence over the entire cell ***(27)***. Cells should not be overloaded as this will buffer changes in $[Ca^{2+}]_{cyt}$.
39. Limit the illumination of the specimen with 340- and 380-nm light to the center of the specimen, using the excitation diaphragm of the microscope, to reduce the potential damage to noninjected guard cells from high-intensity UV excitation.
40. The success rate for microinjection is <10%. Epidermal strips should be discarded after 30–60 min if microinjection is unsuccessful.
41. It is important to use a cold light source, such as the Schott KL 1500, to provide continuous illumination of the perfusion chamber to prevent heating of the specimen.
42. Fura-2-loaded cells should meet all the criteria for estimating guard cell viability before use in measurements of $[Ca^{2+}]_{cyt}$ ***(27,29)***.
43. Occasionally microinjected guard cells lose some or all of the fura-2 from the cytosol during the opening protocol (**Subheading 3.3., step 9**). These cells should be discarded.
44. Limit the area from which the fluorescence is recorded to a single guard cell using the emission diaphragm of the microscope.
45. The signal from fura-2-loaded cells is often quite low following autofluorescence correction, making measurements extremely noisy. The noise can be reduced by averaging both the 340- and 380-nm $Ca^{2+}$-dependent fura-2 fluorescence (510-nm emission) over a number of measurements, increasing the SNR.
46. In imaging studies of guard cell $[Ca^{2+}]_{cyt}$, autofluorescence subtraction is complicated by cell movements owing to stomatal closure making it impossible to subtract the initial image of the unloaded cell from all subsequent images. Ratio images calculated in the absence of autofluorescence correction typically underestimate $[Ca^{2+}]_{cyt}$ by 25% ***(27)***. Therefore, a mean autofluorescence calculated from the cytoplasmic region of an unloaded guard cell at both excitation wavelengths is subtracted from images, pixel by pixel, at the end of each experiment ***(27,29,30,37)***.
47. Similar results are obtained for both in vitro and in vivo calibrations of the 340/380-nm fluorescence ratio in guard cells ***(27,29)***. Consequently, an in vitro calibration can be used routinely.
48. In vivo calibration is performed by perfusing fura-2-loaded guard cells with buffers containing different concentrations of free $Ca^{2+}$ in the presence of a $Ca^{2+}$ ionophore (10 n*M*-10 μ*M* Br-A23187). It is assumed that the $[Ca^{2+}]_{cyt}$ reaches equilibrium with the external concentration of free $Ca^{2+}$ within 10 min. Calibra-

tions can be performed by either constructing a standard curve of the 340/380-nm fluorescence ratio against the concentration of free $Ca^{2+}$ or using the following equation:

$$[Ca^{2+}] = bK_d[(R - R_{min})/(R_{max} - R)]$$

where R = any cell ratio value, $b = Ca^{2+}_{free}/Ca^{2+}_{bound}$ fluorescence (380 nm), $R_{min}$ = ratio in $Ca^{2+}$-free conditions, and $R_{max}$ = ratio value in the presence of high (saturating) external $Ca^{2+}$. Practical difficulties are often encountered during in vivo calibration because of loss of fura-2 from cells following treatment with ionophore, inability to reach a steady $R_{min}$ or $R_{max}$, or extremely slow or zero response to the ionophore.

## Acknowledgments

The author thanks the European Community, The Royal Society, the Natural Environment Research Council (UK), and the Biotechnology and Biological Sciences Research Council (UK) for funding.

## References

1. Rudd, J. J. and franklin-Tong, V. E. (2001) Unravelling response-specificity in $Ca^{2+}$ signalling pathways in plant cells. *New Phytol*. **151,** 7–33.
2. Webb, A. A. R., McAinsh, M. R., Taylor, J. E., and Hetherington, A. M. (1996) Calcium ions as intracellular second messengers in higher plants. *Adv. Botanical Res*. **22,** 45–96.
3. Ogden, D. (1994) *Microelectrode Techniques: The Plymouth Workshop Handbook*, 2nd Ed., Company of Biologists Ltd., Cambridge, UK.
4. Miller, A. J. and Sanders, D. (1987) Depletion of cytosolic free calcium induced by photosynthesis. *Nature* **326,** 397–400.
5. Felle, H. (1988) Auxin causes oscillations of cytosolic free calcium and pH in Zea mays coleoptiles. *Planta* **174,** 495–499.
6. Cobbold, P. H. and Lee, J. A. C. (1991) Aequorin measurements of cytoplasmic free calcium, in *Cellular Calcium: A Practical Approach* (McCormack, J. G. and Cobbold, P. H., eds.), Oxford University Press, New York, NY, pp. 55–82.
7. Gilroy, S., Hughes, W. A., and Trewavas, A. J. (1989) A comparison between Quin-2 and Aequorin as indicators of cytoplasmic calcium levels in higher plant cell protoplasts. *Plant Physiol*. **90,** 482–491.
8. Williamson, R. E. and Ashley, C. C. (1982) Free $Ca^{2+}$ and cytoplasmic streaming in the alga, Chara. *Nature* **296,** 647–651.
9. Knight, M. R., Campbell, A. K., Smith, S. M., and Trewavas, A. J. (1991) Transgenic plant aequorin reports the effects of touch and cold-shock and elicitors on cytoplasmic calcium. *Nature* **352,** 524–526.
10. Knight, H., Trewavas, A. J., and Knight, M. R. (1996) Cold calcium signalling in Arabidopsis involves two cellular pools and a change in calcium signature after acclimation. *Plant Cell* **8,** 489–503.
11. Kiegle, E., Moore, C., Haseloff, J., Tester, M. A., and Knight, M. R. (2000) Cell-type-specific calcium responses to drought, salt and cold in the *Arabidopsis* root. *Plant J*. **23,** 267–278.

12. Miyawaki, A., Lopis, J., Heim, R., et al. (1997) Fluorescent indicators for $Ca^{2+}$ based on green fluorescent proteins and calmodulin. *Nature* **388,** 882–887.
13. Gadella, T. W. J., van der Krongt, G. N. M., and Bisseling, T. (1999) GFP-based FRET microscopy in living plant cells. *Trends Plant Sci*. **4,** 287–291.
14. Emmanouilidou, E., Teschemacher, A. G., Pouli, A. E., Nicholls, L. I., Seward, E. P., and Rutter, G. A. (1999) Imaging $Ca^{2+}$ concentration changes at the secretory vesicle surface with a recombinant targeted cameleon. *Curr. Biol*. **9,** 915–918.
15. Allen, G. J., Kwak, J. M., Chu, S. P., et al. (1999) cameleon calcium indicator reports cytoplasmic calcium dynamics in *Arabidopsis* guard cells. *Plant J*. **19,** 735–747.
16. Allen, G. J., Chu, S. P., Harrington, C. L., et al. (2001) A defined range of guard cell calcium oscillation parameters encodes stomatal movements. *Nature* **411,** 1053–1057.
17. Grynkiewicz, G., Poenie, M., and Tsien, R. Y. (1985) A new generation of $Ca^{2+}$ indicators with greatly improved fluorescence characteristics. *J. Biol. Chem*. **260,** 3440–3450.
18. Callaham, D. A. and Hepler, P. K. (1991) Measurement of free calcium in plant cells, in *Cellular Calcium: A Practical Approach* (McCormack, J. G. and Cobbold, P. H., eds.), Oxford University Press, New York, NY, pp. 383–410.
19. Leckie, C. P., McAinsh, M. R., Allen, G. J., Sanders, D., and Hetherington, A. M. (1998) Abscisic acid-induced stomatal closure mediated by cyclic ADP-ribose. *Proc. Natl. Acad. Sci. USA* **95,** 15,837–15,842
20. Staxen, I., Pical, C., Montgomery, L. T., Gray, J. E., Hetherington, A. M., and McAinsh, M. R. (1999) Abscisic acid induces oscillations in guard cell cytosolic free caclium that involve phosphoinositide-specific phospholipase C. *Proc. Natl. Acad. Sci. USA* **96,** 1779–1784.
21. Ng, C. K-Y., Carr, K., McAinsh, M. R., Powell, B., and Hetherington, A. M. (2001) Drought-induced guard cell signal transduction involves sphingosine-1-phosphate. *Nature* **410,** 596–599.
22. Schroeder, J. I. and Hagiwara, S. (1990) Repetitive increases in cytosolic $Ca^{2+}$ of guard cells by abscisic acid activation of nonselective $Ca^{2+}$ permeable channels. *Proc. Natl. Acad. Sci. USA* **87,** 9305–9309.
23. Lemtiri-Chlieh, F., MacRobbie, E. A. C., Webb, A. A., R., et al. (2003) Inositol hexakisphosphate mobilizes an endomembrane store of calcium in guard cells. *Proc. Natl. Acad. Sci. USA* **100,** 10,091–10,095.
24. Gilroy, S. (1997) Fluorescence microscopy of living plant cells. *Annu. Rev. Plant Physiol. Plant Mol. Biol*. **48,** 165–190.
25. Konig, K. (2000) Multiphoton microscopy in life sciences. *J Microsc*. **200,** 83–104.
26. Gilroy, S., Read, N. D., and Trewavas, A. J. (1990) Elevation of cytoplasmic calcium by caged calcium or caged inositol trisphosphate initiates stomatal closure. *Nature* **346,** 769–771.
27. Gilroy, S., Fricker, M. D., Read, N. D., and Trewavas, A. J. (1991) Role of calcium in signal transduction of Commelina guard cells. *Plant Cell* **3,** 333–344.
28. McAinsh, M. R., Brownlee, C., and Hetherington, A. M. (1990) Abscisic acid-induced elevation of guard cell cytosolic $Ca^{2+}$ precedes stomatal closure. *Nature* **343,** 186–188.

29. McAinsh, M. R., Brownlee, C., and Hetherington A. M. (1992) Visualizing changes in cytosolic-free $Ca^{2+}$ during the response of stomatal guard cells to abscisic acid. *Plant Cell* **4,** 1113–1122.
30. McAinsh, M. R., Webb, A. A. R., Taylor, J. E., and Hetherington, A. M. (1995) Stimulus-induced oscillations in guard cell cytosolic free calcium. *Plant Cell* **7,** 1207–1219.
31. McAinsh, M. R., Clayton, H., Mansfield, T. A., and Hetherington, A. M. (1996) Changes in stomatal behaviour and guard cell cytosolic free calcium in response to oxidative stress. *Plant Physiol.* **111,** 1031–1042.
32. Irving, H. R., Gehring, C. A., and Parish, R. W. (1992) Changes in cytosolic pH and calcium of guard cells precede stomatal movements. *Proc. Natl. Acad. Sci. USA* **89,** 1790–1794.
33. Allan, A. C., Fricker, M. D., Ward, J. L., Beale, M. H., and Trewavas, A. J. (1994) Two transduction pathways mediate rapid effects of abscisic acid in *Commelina* guard cells. *Plant Cell* **6,** 1319–1328.
34. Webb, A. A. R., McAinsh, M. R., Mansfield, T. A., and Hetherington, A. M. (1996) Carbon dioxide induces increases in guard cell cytosolic free calcium. *Plant J.* **9,** 297–304.
35. Grabov, A. and Blatt, M. R. (1997) Parallel control of the inward-rectifier $K^+$ channel by cytosolic free $Ca^{2+}$ and pH in Vicia guard cells. *Planta* **201,** 84–95.
36. Grabov, A. and Blatt, M. R. (1998) Membrane voltage initiates $Ca^{2+}$ waves and potentiates $Ca^{2+}$ increases with abscisic acid in stomatal guard cells. *Proc. Natl. Acad. Sci. USA* **95,** 4778–4783.
37. Webb, A. A. R., Larman, M. G., Montgomery, L. T., Taylor, J. E., and Hetherington, A. M. (2001) The role of calcium in ABA-induced gene expression and stomatal movements. *Plant J.* **26,** 351–362.
38. Garcia-Mata, C., Gay, R., Sokolovski, S., Hills, A., Lamattina, L., and Blatt, M. R. (2003) Nitric oxide regulates $K^+$ and $Cl^-$ channels in guard cells through a subset of abscisic acid-evoked signaling pathways. *Proc. Natl. Acad. Sci. USA* **100,** 11,116–11,121.
39. McAinsh, M. R., Brownlee, C., and Hetherington, A. M. (1991) Partial inhibition of ABA-induced stomatal closure by calcium-channel blockers. *Proc. R. Soc. Lond. B* **243,** 195–201.
40. Oparka, K. J., Murphy, R., Derrick, P. M., Prior, D. A. M., and Smith, J. A. C. (1991) Modification of the pressure-probe technique permits controlled intracellular microinjection of fluorescent-probes. *J. Cell Sci.* **98,** 539–544.
41. Haugland, R. R. (2002) *Molecular Probes Handbook of Fluorescent Probes and Research Chemicals*, 9th Ed. Molecular Probes, Eugene, OR.
42. Trejo, C. L., Clephan, A. L., and Davies, W. J. (1995) How do stomata read abscisic acid-signals. *Plant Physiol.* **109,** 803–811.
43. Brown, K. T. and Flaming, D. G. (1986) *Advanced Micropipet Techniques for Cell Physiology*. John Wiley and Sons, Chichester, UK.

# VI

## $Ca^{2+}$-Sensitive Targets

# 20

# Assay and Purification of Calmodulin-Dependent Protein Kinase

**Rajendra K. Sharma**

## 1. Introduction

Posttranslational modification has long been recognized as a way in which the properties of proteins may be subtly altered after synthesis of the polypeptide chain is complete. Amongst the moieties most commonly encountered covalently attached to proteins are oligosaccharides, phosphate, acetyl, formyl, and nucleosides. Posttranslational covalent modification of protein by phosphorylation is one of the most prevalent and best understood mechanisms employed in cellular regulation ***(1–9)***. Protein kinases catalyze the transfer of the γ-phosphoryl group of adenosine triphosphate (ATP) to an acceptor protein substrate. The activity of the enzyme is determined by the transfer of $^{32}P$ (labeled γ-phosphate) from [γ-$^{32}P$] ATP to protein substrate

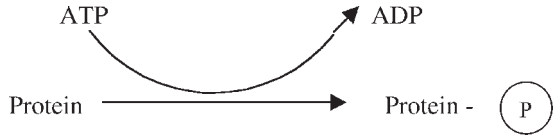


$Ca^{2+}$ is an important intracellular second messenger ***(10–21)*** that regulates cell function through $Ca^{2+}$-dependent phosphorylation of regulatory enzymes and proteins ***(22–35)***. The $Ca^{2+}$-regulatory cascade is mediated by $Ca^{2+}$-binding protein, calmodulin (CaM), and involves a $Ca^{2+}$-dependent reversible association of CaM with its target proteins ***(36–38)***, most notably a large family of $Ca^{2+}$/CaM-dependent protein kinases ***(22–35)***. They are capable of phospho-

From: *Methods in Molecular Biology, vol. 312: Calcium Signaling Protocols: Second Edition*
Edited by: D. G. Lambert © Humana Press Inc., Totowa, NJ

rylating serine and threonine residues on multiple targets and coordinately modifying the activities of several regulatory enzymes and structural proteins ***(29,30,33,35,39)***. CaM kinases have received considerable attention in recent years because they play a pivotal role in various cellular processes, including responses to stimuli that are mediated by $Ca^{2+}$ such as neurotransmitter release, muscle contraction, gene expression, and cell proliferation ***(10,21,29,30, 33,35)***. To identify physiological functions of $Ca^{2+}$ that are mediated by protein phosphorylation, it is essential to purify and characterize each of these kinases and their protein substrates. A number of $Ca^{2+}$/CaM-dependent protein kinases have been characterized ***(22–35)***. $Ca^{2+}$/CaM-dependent protein kinase known as "CaM kinase II" constitutes one of a large family of enzymes known as "multifunctional CaM-dependent protein kinases" ***(29–35)***. The relative amount of CaM-dependent protein kinase II is low compared with other protein kinases; consequently, it is difficult to determine CaM-dependent protein kinase II activity by measuring the existence of the enzyme level in the presence or absence of $Ca^{2+}$ or a CaM antagonist. In addition, like other protein kinases, the CaM-dependent protein kinase II is also autophosphorylated rapidly in the presence of $Ca^{2+}$ and CaM, and it converts to a $Ca^{2+}$-independent form ***(31,40–49)***.

Several investigators have developed purification procedures for the preparation of homogeneous CaM-dependent protein kinase II from various tissues including brain, heart, skeletal muscle, liver, pancreas, and *Aspergillus nidulans* ***(22–28,31,34)***. All these methods involve the use of conventional purification approaches consisting of multiple column chromatographies. This chapter describes the assay method and a rapid purification procedure of CaM kinase II that is suitable for a large-scale preparation.

## 2. Materials

### 2.1. Tissue Material

Fresh bovine hearts were obtained from a local slaughterhouse and transferred to the laboratory in packed ice.

### 2.2. Laboratory Equipments

1. Water bath.
2. Vortex mixer.
3. Spectrophotometer.
4. pH meter.
5. Stainless steel forceps and flat cardboard.
6. Air dryer.
7. Stainless steel wire basket.
8. Magnetic stirrer.
9. Radioactive shield.

10. Geiger-Muller counter.
11. Liquid scintillation counter.

### 2.3. Reagents for CaM-Dependent Protein Kinase Assay

General laboratory chemicals are of analytical grade and are obtained either from Sigma, BDH, or Aldrich.

1. Tris-(hydroxymethyl)-aminomethane (Tris-HCl).
2. Magnesium chloride ($MgCl_2 \cdot 6\ H_2O$).
3. Calcium chloride ($CaCl_2 \cdot 2\ H_2O$).
4. 2-Mercaptoethanol.
5. Ethyleneglycol-*bis*-(β-aminoethyl ether) *N*,*N*′tetraacetic acid (EGTA)
6. ATP.
7. [$\gamma$-$^{32}$P] ATP (ICN Radiochemicals).
8. Substrates: mixed histone, casein.
9. Phosphoric acid.
10. Ethanol.
11. Whatman P81 phosphocellulose filter paper (3 mm) (Whatman Inc., NJ).
12. CaM (Sigma or purify as described by Sharma ***[50]***).
13. Trichloroacetic acid (TCA).
14. Hydrochloric acid (HCL).
15. Sulfuric acid ($H_2SO_4$).
16. Sodium chloride (NaCl).
17. Sodium hydroxide (NaOH).
18. Beckman ready-safe scintillation cocktail.

### 2.4. Preparation of Solution for CaM-Dependent Protein Kinase Assay

1. 1 *M* Tris-HCl: dissolve 60.6 g of Tris-HCl in distilled water, adjust pH 7.0 with HCl, and make the final volume to 500 mL.
2. 1 *M* $MgCl_2$: dissolve 20.3 g of $MgCl_2$ in 100 mL of distilled water.
3. Assay buffer: the standard assay buffer contains 950 µL of 1-*M* Tris-HCl, 50 µL of 1 *M* $MgCl_2$; and 5 µL of 2-mercaptoethanol; mix thoroughly, and it is ready for use.
4. 1 m*M* $CaCl_2$: dissolve 14.7 mg of $CaCl_2$ in 10 mL of distilled water.
5. 1 m*M* EGTA: dissolve 38.0 mg of EGTA in distilled water, adjust pH 7.0 with 0.1 N NaOH, and make the final volume to 10 mL.
6. 10 m*M* ATP: dissolve 31 mg of ATP in distilled water, adjust to pH 7.0, and make the final volume to 5 mL. Calculate correct concentration of ATP, by using molar absorbancy $15.4 \times 10^3$ at 259 nm in 0.1 *N* HCl, and store at –20°C in small aliquots.
7. Working solution of [$\gamma$-$^{32}$P] ATP: 1 m*M* ATP, specific activity 100 cpm/pmol.
8. CaM: make 1 mg/mL of CaM in 20 m*M* Tris-HCl buffer, pH 7.0 containing 0.01 m*M* $CaCl_2$.
9. Substrate: mixed histone, casein, or specific substrate. Make solution of 2 mg/mL; store in small aliquots.

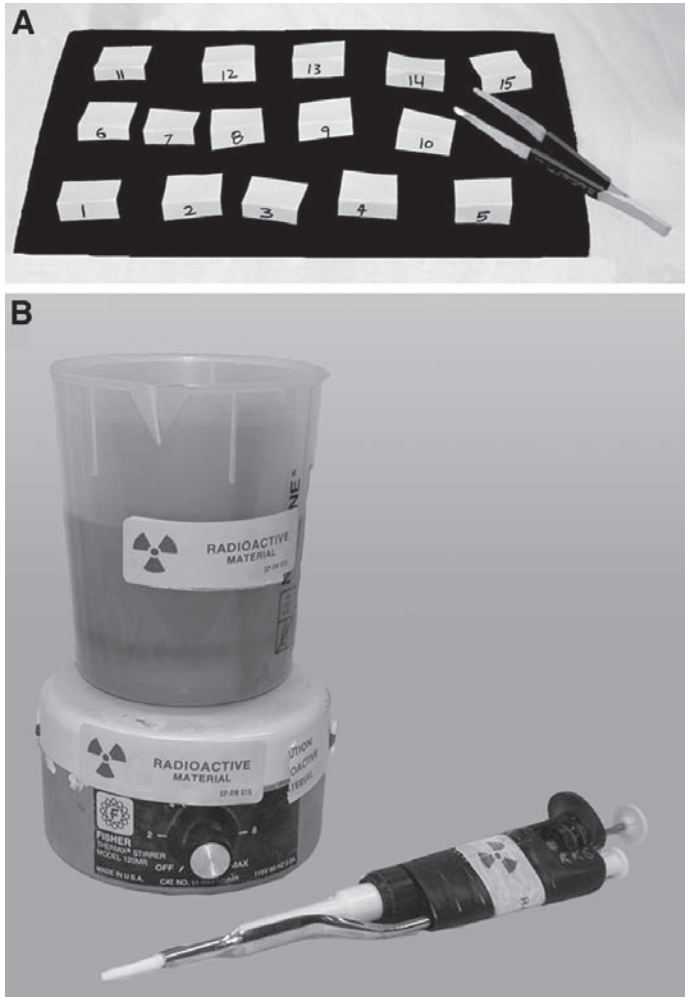


Fig. 1. Termination of calmodulin-dependent protein kinase assay. **(A)** Arrangement of phosphocellulose P81 filter paper discs. **(B)** Washing apparatus for radioactive phosphocellulose P81 filter paper discs.

10. 10% TCA and 2% phosphoric acid: dissolve 100 g of TCA and 20 mL of phosphoric acid in 1 L of distilled water.
11. 5% TCA: dissolve 50 g of TCA in 1 L of distilled water.
12. 95% Ethanol.
13. Whatman P81 phosphocellulose filter paper (3 mm) discs. Phosphocellulose filter paper is cut into 2-cm square discs, and the bottom edge is folded approx 0.5 cm and numbered with a pencil. Place filter paper square on cardboard so that the

bottom folded edge is supporting the filter paper and the number is facing the front (*see* **Fig. 1A**).

All reagents are stable for several months at 4°C. Solutions 6 through 9 are stored in small aliquots at –20°C.

### *2.5. Assay for CaM-Dependent Protein Kinase*

CaM-dependent protein kinase activity is determined by a modification of the filter paper method described by Reimann et al. ***(51)*** (*see* **Note 1**). Units: 1 U of protein kinase activity is defined as the amount of the enzyme that incorporates 1 µmol of phosphate/min at 30°C into substrate. The difference between the phosphorylation observed in the presence of $Ca^{2+}$/CaM and EGTA is used as CaM-dependent phosphorylation activity.

1. CaM-dependent protein kinase assay is carried out in a final volume of 50 µL.
2. Add 5 µL of assay buffer, 5 µL of either $CaCl_2$ or EGTA, 5 µL of CaM, 10 µL of substrate, and crude extract or purified protein kinase as an enzyme source at appropriate dilutions ensuring a linear rate of [$\gamma$-$^{32}$P] ATP incorporation into the protein substrate. (The final concentration of components in the reaction mixture is 100 m*M* of Tris-HCl, pH 7.0, 5 m*M* of $MgCl_2$, 5 m*M* of 2-mercaptoethanol, 0.1 m*M* of $CaCl_2$ or 0.1 m*M* of EGTA, 100 µg/mL of CaM, and 400 µg/mL substrate.)
3. All the reagents and tubes are kept on ice during the additions. The final volume of the reaction is made up to 45 µL with distilled water. The added components are thoroughly mixed, and the tubes are transferred to a water bath at 30°C. Incubate the tubes for approx 1 min.
4. The reaction is initiated by the addition of 5 µL of [$\gamma$-$^{32}$P] ATP to a final concentration of 0.1 to 0.2 m*M* (specific activity, 100–200 cpm/pmol) (*see* **Note 2**).
5. The reaction is terminated after 10 min incubation or after an appropriate time period by spotting 25 µL onto Whatman P81 phosphocellulose filter paper (3 mm) discs (*see* **Fig. 1A**). The discs are dropped by using forceps immediately into a wire basket lying in a beaker containing 10% TCA and 2% phosphoric acid (*see* **Fig. 1B**). The basket provides an easy way of handling the discs during the washing and drying procedure. The beaker should contain washing solution above the level of the filter paper discs. To ensure efficient washing, stir the solution at slow speed and continue washing for 20 min.
6. The filter paper discs are further washed twice with 5% TCA for 20 min and then rinsed in 95% ethanol.
7. The discs are then dried for 5 min with a hair dryer and placed into scintillation vials. Seven milliliters of Beckman ready-safe liquid scintillation cocktail is added to each vial and the radioactivity is quantified in a Beckman liquid scintillation counter.
8. The phosphorylated protein binds to the filter paper discs, which can be removed carefully from the scintillation vials and vials can be reused after checking the background.

### 2.6. Calculation for Protein Kinase Activity

The activity of the enzyme is calculated as follows:

$$\text{pmol phosphate/assay} = \frac{\text{Test-blank}}{\text{Specific activity of } \left[\gamma\text{-}^{32}\text{P}\right]\text{ATP (e.g., 100 cpm/pmol)}} \quad (1)$$

$$\times \frac{\text{Total assay volume (e.g., 50 µL)}}{\text{Volume spotted on P81 filter paper (e.g., 25 µL)}} \quad (2)$$

$$\text{Activity } \left(\mu\text{mol phosphate} \cdot \text{mL}^{-1} \cdot \text{min}^{-1}\right) = \frac{1}{\text{pmol phosphate/assay volume (e.g., 50 µL)}} \quad (3)$$

$$\times \frac{1}{10^6} \times \frac{1}{\text{Incubation time}} \quad (4)$$

$$\text{Specific activity} = \frac{\text{Activity}}{\text{Protein concentration, mg/mL}} \quad (5)$$

## 3. Purification of CaM-Dependent Protein Kinase

### 3.1. Laboratory Equipments, Reagents, and Column Materials

1. Waring blender.
2. Preparative centrifuge.
3. Dialysis bag, 6800 mol-wt cutoff.
4. Amincon centration unit.
5. Diethylaminoethyl (DEAE)—Sepharose CL-6B matrix (Pharmacia Biotech).
6. Sepharcryl S-300 (Pharmacia Biotech).
7. Sepharose 4B (Pharmacia Biotech).
8. Divinyl sulfone.
9. Acetone.
10. Glycine.
11. Phenylmethylsulfonyl fluoride.
12. Partially purified soybean trypsin inhibitor.
13. Leupeptin.
14. Benzamidine.

### 3.2. Preparation of Buffers and Other Solutions for CaM-Dependent Protein Kinase Purification

1. Homogenizing buffer: 20 m*M* Tris-HCl, 2 m*M* ethylene diamine tetraacetic acid (EDTA), pH 7.5: Dissolve 2.42 g of Tris-HCl and 745 mg of EDTA in distilled water, adjust pH to 7.5 with 1 *M* HCl, and make the final volume to 1 L. Add 100 mg of phenylmethylsulfonyl fluoride, 100 mg of partially purified soybean trypsin inhibitor, 700 µg of leupeptin, and 200 mg benzamidine to the buffer (*see* **Note 3**).

2. Buffer A: this buffer will be required throughout the purification procedure. Make 40 times the concentrated stock. Dissolve 96.9 g of Tris-HCl, 2.73 g of imidazole, and 8.58 g of magnesium acetate in distilled water, adjust pH to 7.0 with HCl, and make the final volume to 1 L. Dilute 40 times before use to have final concentration of buffer A (20 m*M* Tris-HCl, 1 m*M* magnesium acetate, and 1 m*M* imidazole, pH 7.0).
3. 100 m*M* $CaCl_2$: dissolve 7.35 g of $CaCl_2$ in 500 mL of distilled water.
4. 100 m*M* EGTA: dissolve 19.02 g of EGTA in distilled water, adjust pH to 7.0 with NaOH solution, and make the final volume to 500 mL.
5. 0.2 *M* Sodium carbonate, pH 9.5: dissolve 24.8 g of sodium carbonate in distilled water, adjust pH to 9.5, and make the final volume to 1 L.
6. 0.5 *M* Sodium carbonate, pH 11.0: dissolve 62.0 g of sodium carbonate in distilled water, adjust pH to 11.0, and make the final volume to 1 L.

### 3.3. Preparation of CaM–Sepharose 4B Affinity Gel

CaM–Sepharose column chromatography is an important step for purification of CaM-binding proteins. CaM is covalently linked to divinyl sulfone activated Sepharose 4B gel.

#### 3.3.1. Preparation of CaM-Affinity Gel Activation of Sepharose 4B

1. Wash Sepharose 4B (400 g) in a glass sintered filter funnel with 4 to 5 L of distilled water and then with 1 L of 0.5 *M* sodium carbonate, pH 11.0.
2. Transfer the washed gel to a 1 L beaker and mix with 400 mL of the same buffer.
3. Under a fume hood, add slowly 22 mL of divinyl sulfone to the gel suspension with gentle stirring. After 2.5 h, add 1 mL aliquots of divinyl sulfone eight times at 15-min intervals.
4. Transfer the gel to a glass filter funnel and wash with 10 L of distilled water until the effluent is close to neutrality.
5. Wash the gel further with 1 L of acetone, and again with 4 L of distilled water. The activated Sepharose 4B gel can be stored for several months at 4°C as a water suspension in the presence of 0.02% sodium azide (*see* **Note 4**).

#### 3.3.2. Conjugation of CaM to Activated Sepharose 4B

1. Wash activated Sepharose 4B (400 g) in a glass sintered filter funnel with 2 L of 0.2 *M* of sodium carbonate, pH 9.5, and then suspend in 400 mL of the same buffer in a 1-L beaker.
2. Mix pure CaM (400 mg/400 mL gel) that has been extensively dialyzed against 0.2 *M* of sodium carbonate, pH 9.5, with the gel suspension. Stir the mixture gently at room temperature for 4 h and then in a cold room for 16 h.
3. Add glycine (1 g) to the gel suspension and stir at room temperature for 4 h.
4. The conjugate Sepharose 4B, after thorough washing with distilled water, can be equilibrated and stored in any neutral buffer at 4°C until use.

CaM-Sepharose 4B column can be stored for several years after regeneration by adding a small amount of sodium azide (0.02%) in equilibration buffer. However, before use, equilibrate the column with buffer A containing 0.25 m*M* $CaCl_2$ and 10 m*M* 2-mercaptoethanol.

### 3.4. Purification of CaM-Dependent Protein Kinase

#### 3.4.1. Extraction

1. All steps are carried out at 4°C. Transfer the fresh bovine hearts obtained from a local slaughterhouse to the laboratory in packed ice.
2. Cut the heart (devoid of vascular tissue) into small pieces, grind 2 kg in a meat grinder, and then homogenize in a Waring blender for 1 min in 2 vol of ice-cold homogenizing buffer containing protease inhibitors (*see* **Notes 3** and **5**).
3. Centrifuge the homogenate at 10,000*g* for 20 min and filter the supernatant through glass wool. Add 2-mercaptoethanol and EGTA to the supernatant to make a final concentration of 10 and 0.1 m*M*, respectively.

#### 3.4.2. DEAE–Sepharose CL-6B Column Chromatography

1. Apply the supernatant from the extraction step to a DEAE-Sepharose CL-6B (8 × 20 cm) column pre-equilibrated with buffer A, pH 7.0, containing 10 m*M* 2-mercaptoethanol and 0.1 m*M* of EGTA (*see* **Note 6**).
2. Wash the column subsequently with two to three bed volumes of buffer A containing 10 m*M* 2-mercaptoethanol, 0.1 m*M* EGTA, and 0.05 *M* NaCl.
3. Elute the proteins with the same buffer containing 0.2 *M* NaCl and pool the fractions containing high protein concentration.

#### 3.4.3. CaM–Sepharose 4B Chromatography

The most efficient purification step in the procedure is the CaM–Sepharose 4B column chromatography, which is used to isolate proteins capable of undergoing $Ca^{2+}$-dependent association with CaM. The purification of the CaM-dependent protein kinase II is based on the manipulation of elution conditions from a CaM–Sepharose 4B column to resolve the CaM-dependent protein kinase II from other CaM-binding proteins. Endogenous CaM has to be removed from the heart supernatant by using DEAE–Sepharose CL-6B column chromatography.

1. Add $CaCl_2$ solution to the pooled sample of DEAE–Sepharose CL-6B column to a final concentration of 0.25 m*M* and stir the solution gently for 20 min (*see* **Note 7**).
2. Apply the sample to a CaM–Sepharose 4B affinity column (6.0 × 15.0 cm) that has been previously equilibrated with buffer A containing 10 m*M* of 2-mercaptoethanol and 0.25 m*M* $CaCl_2$ (*see* **Note 6**).
3. After sample application, wash the column with buffer A containing 10 m*M* 2-mercaptoethanol, 0.1 m*M* $CaCl_2$, and 0.2 *M* NaCl until no protein is detected in the eluate (approx 4 bed volumes). Then, further wash the column with one additional bed volume of the same buffer without NaCl.

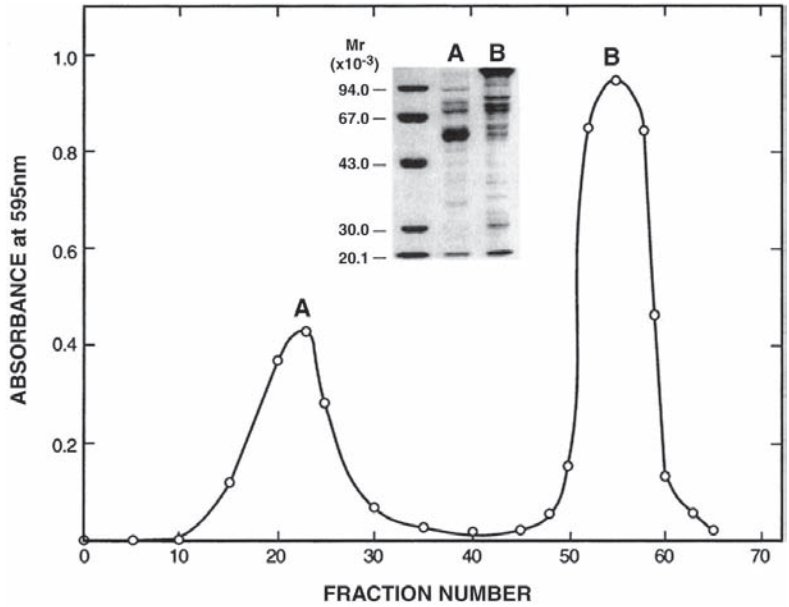


Fig. 2. Chromatography of calmodulin (CaM)-binding proteins on a CaM–Sepharose 4B column. The pooled sample from a DEAE-Sepharose CL-6B column is applied on CaM–Sepharose 4B affinity column. After application, the column is washed with buffer A containing 0.1 of m*M* $Ca^{2+}$ and 0.2 *M* of NaCl (approx 4 bed volumes), and then one bed volume of the same buffer without NaCl. Proteins are eluted initially in buffer A containing 1 m*M* of ethylene glycol tetraacetic acid (EGTA) and subsequently in buffer A containing 1 m*M* of EGTA and 0.5 *M* of NaCl. The fractions in the region of peak A and peak B are pooled separately. Peaks A and B are analyzed by sodium dodecyl sulfate-polyacrylamide gel electrophoresis (**inset**). Lane 1, molecular standards: phosphorylase *b*, bovine serum albumin, ovalbumin, carbonic anhydrase, and soybean trypsin inhibitor. Lanes 2 and 3 are peak A and B, respectively.

4. First, elute the column with buffer A containing 10 m*M* of 2-mercaptoethanol and 1 m*M* of EGTA. When the protein concentration in the column is returned to the basal level, elute the column further with buffer A containing 10 m*M* of 2-mercaptoethanol, 1 m*M* of EGTA, and 0.5 *M* of NaCl. Two protein peaks (peaks A and B) are observed by this elution procedure (*see* **Fig. 2**).
5. Pool both peaks A and B separately and concentrate by ultrafiltration through an Amicon PM-10 membrane. Peaks A and B represent 30 to 35% and 65 to 70% of total CaM-binding proteins, respectively. Peak A contains >85% activity of the CaM-dependent protein kinase II and 90% activity of CaM-dependent cyclic nucleotide phosphodiesterase (*see* **Fig. 2**). CaM-dependent cyclic nucleotide

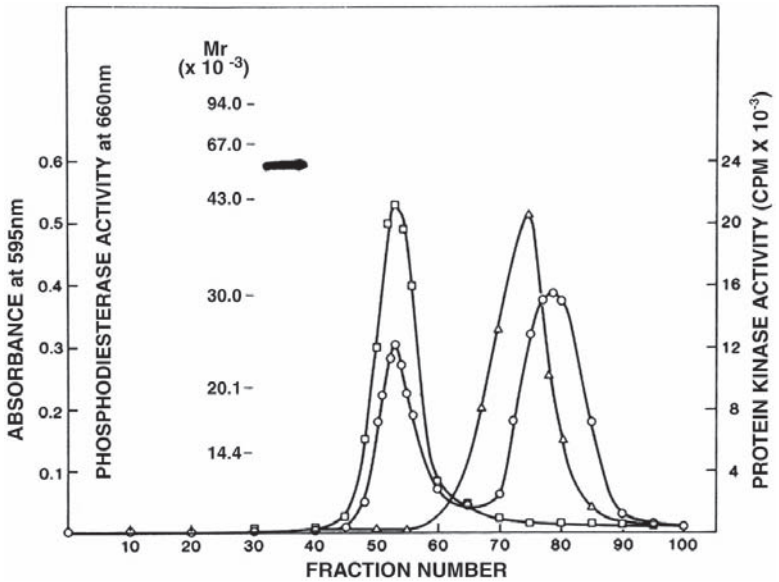


Fig. 3. Gel filtration column chromatography of calmodulin (CaM)-dependent protein kinase II. Peak A is applied to a Sephacryl S-300 column. CaM-dependent protein kinase II (□—□) and CaM-dependent cyclic nucleotide phosphodiesterase (△—△) activity. Protein concentrations are determined by the dye-binding method (○—○) (**inset**). The purity of the pooled sample (fraction 50–57) is analyzed by SDS-PAGE.

phosphodiesterase activities were determined as described in Chapter 21, **Subheading 3.1.**). Using sodium dodecyl sulfate-polyacrylamide gel electrophoresis (SDS-PAGE), it was shown that peak A is enriched with a 56,000-Daltons species, whereas peak B is enriched with the high molecular weight CaM-binding protein ***(50)*** (*see* **Fig. 2 inset**).

### *3.4.4. Sephacryl S-300 Column Chromatography*

1. Prepare a column of Sephacryl S-300 (1.5 × 95 cm), and equilibrate with buffer A containing 10 m*M* of 2-mercaptoethanol, 0.1 m*M* of EGTA, 0.1 *M* of NaCl, and 10% (w/v) sucrose.
2. Apply peak A from the CaM–Sepharose 4B column to the Sephacryl S-300 column.
3. Proteins are eluted with equilibration buffer at a flow rate of 6 mL/h. CaM-dependent protein kinase II activity is detected in a sharp peak that corresponds to the protein peak (*see* **Fig. 3**). The CaM-dependent protein kinase II is separated from the CaM-dependent cyclic nucleotide phosphodiesterase and other CaM-binding proteins.

4. Fractions under the peak region of CaM-dependent protein kinase activity are pooled and concentrated to 2 to 3 mL by ultrafiltration with an Amicon PM-10 membrane and stored in small aliquots at –70°C (*see* **Note 8**).

### *3.5. Other Methods*

SDS-PAGE is carried out according to the method of Laemmli ***(52)***. Coomassie brilliant blue is used to visualize the protein bands on the gel. Protein assay is carried out as described by Bradford ***(53)*** using bovine serum albumin as a standard.

### *3.6. Regeneration of DEAE and CaM–Sepharose 4B Columns*

1. Regenerate the DEAE–Sepharose CL-6B column by washing with two bed volumes of 0.25 *M* of NaCl (14.6 g/L) and 0.25 *M* of NaOH (10 g/L) solution and then twice with distilled water. Wash the column further with one bed volume of 0.1 *M* of HCl (9 mL/L) and then with two to three bed volumes of distilled water until chloride free.
2. Adjust the pH of the gel suspension to 7.0 by washing with buffer A containing 10 m*M* of 2-mercaptoethanol and 0.1 m*M* of EGTA.
3. Regenerate the CaM–Sepharose 4B column by washing with one bed volume of 3 *M* urea to remove tightly bound proteins, followed by three bed volumes of distilled water.
4. Equilibrate the column with buffer A containing 10 m*M* of 2-mercaptoethanol and 0.25 m*M* of $CaCl_2$.

### *3.7. Purity, Molecular Weight, Subunit Structure, and Stability of Cardiac CaM-Dependent Protein Kinase*

The purity of the enzyme preparation is examined by SDS-PAGE. It exhibits essentially a single protein band with a mobility corresponding to a 56,000-Dalton polypeptide (*see* **Fig. 3 inset**). The molecular weight of the CaM-dependent protein kinase II from cardiac muscle determined by the calibrated gel filtration column is 570,000 Daltons, which suggests that the CaM-dependent protein kinase II is composed of 10 identical subunits of 56,000-Daltons ***(34)***. The molecular and subunit weights of the bovine heart CaM-dependent protein kinase II reported here are similar to those reported previously for the bovine brain CaM-dependent protein kinase II ***(31)***. The size of the subunit in various tissues varies because that CaM-dependent protein kinase II may exist as distinct isozymes that possess tissue-specific functions. Like other members of the protein kinase family ***(22–28,31,34)***, the purified bovine heart CaM-dependent protein kinase II also has a relatively broad protein substrate specificity ***(34)***. The purified enzyme shows a specific enzyme activity of 2.4 μmol · $min^{-1}$ · $mg^{-1}$ protein in the presence of mixed histone. The recovery of the CaM-dependent protein kinase II from the gel filtration column is >75%. The purifi-

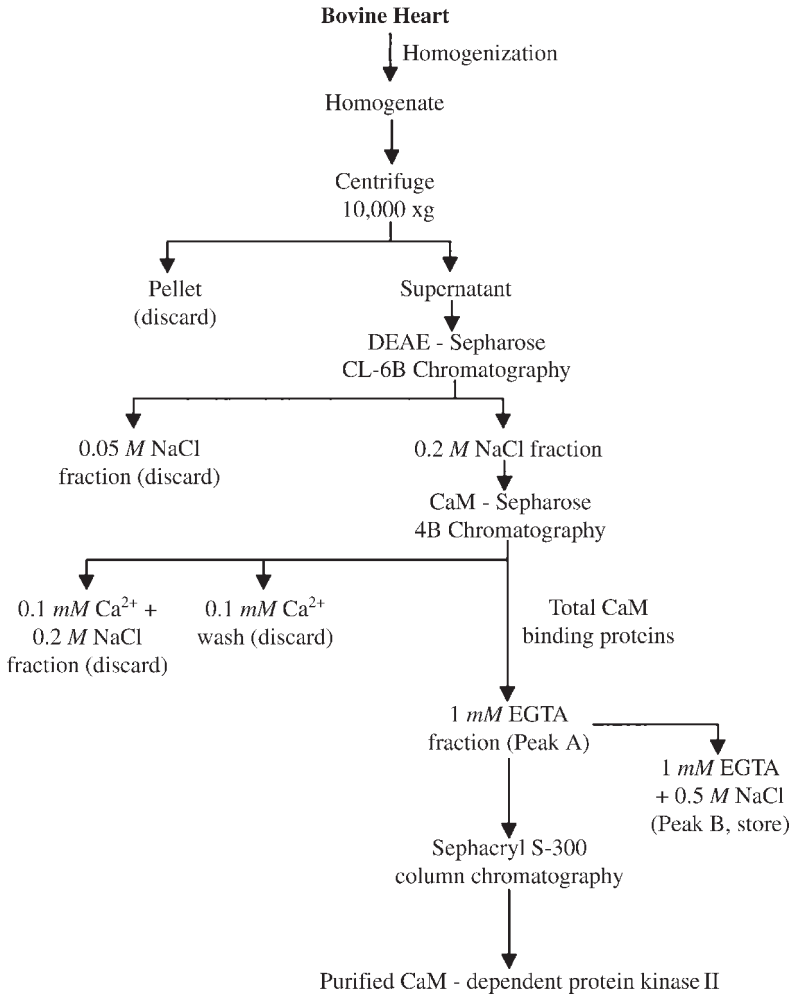


Fig. 4. Purification scheme of calmodulin-dependent protein kinase from bovine heart.

cation scheme (*see* **Fig. 4**) described here is simple, rapid, and suitable for large-scale preparation.

We have observed that storage for several months at –70°C results in the breakdown of the purified bovine cardiac muscle CaM-dependent protein kinase II into several apparent molecular species. The degraded preparation was less sensitive to $Ca^{2+}$/CaM. These results suggest that the enzyme either can be autophosphorylated or is susceptible to protease degradation (*see* **Notes 3** and **8**).

### 3.8. Comments on Purification

Different purification procedures have been used by other investigations for the purification of CaM-dependent protein kinase II ***(22–28,34)***. However, the most efficient purification step in the procedure is the CaM-affinity chromatography that is used to isolate proteins capable of undergoing $Ca^{2+}$-dependent association with CaM. We have also purified bovine brain CaM-dependent protein kinase II from bovine brain with modifications ***(31)***.

### 3.9. Properties of CaM-Dependent Protein Kinase II From Cardiac Muscle

#### 3.9.1. Autophosphorylation

A common, but not universal, feature of protein kinases is that they undergo autophosphorylation. Autophosphorylation is the process in which the holozyme catalyzes the phosphorylation of one or more amino acids within its own structure through intramolecular reaction. It plays an important role in regulating various kinase functions in vivo. Like other members of the CaM-dependent protein kinase II family ***(31,40–49)***, bovine cardiac CaM-dependent protein kinase II also rapidly undergoes autophosphorylation ***(34)***. The autophosphorylation reaction is completely dependent on $Ca^{2+}$ and CaM. The reaction is rapid and completed with a maximal incorporation of 1 mol phosphate/mol subunit of CaM-dependent protein kinase II (*see* **Fig. 5**). Autophosphorylated CaM-dependent protein kinase II becomes a completely $Ca^{2+}$-independent form for the phosphorylation of substrate. The autophosphorylation of CaM-dependent protein kinase can be reversed through dephosphorylation by protein phosphatase I ***(47,54)***. Autophosphorylation of CaM-dependent protein kinase II can be carried out using the same procedure as the protein kinase assay, except a protein substrate is not added.

#### 3.9.2. Phosphorylation as a Function of $Ca^{2+}$ Concentration

The synergistic interaction between $Ca^{2+}$ and CaM in the activation of various CaM-dependent enzymes has been reported repeatedly ***(31,34,55–58)***. The $Ca^{2+}$-dependence of the CaM-dependent protein kinase II was examined at saturating levels of CaM. **Figure 6** shows that $Ca^{2+}$ and CaM interact synergistically in activation of CaM-dependent protein kinase II in the phosphorylation of casein. When the CaM concentration is increased, the $Ca^{2+}$ concentration required for half-maximal activation is decreased. The half-maximal phosphorylation of casein is observed at 6.1, 4.4, and 0.67 $\mu M$ of $Ca^{2+}$ in the presence of 1, 5, and 20 $\mu M$ of CaM, respectively. Although the physiological significance of the observed differential $Ca^{2+}$ sensitivity of the CaM-dependent protein kinase in cardiac muscle is not known, it is noteworthy that the differential

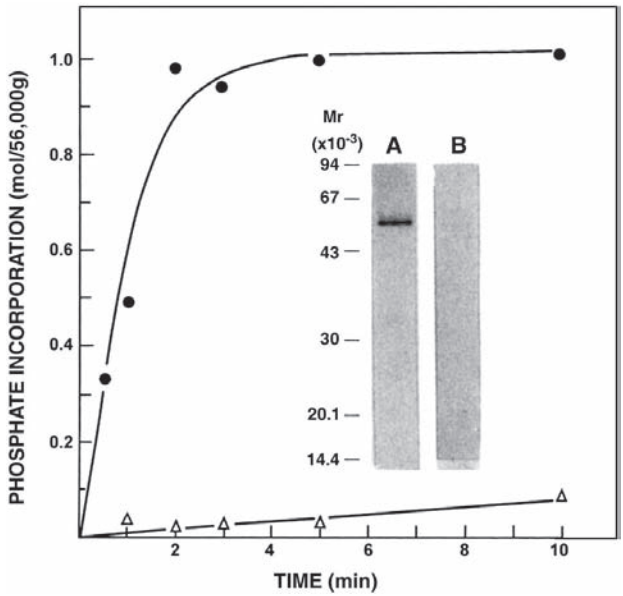


Fig. 5. Time course of stoichiometry of autophosphorylation of calmodulin (CaM)-dependent protein kinase II. The purified CaM-dependent protein kinase II (50 µg/mL) is incubated in a standard reaction mixture containing 200 µg/mL of CaM and 500 µg/mL of bovine serum albumin in the presence of 0.1 m*M* of $CaCl_2$ (●—●) or 0.1 m*M* of ethylene glycol tetraacetic acid (EGTA) (△—△) as described in **Subheading 4.1.** Endogenous phosphorylation is allowed to proceed, and aliquots are taken at various time intervals indicated for $\gamma$-$^{32}P$ incorporation into CaM-dependent protein kinase II. After 10 min of reaction time, aliquots are subjected to electrophoresis followed by autoradiography (inset). Lanes A and B: CaM-dependent protein kinase II in the presence of 0.1 m*M* of $CaCl_2$ (●—●) and 0.1 m*M* of EGTA (△—△), respectively.

$Ca^{2+}$ affinity of CaM-dependent protein kinase II is a mechanism by which the CaM regulatory reactions are adapted to the respective tissues.

### *3.9.3. Immunological Characterization*

To examine whether the cardiac CaM-dependent protein kinase is similar to any other CaM-dependent protein kinase, immunoblotting is carried out by the method of Towbin et al. ***(59)***. A polyclonal antipeptide antibody raised against multifunctional CaM-dependent protein kinase II of rat brain is tested for immunoreactivity with the bovine cardiac muscle CaM-dependent protein kinase II ***(34)***. The antibody is raised against the synthetic peptides of the N- and C-terminal, CTRFTDEYQLFEEL and EETRVWHRRDGKWQNVHFHC corresponding to amino acids 7 to 20 and 514 to 533 of the multifunctional CaM-dependent

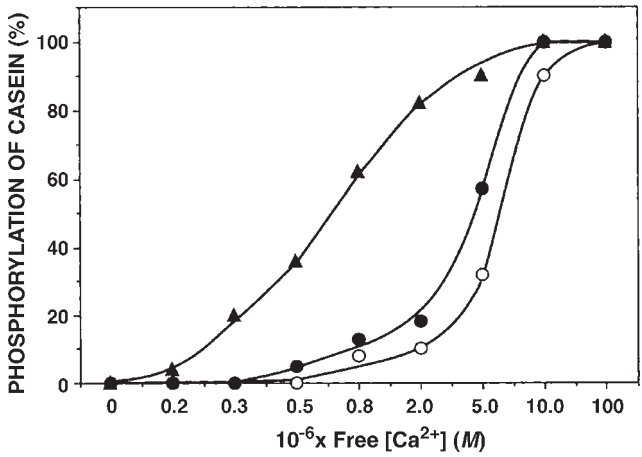


Fig. 6. Phosphorylation of casein by calmodulin (CaM)-dependent protein kinase II as a function of $Ca^{2+}$ concentration at different levels of CaM. The assay is carried out as described in **Subheading 4.2.** The casein is phosphorylated by CaM-dependent protein kinase II (6.4 µg/mL) for 40 min at 1 µ*M* (○—○), 5 µ*M* (●—●), and 20 µ*M* (▲—▲) of CaM. The free $Ca^{2+}$ concentration in the ethylene glycol tetraacetic acid-buffered solution is calculated as described in **ref.** ***34***.

protein kinase II β-isoform of rat brain ***(60,61)***. Western blot of purified cardiac muscle CaM-dependent kinase II showed an immunoreactive band of 56,000-Daltons ***(34)***. This suggested that cardiac muscle enzyme is immunologically similar to that of multifunctional CaM-dependent protein kinase II isozyme of rat brain.

## 4. Notes

1. For protein kinase assay, wear gloves to avoid direct contact with skin from radioactive ATP. After finishing the assay, check working bench with Geiger-Muller counter for any spills, pipet tips, etc. If anything is found contaminated, use appropriate safety procedures to handle the radioactive material.
2. The radioactive ATP has a half-life of 14.3 d, and calculating specific activity decay factor should be considered at each time.
3. Problems may arise by the presence of $Ca^{2+}$-dependent or -independent proteolytic enzymes. It is strongly recommended that the protease inhibitors are included in the buffers at the time of homogenization, up to the CaM–Sepharose 4B affinity chromatography step. (Phenylmethylsulfonyl fluoride should be dissolved in isopropanol with vortex and then added in homogenizing buffer very slowly with continuous stirring.)
4. The binding capacity of activated Sepharose 4B gel must be checked before adding CaM. Take 1 to 2 mL of gel in an Eppendorf tube and add approx 2 to 4 mg of

ferritin; keep for occasional mixing for 4 h. Centrifuge the gel suspension at 320*g* for 2 min, and check the protein concentration of supernatant to see how much is bound to the gel. If protein is bound to the gel and no protein is detected in the supernatant, the gel is activated and ready for use.

5. Before centrifugation, the homogenate should be adjusted to pH 7.5 with 1 *M* Tris-HCl and stirred for 15 to 20 min at 4°C.
6. The DEAE–Sepharose CL-6B column chromatography step is used mainly to remove an endogenous CaM from crude homogenate. If the total CaM-binding proteins do not bind to the CaM–Sepharose 4B column in the presence of $[Ca^{2+}]$, it suggests two possibilities:
   a. The free $Ca^{2+}$ is not high enough to overcome EGTA (*see* **Subheading 3.4.2.**)
   b. Pooled sample from this step is contaminated with an endogenous CaM.

   Therefore, there will be competition between the solid phase (CaM–Sepharose 4B column) and the soluble phase (pooled sample from DEAE–Sepharose CL-6B chromatography step), resulting in poor binding to the CaM–Sepharose 4B column.
7. $CaCl_2$ must be added to a final concentration of 0.25 m*M*.
8. The storage of CaM-dependent protein kinase II at –70°C for several months results in breakdown of the enzyme into several apparent molecular species and freezing and thawing results in the loss of CaM-dependent activity of enzyme. To increase the half-life of enzyme, store in small aliquots at –70°C.

## Acknowledgments

This work was supported by the Heart and Stroke Foundation of Saskatchewan, Canada. I am thankful to my colleagues, postdoctoral fellows, and research assistants who have gratefully contributed to my research endeavors. I wish to express my appreciation to Dr. Gagan Bajaj for the reading of this manuscript. The author is thankful to Mr. Todd Reichert and Ms. Mitch Hesson for the photographic work and Ms. Rosemarie Tollefson for typing the manuscript.

## References

1. Krebs, E. G. and Beavo, J. A. (1979) Phosphorylation-dephosphorylation of enzymes. *Ann. Rev. Biochem.* **48,** 923–959.
2. Cohen, P. (1992) Signal integration at the level of protein kinases, protein phosphatases and their substrates. *Trends Biochem. Sci.* **17,** 408–413.
3. Hunter, T. (1995) Protein kinases and phosphatases: the yin and yang of protein phosphorylation and signalling. *Cell* **80,** 225–236.
4. Seger, R. and Krebs, E. G. (1995) Phosphorylation-dephosphorylation of enzymes. *Ann. Rev. Biochem.* **48,** 923–959.
5. Graves, J. D., Campbell, J. S., and Krebs, E. G. (1995) Protein serine/threonine kinases of the MAPK cascade. *Ann. NY Acad. Sci.* **766,** 320–343.
6. Graves, L. M. Bornfeldt, K. E., and Krebs, E. G. (1997) Historical perspectives and new insights involving the MAP kinase cascades. *Adv. Second Messenger Phosphoprotein Res.* **31,** 49–62.

7. Bornfeldt, K. E. and Krebes, E. G. (1999) Crosstalk between protein kinase A and growth factor receptor signaling pathways in arterial smooth muscle. *Cell Signal*. **11,** 465–477.
8. Graves, J. D. and Krebs, E. G. (1999) Protein phosphorylation and signal transduction. *Pharmacol. Ther.* **82,** 111–121.
9. Rajala, R. V. S., Datla, R. S. S., Carlsen, S., et al. (2001) Phosphorylation of human N-myristoyltransferase by N-myristoylated SRC family tyrosine kinase members. *Biochem. Biophys. Res. Commun.* **288,** 233–239.
10. Carafoli, E. (1987) Intracellular $Ca^{2+}$ homeostasis. *Annu. Rev. Biochem.* **56,** 395–433.
11. Clapham, D. E. (1995) Calcium signalling. *Cell* **80,** 259–268.
12. Berridge, M. J., Bootman, M. D., and Lipp, P. (1998) Calcium a life and death signal. *Nature* **398,** 645–648.
13. Verkhratsky, A. (2002) The endoplasmic reticulum and neuronal calcium signaling. *Cell Calcium* **32,** 393–404.
14. Venkatachalam, K., Van Rossum, D. B., Patterson, R. L., Ma, H.T., and Gill, D. L. (2002) The cellular and molecular basis of store-operated calcium entry. *Nat. Cell Biol.* **4,** E263–272.
15. Peterson, O. H. and Burdakova (2002) The specificity of $Ca^{2+}$ signalling. *Acta Physiol. Hung.* **89,** 439–450.
16. Camello, C., Lomax, R., Petersen, O. H., and Tepikin, A. V. (2002) Calcium leak from intracellular stores—the enigma of calcium signaling. *Cell Calcium* **32,** 355–361.
17. Galione, A. and Churchill, G. C. (2002) Interactions between calcium release pathways: multiple messengers and multiple stores. *Cell Calcium* **32,** 343–354.
18. Hofer, A. M. and Brown, E. M. (2003) Extracellular calcium sensing and signaling. *Nat. Rev. Mol. Cell Biol.* **4,** 530–538.
19. Rudolf, R., Mongillo, M., Rizzuto, R., and Pozzan, T. (2003) Looking forward to seeing calcium. *Nat. Rev. Mol. Cell Biol.* **4,** 579–586.
20. Berridge, M. J., Bootman, M. D., and Roderick, H. L. (2003) Calcium signaling: dynamics, homeostasis and remodeling. *Nat. Rev. Mol. Cell Biol.* **4,** 517–529.
21. Sharma, R. K. (2003) Diversity of calcium action in regulation of calmodulin-dependent cyclic nucleotide phosphodiesterase. *Indian J. Biochm. Biophys.* **40,** 77–91.
22. Kennedy, M. B., McGuiness, T., Greengard, P. (1983) A calcium/calmodulin-dependent protein kinase from mammalian brain that phosphorylates synapsin I: partial purification and characterization. *J. Neurosci.* **3,** 818–831.
23. Goldering, J. R., Gonzalez, B., McGuire, J. S., and DeLorenzo, R. J. (1983) Purification and characterization of a calmodulin-dependent kinase from rat brain cytosol able to phosphorylate tubulin and microtubule-associated proteins. *J. Biol. Chem.* **258,** 12,632–12,640.
24. Bennett, M. K., Erondu, N. E., and Kennedy, M. B. (1983) Purification and characterization of a calmodulin-dependent protein kinase that is highly concentrated in brain. *J. Biol. Chem.* **258,** 12,735–12,744.

25. Gorelick, F.S., Cohn, J. A., Freedman, S. D., Delahunt, N. G., Gershoni, J. M., and Jamisen, J. D. (1983) Calmodulin-stimulated protein kinase activity from rat pancreas. *J. Cell. Biol.* **89,** 440–448.
26. Kuret, J. A. and Schulman, H. (1984) Purification and characterization of a $Ca^{2+}$/calmodulin-dependent protein kinase from rat brain. *Biochemistry* **23,** 5459–5504.
27. Iwasa, T., Inoue, N., Fukunaga, K., Isobe, T., Okuyama, T., and Miyamoto, E. (1986) Purification and characterization of a multifunctional calmodulin-dependent protein kinase from canine myocardial cytosol. *Arch. Biochem. Biophys.* **248,** 21–29.
28. Bartelt, D. C., Fidel, S., Wolff, D. J., and Hammell, R. L. (1988) Calmodulin-dependent multifunctional protein kinase in Aspergillus nidulans. *Proc. Natl. Acad. Sci. USA* **85,** 3279–3283.
29. Schulman, H. (1988) The multifunctional $Ca^{2+}$/calmodulin-dependent protein kinase. *Adv. Second Messenger Phosphoprotein Res.* **22,** 39–112.
30. Kemp, B. E. and Pearson, R. B. (1990) Protein kinase recognition sequence motifs. *Trends Biochem. Sci.* **15,** 342–346.
31. Zhang, G. Y., Wang, J. H., and Sharma, R. K. (1993) Purification and characterization of bovine brain calmodulin-dependent protein kinase II. The significance of autophosphorylation in the regulation of 63 kDa calmodulin-dependent cyclic nucleotide phosphodiesterase isozyme. *Mol. Cell. Biochem.* **122,** 159–169.
32. Nairn, A. C. and Picciotto, M. R. (1994) Calcium/calmodulin dependent protein kinase. *Semin. Cancer Biol.* **5,** 295–303.
33. Soderling, T. R. (1995) Calcium-dependent protein kinases in learning and memory. *Adv. Second Messenger Phosphoprotein Res.* **30,** 175–189.
34. Kakkar, R., Raju, R. V. S., and Sharma, R. K. (1996) Calmodulin-dependent protein kinase II from bovine cardiac muscle: purification and differential activation by calcium. *Cell Calcium* **20,** 347–353.
35. Hudmon, A. and Schulman, H. (2002) Structure-function of multifunctional $Ca^{2+}$/calmodulin-dependent protein kinase II. *Biochem. J.* **364,** 593–611.
36. Cheung, W. Y. (1980) Calmodulin plays a pivotal role in cellular regulation. *Science* **207,** 19–27.
37. Klee, C. B. (1988) Interaction of calmodulin with $Ca^{2+}$ and target proteins, in *Molecular Aspects of Cell Regulation*, vol. 5, (Cohen, P. and Klee, C., eds.), Elsevier Science, New York, NY, pp. 35–56.
38. Vetter, S. W. and Leclerc, E. (2003) Novel aspects of calmodulin target recognition and activation. *Eur. J. Biochem.* **270,** 404–414.
39. Kakkar, R., Raju, R. V. S., and Sharma, R. K. (1999) Calmodulin-dependent cyclic nucleotide phosphodiesterase (PDE1). *Cell Mol. Life Sci.* **55,** 1164–1186.
40. Kuret, J. and Schulman, H. (1985) Mechanism of autophosphorylation of the multifunctional $Ca^{2+}$/calmodulin-dependent protein kinase. *J. Biol. Chem.* **260,** 6427–6433.
41. Yamauchi, T.and Fujisawa, H. (1985) Self-regulation of calmodulin-dependent protein kinase II and glycogen synthase kinase by autophosphorylation. *Biochem. Biophys. Res. Commun.* **129,** 213–219.

42. Schworer, C. M., Colbran, R. J., and Soderling, T. R. (1986) Reversible generation of a $Ca^{2+}$ independent form of $Ca^{2+}$/calmodulin-dependent protein kinase II by an autophosphorylation mechanism. *J. Biol. Chem.* **261,** 8581–8584.
43. Lai, Y., Nairn, A. C., and Greengard, P. (1986) Autophosphorylation reversibly regulates the $Ca^{2+}$/calmodulin-dependence of $Ca^{2+}$/calmodulin-dependent protein kinase II. *Proc. Natl. Acad. Sci. USA* **83,** 4253–4257.
44. Miller, S. G. and Kennedy, M. B. (1986) Regulation of brain type II $Ca^{2+}$/calmodulin-dependent protein kinase by autophosphorylation: A calcium triggered molecular switch. *Cell* **44,** 861–870.
45. Hashimoto, Y., Schworer, C. M., Colbran, R. J., and Soderling, T. R. (1987) Autophosphorylation of $Ca^{2+}$/calmodulin-dependent protein kinase II: effects on total and $Ca^{2+}$-independent activities and kinetic parameters. *J. Biol. Chem.* **262,** 8051–8055.
46. Yang, S. D., Chang, S. Y., and Soderling, T. R. (1987) Characterization of an autophosphorylation-dependent multifunctional protein kinase from liver. *J. Biol. Chem.* **262,** 9421–9427.
47. Saitoh, Y., Yamamato, H., Fukunaga, K., Matsukado, Y., and Miyamoto, E. (1987) Inactivation and reactivation of the multifunctional calmodulin-dependent protein kinase from brain by autophosphorylation and dephosphorylation: involvement of protein phosphatases from brain. *J. Neurochem.* **49,** 1286–1292.
48. Hashimoto, Y., Sharma, R. K. and Soderling, T. R. (1989) Regulation of $Ca^{2+}$/calmodulin-dependent cyclic nucleotide phosphodiesterase by the autophosphorylated form of $Ca^{2+}$/calmodulin-dependent protein kinase II. *J. Biol. Chem.* **264,** 10,884–10,887.
49. Zhang, G. Y., Wang, J. H., and Sharma, R. K. (1993) Bovine brain calmodulin-dependent protein kinase II: molecular mechanisms of autophosphorylation. *Biochem. Biophys. Res. Commun.* **191,** 669–674.
50. Sharma, R. K. (1990) Purification and characterization of novel calmodulin-binding protein from cardiac muscle. *J. Biol. Chem.* **265,** 1152–1157.
51. Reimann, E. M., Walsh, D. A., and Krebs, E. G. (1971) Purification and properties of rabbit skeletal muscle adenosine 3',5'-monophosphate-dependent protein kinases. *J. Biol. Chem.* **246,** 1986–1995.
52. Laemmli, U. K. (1970) Cleavage of structural proteins during the assembly of the head of bacteriophage T4. *Nature* **227,** 680–685.
53. Bradford, M. M. (1976) A rapid and sensitive method for the quantitation of microgram quantities of protein utilizing the principle of protein-dye binding. *Anal. Biochem.* **72,** 248–254.
54. Bronstein, J. M., FFarber, D. B., and Wasterlain, C. G. (1993) Regulation of type II calmodulin kinase: Functional implications. *Brain Res. Rev.* **18,** 135–147.
55. Crouch, T. H. and Klee, C. B. (1980) Positive cooperative binding of calcium to bovine brain calmodulin. *Biochemistry* **19,** 3692–3698.
56. Huang, C. Y., Chau, V., Chock, P. B., Wang, J. H., and Sharma, R. K. (1981) Mechanism of activation of cyclic nucleotide phosphodiesterase: Rquirement of

the binding of four $Ca^{2+}$ to calmodulin for activation. *Proc. Natl. Acad. Sci. USA* **78,** 871–874.

57. Sharma, R. K. and Wang, J. H. (1985) Differential regulationof bovine brain calmodulin-dependent cyclic nucleotide phosphodiesterase isozyme by cAMP-dependednt protein kinase and calmodulin dependent phosphatase. *Proc. Natl. Acad. Sci. USA* **82,** 2603–2607.
58. Sharma, R. K. and Kalra, J. (1994) Characterization of calmodulin-dependent cyclic nucleotide phosphodiesterase isozymes. *Biochem. J.* **299,** 97–100.
59. Towbin, H., Staehelin, T., and Gordon, J. (1979) Electrophoretic transfer of proteins from polyacrylamide gels to nitrocellulose sheets: Procedure and some applications. *Proc. Natl. Acad. Sci. USA* **76,** 4350–4354.
60. Tobimatsu, T. and Fujisawa, H. (1989) Tissue-specific expression of four types of rat calmodulin-dependent protein kinase II mRNAs. *J. Biol. Chem.* **264,** 17,907–17,912.
61. Means, A. R., Cruzalegui, F., Le Magueresse, B., Needleman, D. S., Slaughter, G. R., and Ono, T. (1991) A novel $Ca^{2+}$/calmodulin dependent protein kinase and a male germ cell specific calmodulin binding protein are derived from the same gene. *Mol. Cell. Biol.* **11,** 3960–3971.

# 21

# Assay and Purification of Calmodulin-Dependent Cyclic Nucleotide Phosphodiesterase and Isozyme Separation

**Rajendra K. Sharma**

## 1. Introduction

In general, the action of intracellular second messengers, 3′:5′-cyclic adenosine monophosphate (cAMP) and 3′:5′-cyclic guanosine monophosphate (cGMP), are terminated by cyclic nucleotide phosphodiesterase (PDE). In most mammalian tissues, PDE exists in multiple forms that differ in subcellular localization, catalytic, regulatory, and immunological properties ***(1–4)***. One of these forms of enzyme is activated by $Ca^{2+}$ and calmodulin (CaM) and has a lower apparent $K_m$ for cGMP than for cAMP and higher $V_{max}$ for cAMP than for cGMP ***(2,5,6)***. This CaM-dependent cyclic nucleotide phosphodiesterase (CaMPDE) is widely distributed among mammalian tissues and other eukaryotes ***(7–11)***. CaMPDE is one of the most intensively studied and best characterized PDEs ***(12–19)***.

This chapter describes an assay procedure of CaMPDE and its purification from bovine brain. The most efficient purification step in the procedure is the CaM-affinity chromatography, which is used to isolate proteins capable of undergoing $Ca^{2+}$-dependent association with CaM. The purification procedure used in our laboratory involves the use of column chromatography through diethylaminoethyl (DEAE)–Sepharose CL-6B, Affi-gel Blue, CaM–Sepharose 4B affinity and Sephacryl S-300 ***(14)***.

### *1.1. Assay of CaMPDE*

PDE catalyzes the hydrolysis of cAMP and cGMP to their respective 5′ nucleotide monophosphates. This reaction is stimulated by a $Ca^{2+}$/CaM complex as shown:

From: *Methods in Molecular Biology, vol. 312: Calcium Signaling Protocols: Second Edition*
Edited by: D. G. Lambert © Humana Press Inc., Totowa, NJ

$$Ca^{2+} + \underset{\text{inactive}}{CaM} \rightleftharpoons Ca^{2+} - \underset{\text{active}}{CaM^*}$$

$$Ca^{2+} - CaM^* + \underset{\text{inactive}}{PDE} \rightleftharpoons Ca^{2+} - CaM^* - \underset{\text{active}}{PDE^*}$$

PDE activation is initiated by the binding of $Ca^{2+}$ to the CaM. As a result, an active form of the CaM ($Ca^{2+}$–CaM*) is formed and this active form of CaM* then associates with PDE to convert the active PDE ($Ca^{2+}$–CaM*–PDE*). This assay method is involved in the conversion of the reaction product 5′-AMP or 5′-GMP to their respective nucleoside and inorganic phosphate ($PO_4$) by 5′-nuclotidase and followed by spectrophotometric determination of the $PO_4$ at 660 nm. The amount of $PO_4$ formed is estimated from a standard curve prepared with sodium phosphate solution.

A general PDE reaction is shown:

$$\text{cyclic 3'-5' nucleotide} \xrightarrow{Ca^{2+} - CaM^* - PDE^*} \text{5'nucleotideide} \xrightarrow{\text{5' nucleotidase}} \text{nucleoside} + PO_4$$

In the assay method described above, the formation of $PO_4$ from cyclic 3′-5′ nucleotide is measured. This assay is rapid and inexpensive and suitable for monitoring enzyme activity during purification where the substrate concentrations are in milimolar range.

## 2. Materials

### 2.1. Tissue Material

Fresh bovine brains were obtained from a local slaughterhouse and transferred to the laboratory packed in ice. All tissues were stored at –30°C until use.

### 2.2. Laboratory Equipments and Reagents for CaMPDE Assay

1. Water bath.
2. Vortex mixer.
3. Spectrophotometer.
4. pH meter.
5. Tris-(hydroxymethyl)-aminomethane (Tris-HCl; [EMERCK]).
6. Disodium ethylenediaminetetraacetate (EDTA-$Na_2$).
7. Imidazole (BDH).
8. Magnesium acetate ($Mg[CH_3COO]_2 \cdot 4\ H_2O$).
9. Calcium chloride ($CaCl_2$).
10. 2-Mercaptoethanol (Sigma).
11. Ethyleneglycol-*bis*-(β-aminoethyl ether) *N*,*N*′tetraacetic acid (EGTA; Sigma).
12. cAMP and cGMP (Sigma).
13. 5′-nucleotidase (*Crotalus atrox* venom) (Sigma).
14. CaM (Sigma, or purify as described by Sharma ***[20]***).
15. Trichloroacetic acid (TCA).
16. Ammonium molybdate ($[NH_4]_6Mo_7O_{24} \cdot 4H_2O$).

17. Hydrochloric acid (HCl).
18. Sulfuric acid ($H_2SO_4$).
19. Sodium bisulfite.
20. Sodium sulfite.
21. 1-Amino-1-naphthol-4-sulfonic acid (Sigma).
22. Sodium chloride (NaCl).
23. Sodium hydroxide (NaOH).

### 2.3. CaMPDE Assay Buffers

All solutions are prepared with distilled water. All reagents are stable for several months at 4°C. Solution 4 was stored at 4°C in a brown bottle. Solutions 5 through 8 are stored in 1 mL aliquots at –20°C. Solutions 9 and 10 are stable at room temperature.

1. Assay buffer: 360 m*M* Tris-HCl, 360 m*M* imidazole, and 45 m*M* of Mg $(CH_3COO)_2$, pH 7.5. Dissolve 43.6 g of Tris-HCl, 24.5 g of imidazole, 9.6 g of Mg $(CH_3COO)_2$ in distilled water, adjust pH to 7.5 with HCl and make up to 1000 mL.
2. $CaCl_2$:2 $H_2O$ (4.5 m*M*): dissolve 66.2 mg of $CaCl_2$ in 100 mL distilled water.
3. EGTA (4.5 m*M*): dissolve 171.2 mg of EGTA in 100 mL distilled water.
4. Reducing agent: dissolve 24 g of sodium bisulfite, 2.4 g of sodium sulfite, and 500 mg of 1-amino-2-naphthol-4-sulfonic acid in 200 mL of distilled water and store in dark at 4°C.
5. 5′-Nucleotidase (10 U/mL): dissolve 1000 U in 100 mL 10 m*M* of Tris-HCl containing 0.5 m*M* of $Mg(CH_3COO)_2$, pH 7.0, and divide in 1-mL aliquots.
6. CaM-deficient PDE (*see* **Subheading 3.2.2.**).
7. cAMP (10.8 m*M*): dissolve 355 mg cAMP in distilled water, adjust to pH 7.0, and make up to 100 mL and divide in 1-mL aliquots.
8. CaM (1 mg/mL): dissolve 10 mg of CaM in 10 mL in 20 m*M* of Tris-HCl buffer, pH 7.0, containing 0.01 m*M* of $Ca^{2+}$.
9. TCA (55%): dissolve 55 g of TCA in 100 mL distilled water.
10. Ammonium molybdate (0.55% in 1.1 N $H_2SO_4$): dissolve 550 mg of ammonium molybdate in 100 mL of 1.1 *N* $H_2SO_4$.

### 2.4. Purification of CaMPDE

#### 2.4.1. Laboratory Equipments, Reagents, and Column Materials

1. Waring blender.
2. Preparative centrifuge.
3. Dialysis bag, 6800 mol-wt cutoff.
4. Amicon centration unit.
5. DEAE–Sepharose CL-6B matrix (Pharmacia Biotech).
6. Affi-gel Blue (Biorad).
7. CaM–Sepharose 4 B gel (*see* Chapter 20, **Subheading 3.3.1.**).
8. Sepharcryl S-300 (Pharmacia Biotech).

### 2.4.2. Preparation of Buffers and Other Solutions for CaMPDE Purification

1. Homogenizing buffer (20 m*M* of Tris-HCl, 2 m*M* of ethylene diamine tetraacetic acid (EDTA), pH 7.5): dissolve 2.42 g of Tris-HCl and 745 mg of EDTA in distilled water, adjust pH to 7.5 with 1 *M* of HCl, and make the final volume to 1 L. Add 100 mg of phenylmethylsulfonyl fluoride, 100 mg of partially purified soybean trypsin inhibitor, 700 µg of leupeptin, and 200 mg of benzamidine to the buffer (*see* **Note 1**).
2. Buffer A: this buffer will be required throughout the purification procedure. Make 40 times the concentrated stock. Dissolve 96.9 g of Tris-HCl, 2.73 g of imidazole, and 8.58 g of magnesium acetate in distilled water, adjust pH to 7.0 with HCl, and make the final volume to 1 L. Dilute 40 times before use to have final concentration of buffer A (20 m*M* of Tris-HCl, 1 m*M* of magnesium acetate, and 1 m*M* of imidazole, pH 7.0).
3. 100 m*M* $CaCl_2$: dissolve 7.35 g of $CaCl_2$ in 500 mL of distilled water.
4. 100 m*M* EGTA: dissolve 19.02 g of EGTA in distilled water, adjust pH to 7.0 with NaOH solution, and make the final volume to 500 mL.
5. Buffer B: buffer A containing 10 m*M* of 2-mercaptoethanol and 0.1 m*M* of EGTA.
6. Buffer C: buffer A containing 10 m*M* of 2-mercaptoethanol and 0.1 m*M* of $Ca^{2+}$.
7. Buffer D: buffer A containing 10 m*M* of 2-mercaptoethanol and 1 m*M* of EGTA.

## 3. Methods

### 3.1. Assay for CaMPDE

All biological samples and assay tubes are kept on ice during the additions.

1. CaMPDE assay is carried out in a final volume of 450 µL.
2. Add 50 µL µassay buffer, 10 µL of either $CaCl_2$ or EGTA, 15 µL of 5′-nucleotidase, 5 µL of CaM, and dialyzed sample of crude extract (*see* **Subheading 3.3.1.2.** and **Note 2**) or CaM-deficient PDE (*see* **Subheading 3.3.2., step 4**) as an enzyme source at appropriate dilutions ensuring a linear reaction rate of hydrolysis of cAMP and appropriate amount of water to bring the volume to 400 µL.
3. Mix all assay tubes gently and transfer to a water bath at 30°C. Incubate all tubes for approx 1 min.
4. Initiate the reaction by the addition of 50 µL of cAMP and mix thoroughly.
5. Terminate the reaction after 30 min by the addition of 50 µL of TCA. Centrifuge the assay tubes to remove the protein precipitate and withdraw 250 µL of the supernatant and all 250 µL ammonium molybdate for $PO_4$ determination.
6. Add 25 µL of reducing agent to the supernatant aliquot and mix the contents by vortexing.
7. Read the absorbance of the solution at 660 nm in a spectrophotometer using water as blank.
8. Estimate the amount of $PO_4$ formed from a standard curve prepared with sodium phosphate solution. A typical, standard $PO_4$ curve is given in **Fig. 1**.

The difference between the PDE activity observed in the presence of $Ca^{2+}$/CaM and EGTA is used as CaMPDE activity. One unit of CaMPDE is defined

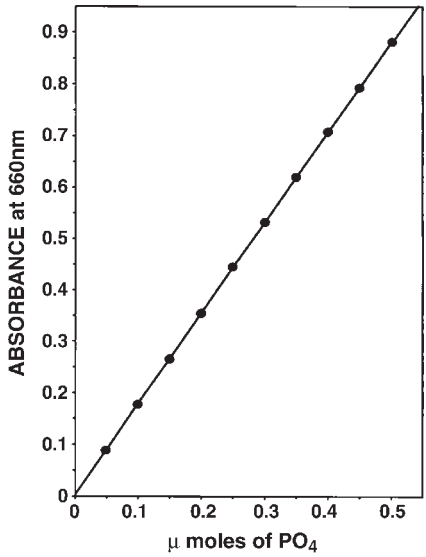


Fig. 1. Standard curve for estimation of $P0_4$.

**Table 1**
**Data for Calculation for CaMPDE Activity**

| Volume of Aliquot (μL) | Absorbance at 660 nm | | | | | |
|---|---|---|---|---|---|---|
| | Crude Extract | | | CaM-deficient PDE | | |
| | $Ca^{2+}$–CaM | $Ca^{2+}$ | EGTA | $Ca^{2+}$–CaM | $Ca^{2+}$ | EGTA |
| 10 | 0.49 | 0.46 | 0.08 | 0.55 | 0.04 | 0.04 |
| 20 | 0.93 | 0.94 | 0.10 | 1.11 | 0.10 | 0.11 |
| 40 | 1.63 | 1.58 | 0.21 | 1.92 | 0.18 | 0.19 |

CaM, camodulin; EGTA, ethylene glycol-*bis*-(β-aminoethyl ether) *N*,*N*′ tetraacetic acid; PDE, phosphodiersterase.

as the amount of enzyme which, when fully activated, hydrolyzes 1 μmol of cAMP/min at 30°C.

### *3.2. Calculation for CaMPDE Activity*

For example, aliquots of 10, 20, and 40 μL of the crude extract and CaM-deficient PDE are used to determine CaMPDE activity from bovine brain. The measurement of the absorbance at 660 nm is given in **Table 1**.

A close look at **Table 1** suggests that the 10 and 20 μL readings are in a linear range. Therefore, these values are useful to calculate the amount of

CaMDPE activity. Because 10 µL of crude extract gives rise to 0.28 µmol $PO_4$/30 min (**Fig. 1**), the CaMPDE activity in crude extract is calculated to be 0.93 µmol $PO_4$/mL/min (0.28 µmol $PO_4$ ÷ 0.01 mL ÷ 30 min). The specific activity can be calculated by dividing units by protein concentration (mg/mL).

### 3.3. Purification of CaMPDE

#### 3.3.1. Extraction

1. All steps are carried out at 4°C.
2. After being partially thawed at room temperature, bovine brain (3 kg) are homogenized in 6 L of ice-cold homogenizing buffer containing protease inhibitors (*see* **Note 1**) in a Waring blender for 30 s. The homogenate is centrifuged at 10,000*g* for 20 min, and the supernatant is filtered through glass wool. The pellet is suspended in 3 L of the homogenizing buffer and again centrifuged at 10,000*g* for 20 min and filtered. Both supernatants are combined, and the pH is adjusted to pH 7.0. To the supernatant, 2-mercaptoethanol and EGTA are added to make a final concentration of 10 m*M* and 0.1 m*M*, respectively. Small aliquot from crude extract is dialyzed overnight against buffer B to remove the endogenous phosphate for CaMPDE activity (*see* **Note 2**).

#### 3.3.2. DEAE–Sepharose CL-6B Column Chromatography

1. Apply the supernatant from the extraction step (**Subheading 3.2.1., step 2**) to a DEAE–Sepharose CL-6B (6 × 70 cm) column pre-equilibrated with buffer B.
2. Wash the column subsequently with 2 to 3 bed volumes of buffer B, containing 0.05 *M* NaCl.
3. Elute the proteins with the same buffer containing 0.2 *M* NaCl and pool the fractions containing high protein concentration.
4. Endogenous CaM is removed from the brain supernatant by using DEAE–Sepharose CL-6B column chromatography and this preparation is referred as the CaM-deficient PDE .

#### 3.3.3. Affi-Gel Blue Column Chromatography

1. Affi-gel Blue Column (4 × 20 cm) is prepared and equilibrated with large volume of buffer B. The pooled sample from DEAE-Sepharose CL-6B column is passed through the column at the rate of 200 to 250 mL/h.
2. Column is washed with a 2.5 bed volume of buffer B containing 0.15 *M* NaCl.
3. CaMPDE activity is eluted with buffer B containing 1.5 *M* of NaCl. Fractions containing the highest CaMPDE activity are pooled and then dialyzed overnight against 8 L of buffer B.

#### 3.3.4. CaM–Sepharose 4B Chromatography

The most efficient purification step in the procedure is the CaM–Sepharose 4B column chromatography, which is used to isolate proteins capable of undergoing $Ca^{2+}$-dependent association with CaM.

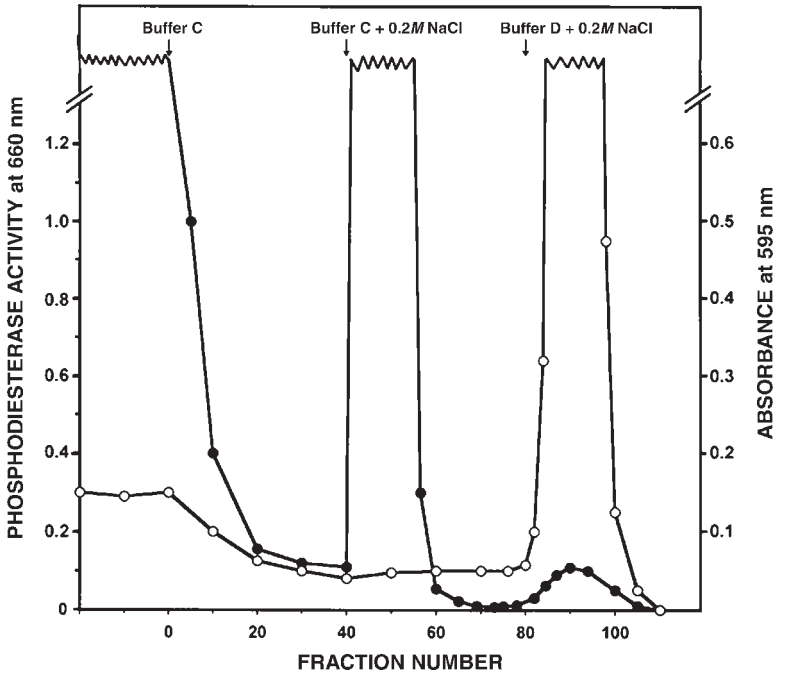


Fig. 2. Chromatography of calmodulin-dependent cyclic nucleotide phosphodiersterase (CaMPDE) on CaM–Sepharose 4B column. The protein concentration was determined by the dye-binding method (●—●) and CaMPDE activity was measured in the presence of 0.1 m*M* of $Ca^{2+}$ with 200 ng of CaM (○—○).

1. Add $CaCl_2$ solution to the pooled sample of Affi-gel Blue column to a final concentration of 0.25 m*M* and stir the solution gently for 20 min (*see* **Note 3**).
2. Apply the sample to a CaM–Sepharose 4B affinity column (6 × 15 cm) that has been previously equilibrated with buffer C and wash with 2 bed volume of the same buffer.
3. Wash the column with 4 bed volumes of buffer C containing 0.2 *M* NaCl until no protein is detected in the eluate (*see* **Note 3**). Most of the proteins within the original sample come through the column without binding or bind with low affinity and can be washed with buffer C containing 0.2 *M* NaCl.
4. Column elution buffer is changed to buffer D containing 0.2 *M* NaCl and CaMPDE activity is eluted from column (*see* **Note 3**).
5. A typical elution profile from CaM–Sepharose 4B is shown in **Fig. 2**. This purification step results in an 80- to 100-fold purification of the CaMPDE (**Fig. 2**). The fractions with the highest activity are pooled and concentrated by ultrafiltration through an Amicon PM-10 membrane to approx 8 mL.

#### 3.3.5. Sephacryl S-300 Column Chromatography

1. Prepare a column of Sepharcryl S-300 (2.5 × 95 cm), and equilibrate with buffer B containing 0.1 *M* NaCl and 10% (w/v) sucrose.
2. Apply concentrated sample from CaM–Sepharose 4B column chromatography to the Sephacryl S-300 column.
3. Proteins are eluted with equilibration buffer at a flow rate of 6 mL/h. CaMPDE activity appears in a sharp peak corresponding to the second protein peak.
4. Fractions under the peak region of CaMPDE activity are pooled and concentrated to an approximate volume of 5 mL by ultrafiltration with Amicon PM-10 membrane and stored in small aliquots at –70°C until further use (*see* **Note 4**).

#### 3.3.6. Purity, Stability, Molecular Weight, and Subunit Structure of Bovine Brain CaMPDE

**Table 2** summarizes the data of a typical preparation of the enzyme from 3 kg of bovine brain. The enzyme is usually purified 3000- to 4000-fold from crude brain extracts with 10 to 15% yield. The specific activity of the purified samples ranged from 320 to 360 U/mg. The enzyme preparation is stable for several months when stored at –70°C. Freezing and thawing for several times often resulted in the loss of CaM-activated activity of the enzyme.

Some of the physicochemical properties of the purified bovine brain CaMPDE are summarized in **Table 3**. The molecular mass of bovine brain CaMPDE is about 120 kDa, and the subunit molecular mass estimated by sodium dodecyl sulfate-polyacrylamide gel electrophoresis (SDS-PAGE) is approx 60 kDa. These results suggest that enzyme is composed of two subunits.

### 3.4. Regeneration of Columns

#### 3.4.1. DEAE–Sepharose CL-6B Column

1. Regenerate the DEAE–Sepharose CL-6B column by washing with two bed volumes of 0.25 *M* of NaCl and 0.25 *M* of NaOH solution and then twice with distilled water. Wash the column further with one bed volume of 0.1 *M* of HCl and then with two to three bed volumes of distilled water until chloride free.
2. Equilibrate the column with buffer B until pH 7.0 is reached.

#### 3.4.2. Affi-Gel Blue Column

1. Regenerate the Affi-gel Blue column by washing with one bed volume of 3 *M* urea to remove tightly bound proteins, followed by three bed volumes of distilled water.
2. Equilibrate the column with buffer B.

#### 3.4.3. CaM–Sepharose 4B Column

1. Regenerate the CaM–Sepharose 4B column by washing with 1 bed volume of buffer D containing 1 *M* NaCl, followed by three bed volumes of distilled water containing 0.1 m*M* $Ca^{2+}$ (*see* **Note 4**).
2. Equilibrate the column with buffer C.

**Table 2**
**Purification of Bovine Brain CaMPDE**

| | Total Activity (μmol $PO_4$/min) | Specific Activity (μmol $PO_4$/min/mg) | Yield (%) | Fold of Purification |
|---|---|---|---|---|
| Crude extract | 7616 | 0.10 | 100 | 1 |
| DEAE-Sepharose CL-6B chromatography | 4000 | 0.38 | 52 | 3.8 |
| Affi-Gel Blue chromatography | 1360 | 2.13 | 18 | 21.3 |
| CaM–Sepharose 4B chromatography | 1583 | 180 | 21 | 1800 |
| Sephacryl S-300 gel filtration chromatography | 746 | 360 | 10 | 3640 |

CaMPDE, calmodulin-dependent cyclic nucleotide phosphodiersterase; $PO_4$, inorganic phosphate.



**Table 3**
**Physical Parameters of Bovine Brain CaMPDE**

| | |
|---|---|
| Free Phosphodiesterase | |
| • Isoelectric point (pI) | 4.85 |
| • Absorbance ($A_{278}$, 1%) | 9.60 |
| • Partial specific volume V (mL/g) | 0.726 |
| • Sedimentation constant (S) | 6.85 |
| • Stokes radius (Å) | 44.20 |
| • Molecular weight | 120,000 |
| • Subunit weight | 60,000 |
| Phosphodiesterase-calmodulin complex | |
| • Sedimentation constant (S) | 8.0 |
| • Stokes radius (Å) | 48.0 |
| • Molecular weight | 159,000 |

CaMPDE, calmodulin-dependent cyclic nucleotide phosphodiersterase.

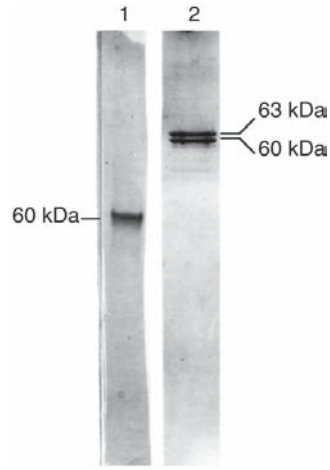


Fig. 3. Sodium dodecyl sulfate-polyacrylamide gel electrophoresis of calmodulin-dependent cyclic nucleotide phosphodiersterase (CaMPDE). Purified CaMPDE was analyzed according to the procedure of Weber and Osborn *(25)*, lane 1, or Laemmli *(22)*, lane 2.

### *3.5. Other Methods*

Protein assay is carried out as described by Bradford *(21)* using bovine serum albumin as a standard. SDS-PAGE is carried out according to the method of Laemmli *(22)*. Coomassie brilliant blue is used to visualize the protein bands on the gel.

### *3.6. Discovery of CaMPDE Isozymes*

Earlier, it was suggested that CaMPDE is existed in a single species *(23)*, but Sharma et al. *(24)* provided direct evidence that CaMPDE exists as tissue-specific and immunological distinct isozymes. A preparation of CaMPDE was initially considered to be homogeneous *(14)* when examined by SDS-PAGE (**Fig. 3**) using the procedure of Weber and Osborn *(25)*. However, when SDS-PAGE was carried out using the procedure of Laemmli *(22)*, two major polypeptides were observed with different molecular mass of 60 and 63 kDa (**Fig. 3**). Using this enzyme preparation as the antigen, several CaMPDE monoclonal antibodies (MAbs) were produced. Western immunoblot analyses have shown that these MAbs can be divided into two groups, one specific toward 60 kDa polypeptide (C1) and the other reacting with both 63- and 60-kDa polypeptides (A6), suggesting that two polypeptides, though related, are immunologically different *(24)*.

In addition, when purified CaMPDE is incubated with a C1 MAb which is specific for the 60-kDa polypeptide and then was subjected to sucrose density

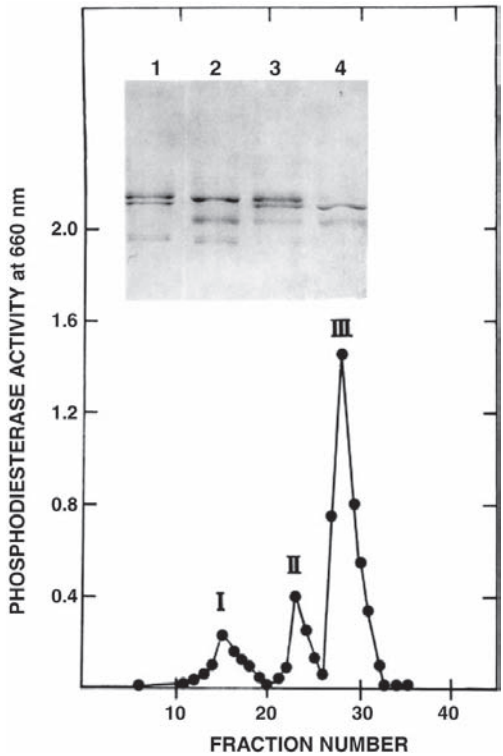


Fig. 4. Sucrose density gradient centrifugation profile of immunocomplexes of bovine brain calmodulin-dependent cyclic nucleotide phosphodiersterase with C1 monoclonal antibody.

gradient centrifugation, three enzyme activity peaks observed (**Fig. 4**) suggesting that bovine brain contains three isozymes: a homodimer of 63-kDa CaMPDE, a homodimer of 60-kDa CaMPDE, and a heterodimer of 63 kDa and 60 kDa. The possibility for the existence of heterodimer form may arise during purification or during storage of the purified CaMPDE ***(24)***. These results suggest that bovine brain contains two major CaMPDE isozymes, designated according to tissue origin and subunit molecular mass as brain 60- and 63-kDa CaMPDE isozymes ***(24)***.

### *3.7. Separation of Bovine Brain CaMPDE Isozymes Using Antibody Affinity Column*

#### *3.7.1. Reagents for Separation of CaMPDE Isozymes*

1. C1 MAb specific for 60 kDa CaMPDE isozyme (*see* **ref. *24***).
2. C1 MAb immunoffinity Sepharose 4B gel.

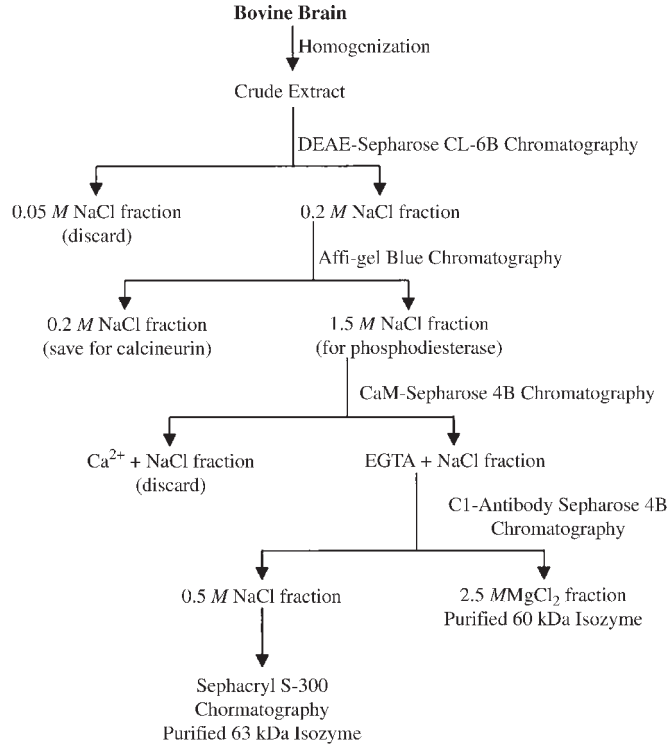


Fig. 5. Flow diagram of the purification of camodulin-dependent cyclic nucleotide phosphodiersterase isozymes from bovine brain.

### *3.7.2. Preparation of C1 MAb–Sepharose 4B Affinity Gel*

1. Prepare activated Sepharose 4B as described (*see* Chapter 20, **Subheading 3.3.1.**).
2. Wash activated Sepharose 4B (200 g) in a glass-sintered filter funnel with 1 L of 0.2 *M* of sodium carbonate, pH 9.5, and then suspend in 200 mL of the same buffer in a 500-mL beaker.
3. Pure C1 MAb, which has been extensively dialyzed against 0.2 *M* of sodium carbonate, pH 9.5, is mixed with the gel suspension (200 mg/200 mL gel).
4. Stir the gel mixture gently first at room temperature for 4 h and then in a cold room for 16 h.
5. Add glycine (500 mg) to the gel suspension and stir at room temperature for 4 h.
6. The conjugated Sepharose 4B, after thorough washing with distilled water, is equilibrated with any neutral buffer and stored at 4°C until use.

### *3.7.3. Separation of Bovine Brain CaMPDE Isozymes*

The major step for separation of bovine brain CaMPDE isozymes, the C1 MAb-affinity gel is used ***(24)***. This purification step will isolate two major bovine brain CaMPDE isozymes: 63-kDa CaMPDE isozyme and 60-kDa CaMPDE isozyme. The purification and separation of bovine brain CaMPDE isozymes is presented in flow chart (**Fig. 5**).

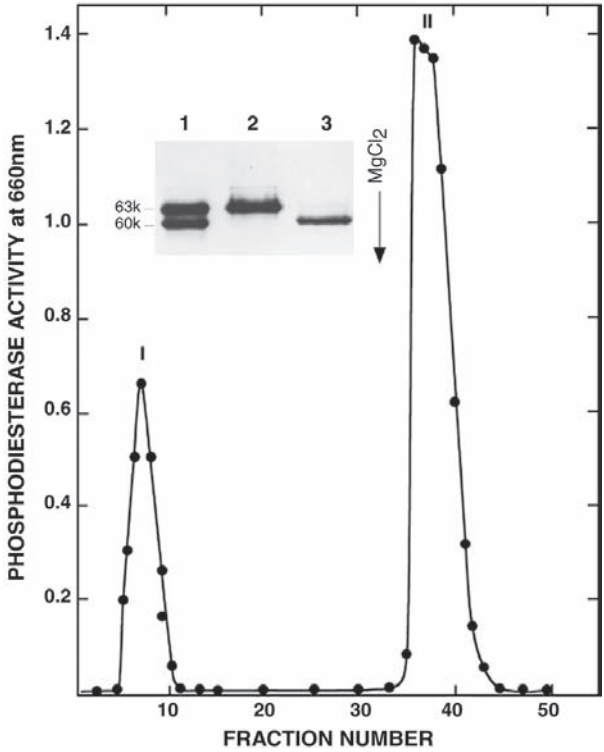


Fig. 6. Separation of calmodulin-dependent cyclic nucleotide phosphodiersterase (CaMPDE) isozymes by C1 monoclonal antibody–Sepharose 4B column chromatography. Inset: Sodium dodecyl sulfate-polyacrylamide gel electrophoresis of original sample of CaMPDE, lane 1; pooled sample of peak I, lane 2; pooled sample of peak II, lane 3.

### 3.7.3.1. C1 MAb–Sepharose 4B Chromatography

1. Sample from CaM–Sepharose 4B column (*see* **Subheading 3.2.4.**) is adjusted to 2 m*M* of EDTA by the addition of 100 m*M* of EDTA solution. Stir the mixture gently for 30 min at 4°C.
2. Sample is applied to C1 MAb–Sepharose 4B column (2.5 × 20 cm), which has been preequalibrated with buffer B containing 2 m*M* of EDTA.
3. Wash column with buffer B, containing 2 m*M* EDTA and 0.5 *M* NaCl until no protein is detected in the eluate (approx 4–5 bed volumes).
4. Elute the column with buffer B containing 0.5 *M* NaCl and 2.5 *M* $MgCl_2$ (**Fig. 6**).
5. Two CaMPDE activity peaks are observed (peak I and peak II). Peak I contains protein which does not react with C1 MAb column, and peak II represents the antibody column-bound protein, which is eluted by buffer B containing 0.5 *M* NaCl and 2.5 *M* $MgCl_2$.

6. Pool both peak I and peak II separately and concentrate by ultrafiltration through an Amincon PM-10 membrane.
7. Dialyze peak II against 2 L of buffer B containing 10% (w/v) sucrose with two changes of buffer. The dialyzed sample is further concentrated to about 250 µg/mL by ultrafiltration through an Amicon PM-10 membrane. This peak II is referred to as the bovine brain 60-kDa CaMPDE isozyme.
8. Peak I is further purified by Sephacryl S-300 gel filtration column.

#### 3.7.3.2. Sephacryl S-300 Column Chromatography

1. Sephacryl S-300 (2.5 × 95 cm) is equilibrated with buffer B containing 0.1 *M* NaCl and 10% (w/v) sucrose.
2. Concentrate peak I is applied to the Sephacryl S-300 column and eluted with the equilibration buffer at a flow rate of 6 mL/h. CaMPDE activity is eluted in a sharp peak corresponding to the second protein peak.
3. Fractions containing the highest enzyme activity are pooled and concentrated by ultrafiltration through an Amicon PM-10 membrane to approx 500 µg/mL. This preparation is referred to as the bovine brain 63-kDa CaMPDE isozyme.
4. Bovine brain 63- and 60-kDa CaPDE isozymes are stored in small aliquots at –70°C; however, repeated freezing and thawing leads to loss of activity.

### *3.8. Different CaMPDE Isozymes From Bovine Tissues*

Five CaMPDE isozymes have been purified to near homogeneity and characterized from bovine brain ***(18,19,24,26,27)***. Two major CaMPDE isozymes, 60- and 63-kDa CaMPDE, are purified from bovine brain using C1 MAb column chromatography (as described in **Subheading 3.6.3., step 5**). In addition CaMPDE from bovine eye, heart and lung are purified in a single step from the total CaM-binding protein fraction, using a C1 MAb that reacts with brain 60-kDa CaMPDE isozyme ***(18,19,26)***.

### *3.9. Kinetic, Inhibition, and Regulatory Properties of Bovine Brain CaMPDE Isozymes*

To understand the physiological role of CaMPDE isozymes, purified CaMPDE isozymes are used to determine kinetic properties in our laboratory ***(27)***. All CaMPDE isozymes have a higher affinity towards cGMP than cAMP. However, brain 63-kDa CaMPDE isozyme exhibits two to three-fold higher affinity for both the substrates, cAMP and cGMP, compared with 60 kDa, heart, and lung CaMPDE isozyme and higher $V_{max}$ for cGMP than for cAMP. It is interesting to note that brain 60-kDa, heart, and lung CaMPDE isozymes have very similar kinetic properties, whereas brain 63-kDa CaMPDE isozyme is kinetically distinct from other CaMPDE isozymes.

Kinetic properties suggest that the 63-kDa brain isozyme is distinct from the brain 60-kDa, heart, and lung CaMPDE isozymes. These isozymes are further distinguished by the effects of pharmacological agents. Heart CaMPDE and

brain 60-kDa CaMPDE isozymes are inhibited by ginsenoside but the brain 63-kDa isozyme is not ***(28)***. Deprenyl (selegeline hydrochloride), a selective inhibitor of monoamine oxidase-B, inhibits brain 60-kDa CaMPDE isozyme but is a poor inhibitor of brain 63-kDa CaMPDE isozyme ***(29)***. Amantadine, which is used for the treatment of Parkinson's disease and is a potent drug for other disorders such as stroke, epilepsy, neuroleptic and malignant syndrome, inhibits brain 60-kDa CaMPDE isozyme but not the brain 63-kDa, heart, and lung CaMPDE isozymes ***(30)***. The inhibition of CaMPDE by these pharmacological agents occurs mostly via $Ca^{2+}$-dependent association with the proteins.

Another main difference which has been observed is that while the heart CaMPDE isozyme, brain 60-kDa CaMPDE isozyme, and eye CaMPDE isozyme are substrates of the cAMP-dependent protein kinase ***(18,31–33)***, the brain 63-kDa isozyme is phosphorylated by CaM-dependent protein kinase II in a $Ca^{2+}$/CaM-dependent manner ***(34–36)***. The CaM-dependent protein kinase II undergoes autophosphorylation, and this autophosphorylated enzyme is active even in the absence of $Ca^{2+}$ and CaM ***(36–38)***. However, the autophosphorylation reaction depends on both $Ca^{2+}$ and CaM. The phosphorylation of CaMPDE isozymes is accompanied by a decrease in the isozyme affinity towards CaM, and can be reversed by a CaM-dependent phosphatase (calcineurin) ***(18,31,34–36)***. The complex regulatory properties of the PDE isozymes suggest that the activity of CaMPDE isozymes are precisely regulated by cross-talk between the $Ca^{2+}$ and cAMP signaling pathways.

We have also demonstrated a potentially novel form of CaMPDE regulation. Polypeptide sequences enriched in proline (P), glutamate (E), serine (S), and threonine (T), are known as PEST motifs. PEST motifs serve as putative intramolecular signals for rapid proteolytic degradation by specific proteases, particulary the calpains ***(39)***. We have reported that the 60-kDa CaMPDE isozyme is proteolyzed by calpain into a 45-kDa catalytic fragment and a 15-kDa fragment. The cleavage occurs between residues $^{126}$Glutamine and $^{127}$Alanine. This eliminates the CaM-dependent activity of carboxy termini of 60-kDa CaMPDE isozyme, resulting in its conversion to a totally CaM-independent form ***(39)***.

## 4. Notes

1. CaMPDE is stimulated by proteolytic enzymes and is not further stimulated by $Ca^{2+}$–CaM ***(40)***. Therefore, it is strongly recommended that the protease inhibitors are included in the homogenizing buffer.
2. Before measuring the CaMPDE activity in the crude extract, it is essential to dialyze a small aliquot overnight against buffer B to remove the endogenous $PO_4$.
3. Do not leave sample in high concentration of $Ca^{2+}$ for longer time because problems may arise by the presence of $Ca^{2+}$-dependent proteolytic enzymes. In addi-

tion, CaM–Sepharose 4B column should not leave in buffer C containing 0.2 *M* of NaCl. Therefore, column is eluted immediately by buffer D containing 0.2 *M* of NaCl.

4. Stored purified CaMPDE isozymes in a small aliquot at –70°C because frequently freezing and thawing often resulted in the loss of CaM-activated activity of the enzyme.

## Acknowledgments

This work was supported by the Heart and Stroke Foundation of Saskatchewan and the Heart and Stroke Foundation of Alberta, Canada. I am thankful to my colleagues, postdoctoral fellows, and research assistants who have gratefully contributed to my research endeavors. I wish to express my appreciation to Dr. Gagan Bajaj for the reading of this manuscript. The author is thankful to Mr. Todd Reichert and Ms. Mitch Hesson for the photographic work and Ms. Rosemarie Tollefson for typing the manuscript.

## References

1. Appleman, M. M., Thompson, W. J., and Russell, T. R. (1973) Cyclic nucleotide phosphodiesterases. *Adv. Cyclic Nucleotide Res.* **3,** 65–98.
2. Wells, J. N. and Hardman, J. G. (1977) Cyclic nucleotide phosphodiesterases. *Adv. Cyclic Nucleotide Res.* **8,** 119–143.
3. Appleman, M. M., Ariano, M. A., Takemoto, D. J., and Whitson, R. H. (1982) Cyclic nucleotide phosphodiesterases, in *Handbook of Experimental Pharmacology*, vol. 58/I (Nathansons, J. A. and Kebabian, J. W., eds.), Springer-Verlag Berlin, New York, NY, pp. 261–299.
4. Beavo, J. A., Conti, M., and Heaslip, R. J. (1994) Multiple cyclic nucleotide phosphodiesterases. *Mol. Pharmacol.* **75,** 399–405.
5. Kakiuchi, S. and Yamazaki, R. (1970) Cacium-dependent phosphodiesterase activity and its activating factor (PAF) from brain studies on cyclic 3′:5′-nucleotide phosphodiesterase. *Biochem. Biophys. Res. Commun.* **41,** 1104–1110.
6. Cheung, W. Y. (1970) Cyclic 3′:5′-nucleotide phosphodiesterase. Determination of an activator. *Biochem. Biophys. Res. Commun.* **38,** 533–538.
7. Sharma, R. K. (2003) Diversity of calcium action in regulation of calmodulin-dependent cyclic nucleotide phosphodiesterase. *Indian J. Biochem. Biophys.* **40,** 77–91.
8. Kakkar, R., Raju, R. V. S., and Sharma, R. K. (1999) Calmodulin-dependent cyclic nucleotide phosphodiesterase (PDE1). *Cell Mol. Life Sci.* **55,** 1164–1186.
9. Sharma, R. K. and Hickie, R. A. (1996) $Ca^{2+}$/calmodulin-dependent cyclic nucleotide phosphodiesterase, in *Phosphodiesterase Inhibitors* (Dent, G., Rabe, K., and Schudt, C., eds.), Academic Press, New York, pp. 65–79.
10. Beavo, J. A. (1995) Cyclic nucleotide phosphodiesterases: functional implications of multiple isoforms. *Physiol. Rev.* **75,** 725–743.
11. Sharma, R. K., Mooibroek, M. J., and Wang, J. H. (1988) Calmodulin-stimulated cyclic nucleotide phosphodiesterase isozymes, in *The Molecular Aspects*

*of Cellular Regulation*, vol. 5 (Cohen, P. and Klee, C. B., eds), Elsevier, Amsterdam, The Netherlands, pp. 265–295.
12. Morrill, M. E., Thompson, S. T., and Stellwagen, E. (1979) Purification of a cyclic nucleotide phosphodiesterase from bovine brain using blue dextran-Sepharose chromatography. *J. Biol. Chem.* **254,** 4371–4374.
13. LaPorte, D. C., Toscano, W. A., and Strom, D. R. (1979) Cross-linking of iodine-125-labelled, calcium-dependent regulatory protein to the $Ca^{2+}$-sensitive phosphodiesterase purified from bovine heart. *Biochemistry* **18,** 2820–2825.
14. Sharma, R. K., Wang, T. H., Wirch, E., and Wang, J. H. (1980) Purification and properties of bovine brain calmodulin-dependent cyclic nucleotide phosphodiesterase. *J. Biol. Chem* **255,** 5916–5923.
15. Hansen, R. S. and Beavo, J. A. (1982) Purification of two calcium-calmodulin-dependent forms of cyclic nucleotide phosphodiesterase by using conformation-specific monoclonal antibody chromatography. *Proc. Natl. Acad. Sci. USA* **79,** 2788–2792.
16. Kincaid, R. L. and Vaughan, M. (1983) Affinity chromatography of brain cyclic nucleotide phosphodiesterase using 3-(2-pyridyldithiol) propionyl-substituted calmodulin linked to thiol-Sepharose. *Biochemistry* **22,** 826–830.
17. Shenolikar, S., Thompson, W. J., and Strada, S. J. (1985) Characterization of $Ca^{2+}$/calmodulin-stimulated cyclic GMP phosphodiesterase from bovine brain. *Biochemistry* **24,** 672–678.
18. Sharma, R. K. (1991) Phosphorylation and characterization of bovine heart calmodulin-dependent phosphodiesterase. *Biochemistry* **30,** 5964–5968.
19. Sharma, R. K., Tan, Y., and Raju, R. V. S. (1997) Calmodulin-dependent cyclic nucleotide phosphodiesterase from bovine eye; high calmodulin affinity isozyme immunologically related to the brain 60 kDa isozyme. *Arch. Biochem. Biophys.* **339,** 40–46.
20. Sharma, R. K. (1990) Purification and characterization of novel calmodulin-binding protein from cardiac muscle. *J. Biol. Chem.* **265,** 1152–1157.
21. Bradford, M. M. (1976) A rapid and sensitive method for the quantitation of microgram quantities of protein utilizing the principle of protein-dye binding. *Anal. Biochem.* **72,** 248–254.
22. Laemmli, U. K. (1970) Cleavage of structural proteins during the assembly of the head of bacteriophage T4. *Nature* **227,** 680–685.
23. Wells, J. N. and Hardman, J. G. (1977) Cyclic nucleotide phosphodiesterases. *Adv. Cyclic Nucleotide Res.* **8,** 119–143.
24. Sharma, R. K., Adachi, A. H., Adachi, K., and Wang, J. H. (1984) Demonstration of bovine brain calmodulin-dependent cyclic nucleotide phosphodiesterase isozyme by monoclonal antibodies. *J. Biol. Chem.* **259,** 9248–9254.
25. Weber, K. and Osborn, M. (1969) The reliability of molecular weight determinations by dodecyl sulfate-polyacrylamide gel electrophoresis. *J. Biol. Chem.* **244,** 4406–4412.
26. Sharma, R. K. and Wang, J. H. (1986) Purification and characterization of bovine lung calmodulin-dependent cyclic nucleotide phosphodiesterase. An enzyme containing calmodulin as a subunit. *J. Biol. Chem.* **261,** 14,160–14,166.

27. Sharma, R. K. and Kalra, J. (1994) Characterization of calmodulin-dependent cyclic nucleotide phosphodiesterase isozymes. *Biochem. J.* **299,** 97–100.
28. Sharma, R. K. and Kalra, J. (1994) Ginsenoides are potent and selective inhibitors of some calmodulin-dependent phosphodiesterase isozymes. *Biochemistry* **32,** 4975–4978.
29. Kakkar, R., Raju, R. V. S., Rajput, A., and Sharma, R. K. (1996) Inhibition of bovine brain calmodulin-dependent cyclic nucleotide phosphodiesterase isozymes by deprenyl. *Life Sci.* **59,** 337–341.
30. Kakkar, R., Raju, R. V. S., Rajput, A., and Sharma, R. K. (1997) Amantadine: an antiparkinsonian agent inhibits bovine brain 60 kDa calmodulin-dependent cyclic nucleotide phosphodiesterase isozyme. *Brain Res.* **749,** 290–294.
31. Sharma, R. K. and Wang, J. H. (1985) Differential regulation of bovine brain calmodulin-dependent cyclic nucleotide phosphodiesterase isozyme by cyclic AMP-dependent protein kinase and calmodulin-dependent phosphatase. *Proc. Natl. Acad. Sci. USA* **82,** 2603–2607.
32. Florio, V, A., Sonnenburg, W. K., Johnson, R., et al. (1994) Phosphorylation of the 61-kDa calmodulin-stimulated cyclic nucleotide phosphodiesterase at serine 120 reduces its affinity for calmodulin. *Biochemistry* **33,** 8948–8954.
33. Sharma, R. K., Seitz, D. P., Singh, B., and Tan, Y. (2002) Localization and regulation of bovine eye calmodulin-dependent cyclic nucleotide phosphodiesterase by cyclic AMP-dependent protein kinase. *Int. J. Mol. Med.* **10,** 17–23.
34. Sharma, R. K. and Wang, J. H. (1986) Regulation of 63 kDa subunit containing isozyme of bovine brain calmodulin-dependent cyclic nucleotide phosphodiesterase by a calmodulin-dependent protein kinase. *J. Biol. Chem.* **261,** 1322–1328.
35. Sharma, R. K. and Wang, J. H. (1986) Regulation of cAMP concentration by calmodulin-dependent cyclic nucleotide phosphodiesterase. *Biochem. Cell Biol.* **64,** 1072–1080.
36. Zhang, G. Y., Wang, J. H., and Sharma, R. K. (1993) Purification and characterization of bovine brain calmodulin-dependent protein kinase II. The significance of autophosphorylation in the regulation of 63 kDa calmodulin-dependent cyclic nucleotide phosphodiesterase isozyme. *Mol. Cell Biochem.* **122,** 159–169.
37. Hashimoto, Y., Sharma, R. K., and Soderling, T. R. (1989) Regulation of $Ca^{2+}$/calmodulin-dependent cyclic nucleotide phosphodiesterase by the autophosphorylated form of $Ca^{2+}$/calmodulin-dependent protein kinase II. *J. Biol. Chem.* **264,** 10,884–10,887.
38. Zhang, G. Y., Wang, J. H., and Sharma, R. K. (1993) Bovine brain calmodulin-dependent protein kinase II: molecular mechanisms of autophosphorylation. *Biochem. Biophys.. Res. Commun.* **191,** 669–674.
39. Kakkar, R., Raju, R. V. S., and Sharma, R. K. (1998) In vitro generation of an active calmodulin-independent phosphodiesterase from brain calmodulin-dependent phosphodiesterase (PDE1A2) by m-calpain. *Arch. Biochem. Biophys.* **358,** 320–328.
40. Cheung, W. Y. (1967) Preparation of cyclic 3′:5′-nucleotide phosphodiesterase from rat brain. *Biochemistry* **6,** 1079–1087.

# 22

# Measurement of $Ca^{2+}$-ATPase Activity (in PMCA and SERCA1)

**Danuta Kosk-Kosicka**

## 1. Introduction

$Ca^{2+}$-ATP pumps play a vital role in intracellular calcium homeostasis and signaling. They remove excess $Ca^{2+}$ from the cytoplasm, either into the lumen of the intracellular sarcoplasmic reticulum/endoplasmic reticulum (SR/ER) network or out of the cell, and fine-tune local calcium concentrations allowing for proper functioning of a variety of $Ca^{2+}$-dependent reactions. They are also integral components of $Ca^{2+}$-dependent cellular events and cascades that are regulated by precisely controlled $Ca^{2+}$ concentrations.

Although $Ca^{2+}$ transport is a physiological function of $Ca^{2+}$ pumps, their $Ca^{2+}$-ATPase activity is so well characterized that it is used as an indicator of their function. In this chapter, three preparations—two membranes and a purified enzyme–best suited for studies of $Ca^{2+}$-ATPase activity are described. The two selected membranes are the human red blood cell (RBC) ghosts, a representative of plasma membranes (PM), and the rabbit skeletal muscle SR, an intracellular membrane. These contain the respective $Ca^{2+}$-ATPase forms: plasma membrane $Ca^{2+}$-ATPase (PMCA; PMCA 4 and 1) and SR $Ca^{2+}$-ATPase (SERCA; SERCA1). These preparations are the simplest, most commonly used, and well characterized in which $Ca^{2+}$-ATPases have been extensively studied. They are easy to prepare without contamination from other membrane types; thus, they contain a single specific $Ca^{2+}$-ATPase activity. In addition, these preparations are devoid of other $Ca^{2+}$-transporting systems, such as $Na^+/Ca^{2+}$ exchanger. Moreover, the $Na^+,K^+$-ATPase activity in RBC membranes is very low, as compared to other plasma membranes. The only enzymatic activity that needs to be considered in the described $P_i$ measurements is that of the $Mg^{2+}$-ATPase, which is also low and easily subtractable.

From: *Methods in Molecular Biology, vol. 312: Calcium Signaling Protocols: Second Edition*
Edited by: D. G. Lambert © Humana Press Inc., Totowa, NJ

Ghost membranes are prepared in hypotonic solutions, and calmodulin (CaM) is removed by EDTA washing ***(1,2)***. Because the resulting ghosts are depleted of endogenous CaM, they are suitable for studies of the calcium-dependent CaM activation of PMCA. The strong interaction of CaM with PMCA has made possible its purification by affinity chromatography following detergent solubilization ***(1,2)***. Preparation of CaM–Sepharose-4B columns is included in the procedure (*see* **Note 1**). The author has extensively modified the originally published purification procedures, and the protocol allows for purification of PMCA soluble in $C_{12}E_8$, which is very stable on storage at –80°C in the presence of 20% glycerol and is easily activated by addition of phospholipids ***(3)***. The preparation is suitable for various studies, including spectroscopic measurements that cannot be conducted on the membranous enzyme owing to its low abundance (0.1% of membrane proteins) and the effects of various phospholipids ***(4)***. Slight modifications allow for application of this procedure to other plasma membranes, as has been recently described for the synaptosomal membranes of rat cerebellum ***(5)***. SERCA1 is conveniently studied in SR, in which it comprises up to 80% of SR membrane protein.

Biochemical characterization of the enzyme in the membrane and at different stages of purification from the membrane always includes determination of its steady-state $Ca^{2+}$-ATPase activity. The assay is especially useful for the purified, soluble PMCA as a rapid functional test to complement structural studies. $Ca^{2+}$-ATPase activity in combination with fluorescence resonance energy transfer, fluorescence polarization, and equilibrium centrifugation measurements performed on such preparations allowed the author to establish that enzyme concentration-dependent dimerization is a mechanism of PMCA activation ***(6–8)***. The enzymatic hydrolysis rate of ATP is determined by quantitation of the inorganic phosphate ($P_i$) resulting from ATP hydrolysis by the pump as a function of time. In the described protocol, $P_i$ released during the ATPase reaction is subsequently measured colorimetrically as a complex of molybdovanadate ***(9,10)***. The method is simple (one-step), fast, sensitive, and reliable (*see* **Note 2**).

## 2. Materials

### 2.1. Reagents

1. Outdated packed human RBCs for preparation of ghost membranes are obtained from the local Red Cross or blood donation center.
2. Skeletal muscle SR is prepared from hind legs of the rabbit (New Zealand White).
3. Unless specified otherwise, the reagents, including egg yolk phosphatidylcholine (PC) (P5763), CNBr-activated Sepharose-4B, aprotinin, bovine brain CaM for affinity chromatography, and divalent cations ionophore A23187 were purchased from Sigma (St. Louis, MO).

4. CaM for $Ca^{2+}$-ATPase activity assays was from Calbiochem (San Diego, CA); standard solution was prepared by dissolving 1 mg of CaM in 1 mL of water and stored at –20°C.
5. 0.2-m*M* ionophore solution is made with ethanol.
6. Glycerol was from Serva (Boehringer Ingelheim Bioproducts Partnership, Heidelberg, Germany) (*see* **Note 3**).
7. Protein microassay and sodium dodecyl sulfate (SDS) were from Bio-Rad (Hercules, CA).
8. Octaethylene glycol mono-*n*-dodecyl ether, $C_{12}E_8$ (*see* **Note 4**), was from Nikkol (Tokyo, Japan). To prepare 0.1 *M* aqueous solution, pour the detergent (melted in a warm water bath) into warm deionized water (do not boil), and stir gently. Store at –4°C in a dark glass bottle.
9. Pellicon Cassette System used in preparation of RBC ghost membranes by molecular filtration is from Millipore (Bedford, MA) ***(2)***. The Cassette contains Millipore Pellicon HVLP filters (pore size 0.5 μm) in 20 sheets and it lasts for approx 15 preparations.
10. All solutions are prepared with deionized water.

### 2.2. Plasma Membranes: Human RBC Ghost Membranes

1. Washing solution: 130 m*M* KCl, 20 m*M* Tris-maleate, pH 7.4 (total volume 7 L).
2. Lysis solution: 5 m*M* Tris-maleate, 1 m*M* EDTA, pH 7.4 (23 L).
3. Ghost storage solution: 10 m*M* Tris-maleate, pH 7.4 (15 L).

### 2.3. Rabbit Skeletal Muscle SR Membranes

1. Solution 1: 10 m*M* MOPS, 10% sucrose, 0.1 m*M* EDTA, pH 7.0 (1 L).
2. Solution 2: 10 m*M* MOPS, 0.6 *M* KCl, pH 7.0 (0.5 L).
3. Solution 3: 10 m*M* MOPS, 30% sucrose, pH 7.0 (0.5 L).

### 2.4. Preparation of CaM–Sepharose-4B for Affinity Chromatography (11)

1. 1 m*M* HCl for swelling (200 mL).
2. Coupling solution: 100 m*M* sodium borate, 100 m*M* NaCl, 50 μ*M* $CaCl_2$, pH 8.2 (10 mL, freshly prepared).
3. Blocking solution: 500 m*M* ethanolamine/HCl (10 mL, freshly prepared).
4. Washing solution: 130 m*M* KCl, 10 m*M* Tris-HCl, pH 7.4 (150 mL).
5. Solution A for column regeneration: 0.1 *M* Tris-HCl, 0.5 *M* NaCl, 0.755 m*M* $C_{12}E_8$, pH 8.5 (100 mL).
6. Solution B for column regeneration: 0.1 *M* $CH_3COONa$, 10-fold diluted acetic acid, 0.5 *M* NaCl, 0.755 m*M* $C_{12}E_8$, pH 4.5 (100 mL).

### 2.5. Purification of PMCA

1. Solubilization solution (2X): 40 m*M* Tris-maleate, pH 7.4, 1 m*M* $MgCl_2$, 260 m*M* KCl, 1.5 m*M* $C_{12}E_8$ (to be added separately), 0.1 m*M* $CaCl_2$, 40% glycerol, 4 m*M* dithiothreitol (DTT) (70 mL).

2. Equilibration solution: 10 m*M* Tris-maleate, pH 7.4, 0.5 m*M* $MgCl_2$, 130 m*M* KCl, 7.55 m*M* $C_{12}E_8$, 0.05 m*M* $CaCl_2$, 20% glycerol, 2 m*M* DTT (250 mL).
3. Washing solution: 10 m*M* Tris-maleate, pH 7.4, 0.5 m*M* $MgCl_2$, 130 m*M* KCl, 0.755 m*M* $C_{12}E_8$, 0.05 m*M* $CaCl_2$, 20% glycerol, 2 m*M* DTT (150 mL).
4. Elution solution: 10 m*M* Tris-maleate, pH 7.4, 0.5 m*M* $MgCl_2$, 130 m*M* KCl, 0.755 m*M* $C_{12}E_8$, 5 m*M* EGTA, 20% glycerol, 2 m*M* DTT (50 mL). PC suspension: Pipet 30 µL of PC solution (100 mg/mL) into a small glass tube and immediately place under a stream of nitrogen delivered slowly through a Pasteur pipet. Blow dry while turning the tube to achieve an even layer of PC on the bottom. Add 300 µL of elution solution and sonicate using a small probe, periodically placing the tube on ice to avoid overheating, until the solution clears (*see* **Note 5**).

### 2.6. $Ca^{2+}$-ATPase Activity Standard Assay Buffers

1. For ghost membranes: 50 m*M* Tris-maleate, pH 7.4, 8 m*M* $MgCl_2$, 120 m*M* KCl, 1 m*M* EGTA, 1.008 m*M* $CaCl_2$ to yield the required 17.5 µ*M* free calcium (*see* **Note 6**). $CaCl_2$ is omitted from the buffer used for $Mg^{2+}$-ATPase activity.
2. For SR membranes: 50 m*M* Tris-maleate, pH 7.4, 8 m*M* $MgCl_2$, 120 m*M* KCl, 1 m*M* EGTA, 10 µ*M* ionophore A23187, 1.008 m*M* $CaCl_2$ to yield the required 17.5 µ*M* free calcium (*see* **Note 7**). $CaCl_2$ is omitted from the buffer used for $Mg^{2+}$-ATPase activity.
3. For purified PMCA: 50 m*M* Tris-maleate, pH 7.4, 8 m*M* $MgCl_2$, 120 m*M* KCl, 1 m*M* EGTA, 0.150 m*M* $C_{12}E_8$, 1.008 m*M* $CaCl_2$ to yield the required 17.5 µ*M* free calcium. When preparing this assay buffer, take into account the composition of the elution solution in which PMCA is stored (*see* **Notes 8** and **9**).

### 2.7. $P_i$ Measurement

1. Ammonium molybdate: Dissolve 5 g of $(NH_4)_6Mo_7O_{24} \cdot 4H_2O$ in water and add 0.5 mL of ammonia (sp gr 0.90) to make 50 mL.
2. Ammonium metavanadate: Dissolve 0.1175 g of $NH_4VO_3$ in 20 mL of boiling water, and cool under tap water immediately after vanadate dissolves; follow with addition of 0.305 mL of concentrated (sp gr 1.42) nitric acid that has been diluted with 0.7 mL of water. Add water up to 50 mL total volume.
3. 20% SDS solution: Dissolve 10 g of SDS in water to make 50 mL.
4. Mixed Lin-Morales reagent: Mix the solutions in **items 1–3** with 17.5 mL of concentrated nitric acid and make up to 0.5 L with water. Store in a dark glass bottle. This solution will keep for 1 to 2 mo; discard when a significant amount of precipitate forms on the bottom. For the assays described in **Subheading 3.3.**, use Lin-Morales solution diluted threefold with water.

## 3. Methods

### 3.1. Preparation of Membranes Containing Either PMCA (RBC Ghosts) or SERCA1 (SR)

All steps are carried out at 4°C either in the cold room or on ice. The solutions can be prepared up to 1 wk ahead of time and kept refrigerated. All glassware is chilled before use.

### 3.1.1. RBC Ghosts

The preparation takes 8–10 h.

1. Start with 3 U of packed erythrocytes (750 mL): Divide them among six 250-mL centrifuge bottles, fill with washing solution, and centrifuge at 4,000*g* for 10 min. Remove the supernatant and the fluffy coat of white blood cells. (Use a Pasteur pipet connected to an aspirator water pump.)
2. Wash two more times with 5 vol of washing solution using 12 centrifuge bottles.
3. Pour the washed cells into an Erlenmeyer flask containing 2 L of the lysis solution while continuously stirring gently by hand. Add lysis solution to a total volume of up to 4 L (the desired volume ratio of lysis solution to the washed erythrocytes is 8–10:1). Leave in a cold room for 15 min.
4. In the meantime, wash the Pellicon with 2 L of lysis solution and subsequently fill with lysate. Wash the RBCs by continuous application of fresh lysis solution (up to 12–15 L total volume), followed by 10–15 L of storage solution until the membranes are light pink (*see* **Note 10**).
5. Transfer the membranes to 40-mL centrifuge tubes (16 tubes). If necessary, fill up with washing solution. Centrifuge at 20,000*g* for 30 min. Aspirate supernatants.
6. Vortex the tubes and transfer the pellets with a Pasteur pipet into a beaker kept on ice. Wash the tubes with small aliquots of storage solution, and by transferring to consecutive tubes recover all material (*see* **Notes 11** and **12**).
7. Measure the total volume and set aside small aliquots for protein and preliminary $Ca^{2+}$-ATPase activity assays. Divide the ghosts into plastic tubes and place in a freezer at –80°C, where they can be stored for a prolonged time (*see* **Notes 13–15**).

### 3.1.2. Light SR Membranes ***(12)***

The preparation takes approx 8 h.

1. Remove muscle from both hind legs of the rabbit and place in a large beaker of 0.1 m*M* EDTA.
2. Cut off the unwanted material and wash once in distilled water.
3. Weigh 170 g of muscle and add 510 mL of solution 1 (*see* **Note 16**). Blend 15 s every 5 min for 1 h. Check pH every 10–20 min; add 10% NaOH solution to maintain pH between 6.5 and 7.0.
4. Divide into four parts and centrifuge in 250-mL centrifuge bottles at 15,000*g* for 20 min.
5. Collect supernatant and filter through 1 to 2 in. of gauze. There should be about 320 mL of filtrate. Divide the filtrate into eight 40-mL tubes, and centrifuge at 40,000*g* for 90 min.
6. Discard supernatant and suspend sediments of alternate tubes in 10 mL of solution 2. Scrape off pellet with a glass rod and pour into next tube; scrape off second pellet and pour suspension into the homogenizer. Repeat with 5 mL of solution 2 again in alternate tubes. Use a total of 60–70 mL of solution 2.
7. Disperse aggregates with a glass homogenizer (40 mL Dounce). Homogenize in portions until uniform, avoiding foam. Incubate in a cold room for 40 min.

8. Divide the suspension into five to six 15-mL Corex tubes and centrifuge at 15,000*g* for 20 min.
9. Collect approx 10 mL of supernatant into each of five to six polycarbonate tubes. Do not take the very top layer or the very thick bottom layer. Centrifuge at 40,000*g* for 90 min.
10. Discard supernatant and dissolve pellet in 18 mL of solution 3 as described in **step 6**. Homogenize and divide into small polypropylene tubes. Quick freeze in liquid nitrogen or by placing in a –80°C freezer (*see* **Notes 17** and **18**).

## 3.2. Purification of PMCA From RBC Ghosts

### 3.2.1. Preparation of CaM–Sepharose-4B Affinity Chromatography Columns

For preparation of three affinity chromatography columns, use 2.8 g of dry Sepharose-4B (which will swell to 9.8 mL) and 8 mg of CaM.

1. Place 1.4 g of CNBr-activated Sepharose-4B in each of two 15-mL Corex tubes. Slowly add 14 mL of 1 m*M* HCl, stirring gently with a thin glass rod. Let this swell for 15 min at room temperature.
2. Spin down at low speed for 5–10 min. Aspirate HCl, taking care not to remove any Sepharose. Repeat five times more.
3. To each tube add 2 mL of coupling solution, hand mix end-to-end, and quickly follow with addition of 2 mL of coupling solution containing CaM at 2 mg/mL (*see* **Note 19**). Mix gently overnight in a cold room using a rotation apparatus (*see* **Note 20**).
4. Spin down at low speed for 10 min. To each tube add 4 mL of blocking solution and incubate for 2 h at room temperature. Determine the amount of unbound CaM (spectrophotometrically, with $E_{1\ mg/mL}$ at 276 nm) in the collected supernatant to calculate the coupling efficiency.
5. Wash the resin six times by alternating distilled water and washing solution. Suspend in washing solution with 0.02% merthiolate for storage at 4°C.
6. Prepare chromatography columns by slowly pouring the resin suspension into 10-mL plastic syringes fitted with plastic tubing and stoppers so that the flow rate can be easily controlled (*see* **Notes 21** and **22**).

### 3.2.2. Purification of PMCA

Two 3-mL columns are used in this 8- to 9-h long purification procedure. All steps are carried out at 4°C, either in a cold room or on ice. Use cold solutions. Include aprotinin in all solutions in **steps 1–4** (*see* **Note 23**).

1. Thaw 500 mg of ghosts by placing them in a water bath at room temperature. In the meantime, cool the centrifuge.
2. Vortex the thawed ghosts and divide into four 40-mL centrifuge tubes. Add the 2X solubilization solution without $C_{12}E_8$, vortex, and pipet $C_{12}E_8$ slowly in, while constantly vortexing the tube, to the final concentration of 0.755 m*M*. Add aprotinin. Keep protein concentration at 8–10 mg/mL (*see* **Note 24**).

3. After 10 min incubation on ice, centrifuge at 40,000*g* for 45 min. Collect the supernatant containing solubilized membrane proteins. Measure the volume, divide into two portions, and load onto two CaM-Sepharose columns at a flow rate of 0.25 mL/1 min. The loading step takes approx 2 h.
4. Wash each column with 30–40 mL of washing solution at a flow rate of 0.25 mL/min until no protein is coming out of the column (absorbance reading at 280 nm equals that of the washing solution).
5. Start adding elution solution and immediately change the flow rate to 0.5 mL/min. Collect 0.8–1-mL fractions, recording absorbance at 280 nm (*see* **Note 25**). Combine fractions with high protein concentration, these are usually fractions 3–5. Perform protein assay (*see* **Note 26**).
6. Supplement the eluted PMCA with PC suspension: 30 µL/1 mL eluent (*see* **Note 27**). Store the preparation in small aliquots (0.2–1 mL, *see* **Note 28**) at –80°C. At this point, 30–40 min have elapsed since initiation of PMCA elution from the column.
7. Run the rest of the elution solution through the column (total volume of 20 mL), and follow with 20 mL of equilibration solution with 0.02% merthiolate (*see* **Note 29**). To regenerate the columns, run 10 bed volumes (30 mL) of solutions A and B. Equilibrate with equilibration solution. Add 0.02% merthiolate if being stored.

### 3.3. Determination of $Ca^{2+}$-ATPase Activity

$Ca^{2+}$-ATPase activity is determined through measurements of $P_i$ resulting from ATP hydrolysis by the $Ca^{2+}$ pump.

1. Prepare 1.7-mL polypropylene tubes with appropriate assay buffer (*see* **Note 30**). Additionally, for determination of the CaM-dependent $Ca^{2+}$-ATPase activity, add 5 µL of CaM solution of appropriate concentration (*see* **Note 31**).
2. Add 2–10 µL membrane or purified enzyme preparation (*see* **Note 32**) to enough appropriate assay buffer and water to a total of 95 µL. Start the $Ca^{2+}$-ATPase reaction 15 s later by adding 5 µL of 60 m*M* ATP, cap the tube, vortex, and place in the rack in the water bath at 37°C (*see* **Note 33**). Start the stopwatch at the moment ATP is added. Repeat the procedure for each tube at 1-min intervals. Perform each data point in duplicates (*see* **Note 34**).
3. Stop the $Ca^{2+}$-ATPase reaction at 15 or 30 minutes (*see* **Note 35**) by adding 300 µL of the diluted Lin-Morales reagent to consecutive tubes at 1-min intervals. Vortex and transfer the whole aliquot to a cuvet, and read the absorbance at 350 nm at 30 s as timed from the addition of the Lin-Morales reagent (*see* **Notes 36** and **37**).
4. To quantify the amount of $P_i$ present in the $Ca^{2+}$-ATPase assay, use a calibration curve obtained by this procedure (no incubation necessary) using $K_2HPO_4$ solutions of known concentrations as standards (*see* **Note 38**).
5. The $Ca^{2+}$-ATPase activity in the membranes is calculated as a difference between the activity determined in the appropriate standard assay buffer and the assay buffer in which calcium is omitted. By contrast, the purified PMCA has no $Ca^{2+}$-independent activity (*see* **Note 39**). The CaM-dependent activation is determined as a dif-

ference in $Ca^{2+}$-ATPase activity in the presence and absence of CaM (*see* **Notes 40** and **41**).

## 4. Notes

1. Commercially available CaM–Sepharose-4B sometimes produces enzyme that is not CaM sensitive, suggesting CaM bleaching.
2. The only drawback to this method is that the solubility of SDS is sensitive to its ionic environment. SDS present in the Lin-Morales solution effectively denatures the assayed protein, thus stopping the reaction and dissolving the protein. Using a threefold-diluted Lin-Morales solution, we seldom encounter problems. Trace amounts of precipitation were observed only with some membranes, such as microvessels, and these could be removed by sedimentation in a countertop centrifuge without affecting the $P_i$ measurement. On some occasions, such as studying the effects of solutes containing phosphate on $Ca^{2+}$-ATPase activity, instead of colorimetric measurement the released $P_i$ may be determined by $^{32}P_i$ radioactivity measurement ***(13,14)***. In this procedure, $^{32}$P-ATP is used to start the $Ca^{2+}$-ATPase reaction. Then, after the reaction is terminated with perchloric acid, $^{32}P_i$ is extracted with charcoal and, following a filtration through Millipore filters, extracted into a 2-methyl-1-propanol/benzene mixture. An aliquot of the organic phase is counted in a scintillation counter.
3. Enzyme purified in the presence of glycerol bought from other companies is often less active.
4. Substitution of $C_{12}E_8$ for Triton X-100 and addition of glycerol results in a stable PMCA preparation. Another advantage of $C_{12}E_8$ over Triton X-100 is lack of interference with protein absorbance at 280 nm, making it easy to monitor protein elution from the column.
5. PC suspension does not totally clarify. It takes some practice to reach exactly the desired point and not further. For future use write down your conditions.
6. Total calcium in solutions needs to be measured by atomic absorption for precise calculations of $CaCl_2$ to be added. This is especially important when $Ca^{2+}$-ATPase activity is measured as a function of free calcium concentration. Our experience shows that 16 μ*M* calcium contamination (from reagents, water, glassware, and so on) should be taken into account. Free $Ca^{2+}$ concentrations are calculated based on the constants given by Schwartzenbach et al. ***(15)***, pH, and the competitive effects of $Mg^{2+}$, $K^+$, and nucleotide as described by Fabiato and Fabiato ***(16)***.
7. The composition of this assay buffer has been modified as compared to buffers used by other investigators. The author wanted it to be as close as possible to the assay buffer used for PMCA activity for the purpose of comparative studies on the two $Ca^{2+}$ pumps. The specific activity of SERCA1 obtained using the author's conditions does not differ from the activity reported in other laboratories.
8. Depending on the volume of PMCA that is added, calculate how much $C_{12}E_8$ and EGTA will be delivered with the enzyme, and add appropriately less of each while preparing the assay buffer. For example, addition of 5 μL of PMCA per assay tube results in 0.0375 m*M* $C_{12}E_8$ and 0.25 m*M* EGTA, i.e., 25% of the

desired final concentrations of both components. To assure good reproducibility, the author prepares separate stock solutions of reaction mixture (RM) for experiments in which various amounts of PMCA are added (such as determination of $Ca^{2+}$-ATPase activity as a function of PMCA concentration, which reflects enzyme activation by self-association ***[6,7,16]***). Thus, for an experiment in which 5 µL of PMCA will be added to the assay tube, prepare 6.5 mL of RM (an amount adequate for 2 d of experiments) comprised of the following: 1 mL of 0.5*M* Tris-maleate, pH 7.4; 1.5 mL of 0.9*M* KCl; 0.8 mL of 0.1 *M* $MgCl_2$, 0.075 mL of 0.1 *M* EGTA, pH 7.4; 1.125 mL of 1 m*M* $C_{12}E_8$, 1.2595 mL of 8 m*M* $CaCl_2$, and 0.7405 mL water. Then to each tube, pipet in the following order: 65 µL of RM, 18–23 µL of water, 5 µL of CaM (if necessary), 2–7 µL of PMCA, and 5 µL of ATP. RM can be refrigerated for several days.

9. When $Ca^{2+}$-ATPase activity is measured as a function of free calcium concentration, prepare RM without calcium and pipet $CaCl_2$ separately to each tube. Since the commercially available standard $CaCl_2$ solutions have a low pH, dilute them with a Tris buffer to keep the pH reproducible in all assay tubes. Titrate calcium solution against EGTA solution.
10. An alternative way to remove hemoglobin after RBC lysis is repetitive centrifugation ***(1)***. This is performed at first in 250-mL centrifuge bottles at 11,000*g* for 20 min. When the pellet becomes fluffy, the material has to be transferred to 40-mL tubes for centrifugation at 20,000*g* for 20 min. A total of five washes with lysis solution is usually followed by four washes with storage solution until the supernatant is no longer red. Having compared the two methods, the author prefers to use the Pellicon because it is less tedious than repetitive centrifugation.
11. The pellet does not have to be white. Some reddish coloration does not interfere with the activity assays. Sometimes a red core is present in the pellets; make sure not to include it in the collected material.
12. At this stage, be very careful to recover all material; it is pure, concentrated ghost membranes.
13. The expected volume is 90–120 mL.
14. In the author's experience, preparations kept for 2 yr were still fully active without loss of $Ca^{2+}$-ATPase activity.
15. The preparation yields 600–800 µg of PMCA protein.
16. One 5–6-lb rabbit yields approx 150–200 g of muscle.
17. SR preparation stored at –80°C remains active for many years.
18. The preparation yields approx 100 mg SR protein.
19. Reactive groups hydrolyze at high pH at which coupling of CaM is performed; thus, perform this step quickly to ensure maximal coupling of CaM. Calculate the efficiency of coupling by comparing the absorbance at 276 nm for CaM solution in the coupling buffer before addition to the Sepharose, and in the supernatant after the coupling (*see* **step 4**). In the author's experience, the coupling efficiency is between 88 and 95%.
20. Alternatively, the coupling could be performed for 2 h at room temperature. We find the overnight incubation more convenient. Also, **step 4** (blocking) could be performed overnight in a cold room.

21. Place a small amount of glass wool on the bottom of the syringe. After packing the column, test different flow rates and make sure that the eluent is clear (if the resin is coming out, one will see it on the wall of the glass tube in which the eluent is collected).
22. The author has used a variety of chromatography columns, including commercially available ones, in different sizes; the described small-scale procedure using syringe columns provides consistently reproducible, active, and CaM-stimulated PMCA preparation. The columns last for 15–20 purifications.
23. Add 100 Kalikrein IU of aprotinin/mL of solution, right before using them. It is especially important at the beginning of the purification procedure when other proteins are still present. There is no need to add aprotinin to the elution solution.
24. For a final protein concentration of 10 mg/mL, the total volume is 12.5 mL. Add 6.25 mL of 2X solubilization solution and 0.95 mL of 10 m*M* $C_{12}E_8$. The volume of ghosts should be 5.3 mL. Ghost preparation is usually less concentrated than 23 mg/mL; thus, centrifuge the thawed ghosts in the four tubes (after filling them with the storage solution) at 20,000*g* for 20 min. Have the desired volume of 5.3 mL marked on the tube so that you will know when to stop aspirating the supernatant.
25. The $UV_{280}$ absorbance of washing and elution solutions needs to be alike in order to observe the elution of the $Ca^{2+}$-ATPase protein. For this reason, we always prepare these solutions at the same time.
26. Before adding PC, determine protein concentration of the combined eluent, using Bio-Rad Protein Micro-assay, based on the Bradford dye-binding procedure. Add 10–20 µL to 790–780 µL of water (total volume 800 µL), and 200 µL of the reagent. The values (80–140 µg protein/mL) are usually close to the expected concentration based on UV readings. PC interferes with the assay. In the first preparation, before combining all fractions, collect small volumes of the eluted PMCA and perform the protein and $Ca^{2+}$-ATPase activity assay. This way the elution profile of the column will be known. One can also keep separately, if desired, the most active PMCA fractions.
27. It is recommended to initially divide the eluted enzyme into small aliquots and add to each of them different amounts of PC. Then, determine $Ca^{2+}$-ATPase activity in the presence and absence of CaM for each to establish optimal PC: enzyme molar ratio for activation of the preparation.
28. The author freezes PMCA in aliquots that can be used in 1-d experiments. It is not advisable to thaw a tube more than two to three times because significant loss of activity may occur.
29. It is safe to leave columns in elution solution until the next day. The columns are usually regenerated the next day, while performing the preliminary characterization of purified PMCA ($Ca^{2+}$-ATPase activity and purity by gel electrophoresis).
30. The reaction can be performed in small glass tubes of appropriate volume that would allow for good mixing of the reaction mixture and the Lin-Morales reagent. The author chose to perform the assay in sealed polypropylene tubes because they are suitable for studies on the effect of volatile anesthetics on the $Ca^{2+}$-ATPase activity.

31. In a typical assay, the author uses 2 μ*M* CaM (final concentration in the reaction is 100 n*M*).
32. The optimal amounts of protein in the assay at 37°C/25°C usually are 10–12/16–20 μg of ghost membranes, 0.20/0.36 μg of SR, and 0.2–0.3/0.4–0.65 μg (i.e., 30–50 n*M* final concentration in the assay) for the CaM-independent dimeric PMCA.
33. When the reaction is performed at a different temperature, the correct range of absorbance readings will be assured by either changing the amount of protein in the assay (an example is shown in **Note 32** for 25 vs 37°C) or the reaction time.
34. Reproducibility of the assay is very good. For some plasma membrane preparations, such as microvessels, there is significant scatter; in such cases, triplicates should be used.
35. The reaction is linear for at least 30–40 min. It is advisable to check first the linearity for your particular preparation before settling on performing the reaction for either 15 or 30 min. The author usually selects a 30-min reaction time, which allows for 30 tubes in one assay performed by one person.
36. Alternatively, the reading could be made at 30–60 min after the addition of the Lin-Morales reagent. In this case, the 1-min intervals between readings do not need to be made.
37. The absorbance of the samples is read against a blank prepared and treated the same way as the samples, with the exclusion of the studied protein. For membranous preparations, it is advisable to double-check that they are not contributing to the reading (at higher protein concentration some plasma membranes do—in such cases subtract the absorbance).
38. The calibration curve that expresses the sensitivity of the method shows linearity in the range of final $P_i$ concentrations up to $1.75 \times 10^{-4}$*M*. 10 nmol of $P_i$ in the tube gives an absorbance reading of 0.25. If desired, the sensitivity can be increased by using the nondiluted Lin-Morales reagent.
39. Specific activities for the $Ca^{2+}$-ATPase in the three preparations at 37°C are 0.8–1.4 μmol $P_i$/(mg protein · h) in ghost membranes, 300 μmol $P_i$/(mg protein · h) for SERCA1 in skeletal SR, and 180–300 μmol $P_i$/(mg protein · h) for the purified PMCA.
40. In a typical CaM-dependent $Ca^{2+}$-ATPase activity assay, CaM is added at 100 n*M* concentration to assure a molar ratio of CaM to PMCA of 2:1 ***(6,17,18)***.
41. By dividing the CaM-dependent by the CaM-independent activity, the CaM stimulation factor is derived. CaM stimulates the PM $Ca^{2+}$-ATPase activity up to five to sevenfold, depending on the particular membrane preparation and calcium as well as potassium concentrations. In the purified PMCA preparations, CaM stimulates only $Ca^{2+}$-ATPase activity of the monomeric enzyme whereas the dimers are fully activated through enzyme self-association ***(6–8,17)***.

## References

1. Niggli, V., Penniston, J. T., and Carafoli, E. (1979) Purification of the ($Ca^{2+}$ + $Mg^{2+}$)-ATPase from human erythrocyte membranes using a calmodulin affinity column. *J. Biol. Chem.* **254,** 9955–9958.

2. Gietzen, K., Tejcka, M., and Wolf, H. V. (1980) Calmodulin affinity chromatography yields a functional purified erythrocyte ($Ca^{2+}$ + $Mg^{2+}$)-dependent adenosine triphosphatase. *Biochem. J.* **189,** 81–88.
3. Kosk-Kosicka, D., Scaillet, S., and Inesi, G. (1986) The partial reactions in the catalytic cycle of the calcium-dependent adenosine triphosphatase purified from erythrocyte membranes. *J. Biol. Chem.* **261,** 3333–3338.
4. Missiaen, L., Raeymaekers, L., Wuytack, F., Vrolix, M., DeSmedt, H., and Casteels, R. (1989) Phospholipid-protein interactions of the plasma-membrane $Ca^{2+}$-transporting ATPase. *Biochem. J.* **263,** 687–694.
5. Kosk-Kosicka, D. and Zylinska, L. (1997) Protein kinase and calmodulin effects on the plasma membrane $Ca^{2+}$-ATPase from excitable and nonexcitable cells. *Mol. Cell. Biochem.* **173,** 79–87.
6. Kosk-Kosicka, D. and Bzdega, T. (1988) Activation of the erythrocyte $Ca^{2+}$-ATPase by either self-association or interaction with calmodulin. *J. Biol. Chem.* **263,** 18,184–18,189.
7. Kosk-Kosicka, D., Bzdega, T., and Wawrzynow, A. (1989) Fluorescence energy transfer studies of purified erythrocyte $Ca^{2+}$-ATPase. *J. Biol. Chem.* **264,** 19,495–19,499.
8. Sackett, D. L. and Kosk-Kosicka, D. (1996) The active species of plasma membrane $Ca^{2+}$-ATPase are a dimer and a monomer-calmodulin complex. *J. Biol. Chem.* **271,** 9987–9991.
9. Lecocq, J. and Inesi, G. (1966) Determination of inorganic phosphate in the presence of adenosine triphosphate by the molybdo-vanadate method. *Anal. Biochem.* **15,** 160–163.
10. Lin, T.-I. and Morales, M. F. (1977) Application of a one-step procedure for measuring inorganic phosphate in the presence of proteins: The actomyosin ATPase system. *Anal. Biochem.* **77,** 10–17.
11. Pharmacia LKB Biotechnology. *Affinity Chromatography: Principles and Methods.* Amersham Pharmacia Biotech instruction booklet (Uppsala, Sweden).
12. Eletr, S. and Inesi, G. (1972) Phospholipid orientation in sarcoplasmic membranes: Spin-label ESR and proton NMR studies. *Biochim. Biophys. Acta* **282,** 174–179.
13. Carvalho, M. G. C., Souza, D. G., and deMeis, L. (1976) On a possible mechanism of energy conservation in sarcoplasmic reticulum membrane. *J. Biol. Chem.* **251,** 3629–3636.
14. Kosk-Kosicka, D., Kurzmack, M., and Inesi, G. (1983) Kinetic characterization of detergent-solubilized sarcoplasmic reticulum adenosinetriphosphatase. *Biochemistry* **22,** 2559–2567.
15. Schwartzenbach, G., Senn, H., and Andereff, G. (1957) *Helvetica Chimica Acta* **40,** 1886–1900.
16. Fabiato, A. and Fabiato, F. (1979) *J. Physiol. (Paris)* **75,** 463,464.
17. Kosk-Kosicka, D., Bzdega, T., and Johnson, J. D. (1990) Fluorescence studies on calmodulin binding to erythrocyte $Ca^{2+}$-ATPase in different oligomerization states. *Biochemistry* **29,** 1875–1879.
18. Kosk-Kosicka, D. (1990) Comparison of the red blood cell $Ca^{2+}$-ATPase in ghost membranes and after purification. *Mol. Cell. Biochem.* **99,** 75–81.

# Index

METHODS IN MOLECULAR BIOLOGY™ • 312
SERIES EDITOR: *John M. Walker*

# Calcium Signaling Protocols

*Second Edition*

Edited by

**David G. Lambert**

*Department of Cardiovascular Sciences, Division of Anaesthesia, Critical Care, and Pain Management, Leicester Royal Infirmary, Leicester, UK*

***From Reviews of the First Edition…***

*"…will find a place on the bench in any lab that is moving into calcium signaling, or expanding its repertoire of techniques in calcium signaling. It will be valuable as a resource for…years to come."* ***—CELL BIOLOGY INTERNATIONAL***

*"This book achieves much…For anyone remotely interested in $Ca^{2+}$ it will be a very valuable resource in their lab."* ***—QUARTERLY REVIEW OF BIOLOGY***

Now extensively updated and expanded, *Calcium Signaling Protocols, Second Edition* continues the excellence of the highly regarded first edition. New to this edition are chapters on the electrophysiological measurement of $Ca^{2+}$ channel activity, enhanced coverage of confocal microscopy, and practical tutorials on two of the most common industrial high-throughput machines, the Fluorometric Imaging Plate Reader (FLIPR), and the FlexStation. All experimental chapters provide readily reproducible techniques for measuring the many facets of $Ca^{2+}$ signaling. The protocols follow the successful *Methods in Molecular Biology*™ series format, each offering step-by-step laboratory instructions, an introduction outlining the principles behind the technique, lists of the necessary equipment and reagents, and tips on troubleshooting and avoiding known pitfalls.

Authoritative and up-to-date, *Calcium Signaling Protocols, Second Edition* provides for novice and expert researchers alike both theoretical and practical information for the optimal design and performance of studies of intracellular $Ca^{2+}$regulation.

## FEATURES

- **Up-to-date and readily reproducible techniques for the study of $Ca^{2+}$ signaling**
- **Proven techniques for measuring $Ca^{2+}$ channel activity**
- **Fully tested methods for assessing the release of stored $Ca^{2+}$**
- **Practical tutorials on the Fluorometric Imaging Plate Reader (FLIPR) and the FlexStation**
- **Step-by-step instructions to ensure successful results**
- **Tricks of the trade and notes on troubleshooting and avoiding known pitfalls**

ISBN 1-58829-442-0

90000

9 781588 294425

Methods in Molecular Biology™ • 312
CALCIUM SIGNALING PROTOCOLS, *SECOND EDITION*
ISBN: 1-58829-442-0 E-ISBN: 1-59259-949-4
ISSN: 1064–3745 humanapress.com